

Optical Sensing and Imaging of pH Values: Spectroscopies, Materials, and Applications

Andreas Steinegger, Otto S. Wolfbeis, and Sergey M. Borisov*

Cite This: *Chem. Rev.* 2020, 120, 12357–12489

Read Online

ACCESS |



Metrics & More

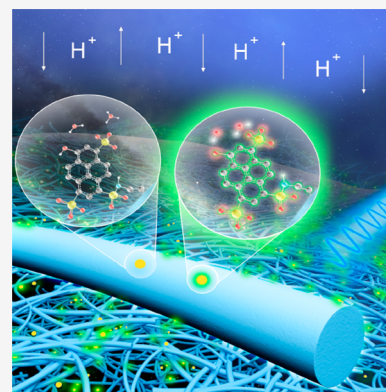


Article Recommendations



Supporting Information

ABSTRACT: This is the first comprehensive review on methods and materials for use in optical sensing of pH values and on applications of such sensors. The Review starts with an introduction that contains subsections on the definition of the pH value, a brief look back on optical methods for sensing of pH, on the effects of ionic strength on pH values and pK_a values, on the selectivity, sensitivity, precision, dynamic ranges, and temperature dependence of such sensors. Commonly used optical sensing schemes are covered in a next main chapter, with subsections on methods based on absorptiometry, reflectometry, luminescence, refractive index, surface plasmon resonance, photonic crystals, turbidity, mechanical displacement, interferometry, and solvatochromism. This is followed by sections on absorptiometric and luminescent molecular probes for use pH in sensors. Further large sections cover polymeric hosts and supports, and methods for immobilization of indicator dyes. Further and more specific sections summarize the state of the art in materials with dual functionality (indicator and host), nanomaterials, sensors based on upconversion and 2-photon absorption, multiparameter sensors, imaging, and sensors for extreme pH values. A chapter on the many sensing formats has subsections on planar, fiber optic, evanescent wave, refractive index, surface plasmon resonance and holography based sensor designs, and on distributed sensing. Another section summarizes selected applications in areas, such as medicine, biology, oceanography, bioprocess monitoring, corrosion studies, on the use of pH sensors as transducers in biosensors and chemical sensors, and their integration into flow-injection analyzers, microfluidic devices, and lab-on-a-chip systems. An extra section is devoted to current challenges, with subsections on challenges of general nature and those of specific nature. A concluding section gives an outlook on potential future trends and perspectives.



CONTENTS

1. Introduction, Definition of the pH Value, and General Considerations	12359	2.2.6. Other Kinds of Energy Transfer	12372
1.1. A Look Back on Optical Sensing of pH Values	12359	2.2.7. Dual Lifetime Referencing (DLR)	12372
1.2. Optical Sensing of pH Values: Specific Features	12363	2.3. Refractive Index Based Sensing	12374
1.3. Definition of the pH Value	12364	2.4. Surface Plasmon Resonance Based Sensing	12375
1.4. Proton Activity versus Concentration	12365	2.5. Photonic Crystal Based Sensing	12375
1.5. Dissociation Constants of Indicators and of Polymers with pH-Dependent Charge	12365	2.6. Sensing of pH Values via the pH-Dependent Turbidity of Hydrogels	12376
1.6. Effect of Ionic Strength on pH Values and pK_a Values	12365	2.7. Infrared and Raman Spectroscopic Sensing	12376
1.7. Selectivity and Interferences	12368	2.8. Sensing of pH Values via Mechanical Displacement	12376
1.8. Sensitivity, Precision, and Dynamic Range	12368	2.9. Interferometric Sensing of pH Values	12377
1.9. Effects of Temperature	12368	2.9.1. Interferometric Sensing of pH Values Using Stimuli-Responsive Polymers, Composites, and Layers	12377
2. Commonly Used Optical Sensing Schemes	12369	2.9.2. Interferometric Sensing (IFS) of pH Values Using pH-Indicators	12378
2.1. Absorptiometry and Reflectometry	12369		
2.2. Measurement of Luminescence	12370		
2.2.1. Luminescence Intensity	12370		
2.2.2. Luminescence Decay Time	12370		
2.2.3. Förster Resonance Energy Transfer	12370		
2.2.4. Inner Filter Effect	12371		
2.2.5. Quenching of Fluorescence	12371		

Received: May 15, 2020

Published: November 4, 2020



2.10. Sensing of pH-Values via Solvatochromic Fluorescent Probes	12378	8.9. Nanofilm Sensors	12413
2.11. Referenced (Ratiometric) Sensing	12378	9. Additives, Coatings, and Other Components	12413
3. Overview of Commonly Used Absorptiometric pH Probes	12380	9.1. Plasticizers	12413
3.1. Sulphophthalein Dyes	12380	9.2. Scattering Particles	12414
3.2. Phthalein Dyes	12381	9.3. Optical Isolations	12414
3.3. Azo Dyes	12381	9.4. Materials Acting As Inert Mechanical Support	12414
3.4. Other Dye Classes	12381	9.5. Photostabilizers	12416
4. Overview of Commonly Used Luminescent pH Probes	12383	10. Luminescent Sensors	12416
4.1. Organic Probes	12384	10.1. Intensity-Based Sensors	12416
4.1.1. HPTS and Derivatives	12385	10.2. Decay Time-Based Sensors	12416
4.1.2. Coumarins and Derivatives	12385	10.3. Fluorescence Anisotropy-Based Sensors	12418
4.1.3. Fluoresceins and Derivatives	12386	10.4. Energy Transfer-Based Sensors	12420
4.1.4. Rhodamine and Rhosamine Dyes	12386	10.5. Other Luminescent Sensing Schemes for pH	12421
4.1.5. 1,8-Naphthalimide Dyes	12387	10.6. pH Sensors Based on Upconversion and 2-Photon Absorption	12423
4.1.6. Perylene Diimides (PDIs)	12387	10.7. Multiparameter Sensors	12424
4.1.7. Boron-dipyrromethenes (BODIPYs)	12387	11. Imaging of pH Values	12427
4.1.8. BF ₂ -Chelated Tetraarylazadipyrromethene Dyes (aza-BODIPYs)	12388	11.1. Intensity-Based Imaging	12427
4.1.9. Diketopyrrolopyrroles (DPPs)	12388	11.2. Lifetime-Based Imaging	12429
4.1.10. Cyanine Dyes	12388	12. pH Sensors for Extreme pH Values	12430
4.1.11. Free-Base Porphyrins	12388	12.1. Sensors for pH Values from 10 to 14	12430
4.1.12. Triangulenium Dyes	12388	12.2. Sensors for pH Values below 3	12433
4.1.13. Miscellaneous Indicator Dyes	12388	13. pH Sensors with Wide Dynamic Range	12434
4.1.14. pK _a and Dynamic Range Adjustment for Fluorescent Indicators	12388	14. Sensing Formats	12438
4.2. Metal–Ligand Complexes	12390	14.1. Planar Sensors	12438
5. Polymeric Hosts and Supports	12391	14.2. Fiber Optic and Other Waveguide Sensors	12439
5.1. General Considerations	12392	14.3. Evanescent Wave Sensing	12439
5.2. Organic Polymers and Supports	12392	14.4. Refractive Index and Surface Plasmon Resonance Based pH Sensors	12440
5.3. Inorganic Supports and Host Materials	12395	14.4.1. Refractive Index Based pH Sensors	12440
5.3.1. Silicates (Including Sol–Gels and Ormosils)	12395	14.4.2. Surface Plasmon Resonance-Based pH Sensors	12441
5.3.2. Mesoporous Materials	12396	14.5. Photonic Crystal-Based pH Sensors	12442
6. Immobilization of Indicator Dyes in Hosts	12396	14.6. Holographic pH Sensors	12443
6.1. Physical Entrapment of Indicators	12396	14.7. Distributed Sensing of pH Values	12444
6.2. Covalent Immobilization of Indicators	12398	15. Selected Applications of Optical pH Sensors	12444
7. Materials with Dual Functionality (Indicator and Host)	12399	15.1. Applications of pH Optodes in Medicine and Test Animals	12444
7.1. Metal–Organic Frameworks	12399	15.1.1. Sensing and Imaging of pH Values in Blood and the Vascular System	12444
7.2. Conjugated Polymers	12401	15.1.2. pH Sensing in Other Biological Fluids	12445
7.3. Genetically Encoded Fluorescent Proteins	12402	15.1.3. Sensing and Imaging of pH Values on Skin and in Wounds	12446
8. Nanomaterials	12403	15.1.4. Sensing and Imaging of pH Values in Tissue and Organs	12446
8.1. Nanoparticle-Based Sensing of pH Values	12403	15.2. Intracellular and Extracellular Measurement of pH Values	12447
8.2. Dendrimers and Biomolecular Conjugates	12405	15.3. Sensing and Imaging of pH Values in Plant Research	12447
8.3. Silica Nanoparticles	12405	15.4. Sensing and Imaging of pH Values in Oceanography and Marine Biology	12448
8.4. Organic Polymer Particles	12407	15.5. Sensing and Imaging of pH Values in Biotechnology	12450
8.4.1. Hydrophilic Polymers	12407	15.6. pH Sensors as Transducers in Biosensors	12450
8.4.2. Hydrophobic Polymers	12407	15.7. pH Sensors as Transducers in Chemical Sensors	12451
8.4.3. Core–Shell Nanoparticles	12407	15.8. Integration of pH Sensors into Flow-Injection Analyzers, Microfluidic Devices, and Lab-on-a-Chip Systems	12451
8.5. Quantum Dots	12407	15.9. pH Sensors in Food Packaging	12453
8.6. Carbon-Based Nanomaterials	12408		
8.6.1. Carbon Dots	12408		
8.6.2. Graphite Oxide Dots	12410		
8.6.3. Single-Walled Carbon Nanotubes	12411		
8.7. Miscellaneous Materials	12411		
8.7.1. Nanosensors Based on Conformational Changes in Polymers	12411		
8.7.2. Inorganic–Organic Hybrids	12412		
8.7.3. Magnetic Nanoparticles	12412		
8.8. Aggregation-Induced Emission	12412		

15.10. Corrosion Studies and Monitoring of pH Values in Concrete	12453
16. Challenges	12454
16.1. Challenges of General Nature	12454
16.2. Challenges of Specific Nature	12455
17. Conclusions and Outlook	12456
Associated Content	12456
Supporting Information	12456
Author Information	12457
Corresponding Author	12457
Authors	12457
Author Contributions	12457
Notes	12457
Biographies	12457
Acknowledgments	12457
List of Abbreviations	12457
References	12458

1. INTRODUCTION, DEFINITION OF THE pH VALUE, AND GENERAL CONSIDERATIONS

The pH value is the chemical parameter most often determined in this world. The glass pH electrode is the gold standard and by far the most widely used tool.¹ It is reliable, precise, covers a wide pH range and is fairly fast (with exceptions). On the other hand, the glass electrode is rather large (>1 mm i.d. even if miniaturized), has a rigid design, and is sensitive to extraneous electrical and microwave fields. Local electrical potentials also can adversely affect the performance of pH electrodes. pH electrodes hardly work in solutions through which an electrical current is flowing, for instance in electrolysis cells and batteries, and they are supposed to present a risk to patients with heart pace makers. Glass electrodes obviously cannot be applied to sense pH values on a nanometer scale, such as inside cells, and not to fast imaging of the distribution of pH values over a certain area.

Many of these problems can be overcome by optically measuring pH values. As will be outlined in section 1.1, the technique dates back to the time when litmus was used to optically indicate the acidity of solutions. Eventually, pH indicator stripe tests (with paper-immobilized pH indicators) have become popular and still are in widespread use. Over the years, optical sensing of pH has become precise enough to be of practical utility not only for visual estimation of pH values but also to perform precise measurements (down to ± 0.01 pH units) so to become competitive to glass electrodes.

It comes as a surprise that there is not a single comprehensive review available on the variety of optical sensors for measurement of pH values, probably a result of the wealth of literature on the subject. Reviews are available that cover specific aspects of the subject. An early book on fiber optic chemical sensors and biosensors, published in 1991, contains a section on pH sensors that also includes the fundamentals of indicator-based pH sensors.² The 16-page review of Wencel et al.³ covers many essentials but obviously cannot reflect the wealth of data and knowledge that does exist in the field. A topical review on fluorescent probes and nanoparticles for use in intracellular sensing of pH values has been presented in 2014 by Shi et al.,⁴ and another one was published in 2019 by the Wang group.⁵ A most informative review was presented by Shamsipur et al.⁶ on fluorometric nanosensors for pH values. While limited to fluorometry and nanoparticles (NPs), it gives a complete account on the various kinds of NPs that have been used in the

past, from quantum dots, nanoclusters, carbonaceous dots, upconversion NPs, frameworks, metal, silica and polymer NPs to proteinic NPs. Other reviews cover optical pH sensors based on swellable polymers on thin film composite optical waveguides for sensor applications (pH sensing included),⁷ and the book series edited by Dakin and Culshaw (mainly on sensors for physical parameters) also contains a section on chemical sensors, pH included.⁸ A rather specific review was presented⁹ on the use of benzimidazole derivatives in various kind of optical detection schemes for various analytes and parameters, such as pH values. Both molecular benzimidazole probes and respective nanomaterial-based detection schemes are covered. A review on optoelectronic noses describes how arrays of chemoresponsive colorants provide high-dimensional data from the color or fluorescence changes of the dyes. It also describes how spot arrays prepared from pH sensitive indicator dyes can be used to identify both acidic and basic gases via changes in reflectance or emission as the spots are exposed to such analytes.¹⁰ Hence, a review that covers the complete subject and discusses the specific features of each of the numerous approaches will certainly be useful for those entering or being working in the field.

It is an unfortunate situation that the rapid progress made in optical sensor technologies has been accompanied by a rather sloppy use of terminology, mainly by organic chemists, who often refer to optical indicators and probes as sensors even though their “sensor” may be a simple dye, for example. The Cambridge definition¹¹ of a chemical sensor is quite clear in that respect: *Chemical sensors are miniaturized devices that can deliver real-time and online information on the presence of specific compounds or ions in complex samples.* Table 1 gives an overview on the typical features of labels versus probes versus sensors.

Research in optical sensor technology (pH sensors included) may be divided into three subdisciplines:

- (1) *Material sciences*: Its main aim consists in the identification of a material that has a strong, selective, and reversible response to the analyte or other parameter of interest. Such materials may consist of indicator dyes in a polymer matrix, of new polymers with intrinsic sensing capabilities, all in the form of coatings, nanoparticles, thin films, and the like.
- (2) *Spectroscopy*: Its aim consists in the design of optical methods (that can range from refraction and reflection to fluorescence, from plasmon resonance to Raman spectroscopy, from lifetime-based sensing to FRET-based sensing, from 2-photon effects to upconversion spectroscopies, and from time-resolved and time-of-flight measurements to sensing schemes based on the (de)-polarization of light or diffraction.
- (3) *Optical Engineering*: This involves smart optical designs that go far beyond classical instrumental arrangements. Examples include the design of detection cells for gases (such as the multireflective White cell for use in IR spectroscopies), evanescent wave sensors, fiber optic distributed sensors, new arrangements in surface plasmon resonance sensors, multiplexed or remote sensors, various kinds of interferometric sensors, and the like.

1.1. A Look Back on Optical Sensing of pH Values

The definition of the pH value by Sørensen (as a parameter for the acidity or basicity of an aqueous solution) may be rather “new”, but it has been recognized in early times that certain solutions taste acidic (Latin: *acidus*; and *acetum* for vinegar),

Table 1. Overview of the Characteristic Features of Optical Labels, Probes, and Sensors¹²

term	features	examples
label (including reagents for derivatization)	<i>supposed not to respond to its environment;</i> acts as a tag to make an analyte detectable usually a conjugatable molecule or particle	electrochemical labels; radioactive labels; optical (fluorescent) labels, such as FITC or quantum dots; Raman labels; fluorescent proteins; derivatization reagents (for use in separation sciences), enzymes (for use in ELISAs); fluorescent aptamers; labels for immunoassays, immunostaining, FISH), etc.
probe (indicator)	<i>supposed to respond to a parameter;</i> usually a molecule; mostly of the optical type (absorptiometric or fluorescent or Raman)	indicators for pH values, probes for calcium(II) and various other ions; intercalating probes for ds-DNA; probes for solvent polarity or lipophilicity; probes for temperature; quencher indicator dyes
sensor	<i>supposed to enable continuous monitoring;</i> supposed to work over hours if not weeks and years (in patients or cars, for example); not just a single molecule, not just a probe or a label; usually solid state	electrochemical or optical solid-phase sensors for pH values, oxygen, nitrite, glucose, methane gas; SO ₂ , NO _x , and others

while others taste burning or exert an aggressive action on certain stones (such as carbonates) and metals. Rather than tasting such fluids (which was soon recognized to imply a certain risk to those testing such fluids), it was found, first around the year 1300, that litmus (a fermented extract of lichens such as *Rocella tinctoria*) responds to acidity by giving a color change from blue to red. The effect is due to the acid–base chemistry of a hydroxyoxazine dye called cudbear or orcein, and it is fully reversible. To prevent addition of the extract to a sample, pH test stripes were designed by soaking paper or cotton with alcoholic solutions of litmus and subsequently gently drying them. These devices (known for some 400 years) were the first optical tests for sensing pH values. Obviously, the dyes were not covalently (but rather electrostatically) immobilized and, therefore, readily leached out. Such tests later were named dry reagent chemistries,¹³ and even later they were referred to as optical sensors.

The 1970s saw test stripes for pH to become commercially available where the pH indicator dye was covalently immobilized on cellulose, usually via vinylsulfonyl chemistry. This early work is difficult to trace because it was mainly performed in industry. An early article by Free et al.¹⁴ describes a triple test stripe for urinary glucose, protein, and pH. In 1975, the immobilization of pH indicator dyes on glass was reported by Harper.¹⁵ Azo dyes were linked to the surface of silicate glass (said to be more stable than cellulosic supports) that was made surface-reactive by treatment with a silane reagent so that the indicator dyes could be covalently immobilized. However, glass-immobilized pH-probes have not had a large success. Two later papers^{16,17} describe fairly well how to chemically immobilize vinylsulfonyl pH indicators on cellulose which still is the method of choice. The resulting nonbleeding test stripes allow for distinctly improved and continuous pH measurement, initially by visual inspection. In the late 1980s, instruments became available that enabled the color (more precisely reflectance) of such sensor stripes to be quantified and related to the actual pH value. They are based on the use of LED light sources and small

enough to be used in field tests. In addition, microtiter plates with pH sensor layers on the bottom of the wells have become available and allow pH changes (for example as a result of metabolic action) to be monitored over time.

All early tests were read visually. Often the color was (and is) compared with a color chart. Results can be surprisingly precise (± 0.05 pH units at around the turning point). Instrumental quantitation of test strips, dry reagent chemistries, and sensor stripes usually is performed by reflectometry, hardly by fluorescence or absorption, simply because fluorescence cannot be easily quantified visually and because practically all sensor stripes are nontransparent.

The absorption (and reflectance) spectra of the most common pH paper stripe typically displays absorption bands at about 460 nm (orange color; acid form) and 580 nm (blue color; base form), respectively. The acid form can be interrogated by a blue LED, and the base form by a yellow LED, thus enabling 2-wavelength ratiometric measurements. However, in the commercial readers, a reference signal obtained with an LED operated at about 670 nm (i.e., beyond the range of dye absorption) is used to compensate for geometrical and scattering effects. This simple and low cost detection system is still superior to many of the complicated, if not expensive pH sensors that have been described in the past years. The law of diffuse reflectance was established by Kubelka and Munk¹⁸ in 1931. It forms the basis for data processing in most instrumental readers.

As the potential of optical sensors (as an alternative to the glass electrode for sensing pH values) was rapidly recognized, several other articles appeared within a few years.^{19–23} Most sensors were reflectance-based, but fluorescent pH sensors were also described rather early.^{24–26} The article by Janata²⁷ on whether pH optical sensors can really measure pH is a “must” in the early literature since it points to aspects hardly addressed in pH sensor work. These issues are still of high significance in terms of precision and accuracy of optical sensors for pH. The dependence on ionic strength is an intrinsic limitation of pH

Table 2. Selected Papers on Early Work on Optical Sensors for pH Values

authors	year	remarks	ref
N.N.	<1970	cellulose-immobilized pH indicators (azo dyes); work performed in industry	
Harper	1975	reusable glass-bound indicators	15
Lübbers et al.	1977	nanoencapsulated fluorescent pH indicators	31
Peterson et al.	1980	first fiber optic pH sensor	32
Goldstein et al.	1980	miniature fiber optic reflectometric pH sensor for blood	33
Tait et al.	1982	fiber optic in vivo pH sensor	34
Saari and Seitz	1982	pH sensor based on immobilized fluorescein	24
Opitz and Lübbers	1983	fluorometric planar sensor for pH and ionic strength	28
Suidan et al.	1983	fiber optic reflectometric pH sensor for blood	35
Wolfbeis et al.	1983	evaluation of fluorescent pH indicator probes for use in optical sensors	36
Kirkbright et al.	1984	immobilization of reflectometric pH indicators on ion exchange polymers	19
Zhujun and Seitz	1984	fluorometric pH sensor using HPTS as an indicator	37
Goldfinch and Lowe	1984	solid-phase optoelectronic pH sensor	38
Offenbacher et al.	1986	fluorometric sensors for near-neutral pH values	25
Wolfbeis et al.	1986	fluorometric sensor for simultaneous monitoring of ionic strength and physiological pH values	29
Scheggi and Baldini	1986	comparison of pH sensing by absorption, reflection, and fluorescence	39
Woods et al.	1986	optical pH sensing at low buffering capacity	40
Gehrich et al.	1986	intravascular blood pH monitoring system (fluorescence based)	41
Janata	1987	assessment of the accuracy and precision of optical pH sensors	27
Grattan et al.	1987	2-wavelength fiber optic pH sensor	21
Kawabata et al.	1987	fiber optic pH sensor with monolayer indicator	42
Boisdé and Pérez	1987	miniature pH sensor (1 mm)	43
Jordan et al.	1987	pH sensor exploiting FRET	44
Monici et al.	1987	pH sensor for seawater monitoring	45
Wolfbeis and Marhold	1987	pH indicators for an extended range	46
Attridge et al.	1987	pH sensing via refractive index	47
Jones and Porter	1988	immobilization of pH indicators on cellulose acetate	23
Knobbe et al.	1988	immobilization of pH probes in sol–gels	48
Posch et al.	1989	gastric pH sensor (pH 0–7)	49
Carey et al.	1989	sensor for high acidities	50
Carey and Jorgensen	1991	sensor for high acidities based on fluorescent polymers	51
Gabor and Walt	1991	pH sensing via inner filter effects	52
Tan et al.	1992	submicrometer intracellular pH sensor	53
Werner et al.	1993	optical sensor for pH 10–13; hydrolyzed cellulose acetate	54
Ge et al.	1993	fiber optic evanescent wave pH sensor	55
Werner et al.	1993	first use of a partially hydrolyzed thin cellulose triacetate film on a polyester support; now widely used in optical pH sensors	54
Parker et al.	1993	pH sensor using the self-referencing dye SNARF	56
Mohr et al.	1994	azo indicators immobilized via vinylsulfonfyl groups on cellulose films (on polyester support)	16, 17
McCurley	1994	optical sensing of pH values based on the use of swelling hydrophilic polymers	57
Bronk and Walt	1994	pH sensor array using fiber bundles	58
Michie et al.	1995	distributed pH sensor using fiber optics and swellable polymers	59
Koncki et al.	1995	pH sensor using near-infrared dye in PVC	60
Schulman et al.	1995	wide-range pH sensor based on photodissociation	61
Zhang et al.	1995	pH sensor based on reflectance of swelling polymers	62
Taib et al.	1996	pH sensor range extended via artificial neural network	63
de Marcos et al.	1996	polypyrrole films as a pH sensor material	64
Draxler and Lippitsch, Werner et al.	1996	first PET-based pH sensing schemes	65–67
Pringsheim et al.	1997	various polyanilines as a sensor material for absorptiometric sensing of pH	68
Papkovsky et al.	1997	PVC sensor membranes containing porphyrins	69
Safavi and Abdollahi	1998	first optical sensor for very high pH values	70

sensors using indicator dyes. It is also noted in this paper that the local environment of an immobilized pH indicator is not purely aqueous (that is, 55 molar in water) so that the definition of pH does not strictly apply and pK_a values may be changed. Limitations due to the adverse effect of ionic strength were overcome by Opitz and Lübbers²⁸ and Offenbacher et al.²⁹ who made use of two indicators whose dependency of their pK_a on

ionic strength is different, so that two independent signals are obtained from two dyes or sensors.

It also was recognized in early work that, in addition to classical indicators, new ones are needed to take advantages of diode lasers and if sensors are to be operated at wavelengths of >600 nm. This can reduce background optical effects and inner filter effects, for example by making use of longwave absorbing

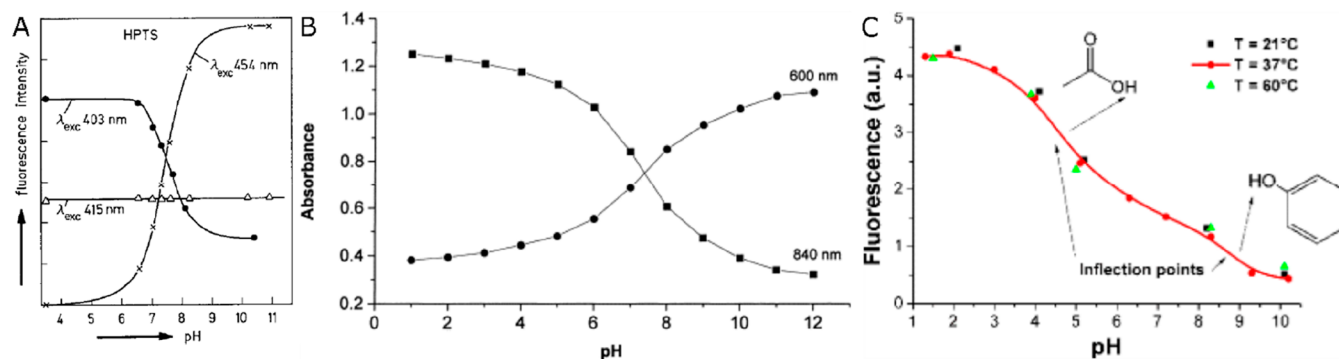


Figure 1. (a) Typical pH titration plot of a pH indicator (HPTS) with a single pH transition (and pK_a value). Reprinted by permission of Springer Nature from ref 36. Copyright Springer Nature 1983. Note that the shape of titration plots depends on the analytical wavelengths in absorption, emission, or excitation: At the isosbestic point (here at 415 nm), the signal is independent of the pH value. (b) Typical titration plot of a pH-dependent conductive polymer (polyaniline) with several overlapping transitions due to the presence of many protonable nitrogen atoms in different microenvironments. This results in a much wider detection range. Reprinted from ref 68 with permission from Elsevier. Copyright Elsevier Science B.V. 1997. (c) Titration plot for a typical nanomaterial (graphite oxide) with two fairly wide transitions that have been attributed to the dissociation of carboxy groups and phenolic hydroxy groups. Reprinted by permission of Springer Nature from ref 98. Copyright Springer Nature 2012.

fluoresceins and rhodamines.³⁰ The fundamental work on pH sensors before the year 2000 is summarized in Table 2.

Conventional electrochemical sensors do not work well at pH values of 11 and higher. It was soon recognized that optical sensors do not suffer from this disadvantage.^{54,70} On the other hand, potentiometric pH sensors cover a large range of pH values, while optical sensor typically cover a range of maximally 3 pH units with adequate accuracy. However, wide range pH sensors are needed in cases, such as measurement of gastric pH values. This is usually overcome by making use of up to 3 indicator dyes,^{49,71} but single indicators with intrinsically wide range (due to the presence of more than one dissociable group) also have been described.⁴⁶ Sensor stripes that cover narrow pH ranges (typically 3 units) or the full pH range (1–14) are commercially available.

A major leap forward was accomplished when fiber optics were coupled to optical sensors for pH because fiber optics enable measurements to be performed at hardly accessible sites (such as in vivo), in harsh environment (such as radioactive areas or in polar regions), and in strong electromagnetic fields. In essence, the sensor chemistry for pH is placed near (or at) the tip of an optical fiber and interrogated remotely. Instruments are now available from various sources. Fiber optic sensors for pH values in nuclear power stations were described in the 1970s by Boisdè and co-workers.^{72,73} The fiber optic pH sensor described by Peterson et al.³² in 1980 was a milestone in optical fiber sensor technology in medicine. The system comprised plastic fibers, a pH chemistry at their ends (composed of a cellulosic dialysis tubing filled with a mixture of polystyrene particles and polyacrylamide beads dyed with phenol red), LED light sources, and photodiode detectors. Surprisingly enough, even multipoint quasi-distributed optical fiber sensing of pH values was reported already back in 1997.⁷⁴ A 2-volume book that appeared in 1991 gives an account of the early work on fiber optic chemical sensors and biosensors.²

In 1984, a fiber optic triple sensor instrument (“GasStat”) became commercially available that can monitor pH values, pCO_2 , and pO_2 during cardiopulmonary bypass operations.^{41,75} It contains 3 fluorescent spots in contact with blood or calibrant, each sensitive for one parameter. Fluorescence intensity is measured at two wavelengths and the signals are then submitted to internal referencing and data processing. The instrument is

still in widespread use (www.terumo.com). A triple sensor was also described for use in bioreactors.⁷⁶ Walt’s group⁷⁷ wrote the milestone paper on the use of fiber arrays for genomic screening which, in turn, became a large commercial success. Microsensors, with diameters of $<50 \mu m$, were first reported in 1995⁷⁸ and enabled submillimeter resolution studies in marine microbiology.

In terms of materials, cellulose is a preferred matrix, but other hydrophilic materials also were introduced including the polyurethane hydrogels,⁷⁹ polyacrylonitrile-*co*-polyacrylamide,⁸⁰ chitosan, agarose, poly(vinyl alcohols),⁸¹ sol-gels,^{48,82,83} and zeolites.⁸⁴ Langmuir–Blodgett films are materials useful for making sensor layers of nanometer dimensions.⁸⁵ Others have used rather hydrophobic polystyrene based ion exchange beads to immobilize negatively or positively charged indicator dyes.¹⁹

Other novel materials for use in optical sensors or probes consist of polymers that have an optical response by themselves, and these were introduced by 1992 and thereafter. These include polypyrroles⁶⁴ and polyanilines.⁶⁸ Their absorption spectra extend far into the near-infrared. Poly(vinyl chloride) is not proton permeable but protons can be carried into a plasticized PVC membrane via carriers. This was used to design ion sensors for ammonium, sodium, potassium and calcium ions.^{86,87} They are based on the ion/proton exchange principle and the use of lipophilic pH indicator dyes. At about the same time, the first infrared based pH sensor that makes use of (de)protonable polymers, and the first refractive index-based sensors that make use of swellable polymers were described.

Optical sensors, unlike potentiometric sensors, do not principally require a reference element. However, optical signals can drift and can be interfered by foreign light. Early methods that have been designed (and still are powerful methods) to overcome such limitations include 2-wavelength referencing²¹ (also by using FRET),⁴⁴ dually emitting dyes,⁸⁸ or lifetime-based sensing.⁸⁹

Aside from measurement of pH values, such sensors also were used as transducers in three major kinds of assays. In the first, sensors for acidic or basic gases have been designed that are based on the changes induced by these gases in an internal buffer system. Typical examples include sensing of carbon dioxide⁹⁰ or ammonia⁹¹ via changes in the pH of a buffer solution entrapped

in a gas-permeable but proton impermeable polymer such as silicone. In the second, pH optical pH sensors are used as transducers in enzymatic reactions during which protons are produced or consumed, for example on oxidation of glucose by glucose oxidase⁹² or hydrolysis of urea by urease.⁶⁰ In the third, a pH sensor is used to monitor bacterial growth via the products of bacterial metabolism that cause pH values to drop or to increase.⁹³

The Lübbers group probably was the first to describe nanosensors.³¹ They immobilized indicators for oxygen and pH in nanocapsules, which retain the probes but are permeable to the analyte. Liebsch et al.⁹⁴ imaged pH, oxygen, and temperature using sensor membranes placed in microtiterplates and by employing decay time-based data acquisition. Kopel-mans group was the first to use sub μm -sized fibers to determine pH values in cells.⁹⁵ A review on optical chemical sensor technology until the year 2000 was presented.⁹⁶ In conclusion, it can be stated that many fundamental ideas for sensing pH values by optical means already have been created in the years before 2000.

1.2. Optical Sensing of pH Values: Specific Features

Most known optical sensors for pH (and all commercially available optical pH sensors) are based on the use of indicator dyes incorporated in some way into a solid support or matrix. However, pH sensors also have been reported that rely on the pH induced (and fully reversible) swelling of certain polymers (which can be detected optically for instance by measuring refractive index), or by making use of photonic crystals which have a *structural* color (very much like butterflies or chameleons) that is affected by the local pH value. Certain polymers (such as polyanilines and polypyrroles) have an intrinsic color that also depends on pH over a rather wide range. Optical sensors based on the use of immobilized pH indicators, in contrast, cover a small dynamic range only (compared to glass electrode), typically 3 pH units unless more than one indicator, or an indicator with more than one pH-transition are being used. Calibration plots have the typical sigmoidal shape of a pH titration plot as shown in Figure 1A (unless the indicator dye has several close-lying pK_a values in immobilized form, for example due to a strongly varying local microenvironment). Other pH-sensitive materials (for example swelling polymers or organic conductive polymers) mostly do not display such a behavior. Rather, these have titration plots that cover a wide range (Figure 1B, C). The limitation of a small analytical range is compensated for by the capability of such sensors to measure pH values with high resolution (defined as optical signal change per pH change; $\Delta S/\Delta\text{pH}$). On the other hand and unlike glass electrodes, optical sensors can measure extreme pH values (such as alkaline pH values between 12 and 14 or Hammett acidities of -1 and lower).

All optical chemical sensors rely on the formation of chemical equilibria between a sensor material and the local pH value of the sample. This makes the approach different from the establishment of a potential at the surface of an electrode. Equilibration requires prior diffusion. Hence, thin sensor layers are preferred to reduce response times if fast responding sensors are required. Most sensors are expected to give a reading within less than 3 min, but sensors that are supposed to work over long periods of time can be slower. Most sensors have response times that are faster in the forward direction than in the back direction. A mathematical model was presented⁹⁷ that explains the nonsymmetrical response times depending on whether an

increase or a decrease in pH values is to be measured. The influence of the pK_a of the indicator, ionic strength, diffusion coefficients, and thickness of the membrane was also investigated.

One may differentiate between three fundamental types of optical sensors for pH. The first is of the planar type, usually a kind of foil that has a coating whose color or fluorescence responds to changes in the pH value of solutions the foil is in contact with. The second is the fiber optic type where the pH-responsive chemistry is placed on or in an optical waveguide. Nanosized particles form the third kind of sensors and have attracted much attention in the past years because they enable pH values to be determined (usually via microscopy) on a microscale, in particular in cells and tissues. It is reminded at this stage that molecular probes (indicators; nowadays sometimes also referred to as “sensors”) are not included in this Review and are described elsewhere.^{4,99}

Optical sensors for pH have several attractive features:

- Planar sensors (i.e., sensor films) can be placed inside vessels, bioreactors, microtiter plates, or microfluidic systems and then be interrogated from outside without direct contact. Planar sensors also have been used to image pH values over certain areas. Planar sensors are readily mass-produced and at low costs by methods known from the film industry and therefore often are of the disposable type.
- Fiber optic devices have tip diameters between 1 mm and $<50\ \mu\text{m}$, and this is distinctly smaller than the size of glass electrodes. They have the additional advantage of being flexible, which offers an attractive possibility for invasive analysis of all kinds of tissues. Possibly more complicated in production, such sensors also can be produced at fair costs without sacrificing accuracy, and hence, they also can be of the disposable type which is important if used in medicine. An additional attractive feature results from the fact that the optical signal can be carried over large distances. This is particularly advantageous if the sample to be measured is inaccessible, for instance in case of remote sensing over hundreds of meters. Other fields include distributed sensing along a fiber optic cable and invasive sensing. Predictably, planar pH sensors and fiber optic pH sensors will replace the use of the glass pH electrodes in many areas.
- The third group of sensors (i.e., nanoparticles with pH-sensing capability) have found particular interest because they allow pH values to be determined inside cells, something that would be impossible even when using the smallest pH electrodes known. This technique also is often combined with (fluorescent) imaging. If incorporated into a nanomaterial, the indicator dye is hardly affected by proteins and other biomolecules. Therefore, nanoparticle-based sensing of pH values is potentially more reliable than using molecular probes for pH which often are bound by proteins upon which their pK_a value can change. Notwithstanding the substantial research going on in nanosensors for pH, such sensors still are, to a wide extent, a research tool. Currently, molecular probes are in much wider use than nanoparticle-based probes, which still have to demonstrate superiority in certain situations. Issues of intracellular delivery, distribution in cells, selectivity, toxicity, and in vivo calibration have to be addressed in each single case.

Given their quite different operating principle (as compared to pH electrodes), pH optical sensors offer quite new possibilities and at the same time are subject to some limitations that are not encountered with electrodes. The fundamental difference between optical techniques and potentiometric measurements of pH is that the optical technique measures the *concentration* of a dye species (that is related to pH), while pH is defined in terms of *activity*, which is what potentiometric measurements are based on. Janata²⁷ has shown the compromises that have to be made in case of optical pH measurements. In essence, it is (a) the discrepancy between activity and concentration of protons and (b) the fact that local pH values in sensor layers may be different from sample pH values because sensor layers do not consist of pure water (for which the definition of pH only is valid). This is discussed further below. A careful comparative study on the performance of optical pH sensors with electrochemical sensors¹⁰⁰ revealed, however, that the agreement between the two kinds of sensors was excellent, the average difference in pH readings in two cell media being 0.04 pH units only.

Because the indicator dye and the sample are in different phases, there is necessarily a mass transfer step required before constant response is reached. This leads to delayed response to pH. Hence, optical sensors for pH usually have a slower response than the glass electrode. Photobleaching, leaching, and interferences by ambient light are further limitations. It is also noted here that pH indicator dyes are weak acids, which can act as buffers, and this may compromise the precise determination of pH values of weakly or unbuffered solutions. And yet: The intrinsic characteristics of small sensor size, electrical isolation, chemical inertness and corrosion resistance offer definite advantages over electrochemical sensors. Figure 2 shows a commercially available optical pH sensor. Such sensors are single-use because they can be fabricated in large quantities at relatively low costs.



Figure 2. Commercially available disposable optical pH sensor attached to a single-use flow-through T-cell (from PreSens). It is connected to the pH meter (not shown) via a polymer optical fiber (top). The sensor spot (diameter = 3 mm) is placed in such a way that it is in contact with the sample solution passing the T-cell. These sensors typically cover the pH range of 5.5–8.5 and are precalibrated. Major applications are in perfusion systems and in process monitoring. Reprinted from <https://www.presens.de/de/produkte/detail/ph-einweg-durchflusszelle-ftc-su-hp5-s> with permission of Presens GmbH (Regensburg, Germany).

1.3. Definition of the pH Value

In simple terms, the pH value is a measure of the degree to which a solution is acidic or alkaline. The pH scale extends from less than 0 to above 14, but values inside this range are most common. Plain water is said to be neutral and to have a pH value of 7 (see below). On addition of an acid, the pH value will drop, while on addition of a base it will rise. The pH value is most often determined, for example in clinical sciences (blood, cells, stomach), environmental sciences (soil, surface waters, acid rain), in food science and oceanography, in engineering and in chemical and biotechnological plants. Blood pH values range between 7.35 and 7.45, and values above 7.8 or below 6.8 are fatal. Urine, gastric fluid, and cancerous cells are acidic, and normal seawater is slightly alkaline (>8).

According to the mathematical definition given by Sørensen in 1909, the pH value is the negative logarithm of the hydrogen ion concentration $[H^+]$:

$$\text{pH} = -\log[H^+] \quad (1)$$

In other words, the concentration of hydrogen ions in plain water is 0.1 μM . The hydrogen ion (also referred to as proton) is not present as such in aqueous solution. Rather, it is bound to a water molecule to form the hydronium ion $[H_3O^+]$, which is important to keep in mind when considering the rate of diffusion of a “proton” through a sensor material.

One liter of water contains around 1.9 μg of hydronium ions because only 2 out of one billion of water molecules dissociate to form H_3O^+ and OH^- ions. Obviously, this is not much and pH values therefore are easily affected by external and environmental factors. For comparison: air-saturated water contains around 8 mg/L of oxygen. The pH value of water is strongly temperature dependent. At the temperature of the human body (37 °C) it is 6.80. One should also keep in mind that the pH scale is logarithmic: Compared to a solution of pH 7, one of pH 6 contains 10-times the number of hydronium ions.

The pH value can be derived from the equilibrium constant of water, which is defined as

$$K = \frac{[H^+][OH^-]}{[H_2O]} \quad (2)$$

In pure water solution, the concentration of water is constant (55.5 M), so that it can be multiplied with K to obtain the dissociation constant (or autoprotolysis constant) (K_w)

$$K_w = [H_3O^+][OH^-] \quad (3)$$

whose numerical value is 10^{-14} at 25 °C. At neutral pH values, the concentrations of $[H^+]$ and $[OH^-]$ are identical, so that both $[H^+]$ and $[OH^-]$ have the numerical value of 10^{-7} . The negative decadic logarithm (that is, the pH and pOH value, respectively), therefore is 7. For purely aqueous solutions, the sum of pH and pOH always is 14.

However, the above assumption of a constant water concentration (55.5 M) is not always warranted, for example:

- If solutions contain organic solvents in fractions of >20%; both the fraction and kind of organic cosolvent exert a large effect on the activity of protons in a solution, and on pK_a values.¹⁰¹
- If solutions contain large fractions of proteins, such as albumin, or polymers, such as poly(ethylene glycol). Both proteins and hydrophilic polymers can bind large fractions of water. Blood, for example, has an apparent

water concentration of around 40 molar only, not 55.5 M, which is assumed when deriving the pH value from the dissociation equilibrium of water. Hence, the definition of blood pH is based on a wrong assumption. In fact, the true pH value (in terms of proton activity) of blood is unknown.

The pH scale is but one example of an acidity function. Other acidity functions have been defined, for example the Hammett acidity (H_0) that has been developed for very strong acids.

1.4. Proton Activity versus Concentration

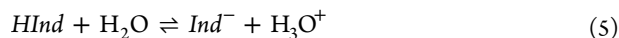
The actual acidity of a solution, however, is not governed by the concentration of hydronium ions ($[H_3O^+]$) but rather by their activity. Therefore, the initial definition was modified by Sørensen and Linderstrøm-Lang by introducing an activity factor a :

$$\text{pH} = -\log a[H^+] \quad (4)$$

It accounts for the fact that the activity of the hydronium ions is compromised by other species that are present in solution, in particular by other inorganic and organic electrolytes, such as salts, charged proteins, or nucleic acids.

1.5. Dissociation Constants of Indicators and of Polymers with pH-Dependent Charge

The applicability of a classical pH probe (indicator or polymers with pH-dependent charge) is best described by its acid dissociation constant, K_a (also known as acidity constant) or its negative logarithm ($\text{p}K_a$). In simple terms, the $\text{p}K_a$ value gives the pH value (± 1.5 pH units) over which an indicator (or polymer) changes its optical properties (or charge) and, hence, is useful in terms of sensing. Most conventional probes can be considered as acids ($HInd$). Their properties can be described in the context of acid–base reactions. In aqueous solution, the equilibrium reaction can be described as



and the respective equilibrium constant K_{eq} is

$$K_{eq} = \frac{[Ind^-][H_3O^+]}{[HInd][H_2O]} \quad (6)$$

By inserting 55.5 for $[H_2O]$, one obtains

$$K_a = \frac{[Ind^-][H_3O^+]}{[HInd]} \quad (7)$$

The negative decadic logarithm of K_a is the widely used $\text{p}K_a$ value of a probe (and this definition, of course, also holds for any other acid).

Again, it is important to keep in mind that $\text{p}K_a$ values usually are given for pure (= 55.5 M) aqueous solutions at low ionic strength. In optical sensors, the indicator dye usually is contained in a polymer, and the microenvironment of such indicators may contain only minute quantities of free (available) water. In this case, the assumption made above (that $[H_2O] = 55.5$ M) is not valid. This is one major reason $\text{p}K_a$ values of pH indicators can be quite different depending on whether they are dissolved in an ideal aqueous solution or in a polymer. The apparent (nonthermodynamic) $\text{p}K_a$ value of a sensor is termed $\text{p}K_a$ in this Review.

Other reasons for shifts in apparent $\text{p}K_a$ values of indicators include (a) effects of ionic strength (see below), (b) binding of indicators to proteins and other charged species, (c) changes in

the hydration number, and (d) dye–polymer interactions of the van der Waals type.

Binding to proteins is a major reason the determination of pH values in protein-containing samples (such as in intracellular fluids) by using plain molecular indicators should be interpreted with caution. Indicators immobilized on (and in) hydrophobic matrices have been found to exhibit acid–base properties that are quite different from those in aqueous solution.^{19,22,102}

Most authors are making use of the Henderson–Hasselbalch equation by using $\text{p}K_a$ values determined by measurement of the activity of protons (via pH electrodes), and these values are then applied in processing data of optical sensors that measure proton concentrations.

The $\text{p}K_a$ value of an (immobilized) indicator can be determined by various methods¹⁰³ but is best determined by photometry or fluorometry by making use of the Eistert equation¹⁰⁴

$$\text{p}K_a = \text{pH} + \log \frac{(A_x - A_b)}{(A_a - A_x)} \quad (8)$$

where A_x is the absorbance of the indicator at a certain wavelength at a given pH value, A_b is the absorbance (at the same wavelength) of the base form of the dye (i.e., in a solution with a pH value that is much higher than the $\text{p}K_a$ value), and A_a is the absorbance (at the same wavelength) of the acid form of the dye (i.e., in a solution with a pH value that is much lower than the $\text{p}K_a$ value).

It is often ignored that many indicators also have an excited state $\text{p}K_a$ value and, therefore, a second pH transition (in fluorometric titrations only). This is due to excited state (adiabatic) photodissociation because phenols are much stronger acids in the first excited singlet state (S_1 state) than in the ground state (S_0). Inversely, amines (like pyridine-derived indicators) are much stronger bases in the first excited singlet state (S_1 state) than in the ground state (S_0). The Förster cycle may be used to calculate excited state $\text{p}K_a$ values. In simplified form, it reads like this for calculating $\text{p}K_a$ values

$$\text{p}K_a(S_1) = \text{p}K_a(S_0) - \frac{0.625}{T}(\tilde{\nu}_{HB} - \tilde{\nu}_B) \quad (9)$$

Here, T is the temperature and $\tilde{\nu}_{HB}$ and $\tilde{\nu}_B$ are the wavenumbers (in cm^{-1} units) of the absorption peaks of the acidic form and of the dissociated form of an indicator dye, respectively. The effect was used⁶¹ to largely extend the response pH range of an optical pH sensor based on the use of 1-hydroxypyrene-3,6,8-trisulfonate.

$\text{p}K_a$ values are thermodynamic parameters and are, therefore, more or less temperature-dependent. This temperature dependency is determined by the structure of the indicator and change in the free enthalpy upon dissociation. For instance, indicators based on phenols typically show $\text{d}K_a/\text{d}T$ values between -0.007 and -0.012 ¹⁰⁵ whereas for those bearing secondary and tertiary amines $\text{d}K_a/\text{d}T$ vary from -0.013 to -0.020 units/K.¹⁰⁶

1.6. Effect of Ionic Strength on pH Values and $\text{p}K_a$ Values

According to Lewis and Randall, the ionic strength I of a solution is defined as

$$I = \frac{1}{2} \sum c_i z_i^2 \quad (10)$$

where c_i is the concentration of each ion present (in mole per liter) and z_i^2 its charge. Ionic strength (IS) affects the activity a of

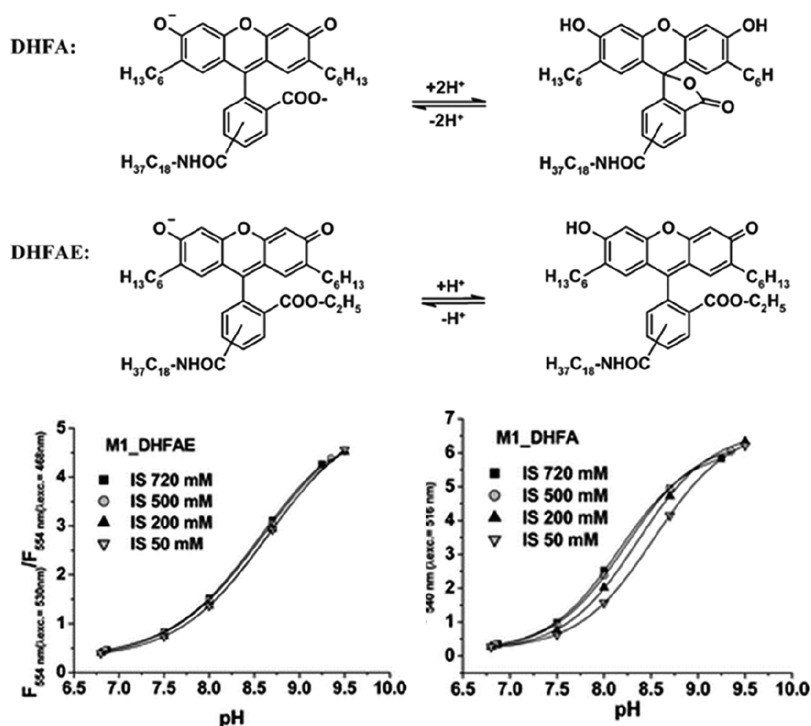


Figure 3. Calibration plots of hydrogel-immobilized fluorescein indicators at different ionic strengths, demonstrating the decrease in the pK_a value with increasing ionic strength of the solution. Reprinted with permission of The Royal Society of Chemistry from ref 110. Copyright Royal Society of Chemistry 2005. Permission conveyed through Copyright Clearance Center, Inc.

any electrolyte in solution (the proton included) so that its true concentration c has to be multiplied by a correction factor γ to obtain the actual activity via

$$a = c\gamma \quad (11)$$

Debye and Hückel have related the activity coefficient γ of a z -valent ion to I by

$$\log \gamma = -0.512z^2I^{1/2} \quad (12)$$

While there is good correlation between theoretical and experimental data for IS-corrected pH values in case of singly charged electrolytes, the situation is more complex in cases of multiple charges and unsymmetrical ions.¹⁰⁷

The activity coefficient depends on the ionic strength of the solution and approaches unity for infinitely dilute solutions. In very dilute solution, pH can be related directly to the concentration of the hydrogen ions.

Ionic strength also affects the dissociation constant of pH indicators.¹⁰³ The following relation is valid between the pK_a value at a given ionic strength I , and the true thermodynamic value (pK_a^{th})

$$pK_a^I = pK_a^{\text{th}} + \frac{0.512(z_B^2 - z_{\text{HB}}^2)I^{1/2}}{(1 + 1.6I^{1/2})} \quad (13)$$

where z_{HB} and z_B are the charges of the acidic form and of the dissociated form of an indicator dye, respectively.

In general, optical sensors for pH values perform much better than electrodes in case of unbuffered solutions.¹⁰⁸ This effect is of particular significance in case of samples with a high variation in ionic strength, for example in case of estuary waters. The effect of ionic strength has to be taken care of when sensing the pH value of seawater or estuaries with their high or varying ionic strength. Edmonds et al.¹⁰⁹ have shown that an increase in ionic

strength from 0.01 to 3 M can shift the pK_a by as much as 1.2 units. Ionic strength (IS) calculators are available on the Internet. However, data on the effects of IS are conflicting in that both increases and decreases in the pK_a values with increasing IS have been reported.

Most pK_a values are determined in buffer solutions with low electrolyte concentrations, typically between 10 and 20 mM, and few authors have studied the effects of IS in detail. An example where the pK_a of fluorescein-based indicator dyes decreases with increasing IS¹¹⁰ is shown in Figure 3 that reflects, exemplarily, the effect of IS (salinity) on the pK_a value. Edmonds et al.¹⁰⁹ have shown that an increase in IS from 0.01 to 3 M can result in strong increase of the pK_a value (bromophenol blue; +0.57 units) and decrease of the pK_a value (phenol red; -1.02 units), whereas for some dyes (bromocresol green, methyl red), the effect was comparably small (see Table 3). Interestingly, phenol red, bromophenol blue, and bromocresol green have rather similar chemical structures.

Table 3. Variation of pK_a Values with Changing Ionic Strength at 25 °C^a

ionic strength [M]	0.01	0.1	0.5	1	1.5	2	3
bromophenol blue	3.94	4.41	4.37	4.40	4.42	4.45	4.51
bromocresol green	4.57	4.65	4.65	4.68	4.71	4.75	4.82
bromocresol purple	6.26	5.67	5.67	5.71	5.74	5.75	5.76
methyl red	4.90	5.04	5.08	5.13	5.31	5.07	5.01
phenol red	7.46	6.96	6.52	6.37	6.39	6.55	6.44

^aFrom ref 109.

Azo dye based pH sensors and test strips are in widespread use. The effect of IS (on going from 0 to 0.1 M NaCl solutions) on a reflectometric azo dye based cellulosic pH sensor (made from the dye that is used in many commercial pH test papers) was also found to be strong, but upon further increase of IS it is less expressed.¹¹¹ Obviously, the concentration of the phosphate buffer only (i.e., in the complete absence of any other electrolyte) also has a remarkable effect on the calibration graph. Given the effects of buffer strength, varying IS and temperature, an accuracy of not better than ± 0.05 pH units at pH values between 6 and 9 was said to be realistic.

Monici et al.⁴⁵ also reported that the pK_a value of the widely used indicator dye phenol red drops by 0.044 units for a 1‰ (1 PSU) increase in salinity. Similar results were found by Robert-Baldo et al.¹¹² who have studied the dependence of the dissociation constant (K_a) of phenol red in seawater at temperatures between 5 and 30 °C.^{113,114} In respect to highly accurate spectrophotometric measurements with aqueous indicators solutions, *m*-cresol purple proved to be the best suitable dye for oceanographic applications ($pK_a = 8.006$ at 25 °C and at 35 PSU).^{115–117} The cross-talk to salinity is already measurable at high salinity (~ 0.00125 pK_a units/PSU at Salinity 35) and dramatically higher at lower salinities (Figure 4).^{116,117}

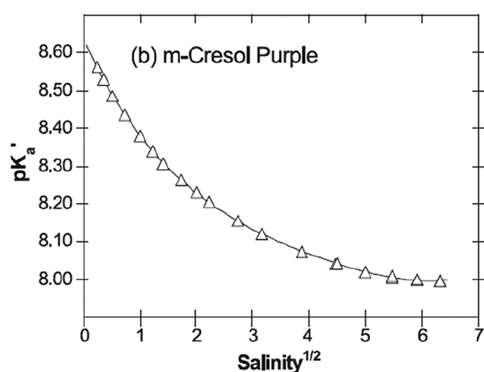


Figure 4. Salinity (in PSU) dependency of the apparent pK_a of *m*-cresol purple in water. Reprinted from ref 116 with permission from Elsevier. Copyright Elsevier B.V. 2004.

The effect of IS increases with the charge of the indicator dye, and it does not come as a surprise that the widely used indicator 1-hydroxypyrene-3,5,8-trisulfonate (HPTS) with its 3–4

negative charges is particularly sensitive to IS. It usually is covalently immobilized via one sulfonamido group on hydrophilic support. The pK_a of the such-immobilized dye drops by as much as 0.4 units if IS increases from 100 to 200 mM. Such a drop is intolerable in case of blood pH sensing, and therefore the effect of IS is compensated for by an algorithm that uses data obtained by ion-selective optodes for sodium¹¹⁸ and potassium¹¹⁹ which cause >90% of the IS of whole blood. Similar material has been evaluated for potential application in oceanography showing 0.2 units change of the pK_a between salinity 15 and 35 PSU.¹²⁰

3-Carboxy-7-hydroxycoumarin (having a single negative charge only in the dissociated form) was conjugated to the amino groups of glass beads and found to have pK_a values that are virtually independent of IS as long as it is surrounded by excess protonated amino groups on the glass surface, which warrant fairly constant local IS. However, if the surface $-NH_3^+$ groups are acetylated (and thus disappear), the pK_a decreases with increasing IS, typically from 7.3 to 7.1 on going from a 0.1 M to a 0.2 M IS. Equations (derived from the Debye–Hückel law) have been presented that allow the effect of IS on the pK_a to be calculated.²⁹

Reducing the charge of the indicator dye (transition between uncharged indicator and a form with charge +1 or –1) has been recognized as an efficient strategy to decrease cross-talk of the sensors to ionic strength. Weidgans et al.¹²¹ and Schröder et al.¹¹⁰ described fluorescein derivatives modified with a long (hydrophobic) alkyl chain and entrapped in an uncharged polyurethane hydrogel showing the transition between the neutral acid form and negatively charged base form of the dye. These dyes show very small cross-talk to ionic strength (Figure 3). In contrast, the cross-talk is much stronger for structurally very similar indicators showing transition between the forms with charges –2 and 0 (Figure 3). The same concept proved to be efficient for indicators of other classes such as perylene dyes^{122,123} and aza-BODIPYs both embedded into uncharged hydrogels.¹²⁴ The perylene dyes bearing amine receptors (showing transition between forms with the charge 0 and +1) showed only slight increase in the apparent pK_a value upon 10-fold increase of the ionic strength (Figure 5, left), and the pK_a of the aza-BODIPY (transition between 0 and –1) was virtually independent of salinity (Figure 5, right).

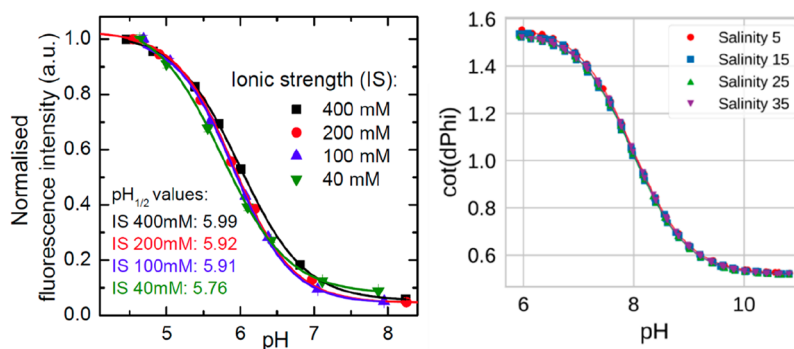


Figure 5. Salinity cross-talk of the pH sensors based on 1-aminopyrene (left) and aza-BODIPY-based indicators (right, salinity in PSU) both embedded into uncharged cross-linked poly(acryloylmorpholine) hydrogel ($T = 25$ °C). Reprinted with permission of The Royal Society of Chemistry from ref 123. Copyright the Royal Society of Chemistry 2013. Permission conveyed through Copyright Clearance Center, Inc. Reprinted from ref 124 with permission from Elsevier. Copyright Elsevier B.V. 2019.

1.7. Selectivity and Interferences

These are issues that are often ignored in papers on sensors for pH values but that decide on whether a sensor is applicable in practice (such as sensing the pH value of blood of the critically ill patients, of bioreactor broths, or of seawater) or not. Unless a sensor is adequately selective, it will have limited scope.

There are several kinds of potential interferences that can compromise the accuracy of optical sensors for pH values. As discussed in section 1, the performance of indicator-based or (de)protonable polymer-based sensors is biased whenever the pK_a value of a pH indicator is compromised by parameters other than the concentration of the hydronium ion, for example by ionic strength, temperature, large fractions of organic solvents, quenchers of fluorescence, such as iodide, by proteins that bind to an indicator, or by polymer–dye interaction in a (solid) sensor matrix.

Temperature and ionic strength also affect polymer swelling (as exploited in all refractive index-based sensors, SPR included). For instance, a typical systematic error would occur if a pH sensor is calibrated with 10 mM phosphate buffer and then applied to the determination the pH value of seawater with its high ionic strength. Temperature and ionic strength also affect (a) the pK_a value of IR-active groups, such as $R-NH_3^+$ (in case of IR sensors), (b) the diffraction of light in photonic crystals if hydrophilic polymers are involved, and (c) the refractive index and swelling of polymer coatings on the gold film of an SPR sensor.

A further major source of error is due to quenching of the fluorescence of pH indicator probes. Bromide, iodide, and sulfide are notorious quenchers that can quench the fluorescence of indicators if they can enter the sensor layer. Fortunately, the above quenchers (unlike chloride) do not occur in substantial concentrations in most biological matrices. Heavy metal ions, such as Fe(III), Pb(II), Hg(II), and Ag(I), also are typical quenchers. It is a misperception that ferric ion does not occur in blood. In fact, it is readily formed in blood by decomposition of heme and subsequent oxidation. It is also present in most surface waters and ground waters.

No (or negligible) interference by quenching has been found for rather inert gases, such noble gases, hydrogen, nitrogen, alkanes (gaseous and fluidic), alcohols (at low level), and most other organic solvents. Chlorine and other strong oxidants may react with (and decolorize) an indicator. Gaseous CO_2 and ammonia may become dissolved in the sample and may change local pH values. All alkali and alkaline earth ions remain inert except for their effect on ionic strength. The anions sulfate, nitrate, nitrite, bicarbonate, carbonate, chlorate, acetate and the like also have virtually never been reported to interfere. Bioorganic species, such as saccharides and lipids (as they occur in blood or bioreactor broths), do not interfere. Proteins (such as traces of albumin) bind most charged indicator probes upon which their pK_a value is changed. This is a major source of error and best prevented by selecting a permeation-selective matrix material for the sensor, examples being hydrogels, such as polyacrylamides and pHEMA, polyacon (pHEMA cross-linked with ethylene glycol dimethacrylate), polyurethanes, chitosan, carrageenan, poly(vinylpyrrolidone), or agarose, in the form of films, coatings or water-insoluble beads. If high mechanical strength is mandatory, (modified) sol–gels may be applied.

Fluorosensors based on the use of UV absorbing indicators can suffer from interferences by inner filter effects in that they screen off excitation light or even fluorescence. Obviously,

colored species such as hemoglobin and chlorophyll can cause the same effect unless excluded via permeation selectivity or by using optical isolations (see section 9.3). Sensors without optical isolations are limited to applications in fairly clear samples such as various kinds of waters. Even seawater may become a problematic matrix because it has a fairly strong intrinsic absorption at wavelengths of below 300 nm.

1.8. Sensitivity, Precision, and Dynamic Range

The term sensitivity is ambiguously used in the scientific literature. Sensitivity is defined by IUPAC as follows: “The sensitivity of an analytical method is the capability of the method to discriminate small differences in concentration of the test analyte.” In plain language, sensitivity is defined as the slope of a plot of signal (signal response) against analyte concentration. Hence, sensitivity is defined as the change in any analytical signal (ΔS) with the change in concentration (Δc). Unfortunately, many authors confuse sensitivity with the limit of detection (the smallest amount of analyte that can be determined with confidence, typically at a signal-to-noise ratio of 3), not so often in case of sensors for pH, but in many others, biosensors included.

The variation in sensitivity (slope; $\Delta S/\Delta pH$) is best demonstrated by looking at the two pH titration plots shown in Figure 3 where pH values are plotted against the optical signal. It should be kept in mind that a pH value by definition is a logarithmic parameter, and hence, such plots—while reflecting concentrations—are logarithmic plots. The sensitivity of all such sensors is highest at the turning point of a plot of pH value versus optical signal (S). At pH values of more than 1.5 units away (+ or –) from the turning point, the slope is approaching zero. This also makes it obvious that even minute changes in the pK_a of an indicator dye or a polymer with pH-dependent IR absorption result in large errors in the optical determination of pH values. The same is true, of course, for calibrations.

A commonly encountered systematic error in the determination of intracellular pH values results from the fact that calibration plots are established with standard buffers that ignore the presence of intracellular proteins. Besides proteins, intracellular pK_a values can also be affected by interaction of indicators with DNA, RNA, lipid structures, and lipoproteins, macromolecular assemblies and even organelles. These can bind indicator dyes and shift their pK_a values so that data for intracellular pH values are heavily biased. In fact, the albumin-induced shift of the pK_a value of an indicator, and thus the change in color at a constant pH value, is used in some tests for albuminuria. In situ calibration is the most efficient strategy, but it is not always feasible.

1.9. Effects of Temperature

Any sensor in this world measures temperature (T) and—ideally quite specifically—another species too. Unless T itself is to be sensed, its effects are not truly welcome. Remarkably, there are relatively few reports on the T dependence of pH sensors. This may be due to the fact that T exerts rather complex effects on fraction of water in hydrophilic polymers used as sensor matrix, and on dissociation constants of indicators and of protonable swellable polymers used in IR based pH sensors, and—in case of fluorescent probes—additionally on fluorescence quantum yields and decay times. As a result, mathematical modeling of its effects is complicated. Temperature is probably the single biggest source of error in such sensors. Ratiometric (2-wavelength) sensing can reduce some effects of T (mainly on fluorescence quantum yield) but not all.

In respect to the temperature dependency of the pK_a value, inorganic, and carboxylic acids show temperature coefficients close to 0.¹⁰⁵ These groups, however, are rarely involved in modulation of fluorescence intensity of the indicators. The secondary and tertiary amines, which are common receptors in indicators based on photoinduced electron transfer, show temperature coefficients dpK_a/dT between -0.013 and -0.020 units/K. Temperature coefficients for the primary amines are higher (-0.012 to -0.028 units/K).¹⁰⁶ Phenols, which represent other important receptors in the fluorescent sensors, typically show the dpK_a/dT values between -0.007 and -0.012 units/K.¹⁰⁵ As an example Figure 6 shows the

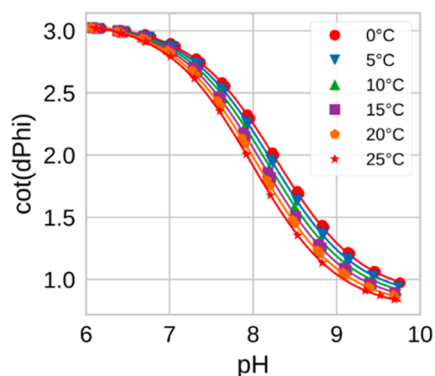


Figure 6. Temperature dependency for the sensor based on azabodipy pH indicator bearing a phenol receptor. Reprinted from ref 124 with permission from Elsevier. Copyright 2019 Elsevier B.V.

temperature dependence for the response of a fluorometric pH sensor. The sensor is based on a pH-indicator of the azabodipy class (bearing a phenol receptor) covalently embedded into an uncharged poly(morpholinoacrylamide) hydrogel with an additional phosphorescent reference material.¹²⁴ As can be seen, the temperature mainly affects the pK_a value of the indicator, other effects (such as thermal quenching of the luminescence of indicator or reference) being either very minor or mostly compensated. The pK_a decreases with temperature showing the coefficient dpK_a/dT of -0.0114 units/K, which is very close to the values reported for phenols.¹⁰⁵

Evidently, the temperature cross-talk can be compensated for providing that the temperature measurement is sufficiently accurate. In practice, it can be not always straightforward since the dynamic response of the optical pH sensor and the temperature probe (e.g., a conventional resistance thermometer) is likely not to be identical. This problem can be particularly pronounced in applications requiring fast measurements in environments showing high temperature and pH gradients (e.g., profiling in seawater). Fortunately, it can be addressed with help of dual sensors based on optical temperature probes¹²⁵ incorporated into the same sensing layer. These dual sensors that can optically detect both pH values and T in the same place.^{126,127}

2. COMMONLY USED OPTICAL SENSING SCHEMES

The following section covers the most common detection schemes that have been described in the past. Despite the variety in terms of spectroscopies, reflectometry and fluorometry are most widespread. They are most often used in planar sensors, in fiber optic sensors, and in imaging of pH values. It may be stated

that fluorometry is expensive (given the price for research fluorimeters), but in fact present day sensor instruments can have the size of a USB stick and can be rather affordable (hand-held imagers included).

2.1. Absorptiometry and Reflectometry

Absorptiometry¹²⁸ is a very established and popular optical method. And yet, absorptiometric continuous sensing of pH values is not common. If the sensor is to be operated in the absorptiometric (transmission) mode, it requires both the sensor layer and the sample to be optically clear (nonscattering and transparent) and free of colored species to warrant lack of light scattering and that no species other than the pH responsive dye are causing absorption. If scattering particles are present in the sensor layer, their concentration must be such that they do not cause scattering to an extent that would make measurement of absorbance impossible. The stipulations of (a) an optically clear sensor material and (b) an optically clear sample are hardly fulfilled in practice. The problem can be circumvented, in part, by making use of evanescent wave absorptiometry (also referred to as ATR; for attenuated total reflection; see section 14.3) where a thin film (typically $<2 \mu\text{m}$) of a pH sensitive material is placed on an optical waveguide. In this configuration, the interrogating beam is totally reflected at the interface between waveguide and pH-sensitive coating, and the attenuation of the light beam is governed by the local pH value in contact with the sensor film on the waveguide.

Reflectometry, in contrast, is quite popular. Most pH sensor stripes are not transparent but based on the use of a fibrous sensor material that is virtually impermeable to visible light. In fact, many sensors are rendered strongly scattering by adding scattering white particles including cellulose, TiO_2 , BaSO_4 , or polystyrene. The relation between the concentration of the indicator and the intensity of diffusely reflected light at the wavelength of absorption follows the law of Kubelka and Munk:

$$c = \frac{S(1 - R_{\text{diff}})^2}{2\epsilon_R R_{\text{diff}}} \quad (14)$$

where c is the concentration of either the acidic form or the conjugated base form of the indicator, S is a constant that is specific for the support (such as cellulose or a TiO_2 -doped hydrogel), R_{diff} is the intensity of light reflected via diffuse reflection; its numerical value can range from 1 (if all light is reflected) to 0 (if no light is reflected), and ϵ is the molar absorbance of the absorbing material at the analytical wavelength. This law forms the basis for all reflectometric read-out schemes using test stripes (not only for pH but also for parameters such as nitrate or glucose) as used in commercially available instrumentation and point-of-care tests. A good review with an updated theory on reflectometry along with representative applications is available.¹²⁹

Most reflectometric sensors are based on ratiometric measurements. Two LEDs are employed, one emitting at a wavelength absorbed by the indicator in its acidic or conjugate base form, the other at a wavelength that is not absorbed or is absorbed by the conjugate base form or acidic form, respectively, of the indicator. Figure 7 gives a schematic of an arrangement as frequently used in industry.

Many sensors now are read-out by making use of RGB imaging. In essence, each present-day camera and each flat-bed color scanner is a 3-color photometer with three channels, one each for red, green and blue (RGB) light. Data are stored in jpg format and channels can be ratioed. This holds for both

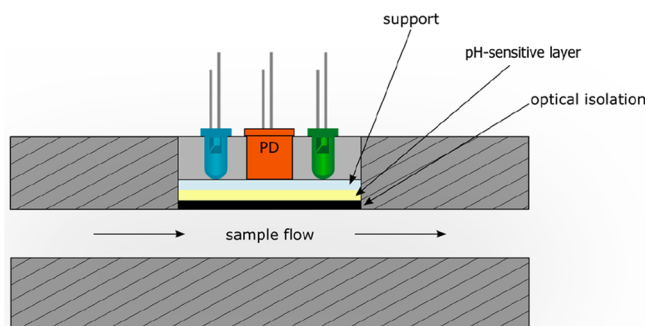


Figure 7. Schematic of an optoelectronic module for continuous sensing of pH values in a flow tube, usually a bypass of a bioreactor fluid, such as in fermenters (beer, wine or production of penicillin). The pH sensitive layer typically is covered with a black optical isolation to prevent sample fluorescence to interfere or to cause inner filter effects. Two LEDs are employed, one serving as a reference. The two LEDs are alternatingly turned on, and the signals of the sensor layer are acquired by a photodiode (PD).

absorption and fluorescence. Methods for referenced luminescent sensing and imaging with digital color cameras have been critically compared.¹³⁰

2.2. Measurement of Luminescence

Fluorometry and phosphorimetry probably are the second most often used methods after reflectometry. Fluorescence commonly originates from the lowest excited singlet state (S_1), while phosphorescence originates from a triplet state (T_1). Both terms are summarized under the general term *luminescence*, along with other kinds of luminescence, which, however, have not yet been applied to pH sensing so far. Luminescence spectroscopy knows more methods of measurement than absorptiometry or reflectometry. This has resulted in quite a number of read-out schemes that shall be discussed in the following.¹³¹

2.2.1. Luminescence Intensity. This is the parameter most often used in research but it is not a robust one as can be shown easily. The ratio between luminescence intensity (F) and the concentration of a fluorophore (which in the case of pH is the concentration of either the base form of the acid form of the indicator probe) is described by Parker's law. In its simplified version—that is valid for absorbances of <0.05 only—it is stating that F is directly related to the intensity of the light source (I), the molar absorbance of the acid form or base form of the indicator (ϵ), its concentration (c), the penetration length (l), and the quantum yield (QY) of the probe (also sometimes referred to as Φ):

$$F = I \cdot \epsilon \cdot c \cdot l \cdot QY \cdot k \quad (15)$$

The geometrical factor k accounts for effects caused by the instrumental arrangement. One can easily see that F not only is affected by the concentration of the pH indicator (in its acidic or conjugate base form). Rather, it is also affected by changes (a) in the geometry of the optical arrangement, (b) of penetration depths (that may change due to swelling), (c) the intensity of the light source, (d) a change in the sensitivity of the photodiode, and (e) a drop in the concentration of the indicator as a result of leaching or photobleaching. There are two main methods that can fully or partially compensate for such potential pitfalls, namely, ratiometric (2-wavelength) measurement of intensity or dual-lifetime referencing (DLR; see below), where intensity is converted into a phase shift or a time shift. In addition to the above sources of error, fluorescence intensity

may also be biased by background fluorescence. It can stem from (a) the fluorescence of samples, such as blood (which can be minimized or completely eliminated by using so-called optical isolations), and (b) the intrinsic fluorescence of optical and other components because most of them are usually made from plastic materials, which display intrinsic (usually blue to green) fluorescence. This background can hardly be compensated for, except by making use of gated fluorescence (see below). However, since the background is mostly constant, it can sometimes be subtracted by performing the measurement without the sensing material (e.g., with attached bare fiber).

Fluorescence intensity (F) can be readily measured with fluorimeters and therefore is the preferred parameter in sensor research. The product of ϵ and QY is sometimes termed brightness (B_s) and represents an important and practical parameter as it indicates how much of the incident light is absorbed and then converted into luminescence. Fluorescent indicators and materials with high B_s are highly desirable. It is remembered here that the Stern–Volmer relationship (SVR) is not applicable to indicator-based pH sensing because acid–base equilibria are ground state equilibria. The SVR is applicable only to dynamic (collisional) quenching that occurs in an excited state.

Fluorimeters may be expensive, but dedicated sensor modules are not. Main components include an LED, a photodiode, a data logger and a port, all of minute size. Main applications of optical pH sensors are in blood pH measurements, online pH monitoring of bioprocesses, in online monitoring of pH values in perfusion systems, and in pH profiling in semisolid (food) samples. Commercial systems do exist for all of these applications.

2.2.1.1. Time-Resolved Measurement of Luminescence Intensity. Measurement of luminescence intensity may be combined with time-resolution if the pH-sensitive materials possess comparably long decay times, typically $>1 \mu\text{s}$. Time-resolved (gated) fluorometry enables background fluorescence (with decay times of less than $1/10$ of the decay time of the pH probe) to be suppressed. In this scheme, luminescence is excited with a short pulse of light and detected only after some delay during which any short-lived background fluorescence has disappeared. Figure 8 shows a schematic of sensing based on time-resolved fluorometry.

2.2.2. Luminescence Decay Time. Decay time is often also referred to as *lifetime* within this context, but this is not a good term because it may also refer to the storage lifetime or operational lifetime of a sensor. The decay profile of a fluorophore affects the temporal course of fluorescence (F) in the following way:

$$F = F_0 e^{-kt} \quad (16)$$

Here, F is the intensity of fluorescence at a certain time (t), F_0 is the intensity at time zero after the light pulse has been terminated, and k is the time constant that is specific for each fluorophore in a given microenvironment. Optical sensors for pH values that are based on the measurement of decay time usually make use of the differences in the decay times of the acidic and conjugate base form of pH indicators, preferably those with long decay times. Both phase fluorometry and pulsed fluorometry are used to measure decay times, each method having its merit.

2.2.3. Förster Resonance Energy Transfer. Förster resonance energy transfer (FRET), often also referred to as “fluorescence” resonance energy transfer (even though no

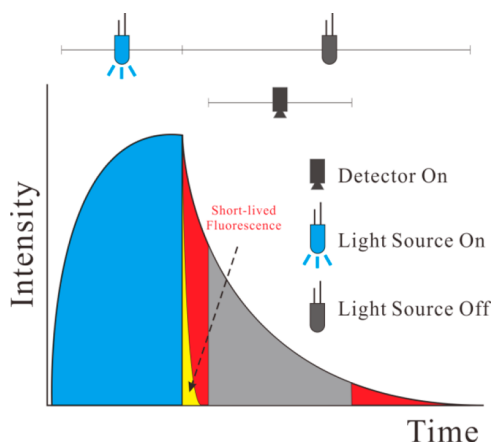


Figure 8. Time-resolved sensing. Following an excitation pulse (during which luminescence rises to a maximum; blue area), the photodetector is opened only after a certain delay time during which background luminescence (yellow) is allowed to decay. The luminescence of the pH-sensitive probe, in contrast, decays much slower (mainly red area) and can be detected after the delay time and with virtually zero background. The method does not compensate, however, for constant levels of ambient light or long-lived background luminescence. Reprinted from ref 132 with public license. Published by The Royal Society of Chemistry.

fluorescence is transferred), is based on classical dipole–dipole interactions between the transition dipoles of a donor dye and an acceptor dye. FRET efficiency inversely depends on the sixth power of the donor–acceptor distance. In case of pH sensors, two dyes are used, one (the “donor” or “acceptor”) being pH-responsive, the other (the “acceptor” or “donor”) usually not (even though it may be so). If in close proximity (typically 7 nm), photonic energy can be transferred from the first to the second dye. In other words, a first fluorophore is photoexcited, and because its emission band overlaps with the absorption band of a second fluorophore, emission occurs from the second fluorophore. A typical example is the fluorescein/rhodamine B pair of dyes: fluorescein has a pH-dependent fluorescence, while rhodamine B is inert to changes in pH. At an excitation wavelength of 488 nm, for example by using the popular argon ion laser, the ratio of green (512 nm) to yellow (550 nm) fluorescence is a parameter for the actual pH value. Molecules are typically kept in close proximity by incorporating them into nanosized hydrophilic polymer particles. It is mandatory, though, that the distance between donor and acceptor remains constant (or is not affected by parameters other than the pH value). FRET is also possible in case of using nanoparticles. The FRET effect has to be clearly differentiated from the inner filter effect. It should be mentioned that some nanosensors that make use of the fluorescein-rhodamine pair do not utilize FRET since these dyes are immobilized into the shell and the core of the nanoparticle, respectively.

2.2.4. Inner Filter Effect. In such sensors, a fluorescent particle (or a dye) is added that displays strong and pH-independent fluorescence, examples being rhodamine B or upconversion nanoparticles. On photoexcitation, these dyes emit fluorescence that is absorbed via an inner filter effect (IFE) by an added pH indicator whose acid form or conjugate base form overlaps the emission of the inert fluorophore (particle).¹³³ Obviously, the inert dye or particle acts as a light source while the pH indicator acts as an absorber of emitted light. Unlike in FRET, there is no need for the inert fluorophore and pH

indicator to be in close proximity, but concentrations usually have to be higher to generate significant pH dependent signal changes. The IFE does not affect the decay time of a fluorophore.

2.2.5. Quenching of Fluorescence. The term quenching is often used but not always in proper form. Many authors refer to quenching whenever fluorescence intensity is reduced. For instance, if the absorbance of a pH indicator dye drops at the wavelength of absorption, fluorescence will also drop, but this is not quenching. Rather, brightness (B_s) is reduced because absorbance (ϵ) drops. Remember that B_s is the product of ϵ and quantum yield. Decrease of luminescence intensity also may occur due to variation in absorption or scattering of the sample. A notorious example is a several-fold decrease in luminescence intensity of a fiber optic sensor (containing no scattering particles, see section 9 for more details) upon going from air into an aqueous solution. According to the IUPAC Gold Book (<https://goldbook.iupac.org>) luminescence quenching can be defined as “Radiationless redistribution of excitation energy via interaction (electronic energy or charge transfer) between an emitting species and the quencher” so that decrease of the luminescence intensity due to change in absorption of the indicator, properties of the probe or hardware (e.g., bending of fibers in fiber-optic sensors) cannot be considered as being quenching.

In classical quenching,¹³¹ a quencher, such as iodide, a metal ion, a nitro compound, or even the hydronium ion (H_3O^+), quenches the fluorescence of a fluorophore or a particle. In other words, photonic energy is no longer emitted by the quencher. Quenching may be static or dynamic. In the former case, the decay time remains unaffected, while in the latter case, it is reduced.

Collisional quenching is best described by a Stern–Volmer plot

$$\frac{F_0}{F} = 1 + K_{sv}[Q] \quad (17)$$

where F_0 and F are the fluorescence intensities (or decay times) in the absence and presence, respectively, of the quencher being present in concentration $[Q]$. The Stern–Volmer constant (K_{sv}) is a quantitative parameter that characterizes quenching efficiency. Plots can be linear, upward curved, or downward curved. In many cases, dynamic and static quenching occur simultaneously.

In this case, a modified Stern–Volmer eq 18 applies

$$\begin{aligned} \frac{F_0}{F} &= (1 + K_d[Q]) \cdot (1 + K_s[Q]) \\ &= 1 + (K_d + K_s)[Q] + K_d K_s [Q]^2 \end{aligned} \quad (18)$$

where K_d is the dynamic quenching constant and K_s is the static quenching constant.

Quenching also can be caused by photoinduced electron transfer (PET). PET is an excited state electron transfer process where a photoexcited electron is transferred from the donor (receptor group) to the fluorophore. With respect to sensing, the PET caused by the unpaired electrons of amino or phenolate groups has received most attention.^{134,135} A representative quenchable fluorophore (naphthalimide) and two typical PET quencher groups (that do not quench when protonated) are shown in the following figure (Figure 9).¹³⁵ The free electron pair at the amino or phenolate group quenches the fluorescence of the fluorophore by PET. If, however, the electron pair binds to

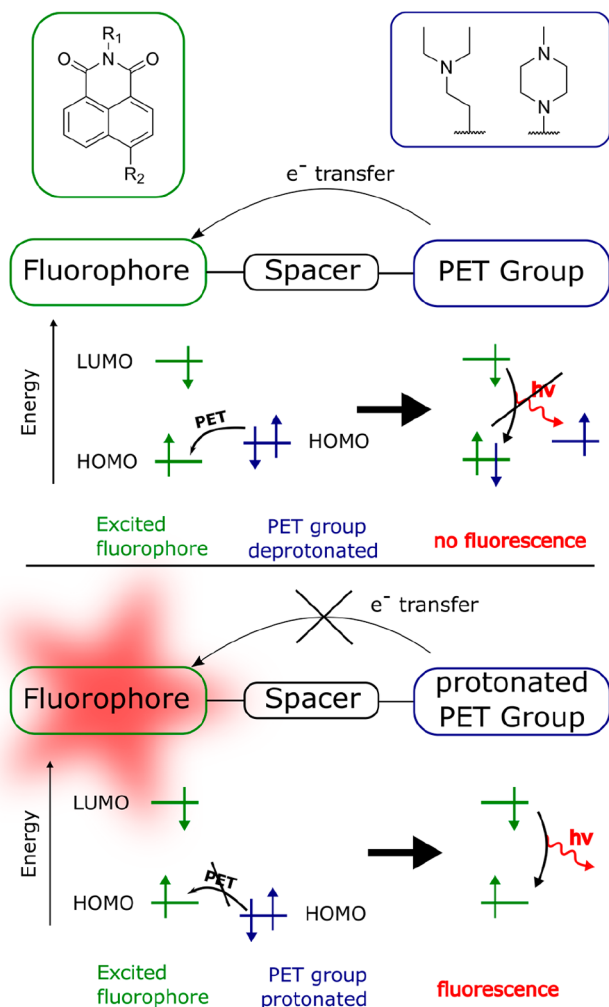


Figure 9. Structures of two PET-based fluorescent probes and illustration of PET-based pH sensing. The PET groups can be attached in R₁ or R₂ position.

a proton, PET is no longer possible, and fluorescence is switched on.

The free enthalpy of the PET process ΔG_{PET} can be estimated by the Weller equation¹³⁶

$$\Delta G_{\text{PET}} = E_{\text{ox}}(\text{rec}) - E_{\text{red}}(\text{fluor}) - \Delta E_{\text{exc}}(\text{fluor}) - E_{\text{IP}} \quad (19)$$

where $E_{\text{ox}}(\text{rec})$ is the first oxidation potential of the receptor group, $E_{\text{red}}(\text{fluor})$ is the first reduction potential of fluorophore, $\Delta E_{\text{exc}}(\text{fluor})$ is the singlet excitation energy of the fluorophore, and E_{IP} the ion pairing energy. Therefore, PET efficiency is high if the PET group is easily oxidized (readily loses an electron in the excited state) and the fluorophore is easily reduced. Moreover, PET is more favorable for short-wavelength fluorophores and in polar solvents.^{137–140}

2.2.6. Other Kinds of Energy Transfer. Dexter ET is another kind of energy transfer. It is a short-range phenomenon that involves electron transfer and whose efficiency drops exponentially with distance (proportional to e^{-kR} where k is a constant that depends on the inverse of the radius of the atom). A further kind of quenching is referred to as surface energy transfer (SET). It is most often observed with (metal) nanoparticles and involves a metallic surface (such as that of gold nanoparticles) and a molecular (organic) dipole. The organic acceptor (quencher) usually does not fluoresce. In a typical example, localized pH measurements were demonstrated by using ratiometric SET.¹⁴¹ A last group of quenchers are called “dark quenchers”. They act very much like FRET pairs, except for the fact that the acceptor dye is nonfluorescent. Hence, ratiometric measurements (which usually are preferred) are not possible in this case. Many authors do not exactly differentiate between FRET, Dexter ET, SET, PET, dark quenching, collisional quenching and even inner filter effects.

2.2.7. Dual Lifetime Referencing (DLR). DLR is a universally applicable scheme for converting fluorescence intensity into a ratiometric signal (Figure 10).¹⁴² Hence, the signal is hardly affected by many parameters except for leaching and bleaching (see Table 4). It is based on the addition of an inert luminescent reference dye/inorganic phosphor having strongly overlapping excitation and emission spectra, but a decay time that is much longer than that of the fluorescent indicator. In case of using a phosphorescent luminophore as the reference dye, the time domain typically is in the microsecond range, and modulation frequencies typically are in the lower kHz range.

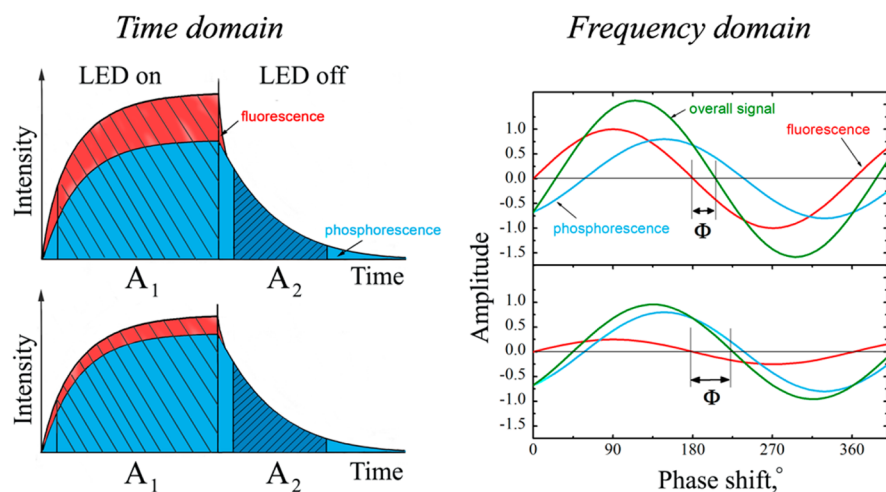


Figure 10. Principle of the DLR referencing for read-out of fluorescent sensors in time domain (left) and in frequency domain (right). The upper and the lower rows reflect the situations with “switched on” and “switched off” pH indicator, respectively.

Table 4. Advantages and Disadvantages of the Various Optical Detection Schemes and How Well They Can Compensate for Various Kinds of Undesired Interferences^a

method	advantages	disadvantages	compensation of interferences by												
			optical components (e.g., filters, optical gratings)	instrumental drift	optical misalignment	background fluorescence from samples	light scattered by sensor materials	intrinsic color of samples	dye leaching and bleaching	inhomogeneous dye loading	temperature				
absorption; reflectance	simple instrumentation; low-cost; portable	moderate sensitivity; many interferences (such as ambient and background light) interfered by many parameters	-	-	-	-	-	-	-	-	-	-	-	-	-
luminescence intensity	sensitive; low-cost; portable devices; enables imaging	relatively expensive; works best in case of OSPs with long lifetime showing oxygen cross-talk	++	++	++	++ ^b	++	++	++	++	++	++	++	++	-
luminescence decay time	sensitive; precise; self-referenced; enables imaging; 1-point calibration	two dyes needed; photodecomposition and leaching of the dyes may be different	-	+	++	-	+	+	+	-	-	-	-	-	+ ^c
two-wavelength referencing	good precision	two dyes needed with different excited-state lifetimes; more complex	++ ^d	++	++	-	++	++	++	++	-	-	++	++	+ ^c
dual lifetime referencing (DLR)	sensitive; precise; enables imaging; simple calibration	two dyes (donor and acceptor dye) needed that have to be in close proximity; and to spectrally overlap	-	+	+	-	+	+	+	-	-	-	-	n.a.	-
Förster resonance energy transfer	low-cost instrumentation		-	+	+	-	+	+	+	-	-	-	-	n.a.	-

^a ++: Efficient compensation. +: Partial compensation. -: No compensation. 0: No effect. n.a.: Not applicable. ^bIn the time domain only. ^cIf both components are thermally quenched to a similar extent. ^dProvided there is excellent spectral overlap.

This enables the use of inexpensive optoelectronic devices and thus provides cost advantages. The method can be equally well applied to conventional sensing, fiber optic sensing and imaging. The scheme works in both the time-domain and the frequency-domain.

In time domain, measurements of luminescence intensity are performed in two windows: (i) during the excitation period in which both the emission of the fluorescent pH indicator and the phosphorescent reference is detected, and (ii) after the light source has been switched off and a certain delay has been applied. This allows complete decay of the short-lived fluorescence so that only the long-lived luminescence of the reference material is measured (Figure 10, left). Evidently, changing of pH will only affect the intensity in the first window, whereas the intensity in the second window is independent of pH. Good examples for time-domain DLR based sensing and imaging of pH values were described by Liebsch et al.¹⁴³ and by Wang et al.¹²⁶

In frequency domain (Figure 10, right), both fluorescence and phosphorescence contribute to overall phase shift. The overall phase shift (or rather its cotangent) reflects the change in the amplitude of the fluorescence and, therefore, the pH changes (eq 20).

$$\frac{A_m \cos \phi_m}{A_m \sin \phi_m} = \cot \phi_m = \frac{A_{\text{ref}} \cos \phi_{\text{ref}} + A_{\text{ind}}}{A_{\text{ref}} \sin \phi_{\text{ref}}} \\ = \cot \phi_{\text{ref}} + \frac{1}{\sin \phi_{\text{ref}}} \cdot \frac{A_{\text{ind}}}{A_{\text{ref}}} \quad (20)$$

Here, A_m represents the overall signal intensity and Φ_m the measurable phase shift. A_{ind} and A_{ref} are the amplitudes of the fluorescence indicator and the reference standard, respectively, and Φ_{ref} is the phase shift of the reference standard. It is mandatory that the decay time of the reference dye is >10 times longer than that of the pH indicator dye.

Ideally, excitation and emission spectra of the indicator and the reference should be almost identical, but it is rarely achieved in practice due to significantly larger Stokes shifts of phosphorescent compounds compared to fluorescent ones. Therefore, a variation of the excitation source or emission filter affects the calibration.

The materials used as references in DLR can be classified in two groups: metal–ligand complexes and inorganic phosphors. Metal–ligand complexes generally possess higher brightness but require immobilization in gas-blocking polymers such as polyacrylonitrile. This eliminates oxygen cross-talk and photodegradation promoted by photosensitized singlet oxygen. Polymeric micro- or nanoparticles with immobilized reference can be dispersed in the matrix used to embed the pH indicator. However, solvent resistance of the nanoparticles and migration of the reference dye into the matrix can cause difficulties. So far, ruthenium(II) polypyridyl complexes have been applied in most cases,^{110,126,143–148} but generally any phosphorescent dye with a decay time between 0.5 and 100 μs is suitable. Luminophores with longer decay times tend to show cross-talk to oxygen even in polymers having low gas permeability. As shown by Demas and co-workers, a combination of two phosphorescent dyes also can be used, providing that the phosphorescence lifetimes are significantly different.¹⁴⁹ The scheme was shown to work both for the combination of an indicator with longer decay time and a reference dye with a shorter lifetime and vice versa for the combination of an indicator with a shorter lifetime and a reference dye with a longer one. Importantly, the phosphor-

escence decay times of all the dyes are >200 ns and thus complete elimination of background fluorescence is possible in a time-resolved measurement. Unfortunately, the set of potential candidates for such a scheme is limited to only a few dye representatives.

In contrast to luminophores, inorganic phosphors are inert in respect to dissolution in solvent, leaching, oxygen quenching and photobleaching. Generally, they can be prepared via solid state synthesis or using a combustion technique and can be further homogenized to give microcrystalline powders. The limitations include lower luminescence brightness and some dependency of the luminescence decay time on the size of phosphor particles (explained by accumulation of defects in crystal structure upon grinding), which results in lower batch-to-batch reproducibility. Some phosphor classes (e.g., Eu(II)-based oxynitride phosphors) show low hydrolytic stability in aqueous media, which disqualifies them for use as reference materials in pH sensors. Red and NIR-emitting phosphors used in DLR referenced sensors include Cr(III)-activated gadolinium aluminum borate,^{150,151} Cr(III)-activated aluminum oxide (Ruby)¹⁵² and calcium copper silicate (Egyptian blue)¹⁵³ (Table S1).

Evidently, both time and frequency domain schemes cannot compensate for varying levels of background fluorescence. Autofluorescence would affect the ratio of intensities in the two windows in the time-domain scheme or the phase shift in the frequency domain and this can be erroneously interpreted as a change of the pH value. The same refers to inelastically scattered excitation light (Raman scattering). Whereas elastically scattered light can be eliminated by appropriate selection of the excitation wavelength and the emission filter, inelastically scattered light may overlap with the emission from the indicator or the reference. Additional optical isolation layer (see section 9.3 for details) shields the sensing material from the probe and thus makes the sensor immune to variations in background fluorescence and scattering. Unfortunately, this is not possible for certain sensor formats such as nanoparticles as used in cells or tissues.

Table 4 shows how efficient the various indicator based optical schemes treated in sections 2.1, 2.2, and 2.2.3 can eliminate potentially interfering optical effects. This summary is valid for indicator-based sensing only.

2.3. Refractive Index Based Sensing

Such sensors are not based on the use of indicator dyes. Rather, the signal is created by a pH-induced change in the refractive index (RI) of a suitable (mostly hydrophilic) material. The sensors are based on the use of a waveguide (fiber optics included) that is coated with a 0.5 to 5 μm thick layer of the pH-responsive material, usually a (de)protonable polymer.¹⁵⁴ The angle of total reflection of light in a waveguide is affected by the ratio of the refractive indices (RIs) of core and cladding. If bent fibers are used, the change in RI may be so strong that light no longer is totally reflected and is lost via a so-called leaky (or lossy) mode. This is schematically shown in Figure 11. The intensity of light will strongly drop when approaching or exceeding a certain pH value.¹⁵⁵ In a typical example, an optical fiber lossy mode pH sensor was generated¹⁵⁶ that measures the differences between transversal (electric; TE) and transversal (magnetic; TM) polarized light. Alternating layers of poly(allylamine hydrochloride) and poly(acrylic acid) were placed on side-polished D-shaped fibers. Two devices were constructed to measure pH from 4.0 to 5.0 and from 7.0 to 8.0, respectively. The sensors based on TE and TM lossy modes show a maximum

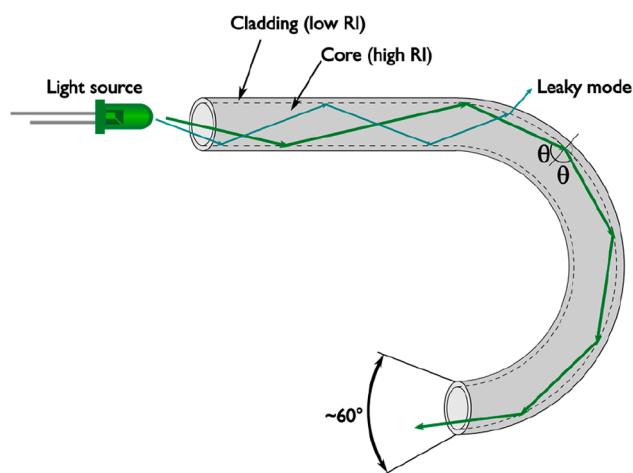


Figure 11. Schematic of a fiber optic pH sensor based on measurement of changes in refractive index (RI). If the RI of the cladding approaches or exceeds the RI of the core, light will not be completely reflected at the interface and get “lost”. This is referred to as a leaky mode.

sensitivity of 69 nm/pH. Numerous other kinds of geometries for use in refractometry are known. By using a polymer whose RI changes with pH value, any refractometer can—in principle at least—be converted into an optical pH sensor.

Various kinds of pH sensors (optical and others) have been described. Most are based on the use of hydrogels, examples being poly(meth)acrylates, poly(meth)acrylamides, polyurethanes, cross-linked polyglycols, chitosan, poly(vinyl alcohols), and copolymers like poly(acrylonitrile-*co*-polyacrylamide) (such as HypanTM; with alternating hydrophilic and hydrophobic domains), to give representative examples only. Figure 12 shows

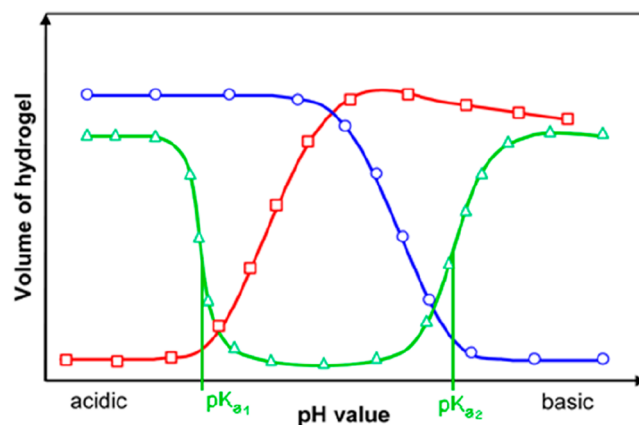


Figure 12. Phase transition behavior of polyelectrolyte hydrogels. Acidic hydrogels (red) swell in basic solution because of ionization by deprotonation; basic hydrogels (blue) swell in acidic solutions and amphiphilic hydrogels (green) contain both acidic and basic groups and therefore show two phase transitions. Adapted from ref 158 with public license. Published by MDPI.

the phase transition of polyelectrolyte hydrogels as a function of pH value. Acidic hydrogels such as poly(methacrylic acid) are dissociated at the carboxy group at pH values above 5 and then swell as a result of electrostatic repulsion. Basic hydrogels, such as polyallylamine, become protonated at the amino group at pH values below 9 and then swell, again as a result of electrostatic repulsion. In case of amphiphilic hydrogels or in case of mixtures

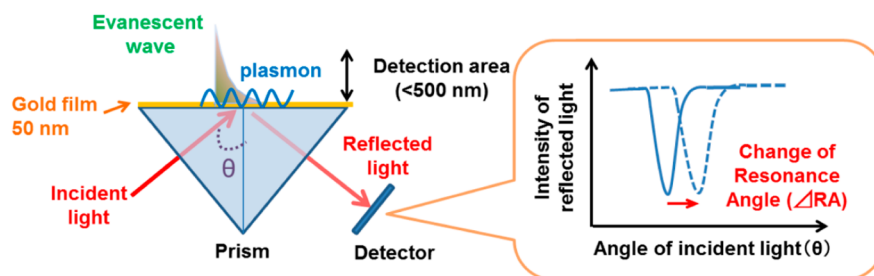


Figure 13. Schematic of an SPR-based sensor. Incident (laser) light hits a gold film placed on a prism. Part of the light wave evanesces into the detection area that consists of a pH-dependently swelling polymer. The angle of reflection depends on the refractive index of the coating, and this is detected by plotting the intensity of reflected light versus the angle of incident light. Reprinted from ref 160 with public license. Published by MDPI.

(or alternating layers), both effects can be seen. A severe disadvantage of certain hydrogels may result from their hysteretic response. This has to be tested in each single case.¹⁵⁷

2.4. Surface Plasmon Resonance Based Sensing

This method also is based on measurement of RI but treated separately because detection is very different from other methods. It is based on an effect referred to as surface plasmon resonance (SPR). Here, the material is placed on a nm-thin film, typically consisting of gold. Two experimental configurations (the so-called Kretschmann and the Otto configuration, respectively; see Figure 13) are widely used. In SPR, the angle of resonance reflection depends on the refractive index (RI) of a swellable coating. If the pH value governs swelling, it also governs the angle of reflection.¹⁵⁹ This method for measurement of changes in RI (unlike the first one) is independent of variations in light intensity as it measures the angle at which the strongest reflection occurs.

A related SPR-based approach is based on the so-called *localized* plasmon resonance of (gold) nanoparticles (rather than of films). Gold nanoparticles and nanorods are known to strongly absorb visible light (and to display colors from red to blue). The color (and absorption maxima) change if such nanoparticles are covered with thin layers of a swellable hydrogel such as poly(methacrylic acid). Any pH-induced swelling or deswelling of the hydrogel will cause a shift of the longitudinal plasmonic absorption peak and, hence, of color.¹⁶¹ Another sensor of that kind was obtained¹⁶² by measurement of the electromagnetic resonances generated in a waveguide-nano-coating interface. The incorporation of gold nanoparticles (AuNPs) into swellable polymeric thin films leads to the generation of two different electromagnetic resonances, namely, localized surface plasmon resonance and lossy mode resonance. These phenomena can be simultaneously observed in the transmitted spectrum. The resulting device works in the pH range from 4.0 to 6.0 and has a fast response.

This special kind of absorptiometry may be extended to almost any combination of nanoparticles undergoing localized plasmonic resonance with any polymer possessing a pH sensitive RI to end up with a pH sensor. One must not forget, however, that this approach in essence is absorbance-based. It suffers from the typical limitations of absorptiometry (see section 2.1) including errors resulting from the presence of other colored absorbers and of light scattering particles, and of variations in the intensity of light sources and the sensitivity of detectors.

2.5. Photonic Crystal Based Sensing

Such sensing schemes have not been widely used but have a large potential because color changes can be readily seen with bare eyes. Their function also relies on changes in refractive index

(RI), but in a way that is quite different from the sensors discussed in sections 2.4 and 2.5. Photonic crystals (PhCs) consist of a periodic arrangement (lattice) of regularly shaped transparent materials whose dielectric constants are different. Only light of a certain wavelength can pass the lattice. If the structure of the lattice is changed (for example due to swelling by varying the pH value of the water penetrating the lattice), the wavelength of light that can pass the structure is changed (Figure 14). This can be detected instrumentally or visually. Fundamentals and applications of PhCs for use in chemical sensing and biosensing have been reviewed by Fenzl et al.¹⁶³

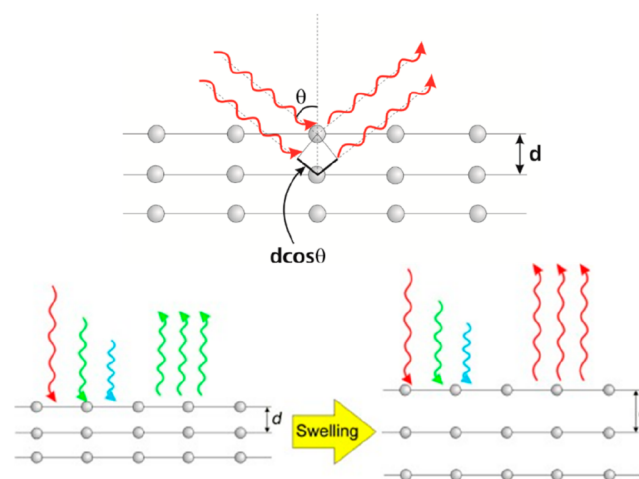


Figure 14. Simplified scheme of light reflection of ordered spheres in a photonic crystal illustrating how the distance in crystals of defined dimensionality (1D, 2D, or 3D) causes a change in the reflected wavelength. Adapted with permission from ref 163. Copyright Wiley-VCH Verlag GmbH & Co., KGaA, Weinheim 2014.

Depending on their dimensionality, PhCs can be subdivided into three groups. One-dimensional PhCs are the simplest variation where the periodicity exists in only one dimension. These are also known as Bragg reflectors or Bragg stacks which reflect one specific wavelength. Two-dimensional PhCs possess periodicity in two spatial directions. Three-dimensional PhCs are most common at present because methods for preparation are simple and cheap. Self-assembly of nanoscopic, monodisperse spheres into a photonic crystal host is most often used. The kinds of spheres include silica (SiO_2), titania (TiO_2), and polyacrylates.

A schematic of a photonic crystal array consisting of dielectric spheres within a dielectric medium (such as the solution whose pH value is to be determined) is shown in Figure 14. By

combining the well-known laws of Bragg (diffraction) and Snell (refraction), the following equation is obtained:

$$2d(n_{\text{eff}}^2 - \sin^2 \theta)^{1/2} = m\lambda \quad (21)$$

where d is the distance between particle planes, n_{eff} is the mean effective refractive index (RI), θ is the angle of incident light, m is the order of reflection, and λ is the wavelength of the reflected light. To sense pH values, a material has to be found whose RI is strongly affected by pH, for instance as a result of swelling. RI can be resolved down to 0.001 units by using one-dimensional PhCs of the Bragg reflector (Bragg stack) type.

It is interesting to note that research on PhCs has almost exponentially grown in physical sciences, but not so far in chemistry. In terms of sensing, PhCs have a very large potential, not the least because sensing can be performed (a) over a wide range of wavelengths (from the UV to the IR), (b) in numerous formats that include fiber optics and fiber resonators, birefringence, polarization, plasmonic resonance, or interferometry, (c) in combination with numerous (bio)chemical receptors that range from enzymes to aptamers, (d) in combination with various kinds of materials including stimulus-responsive polymers and nanomaterials such as noble metal nanoparticles, and (e) by using techniques, such as multiplexing, pillar arrays, or logic gating. It must be stated, however, that selectivity remains a major challenge at least in chemical sensing because most host materials are of the hydrophilic type and therefore will be prone to interference due to changes in pH values and salinity. Temperature also has a strong effect on the distance d between particle planes.

2.6. Sensing of pH Values via the pH-Dependent Turbidity of Hydrogels

Hydrogel films often shrink and then become opaque due to phase separation. Many hydrogels also have a phase transition temperature that is pH-dependent.¹⁶⁴ This can be used to sense pH values via measurement of turbidity.¹⁶⁵ In an approach reported by the Seitz group,¹⁶⁶ colored microspheres were incorporated into a hydrogel whose transmission for light increases if the hydrogel absorbs water which depends on the pH value. The changes of optical properties (absorbance, turbidity) can be monitored as a transmission measurement using a conventional spectrophotometer or a miniature fiber optic spectrometer. Rooney et al.¹⁶⁷ describe another kind of pH sensors based on measurement of turbidity. A membrane was prepared by suspending aminated polystyrene microspheres (1 μm in size) in hydroxyethyl methacrylate, which was then polymerized to form a hydrogel. The resulting membranes are turbid because the RI of the microspheres is larger than the RI of the hydrogel. Turbidity is larger in basic medium and decreases with increasing wavelength. In acidic milieu, protonation of the amino group causes the polymer microspheres to swell. Swelling affects turbidity, both by increasing microsphere diameter and by reducing the microspheres' RI so that it gets closer to the RI of the hydrogel. These membranes can be used for optical sensing in the visible and near-infrared regions, even at wavelengths beyond 1 μm as used for fiber optics telecommunications. They have excellent long-term stability, but response is slow because the required diffusion of protons into the interior of the polymer is rather slow.

2.7. Infrared and Raman Spectroscopic Sensing

Infrared (IR) and Raman spectroscopy are based on the absorption of light that leads to the stimulation of vibration of molecules. In Raman spectroscopy, absorbed light is emitted at a

wavelength whose frequency is smaller by that of a typical vibrational band of the molecule, typically expressed in cm^{-1} units. IR sensors do not require the use of classical indicators. Some sensors for pH values are referred to as near-IR sensors because their analytical wavelength is below 1.5 μm , but in fact they are based on the use of indicators that have NIR electronic absorptions. Such sensors are not treated in this section. Fourier transform IR (FTIR) spectroscopy is a commonly used variant. Unlike in conventional IR spectroscopy, light is guided first through an interferometer and then passes the sample (or vice versa). The resulting "interferogram" represents light output as a function of mirror position. Data are then processed by a technique called Fourier transform, which converts them into the desired spectrum (a plot of transmittance versus wavenumber).

Specifically referring to IR based pH sensing, virtually any material may be used, at least in principle, as a coating, provided its IR absorption varies with pH values. IR-bands with strong transitions obviously are preferred, for example the bands of amino groups or of carboxy groups. Materials, such as amines (polyethylenimine), carboxylic acids (polyacrylates), and even mixtures (which enable ratiometric sensing) typically are used for sensing near-neutral pH values. Examples include ATR-FTIR based sensors¹⁶⁸ and SERS-based sensors (by using the pH-sensitive SERS reporter molecule 4-mercaptopyridine deposited on the surface of single silver nanoparticles that act as plasmonic signal enhancers).^{169,170} More alkaline or more acidic pH values also may be covered by using hydrogels with functional groups that have pK_a values within the pH range of interest. Such pH sensors often are used in combination with nanomaterials to enhance SERS activity. A core-shell nanocomposite consisting of polyaniline and gold nanoparticles (PANI@AuNPs) was shown¹⁷¹ to enable intracellular monitoring of pH values by SERS. The method exploits the pH-responsive property of PANI and the SERS-enhancing effect of AuNPs. The intensity of the PANI Raman peak at 1164 cm^{-1} decreases on increasing the pH value from 4.6 to 7.4. This is the pH range encountered in normal cells and in cancer cells. The NPs were incorporated into HeLa cancer cells and other cells for Raman based imaging of pH values. Generally spoken, the number of Raman spectroscopy based pH sensors remains small.

2.8. Sensing of pH Values via Mechanical Displacement

If a swellable material is coupled to a reflector, its expansion will cause the reflector to move. This can be measured by means of interferometry or by measurement of the intensity of light reflected by a reflector, both often by making use of optical fiber systems. Swelling of a polymer placed on one side of a waveguide also results in a physical stretch and slight bending of the (flexible) waveguide, and this enlarges the grating period, which can be measured by using a Bragg grating based detector. Fiber Bragg grating sensors are fairly simple and in wide use in methods other than chemical sensing. A swellable hydrogel was used in such a sensor¹⁷² to obtain an optical pH sensor based on the effect of pH on RI. On swelling, the hydrogel pushes the clamps fixed on the fiber grating to cause a physical stretch of the fiber, which expands the grating period. Such a sensor resembles the function of displacement sensors. In related work, a polymer was used whose volume reversibly increases and decreases as a function of pH. This causes a reflecting diaphragm to move, and this in turn, changes the intensity of light reflected back into the optical fiber.¹⁷³ This is schematically shown in Figure 15. The scheme was also applied to microcantilevers coated with a swellable polymer. These can convert pH values into a

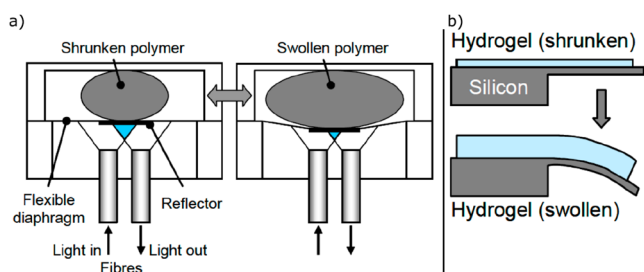


Figure 15. (a) Dual fiber sensor based on measurement of the displacement of a reflector. Changes in polymer volume cause the reflecting diaphragm to move, which in turn changes the intensity of light reflected back into the optical fiber. (b) Principle of a microcantilever-based pH sensor coated with a swellable hydrogel. Adapted from ref 158 with public license. Published by MDPI.

mechanical displacement as shown in Figure 15. The groups of Zhang¹⁷⁴ and Peppas¹⁷⁵ used mechanical cantilever devices with an optical read-out system as transducer element to monitor changes in swelling of hydrogel coatings made from cross-linked 2-dimethylamino ethyl methacrylate or from poly(methacrylic acid)-*co*-poly(ethylene glycol) dimethacrylate, respectively. This causes a pH-induced mechanical displacement of the cantilever. Gerlach et al.¹⁷⁶ have prepared hydrogel blends, such as poly(vinyl alcohol)/poly(acrylic acid) or poly(*N*-isopropylacrylamide), which are sensitive to pH values. They were placed on silicon micromachined sensors and used to electrochemically sense pH values. While not analyzed by an optical method, these materials may work well in various kinds of optical sensors.

A reflection interference system based on displacement was introduced¹⁷⁷ that uses metal island-coated pH-sensitive swelling polymers. Gold nanoparticles coated with a hydrogel layer were placed on top of a mirror to act as an optical thin-film resonance system with reflection properties depending on the thickness of the hydrogel layer. Changes in the thickness of the hydrogel layer can be monitored by the slope of the characteristic reflection minimum.

The Seitz group has studied the diffuse reflected light of swellable hydrogels and found a significant change of the reflection intensity after a change in volume. In one version,¹⁷⁸ an optical reflective device was coupled to the swelling of an amino-modified polystyrene membrane. In another version,¹⁷⁹ a single fiber-optic pH sensor is described based on changes in reflection accompanying polymer swelling. Diffuse reflection occurs at interfaces between regions with a different refractive index (RI), especially between the bulk polymer and the aqueous solution in the pores. During polymer swelling the bulk polymer dilutes with water causing its RI to decrease and become closer to the RI of the water in the pore space. This reduces the reflectance at the polymer–pore interface resulting in a decrease of the reflected intensity. The system includes a light emitting diode as a light source, a photodiode detector, and a fiber optic coupler, which serves as a beam splitter. Yet another chemo-mechanical-optical pH sensing mechanism relies on a Fiber Bragg Grating (FBG) coated with single and multilayers of a hydrogel.¹⁸⁰ The device is based on the ionizable (protonable) chemical functions inside the hydrogel which reversibly dissociate as a function of the local pH value. Consequently, an osmotic pressure difference is generated between the gel and the solution. This pressure gradient causes the hydrogel to deform which in turn induces secondary strain on the FBG sensor and a shift in the Bragg wavelength.

2.9. Interferometric Sensing of pH Values

Numerous methods for interferometric sensing (IFS) are known. Examples include Mach–Zehnder, Michelson, Sagnac, Fabry–Perot, and other configurations). Interferometry can be combined with leaky mode sensing (section 2.3), photonic crystal sensing (see section 2.5), Bragg (fiber) gratings, directional couplers, grating couplers and fiber gratings, twin-core fibers, loop mirror sensors, Fresnel reflection, cascaded microfiber knot resonators, ring resonators and all-fiber ring lasers, and various others. This section differentiates between IFS using stimuli-responsive polymers and IFS using pH-indicators.

While intensity-modulation based IFS for pH are more easily manufactured, they suffer from fluctuations in the light source intensity. Wavelength-modulated sensors are not affected by intensity fluctuations but suffer from a more complex fabrication process.

2.9.1. Interferometric Sensing of pH Values Using Stimuli-Responsive Polymers, Composites, and Layers.

These are most common but also least selective. Stimuli-responsive polymers only in very rare cases respond to pH only. This is because swelling and shrinking not only is affected by pH but also by (a) any salt (ion) contained in a sample, (b) by organic solvents, and (c) by proteins contained in a sample. It does not come as a surprise that many methods for IFS have been described in the scientific literature, but—unlike in case of indicator-based pH sensors—not a single IFS has been commercialized so far. Fiber Bragg grating (FBG) sensors are fairly simple and have been often used. Figure 16 shows a

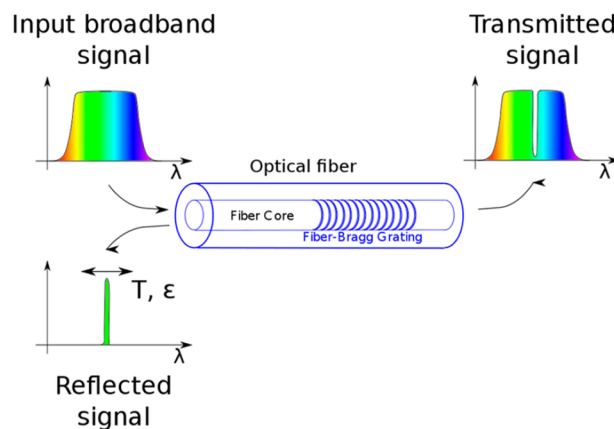


Figure 16. Fiber Bragg grating showing the optical fiber core with the grating, the input spectrum, and the transmitted spectrum, which lacks the fraction that can be found in the reflected signal. The wavelength of the reflected signal is strongly affected if pH (or any other parameter, such as temperature) expands the grating period. Reprinted from ref 181 with public license. Published by MDPI.

schematic presentation of a typical sensor (of which numerous modifications do exist). In essence, it consists of a white (multicolor) light source that passes the core of a fiber possessing a Bragg grating. Depending on the RI of core and fiber, most of the white light will be transmitted and spectrally separated. However, a small band will not be transmitted but reflected.

Interferometric sensing was accomplished,¹⁸² for example, by using a waist-enlarged bitaper modified with a tantalum pentoxide layer that displays high refractive index (RI). It was coated with a poly(vinyl alcohol)/poly(acrylic acid) composite

hydrogel to induce sensitivity to pH in the pH 2.5–6.5 range. In another approach, a poly(vinyl alcohol)/poly(acrylic acid) coating was applied in a photonic crystal sensor with laser interrogation.¹⁸³ Reflective diffraction gratings were coated with a pH-sensitive hydrogel to construct diffraction gratings that swell/shrink reversibly because of changes in pH.¹⁸⁴ Interferometric analysis of the grating enabled detection of the hydrogel's motions with nanoscale precision and resulted in a resolution of 6×10^{-4} pH units. The developed system is remarkably simple both to fabricate and operate and yet is extremely sensitive. Moreover, the concept of the reflective hydrogel grating is generic and can be applied to sense a wide range of other chemical stimuli. Wavelength-modulated pH sensors (that are superior to intensity based interferometric sensors) were described that use a pH-sensitive hydrogel with an optical fiber Bragg grating.¹⁸⁵

Other work includes Fabry-interferometry using optical fibers with pH-sensitive polymeric ultrathin coatings and based on lossy-mode resonance¹⁵⁵ or long-period fiber gratings.¹⁸⁶ In a miniaturized Fabry–Perot pH sensor,¹⁸⁷ an optical fiber was coated with poly(vinyl alcohol)- and poly(acrylic acid)-based hydrogel. A section of a hollow-core photonic crystal fiber was sandwiched between the lead-in single mode fiber and the sensing fiber. Swelling induces optical path modulation when exposed to varying pH solutions. The relative sensitivity is 11 nm per pH unit in the 4.1 to 6.9 pH range. The method was later extended to Mach–Zehnder interferometry using the same materials.¹⁸⁸

Mach–Zehnder interferometric sensing of pH values by using a swellable/shrinkable hydrogel was demonstrated by Tou et al.¹⁸⁹

A hydrogel consisting of poly[2-hydroxyethyl methacrylate-co-2-(dimethylamino)ethyl methacrylate] is used that has basic (protonable) amino groups. These can be protonated/deprotonated, and this changes the interference pattern. The sensor covers the pH range from 6.5 to 8.5 and is claimed to have a pH 0.004 “limit of detection” (which probably should read precision or resolution). In-line Mach–Zehnder interferometry and fiber Bragg gratings in combination with swellable hydrogels was also reported by Lei et al.¹⁹⁰ for simultaneous determination of pH values and temperature. Mohammed¹⁹¹ describes photonic crystal fibers (PhC-Fs) for pH sensing via Mach–Zehnder interferometry. Two PhC-Fs (2 and 4 cm long) were fusion spliced between multimode fibers. The air holes in the adhesive regions completely collapsed to result in a multimedia interference pattern. Response is said to occur between pH 4 and 12, but the reason for the effect of pH is not explained.

2.9.2. Interferometric Sensing (IFS) of pH Values Using pH-Indicators. IFS based on the use of colorimetric or fluorescent probes is more selective but devices are more difficult to make. In a typical experiment, an absorptometric indicator is incorporated in a thin film coating, and changes in absorption or fluorescence are measured by combinations of methods such as evanescent wave sensing and interferometry. Examples include (a) a tapered single-mode optical fiber coated with cellulose and various indicator dyes¹⁹² that allows measurement of pH values from 3 to 7.4 or from 8 to 11, (b) interferometry via laterally adsorbed pH sensitive coatings containing the indicator neutral red,¹⁹³ or (c) fibers coated with a mix of Liquicoat (a metal alkoxide colloidal solution for the deposition of antireflective coatings on surfaces and displays) and various pH indicators;¹⁹⁴ the working range extends from

pH 1 to 6. The work was later extended to fluorometric sensing.¹⁹⁵

2.10. Sensing of pH-Values via Solvatochromic Fluorescent Probes

Many polymers swell and shrink dependent on the local pH values. This is associated with a change in the local polarity of the water-penetrated polymer, and this may be detected by using polarity-sensitive fluorescent probes. McCurley used a swelling material (a copolymer prepared from acrylamide and dimethylaminoethyl methacrylate) that undergoes pH-dependent swelling and shrinking.⁵⁷ The detection principle is based on the protonation of the amino groups in the hydrogel. Electrostatic repulsion between like-charged groups causes the gel to expand. The polymer was doped with a fluorophore, which acts as the transducer that indicates swelling. While the amount of fluorophore remains constant, the gel volume changes in response to a change in the ionization of the hydrogel. This in turn, changes in response to pH. It must be emphasized that the fluorophore used by the authors does not have a pH-dependent fluorescence but is completely inert. Fluorescence increases from 0.37 to 0.74 units on going from pH 3 to 5 but then remains constant. The sensor was also applied to sense glucose via the enzyme glucose oxidase which catalyzes the oxidation of glucose. This is accompanied by a decrease in the local pH value.

2.11. Referenced (Ratiometric) Sensing

The terms referenced sensing and ratiometric sensing relate to techniques, where the analytical (pH-dependent) optical signal is related (referenced) to a second optical signal of the sensor that is differently or not at all affected by pH values. Referencing can eliminate many sources of error, including those resulting from drifts in light source intensity, detector sensitivity, leaching, bleaching, and swelling and from bending effects. Some methods are intrinsically self-referenced, for example refractive index based sensing, decay time based sensing, and the various dual lifetime referenced based sensing schemes. These are discussed in other sections. Also see Table 4.

Most methods for referenced sensing are based on ratioing signals obtained at two wavelengths. The term two-wavelength ratiometry ($2\lambda R$) is used for such methods in the following. $2\lambda R$ works in absorption, reflection, and emission. $2\lambda R$ can be applied to indicator based sensing and to stimulus-responsive polymers possessing pH-dependent IR absorption bands. The main options are summarized in the following.

(A) When using UV/vis absorbing or reflecting indicator dyes:

(1) Measure the intensity of the indicator bands at 2 wavelengths, one going up in intensity with pH, the other going down.

(2) Measure the intensity of the indicator bands at 2 wavelengths, one going up in intensity with pH, the other remaining unaffected (at the so-called isosbestic point).

(3) Measure the intensity at 1 wavelength of the indicator dye, and intensity at 1 wavelength of an added pH-irresponsive reference dye; this is the method of choice if the indicator does not display two distinct absorption bands or an isosbestic point (as, for instance, in case of phenolphthalein).

(B) When using luminescent indicator dyes

(1) Measure the intensities of luminescence at a single emission wavelength at 2 different excitation wavelengths (one going up in intensity with pH, the other going down).

(2) Measure the intensities of luminescence at 2 emission wavelengths at a single excitation wavelength (one going up in

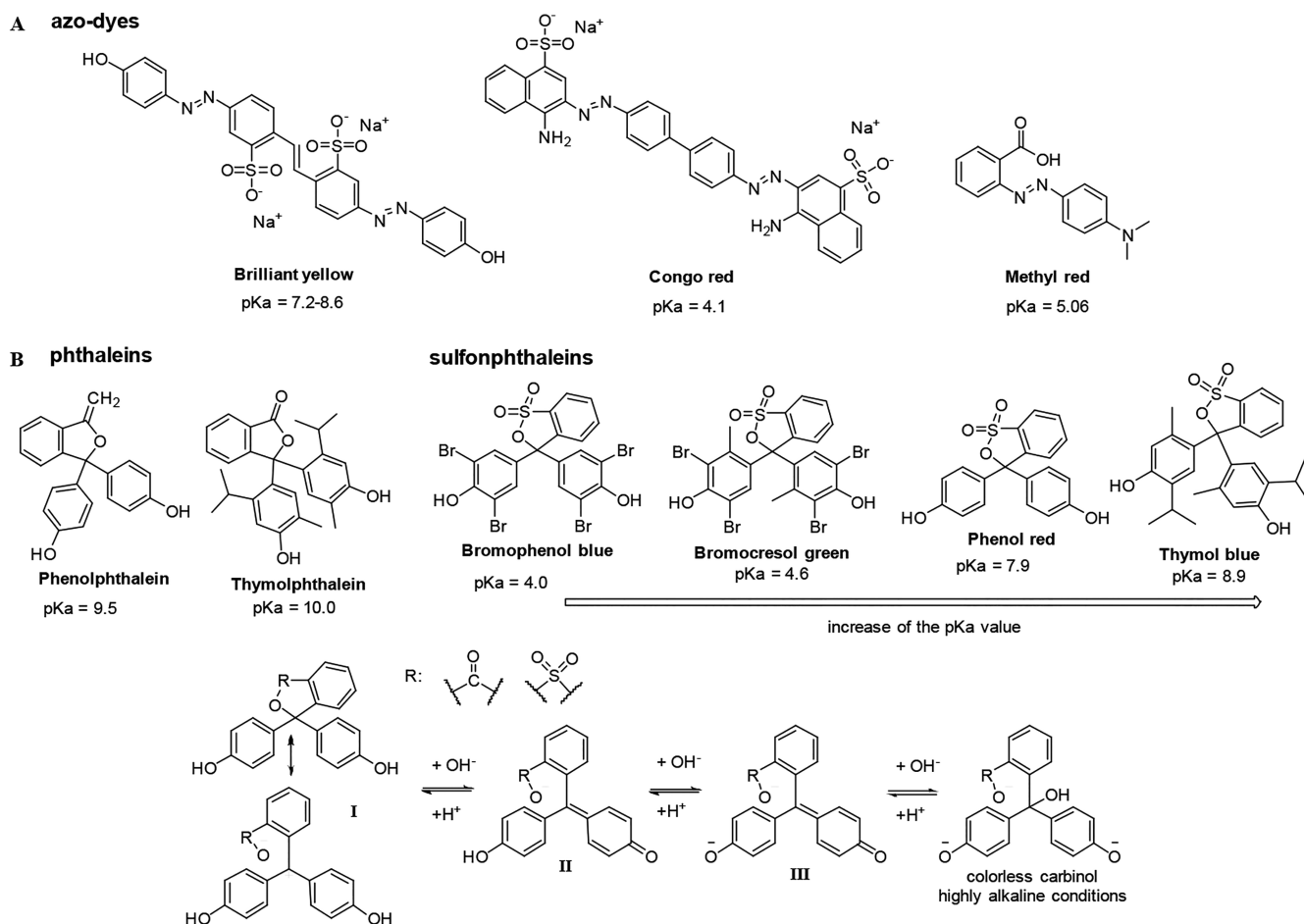


Figure 17. Overview of the most common absorptometric indicators used in optical pH sensors.

intensity with pH, the other going down); this scheme also works in the FRET mode.

(3) Measure the intensities of luminescence at 2 different excitation wavelengths of the indicator dye at 2 emission wavelengths (one going up in intensity with pH, one going down); this method is rarely used because it makes the optical system complex.

(4) Measure the intensities of luminescence at 2 well separated emission wavelengths at a single excitation wavelength; one band is the pH-dependent signal of an indicator, the other is an inert signal caused by an added reference fluorophore.

Other (more complex) combinations also are possible but hardly used in practice.

(C) When using polymers that have pH-dependent absorptions in the infrared (IR)

(1) Measure the intensity of two IR absorption bands, one changing with pH (such as the bands for amino groups or carboxy groups), the other remaining inert (such as those for $-\text{CH}_2-$ groups)

(2) Measure the intensity of (a) any IR absorption band that varies with pH and (b) of IR light scattered by the polymer which is pH-independent.

Other (more complex) combinations also are possible but hardly used in practice.

(D) Less common methods for $2\lambda R$ include

(1) The use of covalently linked pairs of dyes, one has pH-dependent colors, the other not. This is a modification of

scheme A3. Alternatively, the pair of dyes may consist of an ion pair composed of a cationic and an anionic dye.

(2) The use of upconversion nanoparticles (UCNPs) coated with a pH-indicator; UCNPs under NIR excitation display 2 or more emission bands; if one emission band of the UCNPs is screened off by the indicator and the other is not, the ratio of the two signals is a direct parameter for pH.

(3) Measurement of the intensity of scattered light at 2 wavelengths of IR irradiation, one at a wavelength where absorbance varies with pH values (for example that of amino groups), and one at an inert wavelength where scattering is not affected by pH variations.

(4) Raman and SERS based methods for $2\lambda R$, with methods comparable to those used in IR absorptometry.

$2\lambda R$ (and more complex methods of referencing) are widely used in optical sensing schemes. They can be found in this Review by searching for the terms referenced/referencing and ratiometric.

It should be noted that two-wavelength ratiometric techniques do not compensate for variations in the measured sample associated with coloration of the probe, autofluorescence or scattering providing that the sample is "visible" through the sensing material. In certain sensor formats (such as absorptometric and luminescent-based planar optodes and fiber-optic sensors) application of additional optical isolation layer (see section 9.3 for details) represents an efficient way to eliminate these interferences. Evidently, such approach is not feasible for other sensor formats, such as nanoparticle-based sensing.

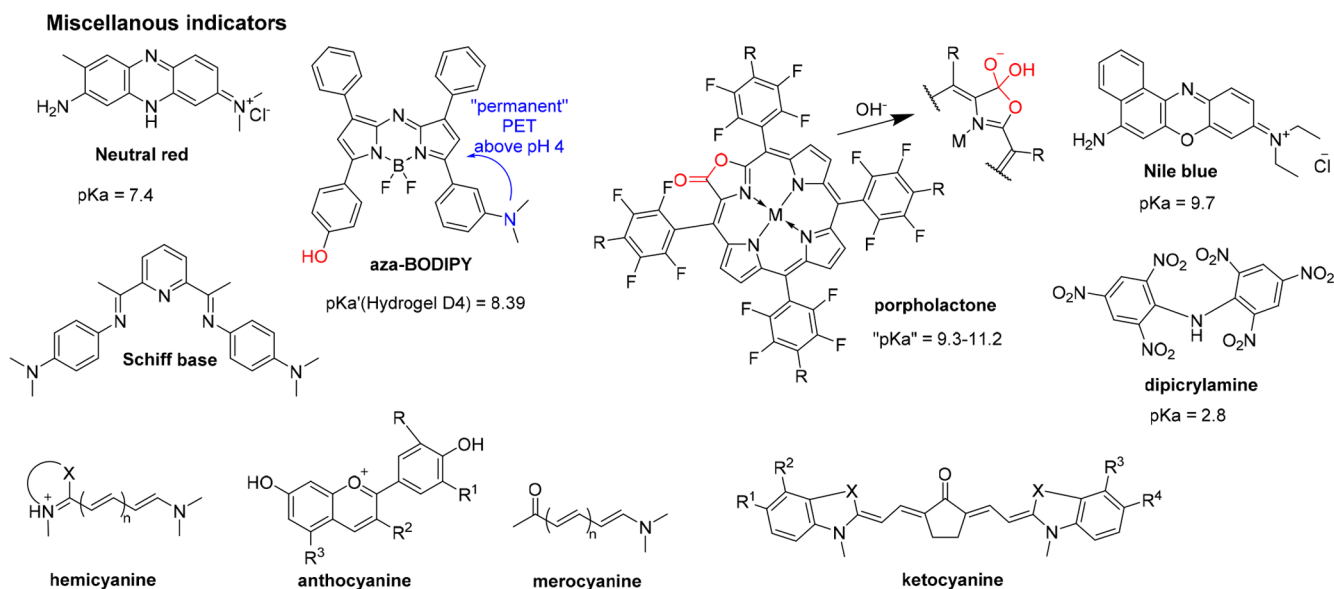


Figure 18. Overview of other absorptiometric indicators used in optical pH sensors.

3. OVERVIEW OF COMMONLY USED ABSORPTIOMETRIC pH PROBES

The book by Bishop¹⁹⁶ and other literature^{197–200} give a wealth of absorptiometric pH indicators (and also indicators for ions) for use at pH ranges that extend from 0 to 14. Only relatively few of them have been considered and applied for preparation of absorptiometric pH sensors (Table S2). Most of them were intended for application in aqueous solutions. The difficulties in finding suitable combinations of indicator and proper host chemistry are mainly due to the requirements and limitations of absorptiometric sensing. Disregarding complex sensing schemes, such as inner-filter effect based read-out (section 2.2.4), the spectral changes of absorptiometric probes upon pH variation can be detected using absorption or reflectance. To achieve sufficient modulation of the signal, high indicator concentrations are used, requiring the dye to be highly soluble in the immobilization matrix without aggregation. The thickness of the sensing layer can be increased which however increases the response time. Alternatively, the optical path through the sensor film can be increased by using different measurement geometries, such as evanescent wave-based read-out (section 14.3). As a trade-off, the size of the sensor is increased significantly.

To enable the best performance, absorptiometric pH probes ideally should not only display pronounced spectral changes upon pH variation but also should possess (a) high molar absorption coefficients, (b) high chemical and photochemical stability, (c) good solubility in immobilization matrices, or (d) have adequate functionality to be covalently coupled in order to prevent leaching (section 6). Similar to luminescent dyes, absorptiometric indicators should not be highly charged to reduce the cross-sensitivity to ionic strength (section 1.6). Depending on the desired application, spectral range and pK_a are the most important selection criteria.

Most popular indicator dyes for application in absorptiometric sensors belong to the group of azo-dyes,^{15–17,23,70,76,194,201–239} phthalein,^{82,194,225,226,240–250} sulfophthalein (ref 19, 22, 32, 34, 35, 38, 43, 45, 63, 71, 102, 194, 213, 222, 226, 232–235, 241, 245–248, 251–321), and other triphenylmethane dyes^{15,50,224,236,252,263,302,322–325} (Figure 17). Less common indicators belong to the groups of

cyanines,^{326–329} porphyrins,^{69,330–339} and other classes (Figure 18; description below).^{60,76,111,340–350}

3.1. Sulfophthalein Dyes

The group of sulfophthalein dyes is based on the chemical structure of phenol red (Figure 17). Prepared by Peterson and co-workers back in 1980,³² the first fiber optic pH sensors used phenol red as indicator embedded into polyacrylamide microspheres. Since then, numerous researchers utilized phenol red in optical pH sensors, which is by far the most commonly used pH probe (22, 32, 33, 43, 45, 222, 226, 232, 234, 241, 247, 284, 288, 306, 307, 309–311, 314, 321, 351, 352). Such popularity can be explained by the response over the physiological pH range and its commercial availability. The properties of the sulfophthalein dyes are typically varied by the substitution pattern on the two phenol rings. In general, the pK_a is increased by electron-rich substituents (such as alkyl) and is decreased by electron withdrawing substituents (such as halogens). Standard sulfophthalein dyes have two protonation equilibria (Figure 17), form I in highly acidic regions, form II in acidic to neutral regions, and form III under alkaline conditions. Contrary to related phthalein dyes, sulfophthaleins are much less inclined toward formation of colorless carbinols under highly alkaline conditions.³⁵³ In aqueous media, the pK_a values of sulfophthaleins span from approximately 1.4 to 9.5. In alkaline media, the indicators exist in the sulfonate form and are, therefore, well water soluble. Because of the negative charge, the sulfonate groups enable strong electrostatic immobilization on ion exchange resins.^{265,273,299,300,317,318} This, however, increases the cross-talk to ionic strength due to high charge of the matrix and may introduce hysteresis and impaired diffusion due to Donnan potential. Leaching of positively or negatively charged indicators can be reduced by replacing the usually inorganic counterion (such as sodium ion or chloride) by an organic counterion.^{354,355} In case of cationic polar indicators (such as those carrying a quaternized pyridinium group or various metal–ligand complexes), the conventional counterion (such as chloride) is replaced by an organic counterion, such as dodecylsulfate or trimethylsilylpropylsulfate. In case of anionic polar indicators (such as those carrying sulfo groups), the conventional counterion (sodium) is replaced by an organic

counterion such as methylpyridinium or trimethyldecylammonium.³⁵⁶ This method also is an excellent method to render ionic dyes soluble in less polar polymer matrices such as polystyrene. In some cases, cationic ruthenium(II) based fluorophores have been ion paired with anionic pH indicator dyes to obtain smart pH indicating ion pairs.³⁵⁷

Sulfophthalein based sensors have been prepared using styrene-divinylbenzene copolymers (refs 19, 22, 43, 45, 102, 245, 253, 265, 273, 288–291, 298, and 306), agarose,³⁰⁹ cellulose,^{38,213,232–234,263,276,302,351} nylon-6 fibers,²⁴¹ PVA,³¹⁰ PVC,^{232–234,296} PVI,^{287–289} sol–gel (refs 194, 226, 252, 254, 255, 257, 259–262, 267, 269, 272, 277, 279, 281–284, 286, 293, 294, 301, 311, 312, 314, 352), SiO₂–TiO₂ composites,^{246,247,266,316} and ormosils^{254,256,258,264,268,270,271,280,321} as immobilization matrices.

Leaching of the dyes can be eliminated via covalent coupling to the immobilization matrix. For instance, carboxy- or glutathione-modified dyes can be coupled via amide linkage to amino TentaGel S, aminopropylated glasses, or aminohydroxypropylated cellophane.^{38,235,251} Azo dyes have been coupled to diazotized glasses,^{15,222} and to cellulose,¹⁶ certain dyes copolymerized with acrylamide,³² amino-modified dyes coupled to chlorosulfonated polystyrene to form sulfonamides³²⁰ and hydroxymethyl-modified dyes have been linked to poly(vinyl alcohol).³¹⁰ Covalent coupling and other immobilization techniques are discussed in detail in section 6.

3.2. Phthalein Dyes

Phthaleins also belong to the triphenylmethane dyes and are structurally similar to sulfophthaleins (Figure 17). Compared to the latter, there is much less structural diversity among phthaleins; the dyes used for preparation of sensors are limited to phenolphthalein, α -naphtholphthalein, *o*-cresolphthalein, and thymolphthalein. Protonation equilibria are similar to the sulfophthaleins, apart from their tendency toward the formation of colorless carbinols under highly alkaline conditions. The analytical range is more in the alkaline pH region with pK_a values from 8.5–10.0. Phthaleins are readily water-soluble in their alkaline form as carboxylates, in contrast to the hardly soluble acidic form. For covalent immobilization, the same procedures as for sulfophthaleins have been used. Additionally, phenolphthaleins were coupled to aminated PAN fibers via Mannich reaction.^{225,240–244} Phthaleins have also been immobilized in or on nylon-6,²⁴¹ PVA,²⁴⁰ PAN/PA6.6 composites,²⁴³ styrene-divinylbenzene copolymers,²⁴⁵ cellulose materials,²⁴⁴ silica–titania sol–gel,^{246–248,250} and silica sol–gel.^{82,194,226,250}

Apart from the phthalein and sulfophthalein dyes, only relatively few other triphenylmethane dyes have been used for the preparation of sensors. Limitations of triphenylmethane dyes include the formation of polyvalent ions introducing strong influence of ionic strength, poor stability in their acidic form, and poor photostability.¹⁹⁶

3.3. Azo Dyes

Azo dyes contain an azo linkage between two sp² carbons in their structure. Dyes used as pH indicators usually have hydroxyl or amino groups, building up the classes of hydroxyazo or aminoazo dyes, respectively (Figure 17). The protonation responsible for the color change can take place at the nitrogen of the azo-group or at peripheral nitrogens.³⁵⁸ Protonation of the azo group results in a bathochromic shift of the absorption peak.³⁵⁸ On the contrary, protonation of peripheral amino nitrogens gives rise to a hypsochromic shift, often into the UV part of the spectrum.³⁵⁸ Among the dyes used for sensors, a wide

pK_a range in solution is covered from 0.5 for a vinylsulfonyl azo dye¹⁷ to 13.5 for Solo chrome dark blue.¹⁹⁶ Because of their origin as indicators for aqueous solutions, many azo dyes have additional polar groups such as carboxylic acid or sulfonic acids to increase solubility in aqueous media. Therefore, covalent immobilization of the dyes is particularly important. Special to azo dyes is the possibility to directly synthesize them onto diazotized glass substrates^{15,222} or onto modified PAN fibers via azo coupling.²²⁵

A popular method for covalent immobilization on cellulose is based on vinylsulfonyl chemistry known from textile industry (where it is known as the Remazol process).^{16,17,76,209,237–239} Numerous pH indicators were mainly immobilized on cellulose materials.^{16,17,76,208,209,237,238} In a typical process,¹¹¹ the azo dye N9 (as used in indicator paper strips from Merck and others) is covalently immobilized on a commercial plotter foil (Hewlett-Packard, product 1770311). The foil is composed of a 100- μ m polyester layer covered, on both sides, with layers of cellulose acetate. One of the two layers was removed by treatment with acetone. The other side of the foil (still coated with cellulose triacetate) served as the substrate for the immobilization of N9 via the Remazol method in strong sulfuric acid. Such sensors were used to manufacture protective clothing and to monitor wound healing or the pH of human body fluids.^{237,274,359} Mohr and co-workers prepared a variety of cellulose-based sensors and textiles, including T-shirts, facecloths, and cotton swabs.^{16,17,209,237,238,360}

Reported covalent immobilization strategies also include reaction of triazine coupled azo dyes with cellulose,²⁰⁶ coupling via an acetal bond between an aldehyde prepared from vinylsulfonyl dyes to PVA,^{207,208} copolymerization of vinylsulfonyl dyes with acrylic monomers,²⁰⁸ coupling of Congo red to agarose after activation with epichlorohydrin,^{214,215} carbodiimide coupling of Congo red to poly-HEMA,²¹⁷ and sol–gel reaction with trimethoxysilane coupled methyl red.²²⁸ Other immobilization matrices used for preparation of sensors are agarose,²¹⁴ SiO₂–ZrO₂ organic polymer composite,^{201,202} poly-HEMA,²¹⁷ PAN fibers,²²⁵ florasil,²³¹ sol–gel,^{194,226–228} nylon-6,^{230,241} styrene-divinylbenzene copolymers,²⁸⁸ polycaprolactone and polycaprolactone/chitosan blends,²²⁹ polyamide 6.6,²³⁰ PVC,^{232–234} hydrogel D4,²³⁸ and most importantly, cellulose materials (c.f. application as dye-stuff).^{16,17,23,76,203–206,209,212,213,215,216,218–221,236–238} In a particularly simple but efficient method, the azo dye calcone [1-(2-hydroxy-1-naphthylazo)-2-naphthol-4-sulfonate; also referred to as Eriochrome blue black] was immobilized on a porous cellulosic polymer film³⁶¹ to obtain a sensor strip for fully reversible pH measurement in the pH range of 4–9 with a response time of <5 min. The color of the membrane changes from pink to blue on going from acidic to basic medium. Ratiometric sensing was accomplished at wavelengths of 510 and 670 nm.

3.4. Other Dye Classes

From other dyes classes, only a few selected representatives have found application for preparation of absorptiometric sensors (Figure 18). Known from staining in histology, neutral red has a pK_a of 7.4 and only a small cross-talk to ionic strength in aqueous solution. The dye has been immobilized into agarose,^{346,362} hydrolyzed cellulose acetate,^{216,218–220} styrene-divinylbenzene copolymers,²⁸⁸ ormosil,³⁴⁸ sol–gel, and sol–gel–Nafion composites^{252,259} and adsorbed onto a support using the layer-by-layer technique.³⁴⁷ Also known from staining and some

extent fluorescence microscopy, Nile blue or its lipophilized derivatives have been used in the preparation of pH sensors for broad ranges in mixtures³⁶³ or sensor arrays^{232–234,302} or to widen the pH range using dynamic approaches.^{217,236} Although explosive, highly toxic and cross sensitive toward potassium, dipicrylamine has been used to measure in the highly acidic pH range from 0 to 3.2, either covalently immobilized or adsorbed on triacetyl cellulose.^{325,364}

In search for NIR pH indicators, Lehmann et al. have developed indicators based on pyridine and aniline units that were connected via methine bridges.³⁴⁹ They have pK_a values of 5.65 and 6.35 in water–isopropanol solutions. The absorption maxima peak at 675 and 850 nm when immobilized in plasticized PVC, and this enables 2-wavelength ratiometric sensing. Hazneci et al. investigated Schiff bases for absorptiometric and fluorometric sensing in the pH 3–7.8 range.³⁶⁵ The Schiff bases, derived from *p*-dimethylaminobenzaldehyde or 2,6-diacetylpyridine, were placed in thin films of plasticized PVC on a polyester support. The display yellow color (absorption peaks near 350 and 415 nm) and the 2,6-diacetylpyridine-derived films also display blue-green fluorescence. Response is adversely affected by ionic strength, and the addition of an antioxidant is required to improve stability beyond a few days. Many Schiff bases are prone to decomposition by slow hydrolysis of the $>C=N-$ double bond.

Porphyrioids attracted attention for use in optical pH sensors due to their high molar absorption coefficients. Among porphyrioids, the free base porphyrioids inherently possess pH sensitive groups. The pyrrolic nitrogens can be protonated, stepwise forming the mono- and dication, which is accompanied by a distinct change in spectral properties. This process typically occurs below pH 5 making porphyrioids potentially interesting only for sensing in acidic conditions. As porphyrioids are capable of forming many different metal complexes, sensors are susceptible to coordination/poisoning of metals that are capable of complexation under mild conditions. The complexation renders the indicator dyes pH insensitive. The copolymerization of protoporphyrin IX with acrylamide and *N,N'*-methylene bis(acrylamide) gives a pH sensitive film for the highly acidic range from 0.15 to 2 molar strong acids.³³⁹ Igarashi electrostatically immobilized a *meso*-tetrakis(4-*N*-trimethylaminophenyl)porphyrin on sulfonated polystyrene and measured pH in the range from 1.5 to 4.5, little data about the sensing performance of the highly charged system was given.³³⁰ Gulino et al. prepared porphyrin monolayers covalently bound to silica surfaces and measured from pH 1 to 5.^{335–337} The performance of the sensor was found to be hampered by Hg(II), Cu(II), and Zn(II) because of the formation of metal complexes. Delmarre and co-workers entrapped 5,10,15,20-tetra(4-sulfonato)porphyrin in a sol gel matrix and measured pH from 3 to 4.4.³³⁸ Below pH 1, they reported formation of *J*-aggregates, due to migration of porphyrins in the sol gel.

In contrast to free-base porphyrins, metalloporphyrins are intrinsically pH insensitive and modification of the porphyrin core is necessary to obtain pH sensitivity. Metal complexes of porpholactones (Figure 18) also lack a protonable group but are susceptible to reversible addition of a hydroxyl ion to the lactone, forming chlorin-like species with different spectral properties.^{331–333} Brückner's group incorporated various PEGylated metal porpholactones into Nafion.³³² The Pt(II) and Ga(III) complexes can indicate pH with a response time of approximately 3 min in ranges from pH 10.5–13 and 8–11,

respectively. The sensors displayed cross sensitivity toward cyanide ions, which nucleophilically attack the lactone. The same Pt(II) porpholactone has been used to prepare a sprayable paint for pH imaging on cement-based materials.³³³

pH sensitive groups also can be introduced into metalloporphyrins by modification of the *meso*-position, such as introduction of a Schiff base or phenol moiety.^{69,334} For example, Blair et al. electropolymerized a cobalt tetrakis(4-hydroxyphenyl)porphyrin onto indium–tin oxide glass slides and measured pH in the range from 8 to 12 within 5 min.³³⁴ Papkovsky and co-workers investigated a Pd(II) porphyrin Schiff base and a free base porphyrin ketone for pH sensing in plasticized PVC membranes covering the ranges 5.5–8.5 and 3.5–7.5, respectively, with response times below 100 s.⁶⁹ Later, the Pd(II) complex and also its Pt(II) analogue were reported to offer unique dual sensitivity acting as an absorptiometric pH indicator and a phosphorescent oxygen probe. Apparent pK_a values shifted 0.15 units increasing the buffer temperature from 20 to 37 °C and 0.1 unit when increasing ionic strength by 0.05 mM.³⁶⁶

Cyanine dyes^{367,368} are known from their use as tunable fluorescent labels with large molar absorptions. Their poor solubility, especially in commonly used plasticizers for PVC membranes,³²⁶ their tendency toward aggregation and their limited photostability hinder practical application. A NIR absorbing cyanine dye immobilized in Nafion³⁶⁹ showing response between pH 10 and 13 belongs to earlier examples of cyanine-based pH sensors. Several groups attempted to overcome some of the above limitations to make this group of dyes more suitable for optical pH sensing. Miltsov and co-workers developed pH sensors based on cyanine structures absorbing in the red to NIR region with increased solubility in organic media.^{326,327,329} Immobilized in plasticized PVC, several hemicyanines (Figure 18) were found to have linear ranges from pH 8.1–10 to 9.8–12 with response times (t_{95}) from 1–2.5 min.³²⁶ The sensor membranes favorably displayed absorption peaks close to the emission wavelengths of laser diodes at 650 and 670 nm, and no hysteresis. Even more red-shifted, differently substituted ketocyanines (Figure 18) possess absorption maxima in the range from 727 to 771 nm when immobilized in plasticized PVC.³²⁷ Response times lie in the range from 0.5 to 3.6 min. PVC membranes doped with NIR nortricyanocyanine dyes cover the pH ranges from pH 2.5–5 to pH 7–9.³²⁹ The immobilized dyes absorb in the range from 793 to 834 nm and pH can be measured within 0.6–1 min. Similar to cyanines, these dyes suffer from poor photostability and rapidly decompose. Hisamoto et al. described a method for sensing of either pseudo-pH values or water content in organic solvents using merocyanines.³²⁸ Copolymerized with HEMA and diethylene glycol monomethyl ether methacrylate, the merocyanines displayed a water content dependent shift of the absorption peak that was also pH independent; for a given solvent/water mixture, the absorbance was a function of pH.

Aza-BODIPYs represent a class of highly fluorescent pH indicators with absorption bands in the red to NIR region with remarkable photostability and molar absorption coefficients (section 4.1). They can be converted to absorptiometric pH indicators by permanently “switching off” the fluorescence at pH higher than 4 (Figure 18).

In food industry, pH sensor foils based on absorptiometric indicator dyes are investigated for unaided eye detection of food spoilage in smart packaging. Food spoilage caused by microbial activity is accompanied by production of metabolites such as

basic nitrogen compounds, which can be detected by pH sensors. To ensure the safety of the consumer, indicator dyes and matrices need to be toxicologically harmless. For this reason, *natural dyes* extracted from foodstuff have been investigated for their suitability as absorptometric probes, among them, curcumin and various anthocyanines.^{340–345} The purification of extracted dyes, however, is either tedious, when pure substances are desired, or gives dye mixtures impairing reproducibility. Application of curcumin and anthocyanines is also limited by their stability. Under given limitations, the sensor foils often may not be suitable for actual sensing, but give only qualitative estimations. For example, Veiga-Santos et al. prepared an edible pH sensitive membrane based on cassava starch and anthocyanines extracted from Merlot grapes, which however was only suitable for visual discrimination between highly acidic and highly basic pH.³⁴⁰ Yoshida et al. also used anthocyanines extracted from grapes but chitosan as immobilization matrix.³⁴¹ Immobilized in the same matrix, anthocyanines responded to pH changes in the range from 2.2 to 9 making the sensor suitable for visual detection.³⁴³ Abolghasemi et al. covalently immobilized anthocyanines on agarose after activation with epichlorohydrin.³⁴² At 540 nm, the sensor film responded to pH changes in the range 1–10 within 3 min. Another food-related pH sensing material is based on curcumin and bacterial cellulose as immobilization matrix and is responsive from pH 6–10.³⁴⁴ For textile application, curcumin was also immobilized on cotton and polyamide 6.6 fabrics, giving pH responsive materials in the ranges from pH 6.5–8.5 and 8.5–13, respectively.³⁴⁵ Apart from natural dyes, also a commercially available Nile blue derivative (Chromoionophore I) has been proposed.³⁷⁰

In contrast to (metal)organic dyes, absorptometric probes based on other materials are very rare. In fact, only a few sensors utilize the pH-dependent absorption in conjugated polymers such as polyanilines and polypyrroles (section 7.2). An uncommon sensor based on inorganic pigment Prussian blue was reported by Koncki and co-workers.^{350,371} The authors utilized the reversible decomposition of Prussian blue to determine pH in the range 5–9. Prussian blue is attacked by hydroxide ions, involving the disappearance of its near-infrared absorption peak at 720 nm. At pH values above 9, the reaction becomes irreversible due to the destruction of the zeolitic structure and escape of $\text{Fe}(\text{CN})_6^{4-}$ from the films. Composite films of Prussian blue and N-substituted polypyrroles were reported to have response times of 30 s and no interference by ionic strength. On the other hand, Prussian blue is known to be easily reduced to Prussian white so that the sensor is likely to suffer from interference by reducing species.³⁷²

4. OVERVIEW OF COMMONLY USED LUMINESCENT pH PROBES

Luminescent molecular probes for pH can be divided into two main groups—fluorescent probes based on organic dyes and phosphorescent probes based on metal–organic complexes. The number of organic fluorescent pH indicators is impressive, while less metal–organic probes have been reported. An overview on commonly used pH-sensitive fluorescent probes was given already in 1983, also with respect to their suitability for use in optical sensors.³⁶ The indicators were divided into two classes. Class A comprises pH indicators that undergo a bathochromic spectral shift on deprotonation. These, typically, are phenols or sulfonamides. Class B comprises indicators that undergo a bathochromic shift on protonation. These, typically,

are nitrogen ring compounds, such as quinines or acridines. Since then, the number of fluorescent pH indicator classes has increased considerably, and numerous systems making use of photoinduced electron transfer (hardly showing any spectral shift upon (de)protonation) have been introduced.

Metal–ligand complexes have long decay times and can be particularly valuable in time-resolved or lifetime-based sensing and imaging. On the other hand, only a few classes of metal–organic dyes show strong room temperature phosphorescence. These comprise primarily porphyrin complexes with platinum group metals but also ruthenium polypyridyl complexes, cyclometalated complexes of platinum(II) and iridium(III), as well as lanthanide chelates. Even within these classes, the choice of suitable systems is further limited due to poor brightness (molar absorption coefficients of most cyclometalated complexes), short wavelength excitation (terbium(III) chelates) or too long phosphorescence lifetime (palladium(II) and platinum(II) porphyrins), which results in strong cross-sensitivity to oxygen in virtually any proton-permeable matrix.

The following characteristics of luminescent probes should be considered apart from the $\text{p}K_a$ value, the compatibility to the matrix material, and the ease of availability:

- Spectral properties. Excitation with UV light is associated with high levels of background fluorescence generated by the sample and optoelectronic components (fibers, filters etc.). Therefore, longer wavelength of excitation is preferred. Far red and NIR (including those based on upconversion) probes are preferred for in vivo applications due to high transparency of tissues to excitation and emission light and low light scattering. In other sensor formats, background fluorescence can be eliminated by using additional coatings (section 9.3). The choice of the indicator is also guided by its spectral compatibility with excitation sources and detectors, such as LEDs or lasers.
- Brightness (B_s). It is defined as a product of molar absorption coefficient ϵ and luminescence quantum yield QY . High brightness ($B_s > 20\,000$) enables preparation of thin sensing layers featuring fast dynamic response. Generally, luminescence brightness of NIR indicators is lower than that of UV–vis probes because of the smaller energy gap between the excited and the ground state and consequently more efficient radiationless deactivation.
- Stokes shift. Symmetrical fluorescent dyes often show very strong overlap between the absorption and emission spectra. Therefore, the “useful brightness” for these dyes is typically much lower than the nominal one. In fact, to avoid crossover of the excitation light into the emission channel, either excitation should be performed at wavelengths that are significantly shorter than the absorption maximum or the emission filter is chosen such that only the long-wavelength part of the emission is collected. Evidently, this results in significant loss of brightness. On the other hand, the dyes, which feature lower ϵ and QY but larger Stokes shifts allow excitation at the absorption maximum and collection of almost entire luminescence. Some fluorescent indicators feature a rather intense shoulder (rhodamines) or even another maximum (perylene) at shorter wavelength in addition to the main maximum of the excitation spectrum, which can also be very useful. Notably, phosphorescent dyes almost always exhibit large Stokes shifts ($>2500\text{ cm}^{-1}$).

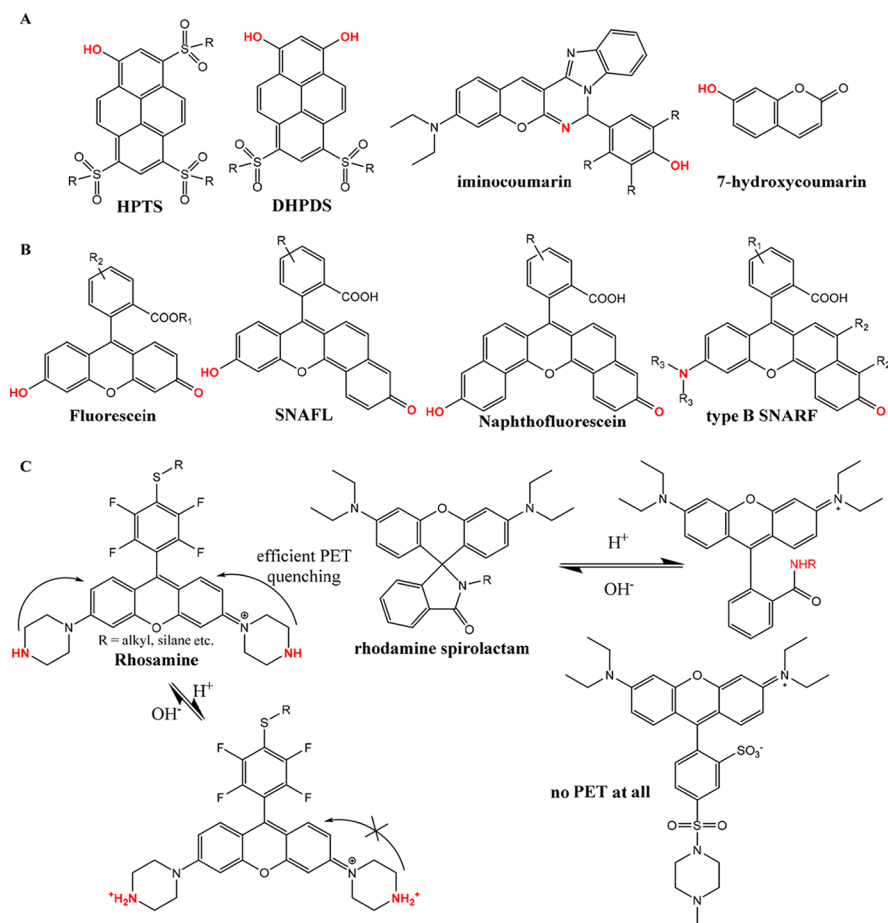


Figure 19. Different classes of pH indicators, which found application in optical sensors (part 1/2, other part see Figure 20). Numerous other dyes reported have been reported as molecular probes and are described in detail elsewhere.^{99,197}

- Photostability. Although high photostability is always desirable, the suitability of the indicator will depend on the application. For instance, even fairly photostable probes can degrade fast at high light intensities, which are characteristic of fiber-optic microsensors and in microscopy.

4.1. Organic Probes

Fluorescent pH probes based on organic dyes can be divided into several groups, namely, (i) fluorophores undergoing classical acid base chemistry; some also undergoing photo-induced proton transfer (PIPT) and (ii) dyes that undergo photoinduced electron transfer (PET).

The first group involves probes that usually have phenol groups as a part of chromophoric system (such as in fluorescein or HPTS) or aromatic rings containing protonable nitrogen atoms (such as in pyridines, quinines, or oxazines), or dissociable groups, such as $-\text{SO}_2-\text{NH}-\text{R}$, attached to a chromophore. The second group consists of dyes that have protonable groups (such as tertiary amino groups or phenols) that are not part of the π -electron system of a fluorophore. The major difference between classical pH indicators of the first type and PET probes is that the absorption and emission spectra of PET probes hardly change with pH values because the quencher group usually is not part of the color-forming system.

Phenolic fluorophores of the first group are often present as a mixture of phenol and phenolate, and the equilibrium between the two is governed by the local pH value. Most often, the fluorescence of the phenolate is photoexcited (such as in case of

fluoresceins or HPTS), and if the absorption of the phenolate form disappears at low pH values, no light is absorbed at this wavelength and the fluorescence of the phenolate also disappears. If the decay time of the phenolic form of the fluorescent pH indicator is long enough, photodissociation may occur. This is due to the fact that many phenols are stronger acids in the first excited singlet state than in the ground state. The excited state $\text{p}K_{\text{a}}$ value can be calculated from absorption and emission spectra via the so-called Förster–Weller cycle (see section 1.5). Hence, even if the phenol becomes photoexcited, fluorescence occurs from the excited state anion due to rapid photodissociation, such as in case of HPTS (Figure 19) or many 7-hydroxycoumarins. The phenol forms of fluoresceins and other xanthenes undergo less efficient photodissociation and have lower quantum yields.

Photoinduced electron transfer (PET; also see section 2.2) occurs with indicators consisting of a pH-insensitive fluorophore and a receptor group, most prominently aliphatic or aromatic amines or phenols (Figure 9). The PET effect occurs if the HOMO of the amine has an energy level that is higher than that of the fluorophore. Electron transfer is associated with quenching of the fluorophore. If the amino group becomes protonated, no electron transfer can occur and quenching is suppressed. The main advantage of PET based indicators is their versatility. Numerous fluorophores may be attached to a receptor group with the desired $\text{p}K_{\text{a}}$ value. However, not every PET group quenches a fluorophore.³⁷³

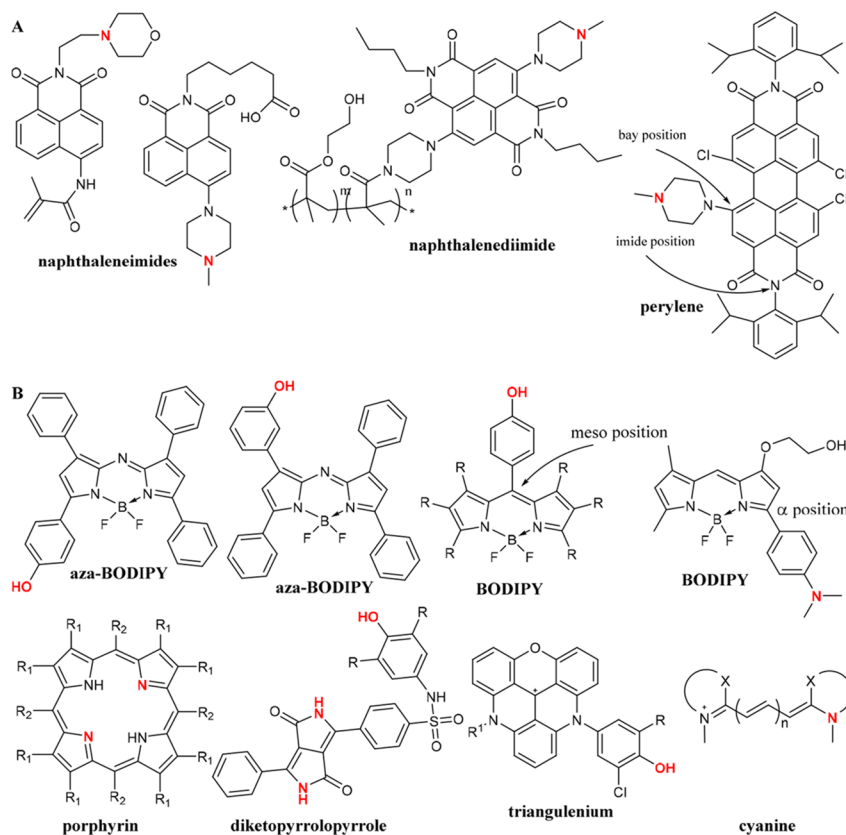


Figure 20. Different classes of pH indicators that have found application in optical sensors (part 2/2, other part see Figure 19). Numerous other dyes have been reported to be viable molecular probes and are described in detail elsewhere.^{99,197}

The aliphatic amines, by far, represent the most common receptor group for PET based indicators. These, however, act as efficient fluorescence quenchers only in combination with certain chromophores, and are not suitable for modulation of fluorescent properties in other dyes. Aigner et al. compared the pH sensing properties of various fluorophores modified with aliphatic amine and phenol receptors at the same position.³⁷³ Among investigated chromophores, fluorescein, rhodamine, diketopyrrolopyrroles and perylene dyes were found to be quenched efficiently solely by phenolate, whereas tertiary amines modulate fluorescence only in case of some perylene dyes. In fact, efficient quenching by amines was possible only for the perylene-diimide (PDI) substituted at the core with electron-withdrawing chlorine atoms (Figure 20).³⁷³ For comparison, perylenes substituted with electron-donating substituents (phenoxy or morpholine) showed moderate (2-fold) or no quenching at all, respectively. A study on model receptor compounds revealed that the oxidation potential of triethylamine is 0.26 V higher than that of deprotonated 2,6-dichlorophenol, which confirms more favorable PET in case of the latter.

4.1.1. HPTS and Derivatives.^{25,37,61,80,374–393} 8-Hydroxypyrene-1,3,6-trisulfonate (Figure 19 R = O⁻Na⁺) is a highly water-soluble pH indicator dye with a pK_a around 7.3 in aqueous solution. HPTS belongs to the class of dyes with photoinduced proton transfer in the excited state. Only the green emission from the deprotonated form around 510 nm is observed upon excitation of the protonated or deprotonated form, absorbing around 405 and 465 nm, respectively. These two absorption bands enable referenced ratiometric measurement. The anion

features a molar absorption of around 20 000 M⁻¹ cm⁻¹ and a quantum yield close to unity. For preparation of sensing membranes, the highly charged dye requires covalent immobilization^{25,61,80,376,377,379,381,384,386,393,394} or derivatization^{382,383,390,395} to minimize leaching to an acceptable level. In this form, HPTS is widely used in commercial pH sensors. In a few cases, anion-exchange resins or cellulose acetate^{375,378,389} were used for electrostatic immobilization, but the indicator immobilized in these matrices is prone to gradual leaching and displays strong sensitivity to ionic strength.^{380,389} Hydrophobic sulfonamide derivatives of HPTS (R = NH-alkyl or N(alkyl))₂, (Figure 19)^{374,382,390,395} can overcome this problem and enable immobilization in hydrogel,^{374,382} PVC,³⁹⁵ or poly(styrene-block-vinylpyrrolidone) nanobeads^{382,390} with negligible leaching. The spectral properties of these dyes, however, are strongly affected by the substitution. In fact, it results in a strong bathochromic shift of absorption of the protonated and deprotonated forms of the dye. Additionally, the emission is observed from both forms. HPTS can also be rendered lipophilic by ion-pairing with quaternary alkylammonium ions.³⁸³ Incorporation in a sol-gel matrix produced a ratiometric pH sensor for the range from 5–8 with a resolution of 0.02 and a response time (*t*₉₀) of 12 s. In 6,8-dihydroxypyrene-1,3-disulfonic acid (DHPDS, Figure 19A),^{386,389,394} the second hydroxy group can be used for covalent immobilization³⁷⁹ or is acting as a second pH sensitive group with a close pK_a (7.33 and 8.53)³⁶ slightly increasing the dynamic range.³⁸⁹ Immobilized, the dye displays dual excitation useful for ratiometric sensing.³⁸⁹

4.1.2. Coumarins and Derivatives.^{25,29,396} 7-Hydroxycoumarins^{25,29} have emission around 455 nm after excitation at

360 or 400 nm for the protonated and the deprotonated form, respectively. Apart from the unfavorable UV to blue region excitation, the dyes display lower brightness compared to HPTS with a similar molar absorption coefficient but lower quantum yield. Additionally, the photostability is slightly inferior to that of HPTS.²⁵ Iminocoumarins (Figure 19A) show a bathochromic shift of the absorption into the blue to green region and higher absorption coefficients compared to 7-hydroxycoumarins.³⁹⁶ The pH-sensitivity of these dyes relies on a different mechanism. The dyes display two protonation equilibria with pK_a values, for example, for one representative of 2.7 and 7.8, associated with deprotonation of an imino group and deprotonation of a phenol PET receptor, respectively. The deprotonation of the imino group results in hypsochromic shift from 510 to 410 nm absorption and a decrease in fluorescence intensity, whereas the deprotonation of the phenol induces PET and results in fluorescence quenching.

4.1.3. Fluoresceins and Derivatives. Xanthene dyes, particularly fluoresceins,^{24,30,44,49,53,56,88,110,121,143,146,150,382,392,397–443} (Figure 19) are the most commonly used pH probes. Wide commercial availability of various derivatives and conjugates offers easy access to various applications especially in biological and medical research. Fluorescein efficiently absorbs at around 490 nm and emits in the green part of the spectrum, typically at 515–520 nm; π -extension (seminaphthofluoresceins (SNAFL)³⁹⁷ and naphthofluorescein)^{30,444,445} results in a bathochromic shift of absorption and emission. The same effect is observed for seminaphthorhodofluor (SNARF) dyes.^{444,445} The brightness is highest for fluoresceins and lowest for naphthofluoresceins, whereas SNAFL occupies an intermediate position (c.f., refs 99 and 445). Fluorescein has several protonation/deprotonation equilibria,⁴⁴⁶ but the most important in aqueous environment are the mono- and dianionic forms with deprotonated carboxylic acid and phenolic groups. In other solvents/polymeric matrices, the closed lactone form becomes more prominent, which, however, is colorless and non-fluorescent. Molar absorption coefficients and fluorescence quantum yields significantly differ between deprotonated and protonated (regarding the phenol) forms.^{99,445} For fluorescein, its derivatives and type B SNARFs (dialkyl SNARF derivatives, Figure 19), the deprotonated form is much brighter compared to the protonated form. For SNAFLs and type A SNARFs (SNARFs with fewer than two alkyl groups, Figure 19B), the base forms have higher molar absorption coefficients but the quantum yields are higher under acidic conditions.⁴⁴⁵ The photostability of fluoresceins and their π -extended derivatives is poor. It can be improved by introduction of electronegative halides in 2' and 7' positions (dichloro- or difluorofluorescein), but the pK_a values also are lowered.^{110,447} Photostability drops if alkyl chains are introduced at the same positions.^{110,447} For preparation of sensing membranes, the commercial availability of various functionalized xanthene dyes simplifies covalent immobilization procedures. Fluorescein isothiocyanate (FITC)^{404,405,411,421,425,441} and fluoresceinamine (FA)^{24,400,401,412,414,429,448} are two commonly used representatives that have been directly immobilized or immobilized after additional functionalization. As the isothiocyanate group is electrophilic, FITC derivatives are useful for covalent coupling via nucleophilic attack. FITC has been coupled to various amino-modified materials such as sol gels,^{404,421} polystyrene beads,⁴⁰⁵ aminoethyl cellulose,^{49,127,425,441} hydrogels,⁴⁹ and controlled pore glass.⁴⁹ The use of oxygen nucleophiles has

been limited to cellulose nanocrystals.⁴¹¹ Fluoresceinamine is the nucleophilic counterpart and has been coupled to materials containing epoxy,^{401,414} cyanuric acid chloride,²⁴ thiophene,⁴¹² isothiocyanate,⁴¹⁴ and alkyl halide⁴⁴⁸ electrophilic groups. The reaction of acryloyl chloride with fluoresceinamine leads to acryloylfluorescein.^{53,400,406,408,417,429,449} This dye-monomer conjugate has been extensively used for copolymerization with acrylic monomers such as acrylamide and hydroxyethyl methacrylate. Both amino- and carboxy-xanthene dyes can easily form amide bonds via coupling reagents or by using reactive succinimidyl esters.^{30,143,397,411,415,420,423,428,448} The carboxy-functionalized dyes were coupled to poly-(acrylamide-co-vinylamine),³⁹⁷ amino-modified cellulose nanocrystals,⁴¹¹ concanavalin A-modified hydrogel,⁴²⁰ amino-functionalized polystyrene microspheres,⁴¹⁵ aminoethyl cellulose,³⁰ amino-modified pHEMA,⁴²³ and amino-containing ORMOSIL.⁴²⁸

A sensing membrane suitable for dual-lifetime referenced measurement of pH values was obtained by coupling a carboxyfluorescein succinimidyl ester to poly(acrylonitrile)-Ru(dpp) particles covered with a hydrogel.¹⁴³ The particles were then dispersed in a hydrogel sensing membrane. Succinimidyl esters of xanthene dyes can also be coupled to amino dextrans. The conjugates have been used for intracellular pH measurement or have been immobilized on silver island films for metal-enhanced fluorescence sensing.⁴¹⁶ Xanthene dyes also allow physical entrapment in hydrogels,^{110,121,398,424,430,438} sol-gels,^{399,402,403,407,414,422,431} poly(styrene-*block*-vinylpyrrolidone) nanobeads,³⁸² cross-linked poly(vinyl alcohol)-silica gel copolymers,⁴³² polyacrylamide,⁸⁸ and pHEMA.^{56,419} To minimize leaching, the dyes can be alkyl substituted,^{110,121,398,424,430,438} directly or via ester bonds, to enhance their hydrophobicity for incorporation into hydrophobic materials. Alkyl core substitution, however, significantly deteriorates photostability. Another approach is to entrap chitosan or dextran conjugates in hydrogel,^{438,450} sol-gels,⁴³¹ or poly(hydroxyethyl methacrylate).^{56,419} Also an electrophoretic deposition procedure has been reported by placing a film of fluorescein and 1-heptanesulfonate cointercalated in a layered double hydroxide matrix.⁴¹³

4.1.4. Rhodamine and Rhosamine Dyes. Rhodamine and rhosamine dyes are bright fluorophores with good photostability,⁴⁵¹ which also were found useful for construction of pH probes. pH-sensitivity usually relies on introduction of PET groups or spirolactam opening. Interestingly, the modulation of fluorescence by PET-active amino groups strongly depends on the position of the receptor. For instance, efficient PET quenching was observed for the rhosamine with PET-groups at the xanthene core (Figure 19C),^{152,452} whereas no modulation of fluorescence occurs for the molecule with the PET group attached to the periphery (Figure 19C).³⁷³ Yet, the PET-groups are not necessarily required to be coupled to the fluorophore. Zhou et al.⁴⁵³ prepared nanoparticles with the rhodamine and the PET-group copolymerized in close proximity. Several rhodamines that explore lactam formation have also been reported (Figure 19C).^{410,454–460} The spirolactam form at neutral pH is colorless, whereas opening of the ring in acidic media yields a highly absorbing and fluorescent rhodamine. The pK_a of spirolactam rhodamines can be tuned by varying the substitution of the group attached to the spirolactam group; the dyes with pK_a values from 2.8 to 6.5 have been reported.^{454,461} Unlike many other systems, the influence depends to a large extent on the steric effects of the substitution.

Substitution on the spirolactam group can also be used for covalent immobilization. Yu et al. have modified a rhodamine spirolactam with an acrylic functional group for free radical polymerization.⁴⁶² The rhodamine monomers were copolymerized with methacrylic acid to prepare pH-sensitive nanoparticles based on the spirolactam opening in acidic media. The nanoparticles with pK_a values of 6.07 and 6.71 were then used to measure lysosomal pH. An interesting approach for measuring acidic pH values consists in the conjugation of a rhodamine to a naphthalimide dye.⁴⁶³ The mechanism involves quenching of the naphthalimide fluorophore by PET from the rhodamine. The dye conjugate was copolymerized with 2-hydroxypropyl methacrylate and enabled pH measurement in the range from pH 1.40 to 3.60.

4.1.5. 1,8-Naphthalimide Dyes.^{139,463–476} These are probably the most common representatives of PET dyes. The PET group (most commonly an amine) can be introduced at the imide position or via core substitution (Figure 20A). The PET efficiency differs significantly for the two positions. PET is inhibited when the electron transfer process to the fluorophore has to occur against a repulsive local electric field (PET quenching from the imide position to the core of 4-amino-naphthalimides).^{134,139} On the contrary, PET quenching is efficient if there are electron withdrawing substituents, usually in 4-position or if the PET-receptor is attached to the 4-position.^{134,139,472} The introduction of electron-donating amino-group into 4-position of the core also generates a push–pull system with an ICT excited state. This results in broad and bathochromically shifted absorption and emission bands and enhances the molar absorption coefficients. For example, the absorption and emission maxima are at 418 and 535 nm, respectively, for the naphthalimide bearing a dimethylamino-group in the position 4, compared to 341 and 370 nm, respectively for unsubstituted naphthalimide.⁴⁷⁷ Nevertheless, even amine-substituted naphthalimides show comparably low brightness, which is due to moderate molar absorption coefficients of about $15\,000\text{ M}^{-1}\text{ cm}^{-1}$, even though the quantum yields can approach unity in organic solvents.^{134,478} On the other hand, the imide position offers simple access to covalent immobilization via copolymerization of acrylic^{467,476} or allylic^{468,470,475} functional groups, amide bond formation,^{469,471,473} or direct bonding via the imide function.^{471,473} Naphthalimide-based PET indicators carrying a 2-hydroxyethylsulfonylethyl function for covalent conjugation to cellulose and textiles were also synthesized and immobilized.⁴⁷⁹

In a typical example,⁴⁶⁹ a piperazine moiety is covalently linked to the naphthalimide fluorophore. Quenching by PET from piperazine to the naphthalimide is modulated by protonation of the piperazine nitrogen. The effect also occurs in a rather rigid sol–gel matrix. The signal increases by >100% upon protonation, and the sensor works in the physiological (pH 5–8) range. New PET-based naphthalimide pH indicators (typically carrying tertiary aliphatic amino groups) and ways for immobilization on arrays have also been presented.⁴⁷³ Majority of reported naphthalimide indicators utilize aliphatic amines as PET quenchers that significantly limits the range of available pK_a values. To address this limitation, Qi et al.⁴⁶⁶ prepared a palette of naphthalimide indicators equipped with aromatic amines and phenols as PET quenchers that show pK_a values from 2.5 to 12. Virtually identical spectral properties of these dyes made possible preparation of wide dynamic range sensors (section 13).

Core-substitution of naphthalene diimides (Figure 20A) allows modulation of spectral properties and introduction of both pH functionalities and groups for covalent immobilization.⁴⁸⁰ For example, Shen et al. modified the chromophore core with two piperazine moieties, one acting as a PET group, the other for copolymerization (after reaction with methacryloyl chloride) of the dye with 2-hydroxyethyl methacrylate.⁴⁸¹ The absorption of the copolymerized purple dye peaked at 570 nm and the emission at 630 nm. The sensing membrane features an apparent pK_a of 6.0.

4.1.6. Perylene Diimides (PDIs). PDIs^{122,123,139,373,482,483} can be viewed as π -extended analogues of naphthalene diimides. However, even core-unsubstituted dyes absorb very efficiently in the green part of the spectrum and emit green-yellow light with QYs close to unity. These dyes are known for their exceptional photostability. The photostability of tetrachloro-derivatives in aqueous solution is poor.¹²² This may be due to photoinduced nucleophilic substitution reactions. Electron-donating substituents introduced in the bay position cause pronounced bathochromic shift of the spectra. For instance, tetraphenoxy-substituted dyes absorb at 578 nm, show emission at 620 nm³⁷³ and retain quantum yields close to unity typical for this group of dyes. Introduction of a single amine donor in the bay position (Figure 20A) results in even stronger bathochromic shift.^{123,484} These dyes absorb in the red and emit in the far-red part of the electromagnetic spectrum making them promising for application in pH sensors where low levels of background fluorescence are of particular importance. Unfortunately, the substitution also results in significant broadening of absorption and emission bands, decrease of ϵ (to about $19\,500\text{ M}^{-1}\text{ cm}^{-1}$)¹²³ and of QYs (to about 0.26).^{123,484} To render PDIs pH sensitive a PET group is introduced in the imide^{122,139,373} or bay^{123,482} position.

The absorption and emission of PDIs can be bathochromically shifted when the dyes are laterally extended in the bay region.⁴⁸³ By condensation with benzo nitriles, one or two pH sensitive imidazole structures are attached to the perylene core. The indicator dyes feature molar absorption coefficients of around $80\,000\text{ M}^{-1}\text{ cm}^{-1}$ and quantum yields close to unity. Deprotonation of the doubly substituted dye results in further bathochromic shift of the absorption, which is 100 and 150 nm for the monoanionic and dianionic forms, respectively. The corresponding pK_a values in a hydrogel matrix are in the range from 9.84 to 10.56.

Exceptional photophysical properties including excellent brightness (albeit not for the perylenes substituted in the bay position with N-donors), multiband absorption spectrum (making efficient separation of excitation and emission possible) and high photostability make PBIs a promising class of pH indicators. On the other hand, the perylene core is highly hydrophobic which results in tendency to aggregate when noncovalently entrapped into hydrophilic matrices, making covalent immobilization of these dyes essential for practical use.¹²³

4.1.7. Boron-dipyrrromethenes (BODIPYs). These dyes are bright fluorophores with highly versatile structures and spectral properties (Figure 20B).^{485–489} The simple BODIPYs absorb in the green region, but absorption can be shifted to the far-red and NIR region by π -extension or introduction of push–pull systems.⁴⁹⁰ The BODIPY-chromophore itself is insensitive to pH but pH sensitive groups can be attached in α or *meso*-position. However, comparably few pH probes on their basis have been reported^{65,491–502} and even fewer have found application in sensing materials.^{65,135,493,503,504} For instance, a

dimethylaniline group acting as a PET receptor has been introduced in *meso*-position of the BODIPY to give a pH indicator for the acidic region.⁶⁵ The BODIPY immobilized in a hydrogel covers the pH range from 0.5 to 2.5. Only some leaching at very low pH was detected. Later, Ando et al. introduced the dimethylaniline receptor in α -position of a BODIPY to prepare a ratiometric pH optode for use in pH range 0.8 to 4.5.⁵⁰³ Ratiometric readout was enabled by a pH-dependent spectral shift due to ICT. The indicator dye was covalently immobilized on activated porous silica glass via formation of a urethane. Response time, however, was comparably slow (>11 min) for a pH change from 1.19 to 1.54. Phenol groups acting as PET receptors for the alkaline region (pH > 9) have been introduced into *meso*-position of the BODIPY to give pH sensors when immobilized in hydrogels matrices.^{493,504}

4.1.8. BF₂-Chelated Tetraarylazadipyrromethene Dyes (aza-BODIPYs). Compared to BODIPY dyes, they show bathochromically shifted absorption and emission spectra but lower quantum yields.⁴⁸⁵ These dyes show excellent photostability and great versatility with regard to the position of the PET receptor which is most commonly a phenol.^{151,505–509} The PET groups can be introduced in 3- and 5-position of both pyrrole rings, and hence, the relatively simple synthesis of asymmetric aza-BODIPYs provides even more flexibility. The other half of the dye can be used to attach substituents improving solubility or to enable covalent immobilization. Generally, deprotonation of phenol receptors bearing hydroxy group in para-position results in virtually complete fluorescence quenching due to PET but also in a bathochromic shift of the absorption spectra due to additional intramolecular charge transfer. Staudinger et al.⁵¹⁰ identified a strategy to prepare aza-BODIPY pH indicator dyes solely based on PET. By consideration of the position of the PET receptor (Figure 20, phenol meta to attachment position) intramolecular charge transfer can be eliminated by avoiding conjugation of the receptor to the chromophore system.

4.1.9. Diketopyrrolopyrroles (DPPs). (Figure 20B)^{511,512} These feature absorption and emission in the green to red region, moderate molar absorption coefficients around 25 000 up to 45 000 M⁻¹ cm⁻¹,⁵¹³ high quantum yields and moderate photostability. Aigner et al. designed DPPs with pH sensitivity based on two different strategies: the use of phenolic PET groups and the deprotonation of the lactam nitrogens of the DPP chromophore.⁵¹¹ The lactam-based strategy enables pH sensing in the pH range 9–12. Co-immobilized with Macrolux Yellow as reference, RL100 nanoparticles were prepared and enabled RGB camera based readout.

4.1.10. Cyanine Dyes. (see Figure 20B)^{367,368} These are versatile tunable fluorescent labels with long wavelength absorption and emission, yet impaired by their poor photostability and poor solubility in most matrices. Probably due to this fact, cyanine dyes have only occasionally been used for fluorescence-based pH sensing.^{329,369} Zen and Patonay investigated the feasibility of using a cationic NIR-cyanine electrostatically immobilized on Nafion for pH sensing.³⁶⁹ The sensing membrane underwent no leaching and covers the pH range 11.5–13. However, the charged matrix introduced strong influence of ionic strength on pH measurement. Puyol et al. developed optodes based on NIR-norcyanine dyes immobilized in plasticized PVC.³²⁹ The sensing membranes displayed pK_a values ranging from 3.89 to 8.02 and response times (t_{90}) of

below 1 min. The practical application, however, is limited due to leaching of the acidic form of the dyes and by photobleaching.

4.1.11. Free-Base Porphyrins. In this case, the pH sensitive groups are the protonable pyrrole moieties of the macrocycle (see Figure 20B). Such porphyrins feature high molar absorption coefficients and large Stokes shifts (if excited in the Soret band). Unfortunately, accessible pK_a values are limited to the acidic range. For instance, sensors based on immobilized free-base porphyrins enabled pH measurements from pH 0.6 to 3.8⁵¹⁴ and 1.5–5.⁵¹⁵ The sensor that utilized a pH-sensitive naphthalimide dye in addition to the porphyrin had an extended range from 1 to 9.5.⁴⁶⁵ Generally, a serious drawback of the sensors based on free base porphyrins is tendency to complexation with metal ions that may be present in a sample. This can render the indicator dyes pH insensitive or change the mechanism of pH sensitivity. For example, a tin porphyrin complex incorporated into a polyethylene glycol hydrogel was found to display pH-responsive fluorescence that was used in an implantable sensor.⁵¹⁶ Here, the axial water molecules of the tin porphyrins can deprotonate to yield a hydroxide-coordinated metal.

4.1.12. Triangulenium Dyes. This rather new class of pH probes (see Figure 20) is based on a cationic triphenylmethylium structure rigidified by bridging hetero atoms, generally oxygen and nitrogen.⁵¹⁷ These highly stable carbenium ions absorb light between 450 and 650 nm. Replacement of one or two oxygen atoms from the trioxa-derivative by nitrogen induces a red shift. All representatives exhibit moderate molar absorption coefficients (10 000–20 000 M⁻¹ cm⁻¹) and moderate to high quantum yields. Mono- and diaza- derivatives are of special interest for optical sensing due to their relatively long fluorescence lifetimes (around 20 ns), which enables elimination of most autofluorescence by making use of time-resolved fluorometry.⁵¹⁸ pH sensitivity is introduced via PET-receptors attached to the aza-position. Analogously to other PET-based systems, the pK_a can be tuned by substitution on the receptor group.⁵¹⁹ The second aza-position can also be used to introduce functional handles for covalent immobilization. Frankær et al. covalently immobilized diaza representatives in ormosil matrices for preparation of ratiometric fiber-optic sensors and biocompatible sensor spots.^{520–523} Dalfen et al.⁵²⁴ prepared diazatriangulenium dyes equipped with different receptors and immobilized them in polyurethane hydrogel. It was found that immobilization induced the decay time (section 10.2) to become pH sensitive. They attributed the pH sensitivity to a homo-FRET process. They also showed that anion composition of the sample has strong influence on the pK_a of the indicator in the hydrogel matrix.

4.1.13. Miscellaneous Indicator Dyes. Various pH indicators from other dye classes have been reported,^{66,525–533} but only found niche application. These are described in the Supporting Information Table S3.

4.1.14. pK_a and Dynamic Range Adjustment for Fluorescent Indicators. Limited dynamic range of the pH indicators implies the necessity of adjusting the pK_a value for a particular application. The pK_a value of an indicator, ideally, is in the middle of the pH range to be measured. It is often desirable to obtain a library of indicator dyes based on a single chromophore class, although indicators of different classes are known that match best different applications. Such approach minimizes the synthetic effort and simplifies the read-out instrumentation due to similar spectral properties of individual indicators. In addition, it allows preparation of wide dynamic

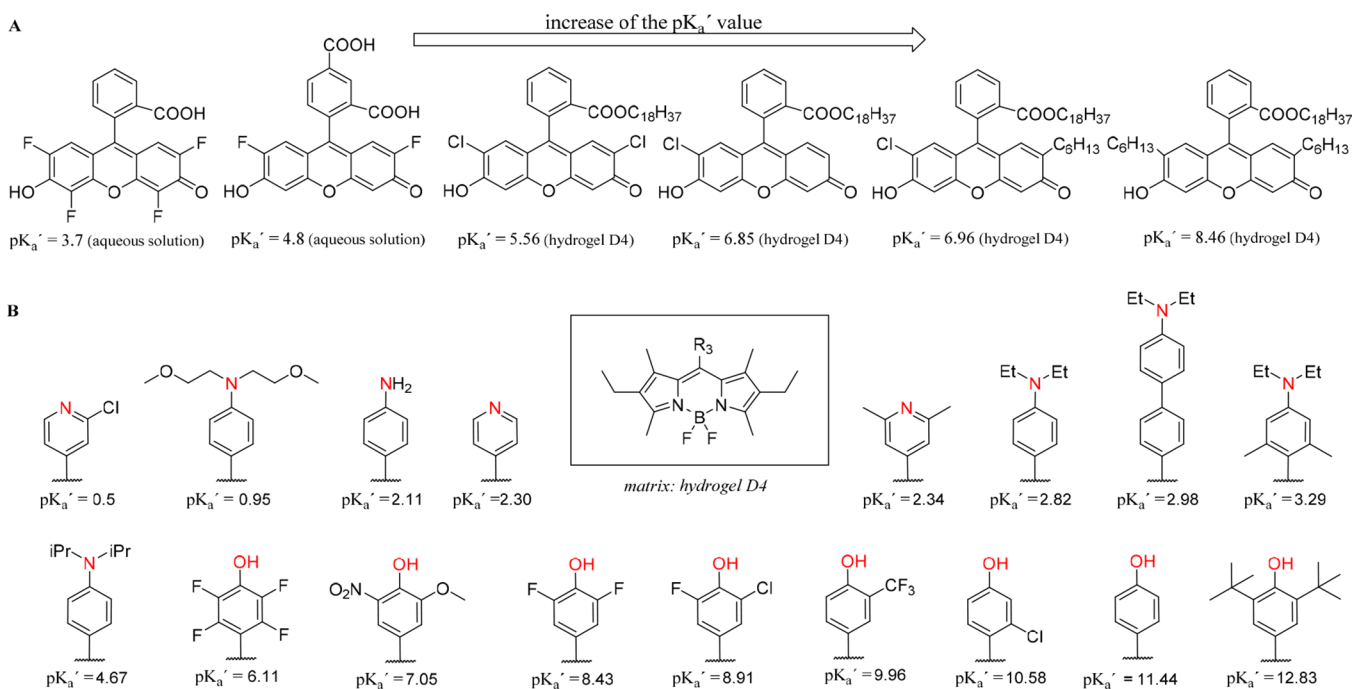


Figure 21. Structure– pK_a' value relationship in fluorescent indicators libraries exemplified for fluoresceins (A) and BODIPY dyes (B).

range pH optodes based on the mixture of indicators with different pK_a' values (see section 13, for more details).

Generally, the acidity of the pH indicators based on deprotonation of hydroxyl group can be tuned over a wide range by introducing electron-withdrawing (halogen atoms, carboxy, sulfo, sulfonamide, or nitro groups) or electron-donating substituents, such as amino or methoxy groups.

Modification of the xanthene structure represents a nice example of tuning the pK_a' value over a broad range. The strategy is essentially similar to that used for triphenylmethane dyes. The electron-withdrawing groups introduced into the 2',7'-positions of the xanthene ring decrease the pK_a' value. For instance, lipophilic octadecyl esters of 2',7'-dichlorofluorescein (DCFODE), 2'-monochlorofluorescein (MCFODE), 2'-chloro-7'-hexylfluorescein (CHFODE), and 2',7'-dihexylfluorescein (DHFODE) reported by Weidgans et al.¹²¹ (Figure 21A) embedded in a hydrogel showed pK_a' values of 5.56, 6.85, 6.96, and 8.5, respectively (ionic strength 0.1 M). The pK_a' value of 5(6)-carboxy-2',7'-difluoro-fluorescein (oregon green) in aqueous solution is 4.8,⁵³⁴ which is similar to that of 2',7'-dichlorofluorescein in the same media (5.19).⁵³⁵ Further fluorination in the 4' and 5' positions (Figure 21A) of the chromophore reduces the pK_a' to 3.7 (aqueous buffer)). The electron-withdrawing substituents improve the photostability of the dyes, but electron-donating alkyl chains, reduce it. In fact, photodegradation of DHFODE-based sensors was reported to be fast.^{110,121}

pH indicators based on quenching via PET are even more versatile with respect to tuneability of the pK_a' values due to a variety of available receptors. For instance, alkylamine receptors render the dyes pH sensitive in slightly basic and near neutral media (pK_a' of morpholine is 8.50,⁵³⁶ but it can decrease upon attachment to the fluorophore). Aromatic amines are protonated in more acidic media (pK_a' values of aniline and *N,N*-diethylaniline are 4.87 and 6.57, respectively).⁵³⁶ Alkylation of aromatic amines in most cases increases the pK_a' value. Rurack and co-workers used PET receptors to create a library of

fluorescent indicators covering the whole pH range from 0 to 14 (Figure 21B).¹³⁵ A hexaalkylated BODIPY core was substituted with PET receptors based on phenol, aniline or pyridine groups. The indicator dyes display pK_a' values (in the hydrogel matrix) increasing from 0.5 to 12.8. The general approach for tuning the pK_a' of the receptor groups was introduction of electron withdrawing substituents to decrease and electron donating substituents to increase the pK_a' . To demonstrate the utility, a sensor array with the dyes incorporated into hydrogel D4 was designed and enabled readout with a smartphone and an uncertainty of only ~ 0.1 pH units. Similar strategies (albeit with a lower number of utilized pH sensitive groups) were adapted to create a palette of pH indicators based on naphthalimides and aza-BODIPY dyes.⁵⁰⁵

In summary, there is already an impressive amount of fluorescent pH indicators that found application in optical sensors (c.f., Table S3). The sensors reported by different groups appear to show adequate performance in described applications. However, it remains open if these systems can also adequately perform in other applications. As was demonstrated above, for several chromophores impressive palettes of pH indicators have been reported with pK_a' values covering a broad pH range. However, designing a material with required performance is much more than just taking a dye with suitable pK_a' value. Whereas stability of the chromophore can be adequate for relatively short-term usage (e.g., in disposable sensors), it may not be the case if the sensor has to maintain high accuracy during many months without possibility of recalibration (like on Argo floats in oceanography). For instance, BF_2 chelated chromophores (BODIPYs and aza-BODIPYs) may exhibit slow decomposition in aqueous media, the drift being temperature-dependent⁵³⁷ and probably pH dependent. Photostability is a critical parameter if high light intensities are involved (e.g., in microscopy or in fiber-optic microsensors). This parameter often is not discussed at all, in the best case some information about sensor drift during continuous interrogation is provided. Evidently, taking into account dramatic differences in the set-ups

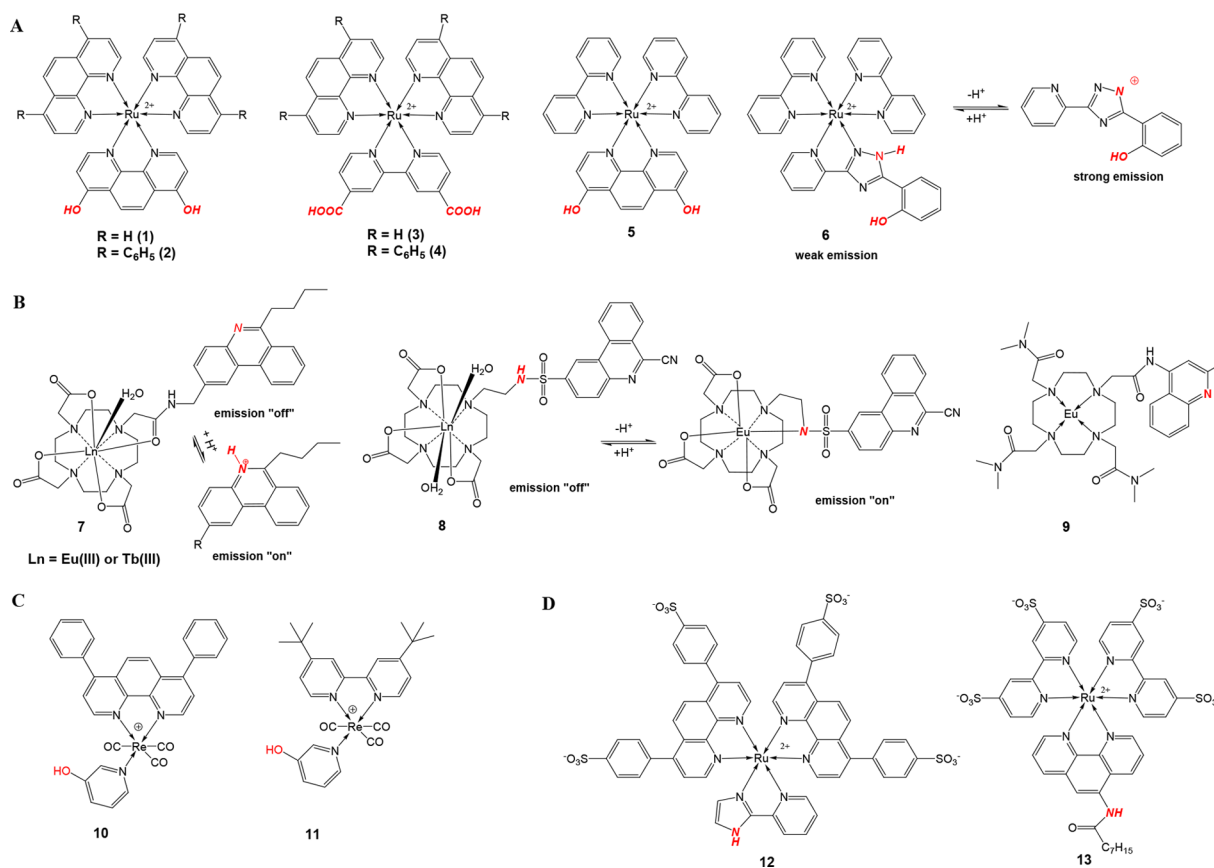


Figure 22. Chemical structures of luminescent ruthenium(II) polypyridyl (1–6) and lanthanide (7–9) complexes used in optical pH sensors, and of model compounds 10, 11 that were used in solution studies.

used such information can only serve for orientation purposes. Therefore, a systematic comparative study of photostability of different chromophores used as pH indicators would be extremely valuable. Surprising discoveries are possible, such as a dramatic enhancement of photostability of some π -extended BODIPY chromophores compared to the “classical” structure shown in Figure 20B.⁵³⁸ Some applications (biotechnology, medicine) require sterilized sensors and the stability of the chromophores in sterilization conditions (e.g., exposure to γ and β radiation) is mostly unknown. Lack of this essential information makes selection of an indicator a difficult and frustrating task, particularly taking into account that most of the reported dyes are not commercially available and can only be accessed in a multistep synthesis.

4.2. Metal–Ligand Complexes

Compared to fluorescent organic probes, most luminescent metal–ligand complexes (MLCs) possess longer decay times, which can be advantageous for discrimination of background fluorescence and even its elimination in a time-resolved measurement. Phosphorescent MLCs also feature larger Stokes shifts compared to fluorescent dyes, because of the lower energy of the triplet state. Finally, pH-sensitive MLCs potentially offer a unique possibility of performing decay time measurement with phase fluorimeters. Unfortunately, several limitations have so far prevented widespread use of MLCs in pH sensors. First, the brightness of most MLCs is often lower than of fluorescent organic dyes. With some exceptions, molar absorption coefficients rarely exceed 40 000 M⁻¹ cm⁻¹, whereas the luminescence quantum yields are typically well below 1 and

are in the range of 0.05–0.5 for most dyes. The second limitation is efficient quenching of long-decaying luminescence by molecular oxygen. The sensitivity of dyes to oxygen is proportional to the luminescence decay time of the indicator and the oxygen permeability of the immobilization matrix that typically is rather good in case of polymers used for pH sensing. The choice of potential candidates is limited to dyes with decay times below 5–10 μ s for which oxygen cross-talk is acceptably weak and can be neglected or compensated for. Europium(III) and terbium(III) chelates represent a notable exception since partly filled f-orbitals only weakly interact with the environment so that the excited states are only marginally quenched by oxygen despite long luminescence decay times typically exceeding 100 μ s. On the other hand, all terbium(III) and most europium(III) chelates require UV excitation, which is often not desirable.

For the above reasons, only a few MLCs have been applied in pH sensing materials (c.f., Table S4) despite many examples of such dyes showing pH-dependent luminescent properties in solutions.^{539–549} The probe reported by Uray and co-workers⁵⁵⁰ is particularly interesting in this respect due to strong lifetime response from pH 4 to 7.5 (about 8-fold decrease), that provides self-referencing capabilities, and successful commercial applicability (Luxcel Biosciences/Agilent).⁵⁴⁹ In contrast to solution behavior, the luminescence of the probe immobilized in a sol-gel matrix is not affected by pH changes (pH 1–11).⁵⁵⁰ The immobilized dye is however useful as large Stokes shift emitter in sensing schemes that utilize energy-transfer or inner-filter effect.

Among metal–ligand complexes applied in optical sensing materials, Ru(II) polypyridyl complexes have been widely

explored. They show broad metal–ligand charge transfer absorption bands in the region of 430–480 nm and are luminescent in the red part of the spectrum. Demas and co-workers⁵⁵¹ have noncovalently immobilized ruthenium(II) polypyridyl complexes (**1** and **2**, Figure 22A) into a cross-linked hydrogel composed of hydrophilic PEG chains and hydrophobic cyclic methylsiloxane rings. The sensors undergo a drastic decrease of luminescence intensity upon deprotonation (~100-fold) and pK_a values are very low (2–4). A similar indicator **5** (Figure 22A) that explores the pH sensitivity of 4,7-dihydroxy-1,10-phenanthroline was embedded in Nafion 117 membrane.⁵⁵² Because of the negative charge of sulfo-groups in Nafion, the pK_a increased to 5.1 compared to the value of 2.6 obtained in solution of the dye and the cross-talk to ionic strength was very strong (decrease of pK_a by ~1 on going from 0.01 to 0.1 M buffer).

Apart from phenols, other functionalities may be useful to induce pH sensitivity of Ru(II) complexes. For instance, Malins et al.⁵⁵³ showed that triazole group introduced into a Ru(II) complex (**6**, Figure 22A) induced luminescence quenching upon protonation.

Suitability of Ru(II) complexes for lifetime-based pH sensing was also investigated.⁵⁵⁴ Complexes **3** and **4** were noncovalently entrapped in a hydrogel. Upon deprotonation, the emission of **4** is enhanced and hypsochromically shifted. Both forms are emissive and this enables lifetime based sensing. The lifetime increases about 3-fold when the pH was increased from 1.5 to 6 (sigmoidal dependency, pK_a 3.75). Significant cross-sensitivity to oxygen is observed in agreement with long decay times (3.25 μ s of base form).

Fiber-optic sensors prepared by Goncalves et al.⁵⁵⁵ made use of complex **3** immobilized into sol–gel glasses. In solution, the dye showed good pH-sensing properties, sigmoidal response of intensity, large dynamics in intensity change (5-fold increase from pH 2 to 6) and acceptable dynamics in the lifetime (increase from 0.4 to 0.6 μ s in the same range). However, immobilization resulted in drastic decrease of the resolution: Intensity increases by only 30% going from pH 2.0 to pH 8.1, and the decay time only increases from 1.05 to 1.16 μ s.

Parker and co-workers⁵⁵⁶ explored the potential of luminescent Eu(III) and Tb(III) complexes for optical sensing of pH. Narrow emission bands of these complexes and the long decay times are particularly attractive. On the other hand, such chelates have to be excited in the UV, which is less favorable. Two different types of Eu(III) complexes were embedded into sol–gel matrix prepared from TEOS. The sensor based on indicator **7** (Figure 22B) showed a ~3-fold decrease of the red luminescence of Eu³⁺ on going from pH 4 to 10. It is caused by quenching via electron transfer from phenanthridine. On the contrary, the luminescence is 3.5 fold enhanced in case of **8** (pH 5 \rightarrow 9) because of the reversible binding of the deprotonated sulfonamide group to the metal ion. Luminescent changes for both sensors can be described with a sigmoidal dependency; the pK_a values were 6.9 and 7.9 for the sensors based on **7** and **8**, respectively. The sensors showed fairly fast response ($t_{95} \sim 80$ s) but required conditioning for 28 days to warrant reproducible response. In contrast to Eu(III)-complex of **7**, the sensor based on Tb(III) complex showed luminescence enhancement (~30%) in the pH range from 4 to 9. This is due to the proximity of the ⁵D₄ level of Tb³⁺ and triplet level of the protonated phenanthridinium, which results in enhanced quenching because of energy back transfer. The brightness of such probes is not good. McCoy and co-workers demonstrated

“on–off” luminescence switching for complex **9** in solution and in a pHEMA matrix.⁵⁵⁷ The complex is luminescent at acidic pH values, but shows virtually no emission at pH 9. Apart from the complexes mentioned above, a Eu(III) complex coordinating thenoyltrifluoroacetone and pyridine dicarboxylic acid was also explored in pH sensors.⁵⁵⁸

Apart from Ru(II) and lanthanide(III) complexes, Re(I) complexes have also been applied as luminescent probes in pH sensors (Figure 22C). Orange-emitting dyes reported by Demas and co-workers featured luminescence decay times of 751 (**10**) and 266 ns (**11**) in cross-linked hydrogel D4J2000 thus enabling elimination of background fluorescence without significant oxygen cross-talk.¹⁴⁹ A 3-hydroxypyridine group coordinated to the central atom induces pH sensitivity. It was observed in an intensity mode since the complexes showed no detectable luminescence in alkaline media. Therefore, a dual lifetime referencing (DLR) technique was implemented. Re(I) complexes can be excited at <400 nm and feature low molar absorption coefficients (<10 000 M⁻¹cm⁻¹).

The above examples clearly show that optical pH sensors based on metal–ligand complexes currently do not favorably compare to optodes based on organic dyes. Low brightness and cross-talk to oxygen remain serious limitations. The Ru(II) polypyridyl-based sensors feature rather low pK_a values and, thus, have limited application potential. While their long luminescence decay times can be useful for elimination of autofluorescence by using time-resolved fluorometry, this aim can be also achieved by optodes based on bright NIR chromophores. The biggest advantage of the luminescent metal–ligand probes can be the unique possibility to quantify pH via measurement of the luminescence decay time. For example, sensors based on indicators **3** and **4** appear to be promising candidates for lifetime read-out. As was demonstrated by Orellana and co-workers,⁵⁵⁹ the situation is significantly more complex. In the first type of a useful lifetime indicator (Figure 22D), the proton exchange in the excited state will be fast and the excited state equilibrium will be established before emission takes place (diabatic equilibration). This indicator type shows a single emission lifetime which varies with the pH value (Figure 23). In the second extreme case, the proton exchange is significantly slower than the respective deactivation rates, so that the protonated and deprotonated excited species decay independently of each other. In this case, the luminescence decay time is biexponential. The luminescence lifetimes do not depend on pH. This is in contrast to the corresponding amplitudes, which reflect the ratio of both species. The authors also showed that comparably fast irreversible excited state proton transfer from or to buffer species renders most luminescent indicators less useful. For instance, indicator **12** (Figure 22D), shows drastic dependency of the response on the buffer type and its concentration due to quenching of the acidic form of the indicator by buffer components (such as hydrogen phosphate). On the contrary, the bulky hydrophobic perfluoroalkyl chain in dye **13** retards the kinetics of the excited state proton transfer at the amide position. Hence, the response of the probe is independent of buffer composition and concentration. This demonstrates the self-referencing capabilities in which only the relative contributions of the overall decay depend on the solution pH (Figure 23).

5. POLYMERIC HOSTS AND SUPPORTS

Polymer chemistry forms an integral part of sensor chemistry. Polymeric materials fulfill any of the following functions:

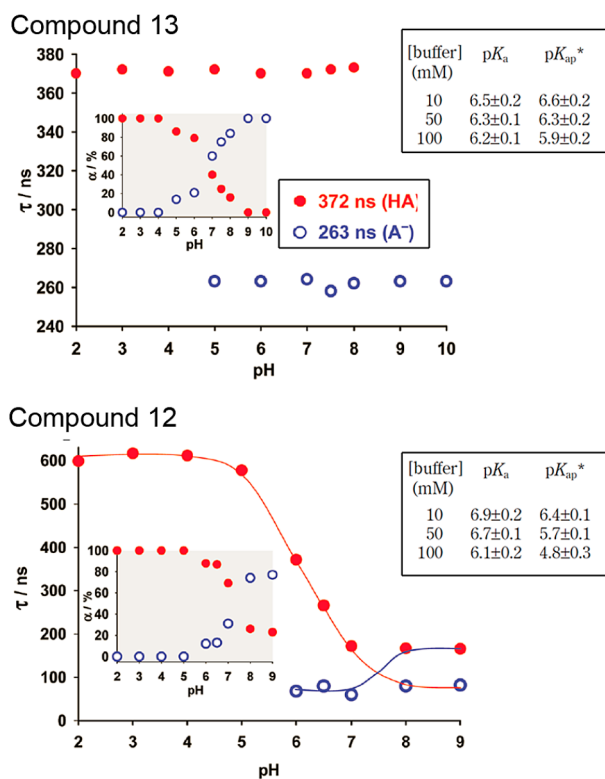


Figure 23. Luminescent lifetimes of the acidic and basic forms of 13 and 12 (Figure 22D) in 10 mM phosphate buffer (air saturation) as a function of pH. The inserts show the corresponding amplitudes of the luminescence lifetimes obtained from the biexponential fits of the emission decays at each pH value. Dependency of the pK_a and apparent pK_a^* values on concentration of the phosphate buffer is given on the right. Adapted with permission from ref 559. Copyright American Chemical Society 2010.

- as a solid support onto which (or in which) an indicator probe is immobilized or dissolved; typical examples being hydrogels and cellulose;
- as a permeation selective material that prevents species other than the proton to enter the sensing layer or a particle;
- as a stimulus-responsive polymer (not treated in this section) examples being polyaniline or poly-(dimethylaminoethylacrylamide) whose absorption in the visible and IR, respectively, change with the pH value;
- as an inert mechanical support for planar sensor layers, examples being thin films of poly(ethylene terephthalate). These materials are treated in section 9.4.

5.1. General Considerations

A polymeric host performs the function of a solvent for the indicator but also acts as a permeation-selective membrane, which can minimize undesired cross-talks. Obviously, the polymeric host has to be permeable to protons. In other words, hydrophobic polymers such as polystyrene, ethyl-cellulose, silicone rubber etc. are not suitable for use in pH sensors. On the other hand, hydrophilic polymers which are able to swell (but are not soluble) in water (hydrogels) represent suitable hosts for pH indicators. The same refers to cross-linked networks built from organic polymers or inorganic materials (sol-gels). Finally, the indicators can also be immobilized on the polymer surface.

Proton transfer in the bulk water is generally accepted to result via proton hopping from H_3O^+ (or $H_5O_2^+$) to a neighboring water molecule (Grotthuss mechanism). Importantly, not an individual proton or a rigid molecular protonic complex is thought to migrate but the bonding situation in the network changes by concerted O–H bond breaking and making, illustrated by the term “structural diffusion”.⁵⁶⁰ Alternatively, a proton can be transported when attached to an uncharged host molecule (“vehicle mechanism” or Stokes diffusion). Obviously, proton transport in highly swollen hydrogels is similar to that in water. In case of sol-gels, hydrogen bonding involving the indicator and the silanol groups appears to have the major influence on the response times rather than proton diffusion.²⁵⁴ However, there is a consensus that proton transport is efficiently hindered by lipophilic substituents, for instance by alkyl and aryl groups in sol-gels.^{254,321} Unfortunately, only few systematic studies revealing the relationship between the structure of the matrix and the dynamic response times have been reported.

5.2. Organic Polymers and Supports

Uncharged hydrophilic linear polymers and cross-linked hydrophilic polymers are most often used in pH optodes. However, also pH sensors based on charged polymers and hydrophobic polymers have been described but they suffer from serious drawbacks (resulting from their charges or poor hydrophilicity) which will be described later. Apart from very few exceptions (such as plasticized poly(vinyl chloride)) the polymers are sufficiently hydrophilic and have high affinity for water. They are insoluble in water because they are physically or chemically cross-linked networks. Theoretical considerations predict that swelling of hydrogels is determined by the thermodynamic equilibrium between the opposing force of mixing and the retractive force of the polymer chains.⁵⁶¹ One of the most important characteristics of a hydrogel is the polymer volume fraction in the swollen state which reflects the amount of water retained by the hydrogel. This parameter will affect proton diffusion in the hydrogel and therefore the response time of the sensor but also its mechanical stability. Hydrogels are elastic materials resembling natural rubbers and generally fully recover to their original dimension from a relatively small deformation (less than 20%).⁵⁶¹ However, swelling of hydrogels is also known to negatively affect the mechanical strength of the materials.⁵⁶² This can result in fast degradation of the sensing layer under mechanical stress, for example when using microsensors in sandy sediments. Such swelling may also result in detachment of the sensing material from the mechanical sensor support.

Among the hydrophilic linear polymers, poly(2-hydroxyethyl methacrylate) (pHEMA) and polyurethane hydrogels (such as hydrogel D4) belong to the most common matrices. Since these polymers are nonionic, the cross-talk of the pH-sensors to ionic strength is mainly determined by the charge of the immobilized indicator. Both polymers are biocompatible and find application in surgical implants and contact lenses and are soluble in a wide range of organic solvents and their mixtures with water (such as ethanol: water = 9:1, v:v). A “cocktail” containing the polymer, the indicator and a solvent can be directly applied onto a mechanical support to result in a pH sensitive sensor layer after solvent evaporation. The simplicity of the process makes it possible to perform high-throughput screening and discovery of optimal polymeric substrates capable of trapping fluorescent pH indicators.⁵⁶³ For instance, more than 100 different polyacrylate and poly(acrylamide) copolymers have been screened using a

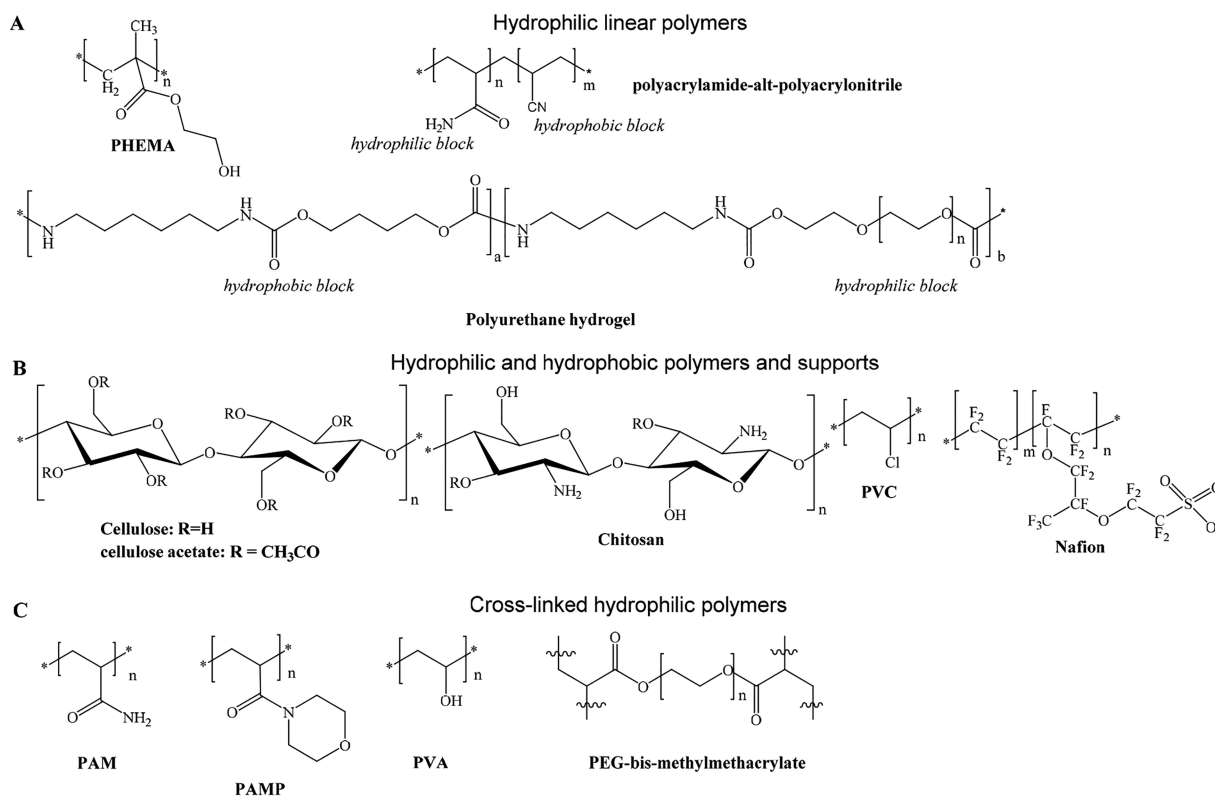


Figure 24. Chemical structures of representative polymers as used in pH-sensing materials.

microarray approach. Poly(methyl methacrylate-*co*-2-dimethylaminoethyl acrylate) was identified as the most promising candidate because it showed the highest dynamics between pH 4 and 10 when used in combination with 5(6)-carboxyfluorescein and allowed, via dip coating, the attachment of fluorescent pH probes to the tip of optical fibers.

pHEMA (Figure 24) is a rather hydrophilic polymer with a water uptake of about 40%. Swelling is significantly enhanced in the presence of urea and slightly reduced when chloride or sulfate ions are added.⁵⁶⁴ pHEMA containing copolymers generally represent good hosts for preparation of pH sensors. However, at extreme pH values (section 12) pHEMA-based materials may deteriorate due to hydrolysis of ester groups. Rather hydrophobic pH indicators tend to aggregate in pHEMA if entrapped noncovalently.¹²² Fortunately, many indicators can be modified with allylic, (meth)acrylate or acrylamide moieties and copolymerized with HEMA monomer. Alternatively, isothiocyanate derivatives of the pH indicators (e.g., fluoresceins or SNARFs) can be covalently attached to pHEMA.⁵⁶ Amino-modified pHEMA variants can also be used for coupling of dyes via amide or sulfonamide bonds.^{381,384,423} The properties of pHEMA can be modified over a wide range via copolymerization of the HEMA monomers with other acrylate monomers. pHEMA does not degrade under physiological conditions.⁵⁶²

Polyurethane hydrogels have been used as matrices for immobilization of pH indicators since almost two decades. They benefit from high chemical stability, biocompatibility and are commercially available (Hydromed series, <http://www.advbiomaterials.com>). Unfortunately, the exact chemical structure of individual representatives is not disclosed. Polyurethane hydrogels reported in literature^{565–567} are composed of hydrophilic poly(ethylene glycol) blocks and hydrophobic domains build by the aliphatic isocyanate and butane-diol or

poly(tetrahydrofuran) (Figure 24A).⁵⁶⁸ Often chemical cross-links are introduced via addition of polyol or polyamine.^{565,566} The commercially available Hydromed hydrogels are linear polymers that have excellent solubility in a wide range of organic solvents. However, their high water uptake, insolubility in aqueous solution and good mechanical stability indicate that microphase separation and physical cross-linking occur, which is typical for polyurethanes. This is due to a combination of hydrophobic interactions (aggregation of hydrophobic domains in order to minimize the surface area contacting with bulk water)⁵⁶⁹ and hydrogen bonding.⁵⁶⁵

Similar to PEG-based hydrogels, which are nontoxic, nonimmunogenic, and are approved for clinical use,^{561,562} polyurethane hydrogels are biocompatible (<http://www.advbiomaterials.com>). Among polyurethane hydrogels, hydrogel D4 (Hydromed D4) has been the most commonly used. It can take up as much as 50% of water.⁵⁷⁰ Hydrogels with higher water content (70%, Hydromed D1) and lower content (30%, Hydromed D7) are also available. Such polymers can well retain hydrophilic indicators carrying hydrophobic anchor groups (e.g., *N*-octadecyl-carboxamidofluoresceins)¹²¹ even without covalent immobilization. On the other hand, rather hydrophobic indicators (such as PDIs) tend to be localized in the hydrophobic domains. This can result in slower response and in hysteresis since the charged protonated form of the dye slowly migrates into more hydrophilic domains.¹²³ The low polarity of the polyurethane hydrogels is also responsible for pronounced increase of the apparent pK_a value upon immobilization of indicators generating negatively charged species upon dissociation (e.g., fluoresceins or HPTS-tris-amides³⁸² or dyes equipped with phenol-based receptors in ref 135) compared to the aqueous solutions and more polar polymers. Analogously, the pK_a value for the indicators, which become positively

charged upon protonation, would decrease compared to aqueous solution due to destabilization of the charged form in less polar environment (c.f., nitrogen based PET-receptors in ref 135).

Thermogelating hydrogels (TGHs), such as poloxamer (a.k.a., pluronic), represent attractive alternative matrix materials. The poloxamer hydrogels are linear triblock copolymers of PEG and poly(propylene oxide). TGHs are highly biocompatible and easy to handle. They are water-soluble, and solutions are sprayable. pH sensor microparticles can be dispersed in Pluronic and sprayed on the surface of interest at temperatures of <math><20\text{ }^\circ\text{C}</math>. At these temperatures, the sensor gel adheres well to the target, even on uneven surfaces such as skin, wounds, and bacterial cultures. If temperature is risen to above $25\text{ }^\circ\text{C}$, the gels form a thin and soft but solid sensing layer, which can be imaged to observe the spatial distribution of pH values on such samples. The gel can be removed from surface by cooling and washing with water. Thermogelating sensor layers present obvious advantages over other sensors by not causing damage to the surface of interest. Such polymers also are applicable to sensors for other species including clinically relevant gases such as oxygen, but also for enzyme substrates (such as glucose or lactate) and ions. TGHs were found to be useful matrices for immobilization of pH indicators. Wang and co-workers demonstrated excellent pH-sensing performance of Pluronic-reinforced silica nanoparticles containing a covalently bound fluorescein dye.⁵⁷¹

Block copolymers of the type polyacrylamide-*alt*-polyacrylonitrile⁵⁷² also have been found to be quite useful and also are used in commercially available optical sensors.⁵⁷³ They have a chemical structure schematically shown in Figure 24A with alternating domains consisting of polyacrylamide and polyacrylonitrile. The former warrants good ion permeability, the latter good mechanical strength and adhesion on non-hydrophilic supports. They are known under the trade name Hypan. Hypan was used in planar sensors for pH⁵⁷⁴ but also for cations, such as potassium,⁵⁷⁵ and for anions, such as nitrate.⁵⁷⁶ Hypan is soluble in DMSO, well penetrated by water, but without strong swelling, and well biocompatible.

Other pH sensors rely on the use of rather hydrophobic hosts such as poly(vinyl chloride) or cellulose acetate (Figure 24B). To improve the ion mobility, addition of a large amount of a plasticizer is necessary (*o*-nitrophenyloctyl ether, dioctyl sebacate, tributyl phosphate etc., typically 1–3-fold the amount in respect to that of the polymer). It was recommended⁵⁷⁷ to replace, in optical sensors, the plasticizer *o*-nitrophenyloctyl ether by *o*-cyanophenylalkyl ethers, which do not act as a quenchers of luminescence and do not cause inner filter effects near 400 nm. The addition of a lipophilic salt (a quaternary ammonium salt for the negatively charged dyes and a lipophilic anion such as tetraphenylborate for the positively charged ones) is essential for solubilization of the indicator in a hydrophobic matrix. These optodes rely on the ion exchange mechanism:⁵⁷⁸ extraction of protons into the polymer results in protonation of the indicator, whereas the potassium ions diffuse out of the membrane to maintain electroneutrality. Such systems not only suffer from rather slow response ($t_{90} = 3\text{--}12\text{ min}$ for $5\text{ }\mu\text{m}$ thick films)⁵⁷⁹ but also are affected by the composition of the buffer used for calibration. Similarly, Hakonen and Hulth⁵⁸⁰ observed a strong shift of the pK_a (from 6.74 to 8.50). It may be due to the change in the environment of the indicator (HPTS in form of the lipophilic ion pair with tetraoctylammonium). Ethylcellulose

films also containing tributyl phosphate as plasticizer show a pK_a of 8.43 for the indicator.⁵⁸¹

Another group of materials represents organic polymers in which the pH indicators are not dissolved but are rather immobilized into a certain domain or on the surface. Nafion 117 is highly chemically and mechanically stable perfluorinated membrane bearing charged sulfonato groups. The combination of a highly hydrophobic polymer backbone and hydrophilic sulfonato groups results in nanoseparation. The membrane, if swollen in water, consists of three different domains: a hydrophobic fluorocarbon backbone, hydrophilic ionic water clusters ($\varnothing \sim 4.5\text{ nm}$) interconnected by short channels ($\varnothing \sim 1\text{ nm}$), and a flexible interfacial region.^{582,583} Optical pH sensors have been manufactured by electrostatic immobilization of cationic pH indicators or of lipophilic indicators in the hydrophilic domains.^{228,332,369,533,552} However, the highly charged character of Nafion 117 results in cross-talk of the sensors to ionic strength⁵⁵² (section 1.6). Hence, this material may not be an optimal choice. Similar to using Nafion as a cation exchange membrane, Zhujun and Seitz immobilized the negatively charged dye HPTS on the anion exchange membrane R-1035.³⁷ Again, the cross-sensitivity to ionic strength was significant.

Cellulose represents another promising organic polymer for preparation of pH optodes. Usually, the dyes are covalently coupled or adsorbed to the polymer, which can be used either in the form of a thin film, or microparticles or nanocrystals.⁴¹¹ Thin cellulose layers can be obtained by hydrolysis of cellulose acetate coatings, for example, covering polyester support in transparency foils.^{16,111,215,239,322} This approach is highly advantageous since the material already contains a mechanically stable and optically transparent inert polyester support.

Agarose is a useful alternative to cellulose and more hydrophilic. Agarose was used, for example, in sensors utilizing orange(II),⁵⁸⁴ Congo red,^{214,215} sulfophthalein,³⁰⁹ neutral red,^{346,362} and anthocyanines³⁴² as pH indicators partially after activation with epichlorohydrin. It was also used to physically immobilize fluorescent pH-sensitive nanoparticles for imaging of bacterial growth and metabolism.⁵⁷¹

Agarose and chitosan (Figure 24B) have been used to coat glass slides.^{214,309,342,346,362} The indicator dyes were covalently immobilized after activation via epichlorohydrin or via simple dye adsorption. Chitosan^{341,343,438} found application as sensor matrix material in food packaging for spoilage indication based on pH-induced visually detectable color changes. Chitosan, however, is prone to biodegradation by enzymes, such as chitosanase or lysozymes.⁵⁸⁵

Alternatively, cellulose microparticles or fibers can be used for immobilization of dyes. Microparticles containing amino groups are promising because many pH indicators can be covalently immobilized on their surface (refs 30, 49, 80, 381, 396, 423, 425, 441, 466). The pK_a value of immobilized fluorescein isothiocyanate on aminoethyl cellulose fibrous particles was reported to be lower (~ 5.2) than for fluorescein.⁴⁹ This may be due to presence of residual protonable amino groups. Cellulose and aminocellulose as biobased materials are prone to degradation by enzymes originating from bacteria or fungi.^{585,586}

Cross-linked hydrophilic polymers as shown in Figure 24 form another important group of organic supports. The linear forms are water-soluble and, therefore, not suitable for preparation of pH sensors. If, however, cross-links are introduced, the resulting hydrogels are mechanically stable and water-insoluble. The hydrophilic character and high water

uptake of these sensors results in fast response. These hydrogels are nonionic, so that cross-talk of the pH optode to ionic strength is mainly guided by the properties of the indicator and not the matrix. Cross-linking also restricts diffusion of large molecules (such as proteins) into the matrix.⁵⁸⁷

Cross-linked polyacrylamide (PAM, Figure 24C) and its derivatives are probably the most common polymeric supports. The polymers have straightforward preparation procedures that give robust materials. Some indicators can be directly copolymerized with acrylamide (e.g., phenol red) without additional modifications. Other polyacrylamide derivatives were also found to be useful. For instance, Aigner et al.^{123,588} demonstrated that polyacryloylmorpholine (PAMP) cross-linked with poly(ethylene glycol diacrylate) represents an excellent matrix for immobilization of perylene dyes. Other matrices include cross-linked PEG gels. To obtain these gels, PEG-bis-methacrylates (Figure 24C) are useful as cross-linkers.⁵⁶¹ The gels can be obtained via photopolymerization and indicators bearing allylic, meth(acrylate), or acrylamide groups can be covalently incorporated into the gels. Even highly cross-linked materials can have a water uptake of about 700%.⁵⁸⁹ Generally, water uptake decreases at higher cross-linking degrees (lower mesh size). The water uptake of cross-linked PVA increases from 400 to 800% when the mesh size (i.e., distance between the cross-links) increases from 1.8 to 6.5 nm.⁵⁹⁰ On the other hand, water uptake of cross-linked pHEMA only marginally depends on the mesh size because water is a rather poor solvent for HEMA.^{590,591}

Micro- and nanoparticles prepared from cross-linked pHEMA or PAM derivatives are also popular. Here, amino-functionality is introduced during polymerization (e.g., via copolymerization with *N*-(3-aminopropyl)-2-methylacrylamide), thereby allowing subsequent covalent attachment of indicators.^{148,152,381,384,396,592} The microparticles can be conveniently dispersed in hydrogel matrices and mixed with other components, such as reference beads. Nanoparticles are valuable for intracellular imaging of pH values. Some linear polymers represent an alternative for these applications. For instance, a polymer on the basis of poly(*N*-(2-hydroxypropyl)-methacrylamide) containing covalently attached ratiometric fluorescent pH indicator, a gadolinium(III) chelate and positively charged poly(2-(methacryloyloxy)ethyl]-trimethylammonium chloride) for enhancing cell permeability was used for simultaneous pH measurement and MRI.⁵⁹³

Poly(vinyl alcohol)^{207,208,240,310,377} was cross-linked with glutaraldehyde, epichlorohydrin, diisocyanates, or via electron beam or γ -irradiation^{562,594} Cross-linked PVA was also used as a mechanical support to obtain a pH-sensitive membrane with immobilized phenol red.⁵⁹⁵ Alternatively, PVA can be cross-linked with tetraalkoxysilanes to obtain an organic–inorganic hybrid material.⁴³² Homogenous crack-free layers obtained with 80–90% of PVA and 20–10% of TEOS showed fast and reversible response to pH. The change in the apparent pK_a value over 2 months was attributed to the ongoing polycondensation reaction that is typical for sol–gels.

Demas and co-workers⁵⁵¹ described hydrogels based on the amino-PEG derivative Jeffamine that was cross-linked with a cyclic siloxane bearing 3 isocyanate moieties. The material forms hydrophobic (siloxane) and hydrophilic domains which was found useful for immobilization of a lipophilic pH indicator without the necessity for covalent immobilization. Despite a high thickness of the films (250 μm), the response times were relatively fast (several minutes).

5.3. Inorganic Supports and Host Materials

5.3.1. Silicates (Including Sol–Gels and Ormosils). The preparation of sol–gel materials involves several steps: hydrolysis of precursors (tetraalkoxysilanes or alkyl-trialkoxysilanes), deposition of the sol onto a support (typically glass), or a waveguide and drying for a prolonged time (24 h) at elevated temperature (e.g., 70 °C). Measurements are typically performed after 1–2 weeks required for stabilization of sensor properties due to slow aging. This is associated with drifts in the pK_a values. In one of the first sol–gel-based pH optical sensors, a 5- and 6-carboxynaphthofluorescein was physically entrapped in a sol–gel matrix and was found to be surprisingly resistive to leaching.³⁰ The sensor works in the pH range 6–9 and uses yellow or orange LEDs as light sources. The indicator dyes were also covalently immobilized on cellulose. However, many of the first sol–gel-based sensors suffered from both leaching of the indicator and long response times, often exceeding 1 h for the bulk monolithic films.⁵⁹⁶ The use of very thin films (>2 μm) along with evanescent field readout (see section 14.3) strongly reduces response time and yet gives good signals.

Most of the reported sol–gel sensors rely on the use of common pH-indicators that are not suitable for covalent immobilization. MacCraith and co-workers²⁷⁹ showed that leaching is affected by many factors, such as the pH of the solution and by conditions affecting the structure of the sol–gel. Base-catalyzed hydrolysis results in materials with large pores, which are less suitable for noncovalent entrapment of indicators due to strong leaching.²⁶⁷ On the contrary, acid-catalyzed hydrolysis and condensation produce microporous structure with small pores (<2 nm).⁵⁹⁷ However, if the pH is too low (<1), the condensation becomes too fast and this results in higher porosity and faster leaching.²⁷⁹ Leaching is much slower from aged films (3 months storage) compared to the freshly prepared. Finally, the introduction of hydrophobic groups (typically methyl or phenyl) results in materials referred to as ormosils (*organically modified silica*). This was demonstrated to efficiently prevent leaching.^{256,414} Unfortunately, such substitution also impairs proton diffusion and slows down the response. For instance, the response times (t_{100}) of bromocresol green embedded into films prepared from tetraethoxysilane (TEOS) and methyltriethoxysilane (MTEOS) were 150 min and >24 h, respectively.²⁵⁴ In materials reported by Wang et al., dye-doped 1 μm thick sol–gel films prepared from TEOS showed surprisingly fast response (t_{95}) of 5 s, whereas it increased to 600 s for an ormosil prepared from an equimolar ratio of TEOS and phenyltriethoxysilane (Ph-TEOS).³²¹ The same effect was observed by Lobnik et al.:⁴¹⁴ introduction of phenyl groups eliminated leaching of noncovalently immobilized amino-fluorescein almost completely, but slowed the response from 90 s for tetramethoxysilane (TMOS) to 30 min for TMOS:PhTMOS (1:1) (t_{95} , ~300 nm-thick films). The decrease of polarity also drastically affected the pK_a values (6.62 and 8.61, respectively).

Immobilization in sol–gels (particularly containing an organic component) affects the pK_a value of the indicator compared to aqueous solution (usually by an increase of the pK_a by 1–5 units for dyes generating negative charge upon deprotonation).^{256,598} It also results in a significant broadening of the dynamic ranges which can span 4–6 pH units^{266,321,407,442,459,469,472,503,599} compared to 3 pH units in solution. Ormosil-type of sol–gels were also doped with pH indicator dyes in order to sense alkaline analytes such as dissolved ammonia.⁶⁰⁰

Postmodification of the sol–gel pores is an efficient strategy for shortening response times.²⁵⁴ In sol–gels, hydrogen bonding between the hydrophilic indicator dyes and the silanol groups appears to be extremely important for the response time. Goddard and co-workers showed that treatment of sol–gel-based sensors with sodium hydroxide shortens the response times from 150 min to 45 s (in case of TEOS) and from 24 h to 22 min in case of MTEOS. Such modification occurs very fast but the risk of damaging of the sol–gel network is high.

During *aging of sol gels*, further hydrolysis and condensation of unreacted groups takes place. This results in an increased density of the sensor films. These structural changes induce *drifts* of the pK_a and can represent a serious problem. For example, Lee and Saavedra observed a large (0.7) increase of the pK_a value of bromophenol blue in TEOS based sensors after 9 months of storage.²⁷⁷ Lobnik et al.⁴¹⁴ noticed the same increase (0.7 units) of the apparent pK_a upon storage of aminofluorescein/TEOS films in air over several months (and much faster change at elevated temperature (70 °C)) whereas storage in aqueous media for the same time hardly affected the sensor properties. McDonagh et al.⁵⁹⁷ demonstrated that aging of sol–gel films at RT continues for many days and even months, which is indicated by decrease in the thickness of the films. 3-glycidioxypropyltrimethoxysilane (GPTMS) has been studied but with mixed results. It was cocondensed with TEOS,⁵⁹⁸ MTEOS,⁴⁰¹ PrTEOS,⁵²⁰ sometimes under catalysis by BF_3 ⁶⁰¹ or aminoalkoxysilanes,⁴⁴² with indicators, such as methyl red, bromocresol green, or fluoresceinamine.

Ion-pairing of a charged indicator with a lipophilic counterion is a common approach to minimize leaching. Rottman et al.^{228,602,603} investigated the influence of coentrapment of surfactants on the properties of pH indicators in sol gel films. The addition of cetyltrimethylammonium bromide (CTAB) strongly affects the pK_a values, which were shifted by up to 3–4 units to more acidic values for azo dyes and to more basic values for phenolphthalein dyes.

Sol–gels based on elements other than silica have also been investigated. Beltran-Perez and co-workers studied sol–gels obtained via hydrolysis and condensation of titanium tetra-isopropoxide.⁶⁰⁴ They were made pH-responsive by doping with Brilliant green, coumarin or rhodamine dyes. However, the paper is of preliminary nature. Yang and Saavedra²⁶⁶ reported a waveguide sensor with a 110 nm sensing layer prepared via hydrolysis of methyltrimethoxysilane (MTMOS) and titanium *tert*-butoxide. Immobilized bromocresol purple responded over a wide range (pH 3.5–9). Islam et al.^{247,249,316} examined the properties of various silica–titania sol–gel composites prepared from TEOS and titanium tetra-isopropoxide as precursors and CTAB as surfactant. Response times were <7 s for both fiber optic and planar sensors, and no dye leaching was observed. A hybrid material for use in pH sensing was reported by Rosenzweig and co-workers.⁶⁰⁵ Carboxyfluorescein-doped liposomes (\varnothing 70 nm) were embedded in a TEOS film. Immobilization did not significantly affect the pK_a value (6.5 in liposomes) but strongly reduced dye leaching and improved response (<1 s for micrometer-thick films).

5.3.2. Mesoporous Materials. Mesoporous materials provide an interesting alternative to sol–gel sensors. They are obtained via hydrolysis and condensation of silicon alkoxide precursors but a surfactant is first added as a structure-directing agent and then removed via extraction. Wirnsberger et al.⁶⁰⁶ prepared sensing films (\sim 0.9 μ m thick) by acidic hydrolysis of TEOS in the presence of a pluronic F127 poloxamer surfactant

and APTS-coupled fluorescein. After aging at room temperature, crack-free films are obtained. The surfactant was removed by treatment with ethanol. The films demonstrated fast response t_{95} of \sim 7s. Similarly, Miled et al.²⁹³ embedded bromothymol blue into a mesoporous material prepared from TEOS in the presence of CTAB as structure-directing agent (which, however, was not removed from the sensing material). The 1.5 μ m-thick sensing layers responded quickly (<20 s) to pH changes in acidic media. Hiruta et al.⁶⁰⁷ covalently immobilized a triethoxysilane-modified BODIPY dye with a protonable dimethylamino group in a mesoporous film prepared via hydrolysis of TEOS in the presence of the surfactant Brij56, which was removed from the sensing film via extraction with hot toluene. The sensor works in the acidic pH range (pH 1–4).

In summary, sol–gel optodes excel by their mechanical stability. They withstand mechanical stress such as wiping with tissue,⁶⁰⁸ which can be useful for sensor cleaning (e.g., from biofouling deposits) also in the presence of detergents.^{599,609} They were also reported to withstand repeating autoclavation without change in sensing properties.⁶⁰⁸ In contrast to organic polymers, the sol–gels do not swell in organic solvents, which can be useful for measurements of proton concentration in solutions containing organic solvents.²⁶¹ On the other hand, sensing properties of the optodes (apparent pK_a value, response time, leaching of the dye) are sensitive to the ratio of the precursors used and reaction conditions (acid or basic catalysis, temperature, and time needed for hydrolysis). Many sol–gel films were reported to crack upon aging and storage. Sol–gel-based sensors also often feature pK_a values, which are largely different from those of dyes in aqueous solutions and also cover a wider dynamic range. Hydrolytic stability of sol–gels should be kept in mind when designing sensors for basic pH range or using harsh sterilization conditions.

6. IMMOBILIZATION OF INDICATOR DYES IN HOSTS

Leaching of pH indicators out of the sensor matrix represents a common problem of optical pH sensors. Leaching severely affects the calibration curves, also for majority of referenced sensors, except for sensors based on measurement of luminescence decay time or luminescence anisotropy. Many pH indicators are hydrophilic and prone to leaching into the aqueous samples. Leaching of the charged forms is particularly likely. There are several useful strategies to overcome leaching. A table with selected examples of immobilization procedures is provided in the [Supporting Information \(Table S5\)](#).

6.1. Physical Entrapment of Indicators

This strategy relies on the *physical entrapment* of pH indicators into a highly cross-linked matrix. It is important that the pore or mesh size (distance between the cross-links) of the cross-linked matrix is smaller than the size of the indicator. Mesh size is comparably high in hydrogels based on cross-linked polymers. For instance, highly cross-linked PEG-diacrylates have mesh sizes varying from about 1 to 14 nm depending on the molecular weight of PEG, its concentration and to a minor extent on the amount of cross-linker.^{589,610} The mesh size of swollen pHEMA hydrogels cross-linked with ethylene glycol dimethacrylate is 1.6–2.4 nm.⁵⁹⁰ Evidently, a mesh size of 1 nm and higher cannot prevent small dye molecules from leaching. This was demonstrated, for example, using tetramethylrhodamine as a model system.⁶¹⁰ However, even in polymers with much smaller mesh sizes of 0.57–0.65 nm (cross-linked pHEMA) the

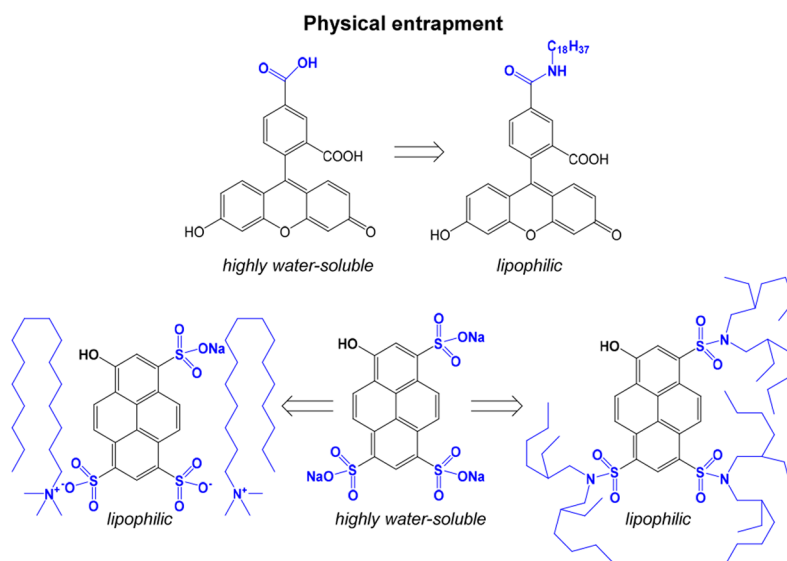


Figure 25. Physical entrapment as strategy for immobilization of pH indicators into matrices

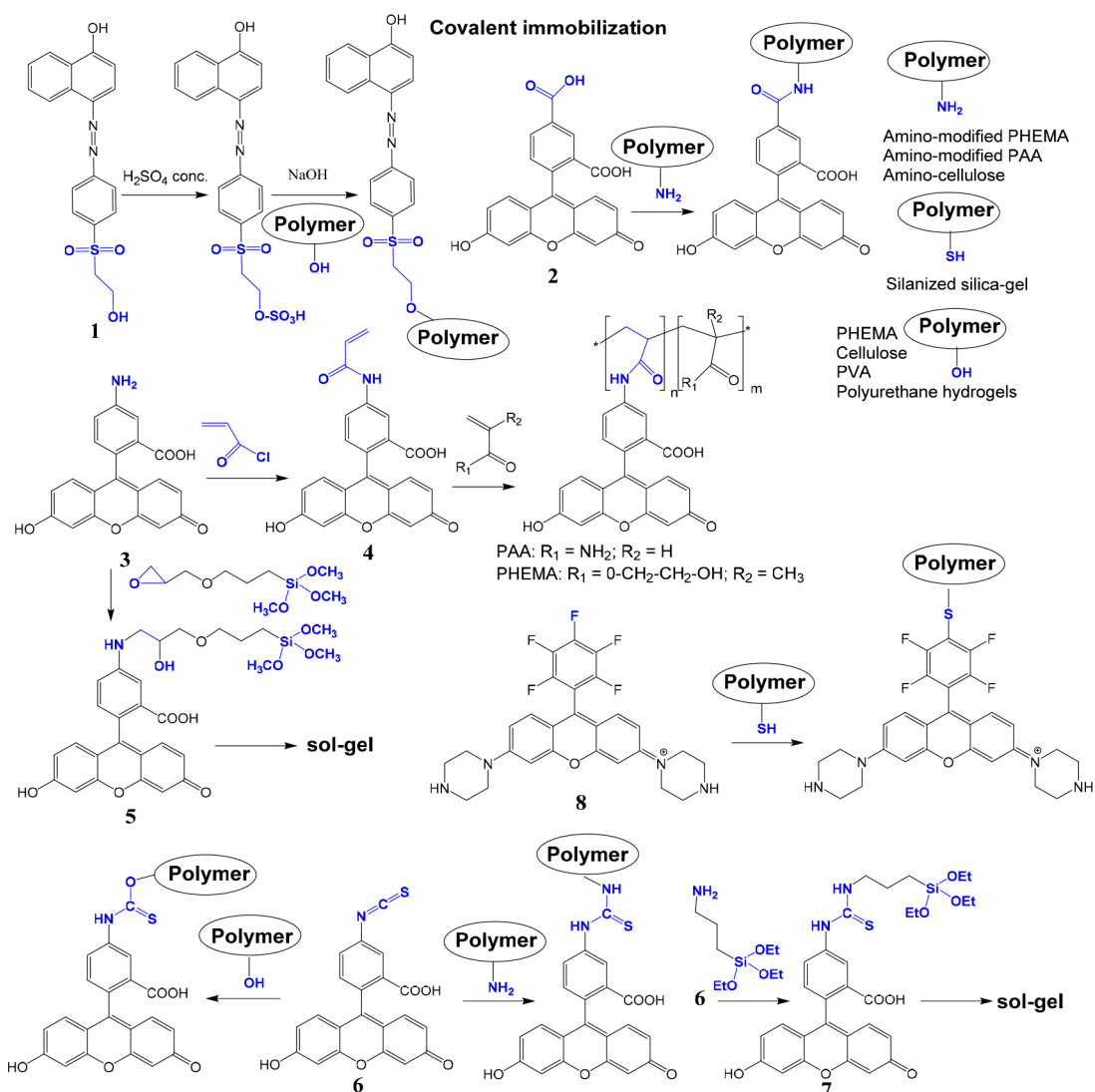


Figure 26. Covalent immobilization for immobilization of pH indicators into matrices.

diffusion of dye molecules, such as alizarin yellow, can be detected although it indeed decreased at lower mesh size.⁶¹¹

Physical entrapment of indicators in nanoporous sol–gel matrixes yields materials that show no leaching even in case of highly water-soluble indicators such as fluorescein or HPTS. For example, no leaching of physically immobilized fluorescein and phenolsafranine was recorded for silica nanoparticles of 30 nm in diameter.⁶¹² McDonagh and co-workers did not observe leaching of HPTS embedded in sol–gel obtained by hydrolysis of a mixture of ethyltriethoxysilane and (3-glycidoxypropyl)-trimethoxysilane.³⁸³ HPTS was used, however, in the form of an ion pair with CTAB, which makes the indicator dye less hydrophilic and more bulky. Modifications of the sensor matrix to minimize leaching may, however, cause adverse effects, such as longer response times.³²¹

Addition of surfactants can also reduce leaching because the amphiphilic molecules with their long alkyl chain tails can create a lipophilic environment for the indicator dye.⁶⁰² In case of the negatively charged indicators, such as HPTS, quaternary alkylammonium ions with long aliphatic chains are preferred (Figure 25).^{354,383} The lipophilic ion pairs have been incorporated into PVC, silicone, hydrogel,³⁵⁴ and sol–gel matrices.³⁸³

Another common strategy relies on *lipophilization* of hydrophilic indicator molecules via *chemical modification* by introducing long-chain alkyl or perfluoroalkyl or *tert*-butyl groups. This is different from the previously discussed modification based on formation of ion pairs. The modified dyes can then also be immobilized by physical entrapment (Figure 25). For example, very hydrophilic fluoresceins are rendered water-insoluble via a long hydrophobic alkyl chain attached via ester bond or amide bond (carboxyfluorescein derivatives, Figure 25). Water-soluble HPTS can be made lipophilic by converting the sulfonate into *N*-alkylsulfonamide groups (Figure 25). Chemical modification, however, can strongly affect photophysical properties of the dyes. Whereas lipophilization of carboxyfluoresceins via modification with alkylamines in the 5(6)-position (Figure 25) has almost no effect on the photophysical properties, introduction of alkyl chains into 2' and 7' position of fluoresceins strongly reduces photostability and increases the pK_a value. Hydrophobic HPTS sulfonamides (Figure 25) display bathochromically shifted absorption and emission maxima of the protonated and deprotonated forms.

Dyes conjugated to dextrans and chitosans have been immobilized in hydrogel,⁴³⁸ sol–gels,⁴³¹ and pHEMA.^{56,419} On the other hand, attachment of such hydrophilic macromolecules may not be sufficient to prevent leaching⁴³¹ even from cross-linked hydrogels. For instance, Kotsmar et al. demonstrated that fluorescein isothiocyanate (FITC) modified with a branched polysaccharide (MW ~ 70 000; hydrodynamic radius 18.5 nm) does not enter cross-linked HEMA hydrogels, while FITC-labeled dextran (MW 20 000; hydrodynamic radius 9.3 nm) penetrates even 3.6 nm mesh size gels, albeit rather slowly.⁶¹³

6.2. Covalent Immobilization of Indicators

Covalent coupling of the indicator to the matrix is the most reliable strategy to avoid leaching and migration of the dye, but often requires tedious synthesis or post modification of dyes. Reactive derivatives of several indicators (such as fluoresceins) are commercially available. The most common possibilities are exemplified in Figure 26. Among the absorptometric indicators,

the vinylsulfonyl chemistry common in textile industry was adopted by Mohr and co-workers^{16,17} to prepare reactive pH indicators such as 1. The 2-hydroxyethylsulfonyl group is then converted to a sulfato-ethyl sulfone in the presence of concentrated sulfuric acid. Subsequent treatment of these intermediates with base results in the formation of reactive vinylsulfonyl dyes. The latter react with polymers containing hydroxyl groups, most commonly cellulose,^{16,239} but also other polymers, such as pHEMA, PVA, or certain polyurethane hydrogels.^{208,238} The method was then extended to naphthalimide-based PET pH indicators with a 2-hydroxyethylsulfonyl function for covalent immobilization to cellulose.⁴⁷⁹ The vinylsulfonyl group also reacts in thiol-Michael additions⁶¹⁴ and can be radically polymerized.²⁰⁸ Azo dyes also were covalently immobilized via (a) triazine coupling to cellulose,²⁰⁶ (b) coupling to PVA via an aldehyde prepared from vinylsulfonyl dyes,^{207,208} (c) copolymerization of vinylsulfonyl dyes with acrylic monomers,²⁰⁸ (d) coupling of Congo red to agarose after activation with epichlorohydrin,^{214,215} (e) carbodiimide coupling of Congo red to pHEMA,²¹⁷ and (f) sol–gel reaction with trimethoxysilane coupled methyl red.²²⁸

Several reactive fluorescein-based pH indicators are commercially available which explains their high popularity in optical sensing despite poor photostability. For instance, 5(6)-carboxyfluorescein 2 (Figure 26) can be coupled to amino-modified pHEMA, PAM or cellulose via standard methods (e.g., DCC/EDC/NHS).^{30,143,397,411,415,420,423,428,448} Other dye classes with carboxy and amino groups have been also immobilized using amide bond formation, for instance azo dyes,^{217,224,228,615} triphenylmethane dyes,²²⁴ Nile Blue,²¹⁷ or xanthene dyes,^{404,615} just to name a few.

Aminofluorescein 3 (Figure 26) can be reacted with acryloyl chloride to give 4, which was copolymerized with a variety of monomers including HEMA or AM.^{53,400,406,408,417,429,449,616} An analogous reaction was reported for piperazine substituted naphthalenediimide.⁴⁸¹ On the other hand, aminofluorescein can also be reacted with 3-glycidyloxypropyltrimethoxysilane or 3-(trimethoxysilyl)-propylisocyanate to give a reactive derivative for immobilization in sol–gels.⁴¹⁴ Interestingly, in case of the former, the pK_a value of aminofluorescein was much higher (7.9) than for the dye in aqueous solution (6.62), whereas for the dye coupled to 3-(trimethoxysilyl)-propylisocyanate it was almost identical (6.73). FITC 6 (Figure 26) is undoubtedly one of the most popular reactive dyes. It can be directly coupled onto polymers containing amino or hydroxy groups (–OH, only under harsh reaction conditions), such as amino-modified polystyrene beads,⁴⁰⁵ aminoethyl cellulose^{49,425,441} and cellulose nanocrystals,⁴¹¹ amino-modified hydrogels,⁴⁹ and amino-containing controlled pore glass,⁴⁹ or reacted with 3-aminopropyltriethoxysilane to give 7 for sol–gel immobilization.^{404,421,606,617,618}

If the polymer and the indicator share the same functional groups, reactive linker units like cyanuric chloride or epichlorohydrin can be used. These have two reactive sites, one for the dye, and one for the polymer. Cyanuric chloride was used to couple aminofluorescein to matrices such as cellulose or PVA,^{24,619} and an iminocoumarin to microbeads of aminocellulose and amino-modified pHEMA.³⁹⁶ Epichlorohydrin allowed coupling of Congo red and anthocyanines to agarose and cellulose films.^{214,215,342}

The widely used pH indicator HPTS was immobilized in many ways. Representative examples include covalent linkage to an amino-modified solid support via chlorosulfonyl groups²⁹

after prior protection of the hydroxy group, or by replacing one sulfo group by a methacryloyl group which then can be copolymerized with poly(ethylene glycol)diacrylate.³⁷⁹

The versatile toolbox of click chemistry offers attractive options in terms of covalent immobilization. For example, the pH-sensitive rosamine derivative **8** (Figure 26) was covalently immobilized into the pores of thiol-modified silica gel beads.¹⁵² Alternatively, it can be reacted with 3-mercaptopropionic acid to introduce carboxy groups for further modification. The thiol-Michael addition is another click reaction that has been used for immobilization of fluorescein on polymer-based nanoparticles.⁶²⁰ In this case, fluorescein-5-maleimide was used as Michael acceptor and coupled to thiol-functionalized particles.

As can be seen (Table S5), the above approaches were widely applied for immobilization of other functionalized pH indicators. Moreover, the same strategies can be adapted for immobilization of reference dyes. For instance, tetramethylrhodamine isocyanate was immobilized on the surface of silica nanoparticles modified with amino groups.⁴⁰⁴ Rhodamine B isothiocyanate was coupled to acrylamide and then copolymerized with **4**.⁶¹⁶

There is a number of less general methods. For instance, Peterson and Goldstein directly copolymerized phenol red with acrylamide.³² Umemura et al. used the vinyl groups of protoporphyrin IX to copolymerize it with acrylamide.³³⁹ A (*p*-hydroxyphenyl)porphyrin was covalently coupled to quartz optical fibers whose surface was modified with trichloro[4-(chloromethyl)-phenyl]silane.³³⁵ Dipicylamine³⁶⁴ and Congo red²¹⁸ were covalently coupled to cellulose that was activated in a two-step procedure. Various azo dyes have been directly synthesized on diazotized quartz and glass surfaces.^{15,222,223} Phenolphthalein was immobilized on amino-modified PAN fibers using the Mannich reaction.^{225,242} Phenolphthalein and *o*-cresolphthalein can be polymerized by reaction with formaldehyde.²⁴⁰ The resulting polymeric indicators were coupled to PVA. One should be aware of possible challenges associated with materials based on covalently immobilized dyes. Immobilization requires introduction of functional groups into the polymer. Many indicator probes are immobilized by covalent binding to amino groups or carboxy groups, but not all are bound to indicator molecules. Quite a few remain unmodified, and this introduces additional local charges (such as $-\text{NH}_3^+$ or $-\text{COO}^-$ groups). Residual charged groups that remain in polymer after coupling may affect apparent pK_a values of the indicator due to formation of ion pairs with oppositely charged dye molecules, increase the cross-talk of the material to ionic strength or even act as fluorescence quenchers (e.g., via PET effect in case of NH_2 groups for certain chromophore classes). Therefore, end-capping of the residual functional groups is advisable to reduce these undesirable effects. For example, the effect of amino groups may be reduced by acetylating them under appropriate conditions so not to acetylate the indicator dye. Excess carboxy groups may be eliminated by converting them into an amido group.

7. MATERIALS WITH DUAL FUNCTIONALITY (INDICATOR AND HOST)

7.1. Metal–Organic Frameworks

Metal–organic frameworks (MOFs) are crystalline solids characterized by extremely high structural diversity due to almost unlimited combination of metal ions and linkers and possibility of postmodification. Featuring high intrinsic porosity,

they have been extensively investigated for gas-separation and gas-storage applications, in catalysis and for chemical sensing.^{621,622} Rocha and co-workers⁶²³ were probably the first who reported preparation of a pH-sensitive metal–organic framework. A material composed of Eu^{3+} and 1,10-phenanthroline-2,9-dicarboxylic acid showed typical lanthanide luminescence upon UV excitation (350 nm). The Eu^{3+} ions have luminescence peaks at 579 and 581 nm. The luminescence of the first peak increases linearly from pH 5 to 7.5 by about 30%. The intensity of the second peak remains constant thus providing the possibility of ratiometric pH measurement. Several limitations of the sensing material should be noted: (i) the peak maxima differ by only 2 nm; (ii) the overall quantum yield is 0.56, but the intensity of the analytically useful transition is about 2 orders of magnitude lower than the inert transition; and (iii) irreversible changes are observed at $\text{pH} < 4$ (due to protonation of the carboxylic groups) and at $\text{pH} > 8$ (formation of europium hydroxide).

Lu and Yan⁶²⁴ modified a bipyridine-containing MOF with Eu^{3+} and 2-thenoyltrifluoroacetone (TTA). Bipyridine binds Eu^{3+} , which acts as an emitter, whereas the TTA ligand coordinates to the Eu^{3+} and acts as an antenna. The Eu^{3+} is located in two different environments, and only one of them is affected by pH changes. In fact, the red luminescence of Eu^{3+} (λ_{max} 614 nm) remained unaffected by pH when excited at 330 nm. If excited at 375 nm a significant decrease of the luminescence intensity occurs on going from pH 7.7 to pH 5.0. Such a change is associated with protonation of the TTA antenna, which becomes only weakly bound to Eu^{3+} so that its sensitization ability decreases. Although such an effect can also be observed for Eu-TTA complexes in solution, the advantage of MOF is in its ability to retain the dissociated TTA molecules. The MOF decomposes at pH values of < 4 and > 8 .

Zhang et al.⁶²⁵ modified silk fibroin powder with pyromellitic acid and Eu^{3+} . In addition to the strong blue fluorescence of silk fibroin originating from amino acids, red luminescence from Eu^{3+} can be detected. The luminescence intensity moderately ($\sim 25\%$) increased on going from pH 3 to 7. The intensity drops if the pH was further increased from 7 to 10 because of formation of europium hydroxide. A MOF composed of Tb^{3+} and viologen-functionalized *m*-benzenedicarboxylate was shown to have a luminescence response from pH 2 to 7.⁶²⁶

Li et al.⁶²⁷ have physically and electrostatically immobilized the Eu(III) thenoylacetonate complex ($\text{Eu}(\text{tta})_n$) on synthetic silicate platelets via ion exchange. The resulting nanocomposites were deposited onto glass slide to form sensing films. Protonation of the antenna in acidic media resulted in complete disappearance of the characteristic red luminescence of Eu^{3+} peaking at 611 nm. The material showed sigmoidal response with a pK_a value of 2.7. This makes it potentially suitable for monitoring very low pH values. The short excitation wavelength (345 nm) is a drawback, but the large Stokes shift is beneficial.

A triple-interpenetrated luminescent lanthanide-organic framework was reported that enables ratiometric measurement in the ranges from pH 2 to 7 and 7 to 10.5.⁶²⁸ The MOF is based on an amphoteric ligand (tetrabenzoic acid with two pyridine rings) and Eu^{3+} . Upon excitation at 300 nm, the emission peaks at 390 and 480 nm are modulated by pH. The MOF can be combined with $\gamma\text{-Fe}_2\text{O}_3$ nanoparticles to allow magnetic manipulation.

Qi and Chen⁶²⁹ reported aggregated MOF nanoparticles ($\varnothing = 30\text{--}40$ nm) composed of Tb^{3+} , dimethylformamide and phenanthroline. The green emission is typical for Tb^{3+} and is

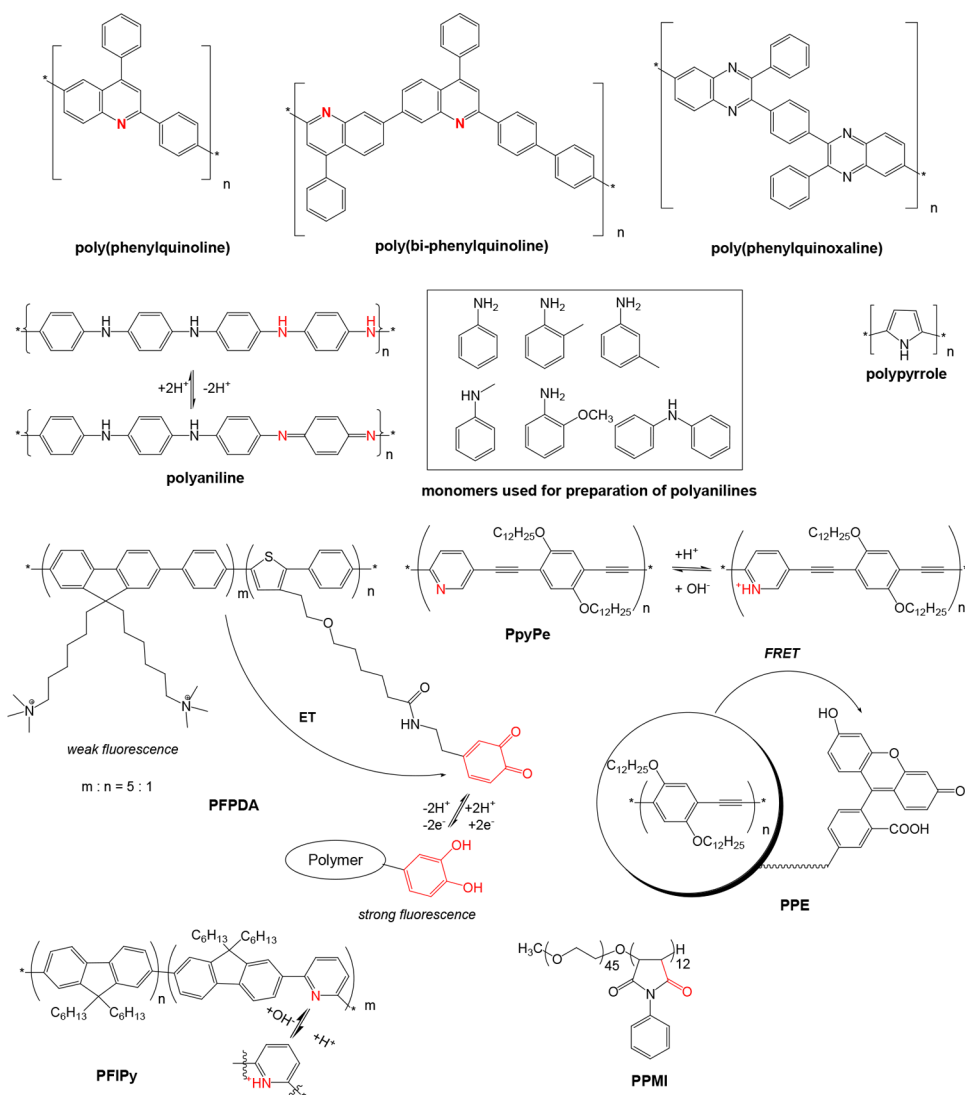


Figure 27. Chemical structures of the pH optodes based on conjugated polymers.

10-fold enhanced in acidic media ($pH < 3.5$). The luminescence lifetime of Tb^{3+} is, however, not affected by pH ($\tau \sim 400 \mu s$). The response of the network to pH is reversible and the stability in water is good. Common metal ions in 1 mM concentration do not interfere. Xia et al.⁶³⁰ prepared a MOF incorporating both Tb^{3+} and Eu^{3+} , which showed ratiometric response from pH 3 to 6. This represents an advantage compared to the materials described above relying only on luminescence intensity, but the stability of MOFs remains a main issue.

As can be seen from the examples above, hydrolytic stability remains the main limitation of pH sensitive MOFs. Aguilera-Sigalat et al.⁶³¹ modified a MOF composed of zirconium(IV) and 2-aminoterephthalic acid with an indole moiety via diazotation of the amino groups. It was attempted to increase the hydrolytic stability of the MOF in basic media, yet the performance in terms of sensing was not impressive. A similar strategy was utilized by Wang and co-workers⁶³² who prepared a MOF on the basis of Zr_6 clusters and 2,2'-bipyridine-5,5'-dicarboxylic acid, responsible for the intrinsic pH sensitivity of the material.

The MOF reported by Zhou and co-workers,⁶³³ in contrast, features exceptional hydrolytic stability even in boiling water and in aqueous solutions with pH values from 1 to 11. The

framework composed on zirconium(IV) and *meso*-tetra(4-carboxyphenyl)porphyrin showed intrinsic NIR fluorescence from the metal-free porphyrin. Fluorescence increases in several steps ($pH 1-6.5$, $6.5-9$, $9-10$) corresponding to the formation of several forms of the porphyrin (dicationic, cationic, neutral and monoanionic). A similar MOF based on $Zr(IV)$ and *meso*-tetra(4-carboxyphenyl)porphyrin was reported by Deibert and Li.⁶³⁴ The authors reported high stability of the network in acidic media and distinct color change from purple to green at $pH \leq 2$ caused by protonation of the pyrrole nitrogens of the porphyrin. On the contrary, Lu and co-workers⁶³⁵ utilized deprotonation of the pyrrole nitrogens in a similar MOF prepared in the form of spherical particles (average size = 330 nm). The intensity of the red emission of the porphyrin increases from pH 9 to 11. Apart from the porphyrin, the MOF also incorporated magnetite nanoparticles and a rhodamine dye, which provided the MOF with magnetic properties and pH sensitivity in the range from 2 to 7, respectively. The main limitation of the porphyrin-based pH sensitive MOFs is potential interference from many metal ions that can be complexed by the metal-free porphyrin thus rendering the receptor pH insensitive.

Wu and co-workers⁶³⁶ described a stable MOF prepared from cadmium(II) and 5,5'-(ethane-1,2-diylbis(oxy))diisophthalic acid. It is stable both in highly acidic (pH 2.0) and highly alkaline (pH 12.2) solutions. Upon UV excitation ($\lambda = 310$ nm), the MOF showed emission band peaking at 350 nm and a shoulder at 410 nm. Fluorescence varies with pH values at <2 or >11. The use of Cd(II) ions makes such a sensor less attractive.

Xu and Yan⁶³⁷ prepared a MOF composed of Al³⁺ and 2-aminoterephthalic acid. Its blue fluorescence increases linearly from pH 4 to 7.5 by 25% and the response is reversible, but heavy metal ions interfere. Nonfluorescent Zr(IV) MOF nanoparticles (112 nm) were postmodified⁶³⁸ with the pH indicator fluorescein. The sensing properties of the pH sensor are similar to those of the dissolved dye. Its high brightness and efficient cellular uptake via endocytosis makes the MOF a promising tool for intracellular imaging of pH.

Nanoscale metal–organic layers were prepared and functionalized with a pH-sensitive fluorescein and an oxygen-sensitive ruthenium(II) bipyridyl complex linked to a hafnium(IV)-based framework to obtain a sensor material for ratiometric determination of both pH values and oxygen in live cells.⁶³⁹ Co-immobilized rhodamine B acts as a reference fluorophore.

In contrast to above MOFs, also a material with pH-dependent emission wavelength was reported.⁶⁴⁰ The MOF is prepared from carbazole based ligands and Zr₆-clusters. Upon excitation at 365 nm, the emission peak shifts linearly from ~420 to 600 nm when going from pH 1 to 8. The MOF degrades in aqueous solution with pH above 9. Interestingly, the pH sensitivity appears not to originate from the NH-group of the carbazole but rather from a conformational change in structurally flexible carbazole-based building block.

A smart approach was presented by Ding et al.⁶⁴¹ who described a light-harvesting MOF nanoprobe for ratiometric fluorescence-based determination of pH values and temperature. The zirconium(IV) derived MOFs are self-assembled and combined with pH-responsive polymers, the MOF acting as the energy donor and the pH-responsive polymer conjugated to fluorophores acting as energy acceptor. In the light-harvesting system, the chain lengths of the stimulus-responsive polymer vary when the local pH value changes. pH values can be sensed between 3 and 8 under 420 nm excitation and by ratioing the emission peaks at 645 and 530 nm. The nanoprobe was applied to image pH values in HeLa cells.

It can be summarized that despite some promising approaches that have been described, the so far known MOF pH probes can hardly compete with better sensing materials. Disadvantages include (i) short wavelength of excitation and emission, (ii) low brightness, (iii) comparably small signal changes, and (iv) poor hydrolytic stability. Some MOFs have been reported to be stable over a broad pH range, but these materials suffer from other drawbacks as mentioned above. It also is often difficult to explain the pH effects on the luminescent properties of MOF, which makes rational design of improved materials challenging.

7.2. Conjugated Polymers

Conjugated (conductive) polymers, such as polyanilines, are colored, and some display fluorescence. If they contain protonable functions (such as amino groups or nitrogen ring atoms), their spectra are pH-dependent. Such materials possess the dual functions of an indicator and a matrix. This can be advantageous due to simplicity of sensor manufacturing and lack of leaching.

Carey and Jorgensen⁵¹ were probably the first who applied conjugated polymers for optical pH sensing. Poly-(phenylquinoline), poly(biphenylquinoline) and poly-(phenylquinoxaline) (Figure 27) were shown to display pH-dependent fluorescence, depending on the polymer, in strongly acidic conditions (0.1–8.4 M HNO₃). The material was used to design fiber optic pH sensors.

Polyaniline (PANI; see Figure 27) is a widely used conjugated polymer that functions as both a solid support and a pH probe. It can be conveniently prepared via oxidative polymerization of aniline in acidic aqueous solution. M_n and M_w values of 22 000 and 74 000 g/mol have been reported,⁶⁴² but they are likely to vary significantly depending on the experimental conditions. PANI is an electrical conductor in the protonated state (Figure 27) and possesses strong NIR absorption (λ_{max} 840 nm)⁶⁸ that extends to beyond 1450 nm. The deprotonated form, in contrast, has an absorption maximum at 600 nm.⁶⁸ Polyaniline has multiple pK_a values. As a consequence, it responds to pH over a wide range (pH 2–12).^{55,68} Ge et al.⁵⁵ were probably the first who deposited polyaniline onto a fiber core directly by polymerization. The thickness of the layer was controlled via the coating time (15–60 min) and the concentration of monomer in solution. Multiple evanescent field absorption was realized to warrant efficient absorbance, which was monitored in the NIR.

Pringsheim et al.⁶⁸ utilized both visible and NIR absorption of various PANIs. The polymers were deposited on the inner wall of polystyrene cuvette. pH values were calculated from the ratio of absorbances at 600 and 840 nm. Unlike PANI, poly(2-bromoaniline), poly(3-chloroaniline), and poly(4-chloroaniline) are not sensitive to pH values between pH 1 and 12. Other conductive polymers possessed spectral properties similar to polyaniline but different pK_a values. For instance, the pK_a values for PANI, poly(2-toluidine), poly(3-toluidine), poly(*N*-methyltoluidine), and poly(diphenylamine) are 7.38, 7.23, 6.61, 5.42, and 10.5, respectively. The pK_a from polyanilines from copolymerization of aniline and *o*-phenylenediamine could be adjusted by changing the molar fraction of *o*-phenylenediamine.⁶⁴³ The films were electrochemically deposited, and their absorbance changed in the range from 400 to 1000 nm with two isosbestic points at 465 and 830 nm. The authors later⁶⁴⁴ also prepared fluorescent beads (360 nm i.d.) coated with PANI that respond to pH values between 5 and 11 via an inner filter effect.

De Paoli and co-workers explored the pH sensing properties of a similar polymer, poly(*o*-methoxyaniline) as a composite with *p*-toluene sulfonic acid and cellulose acetate.⁶⁴⁵ The stability of the composite was high, allowing measurements within 9 months (albeit with recalibration every 10 days), but various salts have a strong effect on the titration plots.

Another group⁶⁴² prepared sensing films by directly casting polyaniline and 10-camphorsulfonic acid from 1,1,1,3,3,3-hexafluoro-2-propanol. 1- μm thick films showed fast response ($t_{90} \sim 1$ s) and operated reversibly for more than 300 h (500 cycles) without noticeable leaching of the polymer. However, the titration curves showed very strong hysteresis (~1.5 units around the pK_a value) on going from pH 2 to pH 10 and back. It should be mentioned that many PANI sensors are slowly decomposed by air. They also are affected by ascorbic acid, ozone, hydrogen sulfide, and NO_x. This limits their applicability.

De Marcos and Wolfbeis investigated the pH sensing properties of polypyrrole.⁶⁴ A thin polymer film (<1 μm) was deposited on the inner walls of polystyrene cuvettes. Polypyrrole possesses broad absorption in the range 400–1100 nm with a minimum at around 550 nm and a maximum in NIR. An

increase of pH causes an increase of the absorbance between 600 and 900 nm and the shift of the absorption minimum from 600 to 500 nm. This corresponds to a color change from dark brown to green that can be observed visually. The pH dependence of the absorbance has sigmoidal shape (pH 5–12, $pK_a = 8.66$) and is attributed to presence of hydroxy groups attached to pyrrole rings in the polymer. The response of the sensor was rather fast (10–20 s) and the calibration independent of the buffer composition. Unfortunately, the response of the material is not reversible at high pH values.

Few fluorescent conjugated polymers are known for use in pH sensing. Wang and co-workers⁶⁴⁶ reported a copolymer of fluorene and thiophene (PFDA, Figure 27) modified with dopamine. The polymer has a strong blue fluorescence at low pH ($\lambda_{max} = 455$ nm). At higher pH, dopamine is converted into a quinone form due to its autooxidation and the fluorescence is quenched via intramolecular electron transfer from conjugated polymer to quinone. Obviously, such a sensor relies on adequate oxygen supply.

Several reported pH-sensitive fluorescent conjugated polymers incorporate pyridine as a pH-sensitive group. Kappaun et al.⁶⁴⁷ reported on an alternating oligomer ($M_n = 2300$ g/mol) of 9,9-dihexylfluorene and pyridine (PFIPy, Figure 27), which showed pH-dependent fluorescence (pH range from -0.2 to $+0.5$) in a solid film triggered by protonation of pyridine.

In a similar work, Adachi et al.⁶⁴⁸ demonstrated reversible modulation of the fluorescence properties of poly(*p*-pyridinium phenylene ethynylene) (PPyPE, Figure 27) by pH. Protonation of pyridine in acidic medium results in about 2-fold decrease of the blue fluorescence ($\lambda_{max} = 455$ nm), which is reversed upon addition of base. Unfortunately, only studies in a mixture of water and tetrahydrofuran were reported, so it remains unclear whether the material also works as a thin sensors film or in the form of nanoparticles. A conjugated hybrid polymer consisting of a polyfluorene-based conjugated backbone with thiophene units and carrying pyridyl moieties was reported to enable fluorometric sensing of pH value in the range from pH 4.8 to 13.⁶⁴⁹ The material was used to prepare sensor nanoparticles. If the pyridyl moieties are omitted, the fluorescence of the material is not affected by pH values.

Park and co-workers⁶⁵⁰ investigated the luminescence of poly(*N*-phenylmaleimides) (PPMI, Figure 27). Although not conjugated in the keto form, these polymers feature conjugated structures in the enol and enolate forms and are fluorescent, although the fluorescence is not very strong (QY of 5–11% depending on the solvent). A water-soluble block copolymer of PPMI and PEG showed ratiometric sensing capabilities in aqueous media (change from green to yellow fluorescence on going from pH 3 to 11) with fully reversible response. Importantly, the pH sensitivity was retained by incorporating the polymer into cross-linked polyethylene glycol diacrylate hydrogel.

In a different approach, Chan et al.⁶⁵⁰ prepared pH sensitive nanoparticles where a conductive polyphenylene-based polymer (PPE, Figure 27) was used as a fluorescent energy donor. pH functionality was introduced via a fluorescein moiety attached to the polystyrene backbone. Strictly spoken, this is not a conducting polymer with dual function, but a fluorescently doped conducting polymer. Both polymers were blended to obtain about 25 nm-large nanoparticles. Upon excitation with UV light, the conjugated polymer emits blue light ($\lambda_{max} \sim 430$ and 460 nm). The blue emission of the polymer is virtually pH-independent. On the other hand, the green emission of

fluorescein is significantly enhanced upon deprotonation and ratiometric read-out becomes possible depending on the efficiency of FRET.

The pH sensing materials based on conjugated polymers are summarized in Table S6.

In summary, the earlier research was mostly focused on investigation of absorptiometric response of polyanilines. Despite reversible response and stability in solution, the performance of these materials is compromised by strong hysteresis of the response, poor stability of the materials on air, and sensitivity of the polymers toward reductants or oxidants. On the other hand, fluorescent conjugated polymers provide significantly higher flexibility in design and properties with potential benefits of high brightness (polymer is a chromophore itself) and absence of leaching. Additionally, nonlinear properties of the conjugated polymers (high two photon absorption cross sections) are particularly attractive for application in microscopy. However, currently their performance is compromised by high hydrophobicity of the backbone, which retards proton diffusion. We envisage that synthesis of significantly more hydrophilic conjugated polymers with pH sensing functionality will represent a significant progress in the field of optical pH sensors.

7.3. Genetically Encoded Fluorescent Proteins

Genetically encoded fluorescent proteins (GFPs) proved to be essential tools for labeling of proteins, cells, tissues and whole organisms.^{651–659} GFPs can be rendered sensitive to different analytes such as metal ions, nitrogen oxide, reactive oxygen species and used for noninvasive imaging of these parameters in vivo.⁶⁵¹ Compared to molecular probes and nanoparticles, GFPs have the advantage that they do not require an invasive procedure in order to be introduced into the cell. In addition, they do not disturb cellular functions, do not leach and can be adjusted to various wavelengths. On the other hand, photostability of GFPs may be poor (in the same order of magnitude as of fluorescein).⁶⁶⁰ The most important class are green fluorescent protein (GFP) homologues. The “Phytofluors”, isolated from phytochrome proteins, form another class of such proteins. They display red and near-infrared fluorescence.⁶⁵⁷

Apart from the pH sensitivity intrinsic to most GFPs, several pH probes have rationally been developed that feature improved fluorescence. These GFPs fulfill the dual function of a pH indicator and a protein matrix. It protects the chromophore from undesired interferences. For intracellular measurements, the GFP probes represent a promising alternative to molecular probes and nanosensors (see section 8 for more details) and benefit from their intracellular expression and high biocompatibility. Similar to fluorophores, the major properties to be considered are spectral properties, brightness, photostability and cross-sensitivity to other parameters.⁶⁵¹ Some additional considerations are necessary to find a suitable GFP for given organism and cell type. The brightness of the sample depends on the kind of protein expression, folding efficiency, chromophore maturation rate and stability of the GFP to environmental parameters and aggregation.^{651,652} For the formation of the chromophore, the GFPs need to reach a near-native conformation.⁶⁵¹ Consequently, to increase the brightness, GFPs with high folding efficiencies were developed.⁶⁵¹ Depending on the targeted organelle, a GFP with a suitable pK_a for the prevailing pH has to be chosen. pH values can range from 4.5, in lysosomes, to around 8 in mitochondria.⁶⁶¹ Most cancer-active cells have pH values of <6 . These ranges are well

Table 5. Characteristics of Nanomaterials Used for pH Sensing

	size (nm)	photostability	modes	advantages	limitations
molecular probes	<1	– to +	A, F	commercial availability, no further modifications, cover a wide spectral range	undefined properties in complex biological environment
genetically encoded fluorescent proteins	~3	– to ~	F	biocompatible; can be used for intra- and extracellular measurements	long maturation times for some proteins
dendrimers	1–14	– to +	A, F	lower interferences compared to molecular probes	only partial protection from environment; high synthetic effort
quantum dots of type MeX	2–10	+	F	high brightness; often relatively long luminescence decay times and FLIM suitability	blinking; toxicity
upconversion nanomaterials	10–100	+	F	complete elimination of background fluorescence	2-wavelength ratiometry often possible; typically photoexcited at 880 or 980 nm
organic polymeric NPs	10–200	– to +	A, F	high versatility in materials, preparation methods, cell penetrating properties and size	robust methods for indicator immobilization are necessary to avoid leaching resulting in higher effort
silica NPs	3–200	– to +	A, F	high versatility in materials, preparation methods, cell penetrating properties and size	robust methods for indicator immobilization are necessary to avoid leaching resulting in higher effort
carbonaceous nanomaterials	3–15	+	F	simple preparation	mostly short-wavelength excitation; emission can depend on exc. wavelength, prone to interferences
polymeric micelles with conformational changes	3–50	– to +	A, F	also pH-insensitive dyes can be used	very narrow dynamic range; concentration dependence of micellar formation except for unimolecular micelles

covered by GEFPs with reported pK_a values ranging from 2.7⁶⁶² to 8.5.⁶⁶³

The pH sensitivity of most GEFPs relies on the deprotonation of a phenol moiety with a pK_a usually between 5.2 and 7.2. Some GEFP representatives, however, have amino acids in the local environment that buffer chromophore ionization and therefore render them unsuitable for pH sensing.⁶⁶⁴ The emissive properties of the undissociated phenol group determine whether GEFP representatives can be used for ratiometric sensing. There is a large number of GEFPs that display only poor emission from the neutral chromophore. As intracellular pH calibration is impractical and the amount of chromophore is unknown, absolute pH values cannot be determined with GEFPs relying solely on fluorescence intensity measurements. These GEFPs are therefore limited to reporting temporal changes of pH.

Ratiometric GEFP probes, in contrast, do not require the knowledge of their concentration for pH values to be measured. Both ratiometric excitation and emission probes have been reported for GEFPs. For example, “pHlourin” displays excitation peaks at 395 and 475 nm for the protonated and deprotonated forms, respectively, and green emission for both forms at 508 nm.⁶⁶⁵ Analogously, the long-wavelength probe “pHRed” emits at 610 nm after excitation at 440 and 585 nm of the deprotonated and protonated forms, respectively.⁶⁶⁶ “deGFP” family represents ratiometric emission probes. The pK_a values range from 6.8 to 8.0 and the proteins show a shift in emission wavelength from 460 to 515 nm upon excitation at 400 nm when going from low to high pH.⁶⁶⁷

The fusion of two GEFP variants having different pH sensitivities is another approach for design of ratiometric GEFP probes. For instance, pH sensitive mutants EGFP and EYFP were separately fused to form GFPuv.⁶⁶⁸ For both variants, dual excitation mode ratiometric sensing was possible, and for one of them also pH dependent FRET was observed. Analogously, the fusion of yellow fluorescent protein (YFP) acceptor variants with enhanced cyan fluorescent protein (ECFP) was used to create a family of FRET-based GEFPs for pH sensing, the “pHlameleons”.⁶⁶⁹ Contrary to development of other GEFPs used as pH indicators where mutagenesis is necessary, these ratiometric probes can be constructed by

ligation of two literature-known GEFPs with known pH dependent characteristics.

The first GEFP probes were based on the use of green fluorescent protein. Given its success, large progress in design and optimization of red and far-red emitting proteins was achieved.^{656,657} These are even better suitable for intracellular imaging due to efficient elimination of (shortwave) autofluorescence, deeper light penetration and reduced phototoxicity. For example, Tantama and co-workers⁶⁶⁶ designed a ratiometric probe for intracellular pH imaging (called “pHRed”) featuring fluorescence peaking at 610 nm and two excitation peaks at 440 and 585 nm for deprotonated and protonated forms, respectively. Another red fluorescent protein (“pHuji”), reported by Shen et al.,⁶⁷⁰ combined attractive spectral properties ($\lambda_{exc} = 566$ nm, $\lambda_{em} = 598$ nm), large fluorescence change between pH 5.5 to 7.5 (22× enhancement of fluorescence) and a sigmoidal calibration curve.

The use of GEFPs with efficient two photon absorption enables even deeper light penetrations and superior signal-overbackground levels. The determined two-photon absorption cross section for various GEFPs vary significantly, but values in the range from 180 to 600 000 Goeppert–Mayer units indicate efficient two-photon absorption despite all controversies.⁶⁷¹ Especially, the probes, deGFP4 and E2GFP, appear to be promising candidates for two-photon fluorescence-based pH-measurement.^{664,667}

8. NANOMATERIALS

8.1. Nanoparticle-Based Sensing of pH Values

Nanoparticle-based sensor materials, commonly referred to as “nanosensors”, represent a comparably new optical sensors format. The definition of a nanosensor is analogous to that of a chemical sensor, with the restriction that its dimensions are supposed to be smaller than 1 μm ⁶⁷² or—in another definition—than 100 nm.⁶⁷³ With increasing size, materials or their aggregates cause increasing light scattering as the intensity of scattering (Rayleigh scattering) scales with the power of sixth of the particle diameter. Table 5 summarizes the different dimensions and characteristics of dyes, fluorescent proteins, and nanomaterials.

Table 6. Nanosensors Based on Dendrimers or Biomolecular Conjugates

class	material	comment	ref	
dendrimers	PAMAM	pH-dependent intrinsic fluorescence	709–711	
	PAMAM–1,8-naphthalimide	PET-based, metal ion cross sensitivity	712–717	
	acetyl-capped G5 PAMAM–SNARF 2 and boronate-caged peroxyfluor-1	dual imaging of pH and H ₂ O ₂	707	
	PAMAM–2 1,8-naphthalimide dyes	light harvesting, PET-based	718	
	PAMAM–1,8-naphthalimide dyes	PET from dendrimer to dye, light harvesting	719–722	
	PAMAM–perylene diimide	PET from dendrimer to dye, metal ion cross sensitivity	723	
	PAMAM–7-hydroxy-4-methyl-3-coumarinylacetic acid, 5(6)-carboxyfluorescein, Oregon green 488	specific subcellular localization	724	
	poly(propyleneamine)–methyl orange	G0 and G1 properties similar to dye	725	
	polyglutamic dendritic porphyrins	ratiometric, pK _a changes with generation number	726	
	tetraaryltetracyclohexenoporphyrrins with 8 Newkome-type dendrons and PEGylated periphery	pK _a in physiological range, no effect of ionic strength	727	
	biomolecular conjugate	bovine serum albumin NPs–ref dye	BSA NPs pH sensitive, ratiometric	728
		bovine serum albumin–energy transfer cassette	temperature dependent localization in cell	729
		DNA–gold NPs	absorption, pH-dep. conformational change	730
fluorescein–DNA–gold NPs		for pH monitoring during application of nanomaterial-based therapeutics, ratio metrically	731	
elastin-like recombinamers and gold NPs		absorption, pH-dep. conformational change	732	
DNA–Alexa-488 and 647		pH-dep. conformational change, FRET based	733	
oligonucleotides, gold NP–dyes		FRET based	734	
DNA–dye, graphene oxide		pH-dep. conformational change and quenching	735	
protein–naphthalimide		pH-dep. conformational change, solvatochromic dye	736	
bacteriophage–cyanine dyes		ratiometric, NIR, imaging	737	
bacteriophage–fluorescein, rhodamine		ratiometric, NIR, imaging	738	
bacteriophage–fluorescein, rhodamine		FRET-based	739	

Nanomaterials and respective sensors can be subdivided into three groups, namely, 1D nanomaterials (nanowires) 2D nanomaterials (nanosheets), and 3D nanomaterials (spherical dots). There has been enormous progress in this field, which is highlighted in several reviews;^{672–702} regarding pH sensing, there is a book section with an extensive review on nanomaterials for intracellular pH sensing and imaging.⁵ Due to their small size, nanosensors are suitable for measurements in small samples, most prominently cells and in tissue cells. This is hardly possible with other sensors. The small dimensions also decrease diffusion pathways of analytes to the “indicator chemistry”. Therefore, they have virtually instantaneous response and qualify for investigation of fast processes.

Molecular probes also feature similar characteristics but they are more prone to various interferences caused by nonspecific binding and effects of the environment. On the other hand, their broad commercial availability, versatility of properties and broad accumulated knowledge on selectivity, cell delivery and distribution, and toxicity, currently make them tools of choice in most biological studies. In situ calibration of such probes enables correction for many interferences.

The matrix in nanosensors fulfills a protective function and improves the robustness of the nanosensors. For instance, the pH response of the nanosensors in the absence and in the presence of proteins is often very similar.⁴³⁶ This is in distinct contrast to molecular probes. Nanosensors, therefore, are more easily calibrated. From another perspective, the matrix protects the cellular environment from direct contact with potentially cytotoxic dyes. Nanosensors with incorporated reference dyes simplify referenced sensing. Yet, leaching and photobleaching effects should be kept in mind for these materials.

The potential of nanosensors has been recognized several decades ago by Lübbbers and co-workers who were probably the first to encapsulate a pH indicator in nanobeads.³¹ The pH-

probe β -methyl-umbelliferone (7-hydroxy-4-methylcoumarin) was embedded into polyacrylamide beads obtained via polymerization of the monomer initiated by γ -irradiation. The nanoparticles (150–200 nm) showed response to pH in the range of 6–8. Kopelman and co-workers later described so-called PEBBLES (probes encapsulated by biologically localized embedding), that is, nanosensors for various parameters including pO₂, Ca²⁺, pH, etc.^{427,433}

Nano- and microparticles have also been used to design optodes of other formats (planar optodes or fiber optic sensors) by dispersing them in proton-permeable hydrogels or in micrometer-sized beads. Also, more than one kind of nanoparticles can be used. This approach allows for simple adjustment of the sensor composition and is particularly useful for preparation of referenced sensors^{126,145,152,438} (section 2.11) and multiparameter sensors^{381,384,441} (section 10.7). In contrast to the situation where all the emitters are dissolved in a single matrix, application of micro- and nanoparticles allows for separation of components and, therefore, minimization or elimination of undesired effect, such as FRET, luminescence quenching, decreased photostability due to formation of reactive oxygen species etc. For each indicator dye or intended purpose, an appropriate matrix can be chosen.^{127,145,425} Considering the rather large number of pH nanosensors reported and their good characteristics, it is rather surprising that their potential has been so scarcely explored for manufacturing of optodes.

Most pH nanosensors have been designed for intra- and extracellular pH imaging. However, other applications of pH nanosensors such as pH sensing in microfluidic devices are gaining popularity.⁷⁰³ For intracellular measurements, particles have to be placed in cells. Methods for delivery include injection with a gene gun, a pico-injector or cell delivery with the help of liposomes have their advantages and disadvantages.⁴³³ Nowadays, most of pH nanosensors can be incorporated into cells via

Table 7. Examples of Nanosensors Based on Silica Particles

class	material	comment	ref
silica particles	Stöber, naphthalimide, and sulforhodamine B	core-shell NPs, ratiometric	471
	rhodamine B isothiocyanate	mechanism of pH sensitivity remains unclear	743
	microemulsion, FITC and Ru(bipy) ₃ ²⁺	ratiometric imaging	744, 745
	microemulsion, FITC and Ru(phen) ₃ ²⁺	core shell, ratiometric imaging	746
	HPTS-polyelectrolyte-SiNPs, rhodamine B SiNPs	raspberry-like assembly of the two SiNPs	747
	poly(ethylene glycol) or hyaluronic acid coated SiNPs	increase of colloidal stability	748
	zeolite core, silica shell, Stöber, fluorescein	ratiometric	436
	ormosil NPs, naphthalenylvinylpyridine	two-photon active	526
	spirohodamineamide	different particle architectures investigated	459
	core-shell SiNPs, acridine orange	linear calibration	749
	core-shell SiNPs, reverse microemulsion; HPTS	indicator physically entrapped in the shell; works in the pH range from 5.5 to 9.0	750
	modified Stöber, fluorescein, tetramethylrhodamine	core-shell NPs, ratiometric imaging	751
	imidazolium salicylaldehyde ionic liquid Schiff base immobilized on SiNPs	60-fold intensity increase as the pH value increases from 5 to 11; method also applied to the determination of ammonia	752
mesoporous silica nanoparticles	fluorescein and rhodamine B	charge neither affected pH response nor cellular uptake, but localization	753
	fluorescein and rhodamine B	FRET-based	618
	fluorescein and Texas red	cell permeable	754
	hollow MSiNPs	extended pH range	755
	MSiNPs pores blocked by polyethylenimine	targeting mitochondria	756

natural uptake (endocytosis), which is facilitated by the presence of positively charged groups on the surface of the nanoparticle. However, positively charged particles often are more cytotoxic than negatively charged ones, which in turn are more cytotoxic than neutral ones.^{681,704} Positive charges are more likely to enhance membrane disruption, while anionic charges are more likely to enhance apoptosis.⁷⁰⁴ Fortunately for cancer research, nanoparticles tend to preferentially accumulate in tumor tissues due to the enhanced permeability and retention effect (EPR) and the poor lymphatic drainage of tumors.^{692,705}

In all cases, aqueous dispersibility of nanosensors is essential. This is usually enabled by introducing charged or uncharged but polar groups on the surface of nanoparticles. Depending on the kind of charged groups present on a surface (examples being carboxy groups or protonated amino groups), the surface charge will be affected by the actual pH value. Consequently, these groups may also have a varying buffering effect and thus perturb pH measurements.

8.2. Dendrimers and Biomolecular Conjugates

Dendrimers are highly branched and mostly symmetrical molecules that are built up via branched monomers from a central multifunctional core. Their size and composition can be systematically varied to tailor the properties. Starting from the core, the number of branching points to the surface defines its generation. Typically, dendrimers with only a few generations can be obtained in a highly monodispersed form; for higher generations, purification is impeded by the similarity of the desired dendrimers and small-defect byproducts.⁷⁰⁶ Most dendrimers are based on the use of polyamidoamines (PAMAMs), and less so of polyimines, polypeptides, polyethers, or polyesters. In dendrimers for optical sensing, the indicator dye core is protected from its environment by the oligomeric/polymeric shell, which is assembled around the chromophore. Alternatively, the indicator dye can be coupled to the surface. Peripheral coupling is chosen when high indicator concentrations without aggregation are desired or when multiple dyes are to be coupled.⁷⁰⁷ Because of the small distances involved,

FRET may occur, especially when using high dye concentrations or dyes with overlapping absorption/emission spectra. From another perspective, dendrimers are useful structures for designing FRET-based systems. Apart from application as self-contained tools for sensing, dendrimers have also been used in composite materials to prevent dye leaching from a sol-gel matrix after physical entrapment.⁷⁰⁸

Another way to generate water-soluble pH sensitive nanoprobes is to couple a pH probe to an oligonucleotide, protein or even viruses. The biomolecule serves to protect the pH probe against its environment and can be used for targeting. Biomolecules can also change their conformation depending on the pH. These changes can be used to modulate the environment of probes based on FRET, quenching or polarity. Table 6 summarizes nanosensors based on dendrimers or biomolecular conjugates.

In the above examples, coupling of an indicator to the surface of biomolecules or dendrimers not always results in strong protection from environmental influence, which may affect the pK_a or photophysical properties. Consequently, for these materials the distinction between sensors and probes is blurred. However, conjugation can significantly improve the applicability of such materials compared to molecular probes as it allows targeting and, analogously to that of the bulk optodes, prevents/minimizes leaching and enables referenced sensing by cocoupling of a pH-insensitive dye.

8.3. Silica Nanoparticles

Silica-based nanoparticles are chemically inert, photostable and thermally stable materials that do not swell when dispersed in water. Due to their surface silanol groups, they are intrinsically hydrophilic and surface modification is straightforward. Generally, dispersibility in water is good but bivalent ions may cause aggregation. The nanomaterials are reported to be biocompatible and are hardly attacked by bacteria. Several reviews illustrate their importance in bioapplications.^{689–693,740,741} Two main approaches are mainly used for

Table 8. Overview of Nanosensors Based on Polymeric Particles

class	material	comment	ref
hydrophilic polymers	polyacrylamide, various fluorescein derivatives	ratiometric, leaching	427
	polyacrylamide, HPTS	two photon excitation	759
	polyacrylamide, fluorescein, rhodamine B	ratiometric, less leaching	616
	polyacrylamide, hyaluronic acid on surface	improved endocytosis	760
	polyacrylamide, fluorescein, Oregon green, rhodamine	extended dynamic range	761
	polyacrylamide, pH indicators Oregon green, Oregon green 488 and fluorescein, pH-insensitive reference fluorophore Alexa 568	analytical range from pH 1.4 to 7.0; spontaneously internalized by HeLa cells, localize at the lysosomes	762
	polyacrylamide, Oregon green fluorescein, rhodamine B	extended dynamic range	763–766
	hydrogel, fluorescein, magnetic particles	miniemulsion solvent evaporation method, magnetic	767
	polyurethane, bromothymol blue, Nile red, coumarin 6	FRET-based	768
	Eudragit RL-100, 1,4-diketopyrrolo-[3,4- <i>c</i>]-pyrroles, Macrolex yellow	ratiometric, imaging	511
	Eudragit RL-100, perylene bisimide	FLIM	482
	Eudragit RL-100, triangulenium dyes	homo-FRET, FLIM	524
	hyperbranched polymer composed of polylactide and PEG, 2 naphthalimide dyes	accumulate in acidic organelles, imaging	769
	hydrophobic polymers	amino modified cross-linked polystyrene, FITC, diphenylanthracene	ratiometric
amino modified cross-linked polystyrene, fluorescein		2 μm particles, yet cellular uptake	415
methyl methacrylate, 2-aminoethyl methacrylate copolymer, 1,8-naphthalimide, fluorescein		FRET-based, localized in the lysosomes	770
polyacrylonitrile, fluorescein, Ru(dpp)		DLR-based, Ru dye temperature sensitive	126
core–shell nanoparticles	PVC, chromoionophore I	absorptiometric and fluorometric	771
	poly(phenylene-1,4-ethynylene), fluorescein	semiconductor polymer dots, FRET-based	620
	polystyrene core, poly(acrylic acid) shell, naphthalene diimide	conjugated to rapid cell-penetrating peptides (HIV-1 TAT) to increase cell-penetration	772
	poly(<i>N,N</i> -dimethylaminopropylacrylamide) core, poly(acrylamide) shell, naphthalimide, rhodamine	ratiometric	773
	polyaniline shell, polystyrene core, dye	pH-dep. polyaniline absorption modulates fluorescence of dye	644
	poly(styrene- <i>block</i> -vinylpyrrolidone), fluorescein derivatives and HPTS	selective staining of core/shell via swelling method	382, 390
	poly(styrene- <i>block</i> -vinylpyrrolidone), porphyrin, aza-BODIPY	simultaneous measurement of oxygen and pH, DLR-based	703
	poly(<i>N</i> -isopropylacrylamide) shell, polystyrene core, 1,8-naphthalimide, ref dye	ratiometric	774
	hollow polymer microcapsules filled with SNARF-1-dextran-conjugates	cellular uptake	775
	poly(2-(methacryloyloxy) ethyl phosphorylcholine- <i>block</i> -2-(diisopropylamino) ethyl methacrylate), Nile blue-based dyes	rapid cellular uptake, absorptiometric	776
	copolymer of poly(methyl methacrylate) and poly(methacrylic acid), 1,8-naphthalimide, rhodamine	FRET-based	777
	triblock copolymer, coumarin, Oregon green 488, 2',7'-bis(2-carboxyethyl)-5-(and-6) carboxyfluorescein, Alexa 633	ratiometric	778
	micelles from poly(vinylpyridine) and poly(vinylphenol) containing polymers, fluorescein, tris(dibenzoylmethanato)europium(III)	cellular uptake	779
	copolymer from poly(<i>ε</i> -caprolactone) and poly(oligo(ethylene glycol) methacrylate) with positively charged ammonium groups on the surface; fluorescein, PtTFPP	dual nanoprobe, intracellular imaging	780
via coprecipitation from polystyrene amino-terminated polystyrene, poly(styrene- <i>co</i> -maleic anhydride) and poly- <i>L</i> -lysine; FITC, PtTFPP	ratiometric, intracellular imaging	781	
liposomes, micelles and emulsions	polypeptide micelles, fluorescein and <i>N</i> -(rhodamine B) lactam	complex pH response, FRET, self-quenching involved	782
	nanoemulsions from perfluoropolyethers, Pluronic F68, polyethylenimine, cyanine dyes	also possible ^{19}F MRI application	783
	liposomes from dimyristoylphosphatidylcholine, cholesterol, dihexadecyl phosphate, fluorescein	no leaching	784
cellulose and dextran	phospholipid coated polystyrene particles, fluorescein, tetramethylrhodamine	micrometer-sized	785
	cellulose nanocrystals, fluorescein, Oregon green, rhodamine	two labeling strategies investigated	411
	cellulose nanocrystals, fluorescein	spacer used to prevent quenching	786
	aminocellulose particles, fluorescein isothiocyanate, Ru(dpp)-PAN	in bulk optodes, imaging	145, 425, 49, 127
	dextran-propionate, fluorescein, sulforhodamine B	nontoxic, incorporated into cells without any additional agent	439, 787, 788

their preparation: the *Stöber process* and *reverse microemulsion techniques*.

Silica-based nanosensors can be illustrated by the work of Burns et al.⁴⁰⁴ who prepared core–shell nanoparticles

composed of a silica core (\varnothing 50 nm) doped with a tetramethylrhodamine dye and a silica shell doped with fluorescein. Both dyes were covalently integrated into the matrix by first reacting the respective isothiocyanates with the

aminopropyltriethoxysilane and subsequent hydrolysis together with TEOS. The aqueous particle suspension (\varnothing 70 nm) was stable against flocculation and leaching of the dyes for several months. The particles penetrated rat basophilic leukemia mast cells in the presence of phorbol-12,13-dibutyrate (which is used to increase endocytotic activity) and allowed ratiometric imaging of pH ($\lambda_{\text{max}} = 525$ and 575 nm for the pH indicator and reference, respectively).

The mesoporous silica NPs are another type of silica-based nanomaterials.⁷⁴² The mesoporous structures exhibit large surface areas and can be heavily loaded with dyes. Several groups have described such nanosensors by incorporating both a fluorescein and a reference dye (in most cases a rhodamine) into mesoporous SiNPs.

pH nanosensors based on silica particles are summarized in Table 7 and more details on their properties are provided in Table S7.

8.4. Organic Polymer Particles

Nanosensor-based on polymeric materials are commonly obtained via emulsion polymerization of the respective monomers (most prominently acrylamide) with a cross-linker and dyes (pH indicator and a reference). Indicator dyes can be immobilized in nanomaterials by physical entrapment or by covalent coupling. For nanomaterials, however, there can be additional limitations to consider. Contrary to the bulk optodes, nanomaterials are generally required to be dispersible in water. Dispersibility is provided by polar polymers or polar groups on the particle surface. Excess reactive groups can make the nanomaterials more prone to aggregation.⁶⁷⁵ Physical entrapment of the indicator and the reference dye is often a method of choice because of its simplicity and reproducibility. Noncovalent dyeing procedures include entrapment during the polymerization process, dyeing after swelling of polymeric beads and coprecipitation. The first method is equally suitable for covalent immobilization of indicators providing that they possess necessary functional groups. For dyeing via swelling, the polymeric nanoparticles are swollen in a mixture of organic solvent and water, which is also a solvent for the dyes. The dye must be water-insoluble to prevent leaching. The indicator dye is then “forced” into the polymer by slowly evaporating the swelling solvent or removing it by dialysis. Among suitable materials, poly(styrene-*block*-vinylpyrrolidone) beads allow straightforward staining and even enable selective dyeing of the core or the shell of the core-shell structured beads.^{382,390}

Hydrophobic pH indicators can also be incorporated into polymeric nanoparticles from solution via nanoprecipitation.⁷⁵⁷ The formation of the nanoparticles relies on the use of two miscible solvents. The polymer and the dye are dissolved in a suitable (organic) solvent and then coprecipitated by addition of the second solvent (water) in which they are insoluble. Afterward, the “good” solvent is removed by evaporation or dialysis. Nanoprecipitation was successfully used to prepare nanoparticles from polymers, such as poly(styrene-*co*-maleic anhydride), poly(methyl methacrylate-*co*-methacrylic acid), RL-100, RS-100, ethylcellulose, poly(vinylidene chloride-*co*-acrylonitrile), polysulfone, hydrogel D4 and D7, Hydrothan H15, PHEMA, cellulose acetate butyrate, and Nafion.⁷⁵⁷

8.4.1. Hydrophilic Polymers. Nanosensors based on hydrophilic polymers generally show high water uptake and are, in essence, hydrogels. Therefore, they are often referred to as *nanogels*. Kopelman and co-workers coined the term PEBBLEs (probes encapsulated by biologically localized embedding) for

nanosensors designed for measurement inside single living cells.^{427,687,758} Allowing the application of well-known indicator dyes, the polymeric embedding protects the dyes from interferences from cellular environment and is supposed to reduce potential toxicity of the dye in the cell. Similar to that of bulk optodes, it also simplifies realization of complex sensing schemes and ratiometric imaging.⁶⁸⁷ PEBBLEs for pH measurement have been prepared mainly from cross-linked polyacrylamide using a water-in-oil microemulsion polymerization technique.

8.4.2. Hydrophobic Polymers. Hydrophobic polymers also are suitable for preparation of pH nanosensors provided that the indicators are attached to the surface of the particles. Due to moderate protection of the indicator the environmental influence is stronger than for the materials containing the dyes incorporated into the bulk of the nanoparticles. In this concept, a reference dye is typically embedded into the bulk of the nanoparticle to minimize environmental effects.

8.4.3. Core-Shell Nanoparticles. Core-shell nanoparticles allow separation of dyes for referencing or multiparameter analysis. The separation can be used to prevent the interaction of dyes or to have each dye immobilized in an appropriate matrix.

pH nanosensors based on polymeric particles are summarized in Table 8. Details on spectral and sensing properties of some representatives of polymeric nanosensors can be found in Table S7.

8.5. Quantum Dots

Semiconductor quantum dots represent promising emitters for biological applications.^{789–797} Traditional quantum dots are nanometer-sized crystals made from metal chalcogenide semiconductors. Their luminescent properties originate from their nanoscale dimensions that induce the “quantum confinement effect”. The consequences are that a variation of the size of the quantum dot controls the energy levels and hence the absorption and emission wavelengths. Correspondingly, the absorption and emission wavelengths can be tuned by variation of size. The QDs are characterized by broad absorption spectra and narrow emission peaks, an exceptionally high brightness, photostability, absence of swelling and longer luminescence lifetimes compared to organic, fluorescent dyes. For instance, the decay time of CdZnS QDs is as long as 1 μs .⁷⁹⁸ Their long lifetimes can be very useful for discrimination of the signal from fluorescence background. Because of the broad absorption spectra, a single excitation wavelength can be used to excite QD with various different emissions. Photostability is generally considered good but can be further improved by using core-shell QDs. Importantly, core-shell architectures also increase quantum yields. The cytotoxicity of QDs is a complex issue and has been the subject of considerable debate.^{790,792} General considerations include the leakage of toxic metal ions into the sample, however, mechanisms of toxicity can vary and are not always clear. It was proposed that toxicity can also arise from polymer coating on the surface of the QD resulting in precipitation on the cell surface.⁷⁹⁹ Surface coating and size are crucial parameters determining cellular uptake but also breakdown of QDs. Concerning the downsides, QDs display fluorescence intermittency, blinking of the single quantum dots. In contrast, dye-doped nanoparticles comprise multiple dye molecules that absorb and emit independently. Therefore, polymeric or silica particles do not display blinking. The “off” states during blinking can be as long as 100 s for some QDs.⁸⁰⁰ However, the blinking is by some regarded as a mean to ensure

Table 9. Overview of Nanosensors Based on Quantum Dots^a

material	sensing mechanism	comments	ref
CdSe/ZnS	deprotonation of COOH groups on the surface	decay time sensing ($\tau = 8.7\text{--}15.5$ ns)	801
Cu-doped CdZnS	deprotonation of COOH groups on the surface	tunable emission, decay time sensing ($\tau = 200\text{--}900$ ns)	798
CdSe/ZnS	deprotonation of COOH groups on the surface	intensity measurement, pH range 4–12, smartphone-based read-out	812
CdSe/ZnS	quenching via hole transfer to phenol, no quenching for phenolate	intensity measurement, decay time measurement ($\tau = 0.65\text{--}4.86$ ns)	804
CdSe/ZnS	quenching via hole transfer to amine, no quenching for protonated amine	intensity measurement, decay time measurement ($\tau = 12.32\text{--}33.74$ ns)	805
CdSe/ZnS	pH-dependent quenching from oxidized dopamine	ratiometric 2- λ sensing	813
CdSe/ZnS + squaraine	FRET from QD to the pH indicator	ratiometric 2- λ sensing	806
CdSe/CdZnS + SNARF	FRET from QD to the pH indicator	ratiometric 2- λ sensing, identical pH response under two-photon excitation	807
CdSe/ZnS + pyrene	FRET from pyrene to QD; polymeric linker undergoes swelling upon protonation	ratiometric 2- λ sensing	807
CdSe/CdZnS + fluorescein	FRET from pH indicator to QD	ratiometric 2- λ sensing	811
CdZnSe/CdZnS/ZnS + fluorescein	FRET from QD to the pH indicator	ratiometric 2- λ sensing	814
CdSe/ZnSe + naphthofluorescein	FRET from QD to the pH indicator	ratiometric 2- λ sensing	815
CdTeSe/ZnS + cyanine dye	FRET from QD to the pH indicator	decay time sensing ($\tau = 12\text{--}29$ ns)	808
mercaptoacetic acid capped CdSe/ZnSe/ZnS	deprotonation of COOH groups on the surface	intensity measurement, loss of surface capping at low pH, resulting in aggregation	816
QD ITK + mOrange ^b	FRET from QD to pH sensitive GEFP	ratiometric 2- λ sensing	660
black phosphorus QDs	protonation and deprotonation of hydroxyl groups causes a different degree of quenching	particle size 5.2 nm; pH range of 1.0–9.0	817

^aA more detailed version of the table can be found in the Table S8. ^bCommercially available QDs.

the observation of a single dot event, for example, observation of a single protein.⁷⁸⁹ Without modification, QDs are poorly soluble, susceptible to quenching, unstable in dispersions and are not intrinsically pH sensitive. Additional modification is necessary for them to overcome these limitations and be useful as pH nanoprobess. QDs can show pH sensitivity due to carboxylic groups on their surface (Table 9).^{798,801,802} The changes in fluorescence intensity are accompanied by modulation of fluorescence decay time of the QDs (see section 10.2 for more details). Analogously, luminescence modulation because of deprotonation of surface defects was observed for Ti₃C₂ QDs.⁸⁰³ This material was modified with a Ru(II) complex to obtain ratiometric response but unfortunately required UV excitation.

Semiconductor QDs can also be rendered pH sensitive via coupling of a sensitive group acting as a hole trapper. Wang and co-workers demonstrated that *p*-mercaptophenol⁸⁰⁴ and *p*-aminothiophenol⁸⁰⁵ coupled to CdSe/ZnS induce fluorescence quenching of the QDs in acidic conditions.

FRET represents another possibility to prepare a pH responsive system using intrinsically pH-insensitive QDs (Table 9). Feasibility of the approach was demonstrated by Nocera and co-workers who covalently bound a pH sensitive squaraine dye⁸⁰⁶ or SNARF⁸⁰⁷ to the surface of CdSe/CdZnS QD. Tang et al.⁸⁰⁸ utilized FRET from NIR emitting CdTeSe/ZnS QD to a cyanine dye, which shows NIR absorption. Remarkable feature of the presented nanosensor is strong response of the fluorescence decay time of the QD ($\tau = 29$ ns at pH > 7 and 12 ns at pH < 5). Dennis et al.⁶⁶⁰ used pH sensitive fluorescent proteins as FRET acceptors instead of organic dyes.

In contrast to above sensors utilizing QDs as energy donors, Kim and co-workers explored FRET from pyrene dye to CdSe/ZnS QD, acting as energy acceptor.⁸⁰⁹

Several researchers utilized fluorescent pH indicators as energy donors for QDs. The luminescence of the QD can be

modulated to a certain extent (for instance if the emission of the donor is “switched off”) and observed ratiometric response can be due to combination of direct excitation of the QD and excitation via FRET from organic dye. Examples include naphthalimide⁸¹⁰ and fluorescein⁸¹¹ coupled to CdSe/ZnS QDs.

8.6. Carbon-Based Nanomaterials

8.6.1. Carbon Dots. Carbon dots (CDs) and graphite oxide nanoparticles (Table 10) feature water solubility/dispersibility, chemical inertness, straightforward surface chemistry, high photostability, and high two-photon absorption cross sections. The luminescence of carbon dots is susceptible to PET quenching making ion sensing possible in principle.⁸¹⁸ Because of the low cytotoxicity, intracellular pH-imaging represents one of the major applications.^{819–827}

Dually emitting carbon dots were shown⁸²⁸ to be viable probes for ratiometric fluorometric sensing of pH values, mercury(II), chloride and chromate. The ratio of fluorescence emissions at 565 and 410 nm strongly depends on the pH value in the range from 4.5–6.5 and 10.0–13.0, respectively. Obviously, the other ions interfere in determination of pH. Green fluorescent carbon dots, probably being doped with nitrogen, also were shown to enable determination and imaging of pH values in in SMMC-7721 cells.⁸²⁹ The dots were prepared from *m*-phenylenediamine, have a 36% quantum yield, an average size of 2.3 nm, excitation/emission peaks at 450/510 nm, and work in the pH range from 6.0 to 10.0.

Carbon dots also found application in pH monitoring of complex 3D cell culture scaffolds in microfluidics, because of their biocompatibility.⁸³⁰ The downsides include low QY and absorption in the UV with only a tail in the VIS region. Absorption can be shifted to longer wavelengths via surface modification. CDs can be obtained via different techniques but hydrothermal synthesis probably represents the most convenient method. The photophysical properties largely depend on

Table 10. Overview of Nanosensors Based on Carbonaceous Materials

material	preparation method	comment	ref
carbon dots	various	a review on CDs for use in pH sensing	851
	hydrothermal method from <i>Agaricus bisporus</i>	in microgels to monitor 3D cell culture scaffolds	820, 830
	from polyethylenimine	pH range 2–12, cellular uptake	819
	from flower (carnation)	pH range 3–12, absorptiometric and fluorometric	821
	from chloroform and diethylamine	coupled to fluorescein, CD as reference	822
	hydrothermal method from β -resorcylic acid and ethylenediamine	linear pH range 3.8–6.2	852
nitrogen- and chloride-doped CD	from urea in choline chloride–glycerine deep eutectic solvent	pH range 5–10, virtually no effect of ionic strength	823
	hydrothermal method from mushrooms	pH range 2–13, linear range 4–8, quenched by hemin	824
	hydrothermal method from ascorbic acid	intensity decrease 10-fold (pH 4–8) emission shift from 441 to 550 nm (pH 2–12)	853
	thermal decomposition of ascorbic acid in DMSO in microfluidic system	absorptiometric, fluorometric, upconversion	825
	hydrothermal method from <i>p</i> -phenylenediamine	excitation-independent emission at 590 nm	826
	from glucose and edible oil	linear range pH 3–13	827
	hydrothermal method from citric acid and dicyandiamide or aniline hydrochloride	high quantum yields 37% 63%	854 855
	hydrothermal method from citric acid and basic fuchsin	dual emission with different pH-dependent behavior allowing ratiometric measurement	856
	hydrothermal method from citric acid and L-serine or monoethanolamine	linear range pH 1.5–7.5	857
CDs doped with Eu(III), Tb(III) and a chelating ligand	from PEG 400	excitation/emission wavelengths of 272/545 (Tb) and 272/614 nm (Eu); effects are due to pH-induced variations in energy transfer; applied to visualize pH values in breast adenocarcinoma, pH 3–10	859
	from aspartic acid and urea	pH range 1–13, sensitive toward oxidation	860
nitrogen and oxygen-rich CD	hydrothermal method from <i>o</i> -phenylenediamine PEG, oxalic acid	dual emission, ratiometric, linear range pH 2.2–4.0	861
	from aminophenylboronic acid	dual emission with different pH-dependent behavior allowing ratiometric measurement	862
nitrogen- and boron-doped CD	hydrothermal method from EDTA and (Eu(NO ₃) ₃ ·6H ₂ O)	ratiometric response to pH from pH 2–10	863
N- and P-doped CD	CD treated with diammonium phosphate	dual emission with different pH-dependent behavior allowing ratiometric measurement, linear range 2–12	864
B- and P-doped CD	CD treated with H ₃ BO ₃ or phosphoric acid	boron doping increased QY, phosphorus doping decreased QY, ratiometric	865
CD	with polyaniline layer	two linear regions from pH 3.5–5.5 and 6–12	866
nitrogen-rich carbon NPs	hydrothermal method from melamine and triethanolamine	PET quenching, linear range 3–12	867
CD with fluorescein	from acrylic acid and 1,2-ethanediamine	FRET-based, ratiometric	834, 835
CD with fluorescein and rhodamine B	from citric acid and 4,7,10-trioxa-1,13-tridecanediamine	ratiometric pH 6–8	836
CD with fluorescein	from kelp juice	CD as reference, linear range 4.6–7.7	831
GO nanosheets		10-fold fluorescence quenching on going from pH 2 to 12, show strong cross-talk to ionic strength	849
	betaine-modified	pH sensitivity from carboxylic and phenolic groups pH range 4–12, quenched by Cu ²⁺ and Fe ³⁺	98 868
GO NPs		bathochromic shift of emission in pH range 1 to 14, strong temperature sensitivity	869
		transducer for urea detection	870
single-walled carbon nanotubes		in wavelength range from 1.1–1.4 μ m, pH range 4.5–8.5, temperature sensitive	850

the preparation procedure and the resulting surface. Various biobased or “green” CDs have been described that are produced from natural products such as kelp juice,⁸³¹ mushrooms,⁸³⁰ and even urine and manure.^{832,833} The composition of these CDs, however, lacks reproducibility compared to procedures using chemicals of known purity/composition. Often, surface passivation or doping increases quantum yields or is necessary for luminescence to occur at all. The pH sensitivity is introduced

via carboxylic groups or nitrogen doping. CDs can also fulfill the dual function as support for a pH probe and as reference. Most commonly fluorescein is attached to the surface of the CDs.^{831,834–836} Temperature sensitivity and selectivity should be considered;^{837–847} cations, such as Ag⁺, Cu²⁺, Fe³⁺, or U⁶⁺, interfere. Also, luminescence quenching from nitrite was reported.⁸⁴⁸ Carbon dots are usually smaller ($\varnothing = 2–8$ nm) than other types of nanosensors and show a broader dynamic

Table 11. Overview of Optical pH Probes Exploring Conformational Changes in Polymers^a

dye	polymer	comments	ref
pyrene + coumarin 343	PAA modified with sulfadimethoxine as a linker	very sharp response; ratiometric 2- λ read-out; short wavelength of excitation and emission	871
7-hydroxy-4-bromomethyl coumarin + coumarin 343	PAA modified with sulfadimethoxine or sulfamethizole as a linker	very sharp response; ratiometric 2- λ read-out; short wavelength of excitation and emission	876
fluorescein + rhodamine B	PAA modified with sulfadimethoxine as a linker	very sharp response; ratiometric 2- λ read-out	876
Cy3 + Cy5	N-palmitoyl chitosan NPs	ratiometric 2- λ read-out	877
Cy5.5 + quencher	poly(oligo(ethylene glycol) methacrylate) and poly(benzyl-L-aspartic acid)	sharp response due to micelle formation	878
CdS/ZnS + CdSe/ZnS QDs	graphene oxide NPs decorated with QD-polymer conjugates	ratiometric 2- λ read-out/lifetime read-out	872
numerous chromophores	block copolymer PEG + alkylamino-modified PMMA	very sharp transitions, high tunability of optical and sensing properties	453, 873, 879
BTPE + coumarin	block copolymer PEG + alkylamino-modified PMMA	ratiometric 2- λ read-out; short wavelength excitation and emission; two-photon read-out possible	880
perylene-bis-imide	PAEMA dendrimer	operates in diluted solutions	874

^aA more detailed version of the table can be found in the Table S9. BTPE = 2-((E)-2-(pyridin-2-yl)vinyl)benzo[d]thiazole, PAEMA = poly(aminoethyl methacrylate), PAA = poly(acrylic acid).

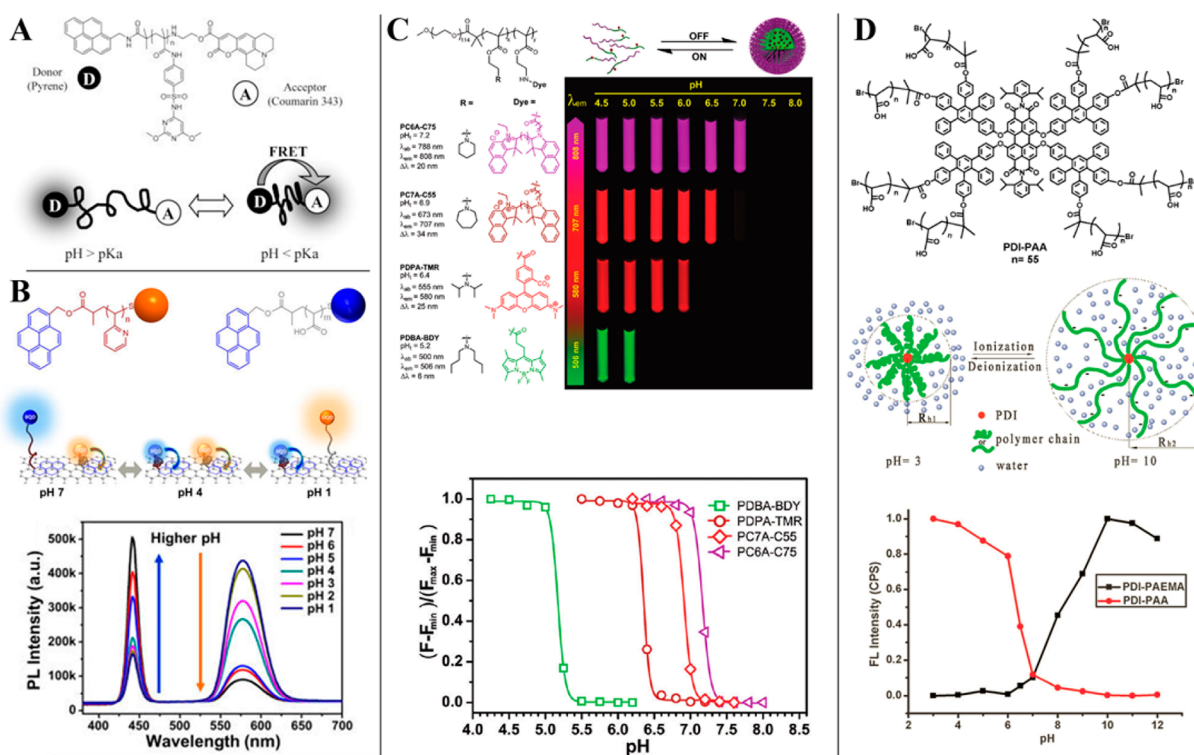


Figure 28. Examples of pH nanosensors exploring conformational changes of polymers. (A) Chemical structure and sensing mechanism of the nanoprobe based on a pyrene energy donor and a coumarin energy acceptor connected via a polyacrylamide linker modified with pH sensitive sulfadimethoxine. Reprinted with permission from ref 871. Copyright American Chemical Society 2005. (B) Chemical structure, sensing mechanism and pH dependency of fluorescence spectra ($\lambda_{\text{exc}} = 365$ nm) for the nanoprobe composed of two quantum dots emitters and graphite oxide acting as a quencher. Reprinted with permission from ref 872. Copyright American Chemical Society 2014. (C) chemical structures of the self-assembled polymeric micelles nanosensors, fluorescent images of their aqueous solutions at the same polymer concentration (100 $\mu\text{g}/\text{mL}$) but different pH values (pseudocolors were used for PC7A-C55 and PC6A-C75 nanoprobes due to their near IR emissions) and the pH response of the nanosensors. Reprinted with permission from ref 873. Copyright American Chemical Society 2012. (D) Chemical structure of a unimolecular polymeric micelle pH probe, schematic representation of the volume phase transition and respective pH response. Reprinted with permission of The Royal Society of Chemistry from ref 874. Copyright The Royal Society of Chemistry 2014. Permission conveyed through Copyright Clearance Center, Inc.

range. They are excited at significantly shorter wavelengths (<450 nm) than most (metal-)organic pH indicators. Most of these materials show emission spectra that depend on the excitation wavelength.

8.6.2. Graphite Oxide Dots. Graphite oxide dots (GODs) are obtained by oxidation of graphene. Similar to carbon dots, GODs do not represent a well-defined material, and the

properties strongly depend on preparation method. Chen and Yan⁸⁴⁹ demonstrated pH sensing properties of graphite oxide for the first time recording ~ 10 -fold fluorescence quenching on going from pH 2 to 12. Hirsch and co-workers⁹⁸ demonstrated that graphite oxide nanoparticles possess carboxylic and phenolic groups which are both responsible for pH sensitivity. Excitation and emission of GODs occurs at significantly longer

Table 12. Overview of pH Nanosensors Based on Miscellaneous Materials

material	pH probe—reference	comment	ref
silica/ γ -Fe ₂ O ₃ core-shell NPs	fluorescein, sulforhodamine B	2- λ emission	887
silica/polymeric core-shell NPs	naphthalimide, rhodamine B	intensity	472
Ag core + silica shell with poly(allyl amine)	HPTS self-referenced	2- λ excitation	884
pluronic F127, TEOS	fluorescein, porphyrin reference	silica-polymer hybrid, no cellular uptake, for monitoring pH during bacterial growth	571
pluronic F127, TEOS	fluorescein, porphyrin reference, Pt(II) porphyrin oxygen indicator	dual sensing of oxygen and pH	881
dendrimer-coated QD	SNARF-5F dye, CdSe/CdZnS QD	FRET-based, two-photon excitation	807
hydroxypropylcellulose-poly(acrylic acid) nanogel	CdSe quantum dots	swelling of the nanogel induces luminescence quenching	882
polyethylenimine coated NaYF ₄ :Yb,Er UCNPs and graphene oxide	NaYF ₄ :Yb,Er UCNPs	graphene oxide acts as quencher depending on strength of the electrostatic interactions	883
metal-organic framework NP (Zr(IV) and amino-triphenyldicarboxylic acid)	fluorescein	high dye loading up to 4% wt. without self-quenching	638
silver core, silica shell, poly(allylamine) coating	HPTS	metal-enhanced fluorescence	884
silver core, silica shell	fluorescein, eosin	dying via click chemistry	889
polythiophene-Au composite		absorption independent of pH, emission linear from pH 3–6	885
gold nanoparticles with thiol spacer	anthracene derivative, rhodamine	ratiometric	141
gold nanoparticles	tetramethylrhodamine	pH dependent dimer formation of rhodamine, pH range 6–10	890
gold nanoparticles	PEGylated porphyrin	ratiometric (absorbance), intensity	891
silica-coated iron oxide nanoparticles with polymer shell	benzo[<i>a</i>]phenoxazine derivative	magnetic, NIR, 40-fold enhancement of luminescence intensity from pH 8.4–3.6	886
maghemite (γ -Fe ₂ O ₃) nanocrystals with 2 silica shells	fluorescein, sulforhodamine B	magnetic, ratiometric	887
nickel core, silver layer, polymer gel shell	silver layer	magnetic, pH-sensitivity due to volume phase	888
NaGdF ₄ :Yb/Er UCNPs	AgS nanodots modified with 3-mercaptopropionic acid and glutathione	NIR excitation (980 nm) and NIR emission (795 nm), ratiometric, pH range 4–9, imaging	892
silica-coated polystyrene NP	fluorescein, CrBPh ₄ , porphyrin or Nile red	simultaneous measurement of T, O ₂ and pH with single excitation	893
silica core and polymeric shell	1,8-naphthalimide with PET group	also for drug release	769
poly(3,4-dihydroxyphenylalanine)		ratiometric, linear pH range 4–8	894
silicon carbide NPs		pH range 5.6–7.4, ratiometric	895
MnO ₂ nanosheets	3-acetyl-7-hydroxy-2H-chromen-2-one	pH range 4–7, dual sensing of pH and glutathione; exc/em maxima at 417/456 nm	896

wavelengths, compared to carbon dots. GODs show strong cross-talk to ionic strength, fluorescence decreases by about 30% upon addition of 50 mM NaCl to pH 4 buffer.⁸⁴⁹

8.6.3. Single-Walled Carbon Nanotubes. Functionalized single-walled carbon nanotubes also display pH-dependent luminescence in wavelength range from 1.1–1.4 μm .⁸⁵⁰ Attachment of an aminoaryl function introduced a defect in the carbon lattice, resulting in red-shifted luminescence. De-/protonation of the aminoaryl function alters the energy level and hence shifts the emission peak introducing pH-sensitivity. The system responds in the range from 4.5 to 8.5 pH units.

8.7. Miscellaneous Materials

8.7.1. Nanosensors Based on Conformational Changes in Polymers. In addition to the major classes of pH nanosensors described above, several other nanomaterials have also been presented. A very interesting approach is a group of nanosensors based on *conformational changes in polymers* (Table 11) in combination with *Förster resonance energy transfer* (FRET). The pH sensitivity of these probes is introduced by FRET modulation because of conformational changes of the polymer backbone or a linker.

For instance, Hong et al.⁸⁷¹ prepared a pH nanoprobe by connecting a pyrene energy donor and a coumarin energy acceptor via a polyacrylamide linker modified with sulfadimethoxine (Figure 28A). Protonation of the sulfadimethoxine

group results in collapse of the linker, which brings the dyes in close proximity, promoting FRET from pyrene to coumarin.

Kim and co-workers⁸⁷² reported a hybrid material exploring quenching properties of graphite oxide. First, pyrene-terminated poly(acrylic acid) (PAA) chains were anchored onto the surface of blue-emitting CdS/ZnS QDs (BQD, $\lambda_{\text{max}} = 440$ nm), whereas pyrene-terminated poly(2-vinylpyridine) (PVP) was anchored onto the surface of orange-emitting CdSe/ZnS QDs (OQD, $\lambda_{\text{max}} = 580$ nm), Figure 28B. Then, both conjugates were anchored onto a single graphite oxide sheet via π interaction of the pyrene and graphene oxide. The resulting nanosensors showed ratiometric response to pH (Figure 28B). In close proximity, graphite oxide quenches the emission of the QDs. The distance between the QDs and the graphite oxide sheet is determined by the conformations of the PAA and PVP parts, which in turn depend on the pH.

Another group of nanosensors explores the properties of pH-switchable self-assembled materials.⁸⁷⁵ Gao and co-workers^{453,873} prepared a library of pH-sensitive self-assembled polymeric micelles based on block copolymer modified with tertiary amino-groups and common pH-insensitive fluorescent dyes (Figure 28C). The conjugates were highly fluorescent in acidic media due to electrostatic repulsion of the polymeric chains bearing protonated amino-groups. At higher pH, micellization greatly enhanced quenching of the dyes via homoFRET mechanism. The materials feature extremely narrow dynamic

ranges with the “on–off” effect achieved within 0.25 pH units (Figure 28C).

Unimolecular polymeric micelles (UPMs) offer the advantage of being stable in very diluted solutions in contrast to self-assembled polymeric micelles. You et al.⁸⁷⁴ reported two fluorescent UPMs probes based on dendrimers bearing a perylene core and cationic or anionic polyelectrolyte shell (Figure 28D). The micelles are compact when the groups are uncharged but undergo a volume phase transition as a result of electrostatic repulsion between the charged chains. The increase in the size of the micelles is accompanied by strong decrease of fluorescence intensity (Figure 28D), which is fully reversible.

8.7.2. Inorganic–Organic Hybrids. Inorganic–organic hybrids (Table 12) are either prepared to improve the performance of the resulting material or to introduce additional functions such as upconverting capability (these materials are treated separately in section 10.6), fluorescence enhancement or additional magnetic properties. For instance, Wang et al.⁵⁷¹ prepared hybrid organic–inorganic pH nanosensors from Pluronic F127, TEOS, and fluorescein. The dye itself is embedded in silica nanoparticles that are entrapped in the micellar structure formed by the Pluronic polymer. Intended for monitoring of pH during bacterial growth, the particles are not ingested by bacteria and are excellently dispersible in standard agarose/nutrient growth media. A similar system was applied for dual sensing of oxygen and pH using a Pt(II) tetraphenyltetra-benzoporphyrin as oxygen indicator.⁸⁸¹ The particles could be delivered to the cytosol of cells via electroporation.

Somers et al.⁸⁰⁷ reported a ratiometric pH sensor prepared from dendrimer-coated quantum dots and pH-sensitive SNARF-5F dye. The CdSe/CdZnS quantum dots were coated to increase robustness against degradation and provide a higher number of coupling sites. Wu et al.⁸⁸² embedded CdSe quantum dots into polysaccharide-based hybrid nanogels. pH dependent swelling of the nanogel induces luminescence quenching.

Yan et al.⁸⁸³ designed a hybrid pH-sensor film based on upconverting nanoparticles and graphene oxide. NaYF₄:Yb,Er UCNPs were coated with polyethylenimine and upon 980 nm excitation displayed emission at 540 and 660 nm. pH sensitivity from pH 5 to 8 is induced by pH-dependent quenching from graphene oxide.

Lin and co-workers⁶³⁸ used metal–organic framework nanoparticles (made of zirconium(IV) and amino-triphenyldicarboxylic acid) for covalent immobilization of fluorescein. High dye loading (up to 4% wt.) could be achieved without self-quenching. High brightness of the material and efficient cellular uptake made the material promising for intracellular imaging of pH. These properties are in contrast to low brightness and short wavelength excitation of other MOFs reported so far (see section 7.1 for more details).

Several groups designed pH nanosensors with a *metal core*. Bai et al.⁸⁸⁴ exploited metal-enhanced fluorescence of HPTS using a hybrid material with a silver core. Panda and Chattopadhyay⁸⁸⁵ reported pH responsive polythiophene–Au composite. Absorption was independent of pH, but emission at 465 nm showed linear pH dependency in the range from pH 3 to 6. Gold nanoparticles were used to fabricate a ratiometric pH-nanosensor material based on PET.¹⁴¹ Anthracene substituted with a PET group and rhodamine as reference were coupled to the surface of the gold nanoparticles via thiol-containing spacer molecule. The system was used for intracellular measurement in the pH range of 3.5–6.

8.7.3. Magnetic Nanoparticles. Magnetic nanoparticles are used to allow manipulation with a magnet or enable magnetic resonance imaging (MRI). Liu et al.⁸⁸⁶ prepared hybrid magnetic nanoparticles by attaching a polymer coating onto silica-coated iron oxide nanoparticles. The coating was added to improve water solubility, prolong the circulation lifetime and reduce nonspecific protein binding. A NIR fluorescent benzo-[a]phenoxazine dye was attached via DCC coupling. Luminescence intensity enhanced 40-fold, when changing pH from 8.4 to 3.6.

Lapresta-Fernandez et al.⁸⁸⁷ reported core–shell nanoparticles that allow manipulation with a magnet. The inner shell contains covalently bound sulforhodamine B, whereas the outer shell covalently bound fluorescein. The material was designed for ratiometric sensing. Wu et al.⁸⁸⁸ prepared magnetic core–shell hybrid nanogels for pH sensing. A fluorescent silver layer was grown onto the magnetic nickel core and then coated with a pH-responsive copolymer gel shell. pH-sensitivity relies on a pH-induced volume phase transition. The material responds in the range from pH 5 to 7.4.

Hybrid materials can also be promising for simultaneous *pH sensing* and *drug release*. In a model system, Wan et al.⁷⁶⁹ prepared hybrid nanoparticles composed of a silica core and polymeric shell with a naphthalimide pH indicator. After loading with guest molecules for drug-release experiments, the pores were closed by cross-linking with cystamine forming disulfide groups. Leaching of guest molecules was low in water. In presence of dithiothreitol, the guest molecules were released, due to cleavage of the disulfide groups.

8.8. Aggregation-Induced Emission

Aggregation-induced emission (AIE) is based on the effect that molecules or nanoparticles (NPs), on aggregation, undergo an increase in fluorescence intensity, which is in contrast to the widely observed phenomenon of emission quenching.⁸⁹⁷ Aggregation makes radiative deactivation the primary pathway from the excited state to the ground state. AIE-based methods may be considered as forming the interface between molecular sensing and NP-based sensing. A review on AIE for use in optical sensors has been presented by the Tang group.⁸⁹⁸ The same group later has described⁸⁹⁹ AIE-based probes/sensors for measurement of intracellular pH values (pHi) that is making use of a tetraphenylethene–cyanine adduct. Upon diffusion into cells, it responds sensitively to pHi over the physiological range, visualizing the acidic and basic compartments with intense red and blue emissions, respectively. The ratiometric signal of the red and blue channels can thus serve as an indicator for local proton concentration. A through-bond energy transfer-based modification of this method was presented later.⁹⁰⁰ Others have used a pyridyl functionalized tetraphenylethylene for ratiometric fluorometric determination of pHi.⁹⁰¹

Another kind of ratiometric AIE-based pH nanosensor material was obtained⁷⁶⁹ by preparing NPs consisting of a hyperbranched polymer with AIE activity. The NPs selectively accumulate in the acidic organelles of living cells by endocytosis. The pHi of HeLa cells was determined by ratiometric sensing. At about the same time, AIE-based probes were introduced where the diketopyrrolopyrrole and the anthracenone chromophores were conjugated to each other.⁹⁰² The diketopyrrolopyrroles containing two diethylamino groups display AIE. At alkaline pH values, the emission is 6.7-fold stronger compared to that at pH 2.5. A dual-emission pH-sensitive fluorescent probe was developed, which displays green fluorescence in alkaline

conditions after deprotonation, while orange emission in acid at aggregated state. This novel probe allows the specific light-on in acidic lysosomes of cancer cells and tumors in nude mice, which indicates its potential application in cancer diagnosis.

Polymers not containing classical dyes or fluorophores were also found to display pH-dependent AIE if they incorporate protonable functions. For example, pH-responsive blue AIE⁹⁰³ can be observed in polymers containing *N,N*-diethylethylenediamine. Similarly, pH-induced AIE was found for an interpenetrating polymer network composed of poly(*N*-isopropylacrylamide-*co*-tetra(phenylethene acrylate)/poly(methacrylic acid) that may be used as a nanosensor materials.⁹⁰⁴

Some Schiff bases and azines appear to readily undergo pH-dependent AIE. A chlorosalicylaldehyde-derived Schiff base was synthesized and used for pH sensing in live cells.⁹⁰⁵ Fluorescence is weak in solution, but strong AIE is found for the nanoaggregated state. This is ascribed to the restriction of the intramolecular rotation of a C–N bond and the nonplanar configuration in the aggregate/solid state. The sensor undergoes a fluorescence color change from orange to green, and the intensity ratio at 516 and 559 nm is enhanced when the pH value is increased from 5.0 to 7.0 (pK_a value 4.8). The same is true for other Schiff bases,^{906,907} salicylaldehyde azines,⁹⁰⁸ and of some hydrazones.⁹⁰⁹ Some show dual emission and therefore enable ratiometric intracellular sensing.⁹¹⁰ Other AIE-based sensors for determination of pHi make use of smartly functionalized anthracenes,⁹¹¹ of BF_2 chelates^{912,913} or of *E/Z* isomers of *N*-methylpyrrole-benzohydrazide-based BF_2 complexes, these also containing $>C=N-$ bonds of the Schiff base type and undergoing pH-induced AIE.⁹¹⁴ They were applied to the determination of the pHi of living cancer cells. It should be mentioned that most of the pH probes based on AIE are expected to show the same limitations as molecular probes, that is, shift of the calibration due to interaction of the biomolecules with the monomeric form of the dye.

8.9. Nanofilm Sensors

The nanomaterials described in the sections 8.1–8.7 are self-contained analytical tools that are mostly applied in the form of an aqueous solution/dispersion for pH quantification in comparably small volumes (e.g., living cells). Only in some cases they have been incorporated into sensors of different formats, such as planar optodes or fiber-optic sensors. Nanofilm sensors represent another type of nanomaterials useful for pH sensing, that, in contrast to self-contained nanosensors, are not self-standing because they are prepared on a support (a planar waveguide or an optical fiber). This section covers the use of classical (soft) lipid nanofilms but not of nanofilms made from materials, such as polyaniline, graphenes, or other solid nanomaterials. There are two common methods for making such nanofilms. Both utilize lipophilic compounds with polar groups at their end. The first is making use of the Langmuir–Blodgett (LB) technique, the other of layer-by-layer (LbL) deposition. Schaffar and Wolfbeis⁸⁵ have used LB films doped with the lipophilic blue fluorescent pH probe 7-hydroxycoumarin-3-carboxylic acid hexadecyl ester ($pK_a = 7.4$). The doped LB film was placed on the surface of a glass platelet, and fluorescence was measured via an evanescent wave technique. In another kind of pH sensor,⁹¹⁵ evanescent coupling between a side-polished single-mode optical fiber and a single-mode, pH-sensitive LB overlay is used. The sensor is intrinsic and does not require the presence of a pH indicator. The sensor shows a wavelength sensitivity of around 19 nm/pH unit and a

transmission sensitivity of 9.7 dB/pH unit when operated at 750 nm. LB films generally suffer from poor mechanical stability and disruption by detergents and many proteins including serum albumin.

The LbL technique has been used more often because LbL layers are more versatile and somewhat more stable. Polyallylamine is widely used. It is present, at neutral pH values, as the hydrochloride and then referred to as PAH (not to be confused with the common acronym for polycyclic aromatic hydrocarbon). PAHs are cationic and form monolayers and bilayers. In addition, layers with alternating charge may be deposited sequentially, for example layers of poly(acrylic acid) (PAA; being anionic) and of PAH (being cationic). Such layers are best deposited on supports by alternating a voltage applied to the support. By incorporating the pH indicator neutral red into alternating layers of PAA and PAH, a pH sensing membrane was obtained for absorptiometric determination of physiological pH values.¹⁹³ In similar work by the Arregui group,³⁴⁷ a thin-core fiber modal interferometer was alternatingly covered with poly(allylamine hydrochloride) and poly(acrylic acid) by LbL electrostatic self-assembly. The response also is fast, the linear range is said to be much wider (pH 2.5–10), and the resolution is ± 0.013 pH units. The group of Grattan²¹¹ showed that six double layers of PAH doped with the pH indicator brilliant yellow showed the best sensitivity in the pH range from 6.8 to 9.0. The method was later extended to fiber optic pH sensing using an unclad silica fiber,⁹¹⁶ and to the use of neutral red deposited on U-shaped fibers.⁹¹⁷ An LbL method for interferometric (indicator-less) sensing was described by Gu et al.⁹¹⁸ The side surface of an optical fiber modal interferometer was self-assembled with alternating layers of sodium alginate (mainly anionic at pH values above 3) and polyethylenimine (mainly cationic at pH values below 10). The sensors have a wide pH sensing range (2 to 11), fairly linear response, and good stability. However, the sensor also has disadvantages including complex fabrication and small signal change.

White light interferometry was used to sense pH values in the range from 3 to 10 and using a halogen lamp as the light source.⁹¹⁹ The Fabry–Perot interference patterns caused by thin polymeric films on standard optical fiber substrates depend on the pH value of the surrounding solution. The films consist of alternating layers of the weak polyelectrolytes poly(allylamine hydrochloride), which is cationic, and of the poly(acrylic acid), which is anionic. The films reversibly swell and shrink as pH values change. Generally spoken, nanofilm sensors are of fundamental interest but have not found wide application, mainly because of difficulties to ensure highly reproducible production of the sensor films, sensitivity of the coatings to detergents and proteins, such as albumin, the adverse effects of many electrolytes, and because of the weak signals provided by extremely thin sensor films, be it absorption (from the visible to the infrared), reflectance, fluorescence, or scattering.

9. ADDITIVES, COATINGS, AND OTHER COMPONENTS

9.1. Plasticizers

Use of plasticizers in pH optodes is rare because pH sensors mostly rely on the use of proton-permeable materials. Plasticizers have been used in pH optodes only in a combination with poly(vinyl chloride), for example in a matrix for a dually responding pH/pO₂ sensor to achieve optimal dynamic range

for pH and oxygen sensing (section 10.7).³⁶⁶ We do not recommend the use of such sensor materials.

9.2. Scattering Particles

The signal of indicator-based sensors can be enhanced via addition of white scattering particles.^{110,146,920} Nano- or microparticles based on materials having high refractive index efficiently enhance the fluorescence signals by increasing the pass-way of excitation light. Titanium dioxide represents a cheap pigment with high refractive index (2.488–2.609 depending on the form) and is thus almost ideally suitable for the signal enhancement. It is available in many modifications (hydrophilic or hydrophobic surface). Potential interaction of the indicator with the surface of the particles should be considered. Hydrophilicity/hydrophobicity of the surface may affect the apparent pK_a value, whereas photocatalytic properties of titanium dioxide may enhance photobleaching or be responsible for fluorescence quenching. It is possible to avoid the above effects by coating an additional light scattering layer (TiO₂ particles dispersed in the matrix) over the sensing layer. Such additional layer reduces the wave guiding to the edges of the foil, which results in additional enhancement of the signal. Overall enhancement can reach 10-fold, which makes even moderately bright indicators competitive. It should be kept in mind that enhancement factor for NIR pH indicators is significantly lower than for UV–vis dyes due to wavelength-dependent nature of light scattering.

Several other scattering materials were proposed. For instance, Moßhammer et al.⁹²¹ used a diamond powder as a light scattering material. Although scattering efficiency of diamond is slightly lower than that of titanium dioxide ($n = 2.418$) diamond does not introduce potential risks due to absence of photocatalytic properties.

Other materials which might be useful include cubic zirconia ($n = 2.13$), zinc oxide ($n = 2.0$), and barium sulfate ($n = 1.64$). White particles have the advantage of being both scatterers and isolators.

9.3. Optical Isolations

Optical isolations (see Figure 29) are recommended to separate the spectral system of the sensor from the spectral characteristics

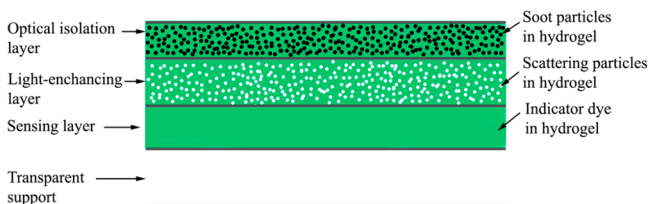


Figure 29. Cross-section of a planar optode with light-enhancing and optical isolation layers. The same design can be adapted for fiber-optic sensors. The upper layers are knife-coated or sprayed onto a dry sensing layer. Dissolution of the upper part of the sensing layer ensures good adhesion but also bears the risk of dye extraction in case of physically entrapped indicators.

of the sample. Note that most genuine samples display strong intrinsic absorption, fluorescence or scattering capability. An optical isolation is essentially an opaque layer (e.g., soot particles dispersed in the matrix), which is coated over the sensor layer. It also prevents external light entering the sensor, for example sunlight, which otherwise may lead to accelerated dye bleaching or result in saturation of the photodetector. Optical isolations are particularly important in case of highly scattering or

absorbing samples, such as blood, sediments, or microbial systems. Most commonly, optical isolations are prepared from lamp black, Fe₂O₃ (red), BaSO₄ (white), or surface-modified TiO₂ (white). The surface modification of TiO₂ is necessary to prevent photocatalytic reactions that may deteriorate the sensing chemistry. White optical isolations do allow some scattered ambient light to penetrate the sensing layer whereas the black ones of adequate thickness completely block it. Black optical isolations are commercially available (<https://www.acktar.com/>).

The design of a sensor with optical isolation is not straightforward. In principle, a black optical isolation layer can be directly coated onto the dry pH sensing layer. On the basis of the same polymer dissolved in the same solvent, the second layer dissolves the upper part of the sensing layer and this warrants excellent adhesion between the two layers. However, it is advisable to add a light-scattering layer between the sensing layer and the black optical isolation layer to enhance the fluorescence signals (3-layer design, Figure 29). Alternatively, to reduce the complexity of the system, it is also possible to coat the optical isolation layer on the sensing layer containing light scattering particles (2-layer design). Obviously, the light-scattering and optical isolation layers should be proton-permeable. If the indicator is noncovalently entrapped into the sensing layer the multilayer design bears the risk of its migration into upper layers that may result in sensor drift. In this case, a proton permeable polymer that is a poor solvent for the indicator is the preferable material for optical isolation. For instance, amphiphilic indicators typically show low solubility in pHEMA which can be coated on polyurethane hydrogel layer using the same solvent mixture. In case of the systems with low or nonexistent risk of indicator migration (indicators covalently embedded into polymeric matrices; indicators entrapped into dense sol–gel network), the two additional layers can be composed of any proton-permeable polymer. It is also possible to obtain an optical isolation layer by spraying a commercially available soot dispersion in isopropanol onto the light-enhancing layer. The residual solvent swells the hydrogel layer, which enhances the adhesion of carbon particles on the surface. The right settings (such as the distance from the spraying head to the sensor foil) are crucial to obtain a homogeneous layer: If the solvent is completely evaporated, the soot particles will not adhere well and too much residual solvent may cause deformation of the sensing layer due to its dissolution.

It should be kept in mind that the additional layers slow down the response of the sensors. Therefore, additional coatings can be omitted if the above-mentioned light interferences are not critical.

9.4. Materials Acting As Inert Mechanical Support

Planar optodes require a support that is supposed to have following properties: (i) mechanical stability, (ii) transparency to the excitation and emission light, (iii) chemical and photochemical inertness, (iv) resistance to solvents used for coating of the pH sensing layer, (v) low or no background fluorescence, and (vi) allow adhesion of the pH sensing layer. Poly(ethylene terephthalates) (PET, such as Mylar or related brands) fulfill virtually all these requirements. It is the support of choice in most planar optodes reported so far, commercial products included. The autofluorescence of PET can only be observed under excitation with UV or violet light, which again underpins the advantage of longwave indicators. The foils

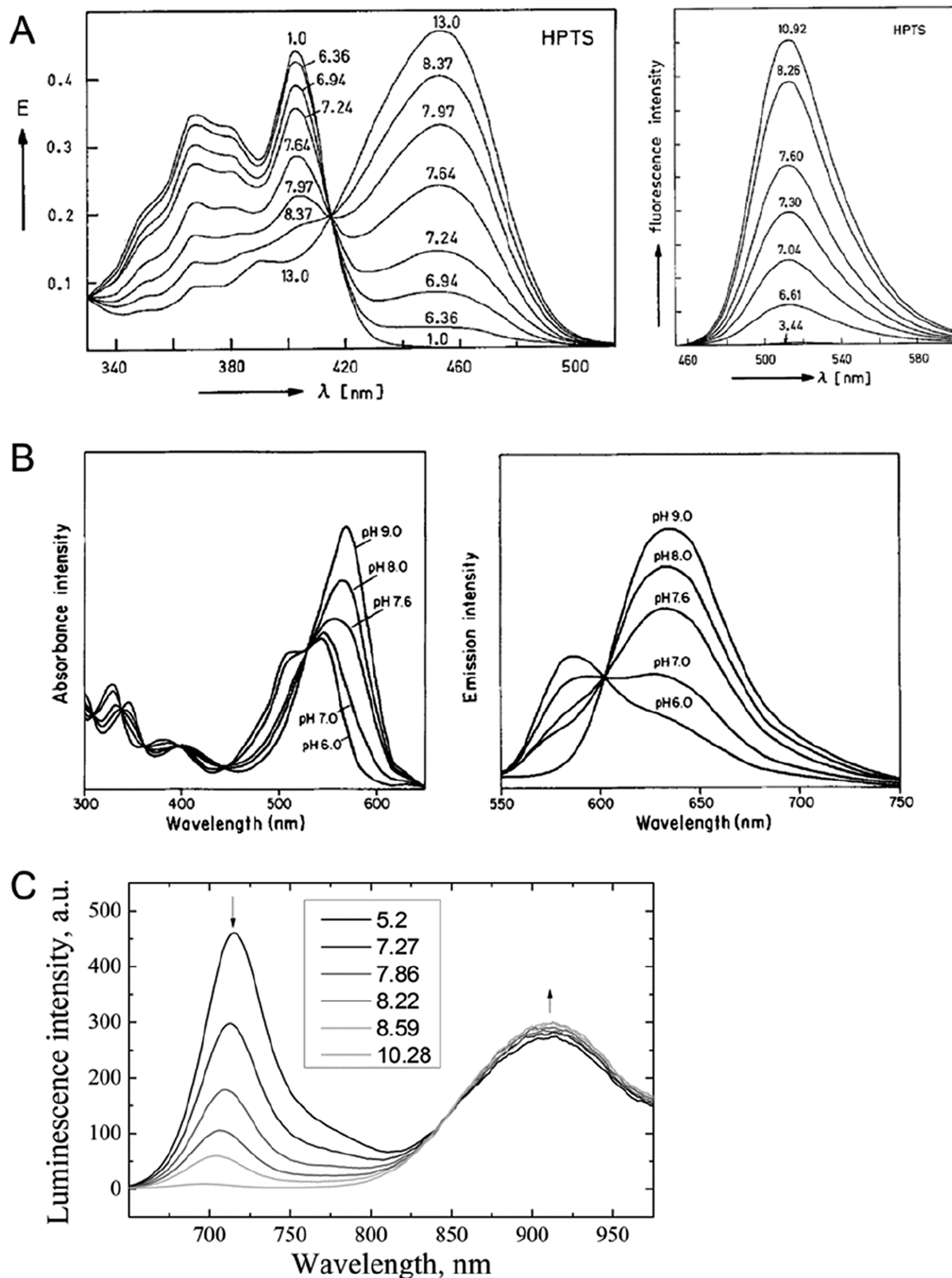


Figure 30. Ratiometric luminescent pH sensing. (A) pH dependency of excitation (left) and emission (right) spectrum of 8-hydroxypyrene-1,3,6-trisulfonate HPTS in an aqueous buffer. Reprinted by permission of Springer Nature from ref 36. Copyright Springer Nature 1983. (B) pH-dependent excitation (left) and emission (right, λ_{exc} 534 nm) spectra of C-SNARF-1 in an aqueous buffer. Reprinted from ref 445 with permission from Elsevier. Copyright Elsevier, Inc., 1991. (C) pH-dependent emission spectra of the sensing material incorporating an aza-BODIPY pH indicator in hydrogel D4 and reference emitter Egyptian blue used in form of microcrystalline powder in the same matrix. Both emitters are excited at 625 nm. Author version of a figure from ref 153. Copyright American Chemical Society 2013.

coated with the sensing material can be conveniently punched or cut into spots of several millimeters in diameter.

The sensing layer may be further treated with an oxygen or nitrogen plasma to result in a more hydrophilic surface and thus to promote adhesion of the hydrogel.^{922,923}

Glass supports are less common in case of planar optodes due to lower flexibility in the dimensions and postprocessing. However, glass surface can be modified in many ways via silanization and sol–gel chemistry.¹²³ This is particularly attractive for covalent coupling of the sensing layer.

In fiber-optic sensors, the fiber acts as a solid support. Glass fibers can be modified as described above, and plastic poly(methyl methacrylate) fibers can be directly coated with the sensing material but adhesion of hydrophilic hydrogels on the hydrophobic surface may not be optimal. It should be kept in mind that PMMA dissolves or swells in many organic solvents.

9.5. Photostabilizers

Oxygen practically is omnipresent. Organic dyes in the first excited singlet state can convert triplet oxygen ($^3\Sigma_g^- \text{O}_2$) to singlet oxygen ($^1\Delta_g, ^1\text{O}_2$) which then can react with indicators to give nonluminescent products of photo-oxidation. Singlet oxygen can also attack polymer backbones. Quenching of the singlet excited state by molecular oxygen is relatively inefficient because of the short lifetime of the former. On the other hand, efficient generation of singlet oxygen is expected from metal–organic phosphorescent indicators and in organic molecules with significant probability of intersystem crossing, such as porphyrins.

Photodecomposition of indicators is particularly efficient under strong UV radiation, when using strong light sources, and under continuous illumination. It can be reduced by applying pulsed light excitation or low radiant powers. Three strategies have been employed to prevent photodecomposition. The first consists in the fluorination of the indicator dye, the second in the incorporation of protective functional groups (such as tertiary amino groups) into the indicator dye, and the third by simply adding a stabilizer to the sensor matrix. This section mainly refers to additives.

It was reported quite some time ago⁹²⁴ that olefinic and aromatic molecules carrying tertiary amino substituents are very stable toward photodegradation by $^1\text{O}_2$. This was exploited to prevent indicators from being oxidized by $^1\text{O}_2$ by addition of tertiary amines⁹²⁵ to the sensor matrix. They physically quench $^1\text{O}_2$, for instance 1,4-diazabicyclo-[2.2.2]octane (DABCO).^{926–928} Other stabilizers (e.g., carotene)⁹²⁹ chemically react with $^1\text{O}_2$ and thus are consumed. Other donors that can decompose $^1\text{O}_2$ include certain sulfur compounds,⁹³⁰ astaxanthin,⁹³¹ allylurea,⁹³² azides.^{933,934} Molecules where a reducing and an oxidizing moiety are covalently linked have been reported.⁹³⁵ Very recently, Demchenko⁹³⁶ has presented a topical review on mechanisms of photobleaching of organic fluorophores, and on ways how to prevent it.

10. LUMINESCENT SENSORS

Luminescent pH sensors are the ones most often reported in recent years. Numerous spectroscopies and read-out schemes have been reported. They are summarized in this section.

10.1. Intensity-Based Sensors

Measurement of luminescence intensity at a single wavelength is common in case of pH sensors but mainly restricted to characterization of the new materials at an early stage of sensor development. It enables fast screening of these materials with

respect to the analytical range, and signal change. However, it is less suitable for practical applications since the signal of the sensor is affected by the intensity of the light source, sensitivity of the photodetector, thickness of the sensing layer, or its distance from the optical fiber (for the sensor spots positioned on the inner wall of a glass window). Self-referenced indicators explore either measurement of luminescence decay time (described in section 10.2) or measurement of luminescence intensity at several wavelengths (ratiometric probes, section 2.11).

The first type of ratiometric pH indicators explores a difference in fluorescence excitation spectra for protonated and deprotonated forms. Such scheme is particularly useful in case of indicators, which feature photodissociation in the singlet excited state, such as HPTS (section 4.1), and therefore having identical emission spectra for the protonated and deprotonated forms of the indicator (Figure 30A).³⁶

Indicators that feature significantly different emission spectra in both forms include seminaphthorhodafluors (SNARFs) (Table S10, Figure 30B). The calibration may alter significantly with the variation of the peak wavelength of the excitation source (e.g., LED) when absorption spectra differ (Figure 30B). In case of spectral overlap of absorption and emission (Table S10, Figure 30B), FRET can occur and shift apparent pK_a values. Then, the calibration of the ratiometric sensor is concentration-dependent, resulting in the shift of the inflection point to higher values at lower concentrations of the dye (less effect of FRET).

Ratiometric indicators are valuable for microscopic imaging of pH, but they have been also applied in pH sensing materials. For instance, SNAFL-2 was covalently immobilized into a photo cross-linked poly(acrylamide-*co*-vinylamine) hydrogel positioned on the tip of optical fiber³⁹⁷ and SNARF-1 isothiocyanate was coupled to pHEMA and immobilized onto a tip of PMMA fiber.⁵⁶

Since self-referenced indicators are comparably rare, optical pH sensors often contain an additional reference emitter with luminescent properties that do not depend on pH. The best candidate will possess the excitation spectrum similar to that of the pH indicator, but different emission spectrum (Figure 30C). The fluorescein/rhodamine system, despite several limitations, has been used most often (refs 404, 411, 618, 753, 755, 763–766, 788, 836, 876, and 887). In fact, a referenced measurement can often only be achieved by using 2 different excitation wavelengths (e.g., 488 nm for fluorescein and about 550 nm for the rhodamine dyes) which does not fully compensate for potential drifts (e.g., in the excitation source). Nevertheless, a combination of fluorescein and rhodamine dyes has been widely used probably due to availability of reactive derivatives. For instance, Lei et al.⁶¹⁸ prepared mesoporous silica nanoparticles from fluorescein and rhodamine B isothiocyanates.

In case of NIR emitting pH indicators, microcrystalline powders of inorganic phosphor Egyptian Blue (broadband excitation from 500 to 900 nm; $\lambda_{\text{max,em}} = 909 \text{ nm}$) were found to be very promising.¹⁵³ Large Stokes shift of the luminescence of the phosphor is responsible for efficient spectral separation from the fluorescence of the indicator (Figure 30C).

10.2. Decay Time-Based Sensors

Measurement of luminescence decay time represents a self-referenced technique, which is free from the drawbacks of the intensity-based read-out. Generally, the fluorescence lifetime can be measured in frequency domain and in time domain.

Phase modulation technique allows calculation of decay time from the fluorescence phase shift Φ ($\tau = \tan \Phi / 2\pi f$). Evidently, in case of indicators with nanosecond decay times, the modulation frequencies have to be very high (10–300 MHz) to measure phase shift reliably. Longer decay times (e.g., typical for some QDs and metal–ligand complexes) require lower modulation frequencies and thus cheaper instrumentation. Importantly, phase modulation technique allows measurement of the average decay time so that the calculated values will be affected by the level of background fluorescence, which, however, can be minimized by using long-wavelength probes. Time domain measurement of fluorescence decay time is usually realized using time correlated single-photon counting technique (TCSPC). Providing that the fluorescence decay time of the probe is much longer than of the background, the background signal can be almost completely eliminated. However, TCSPC, which is widely used for fluorescence lifetime imaging (FLIM), is neither very compact nor very cheap, it requires high quality pulsed light sources and is therefore less suitable for application in compact optical sensor devices.

In contrast to optical oxygen sensors, which rely on dynamic luminescence quenching,¹³² the situation is more complicated in case of fluorescent pH indicators. With the exception of FRET-based systems (section 10.4), measurement of the decay time with a single indicator dye is only possible if (i) both indicator forms are emissive and (ii) they have significantly different fluorescence decay times. Evidently, because two forms with different decay times coexist, the overall signal cannot be described by monoexponential model. An alteration of pH shifts the ratio of the two forms, and this results in the *change of the respective amplitudes* in the biexponential signal. However, for practical purposes it is often sufficient to measure average decay time of the sensor.

Because of the above requirements, the number of pH probes suitable for the decay time read-out is rather limited. Lakowicz and co-workers demonstrated that the fluorescence lifetime of SNARFs can serve as an analytical parameter (Figure 31A).⁹³⁷ Frequency domain measurement of the fluorescence phase shift and decay time revealed dependence of the calibration curves and pK_a on the wavelength at which the fluorescence was excited and detected. Evidently, design of solid state sensors based on dyes like SNARF or SNAFL is more challenging because of relatively high concentration of the dye in matrix and very strong overlap between the emission of the protonated form and the absorption of the deprotonated form of the indicator. This results in an efficient FRET affecting the pH calibration in terms of both fluorescent intensity and decay time response.

Sensors based on *probes exploring photoinduced electron transfer* can be more advantageous since the emission spectra of the protonated and deprotonated forms are very similar and the complications due to concentration-dependent FRET effect are not expected. Indeed, Draxler and Lippitsch showed⁶⁶ that the sensor based on diethylaminomethylpyrene embedded into a polyurethane hydrogel shows no concentration-dependent effects. Unfortunately, numerous “on”–“off” probes are not suitable for this read-out. However, such read-out becomes possible if the PET effect is comparably inefficient. This can be achieved by rational design of the probe by combining a receptor with relatively high oxidation potential and the chromophore with relatively low reduction potential, by shifting the absorption of the chromophore to longer wavelengths or by reducing polarity of the matrix.³⁷³ For example, Aigner et al.⁴⁸² designed a decay time pH probe based on an alkylamine

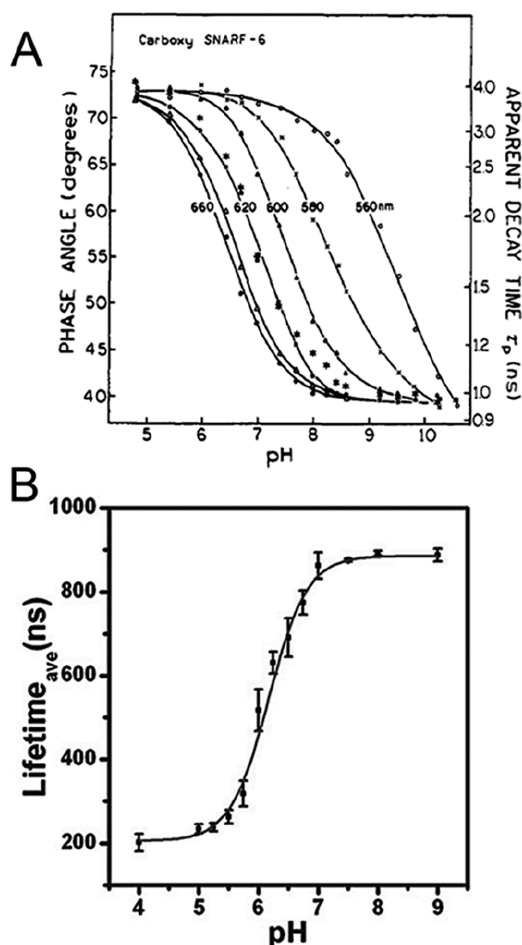


Figure 31. Examples of decay time sensing of pH. (A) Fluorescence phase shift and decay time response of SNARF-6 to pH under 543 nm excitation and emission detected at different wavelengths. Adapted with permission from ref 937. Copyright American Chemical Society 1993. (B) Decay time response of the Cu-doped gradient-alloyed CdZnS nanoparticles to pH. Adapted with permission of The Royal Society of Chemistry from ref 798. Copyright The Royal Society of Chemistry 2015. Permission conveyed through Copyright Clearance Center, Inc.

receptor and perylene chromophore. The negatively charged indicator embedded into positively charged RI-100 nanobeads showed a decrease in fluorescence decay time from 6.7 to 4.6 ns on going from pH 4.5 to pH 8.

The decay times of organic chromophores rarely exceeds 10 ns and is often significantly shorter. Therefore, fluorescence background may significantly affect the lifetime measurement particularly in case of the indicator form with the shortest decay time. Several probes featuring long decay times have been developed. The above-mentioned diethylaminomethylpyrene features decay times of 160 ns for the acid form and 22 ns for the base form.⁶⁶ The protonated form of acridine also features very long fluorescence decay time of 31.6 ns, whereas τ for the deprotonated form is 6.6 ns.⁵³³ Ryder et al.⁵³³ designed a pH sensor based on acridine immobilized into Nafion 117 membrane. The dye retained high lifetime dynamics (33 and 14 ns for the protonated and deprotonated forms, respectively) in the matrix.

Quantum dots represent bright and photostable emitters. Their decay times are significantly longer than those of most organic chromophores. Orte et al.⁸⁰¹ demonstrated that

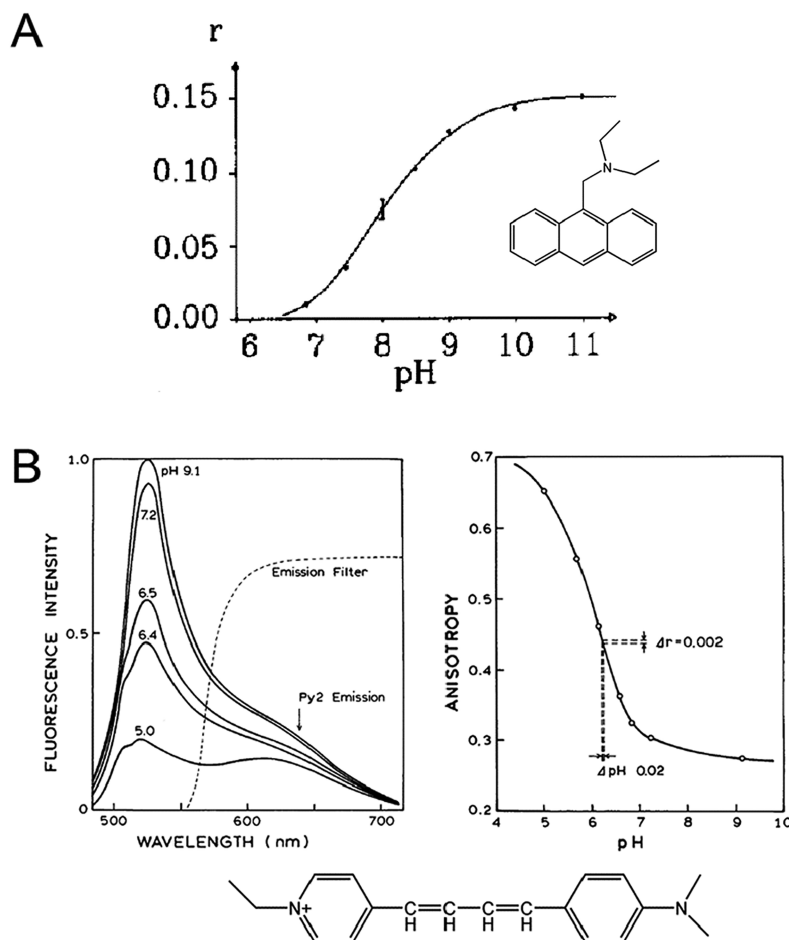


Figure 32. Examples of anisotropy-based pH sensing. (A) pH dependency of fluorescence anisotropy of 10-diethylaminomethylanthracene in an unspecified solvent. Adapted with permission from ref 940. Copyright American Chemical Society 1993. (B) pH dependency of the emission spectra (left) and anisotropy (right) of the stretched films containing Py-2 (structure shown below) and solution of 6-carboxyfluorescein. Adapted with permission of The Royal Society of Chemistry from ref 941. Copyright The Royal Society of Chemistry 2015. Permission conveyed through Copyright Clearance Center, Inc.

modification of commercially available CdSe/ZnS QDs ($\lambda_{\text{max,em}} = 535 \text{ nm}$) with mercaptopropionic acid renders them pH sensitive. The average decay time increases from 8.7 to 15.4 ns on going from pH 5–9.

Cu-doped gradient-alloyed CdZnS QDs ($\varnothing = 3.5 \text{ nm}$) reported by Chen et al.⁷⁹⁸ showed tunable NIR fluorescence (650–750 nm) and very long decay time approaching 1 μs . The luminescence lifetime has a sigmoidal dependence on pH with a linear range from pH 5.5–7.0 (Figure 31B). It changed almost 4-fold (200 ns at pH 4 to 900 ns at pH 8). Other promising QDs nanosensors explore FRET effect (section 10.4).⁸⁰⁸

The decay time of Pt nanoclusters was reported to show strong pH dependence.⁹³⁸ The decay time changes from 21 to 10 ns when going from pH 5 to 9 due to the change of the surface states (zeta potential changes from -0.83 mV to -20.80 mV from acidic to alkaline pH).

Finally, metal–ligand complexes featuring long-lived luminescence (see section 4.2 for more details) appear to be promising candidates for pH sensing and imaging in the lifetime mode. Indeed, the read-out of the relatively long decay times ($>1 \mu\text{s}$) can be realized with very compact and cheap instrumentation (phase fluorometer). Main disadvantage of such probes is their cross-talk to oxygen, which is typically proportional to the luminescence decay time, only lanthanide chelates represent a

notable exception. The number of these probes, however, is limited and the spectral properties, stability and cross-talk to other species are far from being optimal. As was discussed above (section 4.2), only some indicators are in reality suitable for the lifetime read-out,⁵⁵⁹ whereas others show strong dependency of the calibration on buffer concentration and composition and are virtually useless.

Selected examples of lifetime-based sensors and nanosensors can be found in Table S11.

10.3. Fluorescence Anisotropy-Based Sensors

The fluorescence anisotropy upon excitation with a polarized light (r) can be defined as follows: $r = (I_{\parallel} - I_{\perp}) / (I_{\parallel} + 2I_{\perp})$, where I_{\parallel} and I_{\perp} are the emission intensities detected upon orientation of polarizer parallel and perpendicular to direction of the polarized excitation, respectively.¹³¹ Similar to the decay time, anisotropy is a self-referenced parameter which is independent of, for example, intensity of the excitation source or sensitivity of the detector. Importantly, the read-out can be realized with a very simple equipment. Measurement of fluorescence anisotropy is very useful for investigation of binding reactions causing a change in the rotational time of the molecules. The question arises if anisotropy can be a useful parameter in case of pH sensors. For a pH indicator or any other

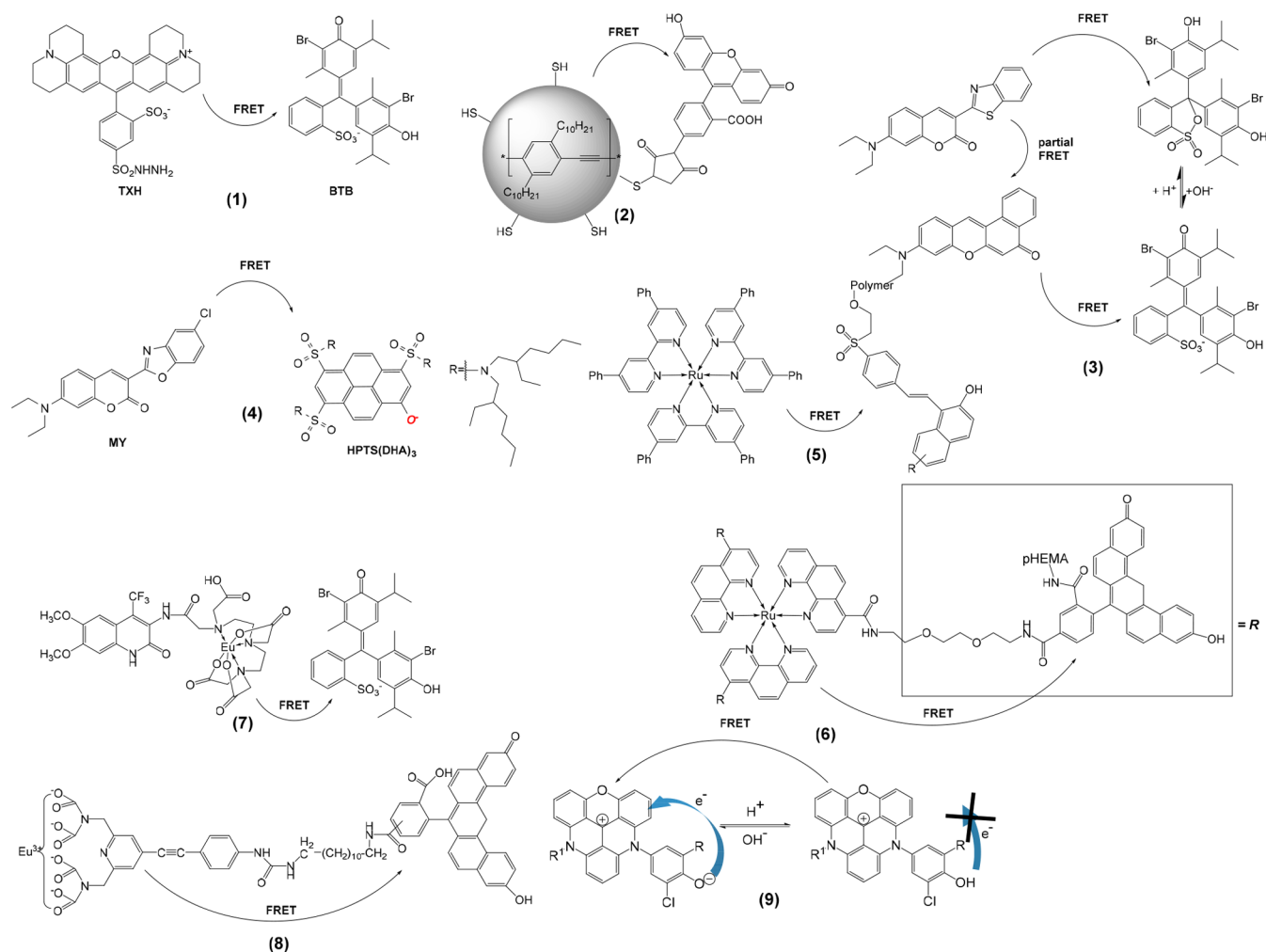


Figure 33. Chemical structures of the optical pH probes utilizing FRET.

fluorescent molecule, the observed anisotropy will be determined by the fluorescence lifetime τ and the rotational correlation time ϕ as follows: $r(t) = r_0 \exp(-t/\phi)$, where r_0 is the intrinsic anisotropy of the molecule.⁹³⁹ Thus, to observe a change in anisotropy the pH indicator should possess a short fluorescence lifetime (well below 1 ns) or be located in a highly viscous environment. It should also show a pronounced change in the fluorescence decay time upon (de)protonation but simultaneously possess comparable fluorescence quantum yields. Evidently, very few fluorescent pH indicators fulfill these requirements; however, viscosity/rigidity of the matrixes (polymeric hydrogels and particularly sol–gels) may be sufficient to observe an effect for fluorophores with decay times of several ns. An example of such system was presented by Lippitsch,⁹⁴⁰ who demonstrated potential suitability of 10-diethylaminomethylanthracene for pH sensing (albeit for dissolved dye) via anisotropy. The dye features a long fluorescence decay time of 20 ns in the acid form but a very short one (<0.1 ns) in the base form. Accordingly, an increase of anisotropy from 0 to 0.15 is observed as pH increases, the dependency almost ideally described by sigmoidal equation. No dependency of the calibration curve on concentration of the indicator was observed but the situation might be different in case of optical sensors where homo FRET can be significant.

Lakowicz et al.⁹⁴¹ proposed anisotropy-based read-out of pH sensors by using a reference luminophore. The measured

anisotropy r is determined by the intensity weighted average of the anisotropies of indicator and reference. Two combinations of an indicator and a reference luminophore has been proposed: (i) a reference with 0 anisotropy (long decay time) and an indicator with short decay time and (ii) a reference with high anisotropy (oriented fluorophores in stretched polymeric films) and a fluorescent indicator with close to 0 anisotropy. As a proof of concept, the authors used stretched poly(vinyl alcohol) films doped with a conjugated dye Py-2 (Figure 32) as a reference, which have anisotropy close to unity. 6-Carboxyfluorescein was used as a pH indicator in solution. Increase of pH resulted in enhancement of fluorescence of fluorescein and consequently in decrease of anisotropy (Figure 32). As in the case of all ratiometric read-out schemes, any variation in concentration of the indicator or a reference but also the excitation wavelength and the spectral window in which the emission is detected, will affect the calibration plot.

Lippitsch discussed the challenges of designing an optical sensor based on anisotropy measurement.⁹⁴⁰ Apart from above limitations in availability of suitable indicators and matrixes, the performance of the anisotropy sensor is compromised by light scattering, since scattered light is polarized. Thus, measurement in a scattering sample is difficult. To be inert to variation of the turbidity of the probe, the optical sensor must contain an additional black optical isolation layer. This, however, will result in a lower brightness since additives such as titanium dioxide

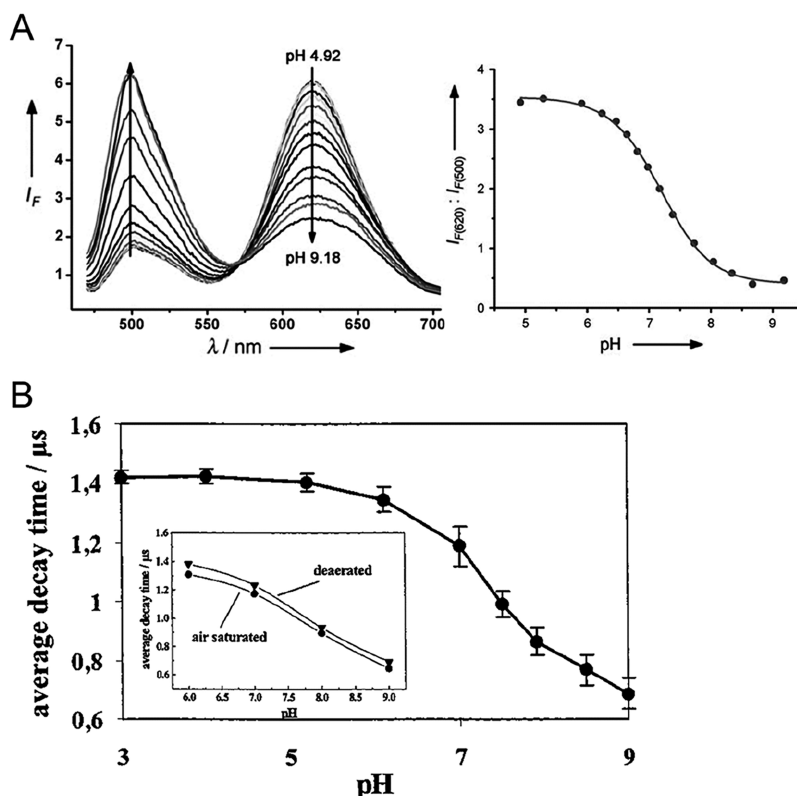


Figure 34. Examples of FRET-based pH sensors. (A) Fluorescence spectra (left) and pH calibration plot (right) for ratiometric pH-sensitive nanoparticles based on coumarin 6, Nile red, and BTB. Reprinted with permission from ref 768. Copyright Wiley-VCH Verlag GmbH & Co., KGaA, Weinheim 2010. (B) Luminescence lifetime-based pH sensing utilizing FRET from the phosphorescent Ru(II) polypyridyl dye to a pH-sensitive azadye. Reprinted with permission from ref 944. Copyright American Chemical Society 1998.

particles (section 9.2) cannot be used to enhance luminescence brightness via scattering. It should also be considered that protonation/deprotonation of the indicator may change the microviscosity of the matrix, which affects anisotropy. Also, reorientation of the fluorophores in the polymer (accelerated at higher temperatures) is likely to compromise the storage stability of such sensors.

10.4. Energy Transfer-Based Sensors

Förster Resonance Energy Transfer (FRET, section 2.2.3) can be very useful in optical pH sensing. It is utilized (i) to convert the response of an absorptiometric indicator (used as a FRET acceptor) into luminescence intensity/decay time change with help of a luminescent energy donor, (ii) to enable ratiometric $2-\lambda$ read-out by using a fluorescent pH-insensitive donor and a fluorescent pH-sensitive acceptor, and (iii) to enhance the luminescence brightness of pH sensors or to increase the Stokes shift via addition of energy donors with high molar absorption coefficients. The use of FRET from a fluorescent donor to a nonfluorescent pH-sensitive acceptor was first proposed by Walt and co-workers.⁴⁴ They prepared a fiber optic sensor containing fluorescent eosin and nonfluorescent pH sensitive phenol red in cross-linked polyacrylamide. Lakowicz and co-workers⁹⁴² pointed out potential limitations of the FRET approach, such as a drift of calibration, because of a change of the acceptor concentration caused by, for example, osmotic effects. Covalent coupling of an acceptor to a donor was indicated as a promising strategy to overcome the above drawback. Later, the same group reported a sol-gel pH sensor (TMOS) exploring FRET from Texas red hydrazide (TXH) to bromothymol blue (BTB) (1, Figure 33).⁶⁰⁸ In fact, the emission spectrum of TXH shows almost

perfect overlap with the absorption band of deprotonated BTB resulting in fluorescence quenching at pH > 6. Surprisingly, the material exhibited an extreme sensitivity to ionic strength and to the nature of the ions added.

FRET was widely used to design pH nanosensors suitable for ratiometric $2-\lambda$ read-out. Chan et al.⁶²⁰ reported semiconducting polymer dots ($\varnothing = 25$ nm) made of fluorescent poly(2,5-di(3',7'-dimethyloctyl)phenylene-1,4-ethynylene) (PPE) acting as energy donor and fluorescein as an energy acceptor (2, Figure 33). Upon excitation of the PPE (390 nm), the nanoparticles showed pH-sensitive green fluorescence from fluorescein and pH-insensitive blue fluorescence from PPE, used for referencing purpose.

Peng et al.⁷⁶⁸ prepared polyurethane nanoparticles ($\varnothing = 137$ nm) doped with pH insensitive dyes coumarin 6 and Nile red and absorptiometric pH indicator bromothymol blue (BTB) (3, Figure 33). The coumarin 6 antenna enables efficient excitation with blue light and partly transfers the energy to Nile red. FRET from the coumarin 6 to the protonated form of BTB results in a decrease of green fluorescence ($\lambda_{\text{max}} = 500$ nm) at low pH (Figure 34). On the other hand, deprotonated form of BTB acts as an energy acceptor for Nile red, resulting in quenching of the red emission at high pH making the nanoparticles suitable for ratiometric read-out.

FRET represents an efficient way to increase the brightness of the optical sensors.⁹⁴³ The energy acceptor is an indicator, which possesses the desired properties but features comparably low molar absorption coefficients and therefore low brightness. Addition of bright antenna fluorophores helps to overcome this limitation. Larsen et al.³⁷⁴ used a coumarin antenna (Macroleux

yellow) to enhance the brightness of 1-hydroxypyrene-3,6,8-tris(2-ethylhexyl)sulfonamide (HPTS(DHA)₃), **4**, Figure 33. The absorption of the deprotonated form of HPTS(DHA)₃ ($\lambda_{\text{max}} = 525$ nm) almost ideally overlaps with the emission of the coumarin ($\lambda_{\text{max}} = 505$ nm) resulting in strong fluorescence enhancement upon excitation with blue light. On the contrary, the protonated form of the pH indicator absorbs at 433 nm, so no FRET is possible and the emission from the coumarin is observed. Thus, the sensor is suitable for ratiometric 2- λ read-out realized via measuring of green fluorescence from the coumarin (low pH) and orange fluorescence from HPTS(DHA)₃ (high pH).

Nanoparticles based on conformational changes in the polymer, which promotes FRET between the chromophores represent a very interesting approach.^{871,877} Also, many nanosensors based on inorganic semiconductor quantum dots employ FRET to render the emission pH sensitive.^{807,808} Often, this allows to generate pH-dependent changes in the fluorescence decay time and makes the probes suitable for FLIM imaging.⁸⁰⁸ Notably, the fluorescence lifetime of QDs is significantly longer than that of organic fluorophores so that the fluorescence background can be efficiently eliminated even in the quenched state.

As was mentioned in section 10.2, measurement of relatively long luminescent lifetimes is attractive from practical point of view. Apart from metal–ligand complexes, which show intrinsic response of their decay time to pH, it is also possible to design optical sensors based on FRET. Here, a bright pH-insensitive luminescent metal complex acts as an energy donor whereas a pH indicator acts as an energy acceptor in one of its forms. Importantly, a wide range of absorptiometric indicators can be used. Kosh et al.⁹⁴⁴ prepared several sensors based on ruthenium(II) tris-4,4-diphenyl-2,2-dipyridyl as an energy donor and a pH-sensitive dye (BTB or an aza-dye) as an energy acceptor (**5**, Figure 33). The efficiency of FRET was highly dependent on BTB concentration, and 10 mmol/kg of BTB was necessary to achieve sufficient response. FRET was efficient at high pH, resulting in decrease of the luminescence lifetime of the Ru(II) complex from 1.44 μs at pH 5 to 0.76 μs at pH 9 (Figure 34). The cross-sensitivity to oxygen was very modest: reduction of the decay time from 1.38 to 1.31 μs at pH 6 was observed on changing from O₂-free to air-saturated solution, which is equivalent in error of 0.16 pH units. Nevertheless, photosensitized singlet oxygen accelerated photodegradation of the pH indicator, particularly in its deprotonated form. More advantageously, the distance between the donor and acceptor can be kept constant with help of a covalently bound spacer (**6**⁹⁴⁵ and **8**,⁹⁴⁶ Figure 33). As energy donors, Eu(III) chelates (**7**^{550,947} and **8**,⁹⁴⁶ Figure 33) represent an interesting alternative to the Ru(II) complexes since their luminescence is only slightly quenched by oxygen despite long decay times of several hundreds of microseconds.

Dalfen et al.⁵²⁴ reported pH sensors utilizing diazaoxotriangulenium (DAOTA) dyes (**9**, Figure 33). In solution, the indicators showed “on”–“off” behavior due to fluorescence quenching via photoinduced electron transfer. In contrast, a clear dependency of the fluorescence decay time was observed for the dyes immobilized into polyurethane hydrogel. The lifetime response was the most pronounced for the sensors using high dye loading (0.5–1 wt %) and was attributed to homo-FRET from the fluorescent protonated to nonfluorescent deprotonated form of the dye.

A comparative table of optical pH sensors based on FRET can be found in the Supporting Information (Table S12).

The above examples demonstrated usefulness of FRET in design of optical pH sensors. Limitations of these sensors arise from the fact that FRET efficiency is determined by the distance between the donor and acceptor and consequently their concentration in the sensing material. Thus, if the pH indicator that acts as a FRET acceptor is leached out of the sensor, a substantial drift of the calibration is expected. Water uptake (swelling) of the polymers might be affected by temperature or ionic strength, which, therefore, may also affect the calibration. Preparation of conjugates in which donor and acceptor are covalently coupled through a spacer, is a preferable strategy to minimize the above effects, but it can be challenging from synthetic point of view. In case of phosphorescent energy donors, photobleaching can be very fast due production of highly reactive singlet oxygen. Evidently, destruction of the donor or acceptor by photosensitized singlet oxygen will result in the sensor drift.

10.5. Other Luminescent Sensing Schemes for pH

Several reported pH optodes rely on the inner-filter effect on fluorescence. These sensors are based on absorptiometric indicators (section 3), which are highly versatile with respect to their chemical structure and acidity constants. Some of the cross-sensitivities of fluorescence (e.g., dynamic quenching) can be avoided. In this method, the intensity of an inert emitter (fluorescent dye, quantum dot, inorganic phosphor) is modulated by the pH-dependent absorption of the indicator, which screens off excitation light or emitted light. To obtain a ratiometric response, a mixture of several emitters can be used. For example, Suzuki and co-workers⁹⁴⁸ fabricated a pH sensor, which contained two types of photostable quantum dots ($\lambda_{\text{em}} = 525$ and 605 nm, respectively) embedded into a sol–gel layer and a colorimetric indicator (Congo red or Basic Fuchsin) immobilized into a second sol–gel layer. Both sensors showed decrease of the red fluorescence at lower pH accompanied by simultaneous enhancement of the green fluorescence. The sensors based on the use of Congo red or Basic Fuchsin showed dynamic ranges between pH 2–6 and 0.2–1.2. A wide-range sensor (containing a mixture of neutral red and methyl yellow) covering the pH range from 4 to 10 was also prepared and showed remarkably linear calibration but also relatively low resolution.

Borisov and Klimant reported a similar approach⁹⁴⁹ but used inorganic phosphor micropowders as luminescent emitters. Compared to metal(organic) dyes and quantum dots, these emitters show exceptional chemical and photochemical stability and inertness to potentially interfering species such as oxygen or ions. On the other hand, the brightness of the phosphors is lower than that of the dyes. Broad-band excitation and/or emission spectra allow using a single phosphor for ratiometric 2-wavelength read-out based inner filter effect. For instance, in the first concept (Figure 35A) the NIR emission of chromium(III)-doped gadolinium aluminum borate (Cr-GAB) was modulated by the pH-dependent absorption of an aza-BODIPY indicator (section 4.1) due to overlap of the protonated and deprotonated forms of the indicator with short-wavelength and long-wavelength components, respectively, of the broad emission of Cr-GAB (Figure 35B). Long luminescence decay time of the phosphor (85 μs) enabled complete elimination of the background fluorescence originating from the protonated form of aza-BODIPY, which otherwise interferes (Figure 35).

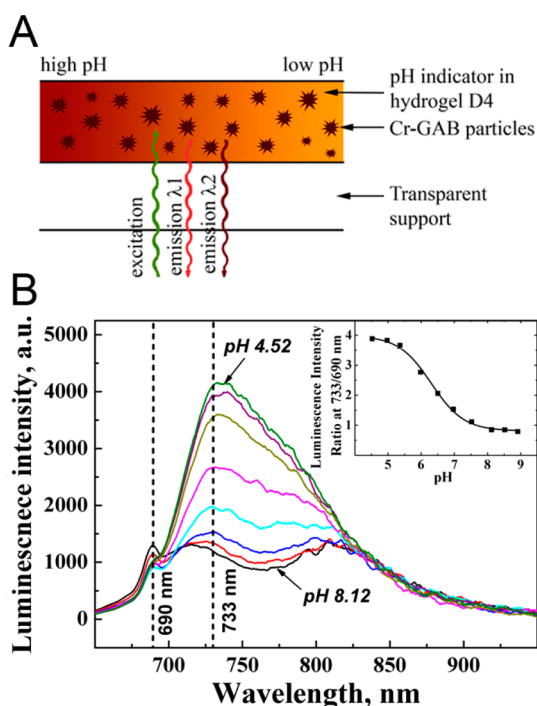


Figure 35. (A) Cross-section of an optical pH sensor based on inner-filter effect read-out. (B) Emission spectra of the pH sensor ($\lambda_{\text{exc}} = 590$ nm) obtained in a time-resolved measurement (delay 20 μs) and resulting calibration curve (inset). Reprinted from ref 949 with permission from Elsevier. Copyright Elsevier B.V. 2013.

Reliable ratiometric 2- λ read-out was possible (Figure 35B, inset). In the second mode, the pH indicator *m*-cresol purple was used. Cr-GAB features two excitation bands in the blue and orange parts of the spectrum. The protonated and deprotonated forms of *m*-cresol purple overlap with the first and the second excitation bands of the phosphor, respectively, thus making ratiometric measurement in the excitation mode possible. The phosphor Egyptian blue features similar properties (broad excitation at 500–700 nm, NIR emission at >800 nm) and also is suitable for the ratiometric read-out in the excitation mode.¹⁵³ It was also shown that simultaneous sensing of pH and temperature is possible.⁹⁴⁹ Cr(III)-activated yttrium aluminum borate is used as a phosphor that has identical excitation spectra at different temperatures but its decay time is highly temperature-dependent.

Wolfbeis and co-workers⁹⁵⁰ made use of the inner-filter effect to design an upconversion-based pH sensor. $\text{NaYF}_4:\text{Er},\text{Yb}$ nanorods (50 nm in diameter and 950 nm in length) show pH-independent green (511–566 nm) and red (635–685 nm) emission under excitation with a 980 nm laser. The nanorods were dispersed in a polyurethane hydrogel containing dissolved bromothymol blue (BTB). The absorption of BTB overlaps the emission, which therefore can be modulated by pH. The effect was found to be different for the two bands, which enables ratiometric measurement. In further work,⁹⁵¹ the indicator was substituted by neutral red, which is more lipophilic and enables better modulation of the green luminescence of the nanorods. Analogous systems were reported by Xi et al.⁹⁵² (section 10.6) and Strobl et al.,⁹⁵³ who used a combination of a molybdate phosphor doped with Yb(III), Ho(III), and Tm(III) and a NIR-absorbing aza-BODIPY indicator.

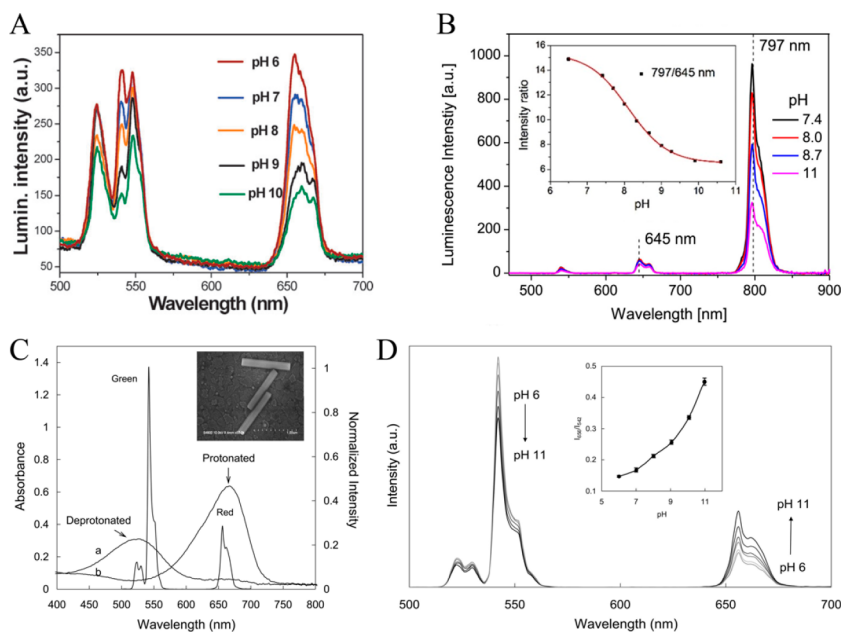


Figure 36. Examples of pH sensors based on lanthanide upconversion. (A) pH-dependent upconversion spectra for the sensor film utilizing $\text{NaYF}_4:\text{Er}^{3+},\text{Yb}^{3+}$ nanorods and bromothymol blue. Reprinted with permission of The Royal Society of Chemistry from ref 950. Copyright The Royal Society of Chemistry 2009. (B) pH-dependent upconversion spectra of the sensor film containing $\text{NaCaY}_{0.2}\text{Yb}_{0.7}\text{Tm}_{0.02}\text{Ho}_{0.08}(\text{MoO}_4)_3$ microcrystalline powder and an aza-BODIPY pH indicator and the respective calibration plot (inset). Reprinted from ref 953 with permission from Elsevier. Copyright Elsevier B.V. 2017. (C) Emission spectra of the $\text{NaYF}_4:\text{Yb}^{3+},\text{Er}^{3+}$ nanorods (inset) together with the absorption spectra of the ETH 5418 pH indicator in protonated and deprotonated forms. Reprinted with permission from ref 952. Copyright American Chemical Society 2012. (D) pH-dependent upconversion spectra for the sensor film containing $\text{NaYF}_4:\text{Yb}^{3+},\text{Er}^{3+}$ nanorods and ETH 5418 in plasticized poly(vinyl chloride) and the respective calibration plot (inset). Reprinted with permission from ref 952. Copyright American Chemical Society 2012.

The red fluorescence of 2 nm gold nanoclusters (AuNCs), with excitation/emission peaks at 470/640 nm, is strongly modulated by the pH indicator BTB.⁹⁵⁴ BTB is present in a bovine serum albumin shell on the AuNCs. Sensitivity to pH results from an inner filter effect due to spectral overlap between the pH-dependent absorption of BTB and the emission of the AuNCs. The method was applied to quantify and to image pH values (between 5 and 9) that occur after the death of red blood cells. Such pH changes are considered as a potential forensic marker for estimating the time passed since death has occurred.

10.6. pH Sensors Based on Upconversion and 2-Photon Absorption

Probes that emit at wavelength shorter than the excitation wavelength, are of high interest for their ability to eliminate fluorescence background. Anti-Stokes luminescence can be generated via three main types: (i) lanthanide upconversion, (ii) triplet–triplet annihilation based upconversion (TTAU), and (iii) multiphoton absorption (most prominently two photon, 2-P). TTAU has been almost exclusively investigated for energy conversion applications and has not been explored for design of pH probes that is explained by strong oxygen quenching of the molecules in the triplet state that are involved in the upconversion process. On the other hand, several pH sensors based on lanthanide upconversion and two-photon excitation have been reported. For these two types, the luminescence quantum yields are much lower than for conventional single-photon probes. Therefore, the required energies of excitation light vary from high (lanthanide upconversion) to very high (2-P excitation). Consequently, the scope of 2-P probes is restricted to microscopic imaging, which is also the main application of the lanthanide upconversion.

Application of lanthanide upconversion in microsensors and planar optodes is still possible but advantages of the anti-Stokes luminescence are balanced by the bulkiness of the setup. In case of bulk optodes, a good NIR probe can deliver very low levels of autofluorescence. pH sensors based on upconverting materials benefit from high chemical and photochemical stability of the inorganic upconverting emitters. Wolfbeis and co-workers⁹⁵⁰ were the first to report a pH sensor relying on lanthanide upconversion. They modulated the upconverted green and red luminescence of NaYF₄:Er³⁺,Yb³⁺ nanorods (emission λ_{\max} = 540 and 660 nm) via an inner-filter effect (section 2.2.4) caused by the pH indicator bromothymol blue (Figure 36A). Both components were embedded into a polyurethane hydrogel layer. Referenced ratiometric measurement is possible since the red emission of the nanorods is modulated to a higher extent (2-fold intensity decrease from pH 6 to 10) than the green one. In further work reported by the same group, bromothymol blue was substituted by neutral red.⁹⁵¹ The protonated form of the latter almost perfectly overlaps the green emission of the upconverting nanoparticles resulting in a strong inner filter effect. Since the indicator does not absorb in the red part of the spectrum, the red emission from the nanorods is not modulated by pH and is suitable for referencing. For the first time, ratiometric RGB imaging (see section 11.1 for more details) with planar optodes under NIR excitation became possible because both green and red emission from the upconverting nanoparticles (UCNPs) almost perfectly overlap with the respective color channels of an RGB camera. Anker and co-workers prepared a rather complex sensor utilizing a layer containing UCNPs and a pH-sensitive layer based on bromocresol green in a sol–gel material.⁹⁵⁵ Since the

deprotonated form of the dye only partly overlaps the red emission band of Er³⁺, the upconverted emissions at 671 and 661 nm are modulated to a different extent. In practice, it is challenging to separate two emission peaks separated by only 10 nm.

Xi et al.⁹⁵² demonstrated that the response of an upconversion sensor can be further improved by using indicators if spectral properties better match the emission of the lanthanide nanorods. The absorption of the protonated form of a lipophilic Nile blue derivative (ETH 5418, Chromoionophore VII, λ_{\max} = 670 nm; designed by Simon et al.^{86,87}) shows almost perfect overlap with the red emission of the nanorods, whereas the absorption of the deprotonated form (λ_{\max} = 525 nm) matches very well with the green emission of the nanorods (Figure 36C). Consequently, the luminescence intensity at 660 nm increases as the pH increases, and the opposite effect is observed for the green emission (Figure 36D). Since the pH indicator and the nanorods were embedded in a matrix consisting of poly(vinyl chloride), sodium tetrakis-[3,5-bis(trifluoromethyl) phenyl] borate and a plasticizer were necessary.

The above nanosensors are based on the NaYF₄:Er³⁺,Yb³⁺ phosphor and utilize the dual emission of the Er³⁺ (green and red). Strobl et al.⁹⁵³ presented an attractive alternative. A molybdate host was doped with Yb³⁺, Ho³⁺, and Tm³⁺ to give dual (red; λ_{\max} = 645 nm and NIR; λ_{\max} = 797 nm) emission under 980 nm excitation (Figure 36B). The NIR emission of the phosphor decreased in basic media due to rise of the NIR absorption of the aza-BODIPY indicator, whereas the red emission of the phosphor remained almost constant and can serve as a reference. Ma et al.⁹⁵⁶ coupled the pH sensitive dye xylenol orange to the amino-modified surface of silica-coated UCNPs (NaYF₄:Yb³⁺,Tm³⁺). Because of an inner filter effect, the protonated form of xylenol orange reduced the fluorescence intensity of the blue upconverted emission, whereas red emission from the beads remained unchanged.

NaYF₄:Yb³⁺,Tm³⁺ UCNPs have inert dual emission (blue, 451 and 475 nm; red, 646 nm) under 980 excitation.⁹⁵⁷ The blue emission can be used to excite a BODIPY dye equipped with a pH-sensitive PET group and is spectrally well separated from the fluorescence (green, 500–600 nm) of the dye. The red UC emission serves as a reference for ratiometric measurement.

Other authors utilized FRET from the upconverted phosphor to a pH sensitive indicator. Schäferling and co-workers⁹⁵⁸ coated NaYF₄:Yb³⁺,Er³⁺ nanocrystals with a silica shell and further modified it with the pH indicator pHrodo Red. Under NIR excitation, the organic dye emitted upconverted emission at 590 nm as a result of the energy transfer from the lanthanide nanoparticles. Unfortunately, sensitization of the fluorescence was very inefficient, most likely because of a too large distance between donor and acceptor. Li et al. noncovalently immobilized a pH sensitive hemicyanine dye onto core–shell–shell upconverting Yb³⁺, Tm³⁺-doped particles to obtain ratiometric green/red emission response.⁹⁵⁹

Tsai et al.⁹⁶⁰ investigated the mechanism of pH-sensitivity of upconversion nanoparticles that are coupled to pH indicators. They electrostatically bound the indicators to UCNPs with polyethylenimine shells of varying thickness. For the thick layer shells, the pH effect was solely due to the inner filter effect. For the thin layer shells, the situation was more complex. Contrary to previous expectation, the main effect remained emission-reabsorption. The resonance energy transfer occurred only with ~10% efficiency. This is attributed to the fact that only Er³⁺

ions close to the surface are within the Förster distance for UC-RET with the dye.

Several groups utilized a common strategy of coating the UCNPs (capped with oleic acid) with polyethylenimine layer to introduce amino groups and subsequent covalent coupling of a pH indicator to the latter. Kong and co-workers used $\text{NaYF}_4:\text{Yb}^{3+},\text{Tm}^{3+}$ nanoparticles in combination with a fluorescein dye.⁹⁶¹ The dye acted as a FRET acceptor, which was confirmed by the strong decrease of the luminescence decay time of the upconverted green emission after dye coupling. Because of the pH-dependent FRET, the blue emission of the nanoparticles ($\lambda_{\text{max}} = 475 \text{ nm}$) decreased and the green emission of fluorescein ($\lambda_{\text{max}} = 510 \text{ nm}$) increased with increasing pH, whereas the red upconverted emission was pH-independent and served as a reference. Another group utilized a similar material but doped Nd^{3+} into the inner shell to enable sensitization at 808 nm in addition to the typical sensitization wavelength of 980 nm because of Yb^{3+} .⁹⁶² Finally, Schäferling and co-workers used polyethylenimine-coated $\text{NaYF}_4:\text{Yb}^{3+},\text{Er}^{3+}$ instead of $\text{NaYF}_4:\text{Yb}^{3+},\text{Tm}^{3+}$ beads and yellow light emitting pHrodo red indicator instead of FITC.⁹⁶³ This material enabled ratiometric sensing and imaging of intracellular pH.⁹⁶³

In contrast to the above upconversion based pH sensors, the pH sensor reported by Zhao and co-workers⁸⁸³ explored the quenching properties of graphite oxide. Positively charged polyethylenimine-coated $\text{NaYF}_4:\text{Yb}^{3+},\text{Er}^{3+}$ nanoparticles were electrostatically immobilized on graphite oxide nanosheets. This resulted in the formation of $\sim 50 \text{ nm}$ large composites, which showed linear decrease of luminescence intensity ($\lambda_{\text{max}} = 540 \text{ nm}$, 980 nm excitation) in the pH range 5.0–8.0. This change was attributed to an increase of the negative charge of graphite oxide and in a shortening of the distance between the UCNPs and the quencher promoted by stronger electrostatic interaction. A bulk optode was constructed by depositing the nanoparticles into the pores of a membrane filter via vacuum filtration. The extent of quenching was rather moderate (35%) but sensing was fully reversible. A similar material modified with APTES has a slightly wider pH range from 5 to 9.⁹⁶⁴

It should be noted that several reported upconverting pH “sensors” are actually only single-shot assays since the UCNPs are simply dispersed in an aqueous solution of a pH sensitive dye.^{965,966} The state of the art in upconversion luminescence based pH nanoprobables has been reviewed by Mahata et al.⁶⁹⁸

The pH probes based on lanthanide upconversion are summarized in Table S13.

Two photon (2-P) excitation is another attractive possibility to eliminate the autofluorescence. In case of 2-P probes, the intensity of the emission is proportional to the square of the excitation light intensity. This makes them attractive for imaging applications due to better resolution and lower photobleaching rates compared to 1-P probes. Additional benefits include better penetration depth of NIR light, which is useful for imaging in tissues and tissue models, such as spheroids. By analogy to the brightness of conventional probes determined by molar absorption coefficient and luminescence quantum yield, the brightness of 2-P probes depends on their quantum yield and 2-P absorption cross-section (σ_2). Unfortunately, most conventional 1-P dyes are poor two photon absorbers with a 2-P cross-section of 1–20 Goeppert Mayer (GM) units. Compared to 2-P excitable pH probes (indicator molecules),^{967,968} the number of 2-P nanosensors is even smaller. For instance, Jia et al.⁸⁵³ reported on carbon dots with 2-photon absorption and pH-sensitive emission. The fluorescence intensity decreases on

going from pH 4 to 8. Kong et al.⁹⁶⁹ prepared carbon dots with a very high 2-P cross-section of $32\,000 \pm 4500 \text{ GM}$ at 800 nm. The carbon dots have surface bound terpyridine units that induce pH sensitivity in the pH range from 6 to 8.5. They allowed imaging in living cells and tissues in depths up to 185 μm . Kim et al.⁵²⁶ designed a fairly bright pH probe for 2-P imaging based on naphthalenylvinylpyridine incorporated into ormosil beads ($\phi = 33 \text{ nm}$). Both the protonated and neutral form of the dyes are emissive ($\lambda_{\text{max}} = 565 \text{ nm}$, $\phi = 0.18$ and $\lambda_{\text{max}} = 460 \text{ nm}$, $\phi = 0.06$). The protonated form can be excited with NIR light ($\lambda_{\text{max}} = 800 \text{ nm}$, $\sigma_2 = 52 \text{ GM}$), whereas excitation of the neutral form is weaker ($\lambda_{\text{max}} = 750 \text{ nm}$, $\sigma_2 = 4 \text{ GM}$). Ratiometric emission read-out in the 2-P mode was demonstrated to be possible, and the calibration plot correlates very well with that obtained under 1-P excitation. Deficiencies of such methods include (a) the lack of dedicated pH sensing materials suitable for 2-P read-out, (b) the lack of an adequate referencing method due to nonlinear dependency of the emission light intensity on the intensity of the excitation light, and (c) loss of the excitation light by scattering, which diminishes the signal. All these effects may result in wrong pH values.

10.7. Multiparameter Sensors

The unique possibility of light to guide multiple information simultaneously can be utilized for multiparameter sensing. Simultaneous monitoring of different parameters, such as pH, pO_2 , and pCO_2 , is of much interest in biotechnology, marine science, medicine, and many other fields. Basic principles are covered in reviews^{970,971} and will be only briefly discussed here. One may distinguish between (a) arrays of several spots or fiber sensors in close spatial proximity (poor spatial resolution, not suited for intracellular sensing), (b) several indicators in the sensor layer (μm resolution), (c) several sensor beads in the same polymer host, and (d) indicators sensitive toward two parameters each with distinct influence on the luminescence properties. The advantages of single material multiparameter sensors include high spatial resolution and compact setup. However, they may suffer from optical cross-talks originating from inadequate signal separation. Often, a combination of several probes with desired photophysical properties can be found, but this requires a compromise between the best optical match and other properties, including brightness, photostability, and sensitivity.

Gehrich et al.⁴¹ described a sensor array for intravascular measurements composed of three fiber-optic sensors (pH, oxygen, and carbon dioxide) and a thermocouple for compensation of the temperature cross-talk. A discontinued Paratrend sensor (Diametrics Medical)⁹⁷² adapted a very similar approach (Figure 37A). Another array reported by Weigl et al.⁷⁶ included a flow-through cell with integrated absorptiometric pH and pCO_2 sensors and pO_2 sensor based on luminescence quenching. Walt and co-workers modified different parts of an imaging fiber ($\phi = 350 \mu\text{m}$) composed of 3000 individual elements with sensing materials for pH, pO_2 , and pCO_2 . The modification was performed via photopolymerization by illuminating different areas of the fiber array to deposit the respective “sensing chemistry”.⁴²⁹

Multianalyte sensors can be realized in a number of formats (section 14) including fiber-optic sensors,^{381,419,423} planar optodes,^{435,921} or nanosensors^{881,974} (section 8). Multiparameter optodes that rely on use of a single sensing material are mostly limited to dual sensors. It becomes increasingly difficult

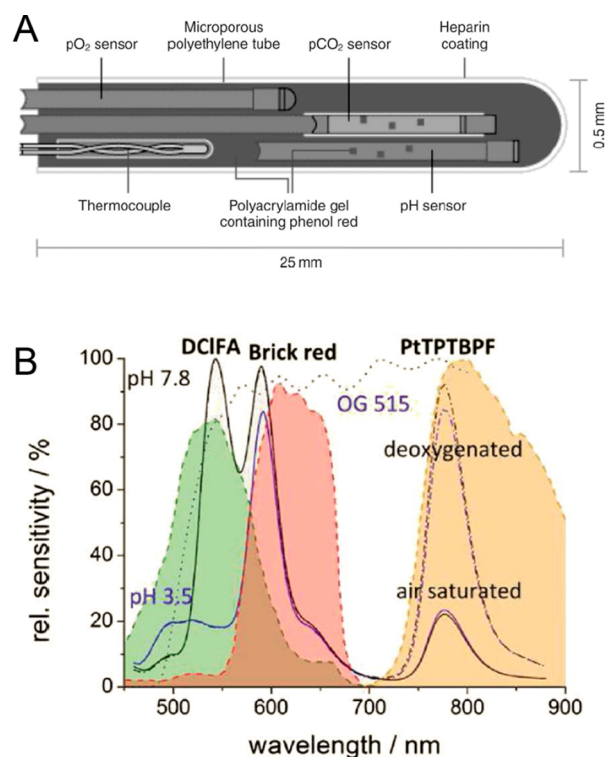


Figure 37. (A) Cross-section of the Paratrend 4-parameter array sensor. Reprinted by permission from Springer Nature from ref 972. Copyright Springer Nature 2004. (B) Spectral properties of the pH/pO₂ dual sensor at different pH and oxygen concentrations as well as the spectral sensitivity of the camera channels. (DCIFA, 2',7'-dichloro-5(6)-N-octadecyl-carboxamidofluorescein; PtTPTBPF, platinum(II) *meso*-tetra(4-fluorophenyl) tetrabenzoporphyrin) Reprinted from ref 973 with public license. Published by The Royal Society of Chemistry.

to find a suitable combination of individual probes but also the complexity of required instrumentation and optical components is increased significantly. In fact, only a few reported sensors can measure 3 or 4 parameters simultaneously.^{384,398} Among dual sensors, combination of pH with oxygen^{115,441,703,975} and pH with temperature is most common. Here, we do not consider some “dual” probes reported in the literature, which apart to their response to pH also show response to another parameter.^{845,976,977} These probes do not allow simultaneous quantification of the analytes since the changes produced by two (or more) analytes are virtually indistinguishable.

The information generated by individual probes is separated either spectrally or via decay time. In the first case, ratiometric approach (section 2.11) is useful. The individual probes and the reference are excited with a single light source but have to have different emission spectra.^{441,973} The information can be separated by emission filters or an RGB camera. Meier et al. reported a planar optode for simultaneous imaging of pH and oxygen with help of an RGB camera.⁴⁴¹ Three types of microparticles (FITC covalently bound to amino-cellulose, Pt(II) porphyrin embedded into polystyrene beads, and diphenylanthracene immobilized into polyacrylonitrile beads) act as probes for pH, oxygen and a reference fluorophore, respectively. All of them are dispersed in a single layer of polyurethane hydrogel, which is permeable for protons and oxygen. The probes show blue (diphenylanthracene), green (FITC), and red (Pt(II) porphyrin) luminescence. In a similar design, Chen and co-workers⁹⁷⁸ prepared a dual-sensor for pH

and oxygen suitable for the read-out with a color chip of a smartphone. Red-emitting oxygen-sensitive nanobeads based on Pt(II) porphyrin were dispersed in a hydrogel composed of cross-linked chitosan. FITC was reacted with the hydrogel to introduce pH sensitivity. Blue-emitting 4,40-bis(2-benzoxazolyl)stilbene served as a reference.

Tian et al.⁹⁷⁹ immobilized green-emitting 4-amino-1,8-naphthalimide-based pH indicator and red-emitting Pt(II) tetraphenylporphyrin-based oxygen indicator into a cross-linked poly(2-hydroxyethyl methacrylate-*co*-acrylamide) hydrogel. Since no reference dye has been added, dual sensing of pH and oxygen is only possible in intensity mode. Referencing of the oxygen indicator against pH probe and vice versa can only be performed if one of the two parameters remains constant during calibration and measurement.

Ehgartner et al.⁹⁷³ designed a dual sensor for pH and oxygen by using lipophilic 2',7'-dichloro-5(6)-N-octadecyl-carboxamidofluorescein (DCIFA) as a pH indicator, platinum(II) *meso*-tetra(4-fluorophenyl) tetrabenzoporphyrin (PtTPTBPF) as an oxygen indicator and fluorescent pigment brick red as a reference. Under excitation with blue light DCIFA, brick red, and PtTPTBPF emit in the green, red, and NIR parts of the spectrum (Figure 37B). It was utilized for the read-out with a dual chip RGB-NIR camera.

Spectral overlap between the emission spectra is difficult to avoid in practice. Hence, probes with narrow emission bands are particularly useful. For instance, the very narrow emission band of Eu(III) complexes is beneficial in a dual pH/O₂ optode⁹²¹ and in a triple pH/pO₂/temperature optode.³⁸⁴ In the former, the red-emitting Eu(III) complex used as an oxygen probe was combined with NIR-emitting aza-BODIPY pH indicator and a green-emitting coumarin reference. The sensor was used for imaging with a dual chip RGB/NIR camera. It was found that the dual sensor relying on a Pt(II)-porphyrin used instead of the Eu(III) complex suffers from optical cross-talks between oxygen and pH and vice versa due to significantly broader emission spectrum of the Pt(II) porphyrin compared to the Eu(III) complex. In contrast to the above material, the triple sensor reported by Stich et al.³⁸⁴ utilizes another Eu(III) complex as a temperature probe, which is immobilized into poly(vinyl chloride) microparticles to minimize oxygen cross-talk. The pH is detected by a hydroxypyrenetrisulfonate (HPTS) derivative immobilized onto pHEMA beads, and oxygen is monitored by a Pt(II) *meso*-tetrapentafluorophenyl-porphyrinlactone (PtTFPPL) in poly(styrene-*co*-acrylonitrile) microparticles. All three probes are dispersed in a polyurethane hydrogel. They are excited with a 405 nm LED and the signals are clearly separated spectrally: the pH, temperature and pO₂ probe emit in the green, red and NIR parts of the spectrum, respectively. Oxygen and temperature are accessed via decay time measurement (imaging in time domain), and pH via ratiometric intensity imaging referenced either to the pO₂ or to the temperature probe.

Another triple sensor⁹⁸⁰ combines HPTS as a pH indicator, ruthenium(II) tris(4,7-diphenyl-1,10-phenanthroline) (Ru-dpp) as an oxygen probe, and CdSeTe quantum dots as a temperature probe. Although the luminescence signals of the indicators are well separated, the sensitivity of the oxygen and temperature probes are rather low (10% intensity change for 0–100% O₂ and about 10% intensity change for the temperature probe in the range 10–45 °C).

The dual lifetime referencing technique (section 2.2.7) can be modified so that simultaneous detection of two parameters

becomes possible. This method is referred to as mDLR. The information on pH values is obtained from the fluorescence of a pH indicator, which is referenced against the slow-decaying luminescence of the reference dye. The lifetime response of the reference delivers information on the second parameter. This method was demonstrated to be useful both in frequency domain^{150,381} and in time domain.⁹⁸¹

Even 4-parameter sensing (pH, pO₂, pCO₂, temperature) has been demonstrated.³⁹⁸ The method utilizes a combination of two pairs of optical probes (fluorescent and phosphorescent) which are spectrally independent of each other. The first layer includes oxygen-sensitive phosphorescent Ir(III)-coumarin embedded in polymeric beads made from cross-linked poly(styrene-*co*-divinylbenzene). They are dispersed in an ethylcellulose layer. Fluorescent HPTS and a quaternary ammonium base are dissolved in ethylcellulose to render the layer CO₂-sensitive. Both dyes are excitable by blue light and emit in 500–600 nm window. The information is extracted by measuring the overall phase shift at two modulation frequencies. The upper layer is composed of temperature-sensitive phosphor (a Cr(III)-activated yttrium aluminum borate) and a lipophilic fluorescent SNARF pH indicator in a hydrogel. Both probes can be excited with red light and emit in far-red; they behave completely independently on the pO₂ and pCO₂ probes. The disadvantages include high complexity of the optical setup and multilayer architecture of the sensing material that combines the hydrophobic lower layer and the hydrophilic upper layer.

Indicators with dual sensitivity reduce the complexity of multiparameter sensors. They eliminate consideration of spectral compatibility and different leaching or photobleaching rates. It can be difficult, however, to find a suitable indicator and a matrix depending on which combination of parameters are to be measured. Wolfbeis⁹⁸² early demonstrated the feasibility of sensing two parameters (pH, oxygen) with one indicator (HPTS) and introduced two approaches for measurement. In the two wavelength approach, the pH is determined via the ratio of intensities measured at the isosbestic point (pH independent) and the emission peak of the anion. As parameter for oxygen, the fluorescence intensity at the isosbestic point is measured. In the second approach, the oxygen content is assessed via the fluorescence decay time that decreases with increasing oxygen concentration. Other indicators for determination of two parameters (pH/O₂, pH/T, CO₂/O₂, pH/Cl⁻) were proposed. Papkovsky and co-workers³⁶⁶ reported metalloporphyrins modified with a Schiff base moiety (Figure 38) as indicators for pH/O₂ determination. Protonation of the Schiff base results in a decrease of the absorption at 400 nm and the formation of a new maxima at 440 nm. This is accompanied by a decrease of phosphorescence. Phosphorescence is also quenched by oxygen, resulting in decrease of phosphorescence intensity and decay

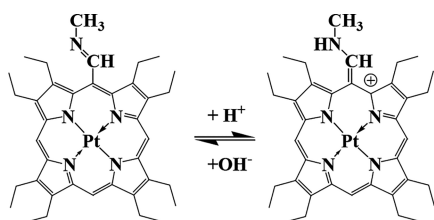


Figure 38. Chemical structure and acid–base equilibrium for Pt(II) porphyrin acting as a dual indicator for oxygen (via phosphorescence quenching) and pH (via absorption changes).

time. Such properties enable simultaneous measurement of pH and oxygen either via (i) measurement of overall emission intensity (influenced by pH and oxygen) and phosphorescence decay time (influenced by oxygen only) or (ii) via measurement of absorbance/reflectance at two wavelengths (the ratio depends only on pH) combined with determination of phosphorescence decay time. The second schema is preferred due to its self-referenced nature. The proper selection of either Pt(II) or Pd(II) complex allows tuning of the dynamic range for oxygen measurement since the decay times of both complexes are largely different.

Multiparameter sensing and imaging with nanosensors (section 8) is also popular.^{881,974} The design of multiparameter nanosensors is challenging; in contrast to bulk optodes, the dyes in nanosensors can be located closer to each other promoting undesired quenching via FRET or accelerated photobleaching. Leaching of the indicators and reference dye may be more critical. Spatial separation of the dyes in a core–shell approach appears to be a promising solution. The dual nanosensors reported by Wang et al.⁸⁸¹ rely on a unique core–shell structure. A lipophilic oxygen indicator and a reference dye (Pt(II) benzoporphyrin and metal-free porphyrin, respectively) are embedded into a soft hydrophobic poly(propylene oxide) core, which is rigidized with a silane agent; pH sensitive FITC is covalently attached to the poly(ethylene glycol) groups of the shell. The core–shell structure warrants good dispersibility and high stability of the nanosensors ($\varnothing = 12$ nm) in aqueous media, whereas PEG chains render them cell-impermeable. The dyes emit in the green (FITC), red (metal-free porphyrin) and NIR (Pt(II) benzoporphyrin) parts of electromagnetic spectrum with virtually no overlap.

Chen and co-workers⁹⁷⁴ also prepared nanosensors for pH and oxygen by combining red-emitting Pt(II) porphyrin as an oxygen indicator and green-emitting FITC as a pH indicator in a single particle composed of poly(9,9-dioctylfluorene). The latter acts as a matrix for the dyes but also as an antenna (partly transferring energy to Pt(II) porphyrin) and as a reference fluorophore since its residual blue fluorescence is neither pH nor oxygen-sensitive. As was shown in a related work,⁹⁸³ such approach enables imaging under two photon excitation due to exceptionally large two-photon cross-section of the conjugated polymer. Importantly, to avoid leaching, FITC is covalently attached to amino-modified polystyrene, which is incorporated into nanoparticles upon precipitation. On the other hand, the Pt(II) porphyrin is sufficiently lipophilic to be retained by the polymers.

A lysosome-targeting nanosensor for simultaneous fluorometric imaging of intracellular pH values and temperature was described,⁹⁸⁴ where three dyes are covalently immobilized in or on 95 nm silica nanoparticles, one acting as a pH probe, one as a temperature indicator, and the third dye (europium(III) complex) as a reference dye. The dual nanosensor responds to pH values in the range from 3.0 to 9.0, and to temperature in the range from 20 to 60 °C. Owing to its good biocompatibility and good sensitivity, the dual nanosensor has been used to monitor changes in local pH values and temperature in the lysosome of HeLa cells.

A dendrimeric nanosensor reported by Srikun et al.⁷⁰⁷ enabled simultaneous imaging of two parameters: pH and hydrogen peroxide. The G5 PANAM dendrimer was functionalized with the pH indicator SNARF2 and a nonfluorescent boronate ether-modified xanthene dye which generates highly emitting fluorescein upon reaction with hydrogen peroxide.

Compensation for the pH effects on fluorescein is necessary and detection of H_2O_2 is not reversible. pH measurement also provides important information on pH regulation in cells.

In some applications, it may be not necessary to combine both probes in a single material. For instance, a luminescent pH probe and a phosphorescent oxygen probe (both commercially available from Luxcel Biosciences/Agilent) were simultaneously used in microplate readers of various manufactures.⁹⁸⁵ Measurement of pH and oxygen along with a chemiluminescent ATP assay and total protein measurement via absorption makes it possible to assess bioenergetics of cells. Similarly, Ehgartner et al.⁷⁰³ performed simultaneous sensing of pH and oxygen in microfluidic chips using a mixture of two types of nanoparticles based on poly(styrene-*block*-vinylpyrrolidone), separately doped with an oxygen indicator (in the hydrophobic core) and a pH indicator (in the hydrophilic shell). Both probes are excited with red light and read out using the mDLR method via phase shift measurement at two modulation frequencies.

Also, a dual sensor was reported that uses 2 different techniques to sense pH and oxygen. The oxygen concentration is accessed via measurement of the phosphorescence decay time of a metalloporphyrin. The pH is measured via surface-enhanced Raman spectroscopy of gold nanoparticles capped with pH-sensitive 4-mercaptobenzoic acid. Microcapsules containing the sensing chemistry for either pH or oxygen were incorporated into a hydrogel. Although being complex, the system proved the feasibility of multimodal optical sensing.

Wang et al.⁸⁹³ designed silica-coated polystyrene nanoparticles for simultaneous measurement of temperature, oxygen, and pH. Fluorescein, CrBPh₄, and 5,10,15,20-tetrakis-(pentafluorophenyl) porphyrin or Nile red were used as pH-, O₂/T-indicator and reference dye, respectively. After amino-modification of the silica coated polystyrene nanoparticles, fluorescein was covalently coupled and used for ratiometric pH measurement around its pK_a of 6.5. The triple parameter nanosensor covered the physiologically relevant parameter ranges with a single excitation wavelength.

A referenced triple sensor for intracellular measurement of temperature, pH, and oxygen concentration was presented by the group of Wang.⁹⁸⁶ Bovine serum albumin (BSA) is selected as the scaffold (support) to which four fluorophores were linked. The following luminophores were used: (a) fluorescein as a probe for pH values, (b) a platinum(II) porphyrin complex for oxygen, (c) a europium(III) clathrate complex for temperature, and (d) rhodamine B as a reference dye. The nanoparticles have a size of 20 nm and show excellent biocompatibility and good brightness. The nanosensors were used for ratiometric imaging of intracellular pH values, oxygen, and temperature in HeLa cells.

Optodes for simultaneous monitoring of pH and other analytes are summarized in Table S14.

11. IMAGING OF pH VALUES

Imaging of pH values is exclusively performed by using optical indicators and nanoprobe, most often via fluorometry. Refractive index based methods and planar plasmon resonance methods play no role, even though photonic crystals may serve the purpose, but this was not shown so far. One may distinguish between 2D imaging (which can be realized with planar optodes in contact with a sample), and 3D imaging (where molecular probes or nanoparticles are placed in a sample such as tumorous tissue). One may also distinguish between conventional imaging and imaging via fiber bundles. Planar optodes are used to

visualize pH distribution in fairly large objects (bacterial cultures, Petri dishes, sediments, microbial mats, etc.; see Figure 39). Imaging with nanoprobe is the method of choice in case of

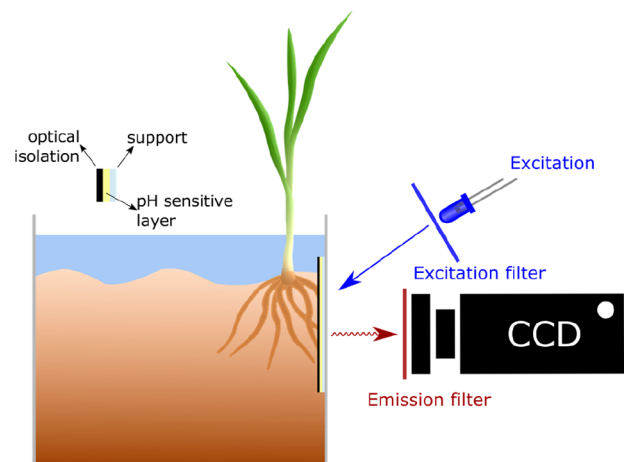


Figure 39. Typical setup for imaging of pH distribution at a water–sand interface with planar optodes.

small objects (such as cells or microfluidic channels). One can also distinguish between intensity-based and lifetime-based imaging. Fluorescence lifetime imaging (FLIM) represents a self-referenced technique, while fluorescence intensity has to be referenced by other means such as ratiometry or DLR (see sections 2.11 and 2.2.7).

Various reviews on imaging based on luminescent materials are available.^{681,699,702} Regarding pH sensing, there is a book chapter with an extensive review on nanomaterials for intracellular pH sensing and imaging.⁵ Methods for self-referenced fluorometric imaging using camera read-outs and the so-called RGB techniques have been described in detail.⁹⁸⁷

11.1. Intensity-Based Imaging

A typical example is pH monitoring in isoelectric focusing.^{430,592,988} For referenced ratiometric read-out, intrinsic properties of some indicators can be utilized. For instance, a ratiometric planar optode reported by Hulth et al. utilized dual excitation of HPTS (protonated and deprotonated forms) immobilized on a cellulose acetate membrane.³⁷⁵ Zhu et al.³⁷⁷ reported imaging of marine sediments with covalently immobilized HPTS dye using excitation with two LEDs (420 and 505 nm) and detection with an RGB camera. Typically for HPTS, the apparent pK_a value of the indicator was heavily affected by the ionic strength and far from being optimal for measurements in seawater.

Fluorescence intensity can also be referenced against that of a pH-insensitive reference luminophore (see section 10.1). Dedicated solutions with movable filters are commercially available. For example, Ocean Optics (<https://oceanoptics.com>) offers a SpectroCam system including a camera in combination with a rotating wheel equipped with 6–8 band-pass filters. The camera system was demonstrated to be useful for imaging of pH distribution in didemnid ascidian with help of a ratiometric sensor material.⁹⁸⁹ In a similar custom-made setup, an RGB camera was used to image pH, pO_2 , and pCO_2 distribution in marine sediments with help of three planar optodes.⁹⁹⁰

RGB cameras are widespread and affordable devices both in industry and in consumer market. The camera filters

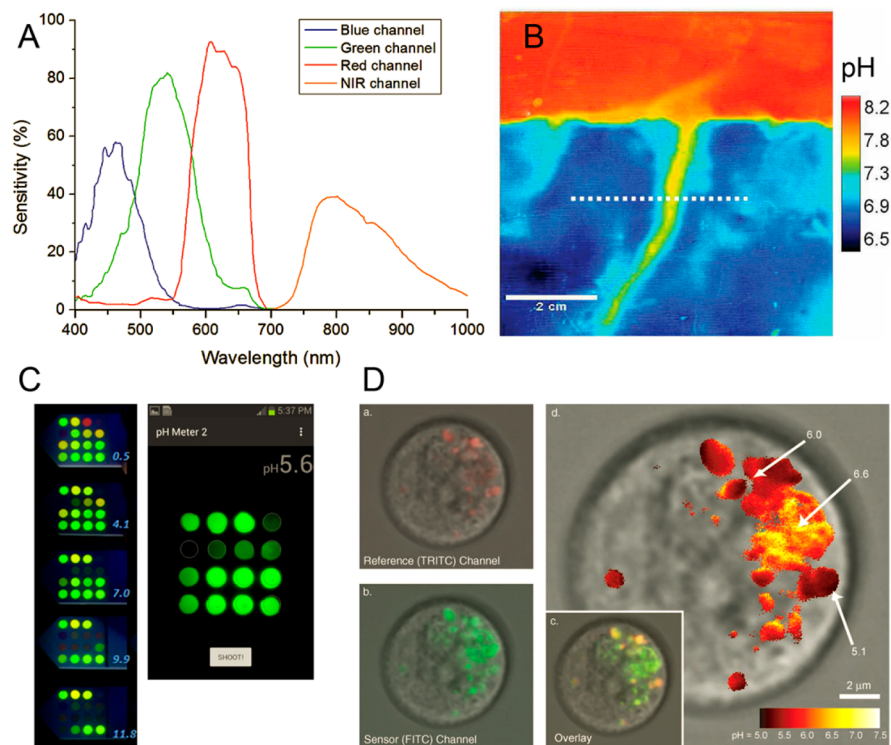


Figure 40. Examples of pH imaging. (A) Spectral response different channels of a dual chip (RGB + NIR) camera. Reprinted from ref 973 with public license. Published by The Royal Society of Chemistry. (B) Example of RGB pH imaging (pseudocolor) with a planar optode in marine sediment containing a burrow. Reprinted with permission from ref 374. Copyright by the Association for the Sciences of Limnology and Oceanography, Inc., 2011. (C) Imaging of a sensor array of immobilized pH indicators with a smartphone. Fluorescence images of the array at different pH values under UV excitation (left) and screenshot of a software for image processing (right). Reprinted with permission from ref 135. Copyright 2017 American Chemical Society. (D) Confocal fluorescence microscopy images (overlaid on bright field) of pH nanosensors in RBL mast cells showing (a) reference dye channel, (b) sensor dye channel, (c) overlaid images, and (d) pseudocolor ratiometric imaging of pH in various intracellular compartments. Reprinted with permission from ref 404. Copyright Wiley-VCH Verlag GmbH & Co., KGaA, Weinheim 2006.

corresponding to the blue, green, and red channels are attractive for isolation of optical signals from the indicator and the reference. For instance, if the excitation is performed with blue light, the green and the red channels can be used for fluorescence of the indicator and the reference, respectively, or vice versa. It is important that one of the emitters possesses significantly larger Stokes shift so that its emission is located in a different channel. Cross-linked polymeric particles doped with a mixture of several fluorophores efficiently increase apparent Stokes shift via FRET, which is beneficial for their use as references.⁴²⁴ It should be kept in mind that the detection channels in the RGB cameras are rather wide and show significant overlap (Figure 40A).

Planar optodes typically utilize visible light for excitation. In contrast, Meier et al.⁹⁵¹ utilized NIR light (980 nm) to excite a planar optode based on upconversion $\text{NaYF}_4:\text{Er}^{3+}, \text{Yb}^{3+}$ nanorods (see section 10.6 for more details). Under this excitation, the nanorods emit strongly both in the green and red part of the spectrum ($\lambda_{\text{max}} = 540$ and 660 nm). These emissions are rather narrow (full widths of the emission bands 25–40 nm) and almost perfectly match the color channels of the RGB camera. Sensing relies on an inner-filter effect (see section 10.5) caused by an organic pH indicator whose absorption overlaps the green emission of the nanorods but shows no overlap with the red emission.

RGB imaging of pH values becomes increasingly popular due to the uncomplicated and low cost equipment required.³⁷⁴ Several reported systems utilize a consumer camera, a high power LED for excitation and a trigger to ensure illumination of

the sensor foil only during the image acquisition time. Planar optodes have been used for imaging of pH values in marine sediments (Figure 40B),^{991,374} seawater,⁹⁹² wounded tissues,⁴⁴¹ and for visualization of bacterial metabolism in Petri dishes.^{127,571} A commercial VisiSens system is available from PreSens GmbH and includes an RGB camera and a set of planar optodes (pH, oxygen, and carbon dioxide). Application of this system for imaging of pH gradients (also pO_2 and pCO_2 gradients) in rhizosphere was demonstrated.⁹⁹⁵

The quality of smartphones cameras improves continuously making them attractive for the RGB imaging of different parameters, including pH. The light torch of a smartphone in combination with a short-pass filter can serve as a suitable excitation source, and the processing capabilities are good enough to convert images into pH values. For instance, Chen and co-workers reported simultaneous imaging of pH and oxygen with a smartphone.⁹⁷⁸ The authors, however, used a UV lamp as an excitation source to photoexcite (a) the reference dye (4,4'-bis(2-benzoxazolyl)stilbene), (b) the pH indicator (fluorescein), and (c) oxygen indicator (platinum(II) pentafluorophenylporphyrin). They emit in the blue, green, and red channels, respectively. Rurack and co-workers¹³⁵ made a step further and presented a self-contained pH measurement system on smartphone basis. A 16 spot array of 10 hydrogel-immobilized fluorescent pH indicators and reference dyes was not only imaged with a smartphone but also processed with a specially designed software running on the same device (Figure 40C). All dyes are based on a BODIPY chromophore and,

therefore, have almost identical excitation and emission spectra. On the other hand, the indicators are decorated with different receptors and show transitions in different pH ranges. Impressively, the sensor array covers the entire pH range from 0 to 14. Although most of the experiments were performed with the UV lamp as an excitation source, the authors also designed an adaptor housing a 470 nm blue LED powered through the smartphone's micro-USB connector. This allows for autonomous on-site and in-field measurements.

The above examples demonstrate high potential of digital cameras and smartphones for RGB imaging. However, three channels may not be sufficient for some applications. For instance, ratiometric imaging of more than one parameter would require three suitable channels for signal detection. Although UV excitation with detection in blue, green, and red channels is possible in principle, it is often undesirable due to high disturbance to biological systems and high levels of generated autofluorescence, which would possibly interfere with ratiometric imaging. The commercially available RGB/NIR camera Jai AD-130GE (www.jai.com) substantially increases the flexibility in choice of pH indicators and reference dyes and their combination with probes for other parameters (Figure 40A). Ehgartner et al.⁹⁷³ used the camera for ratiometric imaging of pH upon excitation with red light (617 nm) with help of the pH indicator and the reference dye emitting in NIR and red part of the spectrum, respectively. In the same work, a dual sensor for pH and oxygen has been described. It utilized a fluorescein-based pH indicator, Pt(II) benzoporphyrin as the oxygen indicator, and dye-doped polymeric reference beads. The materials emit in the green, NIR, and red channels, respectively, under excitation with blue light (458 nm). Later, Moßhammer et al.⁹²¹ used the same camera for simultaneous imaging of pH and oxygen in algal biofilms albeit in combination with different indicator and reference dyes (see section 10.7).

As can be seen from the examples described above, imaging with the planar optodes has been mostly used to visualize pH distribution in marine sediments, soils, tissues, wounds, etc. Since light scattering strongly depends on the wavelength, the effects caused by the sample can severely affect the ratiometric intensity measurements particularly in case of highly scattering sediments for which the optodes are often applied. Therefore, it is essential to use an optical isolation layer. For better contrast and higher fluorescent signals it is advisable to use an additional layer containing scattering particles, such as TiO₂ or BaSO₄, and above it an optical isolation layer containing, for example, carbon black (see section 9.3).

Similar to planar optodes, many nanosensors (section 8) are designed to enable ratiometric imaging (Figure 40D).⁴⁰⁴ In nanosensors, mostly fluorescent compounds are used as reference dyes due to their high brightness, insensitivity to oxygen, and high variety of commercially available derivatives suitable for covalent coupling. The optical setup is significantly different from that used for imaging of planar optodes: in most cases, excitation is performed with a laser and emissions from the indicator and the reference dye are collected by a photomultiplier.

Apart from imaging with fluorescent sensor films, imaging of absorptiometric pH planar optodes with RGB cameras or a scanner was also performed.^{232,233} It was shown that the use of the hue component in the HSV (hue, saturation, value) color space not only reduces the parameter space from three dimensions to one but also makes the read-out more robust against variation in the ambient light conditions compared to the

RGB read-out. The hue value is particularly robust in respect to variations in indicator concentration, membrane thickness, spectral sensitivity of the detector, and illumination conditions and can be easily obtained in a read-out with commercial devices such as scanners and digital cameras.⁹⁹⁴

Optical fiber imaging of pH values is less often used. They can be prepared by using inkjet printing technology.⁹⁹⁵ Microjet printing technology was applied for fabricating imaging sensors by printing an array of photopolymerizable sensing elements, containing a pH sensitive indicator, on the surface of an optical fiber image guide. The reproducibility of the printing process is said to be excellent for micrometer-sized polymers, with sensor diameters of around 90 μm and a height of 35 μm . The sensors were evaluated in terms of pH sensing ability, response time, and hysteresis using a custom fluorescence imaging system.

Table S15 gives an overview of fluorescence intensity based pH imaging using planar optodes.

11.2. Lifetime-Based Imaging

Luminescence lifetime imaging of pH using optical sensors started with work by Liebsch et al.⁹⁴ who presented a modular system for time-resolved two-dimensional luminescence lifetime imaging of planar optical pH sensors (and others). Both luminescence intensity-based and time-resolved images of the sensor spots were evaluated. The combination of optical sensor technology with time-resolved imaging allows for the determination of the distribution of pH values in heterogeneous systems. As discussed in section 10.2, lifetime sensing and imaging is possible with relatively few pH probes only. So called rapid lifetime determination (RLD) represents a simple technique for determination of average decay times.⁹⁹⁶ It also allows autofluorescence to be completely eliminated. The RLD scheme is common for imaging of planar optodes based on phosphorescent oxygen and temperature probes and of course can be adapted for read-out of long decaying pH probes (section 4.2). It can also be applied to pH probes exploring FRET from phosphorescent emitter to an absorptiometric pH indicator. For instance, Nagl and co-workers⁹⁴⁵ reported imaging of pH in a microchamber array with help of a FRET luminescent probe (see section 10.4 for more details). The RLD method requires a gated camera such as discontinued SensiCam from PCO (www.pco.de). On the other hand, imaging of fluorescence lifetime can also be performed in the frequency domain. Commercial cameras support modulation frequencies from 5 kHz to 40 MHz (pco.flim, www.pco.de). This enables imaging both in nanosecond and microsecond time domain. Accordingly, virtually all lifetime-based pH probes (section 10.2) can be read-out with the camera. Both micro- and microscopic pH imaging capabilities of the system were recently demonstrated for the lifetime sensor based on triangulenium indicator⁵²⁴ (see section 10.4 for more details), Figure 41A.

On a microscale, ratiometric 2- λ read-out remains the most popular method. Application of several lifetime nanoprobe for intracellular pH imaging have been reported. Imaging experiments are typically performed in the time domain using the time-correlated single-photon counting (TCSPC) technique and laser scanning microscopy. For instance, several groups demonstrated application of quantum dots^{798,801} and dye-doped polymeric nanoparticles⁴⁸² (see section 10.2 for more details) for intracellular/in vivo imaging (Figure 41B).

Dual lifetime referencing (DLR, section 2.2.7) is equally useful for interrogation of pH sensors in the frequency domain and for imaging in the time domain. pH imaging with DLR

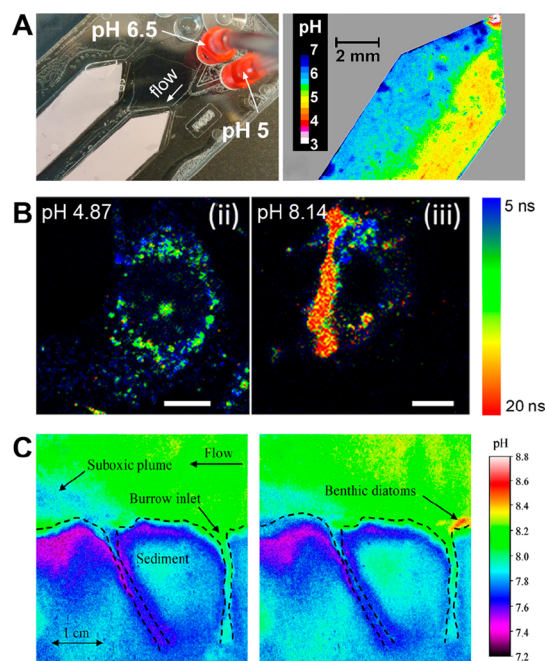


Figure 41. Examples of lifetime-based pH imaging. (A) Frequency domain FLIM imaging of pH with the planar optode via fluorescence decay time of a triangulenium indicator PhOHCl₂-DAOTA. Left: photographic image of the microfluidic chip with integrated sensor foil. Right: false color image of the pH distribution in the chip simultaneously flushed with buffers of pH 6.5 and 5.0 (speed 21 $\mu\text{L min}^{-1}$). Reprinted with permission from ref 524. Copyright 2019 American Chemical Society. (B) Time domain FLIM images of MC3T3-E1 cells incubated with nigericin and buffers mimicking the extracellular medium at pH 4.87 (left) and 8.14 (right). The scale bars (white lines) represent 10 μm . CdZnS quantum dots pH probes were utilized. Reprinted with permission from ref 801. Copyright 2013 American Chemical Society. (C) False color images of pH distribution acquired with time domain DLR technique for a marine sediment after 10 (left) and 40 (right) min light exposure ($\sim 450 \mu\text{mol photons}\cdot\text{m}^{-2}\cdot\text{s}^{-1}$). Reprinted with permission from ref 146. Copyright by the Association for the Sciences of Limnology and Oceanography, Inc., 2006.

sensors in the time domain was pioneered by Klimant and co-workers^{94,143} and has been widely used since then (Table S16). This includes imaging of pH distribution in marine sediments (Figure 41C)^{110,146} and concrete samples,⁹⁹⁷ monitoring of pH dynamics during wound healing,⁴²⁵ and imaging of pH distribution in microfluidic chips as utilized for isoelectric focusing.¹⁴⁸ Although the read-out was performed exclusively using a discontinued SensiCam from PCO, it is certainly possible to interrogate the same materials with frequency domain-based FLIM camera.

It should be considered that imaging of planar optodes that utilize the DLR scheme (both in time and in frequency domains) can be compromised by background fluorescence. Optically dense isolation layer (see section 9.3) is not always possible since the structures behind the optodes cannot be visualized. The problem can be tackled via application of long-wavelength emitters and applying semitransparent optical isolation layer that includes scattering particles in comparably low concentration.

Table S16 gives an overview of lifetime-based pH imaging using planar optodes.

12. pH SENSORS FOR EXTREME PH VALUES

Sensors for extreme pH values are much less numerous compared to those covering the physiological range. Nevertheless, such sensors have important applications, for instance for monitoring of pH in gastric system, the pH value of concrete, or during the production and processing of strong acids and bases. Sensing in highly alkaline conditions is of primary interest in many technological fields, for example, in paper industry, wastewater treatment, leather processing, metal mining and finishing, or microbial production involving alkaliphiles.⁵⁰⁴ It is also of utmost importance for corrosion prediction and detection in steel-reinforced concrete structures, which lifetime strongly depends on the internal pH.

The major challenge in the design is to identify indicator dyes, polymers, and host materials that are stable under rather harsh experimental conditions. Most of these sensors work either at very high or at very low pH values as shown in the following sections. Recently, however, Nawaz et al. have described a sensor for determination of both extreme acidic and strongly basic conditions.⁹⁹⁸ The sensor is based on the use of a cellulose support that is known to resist both strong acids and strong bases. A pH-responsive phenanthroline chromophore (Phen-MDI) was immobilized to obtain a sensor material that allows for visual determination of pH values. In the colorimetric (visual) mode, it can readily discriminate pH values in the pH 11 to 14.0 and in the pH 0.0 to 2.0. In the fluorometric mode, it can differentiate pH values between pH 11.0 and 13.2. Response can be made more distinct by adding a pH-independent reference dye. The material was used to fabricate a pH test strip. The colorful response of the Phen-MDI based test strip is shown in Figure 42.

12.1. Sensors for pH Values from 10 to 14

Optical sensors for high pH values are of interest because they can be prepared at low costs from alkali-resistant materials, such as cellulose and because electrodes, at high pH values, suffer from interferences due to the so-called alkali error. Several *absorptiometric sensors* have been reported. Werner and Wolfbeis⁵⁴ covalently immobilized an azo dye N8 1 (Figure 43) onto cellulose support prepared via partial hydrolysis of cellulose acetate layer under alkaline conditions. The immobilized dye showed absorption maxima at 484 and 560 nm in the neutral and highly alkaline media, respectively, and a pK_a of 11.72. Although the stability was excellent (6 months) for the sensor stored in dry state between the measurements, some delamination of the sensing layer based on cellulose from the polyester support was observed after 7 h of continuous measurement in 0.1 M NaOH.

Safavi and Abdollahi⁷⁰ immobilized thiazole yellow 2 (Figure 43) onto the same support (hydrolyzed cellulose acetate). Advantageously, the absorption bands of the neutral form and the deprotonated forms ($\lambda_{\text{max}} = 423$ and 512 nm, respectively) show only minor overlap. The immobilized dye showed high pK_a of 12.5 and fully reversible response. Interestingly, the sensor showed no cross-talk to Mg^{2+} , which is in contrast to behavior in alkaline aqueous solution where the same dye forms a complex with Mg^{2+} . The same group³²⁵ immobilized a mixture of triphenylmethane dye Victoria blue and dipicrylamine onto cellulose support. The latter shows absorption change in highly acidic media, while immobilized Victoria blue reversibly responds in the range from 8.5 to 13.0 in decreasing the absorption at 621 nm ($\text{pK}_a = 11.2$).

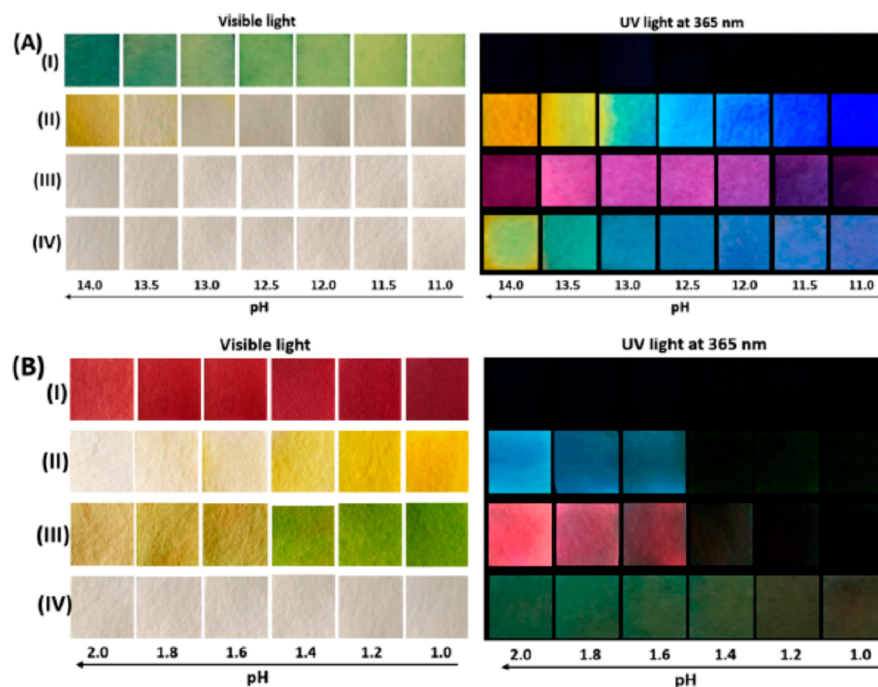


Figure 42. Comparison of the responses of a commercial test strip and the new pH test paper strips to (A) strong bases and (B) strong acids. Row I: Commercial pH test paper strips. Row II: Phen-MDI pH test paper strips. Rows III–IV: Phen-MDI in the presence of two different reference dyes that improve contrast. The photographs on the left were taken under visible light, and those on the right under irradiation with 365 nm light. Reprinted with permission from ref 998. Copyright American Chemical Society 2019.

Thiazole yellow also was the indicator of choice in the sensors reported by Allain and Xue.²⁰¹ The indicator was embedded into a composite of $\text{SiO}_2/\text{ZrO}_2$ and a polar polymer (Nafion, poly(styrene-*co*-methyl methacrylate) or a mixture of both). The indicator showed high pK_a value in all the matrices (13.8–14.1). All the sensors showed excellent stability in highly alkaline solutions and tolerated 30 days of storage in 4 M NaOH. In further work,²⁰² it was indicated that some of the materials remain stable in highly alkaline conditions for up to 120 days after which enhanced indicator leaching was observed. Drastic differences in dynamic response and recovery times have been observed for various sensing materials. The sensors based on dye-doped $\text{SiO}_2/\text{ZrO}_2$ films and those with additional poly(styrene-*co*-methyl methacrylate) showed the response times of up to several hours. In contrast, the composite sensors based on $\text{SiO}_2/\text{ZrO}_2$ with addition of Nafion and on $\text{SiO}_2/\text{ZrO}_2$ with addition of both Nafion and poly(styrene-*co*-methyl methacrylate) demonstrated response times of 5–50 s, which makes these materials particularly promising.

A benzo[*de*]anthracen-7-one indicator **3** (Figure 43),⁹⁹⁹ noncovalently immobilized on viscose fabric, showed a distinct color change from yellow ($\text{pH} \leq 10$) to orange-red ($\text{pH} > 10.7$) with a response time of several minutes. Xu and Sadik¹⁰⁰⁰ described another colorimetric pH sensor based on the indicator 1-(2-pyridazolo)-2-naphthol **4** (Figure 43) immobilized in polystyrene. The absorption of the dye ($\lambda_{\text{max}} = 561 \text{ nm}$) decreased by about 30% when the concentration of NaOH was increased from 0.5 to 10 M. The optode showed high stability in 10 M NaOH (6 months) and reversible response, which was surprisingly fast (several minutes) considering the thickness of the sensing layer ($\sim 20 \mu\text{m}$) and high hydrophobicity of polystyrene.

Porpholactones **5** (Figure 43) are promising absorptometric indicators for sensing pH in alkaline conditions.³³¹ The sensing

mechanism does not involve deprotonation of the pyrroles of the porphyrin macrocycle but rather a nucleophilic attack of the OH^- on the lactone moiety (Figure 43). In fact, both metal-free porpholactone and Pt(II), Zn(II) and Ga(III) complexes show almost identical spectral changes.^{331,332} The Q-band in the red part of the spectrum ($\sim 600 \text{ nm}$) disappears and a new broad band at around $\sim 700 \text{ nm}$ appears in alkaline media. The pH optodes manufactured via immobilization of the metal-free/Pt(II) porpholactones into copolymers of methyl methacrylate, methylenebis-acrylamide and methacrylamidopropyl trimethylammonium chloride have slow response (30–90 min) due to low ion permeability of the polymer.³³¹ In further work, the same group modified the porpholactones with 4 PEG groups via nucleophilic substitution of the para-fluorine atom of the pentafluorophenyl substituents (**6**, Figure 43).³³² The Ga(III) complex showed a strong decrease of the absorption of the Soret and Q-bands (417 and 605 nm, respectively) and a new band at 706 nm appeared. The complex has a pK_a of 11.8.

Fluorescent indicators based on phenol PET groups (photo-induced electron transfer, sections 2.2.5 and 4.1) are good candidates for sensing of very high pH values. The pK_a value of phenol, which is a viable PET quencher in its deprotonated form, is 10.0.¹⁰⁰¹ Gareis et al.⁴⁹³ reported application of phenol-bearing BODIPY dyes **7** and **9** (Figure 43). When immobilized in a hydrogel, the dyes showed pK_a values of 10.4 and 10.8, respectively. Similar systems based on dye dyes **8**⁵⁰⁴ and **10**¹³⁵ (Figure 43) were reported. The methyl groups in the 1 and 7 positions of the BODIPY are important to ensure high fluorescence quantum yields of the indicators, and they also have an effect on the pK_a values. Interestingly, a significant increase of the apparent pK_a was observed after immobilization of dye **8** into the polymer (11.44 and 9.98 for the polymer-supported dye and dye in EtOH– H_2O solution, respectively). This is in contrast to the work of Gareis et al.⁴⁹³ who did not

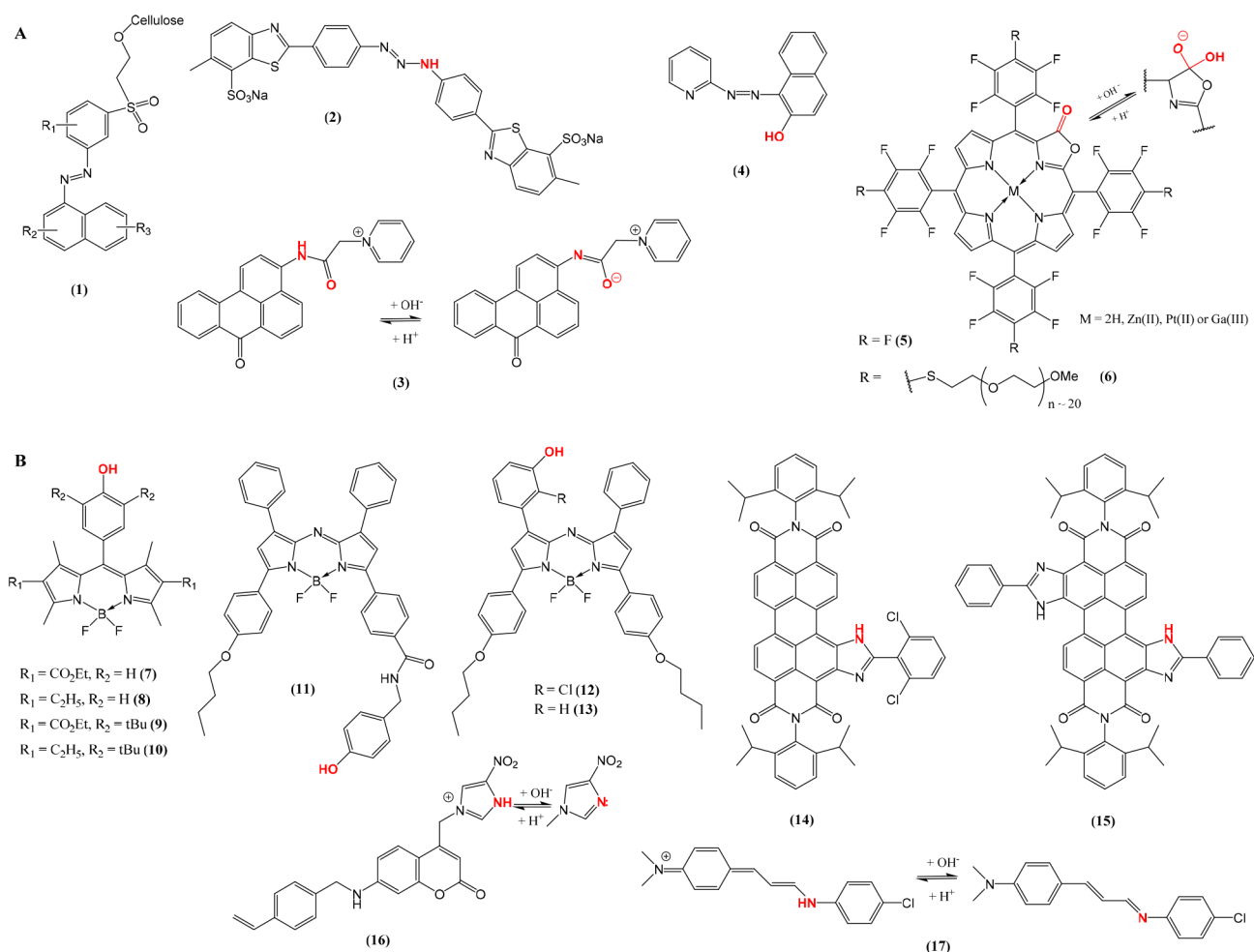


Figure 43. Chemical structures of the indicators used for sensing of high pH. Upper and lower panels: Absorbimetric and fluorescent indicators, respectively. Note that the structure of indicator 1 is not disclosed; one of the R groups is a hydroxy group responsible for the pH sensitivity.

observe any significant change upon immobilization of the dye **10** (pK_a 12.83 and 13.1 for the dye in hydrogel and EtOH–H₂O solution, respectively).

A phenol receptor attached to the aza-BODIPY chromophore **11** (Figure 43) has a pK_a of 11.9 when immobilized in hydrogel.⁵⁰⁵ This is higher compared to EtOH:H₂O buffer solution (11.1). Aza-BODIPY indicators **12** and **13** (Figure 43) have pK_a of 10.8 and 11.7, respectively.⁵¹⁰ A sensor based on dye **12** was recently shown to be very useful for imaging of pH distribution in concrete.⁹⁹⁷

Among fluorescent indicators, π -extended imidazole-substituted perylenes **14** and **15** (Figure 43) represent another promising group of indicators for sensing high pH values. These dyes are equally useful as absorbimetric and fluorescent indicators showing strong change in absorption and emission spectra upon deprotonation of the imidazole group. The apparent pK_a values obtained from the absorption spectra (11.36–11.45) are higher than those obtained in fluorometry (10.15–10.56), which is attributed to FRET from the protonated to the deprotonated form of the dye. Molar absorption coefficients and quantum yields for both perylene dyes are very high ($>75\,000\ M^{-1}\ cm^{-1}$ and $>85\%$, respectively).

Fluorescent coumarin indicator **16** (Figure 43) was covalently embedded into highly cross-linked microparticles prepared from 1,4-bis(acryloyl)piperazine and methacrylic acid.¹⁰⁰² The particles positioned between a quartz disc and a porous nylon

membrane were read-out with a fiber-optic fluorometer. A moderate ($\sim 40\%$) quenching of the fluorescence of the indicator was observed upon pH decrease from 9 to 13.2 (pK_a 11.9) attributed to PET from the neutral imidazole receptor. The material showed excellent photostability and virtually no change in the calibration within 20 months of storage in the dry condition and repeated short-term measurements. Dye leaching was observed at pH > 13.2 , which may be due to hydrolysis of the polymer. It should be mentioned that the dynamic response was very slow ($t_{95} = 50\ min$) which, however, may not be problematic for the intended application (monitoring of pH in the concrete structures).

Derinkuyu et al.⁵⁷⁹ manufactured a high pH sensor via immobilization of the Schiff base **17** (Figure 43) into poly(vinyl chloride). The dye shows fairly strong orange fluorescence ($\lambda_{max} = 593\ nm$, $QY = 0.37$) in the protonated form (pH ≤ 8) which is almost completely quenched in alkaline media ($pK_a = 10.3$). Because of the low permeability of the polymeric matrix to ions, fairly long response and recovery times (up to 13 min) were observed even for rather thin sensing films ($5\ \mu m$).

It can be concluded that sensing of high pH values is undoubtedly challenging since preparing an indicator with suitable spectral properties and pK_a value is only one side of the medal. Stability of the indicator and the matrix at the extreme conditions represents the main challenge particularly for long-term applications, such as pH monitoring in concrete. For

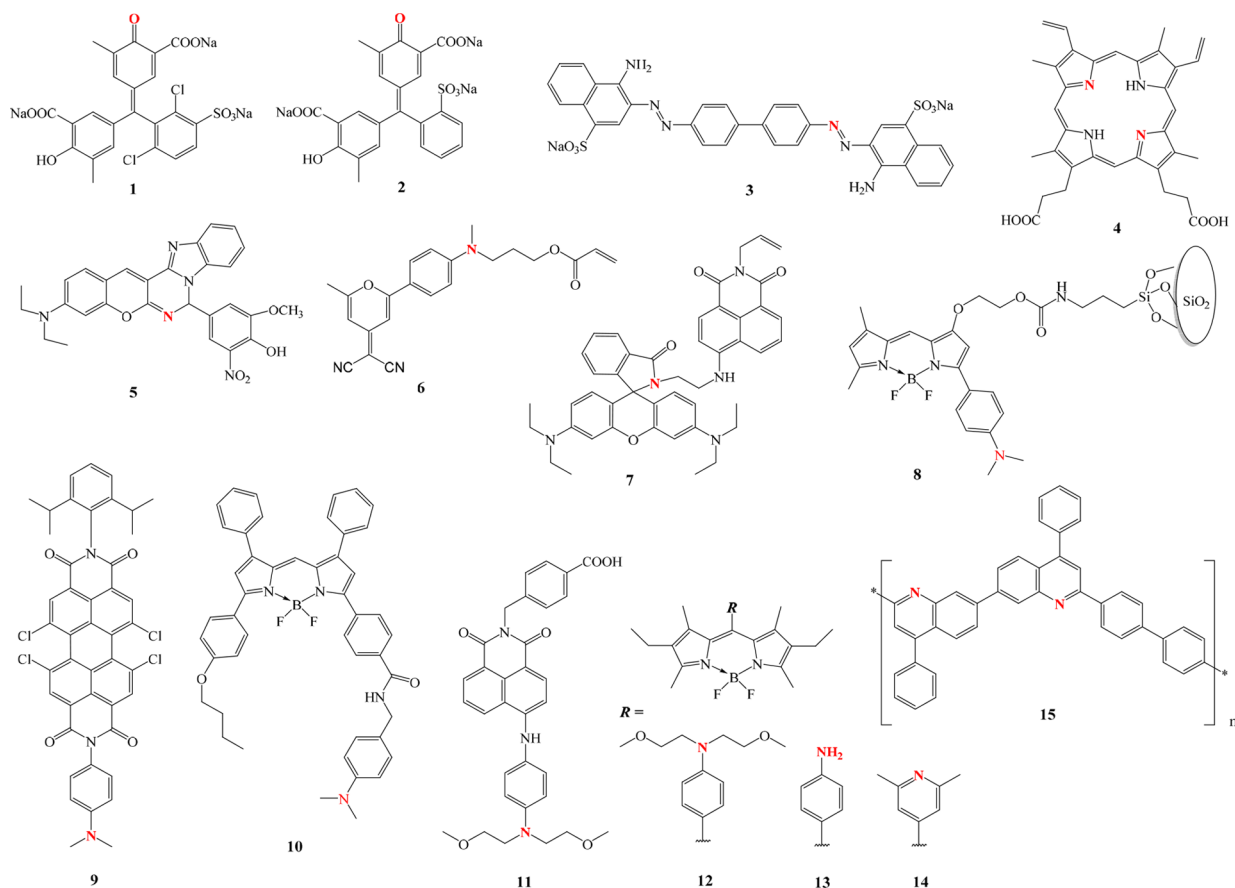


Figure 44. Chemical structures of the indicators used for sensing of low pH. For the structures of other indicators used in sensing of low pH the reader is referred to [section 3](#).

instance, polyacrylate polymers and silica-based matrices tend to degrade in basic media due to hydrolysis of the ester bond, whereas polyacrylamide polymers are more stable. However, even these polymers can be cleaved in very basic conditions. On the other hand, the sensors based on Nafion³³² and SiO₂/ZrO₂ composites²⁰¹ appear to be stable in highly alkaline conditions. One should also keep in mind that the degradation of the optodes is accelerated at higher temperatures.

[Table S17](#) summarizes the composition and properties of optical pH sensors for measurements in highly alkaline conditions.

12.2. Sensors for pH Values below 3

Carey et al.⁵⁰ investigated the ability of several polymer-immobilized *absorptometric indicators* to sense nitric acid from 1 M and stronger. The triphenylmethane dye chromazurol-S **1** ([Figure 44](#)) showed ratiometric response from 2 to 10 M nitric acid when immobilized in a mixture of polybenzimidazole and polyimide. Noire et al.³²⁴ reported an evanescent wave sensor based on a similar dye chromoxane cyanine **2** ([Figure 44](#)) embedded into TEOS sol–gel. It showed reversible response (absorbance at 542 nm) to 1–8 M solutions of nitric acid but, unfortunately, also a decrease of absorption by about 45% after 40 days of continuous measurement (1 M HNO₃) probably due to leaching of the dye.

Baldini et al.⁷¹ immobilized thymol blue ([section 3](#)) on controlled pore glass particles and recorded the changes in reflectance of the probe placed on a distal end of an optical fiber. The absorption of the indicator ($\lambda_{\text{max}} = 565 \text{ nm}$) decreased almost to 0 from pH 0.91 to 4.90. Immobilized in a TEOS-based

sol–gel, bromocresol purple was used for high acidity measurement (1–10 M HCl, $\text{p}K_{\text{a}} = -0.77$).²⁶⁷ The sensor response was very fast (<1 s for 2.7 μm thick films), and only a little leaching was observed (4% in 12 weeks). In later work,^{252,259} the same group investigated the performance of this and other materials in mixtures of strong acids and metal salts. They, then, proposed an algorithm for compensation of variations in ionic strength.

Wang et al.¹⁰⁰³ showed that the pH optode based on phenol red embedded into a TEOS-PhTriEOS sol–gel was suitable for sensing in highly acidic solutions (apparent $\text{p}K_{\text{a}}$ of 0.2). The material shows an increase of the absorption at 510 nm upon protonation. The same material was previously used for sensing in slightly basic conditions³²¹ utilizing the second deprotonation step of the indicator (c.f., [Figure 17](#)). The combined use of indicators rhodamine B and Safranin T entrapped in porous silica glass films prepared by the sol–gel method resulted in sensors for high-acidity ($[\text{H}^+] = 1\text{--}9 \text{ M}$) measurements.¹⁰⁰⁴

Congo red **3** ([Figure 44](#)) was covalently immobilized on an epoxy-activated agarose membrane.²¹⁴ The absorption band at 600 nm observed in highly acidic conditions (pH 0.5), disappeared as the pH was increased to 6 giving rise to a new band peaking at 500 nm. The immobilized indicator showed a $\text{p}K_{\text{a}}$ value of 2.8 and the response of the sensor was fully reversible. Using a similar strategy, Salmani et al.²¹⁵ immobilized Congo red on an epoxy-activated cellulose membrane achieving a dynamic range from pH 0 to pH 4.

Dipicrylamine (2,4,6,2',4',6'-hexanitrodiphenylamine) can be easily covalently immobilized on triacetylcellulose films.³⁶⁴

The membranes can be used for reversible pH measurement in the range of 0.0–3.2 at 450 nm. The sensor is interfered by potassium ion, and bleaching and low sensitivity are main problems in highly acidic media (>1 M of strong acid).

Protonation of pyrrole nitrogens of metal-free porphyrins in acid conditions is well-known. Protoporphyrin IX **4** (Figure 44) was immobilized into cross-linked polyacrylamide gel.³³⁹ The absorption of the Soret band of the porphyrin ($\lambda_{\text{max}} = 410$ nm) is the highest in highly acidic conditions (pH = -0.5) but decreases by more than 10-fold on going to pH 1. The response of the evanescent wave sensor was fast ($t_{90} = 10$ s) because of the thin layer thicknesses (1 μm) and high proton permeability of the polymer. The sensor showed no significant change in the properties after 100 assays and after storage in a dry state over 6 months.

Fluorescent sensors for strongly acidic media have also been reported. Posch et al.⁴⁹ immobilized fluorescein and eosin into different polymers including amino-ethyl cellulose and amino-modified controlled porous glass. Immobilized onto amino-ethyl cellulose, eosin, and fluorescein covered the pH range from 0 to 3 and from 2 to 6, respectively. Tetrafluorofluorescein was applied in a nanosensor based on cross-linked poly(acrylamide). The nanosensors show an apparent pK_{a} of around 3.⁷⁶² A coumarin indicator **5** (Figure 44) showed almost no fluorescence in the neutral form, whereas fluorescence intensity increased strongly in highly acidic media.³⁹⁶ Compared to the EtOH/H₂O buffer, the pK_{a} value slightly increased upon immobilization onto amino-modified cellulose (pK_{a} of 2.8 and 3.36, respectively). Nevertheless, the immobilized indicator showed rather broad fluorescence dynamics (pH 1–7).

Kim and Kim⁵²⁷ prepared pH sensors by covalently immobilizing a dicyanomethylene-4H-pyran dye **6** (Figure 44) into cross-linked pHEMA hydrogels. The neutral form of the dye (pH 3) in the optode features the absorption maximum at 438 nm and emission maximum at 520 nm. Upon protonation of the aniline nitrogen in highly acidic media (pH < 0), the absorption shifts to 370 nm, whereas the fluorescence is completely quenched. The sensor shows reversible response and good stability without significant leaching.

A fluorescent sensor based on pHEMA hydrogel with copolymerized conjugate of rhodamine and 4-amino-1,8-naphthalimide **7** (Figure 44) was reported.⁴⁶³ At pH > 3, the rhodamine dye is present in the colorless spirolactam form, which efficiently quenches the fluorescence of the naphthalimide dye. Opening of the spirolactam ring in the strongly acidic conditions results in a strong enhancement of naphthalimide fluorescence. Such enhancement is rather surprising, since the emission spectrum of the naphthalimide ($\lambda_{\text{max}} = 520$ nm) shows very good overlap with the absorption of the open form of the rhodamine ($\lambda_{\text{max}} = 567$ nm and a shoulder at ~ 520 nm) so that strong FRET from naphthalimide to rhodamine could be expected.

N,N-dialkylaminophenyl receptors are excellent candidates for designing fluorescent indicators for acidic range. The dyes equipped with such receptors typically are not fluorescent in moderately acidic media due to PET effect (see section 4.1 for more details) but the fluorescence is “switched on” upon protonation of the aniline in highly acidic conditions. Particularly, Hiruta et al.⁶⁰⁷ immobilized a BODIPY dye equipped with a *N,N*-dimethylaminophenyl receptor **8** (Figure 44) into mesoporous silica to obtain a sensor operating from pH 0.5 to 4. A far-red aza-BODIPY chromophore was equipped with the same group thus rendering the dye **10** (Figure 44) sensitive

to variation of pH in acidic media (pK_{a} of 2.6 for the dye immobilized into polyurethane hydrogel D4).⁵⁰⁵ A perylene dye modified with dimethylaniline in the imide position **9** (Figure 44) shows favorable properties (λ_{max} ex/em, 520/559 nm), adequate molar absorption coefficient (45 000 $\text{M}^{-1}\text{cm}^{-1}$) and high fluorescence quantum yield in the protonated form (0.81).¹²² The fluorescence of the neutral form is completely quenched due to very efficient PET. It has an apparent pK_{a} of 1.1 when embedded into polyurethane hydrogel D4 and 1.9 when immobilized into poly(hydroxypropyl methacrylate).

4-Amino-1,8-naphthalimide was modified with an aromatic dialkylamino receptor **11** (Figure 44).⁴⁶⁶ The pH optode was prepared via covalent immobilization of the dye onto amino-modified cellulose beads. The beads were incorporated into polyurethane hydrogel D4 and showed a pK_{a} value of 3.1. Rurack and co-workers¹³⁵ attached various aminophenyl receptors (4-bis(2-methoxyethyl)aminophenyl, aniline, *N,N*-diethylaminophenyl, *N,N*-diisopropylaminophenyl) to the BODIPY chromophore (**12**, **13**, Figure 44) to obtain sensors for acidic range. The dye substituted with the 4-bis(2-methoxyethyl)aminophenyl receptor showed the lowest pK_{a} value (0.95). The authors also demonstrated that 2,6-dimethylpyridin-4-yl (**14**, Figure 44) represents another promising PET receptor for sensing pH in acidic range (pK_{a} of 2.34 for the hydrogel-immobilized dye).

Conjugated polymers (poly(phenylquinoline), poly(biphenylquinoline) (**15**, Figure 44), or poly(phenylquinoxaline)) coated onto the tip of an optical fiber showed response (decrease or increase of the fluorescence intensity) in strongly acidic conditions (0.1–8.4 M HNO₃).⁵¹

Table S18 summarizes the composition and properties of optical pH sensors for measurements in highly acidic conditions.

13. pH SENSORS WITH WIDE DYNAMIC RANGE

The dynamic range of pH optodes is much narrower than that of the glass electrode and of pH ion sensitive field effect transistors. Most of the signal change occurs within 2 pH units, which, however, is usually sufficient for the majority of applications. On the other hand, in some applications the pH may show more significant variations making the conventional pH optodes unsuitable. Additionally, one may wish a more universal analytical tool on the basis of optical measurements, which is able to access the pH in a variety of different samples thus reducing the cost of the setup (multiple sensors) and maintenance (exchanging and calibrating the sensors). Therefore, significant effort has been focused on designing a pH optode covering a comparably wide dynamic range.

Four fundamental methods do exist to enlarge the analytical range of optical pH sensors. The first method is making use of indicators with more than one pK_{a} value, for example dyes that have two or more hydroxy groups or have both an acidic group (e.g., a phenol) and basic functions such as pyridine or tertiary amino groups.⁴⁶ The second method is making use of the fact that fluorescent indicators have strongly different pK_{a} values in the electronic ground state and in the first excited singlet state (e.g., HPTS).⁶¹ The third method utilizes the effects of the immobilization matrix on pK_{a} values; by placing the same chromophore in quite different microenvironments, indicators with statistically distributed pK_{a} values are obtained. Finally, the most common approach is to mix several dyes with different pK_{a} values.

The indicators of the first and the second type are rather rare. Several dye classes feature multiple protonation equilibria (e.g.,

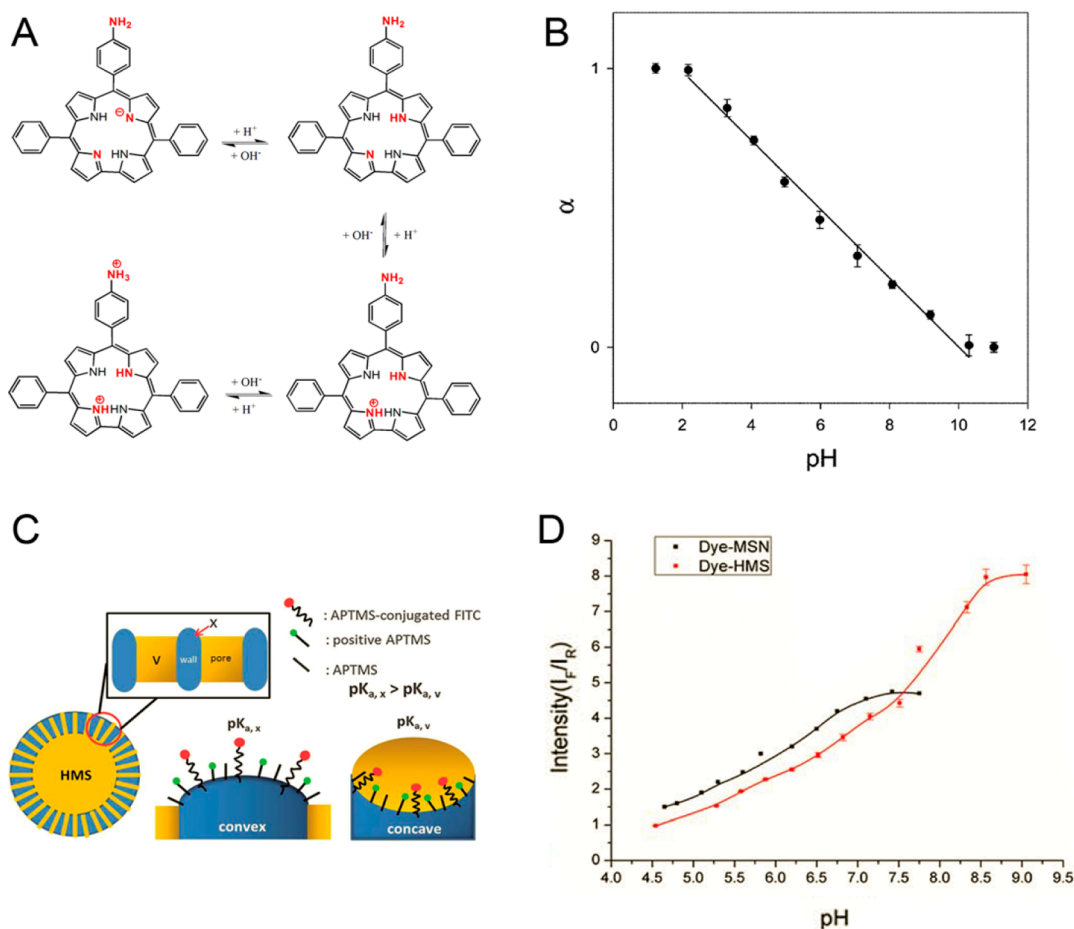


Figure 45. (A) Chemical structure and acid–base equilibria of the corrole indicator. (B) Response of the pH optode based on sol–gel immobilized corrole. $\alpha = (F - F_b)/(F_a - F_b)$, where F , F_b , and F_a are, respectively, the fluorescence intensities at a given pH, in the completely deprotonated form (pH 11) and in the completely protonated form (pH 1). Reprinted with permission of The Royal Society of Chemistry from ref 1005. Copyright The Royal Society of Chemistry 2006. (C) Extended range pH optode utilizing surface curvature of mesoporous silica nanoparticles (MSN) creating different density of positively charged groups originating from aminopropyltrimethoxysilane (AMPMS). Reprinted with permission of The Royal Society of Chemistry from ref 755. Copyright The Royal Society of Chemistry 2013. (D) pH response of mesoporous silica nanoparticles (MSN) and hollow mesoporous silica nanoparticles (HMS) stained with fluorescein and rhodamine dyes. Reprinted with permission of The Royal Society of Chemistry from ref 755. Copyright The Royal Society of Chemistry 2013.

triphenylmethane dyes) and may potentially be used for wide dynamic range sensors. Wolfbeis and Marhold in 1987 designed coumarin probes with both a protonable site (pyridine) and a deprotonable site (a phenolic hydroxy group). This results in a dynamic range from pH 2 to 8.

Uniform response over a wide pH range is rare and a typical response curve is represented by a combination of two sigmoidals,⁶¹ thus making multipoint calibration necessary. The unimolecular indicator 10-(4-aminophenyl)-5,15-dimethylcorrole (Figure 45A)¹⁰⁰⁵ immobilized into a sol–gel is a notable exception. It shows multiple protonation steps: deprotonation of a pyrrole nitrogen in basic conditions, protonation of a pyrrole nitrogen in acidic conditions, and finally protonation of aniline in the strongly acidic media. This is accompanied by the change in the absorption spectrum characterized by the Soret band (380–450 nm) and the Q-bands (500–700 nm). The fluorescence intensity ($\lambda_{\text{max}} = 656$ nm) increased almost linearly in the pH range 2–10 demonstrating a fully reversible response (Figure 45B). It should be noted, however, that the fluorescence response reflects the pH dependency of both the fluorescence QY and the absorption spectra (resulting in different amount of absorbed

light) so that the response curve is likely to be different in shape if the excitation is performed at a different wavelength compared to the experimental conditions (507 nm).

Another way to extend the dynamic range of pH sensors is to utilize the effects of the immobilization matrix on the acid–base equilibrium. These effects are particularly strong for charged matrices so that the dynamic range of a conventional pH indicator can be significantly extended.^{755,1006} For instance, deprotonation of a fluorescein dye is facilitated in the proximity of positively charged groups (e.g., $-\text{NR}_2\text{H}^+$). This results in the decrease of the apparent pK_a value. Evidently, if the indicator is located in many different environments varying in the amount of charged groups, an extended dynamic range is possible. An interesting concept was reported by Mou and co-workers who made use of different surface curvature of hollow mesoporous silica nanoparticles.^{755,1006} Both fluorescein and rhodamine (as a reference dye) were covalently immobilized into the beads. The excess of the latter rendered the surface positively charged in acidic conditions. Different surface curvature in hollow mesoporous nanoparticles (HMS) efficiently extends the dynamic range of the sensor compared to the reference nanoparticles (MSN) (Figure 45C and D). A different

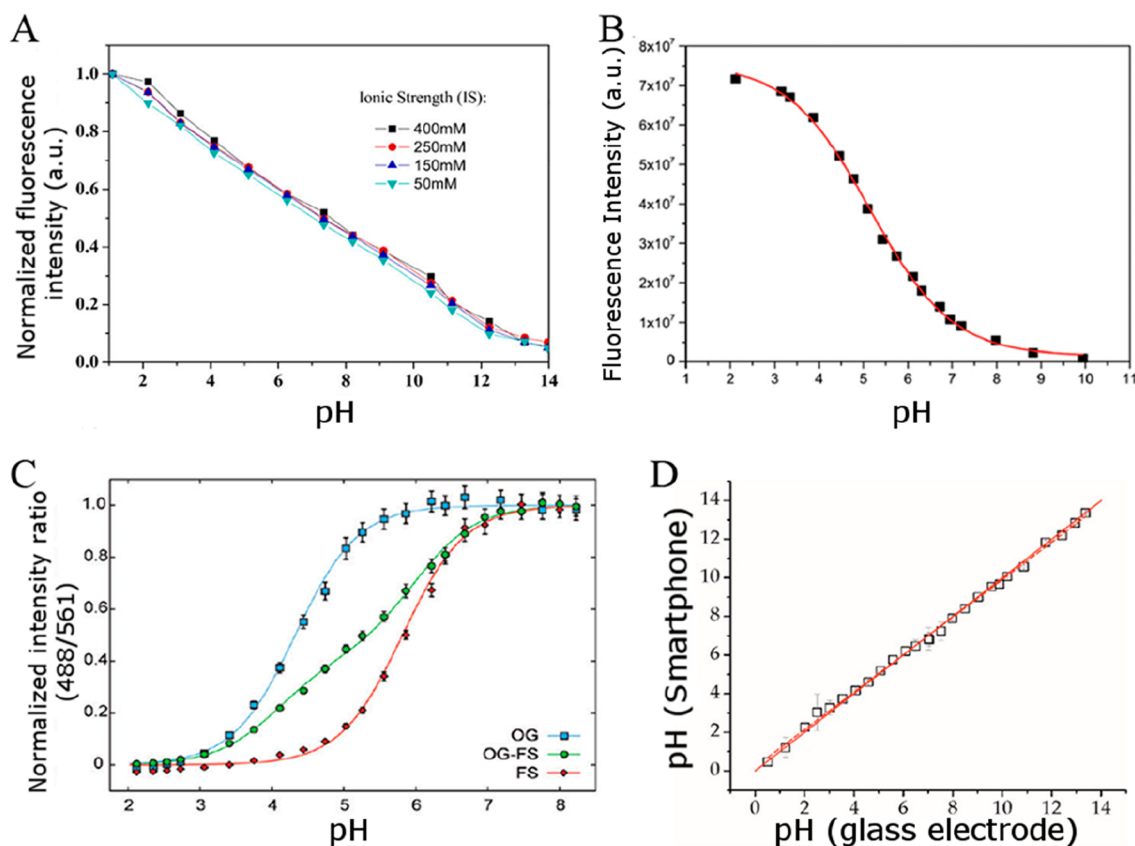


Figure 46. (A) Response of the sensor based on a mixture of 6 4-amino-1,8-naphthalimide pH indicators immobilized onto aminocellulose particles, which were dispersed in polyurethane hydrogel. Adapted with permission from ref 466. Copyright 2015 American Chemical Society. (B) Response of a pH sensor based on a mixture of 4 aza-BODIPY indicators immobilized into polyurethane hydrogel. Adapted from ref 505 with public license. Published by The Royal Society of Chemistry. (C) Response of the nanosensors containing covalently embedded individual indicators (fluorescein FS, Oregon green OG) and their mixture (OG-FS) along with rhodamine reference dye. Adapted with permission from ref 764. Copyright 2011 American Chemical Society. (D) Comparison of pH values obtained with the smartphone photographing the fluorescence of a sensor strip (array of 10 BODIPY indicators) and a conventional pH glass electrode. Adapted with permission from ref 135. Copyright 2017 American Chemical Society.

explanation was proposed for acridine immobilized in amine-modified porous silica.¹⁰⁰⁷ The immobilization matrix itself is subject to protonation equilibria which affects the pK_a of the indicator due to variable microenvironment. For acridine, this result in a lifetime change of 20 ns over the pH range of 2–12. It should be noted here that ionic strength is expected to strongly affect the response of the sensors utilizing charged surfaces, which is a limitation of the approach. Although the effect of ionic strength has not been investigated in the above studies, the material utilizing a similar approach (gold nanoparticles of different sizes modified with carboxylic groups) was demonstrated to have a very high cross-sensitivity to ionic strength.¹⁰⁰⁸

The design of wide dynamic range sensors via combination of several indicators with different pK_a values remains the most common approach.²⁸⁷ Ideally, the indicators should possess very similar spectral properties and comparable photostability and should not leach out of the matrix. Simulations demonstrate²⁵⁷ that if the difference between the pK_a values is too high (≥ 2) even the central part of the calibration curve will not be linear. This is inconvenient in practice since multipoint (re)calibration will be necessary. On the other hand, if the pK_a values differ by only 1, the mixture of the indicators will show sigmoidal response but the broadening of the dynamic range is not very significant. Therefore, the pK_a difference of 1.5 between the individual indicators is optimal. This requirement is difficult to achieve in practice. Additionally, the individual indicators may

differ in their spectral properties and in the signal difference between the protonated and deprotonated forms. Hence, an adjustment of the concentration of individual indicators is necessary. Experiments with the mixture of *absorptiometric indicators* in aqueous media demonstrate excellent correlation with the calculated calibration curves.^{257,1009} For instance, a linear response from pH 4.3 to 8.8 could be obtained by mixing bromocresol green, bromocresol purple, phenol red, and thymol blue (pK_a of 4.59, 6.13, 7.78, and 8.88, respectively).¹⁰⁰⁹ A similar absorptiometric sensor was reported by Gupta and Sharma,²⁸¹ who coated an optical fiber with a thin sol–gel layer containing a mixture of cresol red, bromophenol blue, and chlorophenol red (pK_a in water 8.3, 7.4, and 6.3, respectively). Transmittance, measured at 600 nm (which is the optimal wavelength for the mixture of the dyes), decreased almost linearly from pH 5.5 to 13. However, low hydrolytic stability of sol–gels in alkaline conditions may be problematic. Later, Dong et al.²⁸³ reproduced the same system but added Triton surfactant (~1% wt.) to TEOS. Such a modification resulted in a very smooth sol–gel coating on the optical fiber without cracking defects observed for the material containing no Triton. The authors noticed the reduced hysteresis and also better repeatability of the response. The dynamic range of the sensor (4–13) was not affected by the modification. It should be mentioned here that many pH indicators show wider dynamic range when immobilized in sol–gels. For instance, pH sensitivity

of methyl red immobilized in TMOS-based sol–gel was shown to span over 7 pH units with linear range from about pH 5 to 8.⁵⁹⁹

In another work,³⁶² a mixture of neutral red and thionine was covalently immobilized onto the epoxy-modified surface of agarose-coated glass slide. The sensor showed a nonlinear decrease of absorption at 555 nm in the pH range 0.5 to 12. Interestingly, immobilized neutral red alone already shows a pH response over a very broad range (0.5–7.5). The optode featured good reversibility of the signal and operational stability. However, the immobilization drastically affected the spectral properties and the pH response of the dyes, so that overall absorption decreased only 15% relative to the highest value (pH 0.5).

Six hydroxyazobenzene indicators were prepared and immobilized on cellulose triacetate²⁰⁴ to obtain pH optical sensors with distinct color changes in the visible. These have a linear response in the 7.0 to 11.5 pH range, response times of less than 20 s, and excellent long-term stability.

Several *fluorescent sensors* with extended dynamic range have been presented. Posch et al.⁴⁹ immobilized fluorescein and eosin onto amino ethyl cellulose fibrous particles. The pK_a values of the immobilized dyes were about 5.2 and 1.1, respectively. The beads were mixed in different proportions and fixed on a polyester support to result in broad range sensors covering the pH range between 0 and 7 that is typical for gastric juice. Vasylevska et al.³⁹⁶ reported a pH sensor containing 2 types of microbeads with immobilized iminocoumarin indicators. The sensor membrane showed fluorescence response from pH 1 to 11 but represented a combination of two sigmoidal curves due to very large difference between the pK_a values of the indicators (3.36 and 8.42, respectively). Aigner et al.¹²² extended the dynamic range via combination of two perylene indicators immobilized in hydrogel D4. The fluorescent response was sigmoidal due to rather low difference of the pK_a values of the indicators (5.2 and 6.5).

Suzuki and co-workers⁹⁴⁸ prepared a wide range sensor via combination of colorimetric indicators neutral red and methyl yellow with two types of fluorescent quantum dots ($\lambda_{em} = 525$ and 605 nm, respectively). The sensor operated via the inner-filter effect read-out (see section 2.2.4 for more details) and showed ratiometric response, which was linear in the pH range from 4 to 10.

Combination of more than 2 indicators makes it possible to obtain a smooth response curve over a broad range of pH values. Ideally, all the indicators possess very similar photophysical properties i.e. belong to the same chromophore class. He et al.⁴⁶⁶ used mixtures of 2–6 individual indicators based on a single fluorophore 4-amino-1,8-naphthalimide (see section 4.1 for more details) to obtain pH sensors with wide dynamic range. All the indicators possess similar absorption and emission maxima and photostability, but largely different pK_a values. Carboxylic group enabled covalent binding of the dyes onto aminocellulose microbeads. These were dispersed in a polyurethane hydrogel. Not surprisingly, blending particles doped with different indicators resulted in extension of the dynamic range of the pH sensor reaching maximum when 6 different indicator dyes were used. This sensor was suitable for measurement in the pH range 1–14 showing almost linear decrease of fluorescence intensity (Figure 46A). The extension of the dynamic range was accompanied by the decrease of the resolution. In fact, the slope of the curve decreased from 0.56% signal change/0.01 pH unit for 1 indicator to 0.16%/0.01 pH unit for the mixture of 6 beads.

It is important that all the individual indicators possess very similar (and good) photostability, and show only minor cross-sensitivity to ionic strength, which can be compensated for. The reversibility of the sensor was excellent without a noticeable drift observed upon multiple cycles of switching between pH 1.1 and 14.0 and back. This underlines high hydrolytic stability of the immobilized indicators, aminocellulose, and polyurethane hydrogel used in the sensor.

A wide range sensor presented by Strobl and co-workers⁵⁰⁵ makes use of 4 fluorescent aza-BODIPY indicators (see section 4.1 for more details) immobilized into hydrogel D4. The sensor shows sigmoidal response curve in the pH range of 2–10 (Figure 46B). The aza-BODIPY indicators are advantageous for their long wavelengths of absorption and emission, good fluorescence brightness and excellent photostability, which is particularly important for the application of the dyes in the wide dynamic range sensor.

Frankær et al.⁵¹⁹ also used a palette of diazoxatriangulenium dyes substituted with different aniline or phenol PET receptors. A mixture of four indicators immobilized in a sol–gel matrix resulted in a sensor with a pH range from 1–10.

Nanosensors (see section 8 for more details) with broader dynamic range are also of high interest for instance for imaging of pH in endosomal–lysosomal system. Since the pH varies from 6.0 to 6.5 in endosomes to 4.0 in lysosomes it is almost impossible to maintain adequate resolution in such a range with a single indicator probe. Therefore, probes containing two^{761,764,765} or even three⁷⁶² xanthene-based indicators have been reported. Aylott and co-workers⁷⁶¹ embedded dextran conjugates of fluorescein isothiocyanate, 5(6)-carboxy-2',7'-difluoro-fluorescein (Oregon green) and a reference fluorophore 5-(and-6)-carboxytetramethylrhodamine into poly-(acrylamide) nanoparticles. Andresen and co-workers⁷⁶⁴ covalently immobilized Oregon green and fluorescein into cross-linked poly(acrylamide-co-N(3-aminopropyl)-methacrylamide) nanoparticles. Immobilization of two dyes with substantially different pK_a values (4.7 and 6.4 for Oregon green and fluorescein, respectively) resulted in doubling of the dynamic range of the nanosensor (Figure 46C).^{761,764} In further work, Zhang et al.⁷⁶² added 5(6)-carboxy-2',4',5',7'-tetrafluoro-fluorescein ($pK_a = 3.0$) to Oregon green and fluorescein, which resulted in expansion of the dynamic range to 1.4–7.0. All dyes were covalently immobilized into the nanoparticle along with a reference dye (red-emitting Alexa 568). Since the photostability of xanthene dyes is known to significantly improve with introduction of electron-withdrawing halogen atoms, the nanosensor is likely to show drift in the calibration curve due to photobleaching of less photostable fluorescein. Nevertheless, such nanosensors allow reliable pH monitoring in endosomal–lysosomal system, whereas nanosensors based on a single pH probe provide erroneous results.⁷⁶⁴ A recently reported nanosensor (metal–organic framework incorporating a mixture of porphyrin and rhodamine)⁶³⁵ shows reversible dual response in acidic media (pH 2–7, sensitivity due to rhodamine) and basic media (pH 9.5–11.5, sensitivity due to porphyrin) but almost no sensitivity between pH 7 and 9.5.

Array approaches were described,^{232,233,302} where many individual sensors based on pH indicators covering broad range of pK_a values are combined in an array which is read-out with help of an RGB camera or scanner.^{232,233,302} For instance, Capitan-Vallvey and co-workers^{232,233} combined 11 individual absorptiometric pH sensors embedded in plasticized poly(vinyl chloride) or cellulose acetate with addition of a lipophilic salt

such as tridodecylmethylammonium chloride. Fairly good prediction of pH in the range from 0 to 14 was achieved using hue values obtained from imaging of the sensor array with a calibrated scanner. The use of HSV (hue, saturation, value) color space compared to the RGB technique reduces the parameter space from three dimensions to one. It also makes the read-out more robust against variation in the ambient light conditions. The use of neural networks²³³ improves the quality of the prediction and reduces the requirements on computer memory and processor speed. The application of artificial neural networks can help to extend the dynamic range of sensors based on a single indicator.⁶³

Rurack and co-workers¹³⁵ recently presented an array containing 10 structurally similar fluorescent pH indicators bearing different receptors. The apparent pK_a values of the immobilized indicators vary from 0.5 to 12.8, resulting in the array covering impressive pH range from 0 to 14 (Figure 46D).

The materials described above make use of either absorptiometric or fluorescent pH indicators. Only a few reported optical sensors utilize alternative concepts. Particularly, Pathak and Singh¹⁰¹⁰ presented a fiber-optic sensor in which a small part of the waveguide was removed and substituted with a cross-linked poly(acrylamide) hydrogel. pH sensitive swelling/shrinking of hydrogel results in the change of the refractive index which enables measurements between pH 3 and 10 (see section 2.3). In other work of the group, the cladding of the fiber was removed to be modified with a combination of ZnO nanorods and poly(acrylamide) hydrogel.¹⁰¹¹ The sensor showed response between pH 3 and 11. These sensors operate reversibly and show very little hysteresis. However, no study of potential interferences has been conducted which may be particularly strong in case of temperature and ionic strength.

An uncommon optical fiber pH sensor with wide analytical range was described by Khan et al.¹⁰¹² It is based on an optical fiber pulse width modulation (PWM) technique. The sensing signal's pulse width changes when the unclad sensing element of the fiber comes into contact with buffers of varying pH values. The unclad sensing elements of the array were coated with indicators (methyl red, methyl orange, thymol blue, Nile red, and rhodamine B) that are said to change their refractive index (RI) when contacted with the buffer solution. As a result, the pulse width of the sensing signal also changes. The sensor has a linear response over a wide range of pH values (from 2 to 12). However, such sensors are of quite limited practicability because any other species being present in the sample that would also affect RI and interfere. A more practical optical fiber wide-range pH sensor was obtained by doping a titania sol-gel with organic dyes.⁶⁰⁴ The sensing films were obtained from a precursor solution composed of titanium tetraisopropyl orthosilicate and the dyes brilliant green, rhodamine 6G, rhodamine B, and coumarin. Titania was used because it is more chemically resistant and has a longer lifetime than silica films. The analytical range of the sensor extends from pH 2–12.

The composition and properties of wide dynamic range pH sensors are summarized in Table S19.

14. SENSING FORMATS

14.1. Planar Sensors

Planar optodes (Figure 47A) belong to the most common sensor formats. They represent a sensing layer coated on a transparent support (plastic or glass, see section 9 for more details) and optionally additional layers such as scattering and/

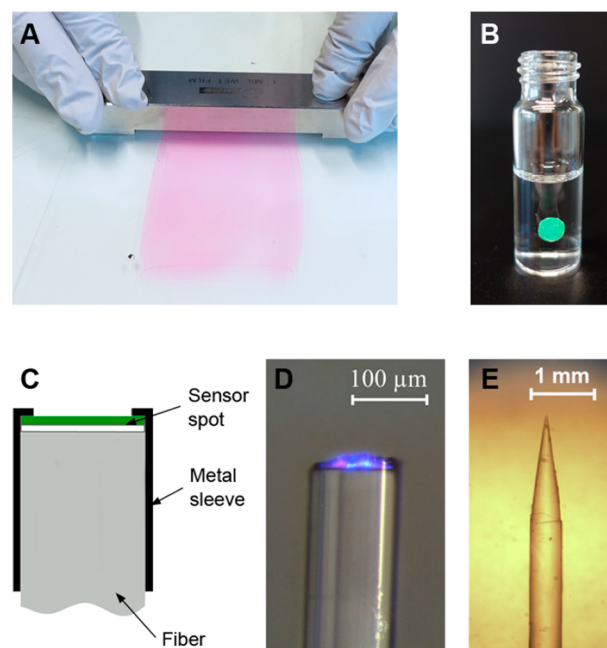


Figure 47. Examples of the planar optodes and fiber-optic sensors. (A) Preparation of a planar optode by knife-coating of a sensor “cocktail” (indicator, polymer, organic solvents, and optionally some additives) onto a transparent poly(ethylene terephthalate) support. (B) Planar sensor spot glued to the inner wall of a transparent glass vial. (C) Fiber-optic sensor manufactured by fixing a planar sensor spot of a small diameter (2 mm) onto a distal end of a plastic optical fiber. (D) Example of a flat-broken fiber-optic pH microsensor for simultaneous measurement of pH and pO_2 . The blue color of a 470 nm LED (used for the excitation), as well as red luminescence from the indicators is visible. Reprinted with permission from ref 381. Copyright 2007 American Chemical Society. (E) Example of a tapered fiber-optic sensor.

or optical isolation layer (section 9). Planar optodes can be manufactured by different methods, preferably by knife coating (Figure 47A), dip-coating, spin coating, spray coating, screen and inject printing. In all these methods, a sensor “cocktail” containing an indicator dye, polymer (or sol-gel), and a solvent is deposited onto the support to give a sensor layer after solvent evaporation. Additional steps (e.g., curing under UV light) may be necessary. The thickness of the sensing layer can be easily adjusted in some methods, for example, by varying viscosity of the “cocktail”, the thickness of the spacer in knife-coating or rotation speed in spin coating. In case of transparent layers, the thickness can be estimated via measurement of the absorbance of the foil assuming that the molar absorption coefficients are not affected by immobilization. Fluorescent pH sensor foils are commercially available.

Planar optodes are well suitable for characterization of the sensing materials even if they later may be used in other formats, such as in fiber optic sensors. Parameters include absorption and emission spectra, luminescence quantum yields, decay times, leaching, and response and recovery times.

Planar optodes also enable *imaging* of pH distribution on two-dimensional surfaces (section 11). One may also punch sensor spots for contactless sensing through a transparent glass wall (Figure 47B). The support side of the spot is glued to the inner part of the chamber (for instance a fermentation flask or a microplate) and the read-out is performed by positioning an optical fiber (or a fiber-less read-out unit) in front of the spot.

Small spots (typical \varnothing 1–3 mm) can be fixed at a distal end of an optical fiber to produce fiber-optic sensors (Figure 47C).

14.2. Fiber Optic and Other Waveguide Sensors

In this format, a sensor spot may be glued onto a distal end of the fiber (Figure 47C). Alternatively, the fibers may be directly coated with the “cocktail” containing indicator, polymer, and organic solvent (Figure 47D and E).^{56,381} Also, the fibers can be coated with a solution of an indicator in a mixture of monomers, cross-linker and photoinitiator, and subsequently photopolymerized.^{88,397,1013,1014} In the case of polymerizable materials, the indicator typically bears a functional group to enable covalent incorporation into the resulting polymers. Fiber-optic sol–gel sensors are manufactured by depositing the sol solution onto the fiber. In most cases, the indicator is covalently coupled to an alkoxy silane before it is mixed with other precursors.⁴⁴²

It is important that the spectral properties of the indicator (and reference material if it is present) match those of the fiber material. Glass and quartz fibers have a numerical aperture (NA) of about 0.2–0.5 and show excellent transparency in visible and NIR parts of the electromagnetic spectrum. Additionally, quartz fibers are transparent to UV light. The NA of much cheaper plastic PMMA fibers is higher (about 0.6), but their transparency in UV and NIR is rather poor. In the red-NIR part of the spectrum, attenuation maxima are observed at ~630 and 730 nm and attenuation minima at ~650 and 760 nm, and light absorption increases continuously at higher wavelength.¹⁰¹⁵ For instance, at 730 nm at least 50% of the light is expected to be lost passing through a 1 m fiber. Thus, in case of NIR indicators, only short (1–2 m) plastic fibers are useful unless deuterated or fluorinated modifications of the polymers (which show much lower attenuation in NIR but have limited commercial availability)¹⁰¹⁶ are used. Concerning mechanical stability, glass fibers are flexible enough at the core diameters of 140 to 400 μm but thicker fibers (e.g., 1 mm in diameter) are inconvenient to use because of the high rigidity and poor stability to bending. In contrast, 1 and 2 mm PMMA fibers have excellent mechanical characteristics. It should be mentioned that fibers of larger diameter are preferable for interrogation of sensor spots through relatively thick walls.

Fiber-optic *microsensors* are popular due to better spatial resolution, suitability for measurements in small volumes and minimal disturbance caused by measurement. Although coating of flat-broken fibers of small diameter is possible (Figure 47D), tapered fibers (Figure 47E) often are preferable because of their higher signals and faster response times. Because of favorable diffusion, the dynamic response of the tapered microsensors is significantly faster than that of the planar optodes and can be in a subsecond range. Additional microstructures on the fiber tip can improve the response times even further.⁴¹⁷ Considering the size, apart from the standard dimensions of hundreds of microns, also sensors based on micrometer-sized⁸⁸ and submicrometer⁵³ fibers have been reported. They enable profiling with 0.1 mm spatial resolution, and fast measurements with response times of <1 s for 3 μm -thick optodes⁸⁸ in very small objects (such as cells). However, they are challenging to manufacture, are mechanically fragile, feature reduced operational stability and faster drift.⁵³ They also require more sophisticated setup for interrogation including laser diodes for the excitation and a photomultiplier for signal detection.⁴⁰⁸ In contrast, microsensors of larger diameter ($\geq 100 \mu\text{m}$) can be conveniently read out using cheap and compact combination of an LED and a photodiode. Such fiber microsensors can also be used for

profiling, for example to analyze pH gradients in saltmarsh ponds at sediment-water interface.¹⁰¹⁷

Most fiber-optic microsensors are capable of measuring pH only, however several multiparameter sensors have also been reported. Ji and Rosenzweig⁴¹⁹ prepared a microsensor ($\varnothing = 50 \mu\text{m}$) for simultaneous measurement of pH and calcium based on SNARF-1-dextran and Oregon green BAPTA-1-dextran conjugates incorporated into PHEMA. Kocincova et al.³⁸¹ reported a fiber-optic microsensor for simultaneous monitoring of pH and oxygen. They used a composite material based on combination of oxygen- and pH-sensitive microbeads dispersed in a hydrogel. Walt and co-workers presented an interesting concept yielding multiparameter fiber-optic sensors.⁴²⁹ They modified an optical imaging fiber¹⁰¹⁸ (i.e., a fiber with the ability to carry a coherent image from one end to the other) of 350 μm in diameter comprising 3000 individual elements with pH, pO_2 and pCO_2 “sensing chemistries”. The photodeposition of the sensing layers was realized via illumination of individual areas ($\varnothing = 40\text{--}50 \mu\text{m}$) of the fiber.

14.3. Evanescent Wave Sensing

In an optical waveguide, light is totally reflected at the interface between an optically denser core and a less dense cladding if the angle of incidence is larger than of the critical angle. The reflected light penetrates the second medium (the so-called evanescent field), which decays exponentially with the distance from the core. Evanescent field read-out makes it possible to obtain sufficient signals from very thin sensing layers. Because of multiple reflections, the increased optical path results in acceptable signals and fast response.^{281,283,284} This read-out type has been applied particularly often in sol–gel-based pH optodes,^{83,277,293,324,609,1019} but several evanescent wave sensor based on polymeric materials have also been reported.^{55,347,1020} The reader is advised to search for the term *evanescent* in other sections of this Review.

In a typical configuration based on a step index multimode fiber (Figure 48), a section of the protective plastic jacket is

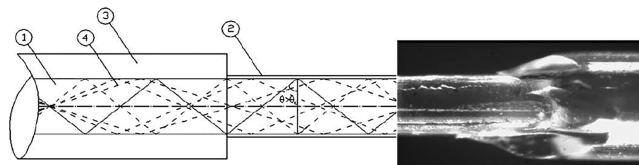


Figure 48. Schematic representation of an evanescent-field sensor (left) and its photographic image (right): 1, fiber core; 2, original cladding; 3, protective jacket; 4, typical propagation modes. Reproduced from ref 1020 with permission from Elsevier. Copyright Published by Elsevier, Ltd., 2004.

removed and the cladding in this part is reduced by polishing or chemical etching. It is then covered with a very thin layer of a pH-sensitive material.

The depth of light penetration (d_p) in evanescent field can be described by the following equation:¹⁰²¹

$$d_p = \frac{\lambda}{2 * \pi * n_{\text{core}} * \sqrt{\sin^2 \theta - \frac{n_{\text{cl}}^2}{n_{\text{core}}^2}}} \quad (22)$$

where λ is the wavelength of the light source, θ is the angle of incidence of the light at the core/cladding interface, and n_{core} and n_{cl} are the refractive indexes of the core and cladding, respectively. In case of a silica fiber (refractive index ~ 1.45) with

removed cladding placed in contact with an aqueous medium and assuming light to enter the core at an angle of 80° , the estimated d_p is $\lambda/3.3$, which is equal to a depth of 170 nm for 550 nm light. The fiber with core diameter of 400 μm will be expected to have 1 reflection each 1 mm or more, resulting in a maximum light path length of 17 μm for the sensing part of the fiber of 10 cm in length. Such path length is expected to result in sufficient signals for both absorptiometric and fluorescence sensors. Interestingly, in case of very thin sensing films, indicators immobilized even in rather hydrophobic polymers such as PMMA can show pH sensing behavior.¹⁰²⁰ Evanescent field sensors based on the use of conductive polymers such as polyaniline (section 7.2), which display pH dependent absorption between 400 and 1000 nm, are also known.⁵⁵ Apart from fiber-optic sensors, evanescent field read-out is also utilized in planar waveguide-based sensors. For instance, Yang and Saavedra²⁶⁶ coated indicator doped sol–gel layer onto a glass substrate (microscope slide).

U-shaped fiber optic pH probes also utilizing evanescent field absorption and dye-doped sol–gels were presented.²⁸² The U-shaped probe was applied to increase the evanescent field in the film and hence the interaction strength with the dyes in the film (Cresol red, bromophenol blue, chlorophenol red). The influences of bending radius of the probe and the numerical aperture of the fiber on the sensitivity of the sensor were studied. As the bending radius of the probe decreases, the sensitivity of the sensor increases. Further, for a given bending radius and the fiber core diameter, increase in the numerical aperture of the fiber increases sensitivity. Similar work on determination of pH values via U-shaped fibers was presented later.¹⁰²² Another kind of optical fiber pH sensor was described¹⁰²³ that is based on surface adsorption of the pH-inert dye methylene blue, producing absorption in the evanescent field surrounding the fiber in a section where the cladding was removed. The linear range of operation is said to be between pH 3 and 9. However, the authors do not explain why the dye (which is not a pH indicator in this pH range) responds to changes in pH values.

Some limitations of evanescent field sensing should be considered. First, changes in the refractive index of the sensing layer (due to swelling, temperature change, etc.) may affect the properties of the sensor.³⁴⁷ Second, since a significant length of the optical fiber/waveguide should be modified, a compact design of the sensor becomes rather challenging. The configuration shown in Figure 48 and the planar waveguide versions²⁶⁶ only allow for measurements in a flow-through cell. This issue can be partially addressed by using a configuration with a mirror positioned on the distal end of the fiber.³⁴⁷ However, even in this case, the total length of the fiber coated with the sensing composition typically exceeds 1 cm.

14.4. Refractive Index and Surface Plasmon Resonance Based pH Sensors

As pointed out in section 2, numerous hydrogels are known that undergo pH-dependent swelling/deswelling. This has resulted in a variety of optical sensing schemes because swelling is associated with changes in the turbidity, refractive index, reflection, color, or fluorescence (for example by using a solvatochromic probe, section 2.10). Detection schemes in pH sensors based on the use of swellable polymers include measurement of refractive index, surface plasmon resonance, holography, or by using hydrogels as a matrix in photonic crystals. Numerous materials have been described that undergo pH-induced swelling/deswelling, and the following are most

common: acrylates and methacrylates (and numerous chemical modifications), polyurethanes, cross-linked polyglycols, chitosan, poly(vinyl alcohols), and copolymers like poly(acrylonitrile-co-polyacrylamide), to give representative examples only. The following sections cover refractive index and surface plasmon resonance-based pH sensors.

14.4.1. Refractive Index Based pH Sensors

The fundamentals of refractive index (RI) based sensing have been outlined in section 2.3. Methods based on measurement of RI do not require a pH indicator to be used. Rather, they are making use of a swellable/shrinkable material. This has certain advantages. On the other hand, changes in RI in such materials often not only depend on the pH value but also on other parameters, such as temperature, salinity or the fraction of organic solvent. There is a substantial wealth of literature on the design of sensor for measurement of RI, but the number of papers specifically devoted to sensing of pH values is moderate. A review covering hydrogel based sensors appeared in 2008. It covers both optical and other sensors.¹⁵⁸ Notwithstanding this, many of the RI sensors described so far (for example in refs.^{1024–1029}) may be converted into pH sensors if coated with a pH-responsive material, and this may result in numerous future papers.

The polymers used in such sensors are often referred to as stimuli-responsive polymers, and the stimulus in this case is the local pH value. During the process of swelling, the fraction of water in the polymer increases, and this causes a decrease in the RI of the hydrogel. Alternatively, swelling may be optically detected via the physical displacement it can induce (see below). The milestone paper by Seitz back in 1999 summarizes the principles and the features of a typical RI-based pH sensor. These include (a) the use of a porous materials to enable fast diffusion of protons, (b) the use of composites consisting of microparticles placed in a hydrogel matrix, and (c) the option of using near-infrared light along with fiber optics technology.¹⁰³⁰ In fact, most such sensors are based on the use of optical fiber waveguides.

Probably the first fiber optic pH sensor based on RI transduction was designed by Attridge et al.⁴⁷ Two methods were used in parallel. The sensing material on the fiber comprises an ion exchange membrane carrying a sulfophthalein dye acting as an indicator. In parallel, changes in the RI are monitored by using a coaxial directional coupler consisting of two monomode waveguides placed a few μm apart over a well-defined interaction length. The two kinds of information are analyzed to assess the practicality of a sensor capable of discriminating against interfering refractive index variations. The response time is as short as a few seconds. A related scheme was presented later¹⁰³¹ by using a thermoresponsive copolymer bearing a pH-responsive solvatochromic dye to result in a dual sensor for temperature and pH value.

The group of Arregui¹⁵⁴ has described pH-sensitive long-period fiber gratings with polymeric nanocoatings. The pH-sensitive films with optimal overlay thickness were deposited by self-assembly poly(allylamine hydrochloride) (which is cationic) and poly(acrylic acid) (which is anionic at pH values above 5). Sensors were also prepared that incorporate the pigment Prussian blue (PB) in the films. Both sensors were compared in terms of sensitivity and response time, and a faster response was obtained in case of sensors with PB particles in the polymer. Linear response is reported for the pH 4–7 range. In related work, multilayered thin poly(allylamine) (PAH) films

containing the pH indicator brilliant yellow (BY) were prepared on a quartz slide by layer-by-layer (LBL) deposition technique.²¹⁰ The spectra and color of the PAH/BY films change in the pH range from 9.0 to 5.0, and the response time is fast because the film is very thin.

Zamarreño et al.¹⁵⁵ have deposited a thin polymeric coating on an optical fiber core. Lossy-mode resonance (LMR) occurs depending on the refractive index of the coating and the thickness of the coating. Poly(allylamine hydrochloride)/poly(acrylic acid) acted as the pH sensitive coating whose thickness reversibly varies with the pH value of the solution due to swelling/deswelling. This LMR-based optical fiber pH sensor is said to have an accuracy of ± 0.001 pH units (at constant temperature) and an average sensitivity (resolution) of 0.027 pH units per nanometer in the range between pH 3 and pH 6, but effects of ionic strength were not tested.

Fiber Bragg grating (FBG, Figure 16) sensors are fairly simple and in wide use. In essence, it consists of a white (multicolor) light source that passes the core of a fiber possessing a Bragg grating. Depending on the RI of core and fiber, most of the white light will be transmitted and spectrally separated. However, a small band will not be transmitted but reflected. Representative examples for such optical pH sensors include an FBG sensor¹⁷² with a swellable hydrogel whose RI is strongly affected by pH values. On swelling, the hydrogel causes a physical stretch on the fiber, which expands the grating period. Such a sensor resembles the function of displacement sensors as described in the section on less common detection schemes. Alternatively, a so-called chirped grating coupler may be used.¹⁰³² Again, pH-induced swelling of a polymer membrane is detected via refractometry using a compact multichannel sensor module. Signal transduction by means of the chirped grating couplers allows for the design of a simple sensor module. Experiments were performed with replicated polycarbonate TiO₂ waveguide sensor chips coated with an ultrathin photopatterned hydrogel membrane carrying amino groups, which reversibly change from the neutral state to a positively charged state upon acidification. The resolution reported by the authors is said to be $< \pm 0.00011$ at pH 7.5 in a dual-channel module, but this is not plausible given the experimental circumstances described and the lack of a more realistic test scenario.

Wavelength interrogation was applied in a no-core fiber optic pH sensor using a polyacrylamide coating.¹⁰¹⁰ A no-core fiber was stubbed between two single-mode fibers with a standard fiber connector before immobilizing the hydrogel. The sensor is placed in a flow cell through which solutions of various pH values are passed. Wavelength shifts, measured with a FBG, can be related to actual pH values. Typically, wavelengths shifts by 1.94 nm per pH unit over the pH range from 3 to 10, with good linearity and fast response.

An example of an interferometric pH sensor is represented by a fiber sensor based on the use of waist-enlarged bitapers and mode excitation.¹⁸² The interferometer, which comprises a waist-enlarged bitaper, a round tip, and a tantalum pentoxide layer displays high refractive index (RI) sensitivity. It was coated with a poly(vinyl alcohol)/poly(acrylic acid) composite hydrogel to induce sensitivity to pH values. The interference fringes shifted with varying pH solutions, and the pH sensitivity is 1.58 nm per pH unit in the pH 2.5–6.5 range. Rise/fall times are as short as 10/11 s.

In another kind of refractometric pH sensor, a pH-sensitive coating was placed on indium tin oxide-coated optical fiber.¹⁰³³ The pH of the external medium modifies the thickness of the

thin polymeric coating and, hence, the effective refractive index. This, in turn, causes a wavelength shift in the near-infrared region. The devices permit wavelength-based pH determination with high sensitivity (17.5 nm/pH unit) and with fast response.

14.4.2. Surface Plasmon Resonance-Based pH Sensors

The fundamentals of surface plasmon resonance (SPR) based sensing have been outlined in section 2.4. Like pH sensors based on (fiber) optic measurement of pH induced effects on refractive index (RI), SPR is another but experimentally entirely different approach to detect changes in RI. **Note:** This section only refers to SPR sensors based on either the Kretschmann or Otto instrumental configurations, not on so-called “SPR sensors” where the color change of gold nanoparticles in colloidal solution (often from red to blue and back) is exploited, usually a result of particle aggregation. This effect often is referred to as localized SPR but is read out visually or by photometry.

SPR-based sensing does not require a pH indicator to be used. Again, a swellable/shrinkable material comes to use. This has several advantages over indicator-based methods (such as the lack of leaching or the need for immobilization of probes), but on the other hand, changes in RI in such materials often not only depend on the pH value but also on other parameters, such as temperature, salinity, or the fraction of organic solvent. The first sensors of this kind were described by the Liedberg group^{1034,1035} back in 1982. Nowadays, SPR based detection is mainly applied to study ligand–receptor interactions of biomolecules by using one of the several commercially available devices. Typically, sensor chips are used, where the gold film is covered with a micrometer film of a hydrophilic polymer. Such films undergo pH-dependent swelling, and hence, all these sensors often are inherently pH-sensitive. Figure 49 shows a typical (fiber optic) arrangement for measurement of changes in RI via SPR using a sensor coating placed on a gold film.

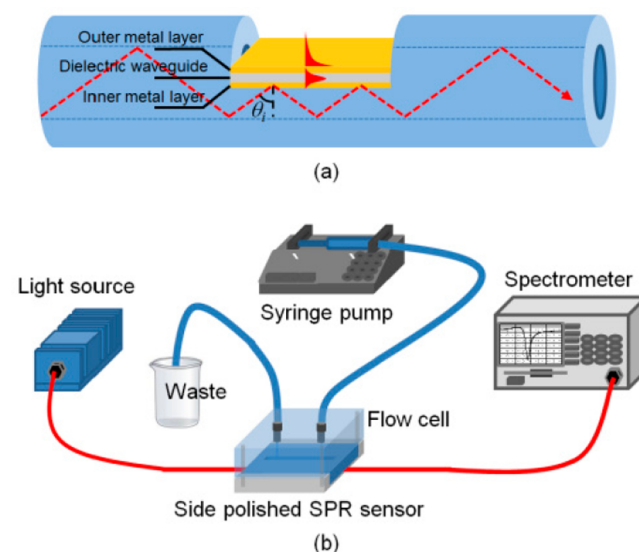


Figure 49. Schematic of a fiber optic sensor for measurement of refractive index by using surface plasmon resonance. The lower panel shows the flow system, including a syringe pump, a flow-through cell, and respective tubings. The upper panel shows an enlarged view of the SPR detection system. The swellable pH-responsive material can be placed on the gold film. The angle of reflection (Φ_r) depends on the RI of the polymer. Reprinted from ref 1036 with public license. Published by the Optical Society of America.

Various kinds of smart nanomaterials have been presented. To achieve an optimal match between the RI of the sensing layer and the waveguide, a sensing probe was prepared¹⁰³⁷ by coating an unclad core of an optical fiber with three consecutive layers of silver, silicon, and a pH-sensitive hydrogel. The change in pH of the fluid around the probe causes the hydrogel layer to reversibly swell and shrink, this in turn resulting in a change in RI. The change in RI causes a change in the resonance wavelength in the transmitted spectrum, and a blue shift is observed in the resonance wavelength (which is in the visible) on increasing the pH value of the solution. The measurement of wavelength rather than of intensity makes the sensor independent of fluctuations of light source intensity, detector sensitivity, and geometrical effects of the optical system. The sensor operates in the low and high pH range, but not at around pH 7. The influence of environmental temperature (between 16–28 °C) is negligible. Other features include a short response time, small size and good temporal stability. Another coating used in SPR based sensing of pH consists of silver, ITO ($\text{In}_2\text{O}_3:\text{SnO}_2$), aluminum and smart hydrogel layers over an unclad core of an optical fiber.¹⁰³⁸ Layers of metallic silver, aluminum and ITO were coated using a thermal evaporation technique, while the hydrogel layer was prepared by dip-coating. The sensor detects changes in the RI of the hydrogel due to its swelling and shrinkage caused by changes in the pH value of the fluid. An increase in the pH value causes swelling of the hydrogel which decreases its RI and results in a shift of the resonance wavelength toward the blue in the spectra. The ITO layer increases the sensitivity while the aluminum layer increases the detection accuracy. Temperature has very little effect in the 25–45 °C range.

An optical fiber SPR pH sensor was reported that is based on the use of multimode and single-mode fibers coated with a carboxylated hydrogel.¹⁰³⁹ Depending on local pH values, the fraction of dissociated carboxy groups in the hydrogel changes and affects the volume and RI of the hydrogel. This results in a shift of the SPR peak wavelength. The sensor works over a wide pH range (from 1 to 12), and at the best sensitivity, the shift is 13 nm/pH (in the pH range 8–10). The influence of temperature (in the range from 20 to 40 °C) on SPR wavelength is weak. The sensor possesses remarkable repeatability and excellent stability, has a wide analytical range, and can be fairly easily fabricated. Another pH-responsive nanoplasmonic pH sensor was fabricated¹⁰⁴⁰ by chemical attachment of poly(allylamine) onto ~28 nm diameter gold nanoprisms bound to a silanized glass surface. The reversible change of polymer structure upon protonation and deprotonation (causing shrinking and swelling) of the amino groups of the polymer alters the localized surface plasmon resonance (LSPR), typically peaking at 694 nm. A spectral shift of the peak can be observed. The pH-induced shrinking and swelling were subsequently applied in an enzymatic glucose sensor.

There is a wealth of literature on the design of sensor for measurement of RI via SPR, but the number of papers specifically devoted to sensing of pH values is moderate. Notwithstanding this, virtually all SPR-based sensors (described, for example, in refs 1041–1046) may be converted to optical sensors for pH values if coated with a pH-response polymer as discussed before. It is also noted, here, that most of the hydrogel based sensors for determination of relative air humidity also are likely to be sensors for pH values of aqueous solutions.¹⁰⁴⁷

14.5. Photonic Crystal-Based pH Sensors

Photonic crystals (PhCs) have so-called structural colors and do not require the use of indicator dyes. Structural colors are widely found in nature, the color of butterflies or chameleons being typical examples. Their color can undergo quick changes by applying a mechanical stress on the system. Color changes may also be induced by changing local pH values because these affect the lattice spacing in PhCs. This has inspired many researchers to mimic nature.

The fundamentals of PhC based sensing have been outlined in section 2.5, and numerous variations of methods for measurement of changes in local diffraction patterns in PhCs have been published in recent years (for example in refs 1048–1051), albeit not for sensing pH values. A review is available on various kinds of photonic hydrogel-based sensors, PhCs included.¹⁰⁵² Virtually all of them may be converted to optical sensors for pH values of combined with a pH-responsive hydrogel as discussed before. The state of the art by the year 2014 in PhC-based chemical sensing and biosensing has been reviewed.¹⁶³

In the simplest (and purely synthetic) version, sensor materials are prepared by incorporating polystyrene nanoparticles into a hydrogel matrix. Hydrogels include acidic polymers, such as poly(meth)acrylates, poly(meth)acrylamides, polyurethanes, and polyethylenimine. Swelling is often due to protonation of basic polymers or due to deprotonation of acidic polymers. Even mixtures (deposited layer-by-layer) have been used. Color effects are quite significant, with spectral shifts as large as 250 nm. Color changes are beautiful and can be observed visually but one has to keep in mind that the colors are so-called structural colors (like those of a butterfly), not like the colors of an indicator dye. Remarkably, some sensors have a rather wide analytical range.

In their milestone papers, the Asher group^{1053,1054} describe PhC-based pH sensors, referred to as a colloidal crystalline array (CCA). Plastic microspheres were incorporated into a stimuli-responsive hydrogel. Visible light is diffracted in the CCA, and the observed color is a function of the lattice spacing d of the plastic microspheres (see Figure 14) which—in turn—is governed by pH-dependent swelling of the gel. Hence, swelling increases the mean separation between the microspheres and shifts the Bragg peak of the diffracted light to longer wavelengths. As a rough rule of thumb, a 0.5% change of the volume of the hydrogel shifts the diffraction wavelength by ~1 nm. The operative pH range of such sensors can be adjusted by proper choice of the hydrogel, but response times can be quite long (>10 min), which is much longer compared to refractive index (RI) based sensors. On the other hand, such sensors can be judged with bare eyes and, therefore, allow for a fast rough estimation of pH values. Instrumental read-out is, of course, more precise.

Various kinds of such sensors for pH values have been reported in subsequent work,^{1055–1060} several based on the use of nanosized particles. Low and high pH sensing capability was achieved by variation of the gel material, for example by functionalization with carboxylates and phenol derivatives, respectively. A mechanically robust and fast responding PhC-based pH sensor was fabricated¹⁰⁶¹ by templated photopolymerization of hydrogel monomers within the interstitial space of a self-assembled colloidal PhC. This pH sensor has a response time of <10 s and a >6 month lifetime without compromising the reproducibility of the pH-driven color change. Similarly, a planar defect layer within an inverse opal hydrogel was used in a tunable PhC-based pH sensor. It was

fabricated by combining the Langmuir–Blodgett technique and the PhC template method. The resulting material consists of a three-dimensional, highly ordered, and interconnected macroporous array of poly(methacrylic acid), which is a hydrogel sensitive to pH values. The optical properties of these inverse opals were investigated using reflection spectroscopy but can also be detected visually.¹⁰⁶² Typical materials and properties of pH sensors are summarized in Table S20.

Even dual sensing of pH values and temperature was shown to be feasible. The diffraction pattern of hybrid particles prepared by copolymerization of *N*-isopropylacrylamide and methacrylic acid in a gel were shown¹⁰⁶³ to be sensitive to temperature in the range from 15 to 40 °C, and to acidity at pH values between 2 and 7. The sensitivity to pH changes leads to a wavelength shift of around 150 nm, while temperature only induces a shift of 50 nm at pH 7 and of 20 nm at pH 2. Unlike in dual sensors where two indicators with different optical properties are used, these sensors can hardly differentiate whether the color changes originate from changes in temperature or pH value.

In more recent bioinspired work, Fei et al.¹⁰⁶⁴ have designed a pH sensing scheme by placing poly(acrylic acid)-*co*-polyacrylamide [P(AAc-*co*-AAM)] via in situ copolymerization onto the wings of the butterfly *Papilio paris*. The wings have a hierarchical, lamellar structure (composed of chitosan) as shown in Figure 50. The structural color of the modified wings is changed by

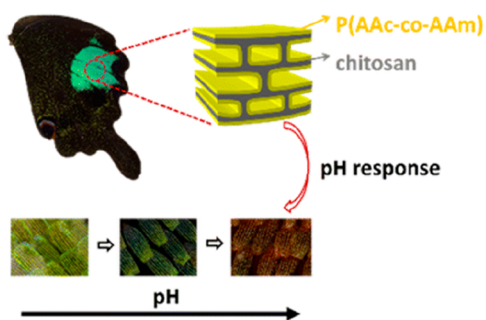


Figure 50. Schematic of a bioinspired photonic crystal based optical sensor for H values. The graph shows the typical chitosan structure of the wing of a butterfly that was coated with a synthetic copolymer that undergoes pH dependent swelling. This results in a change in the structural color of the wing. Reprinted with permission from ref 1064. Copyright American Chemical Society 2016.

local pH values. The introduction of AAM into the system created covalent bonding, which strongly bridges the polymer with the wings and leads to an accurate yet broad variation of reflection wavelength to measure environmental pH values. The reflection wavelength can be tailored by varying the RI of the lamellar interspacing because of the swelling/deswelling of the polymer. The application of covalent cross-linking results in a PhC-based pH sensor with high cycling performance. While interesting from a purely scientific point of view, such sensors are unlikely to be used by others given the fact that simpler sensors have been described that can be made from materials that are readily available at any time and any place in the world.

Liu and co-workers¹⁰⁶⁵ have applied polyaniline in 1D PhCs with a gradient architecture as a material that responds to vapors of acidic or alkaline chemicals. PhC based sensors were also combined with fiber optic sensing schemes in order to enable remote sensing. A pH sensor of that kind is based on the use of a poly(vinyl alcohol)/poly(acrylic acid) coating and interferometric laser interrogation.¹⁸³ The sensor works in reflection

mode, has an average sensitivity of 0.9 nm per pH unit (for the 11 wt % PVA/PAA coated sensor) in the pH range from 2.5 to 6.5 and rise/fall times, respectively, of 12 and 18 s. Inverse opal photonic crystal hydrogels (IOHs) were obtained¹⁰⁶⁶ by polymerization of polyacrylamide and poly(methacrylic acid) along with poly(styrene-*co*-acrylic acid) particles by a “sandwich” method. These IOHs exhibit brilliant structural color that can be tuned by variation of particle size the concentration of monomers and cross-linkers. The color and Bragg diffraction peak of the IOHs responds to pH values (and also to methanol and ethanol). Reflectance is red-shifted at low pH values, and blue-shifted at high pH values.

Various kinds of nanoparticles were also applied in PhC-based sensors. A pH responsive PhC sensor was obtained¹⁰⁶⁷ by incorporating magnetite nanoparticles (Fe_3O_4) into a poly(acrylamide)-poly(2-hydroxyethyl methacrylate) gel. The Fe_3O_4 particles were linearly arranged by polymerization under an external magnetic field. The resulting materials were endowed with pH sensing capability by converting poly-HEMA into PAA units. Other nanomaterials for use in PhC-based colorimetric sensing using hydrogel matrices include porous silicon in poly(2-diethylaminoethyl acrylate) to give a sensor for the pH 3–9 range,¹⁰⁶⁸ silver and gold nanoparticles,¹⁰⁶⁹ various kinds of zeolite nanoparticles, and others. A few other PhC-based methods are known but discussed in another section. These can be found by electronically searching for *photonic crystal*.

All PhC-based pH sensors are strongly interfered by ionic strength, which is disadvantageous and limits their application to defined situations.¹⁰⁶⁰ PhC sensors can also be used as transducers in biosensors, where enzymes cause the production or consumption of hydrogen ions. Examples include organophosphorus hydrolase¹⁰⁷⁰ and urea,¹⁰⁷¹ the determination of the activity of urease.¹⁰⁷² Urease causes an increase in pH, but organophosphorus hydrolase, on the other hand, produces two protons on hydrolyzing the insecticide parathion, and the drop in local pH causes the polymer-based PhC to shrink and to undergo a visually detectable blue-shift. Such sensors also may be used to detect acidic or basic gases.¹⁰⁶⁵ A recent review covers the use of photonic crystals as detectors in microfluidic chips.¹⁰⁷³

14.6. Holographic pH Sensors

This work was pioneered by Chris Lowe and co-workers. In such sensors, changes in the replay wavelength of sensor films are used to characterize the swelling behavior of the matrix as a function of analyte concentration. The various kinds of materials for use in (mainly physical) sensors has been reviewed.¹⁰⁷⁴ In the first holographic pH sensor ever,¹⁰⁷⁵ a 300 nm film of poly(hydroxyethyl methacrylate) was used. The holographic diffraction wavelength (which determines the apparent color) is governed by shrinkage or swelling of the hydrogel as a function of pH. The sensor works best in the pH 5–7 (i.e., physiological) range, and the analytical wavelength changes by up to 165 nm per pH unit. Such large changes make such sensors also well suited for visual estimation of pH values. The sensor, in slightly modified form, was later applied to enzymatic sensing of lactate via the drop in local pH values as the enzymes causes the oxidation of lactate.¹⁰⁷⁶ Several patents also have been issued.

Beiu et al.¹⁰⁷⁷ have introduced photonic crystals (PhCs) embedded into cores of optical fibers, where they undergo mechanical deformation perpendicular to the length of the fiber. While not specifically demonstrated, it may well work as a PhC

based pH sensor when using a swellable polymer matrix whose RI varies with pH values. The near-infrared holographic glucose sensor described by Vezouviou and Lowe¹⁰⁷⁸ is likely also to be a good pH sensor. This is also true for the swelling-based holographic sensors for lead(II),¹⁰⁷⁹ ethanol,¹⁰⁸⁰ temperature,¹⁰⁸¹ cocaine,¹⁰⁸² all based on the use of swellable hydrogels, more recently in combination with molecular imprinting.¹⁰⁸³

14.7. Distributed Sensing of pH Values

Combination of fiber-optic sensor format, evanescent field read-out and time-resolved measurement allows for distributed sensing, that is, obtaining information from different regions along a long fiber-optic waveguide. Evidently, it represents an interesting alternative to the sensor array approach. In the distributed sensors, different parts of the core of optical fiber are coated with the sensing composition. The distance from the fiber front to a fluorophore-doped region is given by $x = (c/2n)\tau_d$, where c is the speed of light in the fiber, n is the refractive index of the fiber core, and τ_d is the time delay between the excitation pulse reflected from the fiber front and the subsequent fluorescence emission from particular sensor region.¹⁰⁸⁴ Consequently, a short laser pulse (e.g., 0.5 ns) and time-resolved fluorescence detection not only allows to access the fluorophore location but also its decay time and, therefore, the analytical information (Figure 51). The spatial resolution of this technique is determined by the fluorophore lifetime and is about 10 cm for a 20 m fiber¹⁰⁸⁵ and 1 m in case of a 100 m fiber.¹⁰⁸⁶

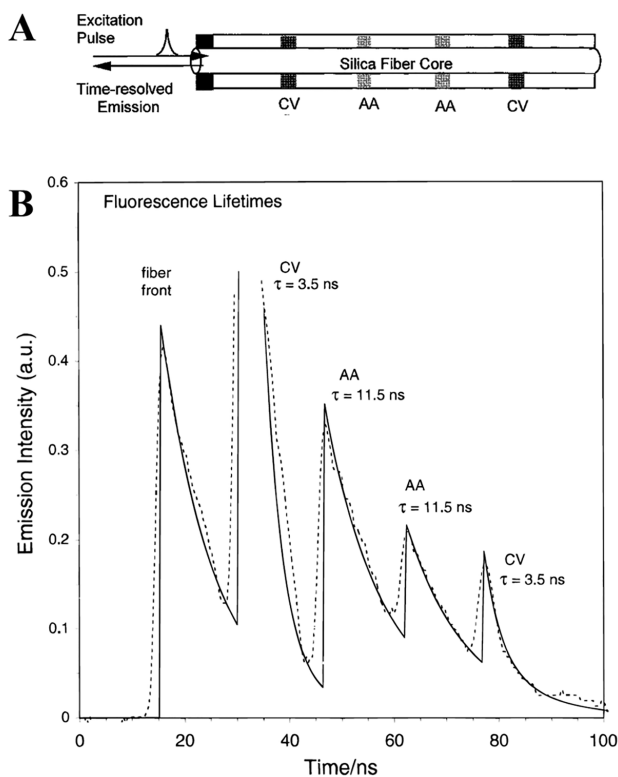


Figure 51. Operating principle of a distributed sensor. (A) Schematic representation of the optical fiber modified with sol-gel layers containing immobilized aminoacridine (AA) and cresyl violet (CV). (B) Corresponding time-resolved emission profiles following pulsed laser excitation for a 9 m fiber. Reprinted with permission from ref 1084. Copyright American Chemical Society 1996.

Time-resolved fluorescence detection following pulsed excitation can be used to probe distributed intrinsic fiber-optic sensors, resolve fluorophore locations along the fiber, and yield the optical dynamics of the chromophore.¹⁰⁸⁴ Potential advantages include possibility of sensing in multiple locations with a single setup and potential suitability for read-out of different “sensing chemistries” (e.g., multiparameter sensing) localized at different fiber regions. However, several factors limit the practical applicability of the technique. Apart from the instrumental requirements (pulsed excitation source and equipment for time-resolved read-out) removing the cladding from a long fiber and coating it with the sensing composition can be very challenging increasing the risk of fiber damage and inhomogeneous coating. Additionally, the technique allows for self-reference read-out only in case of fluorophores showing pronounced response of their fluorescence decay time to pH (section 10.2), which are very rare. Although laser excitation corresponding to the absorption of a protonated or deprotonated form of the pH indicator may be potentially used,¹⁰⁸⁴ it would significantly increase the complexity of the system. Because of these limitations, distributed pH sensing is more suitable for detection of significant pH changes in course of undesired events (e.g., leaks) rather than for precise pH measurements. This is even more true for the sensors that do not use an indicator dye but rather utilize the attenuation in the fiber due to pH-dependent swelling of a hydrogel.⁵⁹

15. SELECTED APPLICATIONS OF OPTICAL pH SENSORS

15.1. Applications of pH Optodes in Medicine and Test Animals

15.1.1. Sensing and Imaging of pH Values in Blood and the Vascular System. The normal blood pH varies between 7.35 and 7.45. Values below and above this range (acidosis and alkalosis, respectively) serve as an indicator of various disorders. Measurement of pH in arterial blood is one of the most frequent tests in monitoring of critically ill patients and is commonly performed intermittently with the help of blood gas analyzers.⁴⁶⁸ Commercial systems are available that make use of an optical pH sensor among 5 other planar sensors (pH, pO₂, pCO₂, K⁺, and Ca²⁺) incorporated in a disposable cassette (Figure 52A).¹⁰⁸⁷ Similarly, a blood parameter monitoring system 500 (Thermo Cardiovascular) incorporates optical sensors for pH, pO₂, pCO₂, and K⁺ and enables continuous monitoring of these parameters during cardiopulmonary bypass. All are mainly based on the early work of the groups of Wolfbeis and of de Silva.

There has been a great interest in developing a system for continuous monitoring of “blood gases” (pH, oxygen, and CO₂) in arterial blood particularly with help of optical sensors because of their high potential for miniaturization and minimally invasive character. The overall requirements are, however, much tighter than in case of in vitro measurements with blood gas analyzers. Particularly, the sensors for intravascular blood gas monitoring should be small enough to pass the artery cannula without affecting blood pressure fidelity, be accurate under all clinical conditions, and have to be biocompatible and nonthrombogenic.¹⁰⁸⁸ Back in 1980, Peterson and co-workers reported the first fiber optic probe for online pH measurements in blood.^{33,1089} The absorptometric probe showed good correlation with the data obtained by a blood gas analyzer and an electrode. Since this pioneering work, the suitability of various

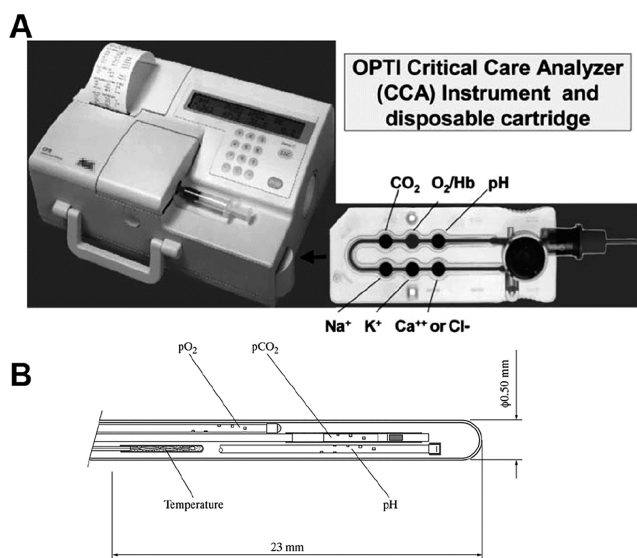


Figure 52. Critical care analyzer developed by AVL Scientific Corporation: instrument (left) and disposable cartridge (right). Blood ($60 \mu\text{L}$) is injected via the Luer port and, then, passes the various optical sensors. The whole sensor kit is placed in a portable instrument for on-site use. The fluorescence of the sensor spots is read by a photodiode after photoexcitation with a blue LED. Reprinted with permission of The Royal Society of Chemistry from ref 1087. Copyright The Royal Society of Chemistry 2005. (B) Schematic cross-section of a multiparameter intravascular blood gas probe. Reproduced from ref 1103 with permission from BMJ Publishing Group, Ltd.

optodes for pH measurement in blood has been tested in humans and animals.^{311,399,468,1090–1093} Gehrlich and co-workers⁴¹ were the first to report a multiparameter intravascular sensor for pH, oxygen and carbon dioxide relying solely on optical principles (Figure 52B). The sensor also included a thermocouple for compensation of the effects of temperature.

Several commercial sensors also incorporating pH sensors have been introduced to the market.^{1088,1094} These sensors share a similar design by representing an array of pO_2 , pH, pCO_2 , and temperature probes in a single compact package.^{1095–1098} The performance of these probes was evaluated in numerous studies,^{1088,1099,1100} which were particularly extensive in case of the Paratrend sensor (Figure 37, section 10.7).¹¹⁰¹ Despite often rather satisfactory *in vitro* performance, further success of such probes was hindered by the strong effect of many factors (thrombosis, reduced flow, etc.) on the accuracy of the intravascular measurements.¹⁰⁸⁸ Furthermore, the cost-effectiveness of intravascular measurements has been disputed,¹¹⁰² and some manufactures faced problems in terms of reproducible and low-cost mass production.¹⁰⁸⁸ As a result, the above optodes for intravascular measurement did not make it to the market, or have been withdrawn.

15.1.2. pH Sensing in Other Biological Fluids.

Monitoring of pH in stomach and esophagus is of importance for diagnostic of peptic ulcer disease and gastroesophageal reflux, respectively, and for assessing the effect of gastric antisecretory drugs.¹¹⁰⁴ Here, fiber-optic sensors can offer higher comfort to patients due to the small size of fiber optic sensors. To qualify, the material should show optimal response in (highly) acidic conditions since the pH value of the gastric juice normally varies from 1.5 to 3.5.¹¹⁰⁵ Several fiber-optic sensors for measurements in gastroenterological system were tested *in vivo*, among them the optodes reported by Baldini and co-workers⁷¹ and Netto et al.²⁸⁵

Because of their compact design, fiber-optic sensors offer significant advantages for *in vivo* measurements in other biological fluids. Schultz et al. recently reported pH measurements in surface liquid of the respiratory tract of patients with cystic fibrosis.¹¹⁰⁶ Assays were performed with a fiber-optic sensor ($\varnothing = 1 \text{ mm}$) inserted through a working channel of a bronchoscope. Sweat represents another medium where pH monitoring is of high interest due to correlation between pH

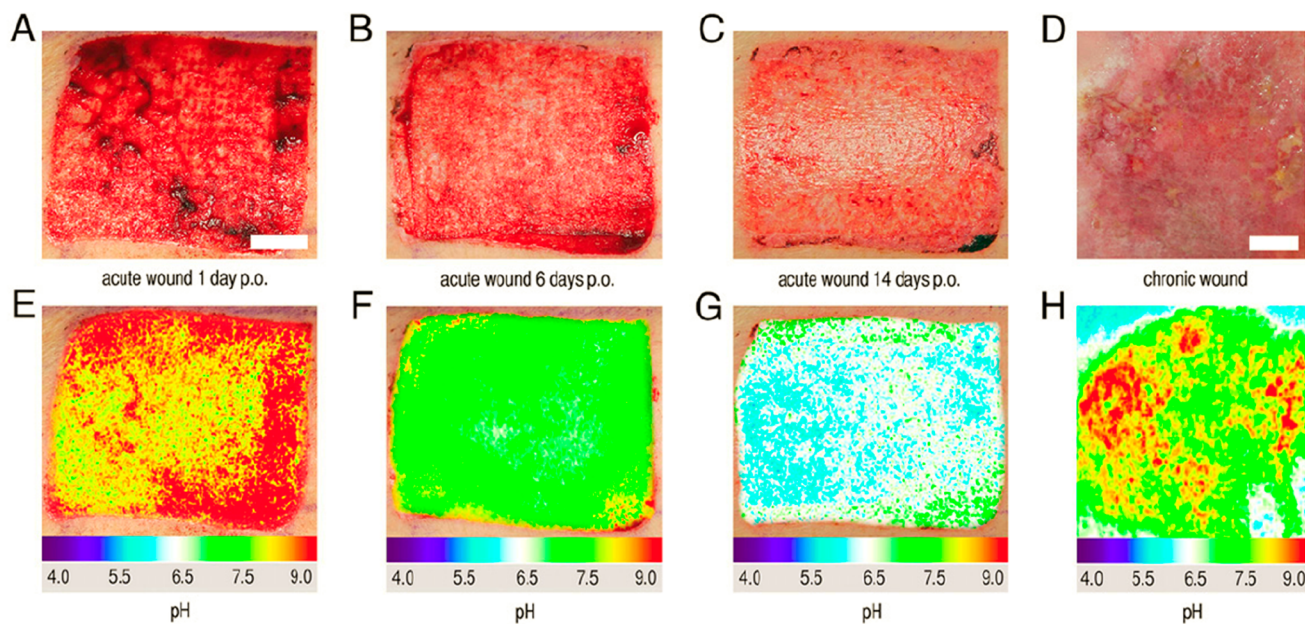


Figure 53. Luminescence imaging of pH during cutaneous wound healing. Upper row: Photographic images of the skin sites. Lower row: Respective pseudocolor images created with optical 2D pH sensors. Scale bars: 1 cm. Reprinted from ref 145 with public license. Published by the United States National Academy of Sciences.

value and health. The typical pH value of sweat is 5 to 7.¹¹⁰⁷ Measuring pH in sweat can be a good indicator of dehydration.¹¹⁰⁸ Curto et al.¹¹⁰⁹ described a microfluidic array of pH sensors based on 4 different absorptiometric indicators, which can be read out with a digital camera to enable semiquantitative pH measurement in sweat. Caldara et al.¹¹¹⁰ designed a wearable pH sensor based on sol–gel immobilized absorptiometric indicator in combination with the dedicated read-out device and used it in body trials.

15.1.3. Sensing and Imaging of pH Values on Skin and in Wounds. Wound healing is a complex process involving many biochemical events and parameters that impair healing. The process is still not fully understood due to the lack of appropriate analytical tools.¹¹¹¹ pH is one of the most important parameters during wound healing because of its regulatory function in numerous processes associated with healing.¹¹¹² pH optodes enable real time 2D monitoring of the healing process via imaging. Schreml et al.¹⁴⁵ imaged pH values during wound healing with the help of a DLR-referenced (section 2.2.7) pH optode. Although the optode follows a common design (pH-sensitive and reference microparticles dispersed in hydrogel layer), the choice of support was of extreme importance for this application. Biologically inert, transparent, and flexible 25- μm poly(vinylidene chloride) foil was found to be the best. Wound healing was accompanied by decrease of pH values (Figure 53).

The same group modified the above pH sensor layer to enable simultaneous imaging of pH and oxygen with an RGB camera⁴⁴¹ since oxygen is another very important parameter in wound healing. A detailed study of chronic wound surfaces with a similar material revealed gradients in extracellular pH in chronic wounds that disrupts epidermal repair.⁴²⁵ The same method was adopted to study postradiogenic wound healing disorders using commercially available pH sensor layers.¹¹¹³

Further development was focused on improvement of material composition and coating techniques to warrant good adhesion of the sensing layer on uneven skin. A fluorescein (with green fluorescence) was used as the indicator, and a red-emitting Ru(II) complex as an inert reference emitter, and the RGB techniques for signal processing.¹¹¹⁴ Spray-coating of the sensing “cocktail” was demonstrated to be promising. A support material (such as polyester) is not needed.

Another group¹¹¹⁵ embedded absorptiometric pH sensitive beads into alginate hydrogel fibers which possessed excellent flexibility and adhesion to the skin surface with the trade-off of losing the spatial information obtained via imaging. In another approach, phenol red was incorporated into an antibiofouling and biocompatible zwitterionic polycarboxybetaine (PCB) hydrogel matrix.¹¹¹⁶ The material allowed smartphone based readout via the blue and green channels of the camera.

The materials described above rely on a single pH indicator and are thus have a limited dynamic range of about 3 pH units. Since the entire range observed in wounds and skin disorders is larger (pH 4–9), further improvement of the indicator chemistry is necessary to achieve optimal resolution in the whole range of interest.

In view of potential applications for treatment of skin diseases via (trans)dermal drug delivery, Haag and co-workers¹¹¹⁷ measured the pH values in hair follicles with help of follicle-penetrating submicroparticles. They found a strong pH gradient in the hair follicle. The pH value is 6.5 on the skin surface but increases to 7.4 in deeper areas with a sharp increase in pH over the first 300 μm . Later, Mohr and co-workers¹¹¹⁸ developed disposable cotton swabs for pH measurements in wounds based

on covalently immobilized colorimetric pH indicators and a reference dye. Although the swabs allowed only semiquantitative pH determination, they combined a number of attractive features such as suitability to gamma sterilization, low toxicity, and low cost. A similar approach was used for a smart bandage that was combined with a small, autonomous analytical instrument that allowed readout with a smartphone using international wireless standards RFID and NFC.³⁶⁰

15.1.4. Sensing and Imaging of pH Values in Tissue and Organs. Monitoring of pH in brain may be beneficial for diagnostics and treatment of neurosurgical patients since pH changes are related to brain damage. Fiber-optic pH microsensors are attractive tools for such studies because of their small size and, therefore, minimal invasiveness. Experiments in test animals performed with a commercial multiparameter sensor (section 10.7) showed that brain pH value decreases by 0.2–0.4 units during brain injury and focal ischemia.¹¹¹⁹ During the brain insult, the pH value of brain parenchymia decreased from 7.13 to 6.75.¹¹²⁰ Similar results were obtained in brain of mice which underwent a stroke.⁴²² The authors used a fiber-optic sensor ($\varnothing = 125 \mu\text{m}$) based on a sol–gel-immobilized seminaphthorhodamine pH indicator. They also studied the response of brain pH to the injections of sodium bicarbonate into the peritoneal cavity and demonstrated excellent correlation between the readings obtained by the optode and a micro-electrode.⁴²² Magnotta et al.¹¹²¹ studied effect of CO₂ inhalation resulting in a decrease in mouse brain pH values with a commercial optical pH microsensor.

The microenvironment of tumorous tissue is characterized by hypoxia, vascular abnormalities and low extracellular pH (pHe).¹¹²² The difference between extracellular and intracellular pH values is particularly distinct. The extracellular pH value near tumor cells is about 0.5 units lower than the intracellular value.^{1123,1124} Low pH, therefore, can be considered as a cancer marker. Typically, pH imaging in tumors is performed with (a) dissolved pH indicators,^{1123,1124} (b) addressable conjugates of pH indicators (e.g., with antibodies),¹¹²⁵ (c) fluorescent proteins,¹¹²⁶ or (d) nanosized sensors.^{782,886,1127} These probes (which are often referred to as “pH activatable”) become highly emissive in tumor microenvironment due to fluorescence “switch on” under acidic conditions. This function is very useful for tumor visualization, but precise pH measurement remains challenging for two reasons: (a) The precision and accuracy of fluorescent pH imaging in tumors and other tissues is strongly affected by scattering and absorption of the excitation and emission light, and (b) calibration is difficult. Chen et al.¹¹²⁸ showed that even in case of NIR pH indicators most fluorescence is lost already at comparably small tissue thicknesses (<1.5 mm). In contrast, the self-assembled nanoprobe based on albumin-immobilized NIR pH indicator and reference dyes were found to be excellently suitable for pH measurement via photoacoustic imaging. Here, ratiometric capabilities were retained even in deeper tissue layers (3 mm).

Compared to in vivo studies, measurement of pH in tumor models is a more convenient and reliable method to study their metabolism, viability, and drug resistance. For instance, Kenney and co-workers performed pH measurements in paper scaffolds containing breast adenocarcinoma cells which were positioned above a planar pH optode.⁴³⁸ Ex vivo, a 250 μm fiber optic probe inside a hollow needle was demonstrated to be applicable for pH measurement in an ovine lung tumor model.¹¹²⁹ The fiber optic probe could distinguish tumorous from healthy tissue with

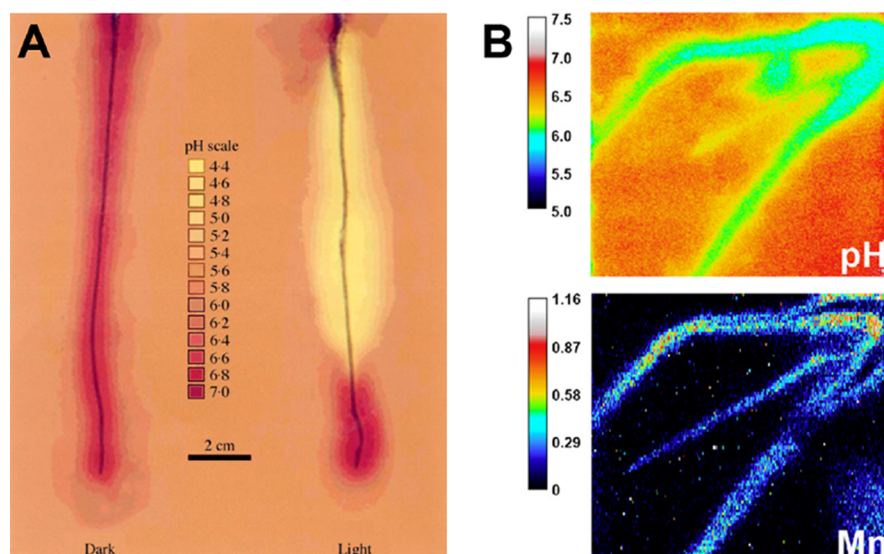


Figure 54. (A) Changes of rhizosphere pH along the root axis in dark (left) and light (right) conditions. Reprinted by permission of Oxford University Press from ref 1140. Copyright Oxford University Press 2002. (B) Combined optical pH imaging and imaging of trace metals with DGT technique in *Salix smithiana* rhizosphere. The bars represent pH and average solute flux to the gel (in $\text{pg}\cdot\text{cm}^{-2}\cdot\text{s}^{-1}$) respectively. Adapted from ref 424 with public license. Published by Elsevier.

statistical significance. For choice of the immobilization matrix, a polymer microarray approach was used that allowed the selection of the material with the best performance from 180 samples.

15.2. Intracellular and Extracellular Measurement of pH Values

Intracellular pH values are typically measured during cell proliferation, apoptosis, endo- and exocytosis, ion transport, or muscle contraction.⁹⁹ Because of the small size of the cells, optical methods are virtually the only possibility to perform measurements. The most common tools include dye-based pH probes, pH sensitive fluorescent proteins, and pH nanosensors. Numerous pH indicators for intracellular measurements, described in detail elsewhere,⁹⁹ have been reported over the past decades are still the most developed and used analytical tools. Fluorescent proteins (section 7.3) can be expressed inside cells and therefore are excellently suitable as biocompatible intracellular probes. The many known pH nanosensors (section 8) are characterized by a large structural variety. The proper choice of materials and functional groups determines their suitability for intra- or extracellular measurements. However, most nanosensors have been designed for intracellular sensing. Their addressable character⁴⁵³ enables accumulations at specific intracellular sites. Since typical pH in cellular compartments differs considerably (cytosol (7.1–7.2); mitochondria (7.5–8), lysosomes (4.5–5.5)), and because optical pH sensors are limited in the dynamic range to 2–3 pH units, different “sensing chemistries” have to be employed to obtain optimal resolution in a particular application. To address broader pH distribution with a single material, nanobeads relying on combination of several pH indicators have been designed (see section 13 for more details).^{762,764}

Read-out of the intracellular pH probes is almost exclusively performed by using microscopy. In most cases, the probes are designed to enable ratiometric (2-wavelength) read-out,^{404,724,744,753,760,834,836,1130,1131} but some lifetime based nanosensors for fluorescence lifetime imaging (FLIM) also have been reported.^{482,801} These probes are advantageous due to

absence of artifacts associated with wavelength-dependent light scattering and also overcome the adverse effects of indicator/reference leaching or photobleaching. Intracellular pH measurement with help of 2-photon^{526,880} and upconverting probes^{956,958} should also be mentioned. It has not been demonstrated in all cases; however, that the $\text{p}K_a$ values of probes and sensors are the same during calibration with buffers and in the intracellular space.

Extracellular pH plays a very important role in biological processes making this parameter useful to study the regulation of bone cell function,¹¹³² in cancer research due to characteristically low extracellular pH of the tumor cells¹¹³³ or to study metabolic perturbations via assessment of glycolytic activity.⁵⁴⁹ The optical tools for measurement of extracellular pH values are versatile, and many materials covered in this Review can be useful. For instance, extracellular pH was accessed with help of planar optodes,⁴⁶⁷ pH sensitive quantum-dots,⁸¹⁴ nanoprobe based on pH indicator-DNA-lipid conjugates that anchor directly on the cell surface¹¹³⁴ or even with water-soluble luminescent pH indicators.⁴⁶⁷ In this kind of applications, combination of extracellular pH measurement with measurement of other parameters, such as concentration of dissolved oxygen, ATP, and total protein, is of particular interest since it allows assessment of cell metabolism.⁹⁸⁵

15.3. Sensing and Imaging of pH Values in Plant Research

Many response systems in plants are linked to complex dynamics in signaling parameters, such as Ca^{2+} , reactive oxygen species, and pH.¹¹³⁵ Most researchers have studied pH in cytoplasm and cell wall of plants with help of genetically encoded fluorescent protein probes.^{1135–1139} For instance, anoxia- and salt stress-induced pH changes in root cells were studied.¹¹³⁹ Optical sensors (planar, fiber optic, or nanosized) have been used more recently. Examples include imaging of pH values in the rhizosphere, that is, an area of soil around a plant root, which is directly influenced by root secretions. Compared to electrodes, planar optodes are much less invasive and allow mapping of different parameters in rhizosphere. Among other parameters, pH is of particular importance due to ability of some

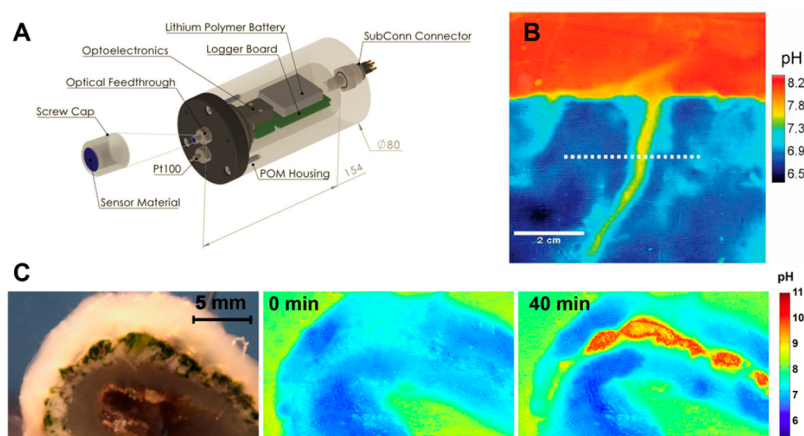


Figure 55. Examples of applications of optical pH sensors in oceanography and marine biology. (A) Stand-alone pH optode for oceanographic applications developed by Staudinger and co-workers. Reprinted from ref 537 with public license. Published by Wiley Periodicals, Inc., on behalf of Association for the Sciences of Limnology and Oceanography. (B) Imaging of pH distribution with planar optode and an RGB camera. The pseudocolor image shows the elevated values around a 2 day old burrow of the polychaete *Hediste diversicolor*. Reprinted from ref 374 with public license. Published by Frontiers. (C) Photograph of cross-section of didemnid ascidian *Lissoclinum patella* containing symbiotic cyanobacterium *Prochloron* (left) and pseudocolor images of the pH distribution in *L. patella* before and under irradiation with visible light (incident photon irradiance of $250 \mu\text{mol photons m}^{-2} \text{s}^{-1}$). Reprinted from ref 1152 with public license. Published by the Association for the Sciences of Limnology and Oceanography, Inc., 2011.

plants to acidify the rhizosphere to enhance the uptake of poorly soluble nutrients. Rao and co-workers¹¹⁴⁰ used a colorimetric system (bromocresol purple in agar gel) to visualize the pH dynamics in rhizosphere of legume roots and found light-induced acidification (Figure 54A). Blossfeld and Gansert demonstrated rhizosphere acidification by mapping pH with a commercial planar optode.¹¹⁴¹ The pH values were read-out point-by-point with help of a micromanipulator. The same sensor system was also used for pH mapping in soils contaminated with trace metals¹¹⁴² and in combination with an oxygen sensor for monitoring of rhizospheric dynamics in short-time flooded plant species.¹¹⁴³

The above drawbacks of the point-by-point read-out can be overcome by using fluorescence imaging. Several groups utilized a combination of a planar optode and a dedicated imaging unit.^{993,1144,1145} Rudolph and co-workers^{430,1146} used hydrogel-immobilized aminofluorescein in combination with a UV lamp and a CCD camera. The pH sensor relies on measurement of fluorescence intensity, which is not the best approach. In several cases, the pH measurement was combined with optical imaging of other parameters, including oxygen,¹¹⁴⁶ carbon dioxide,¹¹⁴⁴ or both oxygen and carbon dioxide.⁹⁹³ Santner and co-workers⁴²⁴ combined imaging of pH (with a ratiometric optode and a consumer RGB camera) and chemical imaging of cationic trace metals (Mn^{2+} , Cd^{2+} , Zn^{2+} , Cu^{2+} , Fe^{3+} , Ni^{2+} , Al^{3+} , Co^{2+} , and Pb^{2+}) as shown in Figure 54B. The latter was realized using diffusive gradients in thin films¹¹⁴⁷ with subsequent analysis of the bound solutes by laser ablation inductively coupled plasma mass spectrometry. A sensor consisted of a thin ($<100 \text{ nm}$) hydrogel film containing anion and cation binding materials, a fluorescent dichlorofluorescein-based pH indicator, and red-emitting reference particles. The experiments demonstrated clear increase in the concentration of several ions (such as Mn^{2+} , Figure 54B) in the rhizosphere due to proton-induced dissolution of metal oxides (Figure 54B). The method was later extended to different plant species and combined imaging of pH and cations with chemical imaging of labile phosphorus.¹¹⁴⁸

15.4. Sensing and Imaging of pH Values in Oceanography and Marine Biology

Such sensors have to be compact enough to be installed on different platforms, enable autonomous sampling and transmission of the data, and possess precision of better than 0.002 pH units¹¹⁴⁹ to enable comparison of data obtained from different locations and time periods. Currently, such precision can only be achieved with systems based on spectrophotometric read-out using dissolved indicators, such as m-cresol purple.^{1149,1150} As pointed out in the section on effects of ionic strength (section 1.6), the varying salinity of samples can heavily compromise the precision of such measurements.¹¹² One of the first studies was presented by Monici et al.⁴⁵ who reported a fiber optic pH sensor for seawater monitoring. Present day (commercial) sensors are still rather bulky (weight of several kilograms).¹¹⁵¹ Several groups have attempted to design/adapt pH optodes for oceanographic applications. Almost three decades ago, Serra et al. designed a colorimetric fiber-optic sensor for seawater measurements,³⁰⁶ which however had moderate reproducibility. Clarke et al.¹²⁰ investigated a commercial pH sensitive sensor spot in a custom-made setup including a LED for the excitation, dichroic beam splitter, and a photomultiplier. The sensor showed a precision of 0.0074 pH units, moderate salinity cross-talk (-0.01 pH/PSU in the salinity range 5–35), a drift of 0.06 pH units in 4 weeks, and good photostability. On the other hand, the limitations included strong cross-talk to temperature (-0.046 pH/K for temperature range from 5 to 25 °C) and the pK_a value of 6.93 at 20 °C, which is about 1 unit below the value optimal for oceanographic applications.

Staudinger et al.⁵³⁷ reported an optode system specially designed for oceanographic applications. It consists of a read-out module and screwable caps with the sensing materials (Figure 55A). The compact reader (length = 154 mm, weight = 970 g) includes an optoelectronic unit, logger, and battery positioned into a pressure-resistant housing and enables autonomous measurements down to 500 m depth. It can be deployed for 1 year, with data provided in intervals of 30 s. The interchangeable sensor caps enable measurements of pH, dissolved oxygen, or

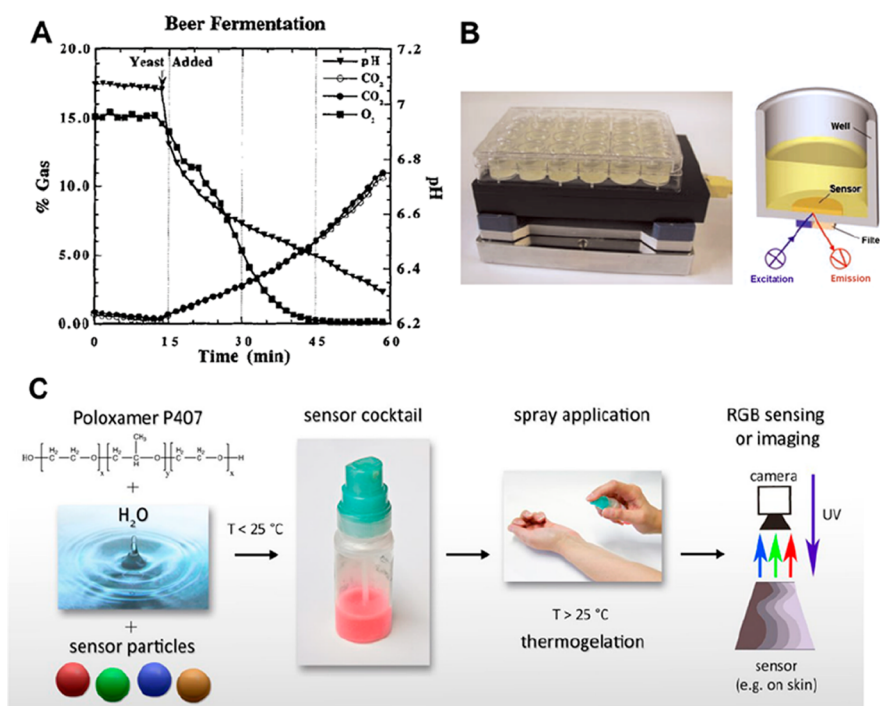


Figure 56. (A) Simultaneous monitoring of pH, carbon dioxide, and oxygen with a fiber-optic multiparameter sensor during fermentation of beer. Reprinted from ref 429 with permission from Elsevier. Copyright Elsevier B.V. 1997. (B) Photograph of a 24-channel SensorDish reader from PreSens on a shaker (left) and cross-section of a well of a microplate with the sensor in its bottom. Reprinted with permission from ref 93 Copyright Wiley Periodicals, Inc., 2008. (C) Scheme for the preparation of a sprayable sensor using a thermogelating hydrogel and its application. Reprinted from ref 127 with permission from Elsevier. Copyright Elsevier B.V. 2015.

dissolved carbon dioxide with the same reader, which is expected to significantly reduce the manufacturing and deployment costs. The pH material based on a far-red aza-BODIPY indicator in a cross-linked hydrogel features almost ideal $\text{p}K_{\text{a}}$ value of 8.05, high precision (0.0023 pH units at pH 8.02), low temperature cross-talk (-0.0114 pH/K), negligible cross-talk to salinities from 15 to 35, and high stability (no drift within 54 days at $10\text{ }^\circ\text{C}$ and a drift of 0.0021 pH units/day at $25\text{ }^\circ\text{C}$).¹²⁴ Later version of the optode system allowing measurements up to 4000 m depth is commercially available from PyroScience (www.pyroscience.com).

In contrast to the pH sensors developed for oceanography, very high precision and stability are not mandatory for short-term applications of optodes in marine biology. Several state-of-the-art systems fulfill the necessary requirements. pH optodes have been used particularly often for studies involving photosynthetic organisms since photosynthetic activity consumes carbon dioxide and thus leads to an increase of pH, while decomposition of organic matter has the opposite effect. Many pH optodes have been designed for imaging of marine sediments. Sensors using HPTS as an indicator embedded in cellulose acetate are far from optimal ($\text{p}K_{\text{a}} = 6.4$)³⁷⁵ and also suffer, not surprisingly, from high cross-talk to salinity. The response of covalently immobilized HPTS^{377,990} was better with respect to the dynamic range ($\text{p}K_{\text{a}} = 7.06$), and the sensor showed more favorable properties (good chemical stability, absence of dye leaching, acceptable cross-talk to salinity), but the "sensing chemistry" was not well described. The group of Klimant¹⁴⁶ reported on a pH optode based on a lipophilic fluorescein derivative with an almost ideal $\text{p}K_{\text{a}}$ value of 8.3. The main drawback of the sensor is the poor photostability of the fluorescein chromophore.

Larsen et al.³⁷⁴ described a ratiometric pH sensor layer for imaging with a digital camera. A light-harvesting system composed of a green-emitting coumarin dye (the energy donor) and yellow-emitting lipophilic HPTS derivative (the energy acceptor) showed response from pH 6 to 9, which makes it suitable for imaging sea sediments (Figure 55B). Specially designed software and hardware (now commercially available) makes it possible to control the illumination with photodiodes and to use virtually any consumer RGB camera for imaging. Han et al.⁹⁹¹ report on a ratiometric optode for imaging slightly alkaline sediments. It is making use of an indicator immobilized in PVC ($\text{p}K_{\text{a}}$ of 9.0 at $15\text{ }^\circ\text{C}$). Good correlation between the profiles obtained with the optode and microelectrode was observed. The drawback of the sensor is rather strong temperature cross-talk ($\sim 0.04\text{ pH units/K}$).

Similar to sediments, planar optodes have been used for pH imaging in marine photosynthetic microbial mats⁹²¹ and rhizosphere of seagrass.¹¹⁵³ In both cases, the sensor based on the indicator aza-BODIPY (section 4.1) showing optimal $\text{p}K_{\text{a}}$ value of 8.0 and excellent photostability was used. The NIR emission of the pH indicator allowed for simultaneous imaging of pH and oxygen distribution with the dual optode.⁹²¹ Planar optodes in combination with a commercial camera were applied for imaging of pH, oxygen, and carbon dioxide in rhizosphere of a saltmarsh plant.⁹⁹³ A pH-optode based on an imaging fiber was used for imaging the release of acids from sea urchin eggs, which was induced by fertilization.¹¹⁵⁴ The group of Kühl explored an alternative approach to imaging pH and oxygen in the rhizosphere of seagrass with help of nanoparticles dispersed in an artificial sediment.¹¹⁵⁵ The same group investigated the photobiology of a didemnid ascidian containing symbiotic cyanobacterium *Prochloron*.¹¹⁵² Upon light exposure strong increase in pH and production of oxygen in the regions

containing the cyanobacterium was observed via imaging (Figure 55C). Also the same group used a fiber-optic pH microsensors to sense pH values in the gastric cavity of corals.¹⁵¹

15.5. Sensing and Imaging of pH Values in Biotechnology

Agayn and Walt¹¹⁵⁶ published one of the earliest reports on application of pH optodes for monitoring of bacterial fermentation (*Escherichia coli*). A fiber-optic sensor based on fluorescein immobilized in pHEMA matrix showed excellent performance in the complex fermentation media and survived steam sterilization without significant alteration of the properties. Shortly later, a triple sensor was described⁷⁶ for measurement of pH, CO₂, and oxygen in bioreactors. Sample fluid was continuously passed through an external flow cell containing the sensors. This reduces the risk of contamination of the bioreactor. However, it is more common now to integrate planar optical sensors into shake flasks and bioreactors, and such products are commercially available. Despite this, other tools (glass pH electrode, ISFET) are still used in many applications. This is explained by the fact that special versions of electrodes offered by main manufactures tolerate harsh cleaning-in-place (CIP) conditions (e.g., 2% NaOH and 80 °C), a process commonly used for cleaning equipment in biotech, pharma, food, and beverage industries. Hardly any state-of-the-art pH optode can survive such conditions without drift due to degradation of the indicator or the matrix. However, most pH optodes tolerate mild sterilization methods including sterilization by steam,¹¹⁵⁶ radiation, or H₂O₂ or simply by dry heat (at 160 °C for 45 min).¹¹¹ A dual excitation ratiometric fluorescent pH sensor was used for noninvasive bioprocess monitoring.³⁸⁰ The fluorescent indicator 8-hydroxy-1,3,6-pyrene trisulfonate was immobilized onto a basic anion exchanger and entrapped into a proton-permeable hydrogel layer. The sensor responded within <9 min and fully reversibly, is sterilizable and can be used for online monitoring of the pH value of an *E. coli* culture. Continuous pH monitoring in a perfused bioreactor system using an optical fiber pH sensor was also demonstrated.¹¹⁵⁷

On the other hand, extreme chemical stability is not needed for application of optodes in microbioreactor systems. Here, optodes offer several unique advantages such as being small (allowing for integration of optodes for different parameters in a single microwell) and low-cost (making the sensors disposable). Most optodes are resistant to sterilization with γ or β radiation and some to sterilization by steam in autoclaves.¹¹¹ Several combined sensor/micro bioreactor systems are available from different manufactures (such as BioLector from m2p-laboratories, ambr 15 system from Sartorius, micro-Matrix from Applikon Biotechnology, bioREACTOR from 2mag). They utilize pH and pO₂ optodes integrated into microplates and minireactors with culture volumes varying from 0.8 to 15 mL. Instrumentation relies on sensors from PreSens (Regensburg, Germany). PreSens also offers a line of products for biotechnology including a microplate system in 24-well format (SensorDish, Figure 56B).¹¹⁵⁸ Other sensor/microbioreactor systems include incubator shaker systems for cultivation and measurement in up to 96 plastic cultivation tubes and shake flasks of larger volume equipped with pH and pO₂ sensor spots.¹¹⁵⁹ These commercial systems have been used in numerous studies, for instance for microorganism cultivation,^{1160,1161} strain screening,^{1162,1163} rapid process optimization,^{1162,1164–1166} and recombinant protein production¹¹⁶⁷ to mention only a few. The main limitation of the above systems is the measurement range from pH 5.5 to 8.0, which does not cover

all potential applications. To address this issue, Janzen et al. presented a pH sensor based on chlorinated fluorescein derivative showing dynamic range from ~4–7 and demonstrated its applicability for anaerobic production of acetone, butanol, and ethanol.¹¹⁶⁸ Unfortunately, application of the sensors in complex medium resulted in a drastic reduction of resolution and dynamic range.

pH values often are measured along with metabolic parameters, such as pO₂ and pCO₂ (Figure 56).⁴²⁹ A dual sensor was described for simultaneous monitoring of pH and oxygen during bacterial fermentation.⁹³ An agarose-coated Petri dish with immobilized pH sensitive nanoparticles was used to image bacterial growth and metabolism with help of an RGB camera.⁵⁷¹ In later work, the same group¹²⁷ used the thermogelating properties of the polymer block-co-polymer Poloxamer407 to spraycoat the Petri dish with a pH sensing layer. pH sensor microparticles were dispersed in the polymer and sprayed on the surface of the Petri dish at below 25 °C (Figure 56C). At these temperatures, the sensor “cocktail” remains fluid and yet adheres well. If temperature is risen to above 25 °C, the gels form a thin and soft but solid sensing film. The method was applied to monitor pH changes caused by the growth and metabolism of a culture of the pathogen *Staphylococcus aureus*. Rao and co-workers integrated optical pH sensors (hydrogel-immobilized 6,8-dihydroxypyrene-1,3-disulfonic acid or Dowex-immobilized HPTS) and oxygen sensors in (micro)bioreactors for mammalian cell culture,^{100,394} cultivation of *E. coli*^{380,1169,1170} and effective clone selection.¹¹⁷¹ Good agreement was found between values obtained by optodes and electrodes, respectively.¹⁰⁰

Although microbioreactors and microplates already allow for dramatic reduction of sample volume compared to shake flasks and lab-scale bioreactor systems, even further miniaturization is possible with microfluidic devices (see section 15.8 for more details). Similar to microbioreactors, optical pH sensors have been integrated into microfluidic devices and used for bioprocess monitoring.¹¹⁷²

Biocatalytic synthesis of fine chemicals often is performed in continuous manner employing enzymes immobilized on insoluble porous carrier particles. In this application, measurement of pH in solution surrounding the particles does not provide desired information about optimal conditions since pH inside the particle may vary considerably from the bulk. The approach proposed by Nidetzky and co-workers addresses this issue by monitoring of local pH with help of enzyme-modified beads (Sepabeads EC-EP) that are stained with a fluorescent pH indicator (or Yellow Fluorescent Protein) and phosphorescent reference material.^{147,1173,1174}

15.6. pH Sensors as Transducers in Biosensors

Many enzymatic reactions involve the formation or consumption of protons and, therefore, can be indirectly monitored with the help of pH sensors. Respective biosensors are composed of a pH sensing layer (typically in the form of a planar optode or a fiber-optic microsensors) and a second layer containing immobilized enzyme. Even better, both components are contained in a single layer, for instance in the form of micro- or nanoparticles. Typical enzymes include glucose oxidase, penicillinase, urease, acetylcholine esterase and organophosphorus hydrolase. It has to be stated here that enzymatic biosensors with pH transduction suffer from two limitations. The first is the varying buffer capacity of an unknown sample,

and the second is the unknown initial pH value of an untreated unknown sample.

Glucose biosensors utilizing optical pH sensors explore classical indicator chemistry,⁹² utilize pH-dependent absorption changes of polyaniline (section 7.2 on conjugated polymers),¹¹⁷⁵ or the swelling of amino-modified hydrogel as induced by pH changes.⁵⁷ Biosensors for penicillin^{38,1176–1181} utilize hydrolysis of the antibiotic catalyzed by penicillinase (β -lactamase). This results in the formation of penicilloic acid and therefore a drop of the pH value. Alternatively, penicillin-G-amidase may be used.¹¹⁸² Ammonia and carbon dioxide are formed upon enzymatic hydrolysis of urea in the presence of urease. This was utilized in numerous biosensors for urea based on optical pH transduction.^{38,177,308,1183–1195} Such biosensors can, in principle, also be used for analysis of metal ions due to their inhibitory action on the activity of urease.¹¹⁹² Ammonia and CO₂ also are formed on hydrolysis of creatinine in the presence of creatinine deiminase which was used for detection of this analyte with help of an optical pH transducer.¹¹⁸⁴ The pH change associated with the production of phosphoric acid upon hydrolysis of *p*-nitrophenyl phosphate catalyzed by alkaline phosphatase was utilized by Koh and Pischko in an enzyme activity assay.¹¹⁹⁵ A biosensor for the herbicide atrazine based on optical pH transduction utilizes the enzyme glutathione S-transferase, which catalyzes the reaction of atrazine with glutathione and results in the release of protons.¹¹⁹⁶

Hydrolysis of acetylcholine, catalyzed by acetylcholinesterase (AChE) and resulting in formation of choline and acetic acid, can be utilized to detect acetylcholine with help of an optical pH transducer.^{1183,1192,1197,1198} All these methods work irreversibly and can be hardly applied to online sensing. The same detection scheme was used in assays for organophosphorus compounds (pesticides and warfare agents), which inhibit the action of AChE.^{268,1188,1199,1200} The selectivity of these methods is poor since action of AChE is inhibited by a wide variety of other toxic compounds and heavy metal ions. Methods based on organophosphorus hydrolase offer much better specificity than those utilizing AChE. The enzyme catalyzes hydrolysis of various organophosphate esters, including pesticides and chemical warfare agents, resulting in a pH change. Several sensors utilizing this enzyme in combination with an optical pH transducer have been reported.^{1201,1202} A biosensor for antiglaucoma drug acetazolamide based on inhibition of bicarbonate dehydration catalyzed by carbonic anhydrase was also described.¹²⁰³ Enzyme-based test stripes for rapid visual or photographic detection of gaseous sulfur mustard by using a hydrolase immobilized on a commercial pH test strip were reported.¹²⁰⁴

15.7. pH Sensors as Transducers in Chemical Sensors

Optical sensors for pH values also were used to quantify acidic or basic chemical species including carbon dioxide, sulfur dioxide, ammonia, and amines. In all these approaches, an existing pH sensor is covered with (or incorporated into) a gas-permeable but proton-impermeable matrix, such as silicone. Typically, the pH sensor consists of a microbead soaked with a solution of a pH indicator probe (such as phenol red or bromothymol blue) in a weak buffer. The pK_a value of the buffer has to be adjusted to the pK_a value of analyte gas (whether acidic or basic), and the capacity of the buffer governs the analytical range. Strong buffers yield wider analytical ranges, but detection limits are higher. The approach has the advantage in enabling both gaseous and dissolved gases to be determined. Sensors based on this

analytical scheme have been reported for carbon dioxide, HCl gas, sulfur dioxide, and ammonia, to give a few examples only. Table S21 summarizes representative examples of pH sensors used as transducers in such sensors.

Optical sensing schemes for pH values may also be used to sense anions or cations via the so-called coextraction or ion-exchange mechanisms, respectively. In this case, lipophilic pH indicators are preferably used. In simplified terms, the coextraction method relies on the extraction of an anion by an anion carrier, such as dodecyltributylammonium ion into a plasticized polymer membrane, which is accompanied by the coextraction of a proton for electroneutrality reasons. The coextracted proton will protonate a lipophilic pH indicator dye also contained in the sensor matrix, and this will cause a detectable color change. The ion-exchange mechanisms relies on the extraction of a cation by a carrier such as a crown ether or valinomycin into a plasticized membrane. To maintain electroneutrality, a proton is released from a lipophilic pH indicator dye also contained in the sensor matrix, and this will also cause a color change. Table S21 also summarizes representative examples of pH sensors used as transducers in optical sensors for cations. Both the coextraction and ion-exchange mechanisms make use of highly lipophilic indicators to warrant solubility in plasticized PVC or ethyl cellulose. Chemical formulas are given in Figure 57. Such lipophilic pH indicators can be used, in

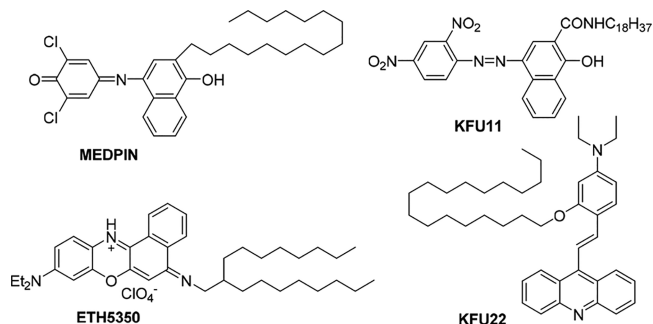


Figure 57. Chemical formula of representative lipophilic pH indicators for use in sensors for pH values and ions.

principle, in optical sensor strips for pH values but were mainly used in sensors for ions, such as K⁺, in serum. MEDPIN [7-(*n*-dodecyl)-2-methyl-4-(3,5-dichlorophen-4-one)-indonaphth-1-ol] was long used in a test commercialized by Ames-Miles.¹²⁰⁵ Its color reversibly changes from orange to pink to blue. The color of the Nile Blue derived probes ETH 5350 or ETH 5418 changes from red to purple to blue,^{86,87,1206} that of KFU 11 from yellow to green to blue,¹²⁰⁷ and that of KFU 22 from blue-green (684 nm) to yellow (420 nm).⁶⁰

15.8. Integration of pH Sensors into Flow-Injection Analyzers, Microfluidic Devices, and Lab-on-a-Chip Systems

Flow-injection analysis (FIA) is a popular and mature tool for high-throughput chemical and biochemical analysis. Various commercial systems are available and can be adapted to numerous kinds of analytical challenges. Numerous (bio)-analytical methods are available. Notably, FIA also is a perfect tool to calibrate optical sensors and to establish the response functions of newly designed sensors. Early uses of pH sensors as detectors in FIA have been reviewed.¹²⁰⁸ A small-volume fiber-optic pH sensor based on evanescent wave excitation and fluorometric detection was adapted such that it can be placed in

a FIA analyzer.¹²⁰⁹ The sensor was fabricated by inserting a deacid fiber into a transparent capillary tube. The microchannel between the optical fiber and the capillary inner wall acts as the flow cell. Flow injection was also used to sense urea via its enzymatic decomposition to ammonium and carbonate and to determine the activity of the enzyme urease.¹²¹⁰

The first microfluidic system of that kind was a product that is on the market ever since 1985. It enables measurement of the pH value and of several other parameters of whole blood (not serum!) via optical sensors placed, one by one, along a microfluidic channel (Figure S2). Blood is injected at one end. On its way to the reservoir at the end contacts the sensors spots as shown. It consists of a microfluidic system comprising an entrance port, flow channels with integrated sensor spots, and a reservoir for excess blood. The channels in the kit come filled with a fluid that is used for 1-point calibration of the sensors spots prior to filling them with a blood sample.

Seemingly simply, the integration of the sensors in a microfluidic chip can be a challenging task since chip materials vary from very hydrophobic (cross-linked polydimethylsiloxane, poly(methyl methacrylate), cyclic polyolefins, such as Zeonor or Topas), to very hydrophilic (glass). In case of pH sensors, good adhesion of the sensing layer on the support is mandatory. This is often accomplished via surface pretreatment or covalent linkage to the surface. The choice of sensing materials and the deposition method is also determined by the technique used to seal and bond the chip. Heat, organic solvents, or UV light as required during the bonding step¹²¹¹ may adversely affect the sensor properties or even lead to malfunction.

Microfluidic channels were functionalized with mesoporous silica films and subsequently surface-modified with covalently linked fluorescein (Figure S8A).¹²¹² Also, polyaniline nanofibers were incorporated into microchannels of a flexible PDMS chip for colorimetric visualization of pH gradients (Figure S8B),¹²¹³ and oxygen and pH sensor arrays for lab-on-a-chip devices were produced by a microfabrication technique.¹²¹⁴ Commercially available microfluidic devices made out of glass can be equipped with pH sensor spots by maskless photopolymerization of suitable prepolymers inside the devices. The method does not require any microfabrication methods and only requires a microscope and a UV-LED.¹¹⁹⁸

Microfluidic devices and lab-on-a-chip systems allow for even further miniaturization of microbioreactors.⁹⁴⁵ Optical pH sensors integrated into microfluidic devices have also been used for fast pesticide detection¹²¹⁵ and for rapid screening of antibiotics.¹²¹⁶ These systems rely on inhibition of metabolism of algae and *E. coli*, respectively. Microarrays for simultaneous measurement of pH values and solvent polarity¹²¹⁷ and simultaneous sensing of pH and glucose have also been reported.¹²¹⁸ Alternatively, microfluidic channels may be modified with pH-sensitive microparticles^{1219–1221} for example in predrilled holes.¹²²¹ Nanoparticles were also dispersed in the flowing sample.^{511,703} In this approach, laborious integration of sensor spots inside the chip is not required so that the commercially available microfluidic chips and particles can be used.

Optical pH sensors integrated into microfluidic chips and flow-injection analysis have also been used for monitoring enzymatic reactions. These sensors are essentially biosensors with optical pH transduction (see section 15.6). The indicator SNAFL-1 was conjugated to alkaline phosphatase (ALP) in PEG-diacrylate-based hydrogel microstructures (Figure S8C).¹¹⁹⁵ ALP hydrolyzes *p*-nitrophenyl phosphate to produce

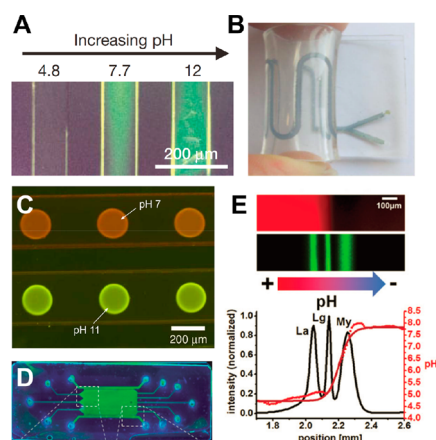


Figure 58. Examples of optical pH sensors integrated into microfluidic devices. (A) pH response of sol-gel immobilized fluorescein in microfluidic channels of a patterned fluidic system. Reprinted by permission from Springer Nature from ref 1212. Copyright Springer Nature 2000. (B) Absorptiometric sensing with polyaniline nanofibers integrated into microfluidic channels of a flexible chip. Adapted with permission of The Royal Society of Chemistry from ref 1213. Copyright The Royal Society of Chemistry 2013. Permission conveyed through Copyright Clearance Center, Inc. (C) Fluorescence images of ratiometric pH sensor spots exposed to different pH. Adapted from ref 1195 with permission from Elsevier. Copyright Elsevier B.V. 2004. (D) Fluorescence image of a chip for isoelectric focusing with integrated pH layer. Adapted with permission of The Royal Society of Chemistry from ref 988. Copyright The Royal Society of Chemistry 2013. Permission conveyed through Copyright Clearance Center, Inc. (E) Simultaneous pH gradient observation and separation of fluorescently labeled proteins lactalbumin (La), lactoglobulin (Lg), and myoglobin (My). Adapted from ref 588 with public license. Published by The Royal Society of Chemistry.

phosphoric acid, which lowers the pH value. The authors also realized a microfluidic biosensor for urea by substituting alkaline phosphatase with urease. In this case, the pH value is increased because of the formation of ammonia. In a different approach, the microfluidic chip was modified only with pH sensors; the enzyme and the substrate were supplied separately.¹²²² The authors monitored synthesis of *L*-erythrulose from hydroxypyruvate and glycolaldehyde catalyzed by transketolase and decomposition of penicillin G into 6-amino penicillanic acid and phenyl acetic acid catalyzed by penicillin G acylase, which are associated with pH changes.

Nagl and co-workers integrated fluorescent pH sensors into microfluidic chips for application in isoelectric focusing (Figure S8D, E).^{148,588,592,988,1223,1224} In this high-resolution variant of electrophoresis, different molecules (typically proteins) are separated due to differences in their isoelectric point (i.e., the pH value at which the molecule has no net charge). The pH gradient created in the gel, together with an applied electrical field, causes migration of the molecules to the position where the isoelectric point is reached. Optical pH sensors were used for direct visualization of the pH gradient. The authors prepared sensor arrays via multistep liquid photolithography on the basis of cross-linked oligo(ethylene glycol diacrylate) hydrogels utilizing fluorescein^{148,592,988} and HPTS⁵⁹² as indicators. They were covalently coupled to pHEMA to avoid leaching.⁵⁹² In further work, the pH sensitive layer was prepared using a photopolymerizable far red perylene bisimide indicator¹²³ incorporated into cross-linked poly(acryloylmorpholine) hydrogel.^{588,1224} pH sensing in the far red spectral range enabled

on-chip labeling of proteins and peptides with fluorescent dyes emitting in visible part of the spectrum and, therefore, visualization of the labeled biomolecules without spectral interference with the pH sensor.⁵⁸⁸ Various kinds of micro-channel based systems (referred to as SensorPlugs) for parameters, such as pH value, oxygen, and carbon dioxide, and an imager (referred to as VisiSens), are commercially available (PreSens) for sensing or imaging, such culture parameters inside microfluidic chips.

15.9. pH Sensors in Food Packaging

The research on intelligent food packaging has seen considerable growth in the last years.¹²²⁵ In intelligent packaging the main function to maintain the quality of the product for extended period of time is complemented by its ability to indicate the changes in the quality. This is often done with help of integrated indicators and sensors because deterioration of food is accompanied by characteristic changes in chemical parameters. Food spoilage can be indicated by change in the gas composition of the headspace (oxygen, carbon dioxide, ammonia). pH represents another important parameter since spoilage of meat and fish is known to result in the increase of the pH value.¹²²⁵ For instance, spoilage of pork and beef meat is accompanied by increase of pH from about 5.1–6.1 to 7.2–7.4.^{1225,1226} Optical sensors are particularly interesting for application in intelligent food packaging due to their ability to operate nondestructively and allow straightforward visualization of changes in the product quality through transparent packaging. Evidently, safety is of utmost importance: the sensors should either not be in contact with food (that is of course not feasible for sensing of pH value) or be nontoxic if contamination with the components of the sensing material may occur. In case of pH sensors for food packaging applications, two main types of materials can be distinguished. The first and largest group of materials relies on absorptiometric indicators and immobilization matrices of natural origin. Typically, these materials are harmless and even edible. Examples of indicators include extracts from blueberries,^{1227,1228} mulberries,¹²²⁹ grape skin,^{341,1230} red cabbage,¹²³¹ black carrot,¹²³² sweet potato,^{1233,1234} nutmeg,¹²³⁵ jamun,¹²³⁵ *Lycium ruthenicum*,¹²³⁶ and curcumin¹²³⁷ that originate from food but also plants (litmus,¹²³⁸ alizarin¹²³⁹) or even microalgae.¹²⁴⁰ These were embedded into gelatin,¹²³⁷ chitosan,^{341,1227,1229,1233} starch^{1228,1234} from different sources, bacterial cellulose,¹²³² starch-cellulose composites,¹²³⁹ tamarind seed polysaccharide,¹²³⁸ tara gum,¹²³⁰ poly(lactic acid)-poly(ethylene oxide) blends,¹²⁴⁰ and κ -carrageenan.¹²³⁶ One can summarize that (i) these materials are mostly intended for visual indication of food freshness and not for precise pH measurements. Moreover, only some of the immobilized dyes show distinct color response, such as, for example, transition from a red-colored form in the acidic conditions to a green-colored form in the basic;¹²³⁴ (ii) the choice of indicators often is determined by their local availability. The utilized indicators mostly belong to anthocyanine dyes. These, however, may strongly vary in the absorptiometric response, chemical stability and photostability. For instance, anthocyanins extracted from red cabbage were found to be more stable and photostable than anthocyanins extracted from black beans; (iii) all the indicators are essentially water-soluble and may leach out of the sensor foil.¹²³¹ Unfortunately, evaluation of the stability of the sensors in respect to leaching, storage in darkness, and upon exposure to light was not performed in most cases.

Less numerous group of materials represents synthetic dyes covalently embedded into natural matrices using established dye chemistry. These include, for instance, aza-dyes covalently attached to regenerated cellulose¹²⁴¹ or aza-anthraquinone hybrid dyes coupled to a paper support¹²⁴² and of course other dyes, such as vinylsulfonyl reactive aza-dyes,¹⁷ can be used as well. Common for these materials is very distinct color response and suitability for ratiometric two wavelength read-out, absence of dye leaching and high chemical and photochemical stability of the immobilized indicators. A fluorescent sensor based on SNARF-1 pH indicator should also be mentioned.⁴³⁷ The sensor showed high accuracy of 0.12 pH units and reliably detected fish spoilage via the pH increase; however, the indicator was not covalently embedded into the matrix material.

Application of optical pH sensors in food packaging is not limited to direct measurement of pH value. pH sensors are utilized as transducers in other sensors (see section 15.7 for more details), and these, in turn, can be applied to monitor food freshness. Sensors detecting ammonia and volatile amines^{1226,1243} that evolve during fish and meat spoilage, as well as carbon dioxide sensors,¹²⁴⁴ can be particularly useful.

15.10. Corrosion Studies and Monitoring of pH Values in Concrete

Corrosion is accompanied by local changes of pH values. Walt and co-workers⁴²¹ demonstrated suitability of an optical pH sensor for monitoring different types of corrosion. They used a fiber-optic array containing a pH sensing material on the distal end of the fiber, which is capable of simultaneous sample visualization and pH imaging.

The pH of concrete is usually between 12.5 and 13 and the most severe concrete damages are associated with dropping of the alkalinity level due several reasons including chloride ingress, carbonation or acid attack.¹²⁴⁵ Decrease of pH is associated with corrosion of steel reinforcing elements, which are originally protected by a passivating oxide layer. Since these elements are passivated only at pH values above 9,¹²⁴⁶ reliable monitoring of pH in concrete in pH range from pH 9 to 13 is important. Fiber-optic sensors provide unique advantages in being compact and cheap, but the need for the long-term stability of the sensor material is challenging. Several absorptiometric sensors based on immobilized azo-dyes,¹²⁴⁷ triphenylmethane dyes¹²⁴⁸ and other indicators¹²⁴⁶ have been investigated. Dantan and co-workers¹²⁴⁶ concluded that among many investigated indicators available for the basic pH range only a few possess the required stability. A functional pH sensor has been configured by using a commercial fiber optic reflectometer and a “sensing chemistry” composed of thymol blue immobilized on Amberlite microbeads and optically isolated with a white layer of TiO₂ particles incorporated into a polymer film. The sensor showed good response in the pH 9–12 range and worked for one year as demonstrated for a concrete anchor in a harbor. A fluorescent fiber-optic sensor for pH monitoring in concrete was described.¹⁰⁰² It is based on a fluorescent coumarin indicator covalently embedded into cross-linked polymeric beads. The sensor showed a pK_a value of 11.9 and long-term stability, but no measurement in concrete was demonstrated.

In contrast to the fiber-optic sensors suitable for point measurements only, planar optodes allow for 2D mapping of pH distribution on surfaces and, therefore, can provide deeper insights in degradation of such heterogeneous material as concrete. Liu et al.³³³ demonstrated pH mapping on concrete surfaces with the help of a platinum porpholactone indicator

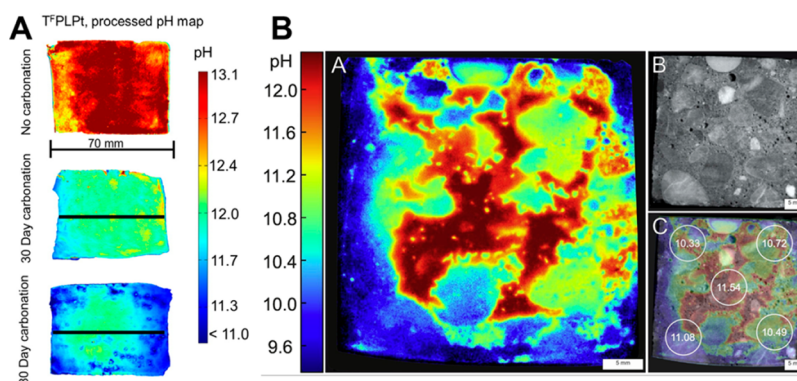


Figure 59. Examples of pH imaging in concrete samples. (A) Pseudocolor images of pH distribution in cement paste specimens at various degrees of carbonation Adapted from ref 333 with permission from Elsevier. Copyright Elsevier, Ltd., 2017. The sensing composition containing a highly viscous solution of an absorptiometric indicator in a mixture of polymers and surfactants was spread over the concrete surface. (B) pH imaging with a planar optode in concrete specimen previously exposed to accelerated carbonation. (B-A) pH image of the sample recorded with t-DLR imaging technique. (B-B) Photographic image of the concrete surface used for pH imaging. (B-C) Combined image of B-A and B-B including reference pH measurements using a flat surface electrode. Reprinted from ref 997 with permission from Elsevier. Copyright Elsevier Ltd. 2018.

(section 12.1) embedded into poly(vinyl alcohol) along with a surfactant. The sensor with a ratiometric absorptiometric response was read out with a digital camera (Figure 59A). A dually lifetime referenced pH optode (section 2.2.7) uses a hydrogel-immobilized fluorescent aza-BODIPY pH indicator (section 12.1) in combination with a phosphorescent reference dye.⁹⁹⁷ High-resolution pH imaging on concrete surfaces revealed strong microscale pH variations within the core regions attributed to the heterogenic mineralogy of the concrete specimens (Figure 59B). In later work, the same group extended the dynamic range of the sensor to 6 units (pH 6.5–12.6) by using a mixture of two pH indicators with different pK_a values.¹²⁴⁹ Also an aza-BODIPY pH indicator was used in a ratiometric approach using a single-lens reflex camera instead of a gated CCD camera.¹²⁵⁰ The system was used to characterize the pH of porewater within cracks of self-healing concrete materials. It enabled imaging of pH with a high resolution (50 μm per pixel) and a gradient of 1.4 pH units per 1 mm.

16. CHALLENGES

Notwithstanding the success of the various optical methods for sensing pH values, substantial challenges remain to be solved. These can be classified into two groups, namely, challenges of general nature and challenges of specific nature.

16.1. Challenges of General Nature

The main challenge of all sensors, be they based on the use of indicators or of swellable polymers, is the inherent sensitivity of pH optical sensors to ionic strength (IS). If good accuracy is required, compensation of the effect of ionic strength is indispensable. In case of sensors for blood pH values (which is the largest application in clinical chemistry), an accuracy of ± 0.01 pH units is required. Since blood electrolyte concentrations vary a lot and are mainly governed by the concentration of sodium ion, the effect of IS can be adequately compensated for by measurement of the concentration of Na^+ (which is wishful anyway) and by correcting pH values for its effect by using proper algorithms. This is a generally applicable method (that may also work for estuary waters) but requires a second if not third sensor. If larger inaccuracies are acceptable, the use of sensors with low sensitivity to IS (as described in previous sections) is recommended. For some reasons, pH sensors based on the use of reversibly protonable/deprotonable (often

referred to as swellable) polymers are more sensitive to IS than most indicator based sensors.

Temperature is the second important parameter that affects accuracy. Any sensor for pH values also is a sensor for temperature. If possible, the sample should be thermostated to ± 1 °C. If not, one has to be aware of the fact that wrong data may be obtained, or temporal drifts may be encountered even at constant pH values.

In case of small sample volumes, one may face the so-called indicator error. In simplified wording, this term refers to the fact that the indicator itself is a (weak) buffer. The same is true for any (de)protonable (and thus swellable) polymer or conductive polymers. The local charge density of both indicator-based sensor layers or—even more so—of (de)protonable polymers can be high, and if small volumes of unbuffered samples are used, the indicator error results in a biased pH measurement. The effect also can be critical (a) in case of unstirred and viscous samples where diffusion of protons and pH equilibration are slow and (b) in intracellular measurements where sample volumes are quite small. One should be aware of the fact that at pH 7.0 a cell with a typical diameter of 1 μm contains around 30 protons only. By ignoring intracellular buffer capacity, one may state that a substantial fraction of protons will be bound by adding a nanosensor containing only a few transducer molecules.

Indicator-based sensors suffer from leaching unless the indicator is firmly retained. However, excellent methods are known to prevent this. Hence, it is not a major challenge any longer. However, all indicator based sensors (unlike swellable polymer based sensors) also suffer from some bleaching, and this can be problematic if sensors are supposed to work over long time or are optically interrogated in short intervals. Bleaching can only be retarded but not suppressed. Organic dyes are more prone to bleaching than inorganic fluorophores like, for example, many quantum dots. Stabilizers, such as diazabicyclooctane (DABCO) or carotene, that are capable of decomposing singlet oxygen formed by the action of some indicators are useful (see section 9.5). Indicators like fluorescein are hardly useful in sensors because they photobleach rather quickly.

On the other hand, optical sensors based on the use of swellable polymers suffer from other disadvantages. Such polymers usually contain numerous protonable sites, and this makes them particularly sensitive to changes in ionic strength

(IS) for two reasons: First, the pK_a value of the system changes with IS, depending on whether charges change from cationic to neutral (for example ammonium groups in polyethyleneimine), or from neutral to anionic (such as in polyacrylic acid). Hence, titration plots strongly shift with IS. Secondly, the extent of swelling also depends on IS. In case of sensors based on measurement of refractive index (SPR included), this is a disastrous interference. Unfortunately, most studies on such sensors ignore such potential effects. The same is true for the effect of organic solvents on refractive index (RI), less so on pK_a values. For example, ethanol — even if present in fractions of only 0.1% — affects the RI such that it fakes a change in local pH value even if it remains constant. These are major reasons why practically all optical sensors based on the use of swellable polymers are not suited for general purpose pH sensing but limited to highly specific situations. Sensors based on the use of optical indicator probes are much less interfered by sample IS or RI.

Sterilization is an issue that relates to all pH sensors for use in vivo and in biotechnology. No perfect method is known for sterilization but heat treatment (autoclaving) is most common. However, many sensors undergo a change in their calibration plot if exposed to steam of temperatures near 130 °C, which is typical for heat sterilization. Sterilization with ethylene oxide (EO) is not recommended because EO is carcinogenic and also can react with hydroxy groups of indicators. The stability of many published pH indicators to sterilization with β - or γ -radiation is unknown.

If intended for later use, sensors usually are stored in buffers containing azide or thimerosal. This also prevents biofouling. In case of biotechnology, the option for contactless sensing turns out to be a unique feature of optical sensors. The sensor membrane can be placed on the inner wall of the window of a reactor and then interrogated through the window. Sterilization, calibration (with sterile buffers) and optical readout then be performed without the need for displacement of the sensors. The same is true for T-shaped sensors in flow-through cells as shown in Figure 2. A commercially available pH sensor membrane is available that is claimed to be sterilizable without the need for subsequent recalibration and yet retaining high precision and accuracy. However, most sensors described in the literature have not been studied in this respect even if intended for use in medicine or bioprocess monitoring.

16.2. Challenges of Specific Nature

Optical sensors for use in blood and serum work well because samples are well buffered and the effect of ionic strength can be compensated for as described above. Rather, sensors for blood pH values suffer from blood clotting, coating with protein and fouling, the latter two in case of online use. Clotting can be widely eliminated by modifying the surface of sensors with heparin. Proteinous coatings can only be removed by treatment with protease but this implies the need for recalibration and resterilization of sensors. Fouling kills sensors.

Optical sensors for intracellular pH values face numerous limitations that are hardly discussed in depth in recent reviews. It may be stated first that most early measurements of intracellular pH values are biased. This has several reasons: (a) Many studies presented so far report average pH value of cells or tissue, ignoring the fact that pH values inside cells vary from site to site. (b) Most earlier studies using optical molecular probes were performed by calibrating the indicator probe in buffers, and pH values were then calculated from data obtained with cells. These

contain proteins and other biomolecules that bind indicator probes and thereby change their pK_a values. This introduces a systematic error. It may be reminded here that the level of albumin in urine is determined by adding, to a buffered urine sample, a pH probe whose color changes because it is bound by albumin. Many of these interferences can be compensated by performing an in situ calibration, which, however, is not always feasible. Nanoparticle-based sensing can overcome such deficiencies. However, many challenges have yet to be addressed to demonstrate superiority of nanoparticles for these applications. The first challenge is to make the NPs membrane-permeable. Another challenge results from the need to place sensors at specific sites such as in the cytosol or near mitochondria. If both are to be measured at the same time, differently modified probes have to be used whose signals can be optically differentiated. The same is true if extracellular acidification is to be determined. In the worst case, sensor NPs are placed in both the intracellular and extracellular space (that is, in the interstitial fluid), and then, an average pH value is recorded.

Site-specific sensing in cells is highly desirable but requires site-specific positioning of sensor NPs. If this is accomplished, it is mandatory that ratiometric methods are used because the plain intensity of fluorescence (at a fixed combination of one excitation and one emission wavelength or of bands) not only depends on the local pH value but also on the local concentration of the sensor probe. Some researchers appear not to be aware of this. Various kind of ratiometric methods have been discussed in previous sections, and any of them may be used. High (nm) resolution imaging (nanoscopy) based on methods, such as STED, PALM, or STORM (that work in the fluorometric mode only), also require special fluorescent probes to work best. No systematic study has been presented so far in terms of their uses in sensor NPs. Finally, to become reliable analytical tools, the reported and new nanoparticle-based sensors have yet to be thoroughly characterized in respect to their selectivity, toxicity, and batch-to-batch reproducibility (evidently more critical compared to molecular probes) that so far was not the case in most studies.

Sensing of pH values in the marine environment and in surface waters faces other challenges. Such sensors usually are operated over prolonged periods of time, and (bio)fouling has become a major challenge that still has to be fully overcome. In addition, most plain water samples are weakly buffered if at all. The effects of varying temperature, ionic strength, and heavy metal ions and of contaminants, such as detergents, oil, or lubricants, can be detrimental. No adequate solution has been found so far (which is also true for pH electrodes). Literature does not offer solutions on how to overcome the problem of biofouling in case of continuously operating pH optodes, but methods based on the use of antifouling agents as used for vessels may be an option. Unfortunately, the most efficient of them (out of the tributyltin group) are very toxic for marine organisms and have been banned by law. Other methods (sterilization with UV light or electrochemically generated chlorine) require extra energy and place a risk of accelerated sensor drift due to photobleaching and chemical reaction, respectively.

Sensing of the (quite high) pH values in concrete has other and partially unsolved challenges. The main issue here is long-term functionality. Such sensors are expected to have life spans exceeding 30 years, which is difficult to test and to achieve. Such sensors preferably are prepared from inorganic sensor materials

(such as pH-sensing quantum dots), which decompose quite slowly even at high pH values. Recalibration is virtually impossible. Sol–gel coatings deteriorate with time. Bacterial attack and fouling are not an issue, on the other hand, and accuracies of less than ± 0.1 pH unit are not required.

Optical fiber sensors are affected by bending effects, and this has to be taken into consideration when using certain configurations. Plastic fibers can become slightly turbid over extended periods of time, which prevents their use, at present, for many long-time applications.

17. CONCLUSIONS AND OUTLOOK

The past years have seen enormous progress in the design of methods other than electrochemical for sensing pH values. Among those, optical approaches have been most successful and have become dominant. This is the result of two attractive features of optical sensors that go far beyond the potential of electrochemical sensors. The first is imaging, and the second is the option of performing measurements on a nanoscale. The results presented in this Review show the impressive progress that has been made in these two fields. Other single features that make such “opt(r)odes” attractive in certain fields include the inertness to interferences by electromagnetic fields, the option to perform remote measurements with even μm -resolution by using fiber optical waveguides and comparably simple design and competitive price of the sensing materials making them attractive for application in disposable sensors.

Progress in pH sensor technology is driven by progress in mainly four fields, namely, (a) new materials, (b) new spectroscopies, (c) new optoelectronic and microelectronic components, and (d) in data processing. This Review covers the first two. Indirectly, progress is also driven by the need for new pH sensors in fields where classical electrodes cannot be applied easily or not at all. The number of publications on the subject is entangling. One additional aim of this Review is to identify the methods that are best suited for a specific problem. Several kinds of sensors have become commercially available. On the other hand, numerous sensing schemes that are also known from literature are interesting from a scientific viewpoint only but unlikely ever to be used in practice or to result in sensors manufactured on a large scale.

Where are we going to? The problem of sensing pH values of various kinds of surface and marine waters, and of blood or urine is solved, in essence. The limitations encountered at present are not related to sensor performance but to limitations resulting from fouling, deterioration, biocompatibility, and calibration. Many authors claiming excellent performance of any new sensors (“new” in terms of indicators and sensors materials; polymers included) ignore the state of the art of commercially available sensors, some intended for measurement of pH values in general, some for use in highly specific situations. Essential progress or fundamentally new ideas cannot be seen here.¹²

The main challenges are of a different kind. All the areas listed below are potentially large markets but unfortunately current research does not focus on these in adequate depth. There is a need for (a) sterilizable sensors, (b) self-calibrated sensors, (c) self-referenced sensors, (d) sensors for pH ranges at which electrochemical sensors do not perform well (or at all), for example at pH values of >12 or at high acidities as defined by the Hammett scale, (e) sensors that reliably work at temperatures between 50 and 150 °C, for example for sensing pH values of hot waters under high external pressure (such as in industry and in the deep sea, or in oil drilling), (f) sensors with very long

operational lifetime, for instance for monitoring the pH value of concrete at pH values above 10.5 over the whole lifetime of the construction, (g) sensors for measurement of acidity in nonaqueous systems such as in used machine oil (which turns acidic at the end of its lifetime), and (h) fast and disposable sensors for rapid testing of all numerous kinds of food and drinks (such as high-priced wines) which undergo changes in pH value when getting spoiled, to mention a few only and ignoring niche markets. In many cases, it will be desirable to integrate sensors for temperature to compensate for its often strong effects on pH values.

In terms of instrumentation, there is a need for approaches and instruments that are inexpensive. Sensors based on the indicator probes already became more affordable due to the availability of optoelectronic components at low costs, examples being LEDs, laser diodes, photodiodes, and optical filters. This is not the case for other methods such as SERS or SPR at present. Refractive index based sensors, fiber optic systems included, seemingly simple and low-cost, still are too expensive at present to enter the pH sensor market on a large scale. This, however, is not a matter of sensing chemistry but of engineering.

ASSOCIATED CONTENT

Supporting Information

The Supporting Information is available free of charge at <https://pubs.acs.org/doi/10.1021/acs.chemrev.0c00451>.

(S1) Examples of pH sensors based on dual-lifetime based referencing; (S2) Absorptiometric pH sensors, their pKa values, polymer matrices, analytical ranges, analytical wavelengths, and the method for immobilization; (S3) Spectral and sensing properties of pH sensors based on luminescent pH probes; (S4) Spectral and sensing properties of pH optodes based on luminescent metal-ligand complexes; (S5) Representative examples of polymers for indicator immobilization; (S6) Overview on pH sensing materials based on conjugated polymers; (S7) Properties of pH nanosensors prepared from various other materials; (S8) Overview on nanosensors based on the use of quantum dots; (S9) Overview on optical pH probes exploring conformational changes in polymers; (S10) Spectral properties of common ratiometric fluorescent pH indicators in aqueous media; (S11) Selected examples of lifetime-based sensors and nanosensors; (S12) Spectral and sensing properties of optical pH sensors based on Förster resonance-energy transfer; (S13) Summary of pH probes based on the use of lanthanide upconversion particles; (S14) Composition and read-out methods of optodes for simultaneous monitoring of pH values and other analytes; (S15) Overview on planar optodes for use in imaging via fluorescence intensity; (S16) Lifetime-based imaging of pH values with planar optodes; (S17) Composition and properties of optical pH sensors for measurements under highly alkaline conditions; (S18) Composition and properties of optical pH sensors for measurements under highly acidic conditions; (S19) Composition and properties of wide dynamic range pH (nano)sensors; (S20) Representative materials for use in pH-sensitive photonic crystals, spectral ranges of optical changes and linear range of their response to pH values; (S21) Overview on optical pH sensors used as transducers in sensors for acidic or basic gases and for ions. (PDF)

AUTHOR INFORMATION

Corresponding Author

Sergey M. Borisov – Institute of Analytical Chemistry and Food Chemistry, Graz University of Technology, A-8010 Graz, Austria; orcid.org/0000-0001-9318-8273; Phone: +43 (316) 873–32516; Email: sergey.borisov@tugraz.at

Authors

Andreas Steinegger – Institute of Analytical Chemistry and Food Chemistry, Graz University of Technology, A-8010 Graz, Austria
Otto S. Wolfbeis – Institute of Analytical Chemistry, Chemo- and Biosensors, University of Regensburg, D-93040 Regensburg, Germany; orcid.org/0000-0002-6124-2842

Complete contact information is available at:

<https://pubs.acs.org/10.1021/acs.chemrev.0c00451>

Author Contributions

All authors have given approval to the final version of the manuscript.

Notes

The authors declare no competing financial interest.

Biographies

Andreas Steinegger studied chemistry at the Graz University of Technology and obtained his diploma in 2016. Currently, he is a PhD student at the Institute of Analytical Chemistry and Food Chemistry, Graz University of Technology within a “DOC” fellowship of the Austrian Academy of Sciences (ÖAW). His research interests include optical chemical sensors, optical thermometry, and indicator synthesis.

Otto S. Wolfbeis was a Full Professor of Analytical and Interface Chemistry at the University of Regensburg, Germany, from 1995–2012. He has authored numerous papers and reviews on optical (fiber) chemical sensors, fluorescent probes, labels, and bioassays, on advanced polymers for use in sensing schemes, on photonic crystals and upconversion particles, and in spectroscopic methods including fluorescence (lifetime) and RGB-based digital imaging. He has (co)edited several books, and acted as the (co)organizer of several conferences related to fluorescence spectroscopy (MAF) and to chemical sensors and biosensors (Europtrode). His current h-index is 107 (June 2020). He was one of the 10 curators of *Angewandte Chemie* (VCH-Wiley, Weinheim), the Editor-in-chief of *Microchimica Acta* (Springer-Nature, Vienna), and one of the three founding editors of *Methods and Applications in Fluorescence* (Inst. Physics Publ., London).

Sergey M. Borisov received his PhD degree in chemistry from Herzen State Pedagogical University (St. Petersburg, Russia) in 2003. From 2004–2006, he was a postdoctoral fellow at the University of Regensburg in the group of Prof. O.S. Wolfbeis. He, then, joined the Institute of Analytical Chemistry and Food Chemistry at the University of Technology in Graz in 2006, where he is currently an associate professor. His research interests are in the chemistry of porphyrins and related systems, synthesis of new luminescent dyes and their application in optical sensing, and in the use of luminescent micro- and nanomaterials in bioanalytical methods.

ACKNOWLEDGMENTS

Financial support was provided by the Austrian Academy of Science (ÖAW) at the Institute of Analytical Chemistry and Food Chemistry, Graz University of Technology (DOC-Fellowship #24945 of A.S.).

LIST OF ABBREVIATIONS

2P = two photon
2λR = two-wavelength ratiometry
AA = acrylic acid
AChE = acetylcholinesterase
AIE = aggregation-induced emission
ALP = alkaline phosphatase
AMPMS = aminopropyltrimethoxysilane
APTS = aminopropyltriethoxysilane
ATR-FTIR = attenuated total reflection FTIR
AuNCs = gold nanoclusters
AuNPs = gold nanoparticles
aza-BODIPY = BF₂-chelated tetraarylazadipyrromethene
BODIPY = boron-dipyrromethene
Bs = brightness
BSA = bovine serum albumin
BTB = bromothymol blue
BTPE = 2-((E)-2-(pyridin-2-yl)vinyl)benzo[d]thiazole
CCA = colloidal crystalline array
CD = carbon dot
CHFODE = 2'-chloro-7'-hexylfluorescein
CIP = cleaning-in-place
Cr-GAB = chromium(III)-doped gadolinium aluminum borate
CTAB = cetyltrimethylammonium bromide
DABCO = 1,4-diazabicyclo-[2.2.2]octane
DAOTA = diazaoxotriangulenium
DCC = N,N'-dicyclohexylcarbodiimide
DCFODE = octadecyl ester of 2',7'-dichlorofluorescein
DCIFA = 2',7'-dichloro-5(6)-N-octadecyl-carboxamido-fluorescein
Dexter ET = Dexter energy transfer
DHFODE = 2',7'-dihexylfluorescein
DHPDS = 6,8-dihydroxypyrene-1,3-disulfonic acid
DLR = dual lifetime referencing
DNA = DNA
DPPs = diketopyrrolopyrroles
ECFP = enhanced cyan fluorescent protein
EDC = 1-ethyl-3-(3-(dimethylamino)propyl)carbodiimide
ELISA = enzyme-linked immunosorbent assay
EPR = enhanced permeability and retention effect
FA = fluoresceinamine
FBG = fiber Bragg grating
FIA = flow-injection analysis
FISH = fluorescence in situ hybridization
FITC = fluorescein isothiocyanate
FLIM = fluorescence lifetime imaging
FRET = Förster resonance energy transfer
FTIR = Fourier transform IR
GFPs = genetically encoded fluorescent proteins
GFP = green fluorescent proteins
GM = Goeppert Mayer
GODs = graphite oxide dots
GPTMS = 3-glycidoxypropyltrimethoxysilane
HEMA = 2-hydroxyethyl methacrylate
HMS = hollow mesoporous nanoparticles
HPTS = 8-hydroxypyrene-1,3,6-trisulfonic acid
HSV = hue, saturation, value
IFE = inner filter effect
IFS = interferometric sensing
IOHs = inverse opal photonic crystal hydrogels
IR = infrared

IS = ionic strength
 ITO = indium tin oxide
 LB = Langmuir–Blodgett
 LbL = layer-by-layer
 LED = light emitting diode
 LMR = lossy-mode resonance
 LSPR = localized surface plasmon resonance
 MCFODE = 2'-monochlorofluorescein
 MLC = metal–ligand complex
 MOF = metal–organic framework
 MRI = magnetic resonance imaging
 MSN = mesoporous silica nanoparticles
 MTEOS = methyltriethoxysilane
 MTMOS = methyltrimethoxysilane
 NFC = near field communication
 NHS = *N*-hydroxysuccinimide
 NIR = near-infrared
 NP = nanoparticle
 NR = neutral red
 ormosil = organically modified silica
 PAA = poly(acrylic acid)
 PAEMA = poly(aminoethyl methacrylate)
 PAH = polyallylamine
 PALM = photoactivated localization microscopy
 PAM = poly(acrylamide)
 PAMAM = polyamidoamine
 PAMP = polyacryloylmorpholine
 PAN = polyacrylonitrile
 PANI = polyaniline
 PANI@AuNPs = polyaniline and gold nanoparticles
 PB = Prussian Blue
 PCB = polycarboxybetaine
 PD = photodiode
 PDI = perylene diimide
 PDMS = polydimethylsiloxane
 PEBBLEs = probes encapsulated by biologically localized embedding
 PET effect, group, receptor, quenching, etc. = photoinduced electron transfer
 PET foil, support, etc. = poly(ethylene terephthalate)
 PFIpy = alternating oligomer 9,9-dihexylfluorene and pyridine
 PFPDA = copolymer of fluorene and thiophene
 PhC-Fs = photonic crystal fibers
 PhCs = photonic crystals
 pHe = extracellular pH values
 pHEMA = poly(2-hydroxyethyl methacrylate)
 pHi = intracellular pH values
 Ph-TEOS = phenyltriethoxysilane
 Ph-TMOS = phenyltrimethoxysilane
 PIPT = photoinduced proton transfer
 PMMA = poly(methyl methacrylate)
 PPE = poly(2,5-di(3',7'-dimethyloctyl)phenylene-1,4-ethynylene)
 PPE = polyphenylene-based polymer
 PPMI = poly(*N*-phenylmaleimides)
 PPyPE = poly(*p*-pyridinium phenylene ethynylene)
 PrTEOS = propyltriethoxysilane
 PSU = practical salinity units
 PtTFPP = Pt(II) meso-tetrapentafluorophenylporphyrin
 PtTFPPL = Pt(II) meso-tetrapentafluorophenylporphyrinlactone

PtTPTBPF = platinum(II) meso-tetra(4-fluorophenyl) tetrabenzoporphyrin
 PVA = poly(vinyl alcohol)
 PVC = poly(vinyl chloride)
 PVP = poly(2-vinylpyridine)
 PWM = pulse width modulation
 QD = quantum dot
 RFID = radio frequency identification
 RGB = red, green, blue
 RI = refractive index
 RLD = rapid lifetime determination
 SERS = surface-enhanced Raman scattering
 SET = surface energy transfer
 SNAFL = seminaphthofluorescein
 SNARF = seminaphthorhodafluor
 SPR = surface plasmon resonance
 STED = stimulated emission depletion microscopy
 STORM = stochastic optical reconstruction microscopy
T = temperature
 TCSPC = time-correlated single photon counting
 TEOS = tetraethoxysilane
 TGHs = thermogelating hydrogels
 TMOS = tetramethoxysilane
 TTA = 2-thenoyltrifluoroacetone
 TTAU = triplet–triplet annihilation based upconversion
 TXH = Texas Red hydrazide
 UCNP = upconverting nanoparticle
 UPMs = unimolecular polymeric micelles
 UV = ultraviolet
 YFP = yellow fluorescent protein

REFERENCES

- (1) Prichard, F. E.; Lawn, R.; Royal Society of Chemistry (Great Britain) *Measurement of pH: A Practical Handbook*; Royal Society of Chemistry: London, 2003.
- (2) Wolfbeis, O. S. *Fiber Optic Chemical Sensors and Biosensors*, Vol. 1 and 2; Wolfbeis, O. S., Ed.; CRC Press: Boca Raton, FL, 1991.
- (3) Wencel, D.; Abel, T.; McDonagh, C. *Optical Chemical pH Sensors. Anal. Chem.* **2014**, *86*, 15–29.
- (4) Shi, W.; Li, X.; Ma, H. Fluorescent Probes and Nanoparticles for Intracellular Sensing of pH Values. *Methods Appl. Fluoresc.* **2014**, *2*, No. 042001.
- (5) Lian, Y.; Zhang, W.; Ding, L.; Zhang, X.; Zhang, Y.; Wang, X. Chapter 8: Nanomaterials for Intracellular pH Sensing and Imaging. In *Novel Nanomaterials for Biomedical, Environmental and Energy Applications*; Wang, X., Chen, X., Eds.; Elsevier, 2019; pp 241–273.
- (6) Shamsipur, M.; Barati, A.; Nematifar, Z. Fluorescent pH Nanosensors: Design Strategies and Applications. *J. Photochem. Photobiol., C* **2019**, *39*, 76–141.
- (7) Yimit, A.; Rossberg, A. G.; Amemiya, T.; Itoh, K. Thin Film Composite Optical Waveguides for Sensor Applications: A Review. *Talanta* **2005**, *65*, 1102–1109.
- (8) Wolfbeis, O. S.; Dakin, J.; Culshaw, B. *Optical Fiber Sensors*, Vol. IV.; Artech House: Boston, 1997.
- (9) Horak, E.; Vianello, R.; Murković Steinberg, I. Optical Sensing (Nano)Materials Based on Benzimidazole Derivatives. In *Chemistry and Applications of Benzimidazole and its Derivatives*; Marinescu, M., Ed.; IntechOpen, 2019.
- (10) Li, Z.; Askim, J. R.; Suslick, K. S. The Optoelectronic Nose: Colorimetric and Fluorometric Sensor Arrays. *Chem. Rev.* **2019**, *119*, 231–292.
- (11) Cammann, K.; Guibault, E.; Hall, H.; Kellner, R.; Wolfbeis, O. *Proceedings of the Cambridge Workshop on Chemical Sensors and Biosensors*, 1996.
- (12) Wolfbeis, O.; Editorial, S. Probes, Sensors, and Labels: Why Is Real Progress Slow? *Angew. Chem., Int. Ed.* **2013**, *52*, 9864–9865.

- (13) Walter, B. Dry Reagent Chemistries in Clinical Analysis. *Anal. Chem.* **1983**, *55*, 498A–514A.
- (14) Free, H. M.; Collins, G. F.; Free, A. H. Triple-Test Strip for Urinary Glucose, Protein, and pH. *Clin. Chem.* **1960**, *6*, 352–361.
- (15) Harper, G. B. Reusable Glass-Bound pH Indicators. *Anal. Chem.* **1975**, *47*, 348–351.
- (16) Mohr, G. J.; Wolfbeis, O. S. Optical Sensors for a Wide pH Range Based on Azo Dyes Immobilized on a Novel Support. *Anal. Chim. Acta* **1994**, *292*, 41–48.
- (17) Mohr, G. J.; Werner, T.; Wolfbeis, O. S.; Janoschek, R. Synthesis of Reactive Vinylsulphonyl Azo Dyes for Application in Optical pH Sensing. *Dyes Pigm.* **1994**, *24*, 223–240.
- (18) Kubelka, V. P.; Munk, F. Ein Beitrag Zur Optik Der Farbanstriche. *Zeits Techn Phys.* **1931**, *12*, 593–601. A translation of this frequently cited paper to the English (Contribution to the Optics of Paints) can be found at http://opticalbioimaging.sbu.ac.ir/wp-content/uploads/2015/10/kubelka_munk.pdf.
- (19) Kirkbright, G. F.; Narayanaswamy, R.; Welti, N. A. Fibre-Optic pH Probe Based on the Use of an Immobilised Colorimetric Indicator. *Analyst* **1984**, *109*, 1025–1028.
- (20) Edmonds, T. E.; Ross, I. D. Low-Cost Fibre Optic Chemical Sensors. *Anal. Proc.* **1985**, No. 22, 206–207.
- (21) Grattan, K. T. V.; Mouaziz, Z.; Palmer, A. W. Dual Wavelength Optical Fibre Sensor for pH Measurement. *Biosensors* **1987**, *3*, 17–25.
- (22) Bacci, M.; Baldini, F.; Scheggi, A. M. Spectrophotometric Investigations on Immobilized Acid-Base Indicators. *Anal. Chim. Acta* **1988**, *207*, 343–348.
- (23) Jones, T. P.; Porter, M. D. Optical pH Sensor Based on the Chemical Modification of a Porous Polymer Film. *Anal. Chem.* **1988**, *60*, 404–406.
- (24) Saari, L. A.; Seitz, W. R. pH Sensor Based on Immobilized Fluoresceinamine. *Anal. Chem.* **1982**, *54*, 821–823.
- (25) Offenbacher, H.; Wolfbeis, O. S.; Furlinger, E. Fluorescence Optical Sensors for Continuous Determination of Near-Neutral pH Values. *Sens. Actuators* **1986**, *9*, 73–84.
- (26) Zhujun, Z.; Seitz, W. R. A Carbon Dioxide Sensor Based on Fluorescence. *Anal. Chim. Acta* **1984**, *160*, 305–309.
- (27) Janata, J. Do Optical Sensors Really Measure pH? *Anal. Chem.* **1987**, *59*, 1351–1356.
- (28) Opitz, N.; Lübbers, D. New Fluorescence Photometric Techniques for Simultaneous and Continuous Measurements of Ionic Strength and Hydrogen Ion Activities. *Sens. Actuators* **1983**, *4*, 473–479.
- (29) Wolfbeis, O. S.; Offenbacher, H. Fluorescence Sensor for Monitoring Ionic Strength and Physiological pH Values. *Sens. Actuators* **1986**, *9*, 85–91.
- (30) Wolfbeis, O. S.; Rodriguez, N. V.; Werner, T. LED-Compatible Fluorosensor for Measurement of near-Neutral pH Values. *Microchim. Acta* **1992**, *108*, 133–141.
- (31) Lübbers, D.; Opitz, N.; Speiser, P.; Bisson, H. Nanoencapsulated Fluorescence Indicator Molecules Measuring pH and pO₂ down to Submicroscopic Regions on the Basis of the Optode-Principle. *Z. Naturforsch., C: J. Biosci.* **1977**, *32*, 133–134.
- (32) Peterson, J. I.; Goldstein, S. R.; Fitzgerald, R. V.; et al. Fiber Optic pH Probe for Physiological Use. *Anal. Chem.* **1980**, *52*, 864–869.
- (33) Goldstein, S. R.; Peterson, J. I.; Fitzgerald, R. V. A Miniature Fiber Optic pH Sensor for Physiological Use. *J. Biomech. Eng.* **1980**, *102*, 141–146.
- (34) Tait, G. A.; Young, R. B.; Wilson, G. J.; Steward, D. J.; MacGregor, D. C. Myocardial pH during Regional Ischemia: Evaluation of a Fiber-Optic Photometric Probe. *Am. J. Physiol.-Heart Circ. Physiol.* **1982**, *243*, H1027–H1031.
- (35) Suidan, J. S.; Young, B. K.; Hetzel, F. W.; Seal, H. R. pH Measurement with a Fiber-Optic Tissue-pH Monitor and a Standard Blood-pH Meter. *Clin. Chem.* **1983**, *29*, 1566–1566.
- (36) Wolfbeis, O. S.; Furlinger, E.; Kroneis, H.; Marsoner, H. Fluorimetric Analysis. *Fresenius' Z. Anal. Chem.* **1983**, *314*, 119–124.
- (37) Zhujun, Z.; Seitz, W. R. A Fluorescence Sensor for Quantifying pH in the Range from 6.5 to 8.5. *Anal. Chim. Acta* **1984**, *160*, 47–55.
- (38) Goldfinch, M. J.; Lowe, C. R. Solid-Phase Optoelectronic Sensors for Biochemical Analysis. *Anal. Biochem.* **1984**, *138*, 430–436.
- (39) Scheggi, A. M.; Baldini, F. pH Sensing by Fibre Optics. *Opt. Acta* **1986**, *33*, 1587–1597.
- (40) Woods, B. A.; Ruzicka, J.; Christian, G. D.; Charlson, R. J. Measurement of pH in Solutions of Low Buffering Capacity and Low Ionic Strength by Optosensing Flow Injection Analysis. *Anal. Chem.* **1986**, *58*, 2496–2502.
- (41) Gehrich, J. L.; Lubbers, D. W.; Opitz, N.; Hansmann, D. R.; Miller, W. W.; Tusa, J. K.; Yafuso, M. Optical Fluorescence and Its Application to an Intravascular Blood Gas Monitoring System. *IEEE Trans. Biomed. Eng.* **1986**, *BME-33* (2), 117–132.
- (42) Kawabata, Y.; Tsuchida, K.; Imasaka, T.; Ishibashi, N. Fiber-Optic pH Sensor with Monolayer Indicator. *Anal. Sci.* **1987**, *3*, 7–9.
- (43) Boisse, G.; Perez, J. J. Miniature Chemical Optical Fiber Sensors for pH Measurements. *Proc. SPIE* **1987**, *798*, 238.
- (44) Jordan, D. M.; Walt, D. R.; Milanovich, F. P. Physiological pH Fiber-Optic Chemical Sensor Based on Energy Transfer. *Anal. Chem.* **1987**, *59*, 437–439.
- (45) Monici, M.; Roniforti, R.; Buzziyoli, G.; De Rossi, B.; Nannini, A. Fibre-Optic pH Sensor for Seawater Monitoring. In *Fiber Optic Sensors II*; International Society for Optics and Photonics, 1987; Vol. 798, pp 294–301.
- (46) Wolfbeis, O. S.; Marhold, H. A New Group of Fluorescent pH-Indicators for an Extended pH-Range. *Fresenius' Z. Anal. Chem.* **1987**, *327*, 347–350.
- (47) Attridge, J. W.; Leaver, K. D.; Cozens, J. R. Design of a Fibre-Optic pH Sensor with Rapid Response. *J. Phys. E: Sci. Instrum.* **1987**, *20*, 548.
- (48) Knobbe, E.; Dunn, B.; Gold, M. Organic Molecules Entrapped in a Silica Host for Use as Biosensor Probe Materials. *Proc. SPIE* **1988**, *906*, 39–41.
- (49) Posch, H. E.; Leiner, M. J.; Wolfbeis, O. S. Towards a Gastric pH-Sensor: An Optrode for the pH 0–7 Range. *Fresenius' Z. Anal. Chem.* **1989**, *334*, 162–165.
- (50) Carey, W. P.; DeGrandpre, M. D.; Jorgensen, B. S. Polymer-Coated Cylindrical Waveguide Absorption Sensor for High Acidities. *Anal. Chem.* **1989**, *61*, 1674–1678.
- (51) Carey, W. P.; Jorgensen, B. S. Optical Sensors for High Acidities Based on Fluorescent Polymers. *Appl. Spectrosc.* **1991**, *45*, 834–838.
- (52) Gabor, G.; Walt, D. R. Sensitivity Enhancement of Fluorescent pH Indicators by Inner Filter Effects. *Anal. Chem.* **1991**, *63*, 793–796.
- (53) Tan, W.; Shi, Z.-Y.; Smith, S.; Birnbaum, D.; Kopelman, R. Submicrometer Intracellular Chemical Optical Fiber Sensors. *Science* **1992**, *258*, 778–781.
- (54) Werner, T.; Wolfbeis, O. S. Optical Sensor for the pH 10–13 Range Using a New Support Material. *Fresenius' J. Anal. Chem.* **1993**, *346*, 564–568.
- (55) Ge, Z.; Brown, C. W.; Sun, L.; Yang, S. C. Fiber-Optic pH Sensor Based on Evanescent Wave Absorption Spectroscopy. *Anal. Chem.* **1993**, *65*, 2335–2338.
- (56) Parker, J. W.; Laksin, O.; Yu, C.; Lau, M. L.; Klima, S.; Fisher, R.; Scott, I.; Atwater, B. W. Fiber-Optic Sensors for pH and Carbon Dioxide Using a Self-Referencing Dye. *Anal. Chem.* **1993**, *65*, 2329–2334.
- (57) McCurley, M. F. An Optical Biosensor Using a Fluorescent, Swelling Sensing Element. *Biosens. Bioelectron.* **1994**, *9*, 527–533.
- (58) Bronk, K. S.; Walt, D. R. Fabrication of Patterned Sensor Arrays with Aryl Azides on a Polymer-Coated Imaging Optical Fiber Bundle. *Anal. Chem.* **1994**, *66*, 3519–3520.
- (59) Michie, W.; Culshaw, B.; McKenzie, I.; Konstantakis, M.; Graham, N.; Moran, C.; Santos, F.; Bergqvist, E.; Carlstrom, B. Distributed Sensor for Water and pH Measurements Using Fiber Optics and Swellable Polymeric Systems. *Opt. Lett.* **1995**, *20*, 103–105.
- (60) Koncki, R.; Mohr, G. J.; Wolfbeis, O. S. Enzyme Biosensor for Urea Based on a Novel pH Bulk Optode Membrane. *Biosens. Bioelectron.* **1995**, *10*, 653–659.
- (61) Schulman, S. G.; Chen, S.; Bai, F.; Leiner, M. J. P.; Weis, L.; Wolfbeis, O. S. Dependence of the Fluorescence of Immobilized 1-

Hydroxypyrene-3,6,8-Trisulfonate on Solution pH: Extension of the Range of Applicability of a pH Fluorosensor. *Anal. Chim. Acta* **1995**, *304*, 165–170.

(62) Zhang, Z.; Shakhsher, Z.; Seitz, W. R. Aminated Polystyrene Membranes for a Fiber Optic pH Sensor Based on Reflectance Changes Accompanying Polymer Swelling. *Microchim. Acta* **1995**, *121*, 41–50.

(63) Taib, M. N.; Andres, R.; Narayanaswamy, R. Extending the Response Range of an Optical Fibre pH Sensor Using an Artificial Neural Network. *Anal. Chim. Acta* **1996**, *330*, 31–40.

(64) de Marcos, S.; Wolfbeis, O. S. Optical Sensing of pH Based on Polypyrrole Films. *Anal. Chim. Acta* **1996**, *334*, 149–153.

(65) Werner, T.; Huber, C.; Heinel, S.; Kollmannsberger, M.; Daub, J.; Wolfbeis, O. S. Novel Optical pH-Sensor Based on a Boradiaza-Indacene Derivative. *Fresenius' J. Anal. Chem.* **1997**, *359*, 150–154.

(66) Draxler, S.; Lippitsch, M. E. pH Sensors Using Fluorescence Decay Time. *Sens. Actuators, B* **1995**, *29*, 199–203.

(67) Draxler, S.; Lippitsch, M. E. Lifetime-Based Sensing: Influence of the Microenvironment. *Anal. Chem.* **1996**, *68*, 753–757.

(68) Pringsheim, E.; Terpetschnig, E.; Wolfbeis, O. S. Optical Sensing of pH Using Thin Films of Substituted Polyanilines. *Anal. Chim. Acta* **1997**, *357*, 247–252.

(69) Papkovsky, D. B.; Ponomarev, G. V.; Wolfbeis, O. S. Protonation of Porphyrins in Liquid PVC Membranes: Effects of Anionic Additives and Application to pH-Sensing. *J. Photochem. Photobiol., A* **1997**, *104*, 151–158.

(70) Safavi, A.; Abdollahi, H. Optical Sensor for High pH Values. *Anal. Chim. Acta* **1998**, *367*, 167–173.

(71) Baldini, F.; Bechi, P.; Bracci, S.; Cosi, F.; Pucciani, F. In Vivo Optical-Fibre pH Sensor for Gastro-Oesophageal Measurements. *Sens. Actuators, B* **1995**, *29*, 164–168.

(72) Boisde, G.; Perez, J. J. Dispositif d'analyse Des Constituants d'une Solution Par Mesure Photometrique. FR2317638B1, December 16, 1977.

(73) Perez, J.; Boisdé, G.; Goujon, de B.; Chevalier, G.; Isaac, M. Automation of Plutonium Spectrophotometry. *Anal. Chim. Acta* **1980**, *8*, 344–351.

(74) Campbell, M.; Yang, Y.; Wallace, P. A.; HOLMES–SMITH, A. S. A Multipoint Quasi-Distributed Optical Fiber pH Sensor. *Opt. Rev.* **1997**, *4*, A111–A113.

(75) Miller, W. W.; Yafuso, M.; Yan, C. F.; Hui, H.; Arick, S. Performance of an In-Vivo, Continuous Blood-Gas Monitor with Disposable Probe. *Clin. Chem.* **1987**, *33*, 1538–1542.

(76) Weigl, B. H.; Holobar, A.; Trettnak, W.; Klimant, I.; Kraus, H.; O'Leary, P.; Wolfbeis, O. S. Optical Triple Sensor for Measuring pH, Oxygen and Carbon Dioxide. *J. Biotechnol.* **1994**, *32*, 127–138.

(77) Steemers, F. J.; Ferguson, J. A.; Walt, D. R. Screening Unlabeled DNA Targets with Randomly Ordered Fiber-Optic Gene Arrays. *Nat. Biotechnol.* **2000**, *18*, 91–95.

(78) Klimant, I.; Meyer, V.; Kühl, M. Fiber-optic Oxygen Microsensors, a New Tool in Aquatic Biology. *Limnol. Oceanogr.* **1995**, *40*, 1159–1165.

(79) Wolfbeis, O. S.; Weis, L. J.; Leiner, M. J.; Ziegler, W. E. Fiber-Optic Fluorosensor for Oxygen and Carbon Dioxide. *Anal. Chem.* **1988**, *60*, 2028–2030.

(80) Leiner, M. J. Optical Sensors for in Vitro Blood Gas Analysis. *Sens. Actuators, B* **1995**, *29*, 169–173.

(81) Wangbai, M.; Zhujun, Z.; Seitz, W. R. Poly(Vinyl Alcohol)-Based Indicators for Optical pH and Mg(II) Sensing. In *Chemical Sensors and Microinstrumentation*; ACS Symposium Series; American Chemical Society, 1989; Vol. 403, pp 273–282.

(82) Ben-David, O.; Shafir, E.; Gilath, I.; Prior, Y.; Avnir, D. Simple Absorption Optical Fiber pH Sensor Based on Doped Sol–Gel Cladding Material. *Chem. Mater.* **1997**, *9*, 2255–2257.

(83) MacCraith, B. D.; Ruddy, V.; Potter, C.; O'Kelly, B.; McGilp, J. F. Optical Waveguide Sensor Using Evanescent Wave Excitation of Fluorescent Dye in Sol-Gel Glass. *Electron. Lett.* **1991**, *27*, 1247–1248.

(84) Meier, B.; Werner, T.; Klimant, I.; Wolfbeis, O. S. Novel Oxygen Sensor Material Based on a Ruthenium Bipyridyl Complex Encapsulated in Zeolite Y: Dramatic Differences in the Efficiency of

Luminescence Quenching by Oxygen on Going from Surface-Adsorbed to Zeolite-Encapsulated Fluorophores. *Sens. Actuators, B* **1995**, *29*, 240–245.

(85) Schaffar, B. B. P.; Wolfbeis, O. S.; Lieberman, R. A.; Wlodarczyk, M. T. New Optical Chemical Sensors Based On The Langmuir-Blodgett Technique. *Proc. SPIE (Soc. Photo-instrum. Eng.)* **1989**, *990*, 122.

(86) Seiler, K.; Morf, W. E.; Rusterholz, B.; Simon, W. Design and Characterization of a Novel Ammonium Ion Selective Optical Sensor Based on Neutral Ionophores. *Anal. Sci.* **1989**, *5*, 557–561.

(87) Spichiger-Keller, U. E.; Seiler, K.; Wang, K.; Suter, G.; Morf, W. E.; Simon, W. Optical Quantification of Sodium, Potassium, and Calcium Ions in Diluted Human Plasma Based on Ion-Selective Liquid Membranes. *Proc. SPIE 1510, Chemical and Medical Sensors* **1991**, 118–130.

(88) Song, A.; Parus, S.; Kopelman, R. High-Performance Fiber-Optic pH Microsensors for Practical Physiological Measurements Using a Dual-Emission Sensitive Dye. *Anal. Chem.* **1997**, *69*, 863–867.

(89) Lippitsch, M. E.; Pusterhofer, J.; Leiner, M. J.; Wolfbeis, O. S. Fibre-Optic Oxygen Sensor with the Fluorescence Decay Time as the Information Carrier. *Anal. Chim. Acta* **1988**, *205*, 1–6.

(90) Lübbers, D.; Opitz, N. The pCO₂/pO₂ Optrode: A New Probe for Measuring pCO₂ and pO₂ of Gases and Liquids. *Z. Naturforsch., C: J. Biosci.* **1975**, *30*, 532–533.

(91) Wolfbeis, O. S.; Posch, H. E. Fibre-Optic Fluorescing Sensor for Ammonia. *Anal. Chim. Acta* **1986**, *185*, 321–327.

(92) Trettnak, W.; Leiner, M. J.; Wolfbeis, O. S. Fibre-Optic Glucose Sensor with a pH Optrode as the Transducer. *Biosensors* **1989**, *4*, 15–26.

(93) Kocincová, A. S.; Nagl, S.; Arain, S.; Krause, C.; Borisov, S. M.; Arnold, M.; Wolfbeis, O. S. Multiplex Bacterial Growth Monitoring in 24-Well Microplates Using a Dual Optical Sensor for Dissolved Oxygen and pH. *Biotechnol. Bioeng.* **2008**, *100*, 430–438.

(94) Liebsch, G.; Klimant, I.; Frank, B.; Holst, G.; Wolfbeis, O. S. Luminescence Lifetime Imaging of Oxygen, pH, and Carbon Dioxide Distribution Using Optical Sensors. *Appl. Spectrosc.* **2000**, *54*, 548–559.

(95) Kopelman, R.; Tan, W.; Shi, Z.-Y. *Nanometer Optical Fiber pH Sensor*; Lieberman, R. A., Ed.; 1993; pp 157–162.

(96) Narayanaswamy, R.; Wolfbeis, O. S. *Optical Sensors: Industrial, Environmental, and Diagnostic Applications*; Springer Series on Chemical Sensors and Biosensors; Springer: Berlin, 2004.

(97) Kostov, Y.; Tzonkov, S.; Yotova, L. Dynamic Model of an Optical Absorption-Based pH Sensor. *Analyst* **1993**, *118*, 987–990.

(98) Kochmann, S.; Hirsch, T.; Wolfbeis, O. S. The pH Dependence of the Total Fluorescence of Graphite Oxide. *J. Fluoresc.* **2012**, *22*, 849–855.

(99) Han, J.; Burgess, K. Fluorescent Indicators for Intracellular pH. *Chem. Rev.* **2010**, *110*, 2709–2728.

(100) Hanson, M. A.; Ge, X.; Kostov, Y.; Brorson, K. A.; Moreira, A. R.; Rao, G. Comparisons of Optical pH and Dissolved Oxygen Sensors with Traditional Electrochemical Probes during Mammalian Cell Culture. *Biotechnol. Bioeng.* **2007**, *97*, 833–841.

(101) Cox, B. G. *Acids and Bases: Solvent Effects on Acid-Base Strength*; Oxford University Press: Oxford, 2013.

(102) Narayanaswamy, R.; Sevilla, F. Reflectometric Study of the Acid-Base Equilibria of Indicators Immobilised on a Styrene/Divinylbenzene Copolymer. *Anal. Chim. Acta* **1986**, *189*, 365–369.

(103) Albert, A.; Serjeant, E. P.; *The Determination of Ionization Constants: A Laboratory Manual*; 3rd ed.; Springer: Berlin, 2012.

(104) Eistert, B.; Merkel, E.; Reiss, W. Halochromie Und Basizität Enolisierbarer B-Diketone. *Chem. Ber.* **1954**, *87*, 1513–1540.

(105) Reijenga, J. C.; Gagliardi, L. G.; Kennndler, E. Temperature Dependence of Acidity Constants, a Tool to Affect Separation Selectivity in Capillary Electrophoresis. *J. Chromatogr. A* **2007**, *1155*, 142–145.

(106) Rayer, A. V.; Sumon, K. Z.; Jaffari, L.; Henni, A. Dissociation Constants (pK_a) of Tertiary and Cyclic Amines: Structural and Temperature Dependences. *J. Chem. Eng. Data* **2014**, *59*, 3805–3813.

- (107) Hammett, L. P. *Physical Organic Chemistry Reaction Rates, Equilibria, and Mechanisms*; McGraw-Hill: New York, 1970.
- (108) Swindlehurst, B. R.; Narayanaswamy, R. Optical Sensing of pH in Low Ionic Strength Waters. In *Optical Sensors*; Springer, 2004; pp 281–308.
- (109) Edmonds, T. Determination of pH with Acid-Base Indicators: Implications for Optical Fibre Probes. *Talanta* **1988**, *35*, 103–107.
- (110) Schröder, C. R.; Weidgans, B. M.; Klimant, I. pH Fluorosensors for Use in Marine Systems. *Analyst* **2005**, *130*, 907–916.
- (111) Holobar, A.; Weigl, B. H.; Trettnak, W.; Beneš, R.; Lehmann, H.; Rodriguez, N. V.; Wollschlager, A.; O'Leary, P.; Raspor, P.; Wolfbeis, O. S. Experimental Results on an Optical pH Measurement System for Bioreactors. *Sens. Actuators, B* **1993**, *11*, 425–430.
- (112) Robert-Baldo, G. L.; Morris, M. J.; Byrne, R. H. Spectrophotometric Determination of Seawater pH Using Phenol Red. *Anal. Chem.* **1985**, *57*, 2564–2567.
- (113) Bockmon, E. E.; Dickson, A. G. An Inter-Laboratory Comparison Assessing the Quality of Seawater Carbon Dioxide Measurements. *Mar. Chem.* **2015**, *171*, 36–43.
- (114) DeGrandpre, M. D.; Spaulding, R. S.; Newton, J. O.; Jaqueth, E. J.; Hamblock, S. E.; Umansky, A. A.; Harris, K. E. Considerations for the Measurement of Spectrophotometric pH for Ocean Acidification and Other Studies. *Limnol. Oceanogr.: Methods* **2014**, *12*, 830–839.
- (115) Clayton, T. D.; Byrne, R. H. Spectrophotometric Seawater pH Measurements: Total Hydrogen Ion Concentration Scale Calibration of m-Cresol Purple and at-Sea Results. *Deep Sea Res., Part I* **1993**, *40*, 2115–2129.
- (116) Mosley, L. M.; Husheer, S. L.; Hunter, K. A. Spectrophotometric pH Measurement in Estuaries Using Thymol Blue and M-Cresol Purple. *Mar. Chem.* **2004**, *91*, 175–186.
- (117) Liu, X.; Patsavas, M. C.; Byrne, R. H. Purification and Characterization of Meta-Cresol Purple for Spectrophotometric Seawater pH Measurements. *Environ. Sci. Technol.* **2011**, *45*, 4862–4868.
- (118) He, H.; Mortellaro, M. A.; Leiner, M. J. P.; Young, S. T.; Fraatz, R. J.; Tusa, J. K. A Fluorescent Chemosensor for Sodium Based on Photoinduced Electron Transfer. *Anal. Chem.* **2003**, *75*, 549–555.
- (119) He, H.; Mortellaro, M. A.; Leiner, M. J. P.; Fraatz, R. J.; Tusa, J. K. A Fluorescent Sensor with High Selectivity and Sensitivity for Potassium in Water. *J. Am. Chem. Soc.* **2003**, *125*, 1468–1469.
- (120) Clarke, J. S.; Achterberg, E. P.; Rérolle, V. M. C.; Abi Kaed Bey, S.; Floquet, C. F. A.; Mowlem, M. C. Characterisation and Deployment of an Immobilised pH Sensor Spot towards Surface Ocean pH Measurements. *Anal. Chim. Acta* **2015**, *897*, 69–80.
- (121) Weidgans, B. M.; Krause, C.; Klimant, I.; Wolfbeis, O. S. Fluorescent pH Sensors with Negligible Sensitivity to Ionic Strength. *Analyst* **2004**, *129*, 645–650.
- (122) Aigner, D.; Borisov, S. M.; Klimant, I. New Fluorescent Perylene Bisimide Indicators—a Platform for Broadband pH Optodes. *Anal. Bioanal. Chem.* **2011**, *400*, 2475–2485.
- (123) Aigner, D.; Borisov, S. M.; Petritsch, P.; Klimant, I. Novel near Infra-Red Fluorescent pH Sensors Based on 1-Aminoperylene Bisimides Covalently Grafted onto Poly(Acryloylmorpholine). *Chem. Commun.* **2013**, *49*, 2139–2141.
- (124) Staudinger, C.; Strobl, M.; Breininger, J.; Klimant, I.; Borisov, S. M. Fast and Stable Optical pH Sensor Materials for Oceanographic Applications. *Sens. Actuators, B* **2019**, *282*, 204–217.
- (125) Wang, X.; Wolfbeis, O. S.; Meier, R. J. Luminescent Probes and Sensors for Temperature. *Chem. Soc. Rev.* **2013**, *42*, 7834–7869.
- (126) Wang, X.; Meier, R. J.; Wolfbeis, O. S. A Fluorophore-Doped Polymer Nanomaterial for Referenced Imaging of pH and Temperature with Sub-Micrometer Resolution. *Adv. Funct. Mater.* **2012**, *22*, 4202–4207.
- (127) Wang, X.; Meier, R. J.; Schmittlein, C.; Schreml, S.; Schäferling, M.; Wolfbeis, O. S. A Water-Sprayable, Thermogelating and Biocompatible Polymer Host for Use in Fluorescent Chemical Sensing and Imaging of Oxygen, pH Values and Temperature. *Sens. Actuators, B* **2015**, *221*, 37–44.
- (128) *Handbook of Applied Photometry*; DeCusatis, C., Optical Society of America, Eds.; AIP Press, Optical Society of America: Woodbury, N.Y., 1997.
- (129) Yang, L.; Kruse, B. Revised Kubelka–Munk Theory. I. Theory and Application. *J. Opt. Soc. Am. A* **2004**, *21*, 1933–1941.
- (130) Meier, R. J.; Fischer, L. H.; Wolfbeis, O. S.; Schäferling, M. Referenced Luminescent Sensing and Imaging with Digital Color Cameras: A Comparative Study. *Sens. Actuators, B* **2013**, *177*, 500–506.
- (131) *Principles of Fluorescence Spectroscopy*; Lakowicz, J. R., Ed.; Springer US: Boston, MA, 2006.
- (132) Wang, X.; Wolfbeis, O. S. Optical Methods for Sensing and Imaging Oxygen: Materials, Spectroscopies and Applications. *Chem. Soc. Rev.* **2014**, *43*, 3666–3761.
- (133) Tomasulo, M.; Yildiz, I.; Raymo, F. M. pH-Sensitive Quantum Dots. *J. Phys. Chem. B* **2006**, *110*, 3853–3855.
- (134) de Silva, A. P.; Gunaratne, H. Q. N.; Habib-Jiwan, J.-L.; McCoy, C. P.; Rice, T. E.; Soumillion, J.-P. New Fluorescent Model Compounds for the Study of Photoinduced Electron Transfer: The Influence of a Molecular Electric Field in the Excited State. *Angew. Chem., Int. Ed. Engl.* **1995**, *34*, 1728–1731.
- (135) Gotor, R.; Ashokkumar, P.; Hecht, M.; Keil, K.; Rurack, K. Optical pH Sensor Covering the Range from pH 0–14 Compatible with Mobile-Device Readout and Based on a Set of Rationally Designed Indicator Dyes. *Anal. Chem.* **2017**, *89*, 8437–8444.
- (136) Weller, A. Electron-Transfer and Complex Formation in the Excited State. *Pure Appl. Chem.* **1968**, *16*, 115–124.
- (137) Bissell, R. A.; de Silva, A. P.; Thilak, W.; Fernando, M.; Patuwathavithana, S. T.; Shantha, T.; Samarasinghe, D. Fluorescent PET (Photoinduced Electron Transfer) Indicators for Solvent Polarity with Quasi-Step Functional Response. *Tetrahedron Lett.* **1991**, *32*, 425–428.
- (138) Bissell, R. A.; de Silva, A. P.; Gunaratne, H. Q. N.; Lynch, P. L. M.; Maguire, G. E. M.; Sandanayake, K. R. A. S. Molecular Fluorescent Signalling with 'Fluor-Spacer-Receptor' Systems: Approaches to Sensing and Switching Devices via Supramolecular Photophysics. *Chem. Soc. Rev.* **1992**, *21*, 187–195.
- (139) Daffy, L. M.; de Silva, A. P.; Gunaratne, H. N.; Huber, C.; Lynch, P. M.; Werner, T.; Wolfbeis, O. S. Arenedicarboximide Building Blocks for Fluorescent Photoinduced Electron Transfer pH Sensors Applicable with Different Media and Communication Wavelengths. *Chem. - Eur. J.* **1998**, *4*, 1810–1815.
- (140) de Silva, A. P.; Gunnlaugsson, T.; Rice, T. E. Recent Evolution of Luminescent Photoinduced Electron Transfer Sensors. A Review. *Analyst* **1996**, *121*, 1759–1762.
- (141) Marin, M. J.; Galindo, F.; Thomas, P.; Russell, D. A. Localized Intracellular pH Measurement Using a Ratiometric Photoinduced Electron-Transfer-Based Nanosensor. *Angew. Chem., Int. Ed.* **2012**, *51*, 9657–9661.
- (142) Klimant, I.; Huber, C.; Liebsch, G.; Neurauder, G.; Stangelmayer, A.; Wolfbeis, O. S. Dual Lifetime Referencing (DLR)—A New Scheme for Converting Fluorescence Intensity into a Frequency-Domain or Time-Domain Information. In *New Trends in Fluorescence Spectroscopy: Applications to Chemical and Life Sciences*; Valeur, B.; Brochon, J.-C., Eds.; Springer: Berlin, 2001; pp 257–274.
- (143) Liebsch, G.; Klimant, I.; Krause, C.; Wolfbeis, O. S. Fluorescent Imaging of pH with Optical Sensors Using Time Domain Dual Lifetime Referencing. *Anal. Chem.* **2001**, *73*, 4354–4363.
- (144) Begemann, J.; Spiess, A. C. Dual Lifetime Referencing Enables pH-Control for Oxidoreductions in Hydrogel-Stabilized Biphasic Reaction Systems. *Biotechnol. J.* **2015**, *10*, 1822–1829.
- (145) Schreml, S.; Meier, R. J.; Wolfbeis, O. S.; Landthaler, M.; Szeimies, R.-M.; Babilas, P. 2D Luminescence Imaging of pH in Vivo. *Proc. Natl. Acad. Sci. U. S. A.* **2011**, *108*, 2432–2437.
- (146) Stahl, H.; Glud, A.; Schröder, C. R.; Klimant, I.; Tengberg, A.; Glud, R. N. Time-Resolved pH Imaging in Marine Sediments with a Luminescent Planar Optode. *Limnol. Oceanogr.: Methods* **2006**, *4*, 336–345.
- (147) Boniello, C.; Mayr, T.; Bolivar, J. M.; Nidetzky, B. Dual-Lifetime Referencing (DLR): A Powerful Method for on-Line Measurement of

Internal pH in Carrier-Bound Immobilized Biocatalysts. *BMC Biotechnol.* **2012**, *12*, No. 11, DOI: 10.1186/1472-6750-12-11.

(148) Poehler, E.; Herzog, C.; Suendermann, M.; Pfeiffer, S. A.; Nagl, S. Development of Microscopic Time-Domain Dual Lifetime Referencing Luminescence Detection for pH Monitoring in Microfluidic Free-Flow Isoelectric Focusing. *Eng. Life Sci.* **2015**, *15*, 276–285.

(149) Bare, W. D.; Mack, N. H.; Xu, W.; Demas, J. N.; DeGraff, B. A. Multicomponent Lifetime-Based pH Sensors Utilizing Constant-Lifetime Probes. *Anal. Chem.* **2002**, *74*, 2198–2209.

(150) Borisov, S. M.; Gatterer, K.; Klimant, I. Red Light-Excitable Dual Lifetime Referenced Optical pH Sensors with Intrinsic Temperature Compensation. *Analyst* **2010**, *135*, 1711.

(151) Jokic, T.; Borisov, S. M.; Saf, R.; Nielsen, D. A.; Kühl, M.; Klimant, I. Highly Photostable Near-Infrared Fluorescent pH Indicators and Sensors Based on BF₂-Chelated Tetraarylazapyrromethene Dyes. *Anal. Chem.* **2012**, *84*, 6723–6730.

(152) Aigner, D.; Borisov, S. M.; Orriach Fernández, F. J.; Fernández Sánchez, J. F.; Saf, R.; Klimant, I. New Fluorescent pH Sensors Based on Covalently Linkable PET Rhodamines. *Talanta* **2012**, *99*, 194–201.

(153) Borisov, S. M.; Würth, C.; Resch-Genger, U.; Klimant, I. New Life of Ancient Pigments: Application in High-Performance Optical Sensing Materials. *Anal. Chem.* **2013**, *85*, 9371–9377.

(154) Corres, J. M.; Matias, I. R.; del Villar, I.; Arregui, F. J. Design of pH Sensors in Long-Period Fiber Gratings Using Polymeric Nanocoatings. *IEEE Sens. J.* **2007**, *7*, 455–463.

(155) Zamarreño, C.; Hernández, M.; Del Villar, I.; Matias, I.; Arregui, F. Optical Fiber pH Sensor Based on Lossy-Mode Resonances by Means of Thin Polymeric Coatings. *Sens. Actuators, B* **2011**, *155*, 290–297.

(156) Zubiate, P.; Zamarreño, C.; Del Villar, I.; Matias, I.; Arregui, F. Tunable Optical Fiber pH Sensors Based on TE and TM Lossy Mode Resonances (LMRs). *Sens. Actuators, B* **2016**, *231*, 484–490.

(157) Suzuki, A.; Suzuki, H. Hysteretic Behavior and Irreversibility of Polymer Gels by pH Change. *J. Chem. Phys.* **1995**, *103*, 4706–4710.

(158) Richter, A.; Paschew, G.; Klatt, S.; Lienig, J.; Arndt, K.-F.; Adler, H.-J. P. Review on Hydrogel-Based pH Sensors and Microsensors. *Sensors* **2008**, *8*, 561–581.

(159) Paynter, S.; Russell, D. A. Surface Plasmon Resonance Measurement of pH-Induced Responses of Immobilized Biomolecules: Conformational Change or Electrostatic Interaction Effects? *Anal. Biochem.* **2002**, *309*, 85–95.

(160) Yanase, Y.; Hiragun, T.; Ishii, K.; Kawaguchi, T.; Yanase, T.; Kawai, M.; Sakamoto, K.; Hide, M. Surface Plasmon Resonance for Cell-Based Clinical Diagnosis. *Sensors* **2014**, *14*, 4948–4959.

(161) Kozlovskaya, V.; Kharlampieva, E.; Khanal, B. P.; Manna, P.; Zubarev, E. R.; Tsukruk, V. V. Ultrathin Layer-by-Layer Hydrogels with Incorporated Gold Nanorods as pH-Sensitive Optical Materials. *Chem. Mater.* **2008**, *20*, 7474–7485.

(162) Rivero, P. J.; Goicoechea, J.; Hernaez, M.; Socorro, A. B.; Matias, I. R.; Arregui, F. J. Optical Fiber Resonance-Based pH Sensors Using Gold Nanoparticles into Polymeric Layer-by-Layer Coatings. *Microsyst. Technol.* **2016**, *22*, 1821–1829.

(163) Fenzl, C.; Hirsch, T.; Wolfbeis, O. S. Photonic Crystals for Chemical Sensing and Biosensing. *Angew. Chem., Int. Ed.* **2014**, *53*, 3318–3335.

(164) Harmon, M. E.; Kuckling, D.; Frank, C. W. Photo-Cross-Linkable PNIPAAm Copolymers. 2. Effects of Constraint on Temperature and pH-Responsive Hydrogel Layers. *Macromolecules* **2003**, *36*, 162–172.

(165) Shakhsher, Z. M.; Odeh, I.; Jabr, S.; Rudolf Seitz, W. An Optical Chemical Sensor Based on Swellable Dicarboxylate Functionalized Polymer Microspheres for pH Copper and Calcium Determination. *Microchim. Acta* **2004**, *144*, 147–153.

(166) Otkar, O.; Caglar, P.; Seitz, W. R. Chemical Modulation of Thermosensitive Poly(*N*-Isopropylacrylamide) Microsphere Swelling: A New Strategy for Chemical Sensing. *Sens. Actuators, B* **2005**, *104*, 179–185.

(167) Rooney, M. T. V.; Rudolf Seitz, W. An Optically Sensitive Membrane for pH Based on Swellable Polymer Microspheres in a Hydrogel. *Anal. Commun.* **1999**, *36*, 267–270.

(168) Müller, M.; Kessler, B.; Houbenov, N.; Bohata, K.; Pientka, Z.; Brynda, E. pH Dependence and Protein Selectivity of Poly (Ethyleneimine)/Poly (Acrylic Acid) Multilayers Studied by in Situ ATR-FTIR Spectroscopy. *Biomacromolecules* **2006**, *7*, 1285–1294.

(169) Jensen, R. A.; Sherin, J.; Emory, S. R. Single Nanoparticle Based Optical pH Probe. *Appl. Spectrosc.* **2007**, *61*, 832–838.

(170) Wang, J.; Geng, Y.; Shen, Y.; Shi, W.; Xu, W.; Xu, S. SERS-Active Fiber Tip for Intracellular and Extracellular pH Sensing in Living Single Cells. *Sens. Actuators, B* **2019**, *290*, 527–534.

(171) Li, Z.; Xia, L.; Li, G.; Hu, Y. Raman Spectroscopic Imaging of pH Values in Cancerous Tissue by Using Polyaniline@gold Nanoparticles. *Microchim. Acta* **2019**, DOI: 10.1007/s00604-019-3265-4.

(172) Liu, X.; Zhang, X.; Cong, J.; Xu, J.; Chen, K. Demonstration of Etched Cladding Fiber Bragg Grating-Based Sensors with Hydrogel Coating. *Sens. Actuators, B* **2003**, *96*, 468–472.

(173) Rudolf Seitz, W. New Directions in Fiber Optic Chemical Sensors: Sensors Based on Polymer Swelling. *J. Mol. Struct.* **1993**, *292*, 105–113.

(174) Zhang, Y.; Ji, H.; Snow, D.; Sterling, R.; Brown, G. M. A pH Sensor Based on a Microcantilever Coated with Intelligent Hydrogel. *Instrum. Sci. Technol.* **2004**, *32*, 361–369.

(175) Bashir, R.; Hilt, J.; Elibol, O.; Gupta, A.; Peppas, N. Micromechanical Cantilever as an Ultrasensitive pH Microsensor. *Appl. Phys. Lett.* **2002**, *81*, 3091–3093.

(176) Gerlach, G.; Guenther, M.; Suchanek, G.; Sorber, J.; Arndt, K.-F.; Richter, A. Application of Sensitive Hydrogels in Chemical and pH Sensors. *Macromol. Symp.* **2004**, *210*, 403–410.

(177) Schalkhammer, T.; Lobmaier, C.; Pittner, F.; Leitner, A.; Brunner, H.; Aussenegg, F. The Use of Metal-Island-Coated pH-Sensitive Swelling Polymers for Biosensor Applications. *Sens. Actuators, B* **1995**, *24*, 166–172.

(178) Zhang, L.; Langmuir, M. E.; Bai, M.; Seitz, W. R. A Sensor for pH Based on an Optical Reflective Device Coupled to the Swelling of an Aminated Polystyrene Membrane. *Talanta* **1997**, *44*, 1691–1698.

(179) Shakhsher, Z.; Seitz, W. R.; Legg, K. D. Single Fiber-Optic pH Sensor Based on Changes in Reflection Accompanying Polymer Swelling. *Anal. Chem.* **1994**, *66*, 1731–1735.

(180) Shivananju, B. N.; Priyadarshi, M. Kr.; Roy Mahapatra, D.; Hegde, G. M.; Asokan, S. pH Sensing = Single and Multi-Layer Hydrogel Coated Fiber Bragg Grating. In *2012 1st International Symposium on Physics and Technology of Sensors (ISPTS-1)*; IEEE: Pune, India, 2012; pp 74–78.

(181) Schenato, L. A Review of Distributed Fibre Optic Sensors for Geo-Hydrological Applications. *Appl. Sci.* **2017**, *7* (896), 896.

(182) Wong, W. C.; Chan, C. C.; Hu, P.; Chan, J. R.; Low, Y. T.; Dong, X.; Leong, K. C. Miniature pH Optical Fiber Sensor Based on Waist-Enlarged Bitaper and Mode Excitation. *Sens. Actuators, B* **2014**, *191*, 579–585.

(183) Hu, P.; Dong, X.; Wong, W. C.; Chen, L. H.; Ni, K.; Chan, C. C. Photonic Crystal Fiber Interferometric pH Sensor Based on Polyvinyl Alcohol/Polyacrylic Acid Hydrogel Coating. *Appl. Opt.* **2015**, *54*, 2647–2652.

(184) Chang, C.-L.; Ding, Z.; Patchigolla, V. N.; Ziaie, B.; Savran, C. A. Reflective Diffraction Gratings with Hydrogels as Biochemical Sensors. *IEEE Sens. J.* **2012**, *12*, 2374–2379.

(185) Liang, X.; Huang, H.; Liu, W.; et al. Study on Sensitivity Improving of Fiber Bragg Grating Based pH Sensor. *Photonic Sens.* **2014**, *4*, 28–33.

(186) Corres, J. M.; Del Villar, I.; Matias, I. R.; Arregui, F. J. Fiber-Optic pH-Sensors in Long-Period Fiber Gratings Using Electrostatic Self-Assembly. *Opt. Lett.* **2007**, *32*, 29–31.

(187) Zheng, Y.; Chen, L. H.; Dong, X.; Yang, J.; Long, H. Y.; So, P. L.; Chan, C. C. Miniature pH Optical Fiber Sensor Based on Fabry–Perot Interferometer. *IEEE J. Sel. Top. Quantum Electron.* **2016**, *22*, 331–335.

(188) Zhou, M.; Dong, X.; Ma, Q.; Chan, C. C. Miniature pH Sensor Based on Thin-Core Fiber Mach-Zehnder Interferometer. In *2017 16th International Conference on Optical Communications and Networks (ICOON)*; IEEE: Wuzhen, 2017; pp 1–3.

- (189) Tou, Z. Q.; Chan, C. C.; Hong, J.; Png, S.; Eddie, K. M. T.; Tan, T. A. H. Double-Pass Mach–Zehnder Fiber Interferometer pH Sensor. *J. Biomed. Opt.* **2014**, *19*, No. 047002.
- (190) Lei, M.; Zhang, Y.-N.; Han, B.; Zhao, Q.; Zhang, A.; Fu, D. In-Line Mach–Zehnder Interferometer and FBG with Smart Hydrogel for Simultaneous pH and Temperature Detection. *IEEE Sens. J.* **2018**, *18*, 7499–7504.
- (191) Mohammed, A. Z. Photonic Crystal Fiber Mach-Zehnder Interferometer pH Sensing. *AIP Conf. Proc.* **2018**, *2045*, No. 020010.
- (192) Arregui, F. J. A Ph Sensor Made Using Cellulosic Coating on a Biconically Tapered Singlemode Optical Fiber. In *Fourteenth International Conference on Optical Fiber Sensors*; Mignani, A. G., Lefèvre, H. C., Eds.; SPIE: Venice, Italy, 2000; p 90.
- (193) Zamarreño, C.; Goicoechea, J.; Matias, I.; Arregui, F. Laterally Selective Adsorption of pH Sensing Coatings Based on Neutral Red by Means of the Electric Field Directed Layer-by-Layer Self Assembly Method. *Thin Solid Films* **2009**, *517*, 3776–3780.
- (194) Arregui, F. J.; Otano, M.; Fernandez-Valdivielso, C.; Matias, I. R. An Experimental Study about the Utilization of Liquicoat® Solutions for the Fabrication of pH Optical Fiber Sensors. *Sens. Actuators, B* **2002**, *87*, 289–295.
- (195) Zamarreño, C. R.; Bravo, J.; Goicoechea, J.; Matias, I.; Arregui, F. Response Time Enhancement of pH Sensing Films by Means of Hydrophilic Nanostructured Coatings. *Sens. Actuators, B* **2007**, *128*, 138–144.
- (196) Bishop, E. *Indicators*, 1st ed.; International Series of Monographs in Analytical Chemistry, Vol. 51; Pergamon Press: Oxford, NY, 1972.
- (197) Sabnis, R. W. *Handbook of Acid-Base Indicators*; CRC Press: Boca Raton, 2008.
- (198) Kolthoff, I. M.; Rosenblum, C. *Acid-Base Indicators*; Lancaster Press, Inc.: Lancaster, PA, 2011.
- (199) Sabnis, R. W.; Ross, E.; Köthe, J.; Naumann, R.; Fischer, W.; Mayer, W.-D.; Wieland, G.; Newman, E. J.; Wilson, C. M. Indicator Reagents. In *Ullmann's Encyclopedia of Industrial Chemistry*; Wiley-VCH Verlag GmbH & Co., KGaA: Weinheim, Germany, 2009.
- (200) *Dictionary of Analytical Reagents*; Springer US: Boston, MA, 1993.
- (201) Allain, L. R.; Xue, Z. Optical Sensors for the Determination of Concentrated Hydroxide. *Anal. Chem.* **2000**, *72*, 1078–1083.
- (202) Canada, T. A.; Beach, D. B.; Xue, Z.-L. Optical Sensors for the Determination of Concentrated Hydroxide. Characterization of the Sensor Materials and Evaluation of the Sensor Performance. *Anal. Chem.* **2005**, *77*, 2842–2851.
- (203) Ensafi, A. A.; Kazemzadeh, A. Optical pH Sensor Based On Chemical Modification of Polymer Film. *Microchem. J.* **1999**, *63*, 381–388.
- (204) Rouhani, S.; Salimi, S.; Haghbeen, K. Development of Optical pH Sensors Based on Derivatives of Hydroxyazobenzene, and the Extended Linear Dynamic Range Using Mixture of Dyes. *Dyes Pigm.* **2008**, *77*, 363–368.
- (205) Cardwell, T. J.; Cattrall, R. W.; Deady, L. W.; Dorkos, M.; O'Connell, G. R. A Fast Response Membrane-Based pH Indicator Optode. *Talanta* **1993**, *40*, 765–768.
- (206) Wolthuis, R.; McCrae, D.; Saaski, E.; Hartl, J.; Mitchell, G. Development of a Medical Fiber-Optic pH Sensor Based on Optical Absorption. *IEEE Trans. Biomed. Eng.* **1992**, *39*, 531–537.
- (207) Makedonski, P.; Brandes, M.; Grahn, W.; Kowalsky, W.; Wichern, J.; Wiese, S.; Johannes, H.-H. Synthesis of New Kinds of Reactive Azo Dyes and Their Application for Fibre-Optical pH-Measurements. *Dyes Pigm.* **2004**, *61*, 109–119.
- (208) Grahn, W.; Makedonski, P.; Wichern, J.; Kowalsky, W.; Wiese, S. Fiber Optic Sensors for an In-Situ Monitoring of Moisture and pH Value in Reinforced Concrete. *Proc. SPIE* **2001**, *4480*, 395–404.
- (209) Trupp, S.; Alberti, M.; Carofiglio, T.; Lubian, E.; Lehmann, H.; Heuermann, R.; Yacoub-George, E.; Bock, K.; Mohr, G. J. Development of pH-Sensitive Indicator Dyes for the Preparation of Micro-Patterned Optical Sensor Layers. *Sens. Actuators, B* **2010**, *150*, 206–210.
- (210) Egawa, Y.; Hayashida, R.; Anzai, J. Multilayered Assemblies Composed of Brilliant Yellow and Poly (Allylamine) for an Optical pH Sensor. *Anal. Sci.* **2006**, *22*, 1117–1119.
- (211) Raoufi, N.; Surre, F.; Sun, T.; Rajarajan, M.; Grattan, K. T. V. Wavelength Dependent pH Optical Sensor Using the Layer-by-Layer Technique. *Sens. Actuators, B* **2012**, *169*, 374–381.
- (212) Sansubrin, A.; Mascini, M. Development of an Optical Fibre Sensor for Ammonia, Urea, Urease and IgG. *Biosens. Bioelectron.* **1994**, *9*, 207–216.
- (213) Wróblewski, W.; Roźniecka, E.; Dybko, A.; Brzózka, Z. Cellulose Based Bulk pH Optomembranes. *Sens. Actuators, B* **1998**, *48*, 471–475.
- (214) Hashemi, P.; Abolghasemi, M. M. Preparation of a Novel Optical Sensor for Low pH Values Using Agarose Membranes as Support. *Sens. Actuators, B* **2006**, *115*, 49–53.
- (215) Salmani G K, M.; Rounaghi, G. H.; Chamsaz, M. An Optical Sensor for Determination of Low pH Values Based on Covalent Immobilization of Congo Red on Triacetyl Cellulose Films via Epichlorohydrin. *Sens. Actuators, B* **2018**, *254*, 177–181.
- (216) Dybko, A.; Wróblewski, W.; Maciejewski, J.; Romaniuk, R.; Brzózka, Z. Efficient Reagent Immobilization Procedure for Ion-Sensitive Optomembranes. *Sens. Actuators, B* **1997**, *39*, 207–211.
- (217) Hisamoto, H.; Tsubuku, M.; Enomoto, T.; Watanabe, K.; Kawaguchi, H.; Koike, Y.; Suzuki, K. Theory and Practice of Rapid Flow-through Analysis Based on Optode Detection and Its Application to pH Measurement as a Model Case. *Anal. Chem.* **1996**, *68*, 3871–3878.
- (218) Kostov, Y.; Tzonkov, S.; Yotova, L.; Krysteva, M. Membranes for Optical pH Sensors. *Anal. Chim. Acta* **1993**, *280*, 15–19.
- (219) Ganesh, A. B.; Radhakrishnan, T. K. Fiber-Optic pH Sensor. *Fiber Integr. Opt.* **2006**, *25*, 403–409.
- (220) Ganesh, A. B.; Radhakrishnan, T. K. Fiber-Optic Sensors for the Estimation of pH within Natural Biofilms on Metals. *Sens. Actuators, B* **2007**, *123*, 1107–1112.
- (221) Liu, J. N.; Shahriari, M. R.; Sigel, G. H. Development of a Porous Polymer pH Optrode. *Opt. Lett.* **1992**, *17*, 1815–1817.
- (222) Bacci, M.; Baldini, F.; Bracci, S. Spectroscopic Behavior of Acid-Base Indicators after Immobilization on Glass Supports. *Appl. Spectrosc.* **1991**, *45*, 1508–1515.
- (223) Mimms, L. T.; McKnight, M. A.; Murray, R. W. Spectrophotometric Study of Coverage and Acid-Base Equilibrium of a Chemically Bonded Base. *Anal. Chim. Acta* **1977**, *89*, 355–361.
- (224) Wong, L. S.; Bradley, M. Immobilisation and Assessment of Aniline Dyes for Non-Fluorescent pH Sensing Applications. *Tetrahedron Lett.* **2005**, *46*, 5731–5734.
- (225) Li, G.; Xiao, J.; Zhang, W. A Novel Dual Colorimetric Fiber Based on Two Acid–Base Indicators. *Dyes Pigm.* **2012**, *92*, 1091–1099.
- (226) Rottman, C.; Ottolenghi, M.; Zusan, R.; Lev, O.; Smith, M.; Gong, G.; Kagan, M. L.; Avnir, D. Doped Sol-Gel Glasses as pH Sensors. *Mater. Lett.* **1992**, *13*, 293–298.
- (227) García-Heras, M.; Gil, C.; Carmona, N.; Faber, J.; Kromka, K.; Villegas, M. A. Optical Behaviour of pH Detectors Based on Sol–Gel Technology. *Anal. Chim. Acta* **2005**, *540*, 147–152.
- (228) Rottman, C.; Turniansky, A.; Avnir, D. Sol-Gel Physical and Covalent Entrapment of Three Methyl Red Indicators: A Comparative Study. *J. Sol-Gel Sci. Technol.* **1998**, *13*, 17–25.
- (229) Van der Schueren, L.; De Meyer, T.; Steyaert, I.; Ceylan, Ö.; Hemelsoet, K.; Van Speybroeck, V.; De Clerck, K. Polycaprolactone and Polycaprolactone/Chitosan Nanofibres Functionalised with the pH-Sensitive Dye Nitrazine Yellow. *Carbohydr. Polym.* **2013**, *91*, 284–293.
- (230) Van der Schueren, L.; Hemelsoet, K.; Van Speybroeck, V.; De Clerck, K. The Influence of a Polyamide Matrix on the Halochromic Behaviour of the pH-Sensitive Azo Dye Nitrazine Yellow. *Dyes Pigm.* **2012**, *94*, 443–451.
- (231) Sakurai, T.; Kurata, S.; Ogino, K. Development of a Novel Optical Sensing Method for Acid Solution Using Oil Red O Supported by Florisil. *Anal. Sci.* **2015**, *31*, 51–54.

- (232) Capel-Cuevas, S.; Cuéllar, M. P.; de Orbe-Payá, I.; Pegalajar, M. C.; Capitán-Vallvey, L. F. Full-Range Optical pH Sensor Based on Imaging Techniques. *Anal. Chim. Acta* **2010**, *681*, 71–81.
- (233) Capel-Cuevas, S.; Cuéllar, M. P.; de Orbe-Payá, I.; Pegalajar, M. C.; Capitán-Vallvey, L. F. Full-Range Optical pH Sensor Array Based on Neural Networks. *Microchem. J.* **2011**, *97*, 225–233.
- (234) Martínez-Olmos, A.; Capel-Cuevas, S.; López-Ruiz, N.; Palma, A. J.; de Orbe, I.; Capitán-Vallvey, L. F. Sensor Array-Based Optical Portable Instrument for Determination of pH. *Sens. Actuators, B* **2011**, *156*, 840–848.
- (235) Wong, L. S.; Brocklesby, W. S.; Bradley, M. Fibre Optic pH Sensors Employing Tethered Non-Fluorescent Indicators on Macroporous Glass. *Sens. Actuators, B* **2005**, *107*, 957–962.
- (236) Safavi, A.; Banazadeh, A. R. Dynamic Method as a Simple Approach for Wide Range pH Measurements Using Optodes. *Anal. Chim. Acta* **2007**, *583*, 326–331.
- (237) Mohr, G. J.; Müller, H. Tailoring Colour Changes of Optical Sensor Materials by Combining Indicator and Inert Dyes and Their Use in Sensor Layers, Textiles and Non-Wovens. *Sens. Actuators, B* **2015**, *206*, 788–793.
- (238) Mohr, G. J.; Müller, H.; Bussemer, B.; Stark, A.; Carofiglio, T.; Trupp, S.; Heuermann, R.; Henkel, T.; Escudero, D.; González, L. Design of Acidochromic Dyes for Facile Preparation of pH Sensor Layers. *Anal. Bioanal. Chem.* **2008**, *392*, 1411–1418.
- (239) Carofiglio, T.; Fregonese, C.; Mohr, G. J.; Rastrelli, F.; Tonellato, U. Optical Sensor Arrays: One-Pot, Multiparallel Synthesis and Cellulose Immobilization of pH and Metal Ion Sensitive Azo-Dyes. *Tetrahedron* **2006**, *62*, 1502–1507.
- (240) Liu, Z.; Liu, J.; Chen, T. Facile Synthesis, Characterization, and Potential Applications of Two Kinds of Polymeric pH Indicators: Phenolphthalein Formaldehyde Ando-Cresolphthalein Formaldehyde. *J. Polym. Sci., Part A: Polym. Chem.* **2005**, *43*, 1019–1027.
- (241) Agarwal, A.; Raheja, A.; Natarajan, T. S.; Chandra, T. S. Development of Universal pH Sensing Electrospun Nanofibers. *Sens. Actuators, B* **2012**, *161*, 1097–1101.
- (242) Zhang, L.; Li, Z.; Chang, R.; Chen, Y.; Zhang, W. Synthesis and Characterization of Novel Phenolphthalein Immobilized Halochromic Fiber. *React. Funct. Polym.* **2009**, *69*, 234–239.
- (243) Zhang, C.; Li, Y.; Wang, W.; Zhan, N.; Xiao, N.; Wang, S.; Li, Y.; Yang, Q. A Novel Two-Nozzle Electrospinning Process for Preparing Microfiber Reinforced pH-Sensitive Nano-Membrane with Enhanced Mechanical Property. *Eur. Polym. J.* **2011**, *47*, 2228–2233.
- (244) Liu, Z.; Luo, F.; Chen, T. Phenolphthalein Immobilized Membrane for an Optical pH Sensor. *Anal. Chim. Acta* **2004**, *510*, 189–194.
- (245) Kirkbright, G. F.; Narayanaswamy, R.; Welti, N. A. Studies with Immobilised Chemical Reagents Using a Flow-Cell for the Development of Chemically Sensitive Fibre-Optic Devices. *Analyst* **1984**, *109*, 15.
- (246) Islam, S.; Rahman, R. A.; Othaman, Z. B.; Riaz, S.; Naseem, S. Synthesis and Characterization of Multilayered Sol–Gel Based Plastic-Clad Fiber Optic pH Sensor. *J. Ind. Eng. Chem.* **2015**, *23*, 140–144.
- (247) Islam, S.; Bidin, N.; Riaz, S.; Rahman, R. A.; Naseem, S.; Marsin, F. M. Mesoporous SiO₂–TiO₂ Nanocomposite for pH Sensing. *Sens. Actuators, B* **2015**, *221*, 993–1002.
- (248) Islam, S.; Bidin, N.; Riaz, S.; Naseem, S.; Marsin, F. M. Correlation between Structural and Optical Properties of Surfactant Assisted Sol–Gel Based Mesoporous SiO₂–TiO₂ Hybrid Nanoparticles for pH Sensing/Optochemical Sensor. *Sens. Actuators, B* **2016**, *225*, 66–73.
- (249) Islam, S.; Bidin, N.; Riaz, S.; Naseem, S. Sol–Gel Based Phenolphthalein Encapsulated Heterogeneous Silica–Titania Optochemical pH Nanosensor. *J. Ind. Eng. Chem.* **2016**, *34*, 258–268.
- (250) Islam, S.; Bidin, N.; Riaz, S.; Naseem, S. Self-Assembled Hierarchical Phenolphthalein Encapsulated Silica Nanoparticles: Structural, Optical and Sensing Response. *Sens. Actuators, A* **2017**, *266*, 111–121.
- (251) Wong, L. S.; Birembaut, F.; Brocklesby, W. S.; Frey, J. G.; Bradley, M. Resin Bead Micro-UV–Visible Absorption Spectroscopy. *Anal. Chem.* **2005**, *77*, 2247–2251.
- (252) Allain, L. R.; Canada, T. A.; Xue, Z. Optical Sensors and the Salt Effect: A Dual-Transducer Approach to Acidity Determination in a Salt-Containing Concentrated Strong Acid. *Anal. Chem.* **2001**, *73*, 4592–4598.
- (253) Motellier, S.; Michels, M. H.; Duréault, B.; Toulhoat, P. Fiber-Optic pH Sensor for in Situ Applications. *Sens. Actuators, B* **1993**, *11*, 467–473.
- (254) Ismail, F.; Malins, C.; Goddard, N. J. Alkali Treatment of Dye-Doped Sol–Gel Glass Films for Rapid Optical pH Sensing. *Analyst* **2002**, *127*, 253–257.
- (255) Wu, S.; Cheng, W.; Qiu, Y.; Li, Z.; Shuang, S.; Dong, C. Fiber Optic pH Sensor Based on Mode-Filtered Light Detection. *Sens. Actuators, B* **2010**, *144*, 255–259.
- (256) Makote, R.; Collinson, M. M. Organically Modified Silicate Films for Stable pH Sensors. *Anal. Chim. Acta* **1999**, *394*, 195–200.
- (257) Lin, J.; Liu, D. An Optical pH Sensor with a Linear Response over a Broad Range. *Anal. Chim. Acta* **2000**, *408*, 49–55.
- (258) Zaggout, F. R. Encapsulation of Bromocresol Green pH Indicator into a Sol-Gel Matrix. *J. Dispersion Sci. Technol.* **2005**, *26*, 757–761.
- (259) Canada, T. A.; Allain, L. R.; Beach, D. B.; Xue, Z. High-Acidity Determination in Salt-Containing Acids by Optical Sensors. The Scope of a Dual-Transducer Approach and the Hammett Acidity Function. *Anal. Chem.* **2002**, *74*, 2535–2540.
- (260) Lee, S. T.; Gin, J.; Nampoori, V. P. N.; Vallabhan, C. P. G.; Unnikrishnan, N. V.; Radhakrishnan, P. A Sensitive Fibre Optic pH Sensor Using Multiple Sol-Gel Coatings. *J. Opt. A: Pure Appl. Opt.* **2001**, *3*, 355–359.
- (261) Ding, J. Y.; Shahriari, M. R.; Sigel, G. H. Fibre Optic pH Sensors Prepared by Sol-Gel Immobilisation Technique. *Electron. Lett.* **1991**, *27*, 1560–1562.
- (262) Thomas Lee, S.; Aneeshkumar, B.; Radhakrishnan, P.; Vallabhan, C.P.G.; Nampoori, V.P.N. A Microbent Fiber Optic pH Sensor. *Opt. Commun.* **2002**, *205*, 253–256.
- (263) Noroozifar, M.; Motlagh, M. K.; Bahmanzadeh, S.; Boroon, S. A Novel Optical Membrane with Extended Detection Range of pH. *Turk. J. Chem.* **2010**, *34*, 719–730.
- (264) Kowada, Y.; Ozeki, T.; Minami, T. Preparation of Silica-Gel Film with pH Indicators by the Sol-Gel Method. *J. Sol-Gel Sci. Technol.* **2005**, *33*, 175–185.
- (265) Motellier, S.; Toulhoat, P. Modified Acid-Base Behaviour of Resin-Bound pH Indicators. *Anal. Chim. Acta* **1993**, *271*, 323–329.
- (266) Yang, L.; Saavedra, S. S. Chemical Sensing Using Sol-Gel Derived Planar Waveguides and Indicator Phases. *Anal. Chem.* **1995**, *67*, 1307–1314.
- (267) Allain, L. R.; Sorasaene, K.; Xue, Z. Doped Thin-Film Sensors via a Sol–Gel Process for High-Acidity Determination. *Anal. Chem.* **1997**, *69*, 3076–3080.
- (268) Andreou, V. G.; Clonis, Y. D. A Portable Fiber-Optic Pesticide Biosensor Based on Immobilized Cholinesterase and Sol–Gel Entrapped Bromocresol Purple for in-Field Use. *Biosens. Bioelectron.* **2002**, *17*, 61–69.
- (269) El-Ashgar, N. M.; El-Basioni, A. I.; El-Nahhal, I. M.; Zourob, S. M.; El-Agez, T. M.; Taya, S. A. Sol-Gel Thin Films Immobilized with Bromocresol Purple pH-Sensitive Indicator in Presence of Surfactants. *ISRN Anal. Chem.* **2012**, *2012*, 1–11.
- (270) Polerecky, L.; Burke, C. S.; MacCraith, B. D. Optimization of Absorption-Based Optical Chemical Sensors That Employ a Single-Reflection Configuration. *Appl. Opt.* **2002**, *41*, 2879–2887.
- (271) Burke, C. S.; Polerecky, L.; MacCraith, B. D. Design and Fabrication of Enhanced Polymer Waveguide Platforms for Absorption-Based Optical Chemical Sensors. *Meas. Sci. Technol.* **2004**, *15*, 1140–1145.
- (272) Butler, T. M.; MacCraith, B. D.; McDonagh, C. M. Development of an Extended-Range Fiber Optic pH Sensor Using Evanescent Wave Absorption of Sol-Gel-Entrapped pH Indicators.

Proc. SPIE 2508, Chemical, Biochemical, and Environmental Fiber Sensors VII **1995**, 168–178.

(273) Andres, R. T.; Sevilla, F. Fibre-Optic Reflectometric Study on Acid–Base Equilibria of Immobilized Indicators: Effect of the Nature of Immobilizing Agents. *Anal. Chim. Acta* **1991**, *251*, 165–168.

(274) Morris, D.; Coyle, S.; Wu, Y.; Lau, K. T.; Wallace, G.; Diamond, D. Bio-Sensing Textile Based Patch with Integrated Optical Detection System for Sweat Monitoring. *Sens. Actuators, B* **2009**, *139*, 231–236.

(275) Sotomayor, P. T.; Raimundo, I. M., Jr; de Oliveira Neto, G.; de Oliveira, W. A. Evaluation of Fibre Optical Chemical Sensors for Flow Analysis Systems. *Sens. Actuators, B* **1998**, *51*, 382–390.

(276) Kostov, Y. V. Immobilized Bromophenol Blue as Sensing Element in Optical pH Sensor. *Sens. Actuators, B* **1992**, *8*, 99–101.

(277) Lee, J. E.; Saavedra, S. S. Evanescent Sensing in Doped Sol-Gel Glass Films. *Anal. Chim. Acta* **1994**, *285*, 265–269.

(278) Baldini, F.; Bracci, S.; Cosi, F.; Bechi, P.; Pucciani, F. Controlled-Pore Glasses Embedded in Plastic Optical Fibers for Gastric pH Sensing Purposes. *Appl. Spectrosc.* **1994**, *48*, 549–552.

(279) Butler, T. M.; MacCraith, B. D.; McDonagh, C. Leaching in Sol-Gel-Derived Silica Films for Optical pH Sensing. *J. Non-Cryst. Solids* **1998**, *224*, 249–258.

(280) Schyrr, B.; Pasche, S.; Scolan, E.; Ischer, R.; Ferrario, D.; Porchet, J.-A.; Voirin, G. Development of a Polymer Optical Fiber pH Sensor for On-Body Monitoring Application. *Sens. Actuators, B* **2014**, *194*, 238–248.

(281) Gupta, B. D.; Sharma, S. A Long-Range Fiber Optic pH Sensor Prepared by Dye Doped Sol-Gel Immobilization Technique. *Opt. Commun.* **1998**, *154*, 282–284.

(282) Gupta, B. D.; Sharma, N. K. Fabrication and Characterization of U-Shaped Fiber-Optic pH Probes. *Sens. Actuators, B* **2002**, *82*, 89–93.

(283) Dong, S.; Luo, M.; Peng, G.; Cheng, W. Broad Range pH Sensor Based on Sol–Gel Entrapped Indicators on Fibre Optic. *Sens. Actuators, B* **2008**, *129*, 94–98.

(284) Gupta, B. D.; Sharma, D. K. Evanescent Wave Absorption Based Fiber Optic pH Sensor Prepared by Dye Doped Sol-Gel Immobilization Technique. *Opt. Commun.* **1997**, *140*, 32–35.

(285) Netto, E. J.; Peterson, J. I.; McShane, M.; Hampshire, V. A Fiber-Optic Broad-Range pH Sensor System for Gastric Measurements. *Sens. Actuators, B* **1995**, *29*, 157–163.

(286) Li, W.; Cheng, H.; Xia, M.; Yang, K. An Experimental Study of pH Optical Sensor Using a Section of No-Core Fiber. *Sens. Actuators, A* **2013**, *199*, 260–264.

(287) Boisdé, G.; Sebillé, B. Co-Immobilization of Several Dyes on Optodes for pH Measurements; *Proc. SPIE 1510. Proc. SPIE* **1991**, *1510*, 80–94.

(288) Boisdé, G.; Biatry, B.; Magny, B.; Dureault, B.; Blanc, F.; Sebillé, B. Comparisons Between Two Dye-Immobilization Techniques On Optodes For The pH - Measurement By Absorption And Reflectance. *Proc. SPIE 1172, Chemical, Biochemical, and Environmental Fiber Sensors* **1990**, *1172*, 239–250.

(289) Boisdé, G.; Blanc, F.; Machuron-Mandard, X. pH Measurements with Dyes Co-Immobilization on Optodes: Principles and Associated Instrumentation. *Intern J. Optoelectr* **1991**, *6*, 407.

(290) Alabbas, S.; Ashworth, D.; Narayanaswamy, R. Design and Performance Features of an Optical-Fibre Reflectance pH Sensor. *Analytical Proceeding* **1989**, *26*, 373–380.

(291) Dybko, A.; Maciejewski, J.; Romaniuk, R. S.; Wroblewski, W. Colorimetric Sensor Based on Two Optical Fiber Couplers. In *Biochemical and Medical Sensors*; International Society for Optics and Photonics, 1994; Vol. 2085, pp 131–137.

(292) Takai, N.; Hirai, T.; Sakuma, I.; Fukui, Y.; Kaneko, A.; Fujie, T. Development of an Optical-Fibre Sensor Using a Functional Membrane. *Sens. Actuators, B* **1993**, *13*, 427–428.

(293) Belhadj Miled, O.; Grosso, D.; Sanchez, C.; Livage, J. An Optical Fibre pH Sensor Based on Dye Doped Mesostructured Silica. *J. Phys. Chem. Solids* **2004**, *65*, 1751–1755.

(294) El Nahhal, I. M.; Zourab, S. M.; Kodeh, F. S.; Qudaih, A. I. Thin Film Optical BTB pH Sensors Using Sol–Gel Method in Presence of Surfactants. *Int. Nano Lett.* **2012**, *2*, 16.

(295) Xie, X.; Suleiman, A. A.; Guilbault, G. G. A Urea Fiber Optic Biosensor Based on Absorption Measurement. *Anal. Lett.* **1990**, *23*, 2143–2153.

(296) Kim, J.; Cho, T. N.; Valdés-Ramírez, G.; Wang, J. A Wearable Fingernail Chemical Sensing Platform: pH Sensing at Your Fingertips. *Talanta* **2016**, *150*, 622–628.

(297) Dafu, C.; Qiang, C.; Jinghong, H.; Jinge, C.; Yating, L.; Zemin, Z. Optical-Fibre pH Sensor. *Sens. Actuators, B* **1993**, *12*, 29–32.

(298) Bacci, M.; Baldini, F.; Scheggi, A. M. Chemical Studies On Acid-Base Indicators For The Development Of An Extrinsic Optical Fiber pH Sensor. *Proc. SPIE 0990, Chemical, Biochemical, and Environmental Applications of Fibers* **1989**, *0990*, 84–87.

(299) Moreno, M. C.; Martinez, A.; Millan, P.; Camara, C. Study of a pH Sensitive Optical Fibre Sensor Based on the Use of Cresol Red. *J. Mol. Struct.* **1986**, *143*, 553–556.

(300) Cruz Moreno, M.; Jiménez, M.; Conde, C. P.; Cámara, C. Analytical Performance of an Optical pH Sensor for Acid-Base Titration. *Anal. Chim. Acta* **1990**, *230*, 35–40.

(301) Seki, A.; Katakura, H.; Kai, T.; Iga, M.; Watanabe, K. A Hetero-Core Structured Fiber Optic pH Sensor. *Anal. Chim. Acta* **2007**, *582*, 154–157.

(302) Safavi, A.; Maleki, N.; Rostamzadeh, A.; Maesum, S. CCD Camera Full Range pH Sensor Array. *Talanta* **2007**, *71*, 498–501.

(303) Abraham, E.; Markle, D. R.; Fink, S.; Ehrlich, H.; Tsang, M.; Smith, M.; Meyer, A. Continuous Measurement of Intravascular pH with a Fiberoptic Sensor. *Anesth. Analg.* **1985**, *64*, 731–736.

(304) Watson, R.; Markle, D.; Ro, Y.; Goldstein, S.; McGuire, D.; Peterson, J.; Patterson, R. Transmural pH Gradient in Canine Myocardial Ischemia. *Am. J. Physiol.-Heart Circ. Physiol.* **1984**, *246*, H232–H238.

(305) Markle, D.; McGuire, D.; Goldstein, S.; Patterson, R.; Watson, R. A pH Measurement System for Use in Tissue and Blood, Employing Miniature Fiber Optic Probes. In *Advances in Bioengineering*; American Society of Mechanical Engineers: New York, 1981, p 123.

(306) Serra, G.; Schirone, A.; Boniforti, R. Fibre-Optic pH Sensor for Sea-Water Monitoring Using a Single Dye. *Anal. Chim. Acta* **1990**, *232*, 337–344.

(307) Motellier, S.; Noiré, M. H.; Pitsch, H.; Duréault, B. pH Determination of Clay Interstitial Water Using a Fiber-Optic Sensor. *Sens. Actuators, B* **1995**, *29*, 345–352.

(308) Gauglitz, G.; Reichert, M. Spectral Investigation and Optimization of pH and Urea Sensors. *Sens. Actuators, B* **1992**, *6*, 83–86.

(309) Hao, T.; Xing, X.; Liu, C.-C. A pH Sensor Constructed with Two Types of Optical Fibers: The Configuration and the Initial Results. *Sens. Actuators, B* **1993**, *10*, 155–159.

(310) Liu, Z.; Liu, J.; Chen, T. Phenol Red Immobilized PVA Membrane for an Optical pH Sensor with Two Determination Ranges and Long-Term Stability. *Sens. Actuators, B* **2005**, *107*, 311–316.

(311) Baldini, F.; Giannetti, A.; Mencaglia, A. A. Optical Sensor for Interstitial pH Measurements. *J. Biomed. Opt.* **2007**, *12*, No. 024024.

(312) El-Nahhal, I. M.; Zourab, S. M.; Kodeh, F. S.; Al-Bawab, A. Behaviour of Phenol Red pH-Sensors in the Presence of Different Surfactants Using the Sol-Gel Process. *Int. J. Environ. Anal. Chem.* **2010**, *90*, 644–656.

(313) Chauhan, S. S.; Jasra, R. V.; Sharma, A. L. Phenol Red Dye Functionalized Nanostructured Silica Films as Optical Filters and pH Sensors. *Ind. Eng. Chem. Res.* **2012**, *51*, 10381–10389.

(314) El-Nahhal, I. M.; Livage, J.; Zourab, S. M.; Kodeh, F. S.; Al swarky, A. Entrapment of Phenol Red (PR) pH Indicator into Sol–Gel Matrix in Presence of Some Surfactants. *J. Sol-Gel Sci. Technol.* **2015**, *75*, 313–322.

(315) Rovati, L.; Fabbri, P.; Ferrari, L.; Pilati, F. Construction and Evaluation of a Disposable pH Sensor Based on a Large Core Plastic Optical Fiber. *Rev. Sci. Instrum.* **2011**, *82*, No. 023106.

(316) Islam, S.; Bidin, N.; Riaz, S.; Krishnan, G.; Naseem, S. Sol–Gel Based Fiber Optic pH Nanosensor: Structural and Sensing Properties. *Sens. Actuators, A* **2016**, *238*, 8–18.

- (317) Baker, M. E. J.; Narayanaswamy, R. The Modelling and Control of the pH Response of an Immobilised Indicator. *Sens. Actuators, B* **1995**, *29*, 368–373.
- (318) Takai, N.; Sakuma, I.; Fukui, Y.; Kaneko, A.; Fujie, T.; Taguchi, K.; Nagaoka, S. Studies of the Development of Optical Fiber Sensors for Biochemical Analysis. *Artif. Organs* **1991**, *15*, 86–89.
- (319) Kuswandi, B.; Narayanaswamy, R. Polymeric Encapsulated Membrane for Optrodes. *Fresenius' J. Anal. Chem.* **1999**, *364*, 605–607.
- (320) Rao, B. S.; Puschett, J. B.; Matyjaszewski, K. Preparation of pH Sensors by Covalent Linkage of Dye Molecules to the Surface of Polystyrene Optical Fibers. *J. Appl. Polym. Sci.* **1991**, *43*, 925–928.
- (321) Wang, E.; Chow, K.-F.; Kwan, V.; Chin, T.; Wong, C.; Bocarsly, A. Fast and Long Term Optical Sensors for pH Based on Sol–Gels. *Anal. Chim. Acta* **2003**, *495*, 45–50.
- (322) Safavi, A.; Sadeghi, M. Development of an Optode Membrane for High pH Values. *Spectrochim. Acta, Part A* **2007**, *66*, 575–577.
- (323) Noire, M. H.; Bouzon, C.; Coustou, L.; Gontier, J.; Marty, P.; Pouyat, D. Optical Sensing of High Acidity Using a Sol–Gel Entrapped Indicator. *Sens. Actuators, B* **1998**, *51*, 214–219.
- (324) Noiré, M. H.; Coustou, L.; Douarre, E.; Pouyat, D.; Bouzon, C.; Marty, P. A New Sol-Gel Derived Optical Fiber Sensor for High Acidity Measurements: Application in Nuclear Fuel Reprocessing. *J. Sol-Gel Sci. Technol.* **2000**, *17*, 131–136.
- (325) Safavi, A.; Bagheri, M. Novel Optical pH Sensor for High and Low pH Values. *Sens. Actuators, B* **2003**, *90*, 143–150.
- (326) Rivera, L.; Puyol, M.; Miltsov, S.; Alonso, J. New Hexamethine–Hemicyanine Dyes for the Development of Integrated Optochemical Sensors. *Anal. Bioanal. Chem.* **2007**, *387*, 2111–2119.
- (327) Puyol, M.; Miltsov, S.; Salinas, I.; Alonso, J. Ketocyanine Dyes: H⁺-Selective Ionophores for Use in Integrated Waveguides Absorbance Optodes. *Anal. Chem.* **2002**, *74*, 570–576.
- (328) Hisamoto, H.; Manabe, Y.; Yanai, H.; Tohma, H.; Yamada, T.; Suzuki, K. Molecular Design, Characterization, and Application of Multiinformation Dyes for Multidimensional Optical Chemical Sensings. 2. Preparation of the Optical Sensing Membranes for the Simultaneous Measurements of pH and Water Content in Organic Media. *Anal. Chem.* **1998**, *70*, 1255–1261.
- (329) Puyol, M.; Encinas, C.; Rivera, L.; Miltsov, S.; Alonso, J. Nortricarbocyanine Dyes as Suitable Long Wavelength pH Indicators for Chemical Sensing. *Sens. Actuators, B* **2007**, *122*, 53–59.
- (330) Igarashi, S.; Kuwae, K.; Yotsuyanagi, T. Optical pH Sensor of Electrostatically Immobilized Porphyrin on the Surface of Sulfonated-Polystyrene. *Anal. Sci.* **1994**, *10*, 821–822.
- (331) Khalil, G. E.; Daddario, P.; Lau, K. S. F.; Imtiaz, S.; King, M.; Gouterman, M.; Sidelev, A.; Puran, N.; Ghandehari, M.; Brückner, C. Meso-Tetraarylporpholactones as High pH Sensors. *Analyst* **2010**, *135*, 2125–2131.
- (332) Worlinsky, J. L.; Halepas, S.; Ghandehari, M.; Khalil, G.; Brückner, C. High pH Sensing with Water-Soluble Porpholactone Derivatives and Their Incorporation into a Nafion® Optode Membrane. *Analyst* **2015**, *140*, 190–196.
- (333) Liu, E.; Ghandehari, M.; Brückner, C.; Khalil, G.; Worlinsky, J.; Jin, W.; Sidelev, A.; Hyland, M. A. Mapping High pH Levels in Hydrated Calcium Silicates. *Cem. Concr. Res.* **2017**, *95*, 232–239.
- (334) Blair, T. L.; Allen, J. R.; Daunert, S.; Bachas, L. G. Potentiometric and Fiber Optic Sensors for pH Based on an Electropolymerized Cobalt Porphyrin. *Anal. Chem.* **1993**, *65*, 2155–2158.
- (335) Gulino, A.; Mineo, P.; Bazzano, S.; Vitalini, D.; Fragalà, I. Optical pH Meter by Means of a Porphyrin Monolayer Covalently Assembled on a Molecularly Engineered Silica Surface. *Chem. Mater.* **2005**, *17*, 4043–4045.
- (336) Gulino, A.; Mineo, P.; Scamporrino, E.; Vitalini, D.; Fragalà, I. Spectroscopic and Microscopic Characterization and Behavior of an Optical pH Meter Based on a Functional Hybrid Monolayer Molecular System: Porphyrin Molecules Covalently Assembled on a Molecularly Engineered Silica Surface. *Chem. Mater.* **2006**, *18*, 2404–2410.
- (337) Gulino, A.; Mineo, P.; Fragalà, I. Spectroscopic and Morphological Investigation of an Optical pH Meter Based on a Porphyrin Monolayer Covalently Assembled on a Engineered Silica Surface. *J. Phys. Chem. C* **2007**, *111*, 1373–1377.
- (338) Delmarre, D.; Méallet-Renault, R.; Bied-Charreton, C.; Pasternack, R. F. Incorporation of Water-Soluble Porphyrins in Sol–Gel Matrices and Application to pH Sensing. *Anal. Chim. Acta* **1999**, *401*, 125–128.
- (339) Umemura, T.; Hotta, H.; Abe, T.; Takahashi, Y.; Takiguchi, H.; Uehara, M.; Otake, T.; Tsunoda, K. Slab Optical Waveguide High-Acidity Sensor Based on an Absorbance Change of Protoporphyrin IX. *Anal. Chem.* **2006**, *78*, 7511–7516.
- (340) Veiga-Santos, P.; Ditchfield, C.; Tadini, C. C. Development and Evaluation of a Novel pH Indicator Biodegradable Film Based on Cassava Starch. *J. Appl. Polym. Sci.* **2011**, *120*, 1069–1079.
- (341) Yoshida, C. M. P.; Maciel, V. B. V.; Mendonça, M. E. D.; Franco, T. T. Chitosan Biobased and Intelligent Films: Monitoring pH Variations. *LWT - Food Sci. Technol.* **2014**, *55*, 83–89.
- (342) Abolghasemi, M. M.; Sobhi, M.; Piryaee, M. Preparation of a Novel Green Optical pH Sensor Based on Immobilization of Red Grape Extract on Bioorganic Agarose Membrane. *Sens. Actuators, B* **2016**, *224*, 391–395.
- (343) Zhang, X.; Lu, S.; Chen, X. A Visual pH Sensing Film Using Natural Dyes from Bauhinia Blakeana Dunn. *Sens. Actuators, B* **2014**, *198*, 268–273.
- (344) Kuswandi, B.; Jayus; Larasati, T. S.; Abdullah, A.; Heng, L. Y. Real-Time Monitoring of Shrimp Spoilage Using On-Package Sticker Sensor Based on Natural Dye of Curcumin. *Food Anal. Methods* **2012**, *5*, 881–889.
- (345) Giachet, F. T.; Vineis, C.; Sanchez Ramirez, D. O.; Carletto, R. A.; Varesano, A.; Mazzuchetti, G. Reversible and Washing Resistant Textile-Based Optical pH Sensors by Dyeing Fabrics with Curcuma. *Fibers Polym.* **2017**, *18*, 720–730.
- (346) Hashemi, P.; Zarjani, R. A.; Abolghasemi, M. M.; Olin, Å. Agarose Film Coated Glass Slides for Preparation of pH Optical Sensors. *Sens. Actuators, B* **2007**, *121*, 396–400.
- (347) Goicoechea, J.; Zamarreño, C. R.; Matías, I. R.; Arregui, F. J. Optical Fiber pH Sensors Based on Layer-by-Layer Electrostatic Self-Assembled Neutral Red. *Sens. Actuators, B* **2008**, *132*, 305–311.
- (348) Jeon, D.; Yoo, W. J.; Seo, J. K.; Shin, S. H.; Han, K.-T.; Kim, S. G.; Park, J.-Y.; Lee, B. Fiber-Optic pH Sensor Based on Sol–Gel Film Immobilized with Neutral Red. *Opt. Rev.* **2013**, *20*, 209–213.
- (349) Lehmann, H.; Schwotzer, G.; Czerney, P.; Mohr, G. J. Fiber-Optic pH Meter Using NIR Dye. *Sens. Actuators, B* **1995**, *29*, 392–400.
- (350) Koncki, R.; Wolfbeis, O. S. Composite Films of Prussian Blue and N-Substituted Polypyrrroles: Fabrication and Application to Optical Determination of pH. *Anal. Chem.* **1998**, *70*, 2544–2550.
- (351) Kuznetsov, V. V.; Yakunina, I. V. The Application of Specific Interaction Theory for Describing the Behaviour of Free and Immobilized Acid–Base Indicators. *Mendeleev Commun.* **1995**, *5*, 52–53.
- (352) Wang, H.; Liu, B.; Li, Z.; Yang, L. Multi-Wavelength Spectrophotometric Determination of pH Using Phenol Red–Doped Sol–Gel Film Sensors. *Spectrosc. Lett.* **2017**, *50*, 307–315.
- (353) Hochberg, S.; LaMer, V. K. Rate and Equilibrium Studies of Carbinol Formation in the Triphenylmethane and Sulphonphthalein Dyes. *J. Am. Chem. Soc.* **1941**, *63*, 3110–3120.
- (354) Mohr, G. J.; Werner, T.; Oehme, I.; Preininger, C.; Klimant, I.; Kovacs, B.; Wolfbeis, O. S. Novel Optical Sensor Materials Based on Solubilization of Polar Dyes in Apolar Polymers. *Adv. Mater.* **1997**, *9*, 1108–1113.
- (355) Klimant, I.; Wolfbeis, O. S. Oxygen-Sensitive Luminescent Materials Based on Silicone-Soluble Ruthenium Diimine Complexes. *Anal. Chem.* **1995**, *67*, 3160–3166.
- (356) Weigl, B. H.; Wolfbeis, O. S. New Hydrophobic Materials for Optical Carbon Dioxide Sensors Based on Ion Pairing. *Anal. Chim. Acta* **1995**, *302*, 249–254.
- (357) Wolfbeis, O. S.; Klimant, I.; Werner, T.; Huber, C.; Kosch, U.; Krause, C.; Neurauder, G.; Dürkop, A. Set of Luminescence Decay Time Based Chemical Sensors for Clinical Applications. *Sens. Actuators, B* **1998**, *51*, 17–24.

- (358) Zollinger, H. *Color Chemistry: Syntheses, Properties, and Applications of Organic Dyes and Pigments*, 3rd rev. ed.; Verlag Helvetica Chimica Acta, Wiley-VCH: Zürich, 2003.
- (359) Van der Schueren, L.; De Clerck, K. Coloration and Application of pH-Sensitive Dyes on Textile Materials: Coloration and Application of pH-Sensitive Dyes. *Color. Technol.* **2012**, *128*, 82–90.
- (360) Kassal, P.; Zubak, M.; Scheipl, G.; Mohr, G. J.; Steinberg, M. D.; Murković Steinberg, I. Smart Bandage with Wireless Connectivity for Optical Monitoring of pH. *Sens. Actuators, B* **2017**, *246*, 455–460.
- (361) Rastegarzadeh, S.; Moradpour, Z. Optical pH Sensor Based on Calcon Immobilization Membrane. *J. Iran. Chem. Soc.* **2009**, *6*, 858–862.
- (362) Hashemi, P.; Zarjani, R. A. A Wide Range pH Optical Sensor with Mixture of Neutral Red and Thionin Immobilized on an Agarose Film Coated Glass Slide. *Sens. Actuators, B* **2008**, *135*, 112–115.
- (363) Vishnoi, G.; Goel, T. C.; Pillai, P. K. C. pH Optrode for the Complete Working Range. *Proc. SPIE 3538, Process Monitoring with Optical Fibers and Harsh Environment Sensors* **1999**, 3538, 319.
- (364) Safavi, A.; Pakniat, M. Dipicyclamine-Modified Triacetylcellulose Membrane for Optical pH and Potassium Ion Measurement. *Anal. Chim. Acta* **1996**, *335*, 227–233.
- (365) Hazneci, C.; Ertekin, K.; Yenigul, B.; Cetinkaya, E. Optical pH Sensor Based on Spectral Response of Newly Synthesized Schiff Bases. *Dyes Pigm.* **2004**, *62*, 35–41.
- (366) Borchert, N. B.; Ponomarev, G. V.; Kerry, J. P.; Papkovsky, D. B. O₂/pH Multisensor Based on One Phosphorescent Dye. *Anal. Chem.* **2011**, *83*, 18–22.
- (367) Mishra, A.; Behera, R. K.; Behera, P. K.; Mishra, B. K.; Behera, G. B. Cyanines during the 1990s: A Review. *Chem. Rev.* **2000**, *100*, 1973–2012.
- (368) Sun, W.; Guo, S.; Hu, C.; Fan, J.; Peng, X. Recent Development of Chemosensors Based on Cyanine Platforms. *Chem. Rev.* **2016**, *116*, 7768–7817.
- (369) Zen, J. M.; Patonay, G. Near-Infrared Fluorescence Probe for pH Determination. *Anal. Chem.* **1991**, *63*, 2934–2938.
- (370) Hasanah, U.; Setyowati, M.; Efendi, R.; Muslem, M.; Md Sani, N. D.; Safitri, E.; Yook Heng, L.; Idroes, R. Preparation and Characterization of a Pectin Membrane-Based Optical pH Sensor for Fish Freshness Monitoring. *Biosensors* **2019**, *9*, 60.
- (371) Koncki, R.; Wolfbeis, O. S. Optical Chemical Sensing Based on Thin Films of Prussian Blue. *Sens. Actuators, B* **1998**, *51*, 355–358.
- (372) Koren, K.; Jensen, P. Ø.; Kühn, M. Development of a Rechargeable Optical Hydrogen Peroxide Sensor – Sensor Design and Biological Application. *Analyst* **2016**, *141*, 4332–4339.
- (373) Aigner, D.; Freunberger, S. A.; Wilkening, M.; Saf, R.; Borisov, S. M.; Klimant, I. Enhancing Photoinduced Electron Transfer Efficiency of Fluorescent pH-Probes with Halogenated Phenols. *Anal. Chem.* **2014**, *86*, 9293–9300.
- (374) Larsen, M.; Borisov, S. M.; Grunwald, B.; Klimant, I.; Glud, R. N. A Simple and Inexpensive High Resolution Color Ratiometric Planar Optode Imaging Approach: Application to Oxygen and pH Sensing. *Limnol. Oceanogr.: Methods* **2011**, *9*, 348–360.
- (375) Hulth, S.; Aller, R. C.; Engström, P.; Selander, E. A pH Plate Fluorosensor (Optode) for Early Diagenetic Studies of Marine Sediments. *Limnol. Oceanogr.* **2002**, *47*, 212–220.
- (376) Strömberg, N.; Mattsson, E.; Hakonen, A. An Imaging pH Optode for Cell Studies Based on Covalent Attachment of 8-Hydroxypyrene-1,3,6-Trisulfonate to Amino Cellulose Acetate Films. *Anal. Chim. Acta* **2009**, *636*, 89–94.
- (377) Zhu, Q.; Aller, R. C.; Fan, Y. High-Performance Planar pH Fluorosensor for Two-Dimensional pH Measurements in Marine Sediment and Water. *Environ. Sci. Technol.* **2005**, *39*, 8906–8911.
- (378) Hakonen, A.; Hulth, S.; Dufour, S. Analytical Performance during Ratiometric Long-Term Imaging of pH in Bioturbated Sediments. *Talanta* **2010**, *81*, 1393–1401.
- (379) Kermis, H. R.; Kostov, Y.; Rao, G. Rapid Method for the Preparation of a Robust Optical pH Sensor. *Analyst* **2003**, *128*, 1181–1186.
- (380) Kermis, H. R.; Kostov, Y.; Harms, P.; Rao, G. Dual Excitation Ratiometric Fluorescent pH Sensor for Noninvasive Bioprocess Monitoring: Development and Application. *Biotechnol. Prog.* **2002**, *18*, 1047–1053.
- (381) Kocincova, A. S.; Borisov, S. M.; Krause, C.; Wolfbeis, O. S. Fiber-Optic Microsensors for Simultaneous Sensing of Oxygen and pH, and of Oxygen and Temperature. *Anal. Chem.* **2007**, *79*, 8486–8493.
- (382) Borisov, S. M.; Herrod, D. L.; Klimant, I. Fluorescent Poly (Styrene-Block-Vinylpyrrolidone) Nanobeads for Optical Sensing of pH. *Sens. Actuators, B* **2009**, *139*, 52–58.
- (383) Wencel, D.; MacCraith, B. D.; McDonagh, C. High Performance Optical Ratiometric Sol–Gel-Based pH Sensor. *Sens. Actuators, B* **2009**, *139*, 208–213.
- (384) Stich, M. I. J.; Schaeferling, M.; Wolfbeis, O. S. Multicolor Fluorescent and Permeation-Selective Microbeads Enable Simultaneous Sensing of pH, Oxygen, and Temperature. *Adv. Mater.* **2009**, *21*, 2216–2220.
- (385) Nivens, D. A.; Schiza, M. V.; Angel, S. M. Multilayer Sol–Gel Membranes for Optical Sensing Applications: Single Layer pH and Dual Layer CO₂ and NH₃ Sensors. *Talanta* **2002**, *58*, 543–550.
- (386) Ge, X.; Kostov, Y.; Tolosa, L.; Rao, G. Study on Low-Cost Calibration-Free pH Sensing with Disposable Optical Sensors. *Anal. Chim. Acta* **2012**, *734*, 79–87.
- (387) Samuel, J.; Strinkovski, A.; Shalom, S.; Lieberman, K.; Ottolenghi, M.; Avnir, D.; Lewis, A. Miniaturization of Organically Doped Sol-Gel Materials: A Microns-Size Fluorescent pH Sensor. *Mater. Lett.* **1994**, *21*, 431–434.
- (388) Zhang, S.; Tanaka, S.; Wickramasinghe, Y.; Rolfe, P. Fibre-Optical Sensor Based on Fluorescent Indicator for Monitoring Physiological pH Values. *Med. Biol. Eng. Comput.* **1995**, *33*, 152–156.
- (389) Hakonen, A.; Hulth, S. A High-Performance Fluorosensor for pH Measurements between 6 and 9. *Talanta* **2010**, *80*, 1964–1969.
- (390) Borisov, S. M.; Mayr, T.; Klimant, I. Poly (Styrene-Block-Vinylpyrrolidone) Beads as a Versatile Material for Simple Fabrication of Optical Nanosensors. *Anal. Chem.* **2008**, *80*, 573–582.
- (391) Wencel, D.; Kaworek, A.; Abel, T.; Efremov, V.; Bradford, A.; Carthy, D.; Coady, G.; McMorrow, R. C. N.; McDonagh, C. Optical Sensor for Real-Time pH Monitoring in Human Tissue. *Small* **2018**, *14*, 1803627.
- (392) Duong, H. D.; Shin, Y.; Rhee, J. I. Development of Fluorescent pH Sensors Based on a Sol-Gel Matrix for Acidic and Neutral pH Ranges in a Microtiter Plate. *Microchem. J.* **2019**, *147*, 286–295.
- (393) Ulrich, S.; Osypova, A.; Panzarasa, G.; Rossi, R. M.; Bruns, N.; Boesel, L. F. Pyranine-Modified Amphiphilic Polymer Conetworks as Fluorescent Ratiometric pH Sensors. *Macromol. Rapid Commun.* **2019**, *40*, 1900360.
- (394) Ge, X.; Hanson, M.; Shen, H.; Kostov, Y.; Brorson, K. A.; Frey, D. D.; Moreira, A. R.; Rao, G. Validation of an Optical Sensor-Based High-Throughput Bioreactor System for Mammalian Cell Culture. *J. Biotechnol.* **2006**, *122*, 293–306.
- (395) Mohr, G. J.; Werner, T.; Wolfbeis, O. S. Application of a Novel Lipophilized Fluorescent Dye in an Optical Nitrate Sensor. *J. Fluoresc.* **1995**, *5*, 135–138.
- (396) Vasylevska, A. S.; Karasyov, A. A.; Borisov, S. M.; Krause, C. Novel Coumarin-Based Fluorescent pH Indicators, Probes and Membranes Covering a Broad pH Range. *Anal. Bioanal. Chem.* **2007**, *387*, 2131–2141.
- (397) Xu, Z.; Rollins, A.; Alcalá, R.; Marchant, R. E. A Novel Fiber-Optic pH Sensor Incorporating Carboxy SNAFL-2 and Fluorescent Wavelength-Ratiometric Detection. *J. Biomed. Mater. Res.* **1998**, *39*, 9–15.
- (398) Borisov, S. M.; Seifner, R.; Klimant, I. A Novel Planar Optical Sensor for Simultaneous Monitoring of Oxygen, Carbon Dioxide, pH and Temperature. *Anal. Bioanal. Chem.* **2011**, *400*, 2463–2474.
- (399) Grant, S. A.; Glass, R. S. A Sol–Gel Based Fiber Optic Sensor for Local Blood pH Measurements. *Sens. Actuators, B* **1997**, *45*, 35–42.
- (400) Bronk, K. S.; Michael, K. L.; Pantano, P.; Walt, D. R. Combined Imaging and Chemical Sensing Using a Single Optical Imaging Fiber. *Anal. Chem.* **1995**, *67*, 2750–2757.

- (401) Duong, H. D.; Sohn, O.-J.; Lam, H. T.; Rhee, J. I. An Optical pH Sensor with Extended Detection Range Based on Fluoresceinamine Covalently Bound to Sol–Gel Support. *Microchem. J.* **2006**, *84*, 50–55.
- (402) Chen, H.; Wang, X.; Song, X.; Zhou, T.; Jiang, Y.; Chen, X. Colorimetric Optical pH Sensor Production Using a Dual-Color System. *Sens. Actuators, B* **2010**, *146*, 278–282.
- (403) Manyam, U.; Shahriari, M. R.; Morris, M. J. *Complete Spectrum Fiber Optic pH Sensor Based on a Novel Fluorescent Indicator Doped Porous Sol-Gel Material*; International Society for Optics and Photonics, 1999; Vol. 3540, pp 10–19.
- (404) Burns, A.; Sengupta, P.; Zedayko, T.; Baird, B.; Wiesner, U. Core/Shell Fluorescent Silica Nanoparticles for Chemical Sensing: Towards Single-Particle Laboratories. *Small* **2006**, *2*, 723–726.
- (405) Allard, E.; Larpent, C. Core-Shell Type Dually Fluorescent Polymer Nanoparticles for Ratiometric pH-Sensing. *J. Polym. Sci., Part A: Polym. Chem.* **2008**, *46*, 6206–6213.
- (406) Medina-Castillo, A. L.; Fernandez-Sanchez, J. F.; Segura-Carretero, A.; Fernandez-Gutierrez, A. Design and Synthesis by ATRP of Novel, Water-Insoluble, Lineal Copolymers and Their Application in the Development of Fluorescent and pH-Sensing Nanofibres Made by Electrospinning. *J. Mater. Chem.* **2011**, *21*, 6742–6750.
- (407) Ferrero Martín, F. J.; Campo Rodríguez, J. C.; Alvarez Anton, J. C.; Viera Perez, J. C.; Sánchez-Barragán, I.; Costa-Fernández, J. M.; Sanz-Medel, A. Design of a Low-Cost Optical Instrument for pH Fluorescence Measurements. *IEEE Trans. Instrum. Meas.* **2006**, *55*, 1215–1221.
- (408) Tan, W.; Shi, Z. Y.; Kopelman, R. Development of Submicron Chemical Fiber Optic Sensors. *Anal. Chem.* **1992**, *64*, 2985–2990.
- (409) Ferrari, L.; Rovati, L.; Fabbri, P.; Pilati, F. Disposable Fluorescence Optical pH Sensor for near Neutral Solutions. *Sensors* **2013**, *13*, 484–499.
- (410) Wu, S.; Li, Z.; Han, J.; Han, S. Dual Colored Mesoporous Silica Nanoparticles with pH Activable Rhodamine-Lactam for Ratiometric Sensing of Lysosomal Acidity. *Chem. Commun.* **2011**, *47*, 11276.
- (411) Nielsen, L. J.; Eyley, S.; Thielemans, W.; Aylott, J. W. Dual Fluorescent Labelling of Cellulose Nanocrystals for pH Sensing. *Chem. Commun.* **2010**, *46*, 8929–8931.
- (412) Millar, D.; Henderson, R.; Keeper, A. Electrochemical Immobilization of a pH Sensitive Fluorescein Derivative: Synthesis and Characterization of a Fluorescein-Derivatized Polythiophene. *Chem. Commun.* **1998**, No. 4, 477–478.
- (413) Shi, W.; He, S.; Wei, M.; Evans, D. G.; Duan, X. Optical pH Sensor with Rapid Response Based on a Fluorescein-intercalated Layered Double Hydroxide. *Adv. Funct. Mater.* **2010**, *20*, 3856–3863.
- (414) Lobnik, A.; Oehme, I.; Murkovic, I.; Wolfbeis, O. S. pH Optical Sensors Based on Sol–Gels: Chemical Doping versus Covalent Immobilization. *Anal. Chim. Acta* **1998**, *367*, 159–165.
- (415) Bradley, M.; Alexander, L.; Duncan, K.; Chennaoui, M.; Jones, A. C.; Sánchez-Martín, R. M. pH Sensing in Living Cells Using Fluorescent Microspheres. *Bioorg. Med. Chem. Lett.* **2008**, *18*, 313–317.
- (416) Aslan, K.; Lakowicz, J. R.; Szmajnski, H.; Geddes, C. D. Enhanced Ratiometric pH Sensing Using SNAFL-2 on Silver Island Films: Metal-Enhanced Fluorescence Sensing. *J. Fluoresc.* **2005**, *15*, 37–40.
- (417) Healey, B. G.; Walt, D. R. Fast Temporal Response Fiber-Optic Chemical Sensors Based on the Photodeposition of Micrometer-Scale Polymer Arrays. *Anal. Chem.* **1997**, *69*, 2213–2216.
- (418) Thompson, R. B.; Lakowicz, J. R. Fiber Optic pH Sensor Based on Phase Fluorescence Lifetimes. *Anal. Chem.* **1993**, *65*, 853–856.
- (419) Ji, J.; Rosenzweig, Z. Fiber Optic pH/Ca²⁺ Fluorescence Microsensor Based on Spectral Processing of Sensing Signals. *Anal. Chim. Acta* **1999**, *397*, 93–102.
- (420) Kuwana, E.; Liang, F.; Sevick-Muraca, E. M. Fluorescence Lifetime Spectroscopy of a pH-sensitive Dye Encapsulated in Hydrogel Beads. *Biotechnol. Prog.* **2004**, *20*, 1561–1566.
- (421) Panova, A. A.; Pantano, P.; Walt, D. R. In Situ Fluorescence Imaging of Localized Corrosion with a pH-Sensitive Imaging Fiber. *Anal. Chem.* **1997**, *69*, 1635–1641.
- (422) Grant, S. A.; Bettencourt, K.; Krulevitch, P.; Hamilton, J.; Glass, R. In Vitro and In Vivo Measurements of Fiber Optic and Electrochemical Sensors to Monitor Brain Tissue pH. *Sens. Actuators, B* **2001**, *72*, 174–179.
- (423) Vasylevska, G. S.; Borisov, S. M.; Krause, C.; Wolfbeis, O. S. Indicator-Loaded Permeation-Selective Microbeads for Use in Fiber Optic Simultaneous Sensing of pH and Dissolved Oxygen. *Chem. Mater.* **2006**, *18*, 4609–4616.
- (424) Hoefler, C.; Santner, J.; Borisov, S. M.; Wenzel, W. W.; Puschenreiter, M. Integrating Chemical Imaging of Cationic Trace Metal Solutes and pH into a Single Hydrogel Layer. *Anal. Chim. Acta* **2017**, *950*, 88–97.
- (425) Schreml, S.; Meier, R. J.; Kirschbaum, M.; Kong, S. C.; Gehmert, S.; Felthaus, O.; Kuchler, S.; Sharpe, J. R.; Wöltje, K.; Weiß, K. T.; Albert, M.; Seidl, U.; Schröder, J.; Morsczeck, C.; Prantl, L.; Duschl, C.; Pedersen, S. F.; Gosau, M.; Berneburg, M.; Wolfbeis, O. S.; Landthaler, M.; Babilas, P. Luminescent Dual Sensors Reveal Extracellular pH-Gradients and Hypoxia on Chronic Wounds That Disrupt Epidermal Repair. *Theranostics* **2014**, *4*, 721–735.
- (426) Carrillo-Carrion, C.; Parak, W. J. Multiplexed Fluorophore–Nanoparticle Hybrids for Extending the Range of pH Measurements. *Small Methods* **2017**, *1*, 1700153.
- (427) Clark, H. A.; Kopelman, R.; Tjalkens, R.; Philbert, M. A. Optical Nanosensors for Chemical Analysis inside Single Living Cells. 2. Sensors for pH and Calcium and the Intracellular Application of PEBBLE Sensors. *Anal. Chem.* **1999**, *71*, 4837–4843.
- (428) Yang, Q.; Wang, H.; Lan, X.; Cheng, B.; Chen, S.; Shi, H.; Xiao, H.; Ma, Y. Reflection-Mode Micro-Spherical Fiber-Optic Probes for in Vitro Real-Time and Single-Cell Level pH Sensing. *Sens. Actuators, B* **2015**, *207*, 571–580.
- (429) Ferguson, J. A.; Healey, B. G.; Bronk, K. S.; Barnard, S. M.; Walt, D. R. Simultaneous Monitoring of pH, CO₂ and O₂ Using an Optical Imaging Fiber. *Anal. Chim. Acta* **1997**, *340*, 123–131.
- (430) Rudolph, N.; Voss, S.; Moradi, A. B.; Nagl, S.; Oswald, S. E. Spatio-Temporal Mapping of Local Soil pH Changes Induced by Roots of Lupin and Soft-Rush. *Plant Soil* **2013**, *369*, 669–680.
- (431) Plaschke, M.; Czolk, R.; Reichert, J.; Ache, H. J. Stability Improvement of Optochemical Sol-Gel Film Sensors by Immobilisation of Dye-Labeled Dextran. *Thin Solid Films* **1996**, *279*, 233–235.
- (432) Cajlakovic, M.; Lobnik, A.; Werner, T. Stability of New Optical pH Sensing Material Based on Cross-Linked Poly(Vinyl Alcohol) Copolymer. *Anal. Chim. Acta* **2002**, *455*, 207–213.
- (433) Clark, H. A.; Barker, S. L.; Brasuel, M.; Miller, M. T.; Monson, E.; Parus, S.; Shi, Z.-Y.; Song, A.; Thorsrud, B.; Kopelman, R.; et al. Subcellular Optochemical Nanobiosensors: Probes Encapsulated by Biologically Localised Embedding (PEBBLEs). *Sens. Actuators, B* **1998**, *51*, 12–16.
- (434) Sanchez-Barragan, I.; Costa-Fernandez, J.; Sanz-Medel, A. Tailoring the pH Response Range of Fluorescent-Based pH Sensing Phases by Sol–Gel Surfactants Co-Immobilization. *Sens. Actuators, B* **2005**, *107*, 69–76.
- (435) Schröder, C. R.; Polerecky, L.; Klimant, I. Time-Resolved pH/PO₂ Mapping with Luminescent Hybrid Sensors. *Anal. Chem.* **2007**, *79*, 60–70.
- (436) Doussineau, T.; Smaïhi, M.; Mohr, G. J. Two-Dye Core/Shell Zeolite Nanoparticles: A New Tool for Ratiometric pH Measurements. *Adv. Funct. Mater.* **2009**, *19*, 117–122.
- (437) Kiryukhin, M. V.; Lau, H. H.; Goh, S. H.; Teh, C.; Korzh, V.; Sadovoy, A. A Membrane Film Sensor with Encapsulated Fluorescent Dyes towards Express Freshness Monitoring of Packaged Food. *Talanta* **2018**, *182*, 187–192.
- (438) Kenney, R. M.; Boyce, M. W.; Whitman, N. A.; Kromhout, B. P.; Lockett, M. R. A pH-Sensing Optode for Mapping Spatiotemporal Gradients in 3D Paper-Based Cell Cultures. *Anal. Chem.* **2018**, *90*, 2376–2383.
- (439) Hornig, S.; Biskup, C.; Gräfe, A.; Wotschadlo, J.; Liebert, T.; Mohr, G. J.; Heinze, T. Biocompatible Fluorescent Nanoparticles for pH-Sensing. *Soft Matter* **2008**, *4*, 1169–1172.

- (440) van Graft, M.; Oosterhuis, B.; van der Werf, K. O.; de Grooth, B. G.; Greve, J. A Simple Optical Fiber Device for Quantitative Fluorescence Microscopy of Single Living Cells. *J. Immunol. Methods* **1993**, *159*, 145–151.
- (441) Meier, R. J.; Schreml, S.; Wang, X.; Landthaler, M.; Babilas, P.; Wolfbeis, O. S. Simultaneous Photographing of Oxygen and pH In Vivo Using Sensor Films. *Angew. Chem., Int. Ed.* **2011**, *50*, 10893–10896.
- (442) Nivens, D. A.; Zhang, Y.; Angel, S. M. A Fiber-Optic pH Sensor Prepared Using a Base-Catalyzed Organo-Silica Sol–Gel. *Anal. Chim. Acta* **1998**, *376*, 235–245.
- (443) Choudhary, S.; Joshi, B.; Pandey, G.; Joshi, A. Application of Single and Dual Fluorophore-Based pH Sensors for Determination of Milk Quality and Shelf Life Using a Fibre Optic Spectrophotometer. *Sens. Actuators, B* **2019**, *298*, 126925.
- (444) Whitaker, J.; Haugland, R.; Prendergast, F. Seminaphtho-Fluoresceins and Seminaphtho-Rhodafuors—Dual Fluorescence pH Indicators. *Biophys. J.* **1988**, *53*, 197.
- (445) Whitaker, J. E.; Haugland, R. P.; Prendergast, F. G. Spectral and Photophysical Studies of Benzo[c]Xanthene Dyes: Dual Emission pH Sensors. *Anal. Biochem.* **1991**, *194*, 330–344.
- (446) Klonis, N.; Sawyer, W. H. Spectral Properties of the Prototropic Forms of Fluorescein in Aqueous Solution. *J. Fluoresc.* **1996**, *6*, 147–157.
- (447) Legrum, W. Influence of the Degree, Position and Nature of the Halide Substitution on the Rate of Photobleaching of Xanthene Dyes. In *Recent Developments in Toxicology: Trends, Methods and Problems*; Chambers, P. L., Chambers, C. M., Wiezorek, W. D., Golbs, S., Eds.; Springer: Berlin, 1991; Vol. 14, pp 298–302.
- (448) Kang, E.-H.; Ham, J.-K.; Shim, J.-M.; Lee, J.-K.; Kim, M.-R. Applications of pH Sensor Using a Covalent Bond Indicator Based on Containing Functional Group Copolymer. *Mol. Cryst. Liq. Cryst.* **2006**, *445*, 285–275.
- (449) Walt, D. R. Fiber Optic Imaging Sensors. *Acc. Chem. Res.* **1998**, *31*, 267–278.
- (450) Huang, S.-H.; Huang, K.-S.; Liou, Y.-M. Simultaneous Monitoring of Oxygen Consumption and Acidification Rates of a Single Zebrafish Embryo during Embryonic Development within a Microfluidic Device. *Microfluid. Nanofluid.* **2017**, *21*, 3.
- (451) Beija, M.; Afonso, C. A. M.; Martinho, J. M. G. Synthesis and Applications of Rhodamine Derivatives as Fluorescent Probes. *Chem. Soc. Rev.* **2009**, *38*, 2410.
- (452) Koide, Y.; Urano, Y.; Hanaoka, K.; Terai, T.; Nagano, T. Evolution of Group 14 Rhodamines as Platforms for Near-Infrared Fluorescence Probes Utilizing Photoinduced Electron Transfer. *ACS Chem. Biol.* **2011**, *6*, 600–608.
- (453) Zhou, K.; Wang, Y.; Huang, X.; Luby-Phelps, K.; Sumer, B. D.; Gao, J. Tunable, Ultrasensitive pH-Responsive Nanoparticles Targeting Specific Endocytic Organelles in Living Cells. *Angew. Chem., Int. Ed.* **2011**, *50*, 6109–6114.
- (454) Yuan, L.; Lin, W.; Feng, Y. A Rational Approach to Tuning the PKA Values of Rhodamines for Living Cell Fluorescence Imaging. *Org. Biomol. Chem.* **2011**, *9*, 1723–1726.
- (455) Li, Z.; Wu, S.; Han, J.; Han, S. Imaging of Intracellular Acidic Compartments with a Sensitive Rhodamine Based Fluorogenic pH Sensor. *Analyst* **2011**, *136*, 3698–3706.
- (456) Best, Q. A.; Xu, R.; McCarroll, M. E.; Wang, L.; Dyer, D. J. Design and Investigation of a Series of Rhodamine-Based Fluorescent Probes for Optical Measurements of pH. *Org. Lett.* **2010**, *12*, 3219–3221.
- (457) Zhang, W.; Tang, B.; Liu, X.; Liu, Y.; Xu, K.; Ma, J.; Tong, L.; Yang, G. A Highly Sensitive Acidic pH Fluorescent Probe and Its Application to HepG2 Cells. *Analyst* **2009**, *134*, 367–371.
- (458) Kim, H. N.; Lee, M. H.; Kim, H. J.; Kim, J. S.; Yoon, J. A New Trend in Rhodamine-Based Chemosensors: Application of Spirolactam Ring-Opening to Sensing Ions. *Chem. Soc. Rev.* **2008**, *37*, 1465–1472.
- (459) Di Paolo, M.; Roberti, M. J.; Bordoni, A. V.; Aramendía, P. F.; Wolosiuk, A.; Bossi, M. L. Nanoporous Silica Nanoparticles Functionalized with a Fluorescent Turn-on Spirorhodamineamide as pH Indicators. *Photochem. Photobiol. Sci.* **2019**, *18*, 155–165.
- (460) Taweetanavanich, T.; Wann, B.; Tuntulani, T.; Pulpoka, B.; Kaewtong, C. A pH Optical and Fluorescent Sensor Based on Rhodamine Modified on Activated Cellulose Paper. *J. Chin. Chem. Soc.* **2019**, *66*, 493–499.
- (461) Stratton, S. G.; Taumoefolau, G. H.; Purnell, G. E.; Rasooly, M.; Czaplinski, W. L.; Harbron, E. J. Tuning the pK_a of Fluorescent Rhodamine pH Probes through Substituent Effects. *Chem. - Eur. J.* **2017**, *23*, 14064–14072.
- (462) Yu, K.-K.; Li, K.; Hou, J.-T.; Yang, J.; Xie, Y.-M.; Yu, X.-Q. Rhodamine Based pH-Sensitive “Intelligent” Polymers as Lysosome Targeting Probes and Their Imaging Applications in Vivo. *Polym. Chem.* **2014**, *5*, 5804–5812.
- (463) Ma, Q.-J.; Li, H.-P.; Yang, F.; Zhang, J.; Wu, X.-F.; Bai, Y.; Li, X.-F. A Fluorescent Sensor for Low pH Values Based on a Covalently Immobilized Rhodamine–Naphthalimide Conjugate. *Sens. Actuators, B* **2012**, *166–167*, 68–74.
- (464) Li, Z.-Z.; Niu, C.-G.; Zeng, G.-M.; Liu, Y.-G.; Gao, P.-F.; Huang, G.-H.; Mao, Y.-A. A Novel Fluorescence Ratiometric pH Sensor Based on Covalently Immobilized Piperazinyl –1,8 -Naphthalimide and Benzothioxanthene. *Sens. Actuators, B* **2006**, *114*, 308–315.
- (465) Wang, X.-Y.; Huang, D.-W.; Niu, C.-G.; Guo, L.-J.; Cui, J.-J.; Hu, L.-Y.; Zeng, G.-M. An Internal Reference Fluorescent pH Sensor with Two pH-Sensitive Fluorophores Carrier. *Sens. Actuators, B* **2016**, *234*, 593–601.
- (466) Qi, J.; Liu, D.; Liu, X.; Guan, S.; Shi, F.; Chang, H.; He, H.; Yang, G. Fluorescent pH Sensors for Broad-Range pH Measurement Based on a Single Fluorophore. *Anal. Chem.* **2015**, *87*, 5897–5904.
- (467) Tian, Y.; Su, F.; Weber, W.; Nandakumar, V.; Shumway, B. R.; Jin, Y.; Zhou, X.; Holl, M. R.; Johnson, R. H.; Meldrum, D. R. A Series of Naphthalimide Derivatives as Intra and Extracellular pH Sensors. *Biomaterials* **2010**, *31*, 7411–7422.
- (468) Jin, W.; Wu, L.; Song, Y.; Jiang, J.; Zhu, X.; Yang, D.; Bai, C. Continuous Intra-Arterial Blood pH Monitoring by a Fiber-Optic Fluorosensor. *IEEE Trans. Biomed. Eng.* **2011**, *58*, 1232–1238.
- (469) Kriltz, A.; Löser, C.; Mohr, G. J.; Trupp, S. Covalent Immobilization of a Fluorescent pH-Sensitive Naphthalimide Dye in Sol–Gel Films. *J. Sol-Gel Sci. Technol.* **2012**, *63*, 23–29.
- (470) Niu, C.-G.; Zeng, G.-M.; Chen, L.-X.; Shen, G.-L.; Yu, R.-Q. Proton “off-on” Behaviour of Methylpiperazinyl Derivative of Naphthalimide: A pH Sensor Based on Fluorescence Enhancement. *Analyst* **2004**, *129*, 20–24.
- (471) Doussineau, T.; Trupp, S.; Mohr, G. J. Ratiometric pH-Nanosensors Based on Rhodamine-Doped Silica Nanoparticles Functionalized with a Naphthalimide Derivative. *J. Colloid Interface Sci.* **2009**, *339*, 266–270.
- (472) Wan, X.; Wang, D.; Liu, S. Fluorescent pH-Sensing Organic/Inorganic Hybrid Mesoporous Silica Nanoparticles with Tunable Redox-Responsive Release Capability. *Langmuir* **2010**, *26*, 15574–15579.
- (473) Trupp, S.; Hoffmann, P.; Henkel, T.; Mohr, G. J. Novel pH Indicator Dyes for Array Preparation via NHS Ester Activation or Solid-Phase Organic Synthesis. *Org. Biomol. Chem.* **2008**, *6*, 4319–4322.
- (474) Gunnlaugsson, T.; McCoy, C. P.; Morrow, R. J.; Phelan, C.; Stomeo, F. Towards the Development of Controllable and Reversible ‘on-off’ Luminescence Switching in Soft-Matter; Synthesis and Spectroscopic Investigation of 1, 8-Naphthalimide-Based PET (Photo-induced Electron Transfer) Chemosensors for pH in Water-Permeable Hydrogels. *Arkivoc* **2003**, *7*, 216–228.
- (475) Grabchev, I.; Qian, X.; Xiao, Y.; Zhang, R. Novel Heterogeneous PET Fluorescent Sensors Selective for Transition Metal Ions or Protons: Polymers Regularly Labelled with Naphthalimide. *New J. Chem.* **2002**, *26*, 920–925.
- (476) Tian, H.; Gan, J.; Chen, K.; He, J.; Song, Q. L.; Hou, X. Y. Positive and Negative Fluorescent Imaging Induced by Naphthalimide Polymers. *J. Mater. Chem.* **2002**, *12*, 1262–1267.
- (477) Jacquemin, D.; Perpète, E. A.; Scalmani, G.; Ciofini, I.; Peltier, C.; Adamo, C. Absorption and Emission Spectra of 1, 8-Naphthalimide Fluorophores: A PCM-TD-DFT Investigation. *Chem. Phys.* **2010**, *372*, 61–66.

- (478) Duke, R. M.; Veale, E. B.; Pfeiffer, F. M.; Kruger, P. E.; Gunnlaugsson, T. Colorimetric and Fluorescent Anion Sensors: An Overview of Recent Developments in the Use of 1,8-Naphthalimide-Based Chemosensors. *Chem. Soc. Rev.* **2010**, *39*, 3936–3953.
- (479) Mohr, G. J. Synthesis of Naphthalimide-Based Indicator Dyes with a 2-Hydroxyethylsulfanyl Function for Covalent Immobilisation to Cellulose. *Sens. Actuators, B* **2018**, *275*, 439–445.
- (480) Al Kobaisi, M.; Bhosale, S. V.; Latham, K.; Raynor, A. M.; Bhosale, S. V. Functional Naphthalene Diimides: Synthesis, Properties, and Applications. *Chem. Rev.* **2016**, *116*, 11685–11796.
- (481) Shen, L.; Lu, X.; Tian, H.; Zhu, W. A Long Wavelength Fluorescent Hydrophilic Copolymer Based on Naphthalenediimide as pH Sensor with Broad Linear Response Range. *Macromolecules* **2011**, *44*, 5612–5618.
- (482) Aigner, D.; Dmitriev, R. I.; Borisov, S. M.; Papkovsky, D. B.; Klimant, I. pH-Sensitive Perylene Bisimide Probes for Live Cell Fluorescence Lifetime Imaging. *J. Mater. Chem. B* **2014**, *2*, 6792–6801.
- (483) Pfeifer, D.; Klimant, I.; Borisov, S. M. Ultrabright Red-Emitting Photostable Perylene Bisimide Dyes: New Indicators for Ratiometric Sensing of High pH or Carbon Dioxide. *Chem. - Eur. J.* **2018**, *24*, 10711–10720.
- (484) Würthner, F.; Stepanenko, V.; Chen, Z.; Saha-Möller, C. R.; Kocher, N.; Stalke, D. Preparation and Characterization of Regioisomerically Pure 1,7-Disubstituted Perylene Bisimide Dyes. *J. Org. Chem.* **2004**, *69*, 7933–7939.
- (485) Loudet, A.; Burgess, K. BODIPY Dyes and Their Derivatives: Syntheses and Spectroscopic Properties. *Chem. Rev.* **2007**, *107*, 4891–4932.
- (486) Boens, N.; Leen, V.; Dehaen, W. Fluorescent Indicators Based on BODIPY. *Chem. Soc. Rev.* **2012**, *41*, 1130–1172.
- (487) Wood, T. E.; Thompson, A. Advances in the Chemistry of Dipyrrins and Their Complexes. *Chem. Rev.* **2007**, *107*, 1831–1861.
- (488) Loudet, A.; Burgess, K. BODIPY Dyes and Their Derivatives: Syntheses and Spectroscopic Properties. In *Handbook of Porphyrin Science*, Vol. 8; World Scientific Publishing Company, 2010; Vol. 10, pp 1–164.
- (489) Kowada, T.; Maeda, H.; Kikuchi, K. BODIPY-Based Probes for the Fluorescence Imaging of Biomolecules in Living Cells. *Chem. Soc. Rev.* **2015**, *44*, 4953–4972.
- (490) Ni, Y.; Wu, J. Far-Red and near Infrared BODIPY Dyes: Synthesis and Applications for Fluorescent pH Probes and Bio-Imaging. *Org. Biomol. Chem.* **2014**, *12*, 3774–3791.
- (491) Baki, C. N.; Akkaya, E. U. Boradiazaindacene-Appended Calix [4] Arene: Fluorescence Sensing of pH near Neutrality. *J. Org. Chem.* **2001**, *66*, 1512–1513.
- (492) Baruah, M.; Qin, W.; Basarić, N.; De Borggraave, W. M.; Boens, N. BODIPY-Based Hydroxyaryl Derivatives as Fluorescent pH Probes. *J. Org. Chem.* **2005**, *70*, 4152–4157.
- (493) Gareis, T.; Huber, C.; Wolfbeis, O. S.; Daub, J. Phenol/Phenolate-Dependent on/off Switching of the Luminescence of 4,4-Difluoro-4-Bora-3a,4a-Diaza-s-Indacenes. *Chem. Commun.* **1997**, No. 18, 1717–1718.
- (494) Tian, M.; Peng, X.; Feng, F.; Meng, S.; Fan, J.; Sun, S. Fluorescent pH Probes Based on Boron Dipyrromethene Dyes. *Dyes Pigm.* **2009**, *81*, 58–62.
- (495) Qin, W.; Baruah, M.; De Borggraave, W. M.; Boens, N. Photophysical Properties of an on/off Fluorescent pH Indicator Excitable with Visible Light Based on a Borondipyrromethene-Linked Phenol. *J. Photochem. Photobiol., A* **2006**, *183*, 190–197.
- (496) Qin, W.; Baruah, M.; Stefan, A.; Van der Auweraer, M.; Boens, N. Photophysical Properties of BODIPY-Derived Hydroxyaryl Fluorescent pH Probes in Solution. *ChemPhysChem* **2005**, *6*, 2343–2351.
- (497) Bartelmess, J.; Weare, W. W.; Latortue, N.; Duong, C.; Jones, D. S. Meso-Pyridyl BODIPYs with Tunable Chemical, Optical and Electrochemical Properties. *New J. Chem.* **2013**, *37*, 2663–2668.
- (498) Rurack, K.; Kollmannsberger, M.; Daub, J. A Highly Efficient Sensor Molecule Emitting in the near Infrared (NIR): 3,5-Distyryl-8-(p-Dimethylaminophenyl)Difluoroboradiazas-Indacene. *New J. Chem.* **2001**, *25*, 289–292.
- (499) Zhang, J.; Yang, M.; Li, C.; Dorh, N.; Xie, F.; Luo, F.-T.; Tiwari, A.; Liu, H. Near-Infrared Fluorescent Probes Based on Piperazine-Functionalized BODIPY Dyes for Sensitive Detection of Lysosomal pH. *J. Mater. Chem. B* **2015**, *3*, 2173–2184.
- (500) Ziessel, R.; Ulrich, G.; Harriman, A.; Alamiry, M. A. H.; Stewart, B.; Retailleau, P. Solid-State Gas Sensors Developed from Functional Difluoroboradiazaindacene Dyes. *Chem. - Eur. J.* **2009**, *15*, 1359–1369.
- (501) Deniz, E.; Isbasar, G. C.; Bozdemir, Ö. A.; Yildirim, L. T.; Siemiarzuk, A.; Akkaya, E. U. Bidirectional Switching of Near IR Emitting Boradiazaindacene Fluorophores. *Org. Lett.* **2008**, *10*, 3401–3403.
- (502) Baruah, M.; Qin, W.; Flors, C.; Hofkens, J.; Vallée, R. A. L.; Beljonne, D.; Van der Auweraer, M.; De Borggraave, W. M.; Boens, N. Solvent and pH Dependent Fluorescent Properties of a Dimethylaminostyryl Borondipyrromethene Dye in Solution. *J. Phys. Chem. A* **2006**, *110*, 5998–6009.
- (503) Ando, Y.; Iino, S.; Yamada, K.; Umezawa, K.; Iwasawa, N.; Citterio, D.; Suzuki, K. A Ratiometric Fluorescent pH Glass Optode Based on a Boron-Dipyrromethene Derivative. *Sens. Actuators, B* **2007**, *121*, 74–82.
- (504) Hecht, M.; Kraus, W.; Rurack, K. A Highly Fluorescent pH Sensing Membrane for the Alkaline pH Range Incorporating a BODIPY Dye. *Analyst* **2013**, *138*, 325–332.
- (505) Strobl, M.; Rappitsch, T.; Borisov, S. M.; Mayr, T.; Klimant, I. NIR-Emitting Aza-BODIPY Dyes – New Building Blocks for Broad-Range Optical pH Sensors. *Analyst* **2015**, *140*, 7150–7153.
- (506) Murtagh, J.; Frimannsson, D. O.; O’Shea, D. F. Azide Conjugatable and pH Responsive Near-Infrared Fluorescent Imaging Probes. *Org. Lett.* **2009**, *11*, 5386–5389.
- (507) McDonnell, S. O.; O’Shea, D. F. Near-Infrared Sensing Properties of Dimethylamino-Substituted BF₂ – Azadipyrromethenes. *Org. Lett.* **2006**, *8*, 3493–3496.
- (508) Killoran, J.; McDonnell, S. O.; Gallagher, J. F.; O’Shea, D. F. A Substituted BF₂ -Chelated Tetraarylazadipyrromethene as an Intrinsic Dual Chemosensor in the 650–850 Nm Spectral Range. *New J. Chem.* **2008**, *32*, 483–489.
- (509) Salim, M. M.; Owens, E. A.; Gao, T.; Lee, J. H.; Hyun, H.; Choi, H. S.; Henary, M. Hydroxylated Near-Infrared BODIPY Fluorophores as Intracellular pH Sensors. *Analyst* **2014**, *139*, 4862–4873.
- (510) Staudinger, C.; Breining, J.; Klimant, I.; Borisov, S. M. Near-Infrared Fluorescent Aza-BODIPY Dyes for Sensing and Imaging of pH from the Neutral to Highly Alkaline Range. *Analyst* **2019**, *144*, 2393–2402.
- (511) Aigner, D.; Ungerböck, B.; Mayr, T.; Saf, R.; Klimant, I.; Borisov, S. M. Fluorescent Materials for pH Sensing and Imaging Based on Novel 1, 4-Diketopyrrolo-[3, 4-c] Pyrrole Dyes. *J. Mater. Chem. C* **2013**, *1*, 5685–5693.
- (512) Schutting, S.; Borisov, S. M.; Klimant, I. Diketo-Pyrrolo-Pyrrole Dyes as New Colorimetric and Fluorescent pH Indicators for Optical Carbon Dioxide Sensors. *Anal. Chem.* **2013**, *85*, 3271–3279.
- (513) Yamagata, T.; Kuwabara, J.; Kanbara, T. Synthesis of Highly Fluorescent Diketopyrrolopyrrole Derivative and Two-Step Response of Fluorescence to Acid. *Tetrahedron Lett.* **2010**, *51*, 1596–1599.
- (514) Veselov, A.; Thür, C.; Efimov, A.; Guina, M.; Lemmetyinen, H.; Tkachenko, N. Acidity Sensor Based on Porphyrin Self-Assembled Monolayers Covalently Attached to the Surfaces of Tapered Fibres. *Meas. Sci. Technol.* **2010**, *21*, 115205.
- (515) Niu, C.-G.; Gui, X.-Q.; Zeng, G.-M.; Guan, A.-L.; Gao, P.-F.; Qin, P.-Z. Fluorescence Ratiometric pH Sensor Prepared from Covalently Immobilized Porphyrin and Benzothioxanthene. *Anal. Bioanal. Chem.* **2005**, *383*, 349–357.
- (516) Huang, H.; Chauhan, S.; Geng, J.; Qin, Y.; Watson, D. F.; Lovell, J. F. Implantable Tin Porphyrin-PEG Hydrogels with pH-Responsive Fluorescence. *Biomacromolecules* **2017**, *18*, 562–567.
- (517) Bosson, J.; Gouin, J.; Lacour, J. Cationic Triangulenes and Helicenes: Synthesis, Chemical Stability, Optical Properties and

Extended Applications of These Unusual Dyes. *Chem. Soc. Rev.* **2014**, *43*, 2824–2840.

(518) Rich, R. M.; Stankowska, D. L.; Maliwal, B. P.; Sørensen, T. J.; Laursen, B. W.; Krishnamoorthy, R. R.; Gryczynski, Z.; Borejdo, J.; Gryczynski, I.; Fudala, R. Elimination of Autofluorescence Background from Fluorescence Tissue Images by Use of Time-Gated Detection and the AzaDiOxaTriAngulenium (ADOTA) Fluorophore. *Anal. Bioanal. Chem.* **2013**, *405*, 2065–2075.

(519) Frankær, C. G.; Rosenberg, M.; Santella, M.; Hussain, K. J.; Laursen, B. W.; Sørensen, T. J. Tuning the pK_a of a pH Responsive Fluorophore and the Consequences for Calibration of Optical Sensors Based on a Single Fluorophore but Multiple Receptors. *ACS Sens.* **2019**, *4*, 764–773.

(520) Frankær, C. G.; Hussain, K. J.; Rosenberg, M.; Jensen, A.; Laursen, B. W.; Sørensen, T. J. Biocompatible Microporous Organically Modified Silicate Material with Rapid Internal Diffusion of Protons. *ACS Sens.* **2018**, *3*, 692–699.

(521) Rosenberg, M.; Laursen, B. W.; Frankær, C. G.; Sørensen, T. J. A Fluorescence Intensity Ratiometric Fiber Optics-Based Chemical Sensor for Monitoring pH. *Adv. Mater. Technol.* **2018**, *3*, 1800205.

(522) Frankær, C. G.; Hussain, K. J.; Dörge, T. C.; Sørensen, T. J. Optical Chemical Sensor Using Intensity Ratiometric Fluorescence Signals for Fast and Reliable pH Determination. *ACS Sens.* **2019**, *4*, 26–31.

(523) Sørensen, T. J.; Rosenberg, M.; Frankær, C. G.; Laursen, B. W. An Optical pH Sensor Based on Diazaoxatriangulenium and Isopropyl-Bridged Diazaoxatriangulenium Covalently Bound in a Composite Sol–Gel. *Adv. Mater. Technol.* **2018**, *4*, 1800561.

(524) Dalfen, I.; Dmitriev, R. I.; Holst, G.; Klimant, I.; Borisov, S. M. Background-Free Fluorescence Decay Time Sensing and Imaging of pH with Highly Photostable Diazaoxatriangulenium Dyes. *Anal. Chem.* **2019**, *91*, 808–816.

(525) Horak, E.; Kassal, P.; Hranjec, M.; Steinberg, I. M. Benzimidazole Functionalised Schiff Bases: Novel pH Sensitive Fluorescence Turn-on Chromoionophores for Ion-Selective Optodes. *Sens. Actuators, B* **2018**, *258*, 415–423.

(526) Kim, S.; Pudavar, H. E.; Prasad, P. N. Dye-Concentrated Organically Modified Silica Nanoparticles as a Ratiometric Fluorescent pH Probe by One- and Two-Photon Excitation. *Chem. Commun.* **2006**, No. 19, 2071–2073.

(527) Kim, D.-Y.; Kim, H. J. pH-Sensitive Optode Membrane Covalently Incorporated with an ICT Dye for Low pH Values. *Sens. Actuators, B* **2015**, *206*, 508–515.

(528) Tian, Y.; Fuller, E.; Klug, S.; Lee, F.; Su, F.; Zhang, L.; Chao, S.; Meldrum, D. R. A Fluorescent Colorimetric pH Sensor and the Influences of Matrices on Sensing Performances. *Sens. Actuators, B* **2013**, *188*, 1–10.

(529) Sreejith, S.; Divya, K. P.; Ajayaghosh, A. A Near-Infrared Squaraine Dye as a Latent Ratiometric Fluorophore for the Detection of Amino-thiol Content in Blood Plasma. *Angew. Chem., Int. Ed.* **2008**, *47*, 7883–7887.

(530) Chen, C.-T.; Marder, S. R.; Cheng, L.-T. Syntheses and Linear and Nonlinear Optical Properties of Unsymmetrical Squaraines with Extended Conjugation. *J. Am. Chem. Soc.* **1994**, *116*, 3117–3118.

(531) Xue, L.; Li, B.; Fei, Q.; Feng, G.; Huan, Y.; Shi, Z. Carboxylate-Modified Squaraine Dye Doped Silica Fluorescent pH Nanosensors. *Nanotechnology* **2010**, *21*, 215502.

(532) Badugu, R.; Kostov, Y.; Rao, G.; Tolosa, L. Development and Application of an Excitation Ratiometric Optical pH Sensor for Bioprocess Monitoring. *Biotechnol. Prog.* **2008**, *24*, 1393–1401.

(533) Ryder, A. G.; Power, S.; Glynn, T. J. Evaluation of Acridine in Nafion as a Fluorescence-Lifetime-Based pH Sensor. *Appl. Spectrosc.* **2003**, *57*, 73–79.

(534) Sun, W.-C.; Gee, K. R.; Klaubert, D. H.; Haugland, R. P. Synthesis of Fluorinated Fluoresceins. *J. Org. Chem.* **1997**, *62*, 6469–6475.

(535) Mchedlov-Petrossyan, N. O.; Rubtsov, M. I.; Lukatskaya, L. L. Ionization and Tautomerism of Chloro-Derivatives of Fluorescein in Water and Aqueous Acetone. *Dyes Pigm.* **1992**, *18*, 179–198.

(536) *CRC Handbook of Chemistry and Physics: A Ready-Reference Book of Chemical and Physical Data*, 96th ed., 2015–2016; Haynes, W. M., Lide, D. R., Eds.; CRC Press: Boca Raton, FL, 2015.

(537) Staudinger, C.; Strobl, M.; Fischer, J. P.; Thar, R.; Mayr, T.; Aigner, D.; Müller, B. J.; Müller, B.; Lehner, P.; Mistlberger, G.; Fritzsche, E.; Ehgartner, J.; Zach, P. W.; Clarke, J. S.; Geißler, F.; Mutzberg, A.; Müller, J. D.; Achterberg, E. P.; Borisov, S. M.; Klimant, I. A Versatile Optode System for Oxygen, Carbon Dioxide, and pH Measurements in Seawater with Integrated Battery and Logger. *Limnol. Oceanogr.: Methods* **2018**, *16*, 459–473.

(538) Pfeifer, D.; Russegger, A.; Klimant, I.; Borisov, S. M. Green to Red Emitting BODIPY Dyes for Fluorescent Sensing and Imaging of Carbon Dioxide. *Sens. Actuators, B* **2020**, *304*, 127312.

(539) Giordano, P.; Bock, C.; Wrighton, M. Excited-State Proton-Transfer of Ruthenium(II) Complexes of 4,7-Dihydroxy-1,10-Phenanthroline - Increased Acidity in Excited-State. *J. Am. Chem. Soc.* **1978**, *100*, 6960–6965.

(540) Nazeeruddin, M.; Kalyanasundaram, K. Acid-Base Behavior in the Ground and Excited-States of Ruthenium(II) Complexes Containing Tetraamines or Dicarboxypyridines as Protonatable Ligands. *Inorg. Chem.* **1989**, *28*, 4251–4259.

(541) Cargill Thompson, A. M. W.; Smailes, M. C. C.; Jeffery, J. C.; Ward, M. D. Ruthenium Tris-(Bipyridyl) Complexes with Pendant Protonatable and Deprotonatable Moieties: pH Sensitivity of Electronic Spectral and Luminescence Properties. *J. Chem. Soc., Dalton Trans.* **1997**, No. 5, 737–744.

(542) Wong, K. M.-C.; Tang, W.-S.; Lu, X.-X.; Zhu, N.; Yam, V. W.-W. Functionalized Platinum(II) Terpyridyl Alkynyl Complexes as Colorimetric and Luminescence pH Sensors. *Inorg. Chem.* **2005**, *44*, 1492–1498.

(543) Zhang, X.; Jiao, Y.; Jing, X.; Wu, H.; He, G.; Duan, C. pH-Sensitive Fluorescent Sensors Based on Europium(III) Complexes. *Dalton Trans.* **2011**, *40*, 2522–2527.

(544) Gunnlaugsson, T.; Leonard, J. P.; Sénéchal, K.; Harte, A. J. pH Responsive Eu(III)-Phenanthroline Supramolecular Conjugate: Novel “off-on-off” Luminescent Signaling in the Physiological pH Range. *J. Am. Chem. Soc.* **2003**, *125*, 12062–12063.

(545) Bai, G.-Y.; Wang, K.-Z.; Duan, Z.-M.; Gao, L.-H. Luminescent pH Sensing and DNA Binding Properties of a Novel Ruthenium(II) Complex. *J. Inorg. Biochem.* **2004**, *98*, 1017–1022.

(546) Wong, K.-H.; Chan, M. C.-W.; Che, C.-M. Modular Cyclometalated Platinum(II) Complexes as Luminescent Molecular Sensors for pH and Hydrophobic Binding Regions. *Chem. - Eur. J.* **1999**, *5*, 2845–2849.

(547) Liu, M.; Ye, Z.; Xin, C.; Yuan, J. Development of a Ratiometric Time-Resolved Luminescence Sensor for pH Based on Lanthanide Complexes. *Anal. Chim. Acta* **2013**, *761*, 149–156.

(548) Higgins, B.; DeGraff, B. A.; Demas, J. N. Luminescent Transition Metal Complexes as Sensors: Structural Effects on pH Response. *Inorg. Chem.* **2005**, *44*, 6662–6669.

(549) Hynes, J.; O’Riordan, T. C.; Zhdanov, A. V.; Uray, G.; Will, Y.; Papkovsky, D. B. In Vitro Analysis of Cell Metabolism Using a Long-Decay pH-Sensitive Lanthanide Probe and Extracellular Acidification Assay. *Anal. Biochem.* **2009**, *390*, 21–28.

(550) Lobnik, A.; Majcen, N.; Niederreiter, K.; Uray, G. Optical pH Sensor Based on the Absorption of Antenna Generated Europium Luminescence by Bromothymolblue in a Sol–Gel Membrane. *Sens. Actuators, B* **2001**, *74*, 200–206.

(551) Price, J. M.; Xu, W. Y.; Demas, J. N.; DeGraff, B. A. Polymer-Supported pH Sensors Based on Hydrophobically Bound Luminescent Ruthenium(II) Complexes. *Anal. Chem.* **1998**, *70*, 265–270.

(552) Chan, C.-M.; Wong, K.-Y. Evaluation of a Luminescent Ruthenium Complex Immobilized inside Nafion as Optical pH Sensor. *Analyst* **1998**, *123*, 1843–1847.

(553) Malins, C.; Glever, H. G.; Keyes, T. E.; Vos, J. G.; Dressick, W. J.; MacCraith, B. D. Sol–Gel Immobilised Ruthenium(II) Polypyridyl Complexes as Chemical Transducers for Optical pH Sensing. *Sens. Actuators, B* **2000**, *67*, 89–95.

- (554) Clarke, Y.; Xu, W.; Demas, J. N.; DeGraff, B. A. Lifetime-Based pH Sensor System Based on a Polymer-Supported Ruthenium(II) Complex. *Anal. Chem.* **2000**, *72*, 3468–3475.
- (555) Gonçalves, H. M. R.; Maule, C. D.; Jorge, P. A. S.; Esteves da Silva, J. C. G. Fiber Optic Lifetime pH Sensing Based on Ruthenium(II) Complexes with Dicarboxypyridine. *Anal. Chim. Acta* **2008**, *626*, 62–70.
- (556) Blair, S.; Lowe, M. P.; Mathieu, C. E.; Parker, D.; Senanayake, P. K.; Katakay, R. Narrow-Range Optical pH Sensors Based on Luminescent Europium and Terbium Complexes Immobilized in a Sol Gel Glass. *Inorg. Chem.* **2001**, *40*, 5860–5867.
- (557) McCoy, C. P.; Stomeo, F.; Plush, S. E.; Gunnlaugsson, T. Soft Matter pH Sensing: From Luminescent Lanthanide pH Switches in Solution to Sensing in Hydrogels. *Chem. Mater.* **2006**, *18*, 4336–4343.
- (558) Al-Qaysi, W. W.; Duerkop, A. Sensor and Sensor Microtiterplate with Expanded pH Detection Range and Their Use in Real Samples. *Sens. Actuators, B* **2019**, *298*, 126848.
- (559) Tormo, L.; Bustamante, N.; Colmenarejo, G.; Orellana, G. Can Luminescent Ru(II) Polypyridyl Dyes Measure pH Directly? *Anal. Chem.* **2010**, *82*, 5195–5204.
- (560) Marx, D. Proton Transfer 200 Years after von Grotthuss: Insights from Ab Initio Simulations. *ChemPhysChem* **2006**, *7*, 1848–1870.
- (561) Peppas, N. A.; Hilt, J. Z.; Khademhosseini, A.; Langer, R. Hydrogels in Biology and Medicine: From Molecular Principles to Bionanotechnology. *Adv. Mater.* **2006**, *18*, 1345–1360.
- (562) Lee, K. Y.; Mooney, D. J. Hydrogels for Tissue Engineering. *Chem. Rev.* **2001**, *101*, 1869–1880.
- (563) Gong, J.; Venkateswaran, S.; Tanner, M. G.; Stone, J. M.; Bradley, M. Polymer Microarrays for the Discovery and Optimization of Robust Optical-Fiber-Based pH Sensors. *ACS Comb. Sci.* **2019**, *21*, 417–424.
- (564) Refojo, M. F. Hydrophobic Interaction in Poly(2-Hydroxyethyl Methacrylate) Homogeneous Hydrogel. *J. Polym. Sci., Part A-1: Polym. Chem.* **1967**, *5*, 3103–3113.
- (565) Furukawa, M.; Kojio, K.; Kugumiya, S.; Uchiba, Y.; Mitsui, Y. Microphase Separation of Bulk and Ultrathin Films of Polyurethane Elastomers. *Macromol. Symp.* **2008**, *267*, 9–15.
- (566) Petrini, P.; Farè, S.; Piva, A.; Tanzi, M. C. Design, Synthesis and Properties of Polyurethane Hydrogels for Tissue Engineering. *J. Mater. Sci.: Mater. Med.* **2003**, *14*, 683–686.
- (567) Barnard, S.; Beckelmann, D.; Berger, J.; Rouilly, M.; Waldner, A. Optical Sensor System for pH Determination Independently of the Ion Strength Using Fluorescein Bound to a Polymer via a Urethane and/or Urea Group. WO9747966 (A1), December 18, 1997.
- (568) Kjær, T. Enzyme Sensor Including a Water-Containing Spacer Layer. US20060275859A1, December 7, 2006.
- (569) Hoare, T. R.; Kohane, D. S. Hydrogels in Drug Delivery: Progress and Challenges. *Polymer* **2008**, *49*, 1993–2007.
- (570) HydroMed Products. <http://www.advbmaterials.com/products/hydrophilic/hydrumed.html> (accessed Jan 31, 2017).
- (571) Wang, X.; Meier, R. J.; Wolfbeis, O. S. Fluorescent pH-Sensitive Nanoparticles in an Agarose Matrix for Imaging of Bacterial Growth and Metabolism. *Angew. Chem., Int. Ed.* **2013**, *52*, 406–409.
- (572) Stoy, V. A. New Type of Hydrogel for Controlled Drug Delivery. *J. Biomater. Appl.* **1988**, *3*, 552–604.
- (573) Huber, C.; Krause, C.; Werner, T.; Wolfbeis, O. S. Serum Chloride Optical Sensors Based on Dynamic Quenching of the Fluorescence of Photo-Immobilized Lucigenin. *Microchim. Acta* **2003**, *142*, 245–253.
- (574) Westover, D.; Rudolf Seitz, W.; Lavine, B. K. Synthesis and Evaluation of Nitrated Poly(4-Hydroxystyrene) Microspheres for pH Sensing. *Microchem. J.* **2003**, *74*, 121–129.
- (575) Krause, C.; Werner, T.; Huber, C.; Wolfbeis, O. S. Emulsion-Based Fluorosensors for Potassium Featuring Improved Stability and Signal Change. *Anal. Chem.* **1999**, *71*, 5304–5308.
- (576) Huber, C.; Klimant, I.; Krause, C.; Werner, T.; Wolfbeis, O. S. Nitrate-Selective Optical Sensor Applying a Lipophilic Fluorescent Potential-Sensitive Dye. *Anal. Chim. Acta* **2001**, *449*, 81–93.
- (577) Papkovsky, D. B.; Mohr, G. J.; Wolfbeis, O. S. New Polar Plasticizers for Luminescence-Based Sensors. *Anal. Chim. Acta* **1997**, *337*, 201–205.
- (578) Bakker, E.; Bühlmann, P.; Pretsch, E. Carrier-Based Ion-Selective Electrodes and Bulk Optodes. 1. General Characteristics. *Chem. Rev.* **1997**, *97*, 3083–3132.
- (579) Derinkuyu, S.; Ertekin, K.; Oter, O.; Denizalti, S.; Cetinkaya, E. Fiber Optic pH Sensing with Long Wavelength Excitable Schiff Bases in the pH Range of 7.0–12.0. *Anal. Chim. Acta* **2007**, *588*, 42–49.
- (580) Hakonen, A.; Hulth, S. A High-Precision Ratiometric Fluorosensor for pH: Implementing Time-Dependent Non-Linear Calibration Protocols for Drift Compensation. *Anal. Chim. Acta* **2008**, *606*, 63–71.
- (581) Choi, M. F. Spectroscopic Behaviour of 8-Hydroxy-1,3,6-Pyrenetrisulphonate Immobilized in Ethyl Cellulose. *J. Photochem. Photobiol., A* **1997**, *104*, 207–212.
- (582) Kreuer, K. D. On the Development of Proton Conducting Polymer Membranes for Hydrogen and Methanol Fuel Cells. *J. Membr. Sci.* **2001**, *185*, 29–39.
- (583) Vasil'ev, V. V.; Borisov, S. M.; Maldotti, A.; Molinari, A. Spectral Properties of Cationic Water-Soluble Metallo-Porphyrins Immobilized in a Perfluorosulfonated Ion-Exchange Membrane. *J. Porphyrins Phthalocyanines* **2003**, *07*, 780–786.
- (584) Heydari, R.; Hosseini, M.; Amraei, A.; Mohammadzadeh, A. Preparation of a Novel pH Optical Sensor Using Orange (II) Based on Agarose Membrane as Support. *Mater. Sci. Eng., C* **2016**, *61*, 333–337.
- (585) Vroman, I.; Tighzert, L. Biodegradable Polymers. *Materials* **2009**, *2*, 307–344.
- (586) Siracusa, V.; Rocculi, P.; Romani, S.; Rosa, M. D. Biodegradable Polymers for Food Packaging: A Review. *Trends Food Sci. Technol.* **2008**, *19*, 634–643.
- (587) Burczak, K.; Fujisato, T.; Hatada, M.; Ikada, Y. Protein Permeation through Poly(Vinyl Alcohol) Hydrogel Membranes. *Biomaterials* **1994**, *15*, 231–238.
- (588) Herzog, C.; Poehler, E.; Peretzki, A. J.; Borisov, S. M.; Aigner, D.; Mayr, T.; Nagl, S. Continuous On-Chip Fluorescence Labelling, Free-Flow Isoelectric Focusing and Marker-Free Isoelectric Point Determination of Proteins and Peptides. *Lab Chip* **2016**, *16*, 1565–1572.
- (589) Browning, M. B.; Wilems, T.; Hahn, M.; Cosgriff-Hernandez, E. Compositional Control of Poly(Ethylene Glycol) Hydrogel Modulus Independent of Mesh Size. *J. Biomed. Mater. Res., Part A* **2011**, *98A*, 268–273.
- (590) Canal, T.; Peppas, N. A. Correlation between Mesh Size and Equilibrium Degree of Swelling of Polymeric Networks. *J. Biomed. Mater. Res.* **1989**, *23*, 1183–1193.
- (591) Peppas, N. A.; Moynihan, H. J.; Lucht, L. M. The Structure of Highly Crosslinked Poly(2-Hydroxyethyl Methacrylate) Hydrogels. *J. Biomed. Mater. Res.* **1985**, *19*, 397–411.
- (592) Herzog, C.; Beckert, E.; Nagl, S. Rapid Isoelectric Point Determination in a Miniaturized Preparative Separation Using Jet-Dispensed Optical pH Sensors and Micro Free-Flow Electrophoresis. *Anal. Chem.* **2014**, *86*, 9533–9539.
- (593) Su, F.; Agarwal, S.; Pan, T.; Qiao, Y.; Zhang, L.; Shi, Z.; Kong, X.; Day, K.; Chen, M.; Meldrum, D.; et al. Multifunctional pHPMA-Derived Polymer for Ratiometric pH Sensing, Fluorescence Imaging, and Magnetic Resonance Imaging. *ACS Appl. Mater. Interfaces* **2018**, *10*, 1556–1565.
- (594) Hennink, W. E.; van Nostrum, C. F. Novel Crosslinking Methods to Design Hydrogels. *Adv. Drug Delivery Rev.* **2002**, *54*, 13–36.
- (595) Luo, F.; Liu, Z.; Chen, T.; Gong, B. Cross-linked Polyvinyl Alcohol pH Sensitive Membrane Immobilized with Phenol Red for Optical pH Sensors. *Chin. J. Chem.* **2006**, *24*, 341–344.
- (596) Shamansky, L. M.; Yang, M.; Olteanu, M.; Chronister, E. L. A Spectroscopic Study of the pH Sensor Response of Fluorescein Doped Silica and Aluminosilica Sol-Gel Glasses. *Mater. Lett.* **1996**, *26*, 113–120.

- (597) McDonagh, C.; Sheridan, F.; Butler, T.; MacCraith, B. D. Characterisation of Sol-Gel-Derived Silica Films. *J. Non-Cryst. Solids* **1996**, *194*, 72–77.
- (598) Jurmanović, S.; Kordić, Š.; Steinberg, M. D.; Steinberg, I. M. Organically Modified Silicate Thin Films Doped with Colourimetric pH Indicators Methyl Red and Bromocresol Green as pH Responsive Sol–Gel Hybrid Materials. *Thin Solid Films* **2010**, *518*, 2234–2240.
- (599) Villegas, M. A.; Pascual, L. Sol–Gel Silica Coatings Doped with a pH-Sensitive Chromophore. *Thin Solid Films* **1999**, *351*, 103–108.
- (600) Lobnik, A.; Wolfbeis, O. S. Sol-Gel Based Optical Sensor for Dissolved Ammonia. *Sens. Actuators, B* **1998**, *51*, 203–207.
- (601) Innocenzi, P.; Brusatin, G.; Guglielmi, M.; Bertani, R. New Synthetic Route to (3-Glycidoxypropyl) Trimethoxysilane-Based Hybrid Organic–Inorganic Materials. *Chem. Mater.* **1999**, *11*, 1672–1679.
- (602) Rottman, C.; Grader, G.; De Hazan, Y.; Melchior, S.; Avnir, D. Surfactant-Induced Modification of Dopants Reactivity in Sol–Gel Matrixes. *J. Am. Chem. Soc.* **1999**, *121*, 8533–8543.
- (603) Rottman, C.; Avnir, D. Getting a Library of Activities from a Single Compound: Tunability and Very Large Shifts in Acidity Constants Induced by Sol–Gel Entrapped Micelles. *J. Am. Chem. Soc.* **2001**, *123*, 5730–5734.
- (604) Beltrán-Pérez, G.; López-Huerta, F.; Muñoz-Aguirre, S.; Castillo-Mixcoatl, J.; Palomino-Merino, R.; Lozada-Morales, R.; Portillo-Moreno, O. Fabrication and Characterization of an Optical Fiber pH Sensor Using Sol–Gel Deposited TiO₂ Film Doped with Organic Dyes. *Sens. Actuators, B* **2006**, *120*, 74–78.
- (605) Nguyen, T.; McNamara, K. P.; Rosenzweig, Z. Optochemical Sensing by Immobilizing Fluorophore-Encapsulating Liposomes in Sol–Gel Thin Films. *Anal. Chim. Acta* **1999**, *400*, 45–54.
- (606) Wirnsberger, G.; Scott, B. J.; Stucky, G. D. pH Sensing with Mesoporous Thin Films. *Chem. Commun.* **2001**, No. 1, 119–120.
- (607) Hiruta, Y.; Ando, Y.; Citterio, D.; Suzuki, K. A Fast-Response pH Optode Based on a Fluoroionophore Immobilized to a Mesoporous Silica Thin Film. *Anal. Sci.* **2010**, *26*, 297–301.
- (608) Bambot, S. B.; Sipiior, J.; Lakowicz, J. R.; Rao, G. Lifetime-Based Optical Sensing of pH Using Resonance Energy Transfer in Sol–Gel Films. *Sens. Actuators, B* **1994**, *22*, 181–188.
- (609) Villegas, M. A.; Pascual, L.; Paje, S. E.; García, M. A.; Llopis, J. Eriochrome Cyanine Doped Sol–Gel Coatings. Optical Behavior against pH. *J. Eur. Ceram. Soc.* **2000**, *20*, 1621–1628.
- (610) Russell, R. J.; Axel, A. C.; Shields, K. L.; Pishko, M. V. Mass Transfer in Rapidly Photopolymerized Poly(Ethylene Glycol) Hydrogels Used for Chemical Sensing. *Polymer* **2001**, *42*, 4893–4901.
- (611) Tufani, A.; Ince, G. O. Permeability of Small Molecules through Vapor Deposited Polymer Membranes. *J. Appl. Polym. Sci.* **2015**, *132*, 42453.
- (612) Gao, F.; Tang, L.; Dai, L.; Wang, L. A Fluorescence Ratiometric Nano-pH Sensor Based on Dual-Fluorophore-Doped Silica Nanoparticles. *Spectrochim. Acta, Part A* **2007**, *67*, 517–521.
- (613) Kotsmar, C.; Sells, T.; Taylor, N.; Liu, D. E.; Prausnitz, J. M.; Radke, C. J. Aqueous Solute Partitioning and Mesh Size in HEMA/MAA Hydrogels. *Macromolecules* **2012**, *45*, 9177–9187.
- (614) Nair, D. P.; Podgórski, M.; Chatani, S.; Gong, T.; Xi, W.; Fenoli, C. R.; Bowman, C. N. The Thiol-Michael Addition Click Reaction: A Powerful and Widely Used Tool in Materials Chemistry. *Chem. Mater.* **2014**, *26*, 724–744.
- (615) Schoolaert, E.; Steyaert, I.; Vancoillie, G.; Geltmeyer, J.; Lava, K.; Hoogenboom, R.; De Clerck, K. Blend Electrospinning of Dye-Functionalized Chitosan and Poly(ϵ -Caprolactone): Towards Biocompatible pH-Sensors. *J. Mater. Chem. B* **2016**, *4*, 4507–4516.
- (616) Sun, H.; Scharff-Poulsen, A. M.; Gu, H.; Almdal, K. Synthesis and Characterization of Ratiometric, pH Sensing Nanoparticles with Covalently Attached Fluorescent Dyes. *Chem. Mater.* **2006**, *18*, 3381–3384.
- (617) Badini, G.; Grattan, K.; Tseung, A. Sol–Gels with Fiber-optic Chemical Sensor Potential: Effects of Preparation, Aging, and Long-term Storage. *Rev. Sci. Instrum.* **1995**, *66*, 4034–4040.
- (618) Lei, J.; Wang, L.; Zhang, J. Ratiometric pH Sensor Based on Mesoporous Silica Nanoparticles and Förster Resonance Energy Transfer. *Chem. Commun.* **2010**, *46*, 8445–8447.
- (619) Zhang, Z.; Zhang, Y.; Ma, W.; Russell, R.; Shakhsher, Z. M.; Grant, C. L.; Seitz, W. R.; Sundberg, D. C. Poly(Vinyl Alcohol) as a Substrate for Indicator Immobilization for Fiber-Optic Chemical Sensors. *Anal. Chem.* **1989**, *61*, 202–205.
- (620) Chan, Y.-H.; Wu, C.; Ye, F.; Jin, Y.; Smith, P. B.; Chiu, D. T. Development of Ultrabright Semiconducting Polymer Dots for Ratiometric pH Sensing. *Anal. Chem.* **2011**, *83*, 1448–1455.
- (621) Kreno, L. E.; Leong, K.; Farha, O. K.; Allendorf, M.; Van Duyne, R. P.; Hupp, J. T. Metal–Organic Framework Materials as Chemical Sensors. *Chem. Rev.* **2012**, *112*, 1105–1125.
- (622) Hu, Z.; Deibert, B. J.; Li, J. Luminescent Metal–Organic Frameworks for Chemical Sensing and Explosive Detection. *Chem. Soc. Rev.* **2014**, *43*, 5815–5840.
- (623) Harbuzaru, B. V.; Corma, A.; Rey, F.; Jordá, J. L.; Ananias, D.; Carlos, L. D.; Rocha, J. A Miniaturized Linear pH Sensor Based on a Highly Photoluminescent Self-Assembled Europium(III) Metal–Organic Framework. *Angew. Chem., Int. Ed.* **2009**, *48*, 6476–6479.
- (624) Lu, Y.; Yan, B. A Ratiometric Fluorescent pH Sensor Based on Nanoscale Metal–Organic Frameworks (MOFs) Modified by Europium(III) Complexes. *Chem. Commun.* **2014**, *50*, 13323–13326.
- (625) Zhang, Y.; Fang, D.; Liu, R.; Zhao, S.; Xiao, X.; Wang, C.; Cao, Y.; Xu, W. Synthesis and Fluorescent pH Sensing Properties of Nanoscale Lanthanide Metal–Organic Frameworks with Silk Fibroin Powder as Polymer Ligands. *Dyes Pigm.* **2016**, *130*, 129–137.
- (626) Li, H.-Y.; Wei, Y.-L.; Dong, X.-Y.; Zang, S.-Q.; Mak, T. C. Novel Tb-MOF Embedded with Viologen Species for Multi-Photofunctionality: Photochromism, Photomodulated Fluorescence, and Luminescent pH Sensing. *Chem. Mater.* **2015**, *27*, 1327–1331.
- (627) Li, Z.; Li, P.; Xu, Q.; Li, H. Europium(III)- β -Diketonate Complex-Containing Nanohybrid Luminescent pH Detector. *Chem. Commun.* **2015**, *51*, 10644–10647.
- (628) Hou, S.-L.; Dong, J.; Tang, M.-H.; Jiang, X.-L.; Jiao, Z.-H.; Zhao, B. Triple-Interpenetrated Lanthanide–Organic Framework as Dual Wave Bands Self-Calibrated pH Luminescent Probe. *Anal. Chem.* **2019**, *91*, 5455–5460.
- (629) Qi, Z.; Chen, Y. Charge-Transfer-Based Terbium MOF Nanoparticles as Fluorescent pH Sensor for Extreme Acidity. *Biosens. Bioelectron.* **2017**, *87*, 236–241.
- (630) Xia, T.; Zhu, F.; Jiang, K.; Cui, Y.; Yang, Y.; Qian, G. A Luminescent Ratiometric pH Sensor Based on a Nanoscale and Biocompatible Eu/Tb-Mixed MOF. *Dalton Trans.* **2017**, *46*, 7549–7555.
- (631) Aguilera-Sigalat, J.; Bradshaw, D. A Colloidal Water-Stable MOF as a Broad-Range Fluorescent pH Sensor via Post-Synthetic Modification. *Chem. Commun.* **2014**, *50*, 4711.
- (632) Wu, S.-H.; Wang, S.; Fang, W.-L.; Guo, X.-F.; Wang, H. An Exceptionally Stable Zr-Based Fluorescent Metal–Organic Framework for Highly Selective Detection of pH. *Anal. Methods* **2019**, *11*, 36–43.
- (633) Jiang, H.-L.; Feng, D.; Wang, K.; Gu, Z.-Y.; Wei, Z.; Chen, Y.-P.; Zhou, H.-C. An Exceptionally Stable, Porphyrinic Zr Metal–Organic Framework Exhibiting pH-Dependent Fluorescence. *J. Am. Chem. Soc.* **2013**, *135* (37), 13934–13938.
- (634) Deibert, B. J.; Li, J. A Distinct Reversible Colorimetric and Fluorescent Low pH Response on a Water-Stable Zirconium–Porphyrin Metal–Organic Framework. *Chem. Commun.* **2014**, *50*, 9636–9639.
- (635) Chen, H.; Wang, J.; Shan, D.; Chen, J.; Zhang, S.; Lu, X. Dual-Emitting Fluorescent Metal–Organic Framework Nanocomposites as a Broad-Range pH Sensor for Fluorescence Imaging. *Anal. Chem.* **2018**, *90*, 7056–7063.
- (636) Wang, J.; Li, Y.; Jiang, M.; Liu, Y.; Zhang, L.; Wu, P. A Highly Chemically Stable Metal–Organic Framework as a Luminescent Probe for the Regenerable Ratiometric Sensing of pH. *Chem. - Eur. J.* **2016**, *22*, 13023–13027.

- (637) Xu, X.-Y.; Yan, B. An Efficient and Sensitive Fluorescent pH Sensor Based on Amino Functional Metal–Organic Frameworks in Aqueous Environment. *Dalton Trans.* **2016**, *45*, 7078–7084.
- (638) He, C.; Lu, K.; Lin, W. Nanoscale Metal–Organic Frameworks for Real-Time Intracellular pH Sensing in Live Cells. *J. Am. Chem. Soc.* **2014**, *136*, 12253–12256.
- (639) Lan, G.; Ni, K.; You, E.; Wang, M.; Culbert, A.; Jiang, X.; Lin, W. Multifunctional Nanoscale Metal–Organic Layers for Ratiometric pH and Oxygen Sensing. *J. Am. Chem. Soc.* **2019**, *141*, 18964–18969.
- (640) Lv, X.-L.; Xie, L.-H.; Wang, B.; Zhao, M.; Cui, Y.; Li, J.-R. Flexible Metal–Organic Frameworks for the Wavelength-Based Luminescence Sensing of Aqueous pH. *J. Mater. Chem. C* **2018**, *6*, 10628–10639.
- (641) Ding, Z.; Wang, C.; Wang, S.; Wu, L.; Zhang, X. Light-Harvesting Metal–Organic Framework Nanoprobes for Ratiometric Fluorescence Energy Transfer-Based Determination of pH Values and Temperature. *Microchim. Acta* **2019**, *186*, 476.
- (642) Grummt, U.-W.; Pron, A.; Zagorska, M.; Lefrant, S. Polyaniline Based Optical pH Sensor. *Anal. Chim. Acta* **1997**, *357*, 253–259.
- (643) Gicevicius, M.; Kucinski, J.; Ramanaviciene, A.; Ramanavicius, A. Tuning the Optical pH Sensing Properties of Polyaniline-Based Layer by Electrochemical Copolymerization of Aniline with o-Phenylenediamine. *Dyes Pigm.* **2019**, *170*, 107457.
- (644) Pringsheim, E.; Zimin, D.; Wolfbeis, O. S. Fluorescent Beads Coated with Polyaniline: A Novel Nanomaterial for Optical Sensing of pH. *Adv. Mater.* **2001**, *13*, 819–822.
- (645) Del Pilar Taboada Sotomayor, M.; De Paoli, M.-A.; de Oliveira, W. A. Fiber-Optic pH Sensor Based on Poly(o-Methoxyaniline). *Anal. Chim. Acta* **1997**, *353*, 275–280.
- (646) Wen, Q.; Liu, L.; Yang, Q.; Lv, F.; Wang, S. Dopamine-Modified Cationic Conjugated Polymer as a New Platform for pH Sensing and Autophagy Imaging. *Adv. Funct. Mater.* **2013**, *23*, 764–769.
- (647) Kappaun, S.; Horner, S.; Kelterer, A.-M.; Waich, K.; Grasse, F.; Graf, M.; Romaner, L.; Niedermair, F.; Müllen, K.; Grimsdale, A. C.; Saf, R.; List, E. J. W.; Zojer, E.; Slugovc, C. The Effect of Protonation on the Optical Properties of Conjugated Fluorene–Pyridine Copolymers. *Macromol. Chem. Phys.* **2008**, *209*, 2122–2134.
- (648) Adachi, N.; Kaneko, Y.; Sekiguchi, K.; Sugiyama, H.; Sugeno, M. pH-Responsive Fluorescence Chemical Sensor Constituted by Conjugated Polymers Containing Pyridine Rings. *Luminescence* **2015**, *30*, 1308–1312.
- (649) Cui, H.; Chen, Y.; Li, L.; Wu, Y.; Tang, Z.; Fu, H.; Tian, Z. Hybrid Fluorescent Nanoparticles Fabricated from Pyridine-Functionalized Polyfluorene-Based Conjugated Polymer as Reversible pH Probes over a Broad Range of Acidity-Alkalinity. *Microchim. Acta* **2014**, *181*, 1529–1539.
- (650) Ahn, H.; Hong, J.; Kim, S. Y.; Choi, I.; Park, M. J. A pH-Responsive Molecular Switch with Tricolor Luminescence. *ACS Appl. Mater. Interfaces* **2015**, *7*, 704–712.
- (651) Newman, R. H.; Fosbrink, M. D.; Zhang, J. Genetically Encodable Fluorescent Biosensors for Tracking Signaling Dynamics in Living Cells. *Chem. Rev.* **2011**, *111*, 3614–3666.
- (652) Chudakov, D. M.; Matz, M. V.; Lukyanov, S.; Lukyanov, K. A. Fluorescent Proteins and Their Applications in Imaging Living Cells and Tissues. *Physiol. Rev.* **2010**, *90*, 1103–1163.
- (653) Ibraheem, A.; Campbell, R. E. Designs and Applications of Fluorescent Protein-Based Biosensors. *Curr. Opin. Chem. Biol.* **2010**, *14*, 30–36.
- (654) Miyawaki, A.; Niino, Y. Molecular Spies for Bioimaging—Fluorescent Protein-Based Probes. *Mol. Cell* **2015**, *58*, 632–643.
- (655) *Fluorescent Protein-Based Biosensors: Methods and Protocols*; Zhang, J., Ni, Q., Newman, R. H., Eds.; Methods in Molecular Biology; Humana Press: New York, 2014.
- (656) Shcherbakova, D. M.; Subach, O. M.; Verkhusha, V. V. Red Fluorescent Proteins: Advanced Imaging Applications and Future Design. *Angew. Chem., Int. Ed.* **2012**, *51*, 10724–10738.
- (657) Rodriguez, E. A.; Campbell, R. E.; Lin, J. Y.; Lin, M. Z.; Miyawaki, A.; Palmer, A. E.; Shu, X.; Zhang, J.; Tsien, R. Y. The Growing and Glowing Toolbox of Fluorescent and Photoactive Proteins. *Trends Biochem. Sci.* **2017**, *42*, 111–129.
- (658) Lukyanov, K. A.; Belousov, V. V. Genetically Encoded Fluorescent Redox Sensors. *Biochim. Biophys. Acta, Gen. Subj.* **2014**, *1840*, 745–756.
- (659) Fan, Y.; Chen, Z.; Ai, H. Monitoring Redox Dynamics in Living Cells with a Redox-Sensitive Red Fluorescent Protein. *Anal. Chem.* **2015**, *87*, 2802–2810.
- (660) Dennis, A. M.; Rhee, W. J.; Sotto, D.; Dublin, S. N.; Bao, G. Quantum Dot–Fluorescent Protein FRET Probes for Sensing Intracellular pH. *ACS Nano* **2012**, *6*, 2917–2924.
- (661) Casey, J. R.; Grinstead, S.; Orłowski, J. Sensors and Regulators of Intracellular pH. *Nat. Rev. Mol. Cell Biol.* **2010**, *11*, 50–61.
- (662) Subach, O. M.; Gundorov, I. S.; Yoshimura, M.; Subach, F. V.; Zhang, J.; Grünwald, D.; Souslova, E. A.; Chudakov, D. M.; Verkhusha, V. V. Conversion of Red Fluorescent Protein into a Bright Blue Probe. *Chem. Biol.* **2008**, *15*, 1116–1124.
- (663) Abad, M. F. C.; Di Benedetto, G.; Magalhães, P. J.; Filippin, L.; Pozzan, T. Mitochondrial pH Monitored by a New Engineered Green Fluorescent Protein Mutant. *J. Biol. Chem.* **2004**, *279*, 11521–11529.
- (664) Bizzarri, R.; Serresi, M.; Luin, S.; Beltram, F. Green Fluorescent Protein Based pH Indicators for in Vivo Use: A Review. *Anal. Bioanal. Chem.* **2009**, *393*, 1107.
- (665) Miesenböck, G.; De Angelis, D. A.; Rothman, J. E. Visualizing Secretion and Synaptic Transmission with pH-Sensitive Green Fluorescent Proteins. *Nature* **1998**, *394*, 192–195.
- (666) Tantama, M.; Hung, Y. P.; Yellen, G. Imaging Intracellular pH in Live Cells with a Genetically Encoded Red Fluorescent Protein Sensor. *J. Am. Chem. Soc.* **2011**, *133*, 10034–10037.
- (667) Hanson, G. T.; McAnaney, T. B.; Park, E. S.; Rendell, M. E.; Yarbrough, D. K.; Chu, S.; Xi, L.; Boxer, S. G.; Montrose, M. H.; Remington, S. J. Green Fluorescent Protein Variants as Ratiometric Dual Emission pH Sensors. 1. Structural Characterization and Preliminary Application. *Biochemistry* **2002**, *41*, 15477–15488.
- (668) Awaji, T.; Hirasawa, A.; Shirakawa, H.; Tsujimoto, G.; Miyazaki, S. Novel Green Fluorescent Protein-Based Ratiometric Indicators for Monitoring pH in Defined Intracellular Microdomains. *Biochem. Biophys. Res. Commun.* **2001**, *289*, 457–462.
- (669) Esposito, A.; Gralle, M.; Dani, M. A. C.; Lange, D.; Wouters, F. S. pHlameleons: A Family of FRET-Based Protein Sensors for Quantitative pH Imaging. *Biochemistry* **2008**, *47*, 13115–13126.
- (670) Shen, Y.; Rosendale, M.; Campbell, R. E.; Perrais, D. pHuji, a pH-Sensitive Red Fluorescent Protein for Imaging of Exo- and Endocytosis. *J. Cell Biol.* **2014**, *207*, 419–432.
- (671) Kirkpatrick, S. M.; Naik, R. R.; Stone, M. O. Nonlinear Saturation and Determination of the Two-Photon Absorption Cross Section of Green Fluorescent Protein. *J. Phys. Chem. B* **2001**, *105*, 2867–2873.
- (672) Borisov, S. M.; Klimant, I. Optical Nanosensors—Smart Tools in Bioanalytics. *Analyst* **2008**, *133*, 1302–1307.
- (673) Lobnik, A.; Korent Urek, Š. Nano-Based Optical Chemical Sensors. *J. Nano Res.* **2011**, *13*, 99–110.
- (674) Wolfbeis, O. S. An Overview of Nanoparticles Commonly Used in Fluorescent Bioimaging. *Chem. Soc. Rev.* **2015**, *44*, 4743–4768.
- (675) Borisov, S. M.; Mayr, T.; Karasyov, A. A.; Klimant, I.; Chojnacki, P.; Moser, C.; Nagl, S.; Schaeferling, M.; Stich, M. L.; Kocincova, A. S.; Wolfbeis, O. S. New Plastic Microparticles and Nanoparticles for Fluorescent Sensing and Encoding. In *Fluorescence of Supramolecules, Polymers, and Nanosystems*; Berberan-Santos, M. N., Ed.; Springer: Berlin, 2007; Vol. 4, pp 431–463.
- (676) Chen, M.; Yin, M. Design and Development of Fluorescent Nanostructures for Bioimaging. *Prog. Polym. Sci.* **2014**, *39*, 365–395.
- (677) Chen, G.; Song, F.; Xiong, X.; Peng, X. Fluorescent Nanosensors Based on Fluorescence Resonance Energy Transfer (FRET). *Ind. Eng. Chem. Res.* **2013**, *52*, 11228–11245.
- (678) Saha, K.; Agasti, S. S.; Kim, C.; Li, X.; Rotello, V. M. Gold Nanoparticles in Chemical and Biological Sensing. *Chem. Rev.* **2012**, *112*, 2739–2779.

- (679) Shen, J.; Zhu, Y.; Yang, X.; Li, C. Graphene Quantum Dots: Emergent Nanolights for Bioimaging, Sensors, Catalysis and Photo-voltaic Devices. *Chem. Commun.* **2012**, *48*, 3686–3699.
- (680) Zhong, W. Nanomaterials in Fluorescence-Based Biosensing. *Anal. Bioanal. Chem.* **2009**, *394*, 47–59.
- (681) Schäferling, M. Nanoparticle-Based Luminescent Probes for Intracellular Sensing and Imaging of pH. *Wiley Interdiscip. Rev. Nanomed. Nanobiotechnol.* **2016**, *8*, 378–413.
- (682) Lu, J.; Rosenzweig, Z. Nanoscale Fluorescent Sensors for Intracellular Analysis. *Fresenius' J. Anal. Chem.* **2000**, *366*, 569–575.
- (683) Srivastava, A. K.; Dev, A.; Karmakar, S. Nanosensors and Nanobiosensors in Food and Agriculture. *Environ. Chem. Lett.* **2018**, *16*, 161–182.
- (684) Doria, G.; Conde, J.; Veigas, B.; Giestas, L.; Almeida, C.; Assunção, M.; Rosa, J.; Baptista, P. V. Noble Metal Nanoparticles for Biosensing Applications. *Sensors* **2012**, *12*, 1657–1687.
- (685) Aylott, J. W. Optical Nanosensors—an Enabling Technology for Intracellular Measurements. *Analyst* **2003**, *128*, 309–312.
- (686) Asefa, T.; Duncan, C. T.; Sharma, K. K. Recent Advances in Nanostructured Chemosensors and Biosensors. *Analyst* **2009**, *134*, 1980–1990.
- (687) Buck, S. Nanoscale Probes Encapsulated by Biologically Localized Embedding (PEBBLEs) for Ion Sensing and Imaging in Live Cells. *Talanta* **2004**, *63*, 41–59.
- (688) Li, K.; Liu, B. Polymer Encapsulated Conjugated Polymer-nanoparticles for Fluorescence Bioimaging. *J. Mater. Chem.* **2012**, *22*, 1257–1264.
- (689) Knopp, D.; Tang, D.; Niessner, R. Review: Bioanalytical Applications of Biomolecule-Functionalized Nanometer-Sized Doped Silica Particles. *Anal. Chim. Acta* **2009**, *647*, 14–30.
- (690) Burns, A.; Ow, H.; Wiesner, U. Fluorescent Core–Shell Silica Nanoparticles: Towards “Lab on a Particle” Architectures for Nanobiotechnology. *Chem. Soc. Rev.* **2006**, *35*, 1028–1042.
- (691) Bae, S. W.; Tan, W.; Hong, J.-I. Fluorescent Dye-Doped Silica Nanoparticles: New Tools for Bioapplications. *Chem. Commun.* **2012**, *48* (17), 2270–2282.
- (692) Wang, K.; He, X.; Yang, X.; Shi, H. Functionalized Silica Nanoparticles: A Platform for Fluorescence Imaging at the Cell and Small Animal Levels. *Acc. Chem. Res.* **2013**, *46*, 1367–1376.
- (693) Peng, F.; Su, Y.; Zhong, Y.; Fan, C.; Lee, S.-T.; He, Y. Silicon Nanomaterials Platform for Bioimaging, Biosensing, and Cancer Therapy. *Acc. Chem. Res.* **2014**, *47*, 612–623.
- (694) Wang, C.; Li, X.; Zhang, F. Bioapplications and Biotechnologies of Upconversion Nanoparticle-Based Nanosensors. *Analyst* **2016**, *141*, 3601–3620.
- (695) DaCosta, M. V.; Doughan, S.; Han, Y.; Krull, U. J. Lanthanide Upconversion Nanoparticles and Applications in Bioassays and Bioimaging: A Review. *Anal. Chim. Acta* **2014**, *832*, 1–33.
- (696) Achatz, D. E.; Ali, R.; Wolfbeis, O. S. Luminescent Chemical Sensing, Biosensing, and Screening Using Upconverting Nanoparticles. In *Luminescence Applied in Sensor Science*; Prodi, L., Montalti, M., Zaccaroni, N., Eds.; Springer: Berlin, 2010; Vol. 300, pp 29–50.
- (697) Doussineau, T.; Schulz, A.; Lapresta-Fernandez, A.; Moro, A.; Körsten, S.; Trupp, S.; Mohr, G. J. On the Design of Fluorescent Ratiometric Nanosensors. *Chem. - Eur. J.* **2010**, *16*, 10290–10299.
- (698) Mahata, M.; Bae, H.; Lee, K. Upconversion Luminescence Sensitized pH-Nanoprobes. *Molecules* **2017**, *22*, 2064.
- (699) Schäferling, M.; Resch-Genger, U. Luminescent Nanoparticles for Chemical Sensing and Imaging. In *Reviews in Fluorescence 2016*; Geddes, C. D., Ed.; Springer International Publishing: Cham, 2017; pp 71–109.
- (700) Canfarotta, F.; Whitcombe, M. J.; Piletsky, S. A. Polymeric Nanoparticles for Optical Sensing. *Biotechnol. Adv.* **2013**, *31*, 1585–1599.
- (701) Wang, L.; Li, C. pH Responsive Fluorescence Nanoprobe Imaging of Tumors by Sensing the Acidic Microenvironment. *J. Mater. Chem.* **2011**, *21*, 15862–15871.
- (702) Moßhammer, M.; Brodersen, K. E.; Kühl, M.; Koren, K. Nanoparticle- and Microparticle-Based Luminescence Imaging of Chemical Species and Temperature in Aquatic Systems: A Review. *Microchim. Acta* **2019**, *186*, 126.
- (703) Ehgartner, J.; Strobl, M.; Bolivar, J. M.; Rabl, D.; Rothbauer, M.; Ertl, P.; Borisov, S. M.; Mayr, T. Simultaneous Determination of Oxygen and pH Inside Microfluidic Devices Using Core–Shell Nanosensors. *Anal. Chem.* **2016**, *88*, 9796–9804.
- (704) Fröhlich, E. The Role of Surface Charge in Cellular Uptake and Cytotoxicity of Medical Nanoparticles. *Int. J. Nanomed.* **2012**, *7*, 5577–5591.
- (705) Nie, S.; Xing, Y.; Kim, G. J.; Simons, J. W. Nanotechnology Applications in Cancer. *Annu. Rev. Biomed. Eng.* **2007**, *9*, 257–288.
- (706) Soršak, E.; Valh, J. V.; Urek, Š. K.; Lobnik, A. Application of PAMAM Dendrimers in Optical Sensing. *Analyst* **2015**, *140*, 976–989.
- (707) Srikun, D.; Albers, A. E.; Chang, C. J. A Dendrimer-Based Platform for Simultaneous Dual Fluorescence Imaging of Hydrogen Peroxide and pH Gradients Produced in Living Cells. *Chem. Sci.* **2011**, *2*, 1156–1165.
- (708) Senarath-Yapa, M. D.; Scott Saavedra, S. Dye Leaching from a Doped Sol–Gel Is Eliminated by Conjugation to a Dendrimer. *Anal. Chim. Acta* **2001**, *432*, 89–94.
- (709) Wang, Y.; Niu, S.; Zhang, Z.; Xie, Y.; Yuan, C.; Wang, H.; Fu, D. Reversible pH Manipulation of the Fluorescence Emission from Sectorial Poly(Amido Amine) Dendrimers. *J. Nanosci. Nanotechnol.* **2010**, *10*, 4227–4233.
- (710) Wang, D.; Imae, T. Fluorescence Emission from Dendrimers and Its pH Dependence. *J. Am. Chem. Soc.* **2004**, *126*, 13204–13205.
- (711) Cao, L.; Jia, D.; Wang, S.; Rong, Y.; Liu, C.; Wang, D. Significant Influence of Distance between Amine Groups on Intrinsic Fluorescence Properties. *Chem. Lett.* **2014**, *43*, 246–248.
- (712) Grabchev, I.; Staneva, D.; Betcheva, R. Sensor Activity, Photodegradation and Photostabilisation of a PAMAM Dendrimer Comprising 1,8-Naphthalimide Functional Groups in Its Periphery. *Polym. Degrad. Stab.* **2006**, *91*, 2257–2264.
- (713) Grabchev, I.; Soumillion, J.-P.; Muls, B.; Ivanova, G. Poly(Amidoamine) Dendrimer Peripherally Modified with 4-N,N-Dimethylaminoethylamine-1,8-Naphthalimide as a Sensor of Metal Cations and Protons. *Photochem. Photobiol. Sci.* **2004**, *3*, 1032–1037.
- (714) Grabchev, I.; Guittonneau, S. Sensors for Detecting Metal Ions and Protons Based on New Green Fluorescent Poly(Amidoamine) Dendrimers Peripherally Modified with 1,8-Naphthalimides. *J. Photochem. Photobiol., A* **2006**, *179*, 28–34.
- (715) Grabchev, I.; Chovelon, J.-M.; Bojinov, V.; Ivanova, G. Poly(Amidoamine) Dendrimers Peripherally Modified with 4-Ethylamino-1,8-Naphthalimide. Synthesis and Photophysical Properties. *Tetrahedron* **2003**, *59*, 9591–9598.
- (716) Grabchev, I. Synthesis and Photophysical Properties of 1,8-Naphthalimide-Labelled PAMAM as PET Sensors of Protons and of Transition Metal Ions. *Polymer* **2002**, *43*, 5731–5736.
- (717) Grabchev, I.; Staneva, D.; Bojinov, V.; Betcheva, R.; Gregoriou, V. Spectral Investigation of Coordination of Cuprum Cations and Protons at PAMAM Dendrimer Peripherally Modified with 1,8-Naphthalimide Units. *Spectrochim. Acta, Part A* **2008**, *70*, 532–536.
- (718) Georgiev, N. I.; Bojinov, V. B. The Design and Synthesis of a Novel 1,8-Naphthalimide PAMAM Light-Harvesting Dendron with Fluorescence “off-on” Switching Core. *Dyes Pigm.* **2010**, *84*, 249–256.
- (719) Bojinov, V. B.; Georgiev, N. I.; Nikolov, P. S. Synthesis and Photophysical Properties of Fluorescence Sensing Ester- and Amidoamine-Functionalized 1,8-Naphthalimides. *J. Photochem. Photobiol., A* **2008**, *193*, 129–138.
- (720) Georgiev, N. I.; Bojinov, V. B.; Nikolov, P. S. Design and Synthesis of a Novel pH Sensitive Core and Peripherally 1,8-Naphthalimide-Labelled PAMAM Dendron as Light Harvesting Antenna. *Dyes Pigm.* **2009**, *81*, 18–26.
- (721) Bojinov, V. B.; Georgiev, N. I.; Nikolov, P. S. Design and Synthesis of Core and Peripherally Functionalized with 1,8-Naphthalimide Units Fluorescent PAMAM Dendron as Light Harvesting Antenna. *J. Photochem. Photobiol., A* **2008**, *197*, 281–289.
- (722) Dodangeh, M.; Gharanjig, K.; Arami, M. Synthesis, Characterization, and Photo-Physical Properties of Dendrimers Modified With

1,8-Naphthalimide Derivatives as Novel Fluorescent pH Sensors. *IEEE Sens. J.* **2014**, *14*, 2889–2896.

(723) Georgiev, N. I.; Sakr, A. R.; Bojinov, V. B. Design and Synthesis of Novel Fluorescence Sensing Perylene Diimides Based on Photo-induced Electron Transfer. *Dyes Pigm.* **2011**, *91*, 332–339.

(724) Albertazzi, L.; Storti, B.; Marchetti, L.; Beltram, F. Delivery and Subcellular Targeting of Dendrimer-Based Fluorescent pH Sensors in Living Cells. *J. Am. Chem. Soc.* **2010**, *132*, 18158–18167.

(725) Dirksen, A.; Zuidema, E.; Williams, R. M.; De Cola, L.; Kauffmann, C.; Vögtle, F.; Roque, A.; Pina, F. Photoactivity and pH Sensitivity of Methyl Orange Functionalized Poly(Propyleneamine) Dendrimers. *Macromolecules* **2002**, *35*, 2743–2747.

(726) Vinogradov, S. A.; Wilson, D. F. Electrostatic Core Shielding in Dendritic Polyglutamic Porphyrins. *Chem. - Eur. J.* **2000**, *6*, 2456–2461.

(727) Thyagarajan, S.; Leiding, T.; Årsköld, S. P.; Cheprakov, A. V.; Vinogradov, S. A. Highly Non-Planar Dendritic Porphyrin for pH Sensing: Observation of Porphyrin Monocation. *Inorg. Chem.* **2010**, *49*, 9909–9920.

(728) Yang, Q.; Ye, Z.; Zhong, M.; Chen, B.; Chen, J.; Zeng, R.; Wei, L.; Li, H.; Xiao, L. Self-Assembled Fluorescent Bovine Serum Albumin Nanoprobes for Ratiometric pH Measurement inside Living Cells. *ACS Appl. Mater. Interfaces* **2016**, *8*, 9629–9634.

(729) Han, J.; Loudet, A.; Barhoumi, R.; Burghardt, R. C.; Burgess, K. A Ratiometric pH Reporter For Imaging Protein-Dye Conjugates In Living Cells. *J. Am. Chem. Soc.* **2009**, *131*, 1642–1643.

(730) Saha, S.; Chakraborty, K.; Krishnan, Y. Tunable, Colorimetric DNA-Based pH Sensors Mediated by A-Motif Formation. *Chem. Commun.* **2012**, *48*, 2513–2515.

(731) Carnevale, K. J. F.; Riskowski, R. A.; Strouse, G. F. A Gold Nanoparticle Bio-Optical Transponder to Dynamically Monitor Intracellular pH. *ACS Nano* **2018**, *12*, 5956–5968.

(732) Alvarez-Rodriguez, R.; Alonso, M.; Girotti, A.; Rebotto, V.; Rodriguez-Cabello, J. C. One-Pot Synthesis of pH and Temperature Sensitive Gold Clusters Mediated by a Recombinant Elastin-like Polymer. *Eur. Polym. J.* **2010**, *46*, 643–650.

(733) Modi, S.; Swetha, M. G.; Goswami, D.; Gupta, G. D.; Mayor, S.; Krishnan, Y. A DNA Nanomachine That Maps Spatial and Temporal pH Changes inside Living Cells. *Nat. Nanotechnol.* **2009**, *4*, 325–330.

(734) Huang, J.; Ying, L.; Yang, X.; Yang, Y.; Quan, K.; Wang, H.; Xie, N.; Ou, M.; Zhou, Q.; Wang, K. Ratiometric Fluorescent Sensing of pH Values in Living Cells by Dual-Fluorophore-Labeled i-Motif Nanoprobes. *Anal. Chem.* **2015**, *87*, 8724–8731.

(735) Luo, F.; Xi, Q.; Jiang, J.; Yu, R. Graphene Oxide Based DNA Nanoswitches as a Programmable pH-Responsive Biosensor. *Anal. Methods* **2016**, *8*, 6982–6985.

(736) Yang, M.; Song, Y.; Zhang, M.; Lin, S.; Hao, Z.; Liang, Y.; Zhang, D.; Chen, P. R. Converting a Solvatochromic Fluorophore into a Protein-Based pH Indicator for Extreme Acidity. *Angew. Chem.* **2012**, *124*, 7794–7799.

(737) Hilderbrand, S. A.; Kelly, K. A.; Niedre, M.; Weissleder, R. Near Infrared Fluorescence-Based Bacteriophage Particles for Ratiometric pH Imaging. *Bioconjugate Chem.* **2008**, *19*, 1635–1639.

(738) Tian, Y.; Wu, M.; Liu, X.; Liu, Z.; Zhou, Q.; Niu, Z.; Huang, Y. Probing the Endocytic Pathways of the Filamentous Bacteriophage in Live Cells Using Ratiometric pH Fluorescent Indicator. *Adv. Healthcare Mater.* **2015**, *4*, 413–419.

(739) Chen, L.; Wu, Y.; Lin, Y.; Wang, Q. Virus-Templated FRET Platform for the Rational Design of Ratiometric Fluorescent Nanosensors. *Chem. Commun.* **2015**, *51*, 10190–10193.

(740) Yan, J.; Estévez, M. C.; Smith, J. E.; Wang, K.; He, X.; Wang, L.; Tan, W. Dye-Doped Nanoparticles for Bioanalysis. *Nano Today* **2007**, *2*, 44–50.

(741) Yao, G.; Wang, L.; Wu, Y.; Smith, J.; Xu, J.; Zhao, W.; Lee, E.; Tan, W. FloDots: Luminescent Nanoparticles. *Anal. Bioanal. Chem.* **2006**, *385*, 518–524.

(742) Tang, F.; Li, L.; Chen, D. Mesoporous Silica Nanoparticles: Synthesis, Biocompatibility and Drug Delivery. *Adv. Mater.* **2012**, *24*, 1504–1534.

(743) Gao, F.; Wang, L.; Tang, L.; Zhu, C. A Novel Nano-Sensor Based on Rhodamine- β -Isothiocyanate – Doped Silica Nanoparticle for pH Measurement. *Microchim. Acta* **2005**, *152*, 131–135.

(744) Peng, J.; He, X.; Wang, K.; Tan, W.; Wang, Y.; Liu, Y. Noninvasive Monitoring of Intracellular pH Change Induced by Drug Stimulation Using Silica Nanoparticle Sensors. *Anal. Bioanal. Chem.* **2007**, *388*, 645–654.

(745) He, X.; Wang, Y.; Wang, K.; Peng, J.; Liu, F.; Tan, W. Research of the Relationship of Intracellular Acidification and Apoptosis in Hela Cells Based on pH Nanosensors. *Sci. China, Ser. B: Chem.* **2007**, *50*, 258–265.

(746) Xu, J.; Sun, L.; Li, J.; Liang, J.; Zhang, H.; Yang, W. FITC and Ru(Phen) $_{32+}$ Co-Doped Silica Particles as Visualized Ratiometric pH Indicator. *Nanoscale Res. Lett.* **2011**, *6*, 561.

(747) Acquah, I.; Roh, J.; Ahn, D. J. Dual-Fluorophore Raspberry-like Nanohybrids for Ratiometric pH Sensing. *Chem. - Asian J.* **2017**, *12*, 1724–1729.

(748) Hu, S.; Sun, L.; Liu, M.; Zhu, H.; Guo, H.; Sun, H.; Sun, H. A Highly Dispersible Silica pH Nanosensor with Expanded Measurement Ranges. *New J. Chem.* **2015**, *39*, 4568–4574.

(749) Liu, J.; Zang, L.; Wang, Y.; Liu, G. Preparation of Acridine Orange-Doped Silica Nanoparticles for pH Measurement. *J. Lumin.* **2014**, *147*, 155–158.

(750) Gao, F.; Chen, X.; Ye, Q.; Yao, Z.; Guo, X.; Wang, L. Core-Shell Fluorescent Silica Nanoparticles for Sensing near-Neutral pH Values. *Microchim. Acta* **2011**, *172*, 327–333.

(751) Mathew, N. D.; Mathew, M. D.; Surawski, P. P. T. Nanoparticle Imaging and Diagnostic of Caenorhabditis Elegans Intracellular pH. *Anal. Biochem.* **2014**, *450*, 52–56.

(752) Ali, R.; Saleh, S. M.; Elshaarawy, R. F. M. Turn-on pH Nano-Fluoresensor Based on Imidazolium Salicylaldehyde Ionic Liquid-Labeled Silica Nanoparticles. *RSC Adv.* **2016**, *6*, 86965–86975.

(753) Chen, Y.-P.; Chen, H.-A.; Hung, Y.; Chien, F.-C.; Chen, P.; Mou, C.-Y. Surface Charge Effect in Intracellular Localization of Mesoporous Silica Nanoparticles as Probed by Fluorescent Ratiometric pH Imaging. *RSC Adv.* **2012**, *2*, 968–973.

(754) Korzeniowska, B.; Woolley, R.; Decourcey, J.; Wencel, D.; Loscher, C. E.; McDonagh, C. Intracellular pH-Sensing Using Core/Shell Silica Nanoparticles. *J. Biomed. Nanotechnol.* **2014**, *10*, 1336–1345.

(755) Tsou, C.-J.; Chu, C.; Hung, Y.; Mou, C.-Y. A Broad Range Fluorescent pH Sensor Based on Hollow Mesoporous Silica Nanoparticles, Utilising the Surface Curvature Effect. *J. Mater. Chem. B* **2013**, *1*, 5557–5563.

(756) Yang, L.; Li, N.; Pan, W.; Yu, Z.; Tang, B. Real-Time Imaging of Mitochondrial Hydrogen Peroxide and pH Fluctuations in Living Cells Using a Fluorescent Nanosensor. *Anal. Chem.* **2015**, *87*, 3678–3684.

(757) Borisov, S. M.; Mayr, T.; Mistleberger, G.; Waich, K.; Koren, K.; Chojnacki, P.; Klimant, I. Precipitation as a Simple and Versatile Method for Preparation of Optical Nanochemosensors. *Talanta* **2009**, *79*, 1322–1330.

(758) Clark, H. A.; Hoyer, M.; Philbert, M. A.; Kopelman, R. Optical Nanosensors for Chemical Analysis inside Single Living Cells. I. Fabrication, Characterization, and Methods for Intracellular Delivery of PEBBLE Sensors. *Anal. Chem.* **1999**, *71*, 4831–4836.

(759) Ray, A.; Koo Lee, Y.-E.; Epstein, T.; Kim, G.; Kopelman, R. Two-Photon Nano-PEBBLE Sensors: Subcellular pH Measurements. *Analyst* **2011**, *136*, 3616–3622.

(760) Sun, H.; Benjaminsen, R. V.; Almdal, K.; Andresen, T. L. Hyaluronic Acid Immobilized Polyacrylamide Nanoparticle Sensors for CD44 Receptor Targeting and pH Measurement in Cells. *Bioconjugate Chem.* **2012**, *23*, 2247–2255.

(761) Chauhan, V. M.; Burnett, G. R.; Aylott, J. W. Dual-Fluorophore Ratiometric pH Nanosensor with Tuneable pK_a and Extended Dynamic Range. *Analyst* **2011**, *136*, 1799–1801.

(762) Zhang, M.; Søndergaard, R. V.; Kumar, E. K. P.; Henriksen, J. R.; Cui, D.; Hammershøj, P.; Clausen, M. H.; Andresen, T. L. A Hydrogel Based Nanosensor with an Unprecedented Broad Sensitivity

Range for pH Measurements in Cellular Compartments. *Analyst* **2015**, *140*, 7246–7253.

(763) Søndergaard, R. V.; Henriksen, J. R.; Andresen, T. L. Design, Calibration and Application of Broad-Range Optical Nanosensors for Determining Intracellular pH. *Nat. Protoc.* **2014**, *9*, 2841–2858.

(764) Benjaminsen, R. V.; Sun, H.; Henriksen, J. R.; Christensen, N. M.; Almdal, K.; Andresen, T. L. Evaluating Nanoparticle Sensor Design for Intracellular pH Measurements. *ACS Nano* **2011**, *5*, 5864–5873.

(765) Sun, H.; Almdal, K.; Andresen, T. L. Expanding the Dynamic Measurement Range for Polymeric Nanoparticle pH Sensors. *Chem. Commun.* **2011**, *47*, 5268–5270.

(766) Sun, H.; Andresen, T. L.; Benjaminsen, R. V.; Almdal, K. Polymeric Nanosensors for Measuring the Full Dynamic pH Range of Endosomes and Lysosomes in Mammalian Cells. *J. Biomed. Nanotechnol.* **2009**, *5*, 676–682.

(767) Mistlberger, G.; Medina-Castillo, A. L.; Borisov, S. M.; Mayr, T.; Fernández-Gutiérrez, A.; Fernandez-Sanchez, J. F.; Klimant, I. Mini-Emulsion Solvent Evaporation: A Simple and Versatile Way to Magnetic Nanosensors. *Microchim. Acta* **2011**, *172*, 299–308.

(768) Peng, H.; Stolwijk, J. A.; Sun, L.-N.; Wegener, J.; Wolfbeis, O. S. A Nanogel for Ratiometric Fluorescent Sensing of Intracellular pH Values. *Angew. Chem., Int. Ed.* **2010**, *49*, 4246–4249.

(769) Bao, Y.; De Keersmaecker, H.; Corneille, S.; Yu, F.; Mizuno, H.; Zhang, G.; Hofkens, J.; Mendrek, B.; Kowalczyk, A.; Smet, M. Tunable Ratiometric Fluorescence Sensing of Intracellular pH by Aggregation-Induced Emission-Active Hyperbranched Polymer Nanoparticles. *Chem. Mater.* **2015**, *27*, 3450–3455.

(770) Chen, J.; Tang, Y.; Wang, H.; Zhang, P.; Li, Y.; Jiang, J. Design and Fabrication of Fluorescence Resonance Energy Transfer-Mediated Fluorescent Polymer Nanoparticles for Ratiometric Sensing of Lysosomal pH. *J. Colloid Interface Sci.* **2016**, *484*, 298–307.

(771) Kisiel, A.; Klucińska, K.; Głębińska, Z.; Gniadek, M.; Maksymiuk, K.; Michalska, A. Alternating Polymer Micelle Nanospheres for Optical Sensing. *Analyst* **2014**, *139*, 2515–2524.

(772) Chang, S.; Wu, X.; Li, Y.; Niu, D.; Gao, Y.; Ma, Z.; Gu, J.; Zhao, W.; Zhu, W.; Tian, H.; Shi, J. A pH-Responsive Hybrid Fluorescent Nanoprobe for Real Time Cell Labeling and Endocytosis Tracking. *Biomaterials* **2013**, *34*, 10182–10190.

(773) Schulz, A.; Wotschadlo, J.; Heinze, T.; Mohr, G. J. Fluorescent Nanoparticles for Ratiometric pH-Monitoring in the Neutral Range. *J. Mater. Chem.* **2010**, *20*, 1475–1482.

(774) Zhou, X.; Su, F.; Tian, Y.; Meldrum, D. R. Dually Fluorescent Core-Shell Microgels for Ratiometric Imaging in Live Antigen-Presenting Cells. *PLoS One* **2014**, *9*, No. e88185.

(775) Kreft, O.; Javier, A. M.; Sukhorukov, G. B.; Parak, W. J. Polymer Microcapsules as Mobile Local pH-Sensors. *J. Mater. Chem.* **2007**, *17*, 4471–4476.

(776) Madsen, J.; Canton, I.; Warren, N. J.; Themistou, E.; Blanz, A.; Ustbas, B.; Tian, X.; Pearson, R.; Battaglia, G.; Lewis, A. L.; Armes, S. P. Nile Blue-Based Nanosized pH Sensors for Simultaneous Far-Red and Near-Infrared Live Bioimaging. *J. Am. Chem. Soc.* **2013**, *135*, 14863–14870.

(777) Georgiev, N. I.; Bryaskova, R.; Tzoneva, R.; Ugrinova, I.; Detrembleur, C.; Miloshev, S.; Asiri, A. M.; Qusti, A. H.; Bojinov, V. B. A Novel pH Sensitive Water Soluble Fluorescent Nanomicellar Sensor for Potential Biomedical Applications. *Bioorg. Med. Chem.* **2013**, *21*, 6292–6302.

(778) Kumar E K, P.; Feldborg, L. N.; Almdal, K.; Andresen, T. L. Synthesis and Characterization of a Micelle-Based pH Nanosensor with an Unprecedented Broad Measurement Range. *Chem. Mater.* **2013**, *25*, 1496–1501.

(779) Li, Y.-Y.; Cheng, H.; Zhu, J.-L.; Yuan, L.; Dai, Y.; Cheng, S.-X.; Zhang, X.-Z.; Zhuo, R.-X. Temperature- and pH-Sensitive Multi-colored Micellar Complexes. *Adv. Mater.* **2009**, *21*, 2402–2406.

(780) Pan, T.; Yang, C.; Shi, J.; Hao, C.; Qiao, Y.; Li, J.; Deng, M.; Tian, Y.; Chen, M. Dual pH and Oxygen Luminescent Nanoprobes Based on Graft Polymers for Extracellular Metabolism Monitoring and Intracellular Imaging. *Sens. Actuators, B* **2019**, *291*, 306–318.

(781) Yao, Q.; Lu, S.; Lin, F.; Zhao, T.; Zhao, L.; Chen, X. A Co-Precipitation Strategy for Making a Ratiometric pH Nanosensor for Intracellular Imaging. *Sens. Actuators, B* **2017**, *250*, 484–490.

(782) Gong, P.; Yang, Y.; Yi, H.; Fang, S.; Zhang, P.; Sheng, Z.; Gao, G.; Gao, D.; Cai, L. Polypeptide Micelles with Dual pH Activatable Dyes for Sensing Cells and Cancer Imaging. *Nanoscale* **2014**, *6*, 5416–5424.

(783) Patrick, M. J.; Janjic, J. M.; Teng, H.; O'Hear, M. R.; Brown, C. W.; Stokum, J. A.; Schmidt, B. F.; Ahrens, E. T.; Waggoner, A. S. Intracellular pH Measurements Using Perfluorocarbon Nanoemulsions. *J. Am. Chem. Soc.* **2013**, *135*, 18445–18457.

(784) McNamara, K. P.; Rosenzweig, N.; Rosenzweig, Z. Liposome-Based Optochemical Nanosensors. *Microchim. Acta* **1999**, *131*, 57–64.

(785) McNamara, K. P.; Nguyen, T.; Dumitrascu, G.; Ji, J.; Rosenzweig, N.; Rosenzweig, Z. Synthesis, Characterization, and Application of Fluorescence Sensing Lipobeads for Intracellular pH Measurements. *Anal. Chem.* **2001**, *73*, 3240–3246.

(786) Tang, L.; Li, T.; Zhuang, S.; Lu, Q.; Li, P.; Huang, B. Synthesis of pH-Sensitive Fluorescein Grafted Cellulose Nanocrystals with an Amino Acid Spacer. *ACS Sustainable Chem. Eng.* **2016**, *4*, 4842–4849.

(787) Horning, S.; Schultz, A.; Mohr, G. J.; Heinze, T. Fluorescent Polysaccharide Nanoparticles for pH-Sensing. *J. Photopolym. Sci. Technol.* **2009**, *22*, 671–673.

(788) Schulz, A.; Hornig, S.; Liebert, T.; Birkner, E.; Heinze, T.; Mohr, G. J. Evaluation of Fluorescent Polysaccharide Nanoparticles for pH-Sensing. *Org. Biomol. Chem.* **2009**, *7*, 1884–1889.

(789) Rosenthal, S. J.; Chang, J. C.; Kovtun, O.; McBride, J. R.; Tomlinson, I. D. Biocompatible Quantum Dots for Biological Applications. *Chem. Biol.* **2011**, *18*, 10–24.

(790) Arya, H.; Kaul, Z.; Wadhwa, R.; Taira, K.; Hirano, T.; Kaul, S. C. Quantum Dots in Bio-Imaging: Revolution by the Small. *Biochem. Biophys. Res. Commun.* **2005**, *329*, 1173–1177.

(791) Li, J.; Zhu, J.-J. Quantum Dots for Fluorescent Biosensing and Bio-Imaging Applications. *Analyst* **2013**, *138*, 2506–2515.

(792) Wang, Y.; Hu, R.; Lin, G.; Roy, I.; Yong, K.-T. Functionalized Quantum Dots for Biosensing and Bioimaging and Concerns on Toxicity. *ACS Appl. Mater. Interfaces* **2013**, *5*, 2786–2799.

(793) Hutter, E.; Maysinger, D. Gold Nanoparticles and Quantum Dots for Bioimaging. *Microsc. Res. Tech.* **2011**, *74*, 592–604.

(794) Jaiswal, J. K.; Simon, S. M. Potentials and Pitfalls of Fluorescent Quantum Dots for Biological Imaging. *Trends Cell Biol.* **2004**, *14*, 497–504.

(795) Bera, D.; Qian, L.; Tseng, T.-K.; Holloway, P. H. Quantum Dots and Their Multimodal Applications: A Review. *Materials* **2010**, *3*, 2260–2345.

(796) Biju, V.; Itoh, T.; Anas, A.; Sujith, A.; Ishikawa, M. Semiconductor Quantum Dots and Metal Nanoparticles: Syntheses, Optical Properties, and Biological Applications. *Anal. Bioanal. Chem.* **2008**, *391*, 2469–2495.

(797) Petryayeva, E.; Algar, W. R.; Medintz, I. L. Quantum Dots in Bioanalysis: A Review of Applications across Various Platforms for Fluorescence Spectroscopy and Imaging. *Appl. Spectrosc.* **2013**, *67*, 215–252.

(798) Chen, C.; Zhang, P.; Zhang, L.; Gao, D.; Gao, G.; Yang, Y.; Li, W.; Gong, P.; Cai, L. Long-Decay near-Infrared-Emitting Doped Quantum Dots for Lifetime-Based in Vivo pH Imaging. *Chem. Commun.* **2015**, *51*, 11162–11165.

(799) Kirchner, C.; Liedl, T.; Kudera, S.; Pellegrino, T.; Muñoz Javier, A.; Gaub, H. E.; Stölzle, S.; Fertig, N.; Parak, W. J. Cytotoxicity of Colloidal CdSe and CdSe/ZnS Nanoparticles. *Nano Lett.* **2005**, *5*, 331–338.

(800) Kuno, M.; Fromm, D. P.; Hamann, H. F.; Gallagher, A.; Nesbitt, D. J. Nonexponential “Blinking” Kinetics of Single CdSe Quantum Dots: A Universal Power Law Behavior. *J. Chem. Phys.* **2000**, *112*, 3117–3120.

(801) Orte, A.; Alvarez-Pez, J. M.; Ruedas-Rama, M. J. Fluorescence Lifetime Imaging Microscopy for the Detection of Intracellular pH with Quantum Dot Nanosensors. *ACS Nano* **2013**, *7*, 6387–6395.

- (802) Ruedas-Rama, M. J.; Orte, A.; Hall, E. A. H.; Alvarez-Pez, J. M.; Talavera, E. M. Quantum Dot Photoluminescence Lifetime-Based pH Nanosensor. *Chem. Commun.* **2011**, *47*, 2898–2900.
- (803) Chen, X.; Sun, X.; Xu, W.; Pan, G.; Zhou, D.; Zhu, J.; Wang, H.; Bai, X.; Dong, B.; Song, H. Ratiometric Photoluminescence Sensing Based on Ti₃C₂MXene Quantum Dots as an Intracellular pH Sensor. *Nanoscale* **2018**, *10*, 1111–1118.
- (804) Xu, H.; Li, D.; Zhao, Y.; Wang, X.; Li, D.; Wang, Y. Sodium 4-mercaptophenolate Capped CdSe/ZnS Quantum Dots as a Fluorescent Probe for pH Detection in Acidic Aqueous Media. *Luminescence* **2018**, *33*, 410–416.
- (805) Li, D.; Xu, H.; Li, D.; Wang, Y. P-Aminothiophenol-Coated CdSe/ZnS Quantum Dots as a Turn-on Fluorescent Probe for pH Detection in Aqueous Media. *Talanta* **2017**, *166*, 54–62.
- (806) Snee, P. T.; Somers, R. C.; Nair, G.; Zimmer, J. P.; Bawendi, M. G.; Nocera, D. G. A Ratiometric CdSe/ZnS Nanocrystal pH Sensor. *J. Am. Chem. Soc.* **2006**, *128*, 13320–13321.
- (807) Somers, R. C.; Lanning, R. M.; Snee, P. T.; Greytak, A. B.; Jain, R. K.; Bawendi, M. G.; Nocera, D. G. A Nanocrystal-Based Ratiometric pH Sensor for Natural pH Ranges. *Chem. Sci.* **2012**, *3*, 2980–2985.
- (808) Tang, R.; Lee, H.; Achilefu, S. Induction of pH Sensitivity on the Fluorescence Lifetime of Quantum Dots by NIR Fluorescent Dyes. *J. Am. Chem. Soc.* **2012**, *134*, 4545–4548.
- (809) Paek, K.; Chung, S.; Cho, C.-H.; Kim, B. J. Fluorescent and pH-Responsive Diblock Copolymer-Coated Core–Shell CdSe/ZnS Particles for a Color-Displaying, Ratiometric pH Sensor. *Chem. Commun.* **2011**, *47*, 10272–10274.
- (810) Ast, S.; Rutledge, P. J.; Todd, M. H. pH-Responsive Quantum Dots (RQDs) That Combine a Fluorescent Nanoparticle with a pH-Sensitive Dye. *Phys. Chem. Chem. Phys.* **2014**, *16*, 25255–25257.
- (811) Jin, T.; Sasaki, A.; Kinjo, M.; Miyazaki, J. A Quantum Dot-Based Ratiometric pH Sensor. *Chem. Commun.* **2010**, *46*, 2408–2410.
- (812) Liu, T.; Wang, W.; Ding, H.; Yi, D. Smartphone-Based Hand-Held Optical Fiber Fluorescence Sensor for On-Site pH Detection. *IEEE Sens. J.* **2019**, *19*, 9441–9446.
- (813) Medintz, I. L.; Stewart, M. H.; Trammell, S. A.; Susumu, K.; Delehanty, J. B.; Mei, B. C.; Melinger, J. S.; Blanco-Canosa, J. B.; Dawson, P. E.; Mattoussi, H. Quantum-Dot/Dopamine Bioconjugates Function as Redox Coupled Assemblies for in Vitro and Intracellular pH Sensing. *Nat. Mater.* **2010**, *9*, 676–684.
- (814) Susumu, K.; Field, L. D.; Oh, E.; Hunt, M.; Delehanty, J. B.; Palomo, V.; Dawson, P. E.; Huston, A. L.; Medintz, I. L. Purple-, Blue-, and Green-Emitting Multishell Alloyed Quantum Dots: Synthesis, Characterization, and Application for Ratiometric Extracellular pH Sensing. *Chem. Mater.* **2017**, *29*, 7330–7344.
- (815) Kurabayashi, T.; Funaki, N.; Fukuda, T.; Akiyama, S.; Suzuki, M. CdSe/ZnS Quantum Dots Conjugated with a Fluorescein Derivative: A FRET-Based pH Sensor for Physiological Alkaline Conditions. *Anal. Sci.* **2014**, *30*, 545–550.
- (816) Liu, Y.-S.; Sun, Y.; Vernier, P. T.; Liang, C.-H.; Chong, S. Y. C.; Gundersen, M. A. pH-Sensitive Photoluminescence of CdSe/ZnSe/ZnS Quantum Dots in Human Ovarian Cancer Cells. *J. Phys. Chem. C* **2007**, *111*, 2872–2878.
- (817) Yue, Q.; Hu, Y.; Tao, L.; Zhang, B.; Liu, C.; Wang, Y.; Chen, C.; Zhao, J.; Li, C.-Z. Fluorometric Sensing of pH Values Using Green-Emitting Black Phosphorus Quantum Dots. *Microchim. Acta* **2019**, *186*, 640.
- (818) Zu, F.; Yan, F.; Bai, Z.; Xu, J.; Wang, Y.; Huang, Y.; Zhou, X. The Quenching of the Fluorescence of Carbon Dots: A Review on Mechanisms and Applications. *Microchim. Acta* **2017**, *184*, 1899–1914.
- (819) Shen, L.; Zhang, L.; Chen, M.; Chen, X.; Wang, J. The Production of pH-Sensitive Photoluminescent Carbon Nanoparticles by the Carbonization of Polyethylenimine and Their Use for Bioimaging. *Carbon* **2013**, *55*, 343–349.
- (820) Chandra, A.; Singh, N. Biocompatible Fluorescent Carbon Dots for Ratiometric Intracellular pH Sensing. *ChemistrySelect* **2017**, *2*, 5723–5728.
- (821) Zhong, D.; Miao, H.; Yang, K.; Yang, X. Carbon Dots Originated from Carnation for Fluorescent and Colorimetric pH Sensing. *Mater. Lett.* **2016**, *166*, 89–92.
- (822) Nie, H.; Li, M.; Li, Q.; Liang, S.; Tan, Y.; Sheng, L.; Shi, W.; Zhang, S. X.-A. Carbon Dots with Continuously Tunable Full-Color Emission and Their Application in Ratiometric pH Sensing. *Chem. Mater.* **2014**, *26*, 3104–3112.
- (823) Wang, N.; Zheng, A.-Q.; Liu, X.; Chen, J.-J.; Yang, T.; Chen, M.-L.; Wang, J.-H. Deep Eutectic Solvent-Assisted Preparation of Nitrogen/Chloride-Doped Carbon Dots for Intracellular Biological Sensing and Live Cell Imaging. *ACS Appl. Mater. Interfaces* **2018**, *10*, 7901–7909.
- (824) Wang, W.-J.; Xia, J.-M.; Feng, J.; He, M.-Q.; Chen, M.-L.; Wang, J.-H. Green Preparation of Carbon Dots for Intracellular pH Sensing and Multicolor Live Cell Imaging. *J. Mater. Chem. B* **2016**, *4*, 7130–7137.
- (825) Pedro, S. G.; Salinas-Castillo, A.; Ariza-Avidad, M.; Lapresta-Fernández, A.; Sánchez-González, C.; Martínez-Cisneros, C. S.; Puyol, M.; Capitan-Vallvey, L. F.; Alonso-Chamarro, J. Microsystem-Assisted Synthesis of Carbon Dots with Fluorescent and Colorimetric Properties for pH Detection. *Nanoscale* **2014**, *6*, 6018–6024.
- (826) Jiao, Y.; Gong, X.; Han, H.; Gao, Y.; Lu, W.; Liu, Y.; Xian, M.; Shuang, S.; Dong, C. Facile Synthesis of Orange Fluorescence Carbon Dots with Excitation Independent Emission for pH Sensing and Cellular Imaging. *Anal. Chim. Acta* **2018**, *1042*, 125–132.
- (827) Liu, X.; Yang, C.; Zheng, B.; Dai, J.; Yan, L.; Zhuang, Z.; Du, J.; Guo, Y.; Xiao, D. Green Anhydrous Synthesis of Hydrophilic Carbon Dots on Large-Scale and Their Application for Broad Fluorescent pH Sensing. *Sens. Actuators, B* **2018**, *255*, 572–579.
- (828) Li, B.; Ma, H.; Zhang, B.; Qian, J.; Cao, T.; Feng, H.; Li, W.; Dong, Y.; Qin, W. Dually Emitting Carbon Dots as Fluorescent Probes for Ratiometric Fluorescent Sensing of pH Values, Mercury (II), Chloride and Cr (VI) via Different Mechanisms. *Microchim. Acta* **2019**, *186*, 341.
- (829) Wang, Q.; Yang, H.; Zhang, Q.; Ge, H.; Zhang, S.; Wang, Z.; Ji, X. Strong Acid-Assisted Preparation of Green-Emissive Carbon Dots for Fluorometric Imaging of pH Variation in Living Cells. *Microchim. Acta* **2019**, *186*, 468.
- (830) Chandra, A.; Singh, N. Cell Microenvironment pH Sensing in 3D Microgels Using Fluorescent Carbon Dots. *ACS Biomater. Sci. Eng.* **2017**, *3*, 3620–3627.
- (831) Zhu, X.; Jin, H.; Gao, C.; Gui, R.; Wang, Z. Ratiometric, Visual, Dual-Signal Fluorescent Sensing and Imaging of pH/Copper Ions in Real Samples Based on Carbon Dots-Fluorescein Isothiocyanate Composites. *Talanta* **2017**, *162*, 65–71.
- (832) Essner, J. B.; Laber, C. H.; Ravula, S.; Polo-Parada, L.; Baker, G. A. Pee-Dots: Biocompatible Fluorescent Carbon Dots Derived from the Upcycling of Urine. *Green Chem.* **2016**, *18*, 243–250.
- (833) D'Angelis do E. S. Barbosa, C.; Correa, J. R.; Medeiros, G. A.; Barreto, G.; Magalhães, K. G.; de Oliveira, A. L.; Spencer, J.; Rodrigues, M. O.; Neto, B. A. D. Carbon Dots (C-dots) from Cow Manure with Impressive Subcellular Selectivity Tuned by Simple Chemical Modification. *Chem. - Eur. J.* **2015**, *21*, 5055–5060.
- (834) Du, F.; Ming, Y.; Zeng, F.; Yu, C.; Wu, S. A Low Cytotoxic and Ratiometric Fluorescent Nanosensor Based on Carbon-Dots for Intracellular pH Sensing and Mapping. *Nanotechnology* **2013**, *24*, 365101.
- (835) Liu, W.; Li, C.; Sun, X.; Pan, W.; Wang, J. Carbon-Dot-Based Ratiometric Fluorescent pH Sensor for the Detections of Very Weak Acids Assisted by Auxiliary Reagents That Contribute to the Release of Protons. *Sens. Actuators, B* **2017**, *244*, 441–449.
- (836) Shi, W.; Li, X.; Ma, H. A Tunable Ratiometric pH Sensor Based on Carbon Nanodots for the Quantitative Measurement of the Intracellular pH of Whole Cells. *Angew. Chem., Int. Ed.* **2012**, *51*, 6432–6435.
- (837) Qu, S.; Chen, H.; Zheng, X.; Cao, J.; Liu, X. Ratiometric Fluorescent Nanosensor Based on Water Soluble Carbon Nanodots with Multiple Sensing Capacities. *Nanoscale* **2013**, *5*, 5514–5518.

- (838) Zhang, C.; Cui, Y.; Song, L.; Liu, X.; Hu, Z. Microwave Assisted One-Pot Synthesis of Graphene Quantum Dots as Highly Sensitive Fluorescent Probes for Detection of Iron Ions and pH Value. *Talanta* **2016**, *150*, 54–60.
- (839) Wang, C.; Xu, Z.; Cheng, H.; Lin, H.; Humphrey, M. G.; Zhang, C. A Hydrothermal Route to Water-Stable Luminescent Carbon Dots as Nanosensors for pH and Temperature. *Carbon* **2015**, *82*, 87–95.
- (840) Yao, C.; Xu, Y.; Xia, Z. A Carbon Dot-Encapsulated UiO-Type Metal Organic Framework as a Multifunctional Fluorescent Sensor for Temperature, Metal Ion and pH Detection. *J. Mater. Chem. C* **2018**, *6*, 4396–4399.
- (841) Liu, G.; Li, S.; Cheng, M.; Zhao, L.; Zhang, B.; Gao, Y.; Xu, Y.; Liu, F.; Lu, G. Facile Synthesis of Nitrogen and Sulfur Co-Doped Carbon Dots for Multiple Sensing Capacities: Alkaline Fluorescence Enhancement Effect, Temperature Sensing, and Selective Detection of Fe³⁺ Ions. *New J. Chem.* **2018**, *42*, 13147–13156.
- (842) Wang, Z.; Lu, Y.; Yuan, H.; Ren, Z.; Xu, C.; Chen, J. Microplasma-Assisted Rapid Synthesis of Luminescent Nitrogen-Doped Carbon Dots and Their Application in pH Sensing and Uranium Detection. *Nanoscale* **2015**, *7*, 20743–20748.
- (843) Moniruzzaman, M.; Kim, J. Mechanistic Studies on the β -Resorcylic Acid Mediated Carbon Dots for the pH-Induced Fluorescence Switch and Sensing Application. *Dyes Pigm.* **2019**, *163*, 538–546.
- (844) Wang, L.; Li, M.; Li, W.; Han, Y.; Liu, Y.; Li, Z.; Zhang, B.; Pan, D. Rationally Designed Efficient Dual-Mode Colorimetric/Fluorescence Sensor Based on Carbon Dots for Detection of pH and Cu²⁺ Ions. *ACS Sustainable Chem. Eng.* **2018**, *6*, 12668–12674.
- (845) Park, C. H.; Yang, H.; Lee, J.; Cho, H.-H.; Kim, D.; Lee, D. C.; Kim, B. J. Multicolor Emitting Block Copolymer-Integrated Graphene Quantum Dots for Colorimetric, Simultaneous Sensing of Temperature, pH, and Metal Ions. *Chem. Mater.* **2015**, *27*, 5288–5294.
- (846) Wang, Y.; Xu, J.; Lei, L.; Wang, F.; Xu, Z.; Zhang, W. Multi-Functional Carbon Dots-Based Nanoprobe for Ratiometric Enzyme Reaction Monitoring and Biothiol Analysis. *Sens. Actuators, B* **2018**, *264*, 296–303.
- (847) Shi, B.; Zhang, L.; Lan, C.; Zhao, J.; Su, Y.; Zhao, S. One-Pot Green Synthesis of Oxygen-Rich Nitrogen-Doped Graphene Quantum Dots and Their Potential Application in pH-Sensitive Photoluminescence and Detection of Mercury(II) Ions. *Talanta* **2015**, *142*, 131–139.
- (848) Doroodmand, M. M.; Askari, M. Synthesis of a Novel Nitrogen-Doped Carbon Dot by Microwave-Assisted Carbonization Method and Its Applications as Selective Probes for Optical pH (Acidity) Sensing in Aqueous/Nonaqueous Media, Determination of Nitrate/Nitrite, and Optical Recognition of NO_x Gas. *Anal. Chim. Acta* **2017**, *968*, 74–84.
- (849) Chen, J.-L.; Yan, X.-P. Ionic Strength and pH Reversible Response of Visible and Near-Infrared Fluorescence of Graphene Oxide Nanosheets for Monitoring the Extracellular pH. *Chem. Commun.* **2011**, *47*, 3135–3137.
- (850) Kwon, H.; Kim, M.; Meany, B.; Piao, Y.; Powell, L. R.; Wang, Y. Optical Probing of Local pH and Temperature in Complex Fluids with Covalently Functionalized, Semiconducting Carbon Nanotubes. *J. Phys. Chem. C* **2015**, *119*, 3733–3739.
- (851) Ehtesabi, H.; Hallaji, Z.; Najafi Nobar, S.; Bagheri, Z. Carbon Dots with pH-Responsive Fluorescence: A Review on Synthesis and Cell Biological Applications. *Microchim. Acta* **2020**, *187*, No. 150.
- (852) Moniruzzaman, M.; Kim, J. N-Doped Carbon Dots with Tunable Emission for Multifaceted Application: Solvatochromism, Moisture Sensing, pH Sensing, and Solid State Multicolor Lighting. *Sens. Actuators, B* **2019**, *295*, 12–21.
- (853) Jia, X.; Li, J.; Wang, E. One-Pot Green Synthesis of Optically pH-Sensitive Carbon Dots with Upconversion Luminescence. *Nanoscale* **2012**, *4*, 5572–5575.
- (854) Wu, Z. L.; Gao, M. X.; Wang, T. T.; Wan, X. Y.; Zheng, L. L.; Huang, C. Z. A General Quantitative pH Sensor Developed with Dicyandiamide N-Doped High Quantum Yield Graphene Quantum Dots. *Nanoscale* **2014**, *6*, 3868–3874.
- (855) Yang, S.; Chen, X.; Liu, S.; Wang, F.; Ouyang, G. Microwave-Assisted Solid-Phase Synthesis of Highly Fluorescent Carbon Nanoparticles and Its Application in Intracellular pH Sensing. *Talanta* **2018**, *186*, 80–87.
- (856) Shangguan, J.; He, D.; He, X.; Wang, K.; Xu, F.; Liu, J.; Tang, J.; Yang, X.; Huang, J. Label-Free Carbon-Dots-Based Ratiometric Fluorescence pH Nanoprobes for Intracellular pH Sensing. *Anal. Chem.* **2016**, *88*, 7837–7843.
- (857) Yang, M.; Li, B.; Zhong, K.; Lu, Y. Photoluminescence Properties of N-Doped Carbon Dots Prepared in Different Solvents and Applications in pH Sensing. *J. Mater. Sci.* **2018**, *53*, 2424–2433.
- (858) Sun, Y.; Wang, X.; Wang, C.; Tong, D.; Wu, Q.; Jiang, K.; Jiang, Y.; Wang, C.; Yang, M. Red Emitting and Highly Stable Carbon Dots with Dual Response to pH Values and Ferric Ions. *Microchim. Acta* **2018**, *185*, 83.
- (859) Wang, L.; Chen, Y. Lanthanide Doped Carbon Dots as a Fluorescence Chromaticity-Based pH Probe. *Microchim. Acta* **2018**, *185*, 489.
- (860) Mondal, T. K.; Saha, S. K. Facile Approach To Synthesize Nitrogen- and Oxygen-Rich Carbon Quantum Dots for pH Sensor, Fluorescent Indicator, and Invisible Ink Applications. *ACS Sustainable Chem. Eng.* **2019**, *7*, 19669–19678.
- (861) Xia, C.; Cao, M.; Xia, J.; Zhou, G.; Jiang, D.; Zhang, D.; Wang, J.; Li, H. An Ultrafast Responsive and Sensitive Ratiometric Fluorescent pH Nanoprobe Based on Label-Free Dual-Emission Carbon Dots. *J. Mater. Chem. C* **2019**, *7*, 2563–2569.
- (862) Wang, Y.; Lu, L.; Peng, H.; Xu, J.; Wang, F.; Qi, R.; Xu, Z.; Zhang, W. Multi-Doped Carbon Dots with Ratiometric pH Sensing Properties for Monitoring Enzyme Catalytic Reactions. *Chem. Commun.* **2016**, *52*, 9247–9250.
- (863) Zhang, T.; Zhai, Y.; Wang, H.; Zhu, J.; Xu, L.; Dong, B.; Song, H. Facilely Prepared Carbon Dots and Rare Earth Ion Doped Hybrid Composites for Ratio-Metric pH Sensing and White-Light Emission. *RSC Adv.* **2016**, *6*, 61468–61472.
- (864) Hu, S.; Meng, X.; Tian, F.; Yang, W.; Li, N.; Xue, C.; Yang, J.; Chang, Q. Dual Photoluminescence Centers from Inorganic-Salt-Functionalized Carbon Dots for Ratiometric pH Sensing. *J. Mater. Chem. C* **2017**, *5*, 9849–9853.
- (865) Pal, A.; Ahmad, K.; Dutta, D.; Chattopadhyay, A. Boron Doped Carbon Dots with Unusually High Photoluminescence Quantum Yield for Ratiometric Intracellular pH Sensing. *ChemPhysChem* **2019**, *20*, 1018–1027.
- (866) Mao, Y.; Bao, Y.; Yan, L.; Li, G.; Li, F.; Han, D.; Zhang, X.; Niu, L. pH-Switched Luminescence and Sensing Properties of a Carbon Dot–Polyaniline Composite. *RSC Adv.* **2013**, *3*, 5475–5482.
- (867) Shi, B.; Su, Y.; Zhang, L.; Liu, R.; Huang, M.; Zhao, S. Nitrogen-Rich Functional Groups Carbon Nanoparticles Based Fluorescent pH Sensor with Broad-Range Responding for Environmental and Live Cells Applications. *Biosens. Bioelectron.* **2016**, *82*, 233–239.
- (868) Lu, L.; Liu, C.; Li, G.; Liu, L.-J.; Leung, C.-H.; Ma, D.-L. Low Toxic Fluorescent Nanoprobe Applicable for Sensing pH Changes in Biological Environment. *Sens. Actuators, B* **2018**, *257*, 860–865.
- (869) Yuan, F.; Ding, L.; Li, Y.; Li, X.; Fan, L.; Zhou, S.; Fang, D.; Yang, S. Multicolor Fluorescent Graphene Quantum Dots Colorimetrically Responsive to All-pH and a Wide Temperature Range. *Nanoscale* **2015**, *7*, 11727–11733.
- (870) Shao, T.; Zhang, P.; Tang, L.; Zhuo, S.; Zhu, C. Highly Sensitive Enzymatic Determination of Urea Based on the pH-Dependence of the Fluorescence of Graphene Quantum Dots. *Microchim. Acta* **2015**, *182*, 1431–1437.
- (871) Hong, S. W.; Kim, K. H.; Huh, J.; Ahn, C.-H.; Jo, W. H. Design and Synthesis of a New pH Sensitive Polymeric Sensor Using Fluorescence Resonance Energy Transfer. *Chem. Mater.* **2005**, *17*, 6213–6215.
- (872) Paek, K.; Yang, H.; Lee, J.; Park, J.; Kim, B. J. Efficient Colorimetric pH Sensor Based on Responsive Polymer–Quantum Dot Integrated Graphene Oxide. *ACS Nano* **2014**, *8*, 2848–2856.
- (873) Zhou, K.; Liu, H.; Zhang, S.; Huang, X.; Wang, Y.; Huang, G.; Sumer, B. D.; Gao, J. Multicolored pH-Tunable and Activatable

Fluorescence Nanoplatfom Responsive to Physiologic pH Stimuli. *J. Am. Chem. Soc.* **2012**, *134*, 7803–7811.

(874) You, S.; Cai, Q.; Müllen, K.; Yang, W.; Yin, M. pH-Sensitive Unimolecular Fluorescent Polymeric Micelles: From Volume Phase Transition to Optical Response. *Chem. Commun.* **2014**, *50*, 823–825.

(875) Frisch, H.; Besenius, P. pH-Switchable Self-Assembled Materials. *Macromol. Rapid Commun.* **2015**, *36*, 346–363.

(876) Hong, S. W.; Jo, W. H. A Fluorescence Resonance Energy Transfer Probe for Sensing pH in Aqueous Solution. *Polymer* **2008**, *49*, 4180–4187.

(877) Chiu, Y.-L.; Chen, S.-A.; Chen, J.-H.; Chen, K.-J.; Chen, H.-L.; Sung, H.-W. A Dual-Emission Förster Resonance Energy Transfer Nanoprobe for Sensing/Imaging pH Changes in the Biological Environment. *ACS Nano* **2010**, *4*, 7467–7474.

(878) Fu, L.; Yuan, P.; Ruan, Z.; Liu, L.; Li, T.; Yan, L. Ultra-pH-Sensitive Polypeptide Micelles with Large Fluorescence off/on Ratio in near Infrared Range. *Polym. Chem.* **2017**, *8*, 1028–1038.

(879) Ma, X.; Wang, Y.; Zhao, T.; Li, Y.; Su, L.-C.; Wang, Z.; Huang, G.; Sumer, B. D.; Gao, J. Ultra-pH-Sensitive Nanoprobe Library with Broad pH Tunability and Fluorescence Emissions. *J. Am. Chem. Soc.* **2014**, *136*, 11085–11092.

(880) Liu, T.; Hu, J.; Jin, Z.; Jin, F.; Liu, S. Two-Photon Ratiometric Fluorescent Mapping of Intracellular Transport Pathways of pH-Responsive Block Copolymer Micellar Nanocarriers. *Adv. Healthcare Mater.* **2013**, *2*, 1576–1581.

(881) Wang, X.; Stolwijk, J. A.; Lang, T.; Sperber, M.; Meier, R. J.; Wegener, J.; Wolfbeis, O. S. Ultra-Small, Highly Stable, and Sensitive Dual Nanosensors for Imaging Intracellular Oxygen and pH in Cytosol. *J. Am. Chem. Soc.* **2012**, *134*, 17011–17014.

(882) Wu, W.; Aiello, M.; Zhou, T.; Berliner, A.; Banerjee, P.; Zhou, S. In-Situ Immobilization of Quantum Dots in Polysaccharide-Based Nanogels for Integration of Optical pH-Sensing, Tumor Cell Imaging, and Drug Delivery. *Biomaterials* **2010**, *31*, 3023–3031.

(883) Yan, L.; Chang, Y.-N.; Yin, W.; Liu, X.; Xiao, D.; Xing, G.; Zhao, L.; Gu, Z.; Zhao, Y. Biocompatible and Flexible Graphene Oxide/Upconversion Nanoparticle Hybrid Film for Optical pH Sensing. *Phys. Chem. Chem. Phys.* **2014**, *16*, 1576–1582.

(884) Bai, Z.; Chen, R.; Si, P.; Huang, Y.; Sun, H.; Kim, D.-H. Fluorescent pH Sensor Based on Ag@SiO₂ Core–Shell Nanoparticle. *ACS Appl. Mater. Interfaces* **2013**, *5*, 5856–5860.

(885) Panda, B. R.; Chattopadhyay, A. A Water-Soluble Polythiophene–Au Nanoparticle Composite for pH Sensing. *J. Colloid Interface Sci.* **2007**, *316*, 962–967.

(886) Liu, X.; Chen, Q.; Yang, G.; Zhang, L.; Liu, Z.; Cheng, Z.; Zhu, X. Magnetic Nanomaterials with Near-Infrared pH-Activatable Fluorescence via Iron-Catalyzed AGET ATRP for Tumor Acidic Microenvironment Imaging. *J. Mater. Chem. B* **2015**, *3*, 2786–2800.

(887) Lapresta-Fernández, A.; Doussineau, T.; Moro, A. J.; Dutz, S.; Steiniger, F.; Mohr, G. J. Magnetic Core–Shell Fluorescent pH Ratiometric Nanosensor Using a Stöber Coating Method. *Anal. Chim. Acta* **2011**, *707*, 164–170.

(888) Wu, W.; Shen, J.; Gai, Z.; Hong, K.; Banerjee, P.; Zhou, S. Multi-Functional Core-Shell Hybrid Nanogels for pH-Dependent Magnetic Manipulation, Fluorescent pH-Sensing, and Drug Delivery. *Biomaterials* **2011**, *32*, 9876–9887.

(889) Asselin, J.; Roy, C.; Boudreau, D.; Messaddeq, Y.; Bouchareb, R.; Mathieu, P. Supported Core–Shell Nanobiosensors for Quantitative Fluorescence Imaging of Extracellular pH. *Chem. Commun.* **2014**, *50*, 13746–13749.

(890) Sun, S.; Ning, X.; Zhang, G.; Wang, Y.-C.; Peng, C.; Zheng, J. Dimerization of Organic Dyes on Luminescent Gold Nanoparticles for Ratiometric pH Sensing. *Angew. Chem., Int. Ed.* **2016**, *55*, 2421–2424.

(891) Mineo, P. G.; Abbadessa, A.; Rescifina, A.; Mazzaglia, A.; Nicosia, A.; Scamporrino, A. A. PEGylate Porphyrin-Gold Nanoparticles Conjugates as Removable pH-Sensor Nano-Probes for Acidic Environments. *Colloids Surf., A* **2018**, *546*, 40–47.

(892) Ding, C.; Cheng, S.; Zhang, C.; Xiong, Y.; Ye, M.; Xian, Y. Ratiometric Upconversion Luminescence Nanoprobe with Near-

Infrared Ag₂S Nanodots as the Energy Acceptor for Sensing and Imaging of pH in Vivo. *Anal. Chem.* **2019**, *91*, 7181–7188.

(893) Wang, C.; Otto, S.; Dorn, M.; Heinze, K.; Resch-Genger, U. Luminescent TOP Nanosensors for Simultaneously Measuring Temperature, Oxygen, and pH at a Single Excitation Wavelength. *Anal. Chem.* **2019**, *91*, 2337–2344.

(894) Zhao, Y.; Chang, C.; Gai, P.; Han, L.; Li, F.; Li, B. One-Step Synthesis of Fluorescent Organic Nanoparticles: The Application to Label-Free Ratiometric Fluorescent pH Sensor. *Sens. Actuators, B* **2018**, *273*, 1479–1486.

(895) Guo, J.; Xiong, S.; Wu, X.; Shen, J.; Chu, P. K. In Situ Probing of Intracellular pH by Fluorescence from Inorganic Nanoparticles. *Biomaterials* **2013**, *34*, 9183–9189.

(896) Fu, L.; Du, Y.; Zhang, Z.; Sun, H.; Zheng, A.; Liu, X. Dual Sensing of Glutathione and Acidic pH Values by Using MnO₂ Nanosheets and 3-Acetyl-7-Hydroxy-2H-Chromen-2-One as a Fluorescent pH Probe. *Microchim. Acta* **2019**, *186*, 491.

(897) Luo, J.; Xie, Z.; Lam, J. W.; Cheng, L.; Chen, H.; Qiu, C.; Kwok, H. S.; Zhan, X.; Liu, Y.; Zhu, D.; et al. Aggregation-Induced Emission of 1-Methyl-1, 2, 3, 4, 5-Pentaphenylsilole. *Chem. Commun.* **2001**, *18*, 1740–1741.

(898) Hong, Y.; Lam, J. W.; Tang, B. Z. Aggregation-Induced Emission: Phenomenon, Mechanism and Applications. *Chem. Commun.* **2009**, *29*, 4332–4353.

(899) Chen, S.; Hong, Y.; Liu, Y.; Liu, J.; Leung, C. W.; Li, M.; Kwok, R. T.; Zhao, E.; Lam, J. W.; Yu, Y.; et al. Full-Range Intracellular pH Sensing by an Aggregation-Induced Emission-Active Two-Channel Ratiometric Fluorogen. *J. Am. Chem. Soc.* **2013**, *135*, 4926–4929.

(900) Fang, M.; Xia, S.; Bi, J.; Wigstrom, T. P.; Valenzano, L.; Wang, J.; Mazi, W.; Tanasova, M.; Luo, F.-T.; Liu, H. A Cyanine-Based Fluorescent Cassette with Aggregation-Induced Emission for Sensitive Detection of pH Changes in Live Cells. *Chem. Commun.* **2018**, *54*, 1133–1136.

(901) Rananaware, A.; Bhosale, R. S.; Patil, H.; Al Kobaisi, M.; Abraham, A.; Shukla, R.; Bhosale, S. V.; Bhosale, S. V. Precise Aggregation-Induced Emission Enhancement via H⁺ Sensing and Its Use in Ratiometric Detection of Intracellular pH Values. *RSC Adv.* **2014**, *4*, 59078–59082.

(902) Wang, L.; Yang, L.; Cao, D. Probes Based on Diketopyrrolopyrrole and Anthracenone Conjugates with Aggregation-Induced Emission Characteristics for pH and BSA Sensing. *Sens. Actuators, B* **2015**, *221*, 155–166.

(903) Zhao, Y.; Zhu, W.; Ren, L.; Zhang, K. Aggregation-Induced Emission Polymer Nanoparticles with pH-Responsive Fluorescence. *Polym. Chem.* **2016**, *7*, 5386–5395.

(904) Zhou, H.; Liu, F.; Wang, X.; Yan, H.; Song, J.; Ye, Q.; Tang, B. Z.; Xu, J. Aggregation Induced Emission Based Fluorescence pH and Temperature Sensors: Probing Polymer Interactions in Poly (N-Isopropyl Acrylamide-Co-Tetra (Phenyl) Ethene Acrylate)/Poly (Methacrylic Acid) Interpenetrating Polymer Networks. *J. Mater. Chem. C* **2015**, *3*, 5490–5498.

(905) Song, P.; Chen, X.; Xiang, Y.; Huang, L.; Zhou, Z.; Wei, R.; Tong, A. A Ratiometric Fluorescent pH Probe Based on Aggregation-Induced Emission Enhancement and Its Application in Live-Cell Imaging. *J. Mater. Chem.* **2011**, *21*, 13470–13475.

(906) Wang, A.; Fan, R.; Zhou, Y.; Zheng, X.; Zhou, X.; Hao, S.; Yang, Y. Multiple-Color Aggregation-Induced Emission-Based Schiff Base Sensors for Ultrafast Dual Recognition of Hg²⁺ and pH Integrating Boolean Logic Operations. *J. Coord. Chem.* **2019**, *72*, 102–118.

(907) Yan, L.; Qing, T.; Li, R.; Wang, Z.; Qi, Z. Synthesis and Optical Properties of Aggregation-Induced Emission (AIE) Molecules Based on the ESIPT Mechanism as pH- and Zn²⁺-Responsive Fluorescent Sensors. *RSC Adv.* **2016**, *6*, 63874–63879.

(908) Ma, X.; Cheng, J.; Liu, J.; Zhou, X.; Xiang, H. Ratiometric Fluorescent pH Probes Based on Aggregation-Induced Emission-Active Salicylaldehyde Azines. *New J. Chem.* **2015**, *39*, 492–500.

(909) Tian, D.; Zheng, X.; Li, X.; Liu, X.; Zhao, J.; Wang, J. Tunable Aggregation-Induced Emission of Imidazole Hydrazones by pH and Anions. *Chem. - Eur. J.* **2019**, *25*, 16519–16522.

- (910) Lin, N.; Chen, X.; Yan, S.; Wang, H.; Lu, Z.; Xia, X.; Liang, M.; Wu, Y.-L.; Zheng, L.; Cao, Q.; et al. An Aggregation-Induced Emission-Based pH-Sensitive Fluorescent Probe for Intracellular Acidity Sensing. *RSC Adv.* **2016**, *6*, 25416–25419.
- (911) Lu, H.; Xu, B.; Dong, Y.; Chen, F.; Li, Y.; Li, Z.; He, J.; Li, H.; Tian, W. Novel Fluorescent pH Sensors and a Biological Probe Based on Anthracene Derivatives with Aggregation-Induced Emission Characteristics. *Langmuir* **2010**, *26*, 6838–6844.
- (912) Wu, D.; Shao, L.; Li, Y.; Hu, Q.; Huang, F.; Yu, G.; Tang, G. A Boron Difluoride Dye Showing the Aggregation-Induced Emission Feature and High Sensitivity to Intra- and Extra-Cellular pH Changes. *Chem. Commun.* **2016**, *52*, 541–544.
- (913) Bai, Y.; Liu, D.; Han, Z.; Chen, Y.; Chen, Z.; Jiao, Y.; He, W.; Guo, Z. BODIPY-Derived Ratiometric Fluorescent Sensors: pH-Regulated Aggregation-Induced Emission and Imaging Application in Cellular Acidification Triggered by Crystalline Silica Exposure. *Sci. China: Chem.* **2018**, *61*, 1413–1422.
- (914) Yu, Y.; Yu, C.; Wu, Q.; Wang, H.; Jiao, L.; Wong, W.-Y.; Hao, E. Pure E/Z Isomers of N-Methylpyrrole-Benzohydrazide-Based BF₂ Complexes: Remarkable Aggregation-, Crystallization-Induced Emission Switching Properties and Application in Sensing Intracellular pH Microenvironment. *J. Mater. Chem. C* **2019**, *7*, 4533–4542.
- (915) Flannery, D.; James, S. W.; Tatam, R. P.; Ashwell, G. J. pH Sensor Using Langmuir–Blodgett Overlays on Polished Optical Fibers. *Opt. Lett.* **1997**, *22*, 567–569.
- (916) Raoufi, N.; Surre, F.; Rajarajan, M.; Sun, T.; Grattan, K. T. Fiber Optic pH Sensor Using Optimized Layer-by-Layer Coating Approach. *IEEE Sens. J.* **2014**, *14*, 47–54.
- (917) Surre, F.; Lyons, W.; Sun, T.; Grattan, K.; O’Keeffe, S.; Lewis, E.; Elosua, C.; Hernaez, M.; Barian, C. *U-Bend Fibre Optic pH Sensors Using Layer-by-Layer Electrostatic Self-Assembly Technique*; IOP Publishing, 2009; Vol. 178, p 012046.
- (918) Gu, B.; Yin, M.; Zhang, A. P.; Qian, J.; He, S. Biocompatible Fiber-Optic pH Sensor Based on Optical Fiber Modal Interferometer Self-Assembled with Sodium Alginate/Polyethylenimine Coating. *IEEE Sens. J.* **2012**, *12*, 1477–1482.
- (919) Goicoechea, J.; Zamarreño, C.; Matias, I.; Arregui, F. Utilization of White Light Interferometry in pH Sensing Applications by Mean of the Fabrication of Nanostructured Cavities. *Sens. Actuators, B* **2009**, *138*, 613–618.
- (920) Zhou, Z.; Shinar, R.; Allison, A. J.; Shinar, J. Enhanced Photoluminescence of Oxygen Sensing Films through Doping with High Dielectric Constant Particles. *Adv. Funct. Mater.* **2007**, *17*, 3530–3537.
- (921) Moßhammer, M.; Strobl, M.; Köhl, M.; Klimant, I.; Borisov, S. M.; Koren, K. Design and Application of an Optical Sensor for Simultaneous Imaging of pH and Dissolved O₂ with Low Cross-Talk. *ACS Sens.* **2016**, *1*, 681–687.
- (922) Vesel, A.; Junkar, I.; Cvelbar, U.; Kovac, J.; Mozetic, M. Surface Modification of Polyester by Oxygen- and Nitrogen-plasma Treatment. *Surf. Interface Anal.* **2008**, *40*, 1444–1453.
- (923) Chan, C.-M.; Ko, T.-M.; Hiraoka, H. Polymer Surface Modification by Plasmas and Photons. *Surf. Sci. Rep.* **1996**, *24*, 1–54.
- (924) Atkinson, R. S.; Brimage, D. R. G.; Davidson, R. S.; Gray, E. Use of Tertiary Amino-Groups as Substituents to Stabilise Compounds towards Attack by Singlet Oxygen. *J. Chem. Soc., Perkin Trans. 1* **1973**, 960–964.
- (925) Matheson, I.; Lee, J. Quenching of Photophysically Formed Singlet (1. DELTA. 4g) Oxygen in Solution by Amines. *J. Am. Chem. Soc.* **1972**, *94*, 3310–3313.
- (926) Ricketts, S. R.; Douglas, P. A Simple Colorimetric Luminescent Oxygen Sensor Using a Green LED with Pt Octaethylporphyrin in Ethyl Cellulose as the Oxygen-Responsive Element. *Sens. Actuators, B* **2008**, *135*, 46–51.
- (927) Ouannes, C.; Wilson, T. Quenching of Singlet Oxygen by Tertiary Aliphatic Amines. Effect of DABCO (1,4-Diazabicyclo [2.2.2] Octane). *J. Am. Chem. Soc.* **1968**, *90*, 6527–6528.
- (928) Goicoechea, J.; Zamarreño, C. R.; Matias, I. R.; Arregui, F. J. Study and Optimization of the Photobleaching in Self-Assembled Optical Fiber pH Sensors Based on HPTS Using DABCO Antifading Agent. In *Optical Fiber Sensors*; Optical Society of America, 2006; p TuE66.
- (929) Guillory, J.; Cook, C. Energy Transfer Processes Involving Ultraviolet Stabilizers. Quenching of Singlet Oxygen. *J. Polym. Sci., Polym. Chem. Ed.* **1973**, *11*, 1927–1937.
- (930) Ackerman, R.; Rosenthal, I.; Pitts, J., Jr Singlet Oxygen in the Environmental Sciences. X. Absolute Rates of Deactivation of O₂ (¹Δ_g) in the Gas Phase by Sulfur Compounds. *J. Chem. Phys.* **1971**, *54*, 4960–4961.
- (931) Bregnhøj, M.; Prete, M.; Turkovic, V.; Petersen, A. U.; Nielsen, M. B.; Madsen, M.; Ogilby, P. R. Oxygen-Dependent Photophysics and Photochemistry of Prototypical Compounds for Organic Photovoltaics: Inhibiting Degradation Initiated by Singlet Oxygen at a Molecular Level. *Methods Appl. Fluoresc.* **2020**, *8*, No. 014001.
- (932) Foote, C. S.; Fujimoto, T. T.; Chang, Y. C. Chemistry of Singlet Oxygen. XV. Irrelevance of Azide Trapping to Mechanism of the Ene Reaction. *Tetrahedron Lett.* **1972**, *13*, 45–48.
- (933) Hasty, N.; Merkel, P. B.; Radlick, P.; Kearns, D. R. Role of Azide in Singlet Oxygen Reactions: Reaction of Azide with Singlet Oxygen. *Tetrahedron Lett.* **1972**, *13*, 49–52.
- (934) Engel, E.; Schraml, R.; Maisch, T.; Kobuch, K.; König, B.; Szeimies, R.-M.; Hillenkamp, J.; Bäuml, W.; Vasold, R. Light-Induced Decomposition of Indocyanine Green. *Invest. Ophthalmol. Visual Sci.* **2008**, *49*, 1777–1783.
- (935) van der Velde, J. H.; Oelerich, J.; Huang, J.; Smit, J. H.; Hiermaier, M.; Ploetz, E.; Herrmann, A.; Roelfes, G.; Cordes, T. The Power of Two: Covalent Coupling of Photostabilizers for Fluorescence Applications. *J. Phys. Chem. Lett.* **2014**, *5*, 3792–3798.
- (936) Demchenko, A. P. Photobleaching of Organic Fluorophores: Quantitative Characterization, Mechanisms. *Methods Appl. Fluoresc.* **2020**, *8*, No. 022001.
- (937) Szmajcinski, H.; Lakowicz, J. R. Optical Measurements of pH Using Fluorescence Lifetimes and Phase-Modulation Fluorimetry. *Anal. Chem.* **1993**, *65*, 1668–1674.
- (938) Jin, L.; Shi, L.; Shi, W.; Meng, Z.; Shang, L.; Shen, Y. Fluorescence Lifetime-Based pH Sensing by Platinum Nanoclusters. *Analyst* **2019**, *144*, 3533–3538.
- (939) Valeur, B. *Molecular Fluorescence: Principles and Applications*; Wiley-VCH: Weinheim, 2001.
- (940) Lippitsch, M. E. Optical Sensors Based on Fluorescence Anisotropy. *Sens. Actuators, B* **1993**, *11*, 499–502.
- (941) Lakowicz, J. R.; Gryczynski, I.; Gryczynski, Z.; Dattelbaum, J. D. Anisotropy-Based Sensing with Reference Fluorophores. *Anal. Biochem.* **1999**, *267*, 397–405.
- (942) Lakowicz, J. R.; Szmajcinski, H.; Karakelle, M. Optical Sensing of pH and pCO₂ Using Phase-Modulation Fluorimetry and Resonance Energy Transfer. *Anal. Chim. Acta* **1993**, *272*, 179–186.
- (943) Mayr, T.; Borisov, S. M.; Abel, T.; Enko, B.; Waich, K.; Mistlberger, G.; Klimant, I. Light Harvesting as a Simple and Versatile Way to Enhance Brightness of Luminescent Sensors. *Anal. Chem.* **2009**, *81*, 6541–6545.
- (944) Kosch, U.; Klimant, I.; Werner, T.; Wolfbeis, O. S. Strategies To Design pH Optodes with Luminescence Decay Times in the Microsecond Time Regime. *Anal. Chem.* **1998**, *70*, 3892–3897.
- (945) Poehler, E.; Pfeiffer, S. A.; Herm, M.; Gaebler, M.; Busse, B.; Nagl, S. Microchamber Arrays with an Integrated Long Luminescence Lifetime pH Sensor. *Anal. Bioanal. Chem.* **2016**, *408*, 2927–2935.
- (946) Meier, R. J.; Simbürger, J. M. B.; Soukka, T.; Schäferling, M. A FRET Based pH Probe with a Broad Working Range Applicable to Referenced Ratiometric Dual Wavelength and Luminescence Lifetime Read Out. *Chem. Commun.* **2015**, *51*, 6145–6148.
- (947) Turel, M.; Cajlakovic, M.; Austin, E.; Dakin, J. P.; Uray, G.; Lobnik, A. Direct UV-LED Lifetime pH Sensor Based on a Semi-Permeable Sol-Gel Membrane Immobilized Luminescent Eu³⁺ Chelate Complex. *Sens. Actuators, B* **2008**, *131*, 247–253.
- (948) Hiruta, Y.; Yoshizawa, N.; Citterio, D.; Suzuki, K. Highly Durable Double Sol–Gel Layer Ratiometric Fluorescent pH Optode

Based on the Combination of Two Types of Quantum Dots and Absorbing pH Indicators. *Anal. Chem.* **2012**, *84*, 10650–10656.

(949) Borisov, S. M.; Klimant, I. A Versatile Approach for Ratiometric Time-Resolved Read-out of Colorimetric Chemosensors Using Broadband Phosphors as Secondary Emitters. *Anal. Chim. Acta* **2013**, *787*, 219–225.

(950) Sun, L.-N.; Peng, H.; Stich, M. I. J.; Achatz, D.; Wolfbeis, O. S. pH Sensor Based on Upconverting Luminescent Lanthanide Nanorods. *Chem. Commun.* **2009**, No. 33, 5000–5002.

(951) Meier, R. J.; Simbürger, J. M. B.; Soukka, T.; Schäferling, M. Background-Free Referenced Luminescence Sensing and Imaging of pH Using Upconverting Phosphors and Color Camera Read-Out. *Anal. Chem.* **2014**, *86*, 5535–5540.

(952) Xie, L.; Qin, Y.; Chen, H.-Y. Polymeric Optodes Based on Upconverting Nanorods for Fluorescent Measurements of pH and Metal Ions in Blood Samples. *Anal. Chem.* **2012**, *84*, 1969–1974.

(953) Strobl, M.; Mayr, T.; Klimant, I.; Borisov, S. M. Photostable Upconverting and Downconverting pH Sensors Based on Combination of a Colorimetric NIR Indicator and Stable Inorganic Phosphors as Secondary Emitters. *Sens. Actuators, B* **2017**, *245*, 972–979.

(954) Ali, R.; Saleh, S. M.; Aly, S. M. Fluorescent Gold Nanoclusters as pH Sensors for the pH 5 to 9 Range and for Imaging of Blood Cell pH Values. *Microchim. Acta* **2017**, *184*, 3309–3315.

(955) Wang, F.; Raval, Y.; Chen, H.; Tzeng, T. J.; DesJardins, J. D.; Anker, J. N. Development of Luminescent pH Sensor Films for Monitoring Bacterial Growth through Tissue. *Adv. Healthcare Mater.* **2014**, *3*, 197–204.

(956) Ma, T.; Ma, Y.; Liu, S.; Zhang, L.; Yang, T.; Yang, H.-R.; Lv, W.; Yu, Q.; Xu, W.; Zhao, Q.; Huang, W. Dye-Conjugated Upconversion Nanoparticles for Ratiometric Imaging of Intracellular pH Values. *J. Mater. Chem. C* **2015**, *3*, 6616–6620.

(957) Radunz, S.; Andresen, E.; Würth, C.; Koerdt, A.; Tschiche, H. R.; Resch-Genger, U. Simple Self-Referenced Luminescent pH Sensors Based on Upconversion Nanocrystals and pH-Sensitive Fluorescent BODIPY Dyes. *Anal. Chem.* **2019**, *91*, 7756–7764.

(958) Arppe, R.; Näreoja, T.; Nylund, S.; Mattsson, L.; Koho, S.; Rosenholm, J. M.; Soukka, T.; Schäferling, M. Photon Upconversion Sensitized Nanoprobes for Sensing and Imaging of pH. *Nanoscale* **2014**, *6*, 6837–6843.

(959) Li, H.; Dong, H.; Yu, M.; Liu, C.; Li, Z.; Wei, L.; Sun, L.-D.; Zhang, H. NIR Ratiometric Luminescence Detection of pH Fluctuation in Living Cells with Hemicyanine Derivative-Assembled Upconversion Nanophosphors. *Anal. Chem.* **2017**, *89*, 8863–8869.

(960) Tsai, E. S.; Himmelstoß, S. F.; Wiesholler, L. M.; Hirsch, T.; Hall, E. A. H. Upconversion Nanoparticles for Sensing pH. *Analyst* **2019**, *144*, 5547–5557.

(961) Li, C.; Zuo, J.; Zhang, L.; Chang, Y.; Zhang, Y.; Tu, L.; Liu, X.; Xue, B.; Li, Q.; Zhao, H.; et al. Accurate Quantitative Sensing of Intracellular pH Based on Self-Ratiometric Upconversion Luminescent Nanoprobe. *Sci. Rep.* **2016**, *6*, 38617.

(962) Du, S.; Hernández-Gil, J.; Dong, H.; Zheng, X.; Lyu, G.; Bañobre-López, M.; Gallo, J.; Sun, L.; Yan, C.; Long, N. J. Design and Validation of a New Ratiometric Intracellular pH Imaging Probe Using Lanthanide-Doped Upconverting Nanoparticles. *Dalton Trans* **2017**, *46*, 13957–13965.

(963) Näreoja, T.; Deguchi, T.; Christ, S.; Peltomaa, R.; Prabhakar, N.; Fazeli, E.; Perälä, N.; Rosenholm, J. M.; Arppe, R.; Soukka, T.; Schäferling, M. Ratiometric Sensing and Imaging of Intracellular pH Using Polyethylenimine-Coated Photon Upconversion Nanoprobes. *Anal. Chem.* **2017**, *89*, 1501–1508.

(964) Dutta, J.; Rai, V. K. APTES Modified GO-PEI-Er³⁺/Yb³⁺:NaYF₄ Upconverting Nanoparticles Hybrid Film-Based Optical pH Sensor and NIR Photoelectric Response. *IEEE Sens. J.* **2019**, *19*, 3609–3615.

(965) Wang, S.; Feng, J.; Song, S.; Zhang, H. A Long-Wave Optical pH Sensor Based on Red Upconversion Luminescence of NaGdF₄ Nanotubes. *RSC Adv.* **2014**, *4*, 55897–55899.

(966) Liu, X.; Zhang, S.-Q.; Wei, X.; Yang, T.; Chen, M.-L.; Wang, J.-H. A Novel “Modularized” Optical Sensor for pH Monitoring in Biological Matrixes. *Biosens. Bioelectron.* **2018**, *109*, 150–155.

(967) Xu, D.; Li, Y.; Poon, C.-Y.; Chan, H.-N.; Li, H.-W.; Wong, M. S. A Zero Cross-Talk Ratiometric Two-Photon Probe for Imaging of Acid pH in Living Cells and Tissues and Early Detection of Tumor in Mouse Model. *Anal. Chem.* **2018**, *90*, 8800–8806.

(968) Han, Z.; Tan, J.; Wei, T.; Zhang, Y.; Xiao, H.; Xu, L.; He, B. Two Novel Two-Photon Fluorescent Probes for Low pH Values and Cell Imaging Based on Spirobifluorene Motif. *Sens. Actuators, B* **2018**, *255*, 2290–2297.

(969) Kong, B.; Zhu, A.; Ding, C.; Zhao, X.; Li, B.; Tian, Y. Carbon Dot-Based Inorganic-Organic Nanosystem for Two-Photon Imaging and Biosensing of pH Variation in Living Cells and Tissues. *Adv. Mater.* **2012**, *24*, 5844–5848.

(970) Nagl, S.; Wolfbeis, O. S. Optical Multiple Chemical Sensing: Status and Current Challenges. *Analyst* **2007**, *132*, 507–511.

(971) Stich, M. I. J.; Fischer, L. H.; Wolfbeis, O. S. Multiple Fluorescent Chemical Sensing and Imaging. *Chem. Soc. Rev.* **2010**, *39*, 3102–3114.

(972) Hwang, E. Y.; Pappas, D.; Jeevarajan, A. S.; Anderson, M. M. Evaluation of the Paratrend Multi-Analyte Sensor for Potential Utilization in Long-Duration Automated Cell Culture Monitoring. *Biomed. Microdevices* **2004**, *6*, 241–249.

(973) Ehgartner, J.; Wiltsche, H.; Borisov, S. M.; Mayr, T. Low Cost Referenced Luminescent Imaging of Oxygen and pH with a 2-CCD Colour near Infrared Camera. *Analyst* **2014**, *139*, 4924–4933.

(974) Xu, W.; Lu, S.; Xu, M.; Jiang, Y.; Wang, Y.; Chen, X. Simultaneous Imaging of Intracellular pH and O₂ Using Functionalized Semiconducting Polymer Dots. *J. Mater. Chem. B* **2016**, *4*, 292–298.

(975) Chauhan, V. M.; Giuntini, F.; Aylott, J. W. Quadruple Labelled Dual Oxygen and pH-Sensitive Ratiometric Nanosensors. *Sens. Bio-Sens. Res.* **2016**, *8*, 36–42.

(976) Wan, X.; Liu, S. Fluorescent Water-Soluble Responsive Polymers Site-Specifically Labeled with FRET Dyes Possessing pH- and Thermo-Modulated Multicolor Fluorescence Emissions as Dual Ratiometric Probes. *J. Mater. Chem.* **2011**, *21*, 10321–10329.

(977) Yin, L.; He, C.; Huang, C.; Zhu, W.; Wang, X.; Xu, Y.; Qian, X. A Dual pH and Temperature Responsive Polymeric Fluorescent Sensor and Its Imaging Application in Living Cells. *Chem. Commun.* **2012**, *48*, 4486–4488.

(978) Xu, W.; Lu, S.; Chen, Y.; Zhao, T.; Jiang, Y.; Wang, Y.; Chen, X. Simultaneous Color Sensing of O₂ and pH Using a Smartphone. *Sens. Actuators, B* **2015**, *220*, 326–330.

(979) Tian, Y.; Shumway, B. R.; Cody Youngbull, A.; Li, Y.; Jen, A. K.-Y.; Johnson, R. H.; Meldrum, D. R. Dually Fluorescent Sensing of pH and Dissolved Oxygen Using a Membrane Made from Polymerizable Sensing Monomers. *Sens. Actuators, B* **2010**, *147*, 714–722.

(980) Kim, C.-K.; Duong, H. D.; Rhee, J. I. Preparation of an Optical Sensing Membrane for Triple Detection of Oxygen, pH, and Temperature Using Response Surface Methodology. *Microchem. J.* **2013**, *110*, 702–710.

(981) Schroder, C.; Polerecky, L.; Klimant, I. Time-Resolved pH/PO₂ Mapping with Luminescent Hybrid Sensors. *Anal. Chem.* **2007**, *79*, 60–70.

(982) Wolfbeis, O. S. *Feasibility of Optically Sensing Two Parameters Simultaneously Using One Indicator*; International Society for Optics and Photonics, 1991; Vol. 1368, pp 218–222.

(983) Dmitriev, R. I.; Borisov, S. M.; Dussmann, H.; Sun, S.; Müller, B. J.; Prehn, J.; Baklaushev, V. P.; Klimant, I.; Papkovsky, D. B. Versatile Conjugated Polymer Nanoparticles for High-Resolution O₂ Imaging in Cells and 3D Tissue Models. *ACS Nano* **2015**, *9*, 5275–5288.

(984) Zhang, W.; Abou El-Reash, Y. G.; Ding, L.; Lin, Z.; Lian, Y.; Song, B.; Yuan, J.; Wang, X.-d. A Lysosome-Targeting Nanosensor for Simultaneous Fluorometric Imaging of Intracellular pH Values and Temperature. *Microchim. Acta* **2018**, *185*, 533.

(985) Papkovsky, D. B.; Zhdanov, A. V. Cell Energy Budget Platform for Assessment of Cell Metabolism. In *Mitochondrial Medicine: Vol. II*,

Manipulating Mitochondrial Function; Weissig, V., Edeas, M., Eds.; Springer New York: New York, NY, 2015; pp 333–348.

(986) Zhang, X.; Zhang, W.; Wang, Q.; Wang, J.; Ren, G.; Wang, X. Quadruply-Labeled Serum Albumin as a Biodegradable Nanosensor for Simultaneous Fluorescence Imaging of Intracellular pH Values, Oxygen and Temperature. *Microchim. Acta* **2019**, *186*, 584.

(987) Fischer, L. H.; Karakus, C.; Meier, R. J.; Risch, N.; Wolfbeis, O. S.; Holder, E.; Schäferling, M. Referenced Dual Pressure- and Temperature-Sensitive Paint for Digital Color Camera Read Out. *Chem. - Eur. J.* **2012**, *18*, 15706–15713.

(988) Jezierski, S.; Belder, D.; Nagl, S. Microfluidic Free-Flow Electrophoresis Chips with an Integrated Fluorescent Sensor Layer for Real Time pH Imaging in Isoelectric Focusing. *Chem. Commun.* **2013**, *49*, 904–906.

(989) Köhl, M.; Behrendt, L.; Trampe, E. C. L. E.; Qvortrup, K.; Schreiber, U.; Borisov, S. M.; Klimant, I.; Larkum, A. W. Micro-environmental Ecology of the Chlorophyll B-Containing Symbiotic Cyanobacterium *Prochloron* in the Didemnid Ascidian *Lissoclinum Patella*. *Front. Microbiol.* **2012**, *3*, 402.

(990) Fan, Y.; Zhu, Q.; Aller, R. C.; Rhoads, D. C. An In Situ Multispectral Imaging System for Planar Optodes in Sediments: Examples of High-Resolution Seasonal Patterns of pH. *Aquat. Geochem.* **2011**, *17*, 457–471.

(991) Han, C.; Yao, L.; Xu, D.; Xie, X.; Zhang, C. High-Resolution Imaging of pH in Alkaline Sediments and Water Based on a New Rapid Response Fluorescent Planar Optode. *Sci. Rep.* **2016**, *6*, 26417.

(992) Jiang, Z.; Yu, X.; Hao, Y. Design and Fabrication of a Ratiometric Planar Optode for Simultaneous Imaging of pH and Oxygen. *Sensors* **2017**, *17*, 1316.

(993) Koop-Jakobsen, K.; Mueller, P.; Meier, R. J.; Liebsch, G.; Jensen, K. Plant-Sediment Interactions in Salt Marshes – An Optode Imaging Study of O₂, pH, and CO₂ Gradients in the Rhizosphere. *Front. Plant Sci.* **2018**, *9*, 541.

(994) Cantrell, K.; Erenas, M. M.; de Orbe-Payá, I.; Capitán-Vallvey, L. F. Use of the Hue Parameter of the Hue, Saturation, Value Color Space As a Quantitative Analytical Parameter for Bitonal Optical Sensors. *Anal. Chem.* **2010**, *82*, 531–542.

(995) Carter, J. C.; Alvis, R. M.; Brown, S. B.; Langry, K. C.; Wilson, T. S.; McBride, M. T.; Myrick, M.; Cox, W. R.; Grove, M. E.; Colston, B. W. Fabricating Optical Fiber Imaging Sensors Using Inkjet Printing Technology: A pH Sensor Proof-of-Concept. *Biosens. Bioelectron.* **2006**, *21*, 1359–1364.

(996) Sharman, K. K.; Periasamy, A.; Ashworth, H.; Demas, J. N. Error Analysis of the Rapid Lifetime Determination Method for Double-Exponential Decays and New Windowing Schemes. *Anal. Chem.* **1999**, *71*, 947–952.

(997) Grengg, C.; Müller, B.; Staudinger, C.; Mittermayr, F.; Breininger, J.; Ungerböck, B.; Borisov, S. M.; Mayr, T.; Dietzel, M. High-Resolution Optical pH Imaging of Concrete Exposed to Chemically Corrosive Environments. *Cem. Concr. Res.* **2019**, *116*, 231–237.

(998) Nawaz, H.; Tian, W.; Zhang, J.; Jia, R.; Yang, T.; Yu, J.; Zhang, J. Visual and Precise Detection of pH Values under Extreme Acidic and Strong Basic Environments by Cellulose-Based Superior Sensor. *Anal. Chem.* **2019**, *91*, 3085–3092.

(999) Staneva, D.; Betcheva, R. Synthesis and Functional Properties of New Optical pH Sensor Based on Benzo[*de*]Anthracen-7-One Immobilized on the Viscose. *Dyes Pigm.* **2007**, *74*, 148–153.

(1000) Xu, H.; Sadik, O. A. Design of a Simple Optical Sensor for the Detection of Concentrated Hydroxide Ions in an Unusual pH Range. *Analyst* **2000**, *125*, 1783–1786.

(1001) Raamat, E.; Kaupmees, K.; Ovsjannikov, G.; Trummal, A.; Kütt, A.; Saame, J.; Koppel, I.; Kaljurand, I.; Lipping, L.; Rodima, T.; Pihl, V.; Koppel, I. A.; Leito, I. Acidities of Strong Neutral Brønsted Acids in Different Media. *J. Phys. Org. Chem.* **2013**, *26*, 162–170.

(1002) Nguyen, T. H.; Venugopala, T.; Chen, S.; Sun, T.; Grattan, K. T. V.; Taylor, S. E.; Basheer, P. A. M.; Long, A. E. Fluorescence Based Fibre Optic pH Sensor for the pH 10–13 Range Suitable for Corrosion

Monitoring in Concrete Structures. *Sens. Actuators, B* **2014**, *191*, 498–507.

(1003) Wang, E.; Chow, K.-F.; Wang, W.; Wong, C.; Yee, C.; Persad, A.; Mann, J.; Bocarsly, A. Optical Sensing of HCl with Phenol Red Doped Sol–Gels. *Anal. Chim. Acta* **2005**, *534*, 301–306.

(1004) Shamsipur, M.; Azimi, G. High-Acidity Optical Sensors Based on Sol-Gel-Derived Thin Films. *Anal. Lett.* **2001**, *34*, 1603–1616.

(1005) Li, C.-Y.; Zhang, X.-B.; Han, Z.-X.; Åkermark, B.; Sun, L.; Shen, G.-L.; Yu, R.-Q. A Wide pH Range Optical Sensing System Based on a Sol–Gel Encapsulated Amino-Functionalised Corrole. *Analyst* **2006**, *131*, 388–393.

(1006) Tsou, C.-J.; Hung, Y.; Mou, C.-Y. Hollow Mesoporous Silica Nanoparticles with Tunable Shell Thickness and Pore Size Distribution for Application as Broad-Ranging pH Nanosensor. *Microporous Mesoporous Mater.* **2014**, *190*, 181–188.

(1007) Totland, C.; Thomas, P. J.; Holst, B.; Akhtar, N.; Hovdenes, J.; Skodvin, T. A Broad-Range Fluorescence Lifetime pH Sensing Material Based on a Single Organic Fluorophore. *J. Fluoresc.* **2019**, *29*, 1125–1131.

(1008) Wang, D.; Nap, R. J.; Lagzi, I.; Kowalczyk, B.; Han, S.; Grzybowski, B. A.; Szeleifer, I. How and Why Nanoparticle's Curvature Regulates the Apparent pK_a of the Coating Ligands. *J. Am. Chem. Soc.* **2011**, *133*, 2192–2197.

(1009) Lin, J. Recent Development and Applications of Optical and Fiber-Optic pH Sensors. *TrAC, Trends Anal. Chem.* **2000**, *19*, 541–552.

(1010) Pathak, A. K.; Singh, V. K. A Wide Range and Highly Sensitive Optical Fiber pH Sensor Using Polyacrylamide Hydrogel. *Opt. Fiber Technol.* **2017**, *39*, 43–48.

(1011) Pathak, A. K.; Chaudhary, D. K.; Singh, V. K. Broad Range and Highly Sensitive Optical pH Sensor Based on Hierarchical ZnO Microflowers over Tapered Silica Fiber. *Sens. Actuators, A* **2018**, *280*, 399–405.

(1012) Khan, Md.; Kang, S.-W. Highly Sensitive and Wide-Dynamic-Range Multichannel Optical-Fiber pH Sensor Based on PWM Technique. *Sensors* **2016**, *16*, 1885.

(1013) Munkholm, C.; Walt, D. R.; Milanovich, F. P.; Klainer, S. M. Polymer Modification of Fiber Optic Chemical Sensors as a Method of Enhancing Fluorescence Signal for pH Measurement. *Anal. Chem.* **1986**, *58*, 1427–1430.

(1014) Mohamad, F.; Tanner, M. G.; Choudhury, D.; Choudhary, T. R.; Wood, H. A.; Harrington, K.; Bradley, M. Controlled Core-to-Core Photo-Polymerisation–Fabrication of an Optical Fibre-Based pH Sensor. *Analyst* **2017**, *142*, 3569–3572.

(1015) Schubert, E. F. *Light-Emitting Diodes*, 2nd ed.; Cambridge University Press, 2006.

(1016) Ioannides, N.; Chunga, E. B.; Bachmatiuk, A.; Gonzalez-Martinez, I. G.; Trzebicka, B.; Adebimpe, D. B.; Kalymnios, D.; Rümeli, M. H. Approaches to Mitigate Polymer-Core Loss in Plastic Optical Fibers: A Review. *Mater. Res. Express* **2014**, *1*, No. 032002.

(1017) Koop-Jakobsen, K.; Gutbrod, M. S. Shallow Salt Marsh Tidal Ponds—An Environment With Extreme Oxygen Dynamics. *Front. Environ. Sci.* **2019**, *7*, 137.

(1018) Pantano, P.; Walt, D. R. Analytical Applications of Optical Imaging Fibers. *Anal. Chem.* **1995**, *67*, 481A–487A.

(1019) Sharma, N. K.; Gupta, B. Fabrication and Characterization of pH Sensor Based on Side Polished Single Mode Optical Fiber. *Opt. Commun.* **2003**, *216*, 299–303.

(1020) Ghandehari, M.; Vimer, C. S. In Situ Monitoring of pH Level with Fiber Optic Evanescent Field Spectroscopy. *NDT&E Int.* **2004**, *37*, 611–616.

(1021) Mizaikoff, B.; Lendl, B. Sensor Systems Based on Mid-Infrared Transparent Fibers. In *Handbook of Vibrational Spectroscopy*; John Wiley & Sons, Ltd., 2006.

(1022) Zajić, J.; Traplová, L.; Matějček, V.; Pospíšilová, M.; Bartoň, I. *Optical pH Detection with U-Shaped Fiber-Optic Probes and Absorption Transducers*, Conference Papers in Science; Hindawi, 2015, Vol. 2015.

(1023) Deboux, B.-C.; Lewis, E.; Scully, P.; Edwards, R. A Novel Technique for Optical Fiber pH Sensing Based on Methylene Blue Adsorption. *J. Lightwave Technol.* **1995**, *13*, 1407–1414.

- (1024) Xiao, S.; Wang, T.; Liu, Y.; Han, X.; Yan, X. An Ultrasensitive and Multispectral Refractive Index Sensor Design Based on Quad-Supercell Metamaterials. *Plasmonics* **2017**, *12*, 185–191.
- (1025) Ji, L.; Sun, X.; He, G.; Liu, Y.; Wang, X.; Yi, Y.; Chen, C.; Wang, F.; Zhang, D. Surface Plasmon Resonance Refractive Index Sensor Based on Ultraviolet Bleached Polymer Waveguide. *Sens. Actuators, B* **2017**, *244*, 373–379.
- (1026) An, G.; Li, S.; Wang, H.; Zhang, X.; Yan, X. Quasi-D-Shaped Optical Fiber Plasmonic Refractive Index Sensor. *J. Opt.* **2018**, *20*, No. 035403.
- (1027) Chen, C.; Yang, R.; Zhang, X.; Wei, W.; Guo, Q.; Zhang, X.; Qin, L.; Ning, Y.; Yu, Y. Compact Refractive Index Sensor Based on an S-Tapered Fiber Probe. *Opt. Mater. Express* **2018**, *8*, 919–925.
- (1028) Zhou, X.; Sheng, L.; Ling, X. Photonic Spin Hall Effect Enabled Refractive Index Sensor Using Weak Measurements. *Sci. Rep.* **2018**, *8*, 1221.
- (1029) Wang, Y.; Gao, B.; Zhang, K.; Yuan, K.; Wan, Y.; Xie, Z.; Xu, X.; Zhang, H.; Song, Q.; Yao, L.; et al. Refractive Index Sensor Based on Leaky Resonant Scattering of Single Semiconductor Nanowire. *ACS Photonics* **2017**, *4*, 688–694.
- (1030) Seitz, W. R.; Rooney, M. T.; Miele, E. W.; Wang, H.; Kaval, N.; Zhang, L.; Doherty, S.; Milde, S.; Lenda, J. Derivatized, Swellable Polymer Microspheres for Chemical Transduction. *Anal. Chim. Acta* **1999**, *400*, 55–64.
- (1031) Pietsch, C.; Hoogenboom, R.; Schubert, U. S. Soluble Polymeric Dual Sensor for Temperature and pH Value. *Angew. Chem.* **2009**, *121*, 5763–5766.
- (1032) Dübendorfer, J.; Kunz, R.; Jobst, G.; Moser, I.; Urban, G. Integrated Optical pH Sensor Using Replicated Chirped Grating Coupler Sensor Chips. *Sens. Actuators, B* **1998**, *50*, 210–219.
- (1033) Zamarreño, C.; Hernández, M.; Del Villar, I.; Fernandez-Valdivielso, C.; Arregui, F.; Matias, I. Optical Fiber pH Sensor Fabrication by Means of Indium Tin Oxide Coated Optical Fiber Refractometers. *Phys. Status Solidi C* **2010**, *7*, 2705–2707.
- (1034) Nylander, C.; Liedberg, B.; Lind, T. Gas Detection by Means of Surface Plasmon Resonance. *Sens. Actuators* **1982**, *3*, 79–88.
- (1035) Liedberg, B.; Nylander, C.; Lunström, I. Surface Plasmon Resonance for Gas Detection and Biosensing. *Sens. Actuators* **1983**, *4*, 299–304.
- (1036) Ahn, J. H.; Seong, T. Y.; Kim, W. M.; Lee, T. S.; Kim, I.; Lee, K.-S. Fiber-Optic Waveguide Coupled Surface Plasmon Resonance Sensor. *Opt. Express* **2012**, *20*, 21729–21738.
- (1037) Singh, S.; Gupta, B. D. Fabrication and Characterization of a Highly Sensitive Surface Plasmon Resonance Based Fiber Optic pH Sensor Utilizing High Index Layer and Smart Hydrogel. *Sens. Actuators, B* **2012**, *173*, 268–273.
- (1038) Mishra, S. K.; Gupta, B. D. Surface Plasmon Resonance Based Fiber Optic pH Sensor Utilizing Ag/ITO/Al/Hydrogel Layers. *Analyst* **2013**, *138*, 2640–2646.
- (1039) Zhao, Y.; Lei, M.; Liu, S.-X.; Zhao, Q. Smart Hydrogel-Based Optical Fiber SPR Sensor for pH Measurements. *Sens. Actuators, B* **2018**, *261*, 226–232.
- (1040) Joshi, G. K.; Johnson, M. A.; Sardar, R. Novel pH-Responsive Nanoplasmonic Sensor: Controlling Polymer Structural Change to Modulate Localized Surface Plasmon Resonance Response. *RSC Adv.* **2014**, *4*, 15807–15815.
- (1041) Gangwar, R. K.; Singh, V. K. Highly Sensitive Surface Plasmon Resonance Based D-Shaped Photonic Crystal Fiber Refractive Index Sensor. *Plasmonics* **2017**, *12*, 1367–1372.
- (1042) Fan, J.; Li, Z.; Chen, Z.; Wu, W. Standing-Wave Resonances in Plasmonic Nanoumbrella Cavities for Color Generation and Colorimetric Refractive Index Sensor. *Appl. Surf. Sci.* **2016**, *384*, 534–538.
- (1043) Tang, Y.; Zhang, Z.; Wang, R.; Hai, Z.; Xue, C.; Zhang, W.; Yan, S. Refractive Index Sensor Based on Fano Resonances in Metal-Insulator-Metal Waveguides Coupled with Resonators. *Sensors* **2017**, *17*, 784.
- (1044) Velázquez-González, J. S.; Monzón-Hernández, D.; Moreno-Hernández, D.; Martínez-Piñón, F.; Hernández-Romano, I. Simultaneous Measurement of Refractive Index and Temperature Using a SPR-Based Fiber Optic Sensor. *Sens. Actuators, B* **2017**, *242*, 912–920.
- (1045) An, G.; Li, S.; Yan, X.; Zhang, X.; Yuan, Z.; Wang, H.; Zhang, Y.; Hao, X.; Shao, Y.; Han, Z. Extra-Broad Photonic Crystal Fiber Refractive Index Sensor Based on Surface Plasmon Resonance. *Plasmonics* **2017**, *12*, 465–471.
- (1046) Dash, J. N.; Jha, R. Graphene-Based Birefringent Photonic Crystal Fiber Sensor Using Surface Plasmon Resonance. *IEEE Photonics Technol. Lett.* **2014**, *26*, 1092–1095.
- (1047) Wong, W. C.; Chan, C. C.; Chen, L. H.; Li, T.; Lee, K. X.; Leong, K. C. Polyvinyl Alcohol Coated Photonic Crystal Optical Fiber Sensor for Humidity Measurement. *Sens. Actuators, B* **2012**, *174*, 563–569.
- (1048) Zhang, W.; Lian, Z.; Benson, T.; Wang, X.; Lou, S. A Refractive Index Sensor Based on a D-Shaped Photonic Crystal Fiber with a Nanoscale Gold Belt. *Opt. Quantum Electron.* **2018**, *50*, 29.
- (1049) Chen, X.; Xia, L.; Li, C. Surface Plasmon Resonance Sensor Based on a Novel D-Shaped Photonic Crystal Fiber for Low Refractive Index Detection. *IEEE Photonics J.* **2018**, *10*, 1–9.
- (1050) Yang, Q.; Qin, L.; Cao, G.; Zhang, C.; Li, X. Refractive Index Sensor Based on Graphene-Coated Photonic Surface-Wave Resonance. *Opt. Lett.* **2018**, *43*, 639–642.
- (1051) Maurya, J. B.; François, A.; Prajapati, Y. K. Two-Dimensional Layered Nanomaterial-Based One-Dimensional Photonic Crystal Refractive Index Sensor. *Sensors* **2018**, *18*, 857.
- (1052) Yetisen, A. K.; Butt, H.; Volpatti, L. R.; Pavlichenko, I.; Humar, M.; Kwok, S. J.; Koo, H.; Kim, K. S.; Naydenova, I.; Khademhosseini, A.; et al. Photonic Hydrogel Sensors. *Biotechnol. Adv.* **2016**, *34*, 250–271.
- (1053) Holtz, J. H.; Asher, S. A. Polymerized Colloidal Crystal Hydrogel Films as Intelligent Chemical Sensing Materials. *Nature* **1997**, *389*, 829–832.
- (1054) Lee, K.; Asher, S. A. Photonic Crystal Chemical Sensors: pH and Ionic Strength. *J. Am. Chem. Soc.* **2000**, *122*, 9534–9537.
- (1055) Xu, X.; Goponenko, A. V.; Asher, S. A. Polymerized PolyHEMA Photonic Crystals: pH and Ethanol Sensor Materials. *J. Am. Chem. Soc.* **2008**, *130*, 3113–3119.
- (1056) Asher, S. A.; Kimble, K. W.; Walker, J. P. Enabling Thermoreversible Physically Cross-Linked Polymerized Colloidal Array Photonic Crystals. *Chem. Mater.* **2008**, *20*, 7501–7509.
- (1057) Zhang, J.-T.; Wang, L.; Luo, J.; Tikhonov, A.; Kornienko, N.; Asher, S. A. 2-D Array Photonic Crystal Sensing Motif. *J. Am. Chem. Soc.* **2011**, *133*, 9152–9155.
- (1058) Li, C.; Lotsch, B. V. Stimuli-Responsive 2D Polyelectrolyte Photonic Crystals for Optically Encoded pH Sensing. *Chem. Commun.* **2012**, *48*, 6169–6171.
- (1059) Yang, Q.; Zhu, S.; Peng, W.; Yin, C.; Wang, W.; Gu, J.; Zhang, W.; Ma, J.; Deng, T.; Feng, C.; et al. Bioinspired Fabrication of Hierarchically Structured, pH-Tunable Photonic Crystals with Unique Transition. *ACS Nano* **2013**, *7*, 4911–4918.
- (1060) Fenzl, C.; Wilhelm, S.; Hirsch, T.; Wolfbeis, O. S. Optical Sensing of the Ionic Strength Using Photonic Crystals in a Hydrogel Matrix. *ACS Appl. Mater. Interfaces* **2013**, *5*, 173–178.
- (1061) Shin, J.; Braun, P. V.; Lee, W. Fast Response Photonic Crystal pH Sensor Based on Templated Photo-Polymerized Hydrogel Inverse Opal. *Sens. Actuators, B* **2010**, *150*, 183–190.
- (1062) Griffete, N.; Frederich, H.; Maitre, A.; Chehimi, M. M.; Ravaine, S.; Mangeney, C. Photonic Crystal pH Sensor Containing a Planar Defect for Fast and Enhanced Response. *J. Mater. Chem.* **2011**, *21*, 13052–13055.
- (1063) Honda, M.; Seki, T.; Takeoka, Y. Dual Tuning of the Photonic Band-Gap Structure in Soft Photonic Crystals. *Adv. Mater.* **2009**, *21*, 1801–1804.
- (1064) Fei, X.; Lu, T.; Ma, J.; Wang, W.; Zhu, S.; Zhang, D. Bioinspired Polymeric Photonic Crystals for High Cycling pH-Sensing Performance. *ACS Appl. Mater. Interfaces* **2016**, *8*, 27091–27098.
- (1065) Liu, C.; Zhu, Y.; Ma, T.; Yao, C.; Ren, J.; Peng, H.; Zhao, X.; Ge, L. Acidic/Alkali Vapor Sensitive One Dimensional Photonic

Crystals with a Gradient Architecture. *Mater. Today Proc.* **2015**, *2*, 261–270.

(1066) Shi, D.; Zhang, X.; Yang, Z.; Liu, S.; Chen, M. Fabrication of PAM/PMAA Inverse Opal Photonic Crystal Hydrogels by a “Sandwich” Method and Their pH and Solvent Responses. *RSC Adv.* **2016**, *6*, 85885–85890.

(1067) Jia, X.; Wang, K.; Wang, J.; Hu, Y.; Shen, L.; Zhu, J. Full-Color Photonic Hydrogels for pH and Ionic Strength Sensing. *Eur. Polym. J.* **2016**, *83*, 60–66.

(1068) Pace, S.; Vasani, R. B.; Zhao, W.; Perrier, S.; Voelcker, N. H. Photonic Porous Silicon as a pH Sensor. *Nanoscale Res. Lett.* **2014**, *9*, 420.

(1069) Pidenko, P. S.; Borzov, V. M.; Savenko, O. A.; Skaptsov, A. A.; Skibina, Y. S.; Goryacheva, I. Y.; Rusanova, T. Y. *Modification of the Internal Surface of Photonic Crystal Fibers with Ag and Au Nanoparticles for Application as Sensor Elements*; International Society for Optics and Photonics, 2017; Vol. 10336, p 103360T.

(1070) Walker, J. P.; Kimble, K. W.; Asher, S. A. Photonic Crystal Sensor for Organophosphate Nerve Agents Utilizing the Organophosphorus Hydrolase Enzyme. *Anal. Bioanal. Chem.* **2007**, *389*, 2115–2124.

(1071) Li, L.; Long, Y.; Gao, J.-M.; Song, K.; Yang, G. Label-Free and pH-Sensitive Colorimetric Materials for the Sensing of Urea. *Nanoscale* **2016**, *8*, 4458–4462.

(1072) Arunbabu, D.; Sannigrahi, A.; Jana, T. Photonic Crystal Hydrogel Material for the Sensing of Toxic Mercury Ions (Hg 2+) in Water. *Soft Matter* **2011**, *7*, 2592–2599.

(1073) Zhang, Y.; Zhao, Y.; Zhou, T.; Wu, Q. Applications and Developments of On-Chip Biochemical Sensors Based on Optofluidic Photonic Crystal Cavities. *Lab Chip* **2018**, *18*, 57–74.

(1074) Zawadzka, M.; Mikulchuk, T.; Cody, D.; Martin, S.; Yetisen, A. K.; Martinez-Hurtado, J. L.; Butt, H.; Mihaylova, E.; Awala, H.; Mintova, S. Photonic Materials for Holographic Sensing. In *Photonic Materials for Sensing, Biosensing and Display Devices*; Springer, 2016; pp 315–359.

(1075) Marshall, A. J.; Blyth, J.; Davidson, C. A.; Lowe, C. R. pH-Sensitive Holographic Sensors. *Anal. Chem.* **2003**, *75*, 4423–4431.

(1076) Sartain, F. K.; Yang, X.; Lowe, C. R. Holographic Lactate Sensor. *Anal. Chem.* **2006**, *78*, 5664–5670.

(1077) Beiu, R.-M.; Beiu, V.; Duma, V.-F. Fiber Optic Mechanical Deformation Sensors Employing Perpendicular Photonic Crystals. *Opt. Express* **2017**, *25*, 23388–23398.

(1078) Vezouviou, E.; Lowe, C. R. A near Infrared Holographic Glucose Sensor. *Biosens. Bioelectron.* **2015**, *68*, 371–381.

(1079) Bianco, G.; Ferrara, M. A.; Borbone, F.; Zuppari, F.; Roviello, A.; Striano, V.; Coppola, G. *Volume Holographic Gratings as Optical Sensor for Heavy Metal in Bathing Waters*; Baldini, F., Homola, J., Lieberman, R. A., Eds.; Prague, Czech Republic, 2015; p 95062B.

(1080) Ye, H.; Nilsen, O.; Bright, V. M.; Anderson, D. Z. Holographic Chemical Vapor Sensor. *Opt. Lett.* **2005**, *30*, 1467–1469.

(1081) Liu, H.; Yu, D.; Zhou, K.; Wang, S.; Luo, S.; Wang, W.; Song, Q. Improvement of Temperature-Induced Spectrum Characterization in a Holographic Sensor Based on N-Isopropylacrylamide Photopolymer Hydrogel. *Appl. Opt.* **2017**, *56*, 9006–9013.

(1082) Oliveira, N. C.; El Khoury, G.; Versnel, J. M.; Moghaddam, G. K.; Leite, L. S.; Lima-Filho, J. L.; Lowe, C. R. A Holographic Sensor Based on a Biomimetic Affinity Ligand for the Detection of Cocaine. *Sens. Actuators, B* **2018**, *270*, 216–222.

(1083) Khalili Moghaddam, G.; Margerison, H.; Suzuki, J.; Blyth, J.; Lowe, C. R. A Transparent Glucose-Sensitive Double Polymerised Holographic Sensor. *Sens. Actuators, B* **2018**, *267*, 1–4.

(1084) Browne, C. A.; Tarrant, D. H.; Olteanu, M. S.; Mullens, J. W.; Chronister, E. L. Intrinsic Sol–Gel Clad Fiber-Optic Sensors with Time-Resolved Detection. *Anal. Chem.* **1996**, *68*, 2289–2295.

(1085) Mendoza, E. A.; Sorenson, J. A.; Iossi, A.; Sun, Z.; Robinson, D. P.; Lieberman, R. A. *Demonstration of Self-Referenced Fiber Optic Moisture and pH Sensors Using Optical Time Domain Reflectometry (OTDR)*; Lieberman, R. A., Ed.; Denver, CO, 1996; pp 242–249.

(1086) Wallace, P. A.; Campbell, M.; Yang, Y.; Holmes-Smith, A. S.; Uttamral, M. A. Distributed Optical Fibre Fluorosensor for pH Measurement. *J. Lumin.* **1997**, *72*, 1017–1019.

(1087) Tusa, J. K.; He, H. Critical Care Analyzer with Fluorescent Optical Chemosensors for Blood Analytes. *J. Mater. Chem.* **2005**, *15*, 2640–2647.

(1088) Mahutte, C. K. On-Line Arterial Blood Gas Analysis With Optodes: Current Status. *Clin. Biochem.* **1998**, *31*, 119–130.

(1089) Peterson, J. L.; Goldstein, S. R.; Fitzgerald, R. V.; Buckhold, D. K. Fiber optic pH probe for physiological use. *Anal. Chem.* **1980**, *52*, 864–869.

(1090) Leiner, M. J. P. Optical Sensors for in Vitro Blood Gas Analysis. *Sens. Actuators, B* **1995**, *29*, 169–173.

(1091) Ferrari, L.; Rovati, L.; Fabbri, P.; Pilati, F. Continuous Haematic pH Monitoring in Extracorporeal Circulation Using a Disposable Fluorescence Sensing Element. *J. Biomed. Opt.* **2013**, *18*, No. 027002.

(1092) Pakulla, M.; Obal, D.; Loer, S. Continuous Intra-Arterial Blood Gas Monitoring in Rats. *Lab. Anim.* **2004**, *38*, 133–137.

(1093) Bromberg, A.; Zilberstein, J.; Riesemberg, S.; Benori, E.; Silberstein, E.; Zimnavoda, J.; Frishman, G.; Kritzman, A. Optical-Fibre Sensors for Blood Gases and pH, Based on Porous Glass Tips. *Sens. Actuators, B* **1996**, *31*, 181–191.

(1094) McKinley, B. A. ISFET and Fiber Optic Sensor Technologies: In Vivo Experience for Critical Care Monitoring. *Chem. Rev.* **2008**, *108*, 826–844.

(1095) Miller, W. W.; Yafuso, M.; Yan, C. F.; Hui, H. K.; Arick, S. Performance of an In-Vivo, Continuous Blood-Gas Monitor with Disposable Probe. *Clin. Chem.* **1987**, *33*, 1538–1542.

(1096) Smith, B. E.; King, P. H.; Schlain, L. Clinical Evaluation–Continuous Real-Time Intra-Arterial Blood Gas Monitoring during Anesthesia and Surgery by Fiber Optic Sensor. *Int. J. Clin. Monit. Comput.* **1992**, *9*, 45–52.

(1097) Lumsden, T.; Marshall, W. R.; Divers, G. A.; Riccitelli, S. D. The PB3300 Intraarterial Blood Gas Monitoring System. *J. Clin. Monit.* **1994**, *10*, 59–66.

(1098) VENKATESH, B.; CLUTTON BROCK, T. H.; HENDRY, S. P. A Multiparameter Sensor for Continuous Intra-Arterial Blood Gas Monitoring: A Prospective Evaluation. *Crit. Care Med.* **1994**, *22*, 588–594.

(1099) Christiansson, L.; Hellberg, A.; Koga, I.; Thelin, S.; Bergqvist, D.; Wiklund, L.; Karacagil, S. A New Method of Intrathecal PO₂, PCO₂, and pH Measurements for Continuous Monitoring of Spinal Cord Ischemia during Thoracic Aortic Clamping in Pigs. *Surgery* **2000**, *127*, 571–576.

(1100) Venkatesh, B.; Clutton-Brock, T. H.; Hendry, S. P. Evaluation of the Paratrend 7 Intravascular Blood Gas Monitor during Cardiac Surgery: Comparison with the C4000 in-Line Blood Gas Monitor during Cardiopulmonary Bypass. *J. Cardiothorac. Vasc. Anesth.* **1995**, *9*, 412–419.

(1101) Ganter, M.; Zollinger, A. Continuous Intravascular Blood Gas Monitoring: Development, Current Techniques, and Clinical Use of a Commercial Device. *Br. J. Anaesth.* **2003**, *91*, 397–407.

(1102) Venkatesh, B. Continuous Intra-Arterial Blood Gas Monitoring. *Crit. Care Resusc.* **1999**, *1*, 140.

(1103) Morgan, C.; Newell, S. J.; Ducker, D. A.; Hodgkinson, J.; White, D. K.; Morley, C. J.; Church, J. M. Continuous Neonatal Blood Gas Monitoring Using a Multiparameter Intra-Arterial Sensor. *Arch. Dis. Child. - Fetal Neonatal Ed.* **1999**, *80*, F93–F98.

(1104) Baldini, F. In Vivo Monitoring of the Gastroesophageal System Using Optical Fibre Sensors. *Anal. Bioanal. Chem.* **2003**, *375*, 732–743.

(1105) Marieb, E. N.; Hoehn, K. *Human Anatomy & Physiology*; Pearson Education, 2007.

(1106) Schultz, A.; Puvvadi, R.; Borisov, S. M.; Shaw, N. C.; Klimant, I.; Berry, L. J.; Montgomery, S. T.; Nguyen, T.; Kreda, S. M.; Kicic, A.; Noble, P. B.; Button, B.; Stick, S. M. Airway Surface Liquid pH Is Not Acidic in Children with Cystic Fibrosis. *Nat. Commun.* **2017**, *8*, 1409.

- (1107) Sato, K.; Kang, W. H.; Saga, K.; Sato, K. T. Biology of Sweat Glands and Their Disorders. I. Normal Sweat Gland Function. *J. Am. Acad. Dermatol.* **1989**, *20*, 537–563.
- (1108) Nakata, S.; Arie, T.; Akita, S.; Takei, K. Wearable, Flexible, and Multifunctional Healthcare Device with an ISFET Chemical Sensor for Simultaneous Sweat pH and Skin Temperature Monitoring. *ACS Sens.* **2017**, *2*, 443–448.
- (1109) Curto, V. F.; Fay, C.; Coyle, S.; Byrne, R.; O'Toole, C.; Barry, C.; Hughes, S.; Moyna, N.; Diamond, D.; Benito-Lopez, F. Real-Time Sweat pH Monitoring Based on a Wearable Chemical Barcode Micro-Fluidic Platform Incorporating Ionic Liquids. *Sens. Actuators, B* **2012**, *171–172*, 1327–1334.
- (1110) Caldara, M.; Colleoni, C.; Guido, E.; Re, V.; Rosace, G. Optical Monitoring of Sweat pH by a Textile Fabric Wearable Sensor Based on Covalently Bonded Litmus-3-Glycidoxypolytrimethoxysilane Coating. *Sens. Actuators, B* **2016**, *222*, 213–220.
- (1111) Dargaville, T. R.; Farrugia, B. L.; Broadbent, J. A.; Pace, S.; Upton, Z.; Voelcker, N. H. Sensors and Imaging for Wound Healing: A Review. *Biosens. Bioelectron.* **2013**, *41*, 30–42.
- (1112) Jones, E. M.; Cochrane, C. A.; Percival, S. L. The Effect of pH on the Extracellular Matrix and Biofilms. *Adv. Wound Care* **2015**, *4*, 431–439.
- (1113) Auerswald, S.; Schreml, S.; Meier, R.; Blancke Soares, A.; Niyazi, M.; Marschner, S.; Belka, C.; Canis, M.; Haubner, F. Wound Monitoring of pH and Oxygen in Patients after Radiation Therapy. *Radiat. Oncol.* **2019**, *14*, 199.
- (1114) Schreml, S.; Meier, R. J.; Weiß, K. T.; Cattani, J.; Flittner, D.; Gehmert, S.; Wolfbeis, O. S.; Landthaler, M.; Babilas, P. A Sprayable Luminescent pH Sensor and Its Use for Wound Imaging in Vivo. *Exp. Dermatol.* **2012**, *21*, 951–953.
- (1115) Tamayol, A.; Akbari, M.; Zilberman, Y.; Comotto, M.; Lasha, E.; Serex, L.; Bagherifard, S.; Chen, Y.; Fu, G.; Ameri, S. K.; Ruan, W.; Miller, E. L.; Dokmeci, M. R.; Sonkusale, S.; Khademhosseini, A. Flexible pH-Sensing Hydrogel Fibers for Epidermal Applications. *Adv. Healthcare Mater.* **2016**, *5*, 711–719.
- (1116) Zhu, Y.; Zhang, J.; Song, J.; Yang, J.; Du, Z.; Zhao, W.; Guo, H.; Wen, C.; Li, Q.; Sui, X.; Zhang, L. A Multifunctional Pro-Healing Zwitterionic Hydrogel for Simultaneous Optical Monitoring of pH and Glucose in Diabetic Wound Treatment. *Adv. Funct. Mater.* **2020**, *30*, 1905493.
- (1117) Dimde, M.; Sahle, F. F.; Wycisk, V.; Steinhilber, D.; Camacho, L. C.; Licha, K.; Lademann, J.; Haag, R. Synthesis and Validation of Functional Nanogels as pH-Sensors in the Hair Follicle. *Macromol. Biosci.* **2017**, *17*, 1600505.
- (1118) Schaude, C.; Fröhlich, E.; Meindl, C.; Attard, J.; Binder, B.; Mohr, G. J. The Development of Indicator Cotton Swabs for the Detection of pH in Wounds. *Sensors* **2017**, *17*, 1365.
- (1119) Zauner, A.; Bullock, R.; Di, X.; Young, H. F. Brain Oxygen, CO₂, pH, and Temperature Monitoring: Evaluation in the Feline Brain. *Neurosurgery* **1995**, *37*, 1168–1176 discussion 1176–1177.
- (1120) McKinley, B. A.; Morris, W. P.; Parmley, C. L.; Butler, B. D. Brain Parenchyma pO₂, pCO₂, and pH during and after Hypoxic, Ischemic Brain Insult in Dogs. *Crit. Care Med.* **1996**, *24*, 1858–1868.
- (1121) Magnotta, V. A.; Heo, H.-Y.; Dlouhy, B. J.; Dahdaleh, N. S.; Follmer, R. L.; Thedens, D. R.; Welsh, M. J.; Wemmie, J. A. Detecting Activity-Evoked pH Changes in Human Brain. *Proc. Natl. Acad. Sci. U. S. A.* **2012**, *109*, 8270–8273.
- (1122) Ramamonjisoa, N.; Ackerstaff, E. Characterization of the Tumor Microenvironment and Tumor–Stroma Interaction by Non-Invasive Preclinical Imaging. *Front. Oncol.* **2017**, *7*, 3.
- (1123) Tung, C.-H.; Qi, J.; Hu, L.; Han, M. S.; Kim, Y. A Quick Responsive Fluorogenic pH Probe for Ovarian Tumor Imaging. *Theranostics* **2015**, *5*, 1166–1174.
- (1124) Martin, G. R.; Jain, R. K. Noninvasive Measurement of Interstitial pH Profiles in Normal and Neoplastic Tissue Using Fluorescence Ratio Imaging Microscopy. *Cancer Res.* **1994**, *54*, 5670–5674.
- (1125) Urano, Y.; Asanuma, D.; Hama, Y.; Koyama, Y.; Barrett, T.; Kamiya, M.; Nagano, T.; Watanabe, T.; Hasegawa, A.; Choyke, P. L.; Kobayashi, H. Selective Molecular Imaging of Viable Cancer Cells with pH-Activatable Fluorescence Probes. *Nat. Med.* **2009**, *15*, 104–109.
- (1126) Shirmanova, M. V.; Druzhkova, I. N.; Lukina, M. M.; Matlashov, M. E.; Belousov, V. V.; Snopova, L. B.; Prodanetz, N. N.; Dudenkova, V. V.; Lukyanov, S. A.; Zagaynova, E. V. Intracellular pH Imaging in Cancer Cells in Vitro and Tumors in Vivo Using the New Genetically Encoded Sensor SypHer2. *Biochim. Biophys. Acta, Gen. Subj.* **2015**, *1850*, 1905–1911.
- (1127) Li, C.; Xia, J.; Wei, X.; Yan, H.; Si, Z.; Ju, S. pH-Activated Near-Infrared Fluorescence Nanoprobe Imaging Tumors by Sensing the Acidic Microenvironment. *Adv. Funct. Mater.* **2010**, *20*, 2222–2230.
- (1128) Chen, Q.; Liu, X.; Chen, J.; Zeng, J.; Cheng, Z.; Liu, Z. A Self-Assembled Albumin-Based Nanoprobe for In Vivo Ratiometric Photoacoustic pH Imaging. *Adv. Mater.* **2015**, *27*, 6820–6827.
- (1129) Gong, J.; Tanner, M. G.; Venkateswaran, S.; Stone, J. M.; Zhang, Y.; Bradley, M. A Hydrogel-Based Optical Fibre Fluorescent pH Sensor for Observing Lung Tumor Tissue Acidity. *Anal. Chim. Acta* **2020**, *1134*, 136.
- (1130) Stromer, B. S.; Kumar, C. V. White-Emitting Protein Nanoparticles for Cell-Entry and pH Sensing. *Adv. Funct. Mater.* **2017**, *27*, 1603874.
- (1131) Ma, J.; Ding, C.; Zhou, J.; Tian, Y. 2D Ratiometric Fluorescent pH Sensor for Tracking of Cells Proliferation and Metabolism. *Biosens. Bioelectron.* **2015**, *70*, 202–208.
- (1132) Arnett, T. R. Extracellular pH Regulates Bone Cell Function. *J. Nutr.* **2008**, *138*, 415S–418S.
- (1133) Zhang, X.; Lin, Y.; Gillies, R. J. Tumor pH and Its Measurement. *J. Nucl. Med.* **2010**, *51*, 1167–1170.
- (1134) Ke, G.; Zhu, Z.; Wang, W.; Zou, Y.; Guan, Z.; Jia, S.; Zhang, H.; Wu, X.; Yang, C. J. A Cell-Surface-Anchored Ratiometric Fluorescent Probe for Extracellular pH Sensing. *ACS Appl. Mater. Interfaces* **2014**, *6*, 15329–15334.
- (1135) Choi, W.-G.; Swanson, S. J.; Gilroy, S. High-Resolution Imaging of Ca²⁺, Redox Status, ROS and pH Using GFP Biosensors. *Plant J.* **2012**, *70*, 118–128.
- (1136) Gao, D.; Knight, M. R.; Trewavas, A. J.; Sattelmacher, B.; Plieth, C. Self-Reporting Arabidopsis Expressing pH and [Ca²⁺] Indicators Unveil Ion Dynamics in the Cytoplasm and in the Apoplast under Abiotic Stress. *Plant Physiol.* **2004**, *134*, 898–908.
- (1137) Gjetting, S. K.; Ytting, C. K.; Schulz, A.; Fuglsang, A. T. Live Imaging of Intra- and Extracellular pH in Plants Using pHusion, a Novel Genetically Encoded Biosensor. *J. Exp. Bot.* **2012**, *63*, 3207–3218.
- (1138) Michard, E.; Dias, P.; Feijó, J. A. Tobacco Pollen Tubes as Cellular Models for Ion Dynamics: Improved Spatial and Temporal Resolution of Extracellular Flux and Free Cytosolic Concentration of Calcium and Protons Using pHluorin and YC3.1 CaMeleon. *Sex. Plant Reprod.* **2008**, *21*, 169–181.
- (1139) Schulte, A.; Lorenzen, I.; Böttcher, M.; Plieth, C. A Novel Fluorescent pH Probe for Expression in Plants. *Plant Methods* **2006**, *2*, 7.
- (1140) Rao, T. P.; Yano, K.; Iijima, M.; Yamauchi, A.; Tatsumi, J. Regulation of Rhizosphere Acidification by Photosynthetic Activity in Cowpea (*Vigna unguiculata* L. Walp.) Seedlings. *Ann. Bot.* **2002**, *89*, 213–220.
- (1141) Blossfeld, S.; Gansert, D. A Novel Non-Invasive Optical Method for Quantitative Visualization of pH Dynamics in the Rhizosphere of Plants. *Plant, Cell Environ.* **2007**, *30*, 176–186.
- (1142) Blossfeld, S.; Perriguet, J.; Sterckeman, T.; Morel, J.-L.; Lösch, R. Rhizosphere pH Dynamics in Trace-Metal-Contaminated Soils, Monitored with Planar pH Optodes. *Plant Soil* **2010**, *330*, 173–184.
- (1143) Schreiber, C. M.; Zeng, B.; Blossfeld, S.; Rascher, U.; Kazda, M.; Schurr, U.; Höltkemeier, A.; Kuhn, A. J. Monitoring Rhizospheric pH, Oxygen, and Organic Acid Dynamics in Two Short-Time Flooded Plant Species. *J. Plant Nutr. Soil Sci.* **2012**, *175*, 761–768.
- (1144) Blossfeld, S.; Schreiber, C. M.; Liebsch, G.; Kuhn, A. J.; Hinsinger, P. Quantitative Imaging of Rhizosphere pH and CO₂ Dynamics with Planar Optodes. *Ann. Bot.* **2013**, *112*, 267–276.

- (1145) Buss, W.; Shepherd, J. G.; Heal, K. V.; Mašek, O. Spatial and Temporal Microscale pH Change at the Soil-Biochar Interface. *Geoderma* **2018**, *331*, 50–52.
- (1146) Rudolph-Mohr, N.; Tötze, C.; Kardjilov, N.; Oswald, S. E. Mapping Water, Oxygen, and pH Dynamics in the Rhizosphere of Young Maize Roots. *J. Plant Nutr. Soil Sci.* **2017**, *180*, 336–346.
- (1147) Santner, J.; Larsen, M.; Kreuzeder, A.; Glud, R. N. Two Decades of Chemical Imaging of Solutes in Sediments and Soils – a Review. *Anal. Chim. Acta* **2015**, *878*, 9–42.
- (1148) Kreuzeder, A.; Santner, J.; Scharching, V.; Oburger, E.; Hofer, C.; Hann, S.; Wenzel, W. W. In Situ Observation of Localized, Sub-Mm Scale Changes of Phosphorus Biogeochemistry in the Rhizosphere. *Plant Soil* **2018**, *424*, 573–589.
- (1149) Rérolle, V. M. C.; Floquet, C. F. A.; Mowlem, M. C.; Connelly, D. P.; Achterberg, E. P.; Bellerby, R. R. G. J. Seawater-pH Measurements for Ocean-Acidification Observations. *TrAC, Trends Anal. Chem.* **2012**, *40*, 146–157.
- (1150) Rérolle, V. M. C.; Floquet, C. F. A.; Harris, A. J. K.; Mowlem, M. C.; Bellerby, R. R. G. J.; Achterberg, E. P. Development of a Colorimetric Microfluidic pH Sensor for Autonomous Seawater Measurements. *Anal. Chim. Acta* **2013**, *786*, 124–131.
- (1151) Lai, C.-Z.; DeGrandpre, M. D.; Darlington, R. C. Autonomous Optofluidic Chemical Analyzers for Marine Applications: Insights from the Submersible Autonomous Moored Instruments (SAMI) for pH and pCO₂. *Front. Mar. Sci.* **2018**, *4*, 438.
- (1152) Kühl, M.; Behrendt, L.; Trampe, E. C. L. E.; Qvortrup, K.; Schreiber, U.; Borisov, S. M.; Klimant, I.; Larkum, A. W. D. Microenvironmental Ecology of the Chlorophyll B-Containing Symbiotic Cyanobacterium *Prochloron* in the Didemnid Ascidian *Lissoclinum Patella*. *Front. Microbiol.* **2012**, *3*, 402.
- (1153) Brodersen, K. E.; Koren, K.; Moßhammer, M.; Ralph, P. J.; Kühl, M.; Santner, J. Seagrass-Mediated Phosphorus and Iron Solubilization in Tropical Sediments. *Environ. Sci. Technol.* **2017**, *51*, 14155–14163.
- (1154) Michael, K. L.; Walt, D. R. Combined Imaging and Chemical Sensing of Fertilization-Induced Acid Release from Single Sea Urchin Eggs. *Anal. Biochem.* **1999**, *273*, 168–178.
- (1155) Elgetti Brodersen, K.; Koren, K.; Lichtenberg, M.; Kühl, M. Nanoparticle-Based Measurements of pH and O₂ Dynamics in the Rhizosphere of *Zostera Marina* L.: Effects of Temperature Elevation and Light-Dark Transitions. *Plant, Cell Environ.* **2016**, *39*, 1619–1630.
- (1156) Agayn, V. I.; Walt, D. R. Fiber-Optic Sensor for Continuous Monitoring of Fermentation pH. *Nat. Biotechnol.* **1993**, *11*, 726–729.
- (1157) Jeevarajan, A. S.; Vani, S.; Taylor, T. D.; Anderson, M. M. Continuous pH Monitoring in a Perfused Bioreactor System Using an Optical pH Sensor. *Biotechnol. Bioeng.* **2002**, *78*, 467–472.
- (1158) Kensy, F.; John, G. T.; Hofmann, B.; Büchs, J. Characterisation of Operation Conditions and Online Monitoring of Physiological Culture Parameters in Shaken 24-Well Microtiter Plates. *Bioprocess Biosyst. Eng.* **2005**, *28*, 75–81.
- (1159) Schneider, K.; Schütz, V.; John, G. T.; Heinzle, E. Optical Device for Parallel Online Measurement of Dissolved Oxygen and pH in Shake Flask Cultures. *Bioprocess Biosyst. Eng.* **2010**, *33*, 541–547.
- (1160) Isett, K.; George, H.; Herber, W.; Amanullah, A. Twenty-Four-Well Plate Miniature Bioreactor High-Throughput System: Assessment for Microbial Cultivations. *Biotechnol. Prog.* **2007**, *98*, 1017–1028.
- (1161) Naciri, M.; Kuystermans, D.; Al-Rubeai, M. Monitoring pH and Dissolved Oxygen in Mammalian Cell Culture Using Optical Sensors. *Cytotechnology* **2008**, *57*, 245–250.
- (1162) Velez-Suberbie, M. L.; Betts, J. P. J.; Walker, K. L.; Robinson, C.; Zoro, B.; Keshavarz-Moore, E. High Throughput Automated Microbial Bioreactor System Used for Clone Selection and Rapid Scale-down Process Optimization. *Biotechnol. Prog.* **2018**, *34*, 58–68.
- (1163) Hsu, W.-T.; Aulakh, R. P. S.; Traul, D. L.; Yuk, I. H. Advanced Microscale Bioreactor System: A Representative Scale-down Model for Bench-Top Bioreactors. *Cytotechnology* **2012**, *64*, 667–678.
- (1164) Puskeiler, R.; Kaufmann, K.; Weuster-Botz, D. Development, Parallelization, and Automation of a Gas-Inducing Milliliter-Scale Bioreactor for High-Throughput Bioprocess Design (HTBD). *Biotechnol. Bioeng.* **2005**, *89*, 512–523.
- (1165) Chen, A.; Chitta, R.; Chang, D.; Amanullah, A. Twenty-Four Well Plate Miniature Bioreactor System as a Scale-down Model for Cell Culture Process Development. *Biotechnol. Bioeng.* **2009**, *102*, 148–160.
- (1166) Moses, S.; Manahan, M.; Ambrogely, A.; Ling, W. L. W. Assessment of AMBRTM as a Model for High-Throughput Cell Culture Process Development Strategy. *Adv. Biosci. Biotechnol.* **2012**, *03*, 918–927.
- (1167) Schmideder, A.; Weuster-Botz, D. High-Performance Recombinant Protein Production with *Escherichia Coli* in Continuously Operated Cascades of Stirred-Tank Reactors. *J. Ind. Microbiol. Biotechnol.* **2017**, *44*, 1021–1029.
- (1168) Janzen, N. H.; Schmidt, M.; Krause, C.; Weuster-Botz, D. Evaluation of Fluorimetric pH Sensors for Bioprocess Monitoring at Low pH. *Bioprocess Biosyst. Eng.* **2015**, *38*, 1685–1692.
- (1169) Sardesai, N.; Rao, G.; Kostov, Y. Versatile Common Instrumentation for Optical Detection of pH and Dissolved Oxygen. *Rev. Sci. Instrum.* **2015**, *86*, No. 074302.
- (1170) Ge, X.; Rao, G. Real-time Monitoring of Shake Flask Fermentation and off Gas Using Triple Disposable Noninvasive Optical Sensors. *Biotechnol. Prog.* **2012**, *28*, 872–877.
- (1171) Kondragunta, B.; Drew, J. L.; Brorson, K. A.; Moreira, A. R.; Rao, G. Advances in Clone Selection Using High-Throughput Bioreactors. *Biotechnol. Prog.* **2010**, *26*, 1095–1103.
- (1172) Lee, S.; Ibey, B. L.; Coté, G. L.; Pishko, M. V. Measurement of pH and Dissolved Oxygen within Cell Culture Media Using a Hydrogel Microarray Sensor. *Sens. Actuators, B* **2008**, *128*, 388–398.
- (1173) Boniello, C.; Mayr, T.; Klimant, I.; Koenig, B.; Riethorst, W.; Nidetzky, B. Intraparticle Concentration Gradients for Substrate and Acidic Product in Immobilized Cephalosporin C Amidase and Their Dependencies on Carrier Characteristics and Reaction Parameters. *Biotechnol. Bioeng.* **2010**, *106*, 528–540.
- (1174) Consolati, T.; Bolivar, J. M.; Petrasek, Z.; Berenguer, J.; Hidalgo, A.; Guisán, J. M.; Nidetzky, B. Biobased, Internally pH-Sensitive Materials: Immobilized Yellow Fluorescent Protein as an Optical Sensor for Spatiotemporal Mapping of pH Inside Porous Matrices. *ACS Appl. Mater. Interfaces* **2018**, *10*, 6858–6868.
- (1175) Piletsky, S. A.; Panasyuk, T. L.; Piletskaya, E. V.; Sergeeva, T. A.; El'skaya, A. V.; Pringsheim, E.; Wolfbeis, O. S. Polyaniline-Coated Microtiter Plates for Use in Longwave Optical Bioassays. *Fresenius' J. Anal. Chem.* **2000**, *366*, 807–810.
- (1176) Busch, M.; Höbel, W.; Polster, J. Software FIACRE: Bioprocess Monitoring on the Basis of Flow Injection Analysis Using Simultaneously a Urea Optode and a Glucose Luminescence Sensor. *J. Biotechnol.* **1993**, *31*, 327–343.
- (1177) Kulp, T. J.; Camins, I.; Angel, S. M.; Munkholm, C.; Walt, D. R. Polymer Immobilized Enzyme Optodes for the Detection of Penicillin. *Anal. Chem.* **1987**, *59*, 2849–2853.
- (1178) Fuh, M. R. S.; Burgess, L. W.; Christian, G. D. Single Fiber-Optic Fluorescence Enzyme-Based Sensor. *Anal. Chem.* **1988**, *60*, 433–435.
- (1179) Xie, X.; Suleiman, A. A.; Guilbault, G. G. A Fluorescence-based Fiber Optic Biosensor for the Flow-injection Analysis of Penicillin. *Biotechnol. Bioeng.* **1992**, *39*, 1147–1150.
- (1180) Healey, B. G.; Walt, D. R. Improved Fiber-Optic Chemical Sensor for Penicillin. *Anal. Chem.* **1995**, *67*, 4471–4476.
- (1181) Yerian, T. D.; Christian, G. D.; Ruzicka, J. Flow Injection Analysis as a Diagnostic Tool for Development and Testing of a Penicillin Sensor. *Anal. Chem.* **1988**, *60*, 1250–1256.
- (1182) Scheper, Th.; Brandes, W.; Maschke, H.; Plötz, F.; Müller, C. Two FIA-Based Biosensor Systems Studied for Bioprocess Monitoring. *J. Biotechnol.* **1993**, *31*, 345–356.
- (1183) Yadavalli, V. K.; Koh, W.-G.; Lazur, G. J.; Pishko, M. V. Microfabricated Protein-Containing Poly (Ethylene Glycol) Hydrogel Arrays for Biosensing. *Sens. Actuators, B* **2004**, *97*, 290–297.
- (1184) Tsai, H.; Doong, R. Simultaneous Determination of Renal Clinical Analytes in Serum Using Hydrolase- and Oxidase-Encapsulated Optical Array Biosensors. *Anal. Biochem.* **2004**, *334*, 183–192.

- (1185) Koncki, R.; Lenarczuk, T.; Radomska, A.; Głab, S. Optical Biosensors Based on Prussian Blue Films. *Analyst* **2001**, *126*, 1080–1085.
- (1186) Brennan, J. D.; Brown, R. S.; Della Manna, A.; Kallury, K. M.; Piunno, P. A.; Krull, U. J. Covalent Immobilization of Amphiphilic Monolayers Containing Urease onto Optical Fibers for Fluorimetric Detection of Urea. *Sens. Actuators, B* **1993**, *11*, 109–119.
- (1187) Yerian, T. D.; Christian, G. D.; Růžička, J. Enzymatic Determination of Urea in Water and Serum by Optosensing Flow Injection Analysis. *Analyst* **1986**, *111*, 865–873.
- (1188) Koncki, R.; Wolfbeis, O. S. Composite Films of Prussian Blue and *N*-Substituted Polypyrrroles: Covalent Immobilization of Enzymes and Application to near Infrared Optical Biosensing. *Biosens. Bioelectron.* **1999**, *14*, 87–92.
- (1189) Scheper, T.; Brandes, W.; Maschke, H.; Plötz, F.; Müller, C. Two FIA-Based Biosensor Systems Studied for Bioprocess Monitoring. *J. Biotechnol.* **1993**, *31*, 345–356.
- (1190) de Marcos, S.; Hortigüela, R.; Gatbán, J.; Castillo, J. R.; Wolfbeis, O. S. Characterization of a Urea Optical Sensor Based on Polypyrrrole. *Microchim. Acta* **1999**, *130*, 267–272.
- (1191) Busch, M.; Gutberlet, F.; Hoebel, W.; Polster, J.; Schmidt, H.-L.; Schwenk, M. The Application of Optodes in FIA-Based Fermentation Process Control Using the Software Package FIACRE. *Sens. Actuators, B* **1993**, *11*, 407–412.
- (1192) Tsai, H.; Doong, R. Simultaneous Determination of pH, Urea, Acetylcholine and Heavy Metals Using Array-Based Enzymatic Optical Biosensor. *Biosens. Bioelectron.* **2005**, *20*, 1796–1804.
- (1193) Esmaeili, C.; Heng, L. Y.; Ling, T. L. Nile Blue Chromoionophore-Doped Kappa-Carrageenan for a Novel Reflectometric Urea Biosensor. *Sens. Actuators, B* **2015**, *221*, 969–977.
- (1194) Kazakova, L. I.; Shabarchina, L. I.; Sukhorukov, G. B. Co-Encapsulation of Enzyme and Sensitive Dye as a Tool for Fabrication of Microcapsule Based Sensor for Urea Measuring. *Phys. Chem. Chem. Phys.* **2011**, *13*, 11110–11117.
- (1195) Koh, W.-G.; Pishko, M. Immobilization of Multi-Enzyme Microreactors inside Microfluidic Devices. *Sens. Actuators, B* **2005**, *106*, 335–342.
- (1196) Andreou, V. G.; Clonis, Y. D. Novel Fiber-Optic Biosensor Based on Immobilized Glutathione S-Transferase and Sol–Gel Entrapped Bromocresol Green for the Determination of Atrazine. *Anal. Chim. Acta* **2002**, *460*, 151–161.
- (1197) Vamvakaki, V.; Fournier, D.; Chaniotakis, N. A. Fluorescence Detection of Enzymatic Activity within a Liposome Based Nano-Biosensor. *Biosens. Bioelectron.* **2005**, *21*, 384–388.
- (1198) Pfeiffer, S. A.; Borisov, S. M.; Nagl, S. In-Line Monitoring of pH and Oxygen during Enzymatic Reactions in off-the-Shelf All-Glass Microreactors Using Integrated Luminescent Microsensors. *Microchim. Acta* **2017**, *184*, 621–626.
- (1199) Xavier, M. P.; Vallejo, B.; Marazuela, M. D.; Moreno-Bondi, M. C.; Baldini, F.; Falai, A. Fiber Optic Monitoring of Carbamate Pesticides Using Porous Glass with Covalently Bound Chlorophenol Red. *Biosens. Bioelectron.* **2000**, *14*, 895–905.
- (1200) Doong, R.-A.; Tsai, H.-C. Immobilization and Characterization of Sol–Gel-Encapsulated Acetylcholinesterase Fiber-Optic Biosensor. *Anal. Chim. Acta* **2001**, *434*, 239–246.
- (1201) Russell, R. J.; Pishko, M. V.; Simonian, A. L.; Wild, J. R. Poly(Ethylene Glycol) Hydrogel-Encapsulated Fluorophore–Enzyme Conjugates for Direct Detection of Organophosphorus Neurotoxins. *Anal. Chem.* **1999**, *71*, 4909–4912.
- (1202) Viveros, L.; Paliwal, S.; McCrae, D.; Wild, J.; Simonian, A. A Fluorescence-Based Biosensor for the Detection of Organophosphate Pesticides and Chemical Warfare Agents. *Sens. Actuators, B* **2006**, *115*, 150–157.
- (1203) Jerónimo, P. C. A.; Araújo, A. N.; Montenegro, M. C. B. S. M.; Satinský, D.; Solich, P. Flow-through Sol–Gel Optical Biosensor for the Colorimetric Determination of Acetazolamide. *Analyst* **2005**, *130*, 1190–1197.
- (1204) Bidmanova, S.; Steiner, M.-S.; Stepan, M.; Vymazalova, K.; Gruber, M. A.; Duerkop, A.; Damborsky, J.; Prokop, Z.; Wolfbeis, O. S. Enzyme-Based Test Strips for Visual or Photographic Detection and Quantitation of Gaseous Sulfur Mustard. *Anal. Chem.* **2016**, *88*, 6044–6049.
- (1205) Charlton, S. C.; Fleming, R. L.; Zipp, A. Solid-Phase Colorimetric Determination of Potassium. *Clin. Chem.* **1982**, *28*, 1857–1861.
- (1206) Lerchi, M.; Bakker, E.; Rusterholz, B.; Simon, W. Lead-Selective Bulk Optodes Based on Neutral Ionophores with Subnanomolar Detection Limits. *Anal. Chem.* **1992**, *64*, 1534–1540.
- (1207) He, H.; Li, H.; Mohr, G.; Kovacs, B.; Werner, T.; Wolfbeis, O. S. Novel Type of Ion-Selective Fluorosensor Based on the Inner Filter Effect: An Optrode for Potassium. *Anal. Chem.* **1993**, *65*, 123–127.
- (1208) Wolfbeis, O. S. Optical Sensors in Flow Injection Analysis. *J. Mol. Struct.* **1993**, *292*, 133–140.
- (1209) Xiong, Y.; Huang, Y.; Ye, Z.; Guan, Y. Flow Injection Small-Volume Fiber-Optic pH Sensor Based on Evanescent Wave Excitation and Fluorescence Determination. *J. Fluoresc.* **2011**, *21*, 1137–1142.
- (1210) Li, H.; Wolfbeis, O. S. Determination of Urease Activity by Flow-Injection Analysis Using an Ammonium-Selective Optrode as the Detector. *Anal. Chim. Acta* **1993**, *276*, 115–119.
- (1211) Gruber, P.; Marques, M. P. C.; Szita, N.; Mayr, T. Integration and Application of Optical Chemical Sensors in Microbioreactors. *Lab Chip* **2017**, *17*, 2693–2712.
- (1212) Fan, H.; Lu, Y.; Stump, A.; Reed, S. T.; Baer, T.; Schunk, R.; Perez-Luna, V.; López, G. P.; Brinker, C. J. Rapid Prototyping of Patterned Functional Nanostructures. *Nature* **2000**, *405*, 56–60.
- (1213) Florea, L.; Fay, C.; Lahiff, E.; Phelan, T.; O'Connor, N. E.; Corcoran, B.; Diamond, D.; Benito-Lopez, F. Dynamic pH Mapping in Microfluidic Devices by Integrating Adaptive Coatings Based on Polyaniline with Colorimetric Imaging Techniques. *Lab Chip* **2013**, *13*, 1079–1085.
- (1214) Zhu, H.; Zhou, X.; Su, F.; Tian, Y.; Ashili, S.; Holl, M. R.; Meldrum, D. R. Micro-Patterning and Characterization of pHEMA-Co-PAM-Based Optical Chemical Sensors for Lab-on-a-Chip Applications. *Sens. Actuators, B* **2012**, *173*, 817–823.
- (1215) Tahirbegi, I. B.; Ehgartner, J.; Sulzer, P.; Zieger, S.; Kasjanow, A.; Paradiso, M.; Strobl, M.; Bouwes, D.; Mayr, T. Fast Pesticide Detection inside Microfluidic Device with Integrated Optical pH, Oxygen Sensors and Algal Fluorescence. *Biosens. Bioelectron.* **2017**, *88*, 188–195.
- (1216) Tang, Y.; Zhen, L.; Liu, J.; Wu, J. Rapid Antibiotic Susceptibility Testing in a Microfluidic pH Sensor. *Anal. Chem.* **2013**, *85*, 2787–2794.
- (1217) Thete, A. R.; Gross, G. A.; Henkel, T.; Koehler, J. M. Microfluidic Arrangement with an Integrated Micro-Spot Array for the Characterization of pH and Solvent Polarity. *Chem. Eng. J.* **2008**, *135*, S327–S332.
- (1218) Zhan, W.; Seong, G. H.; Crooks, R. M. Hydrogel-Based Microreactors as a Functional Component of Microfluidic Systems. *Anal. Chem.* **2002**, *74*, 4647–4652.
- (1219) Klauke, N.; Monaghan, P.; Sinclair, G.; Padgett, M.; Cooper, J. Characterisation of Spatial and Temporal Changes in pH Gradients in Microfluidic Channels Using Optically Trapped Fluorescent Sensors. *Lab Chip* **2006**, *6*, 788–793.
- (1220) Funfak, A.; Cao, J.; Wolfbeis, O. S.; Martin, K.; Köhler, J. M. Monitoring Cell Cultivation in Microfluidic Segments by Optical pH Sensing with a Micro Flow-through Fluorometer Using Dye-Doped Polymer Particles. *Microchim. Acta* **2009**, *164*, 279–286.
- (1221) Brigo, L.; Carofiglio, T.; Fregonese, C.; Meneguzzi, F.; Mistura, G.; Natali, M.; Tonellato, U. An Optical Sensor for pH Supported onto Tentagel Resin Beads. *Sens. Actuators, B* **2008**, *130*, 477–482.
- (1222) Gruber, P.; Marques, M. P. C.; Sulzer, P.; Wohlgemuth, R.; Mayr, T.; Baganz, F.; Szita, N. Real-Time pH Monitoring of Industrially Relevant Enzymatic Reactions in a Microfluidic Side-Entry Reactor (MSER) Shows Potential for pH Control. *Biotechnol. J.* **2017**, *12*, 1600475.
- (1223) Nagl, S. Micro Free-Flow Isoelectric Focusing with Integrated Optical pH Sensors. *Eng. Life Sci.* **2018**, *18*, 114–123.

- (1224) Poehler, E.; Herzog, C.; Lotter, C.; Pfeiffer, S. A.; Aigner, D.; Mayr, T.; Nagl, S. Label-Free Microfluidic Free-Flow Isoelectric Focusing, pH Gradient Sensing and near Real-Time Isoelectric Point Determination of Biomolecules and Blood Plasma Fractions. *Analyst* **2015**, *140*, 7496–7502.
- (1225) Kalpana, S.; Priyadarshini, S. R.; Maria Leena, M.; Moses, J. A.; Anandharamakrishnan, C. Intelligent Packaging: Trends and Applications in Food Systems. *Trends Food Sci. Technol.* **2019**, *93*, 145–157.
- (1226) Kuswandi, B.; Nurfawaidi, A. On-Package Dual Sensors Label Based on pH Indicators for Real-Time Monitoring of Beef Freshness. *Food Control* **2017**, *82*, 91–100.
- (1227) Kurek, M.; Garofulić, I. E.; Bakić, M. T.; Šćetar, M.; Uzelac, V. D.; Galić, K. Development and Evaluation of a Novel Antioxidant and pH Indicator Film Based on Chitosan and Food Waste Sources of Antioxidants. *Food Hydrocolloids* **2018**, *84*, 238–246.
- (1228) Luchese, C. L.; Abdalla, V. F.; Spada, J. C.; Tessaro, I. C. Evaluation of Blueberry Residue Incorporated Cassava Starch Film as pH Indicator in Different Simulants and Foodstuffs. *Food Hydrocolloids* **2018**, *82*, 209–218.
- (1229) Ma, Q.; Liang, T.; Cao, L.; Wang, L. Intelligent Poly (Vinyl Alcohol)-Chitosan Nanoparticles-Mulberry Extracts Films Capable of Monitoring pH Variations. *Int. J. Biol. Macromol.* **2018**, *108*, 576–584.
- (1230) Ma, Q.; Wang, L. Preparation of a Visual pH-Sensing Film Based on Tara Gum Incorporating Cellulose and Extracts from Grape Skins. *Sens. Actuators, B* **2016**, *235*, 401–407.
- (1231) Prietto, L.; Mirapallete, T. C.; Pinto, V. Z.; Hoffmann, J. F.; Vanier, N. L.; Lim, L.-T.; Guerra Dias, A. R.; da Rosa Zavareze, E. pH-Sensitive Films Containing Anthocyanins Extracted from Black Bean Seed Coat and Red Cabbage. *LWT* **2017**, *80*, 492–500.
- (1232) Moradi, M.; Tajik, H.; Almasi, H.; Forough, M.; Ezati, P. A Novel pH-Sensing Indicator Based on Bacterial Cellulose Nanofibers and Black Carrot Anthocyanins for Monitoring Fish Freshness. *Carbohydr. Polym.* **2019**, *222*, 115030.
- (1233) Yong, H.; Wang, X.; Bai, R.; Miao, Z.; Zhang, X.; Liu, J. Development of Antioxidant and Intelligent pH-Sensing Packaging Films by Incorporating Purple-Fleshed Sweet Potato Extract into Chitosan Matrix. *Food Hydrocolloids* **2019**, *90*, 216–224.
- (1234) Choi, I.; Lee, J. Y.; Lacroix, M.; Han, J. Intelligent pH Indicator Film Composed of Agar/Potato Starch and Anthocyanin Extracts from Purple Sweet Potato. *Food Chem.* **2017**, *218*, 122–128.
- (1235) Jayakumar, A.; Heera, K. V.; Sumi, T. S.; Joseph, M.; Mathew, S.; Praveen, G.; Nair, I. C.; Radhakrishnan, E. K. Starch-PVA Composite Films with Zinc-Oxide Nanoparticles and Phytochemicals as Intelligent pH Sensing Wraps for Food Packaging Application. *Int. J. Biol. Macromol.* **2019**, *136*, 395–403.
- (1236) Liu, J.; Wang, H.; Guo, M.; Li, L.; Chen, M.; Jiang, S.; Li, X.; Jiang, S. Extract from Lycium Ruthenicum Murr. Incorporating κ -Carrageenan Colorimetric Film with a Wide pH-Sensing Range for Food Freshness Monitoring. *Food Hydrocolloids* **2019**, *94*, 1–10.
- (1237) Musso, Y. S.; Salgado, P. R.; Mauri, A. N. Smart Edible Films Based on Gelatin and Curcumin. *Food Hydrocolloids* **2017**, *66*, 8–15.
- (1238) Liang, T.; Wang, L. A pH-Sensing Film from Tamarind Seed Polysaccharide with Litmus Lichen Extract as an Indicator. *Polymers* **2018**, *10*, 13.
- (1239) Ezati, P.; Tajik, H.; Moradi, M.; Molaei, R. Intelligent pH-Sensitive Indicator Based on Starch-Cellulose and Alizarin Dye to Track Freshness of Rainbow Trout Fillet. *Int. J. Biol. Macromol.* **2019**, *132*, 157–165.
- (1240) Moreira, J. B.; Terra, A. L. M.; Costa, J. A. V.; Greque de Morais, M. G. Development of pH Indicator from PLA/PEO Ultrafine Fibers Containing Pigment of Microalgae Origin. *Int. J. Biol. Macromol.* **2018**, *118*, 1855–1862.
- (1241) Ding, L.; Li, X.; Hu, L.; Zhang, Y.; Jiang, Y.; Mao, Z.; Xu, H.; Wang, B.; Feng, X.; Sui, X. A Naked-Eye Detection Polyvinyl Alcohol/Cellulose-Based pH Sensor for Intelligent Packaging. *Carbohydr. Polym.* **2020**, *233*, 115859.
- (1242) Zhang, H.; Hou, A.; Xie, K.; Gao, A. Smart Color-Changing Paper Packaging Sensors with pH Sensitive Chromophores Based on Azo-Anthraquinone Reactive Dyes. *Sens. Actuators, B* **2019**, *286*, 362–369.
- (1243) Pacquit, A.; Lau, K. T.; McLaughlin, H.; Frisby, J.; Quilty, B.; Diamond, D. Development of a Volatile Amine Sensor for the Monitoring of Fish Spoilage. *Talanta* **2006**, *69*, 515–520.
- (1244) Borchert, N. B.; Kerry, J. P.; Papkovsky, D. B. A CO₂ Sensor Based on Pt-Porphyrin Dye and FRET Scheme for Food Packaging Applications. *Sens. Actuators, B* **2013**, *176*, 157–165.
- (1245) Behnood, A.; Van Tittelboom, K.; De Belie, N. Methods for Measuring pH in Concrete: A Review. *Constr. Build. Mater.* **2016**, *105*, 176–188.
- (1246) Dantan, N.; Habel, W. R.; Wolfbeis, O. S. Fiber Optic pH Sensor for Early Detection of Danger of Corrosion in Steel-Reinforced Concrete Structures. In *Smart Structures and Materials 2005: Smart Sensor Technology and Measurement Systems*; International Society for Optics and Photonics, 2005; Vol. 5758, pp 274–285.
- (1247) Blumentritt, M.; Melhorn, K.; Flachsbarth, J.; Kroener, M.; Kowalsky, W.; Johannes, H.-H. A Novel Fabrication Method of Fiber-Optical Planar Transmission Sensors for Monitoring pH in Concrete Structures. *Sens. Actuators, B* **2008**, *131*, 504–508.
- (1248) McPolin, D. O.; Basheer, P. A. M.; Grattan, K. T. V.; Long, A. E.; Sun, T.; Xie, W. Preliminary Development and Evaluation of Fiber-Optic Chemical Sensors. *J. Mater. Civ. Eng.* **2011**, *23*, 1200–1210.
- (1249) Müller, B.; Grengg, C.; Schallert, V.; Sakoparnig, M.; Staudinger, C.; Breininger, J.; Mittermayr, F.; Ungerböck, B.; Borisov, S. M.; Dietzel, M.; et al. Wide-Range Optical pH Imaging of Cementitious Materials Exposed to Chemically Corrosive Environments. *RILEM Technol. Lett.* **2018**, *3*, 39–45.
- (1250) Nielsen, S. D.; Paegle, L.; Borisov, S. M.; Kjeldsen, K. U.; Røy, H.; Skibsted, J.; Koren, K. Optical Sensing of pH and O₂ in the Evaluation of Bioactive Self-Healing Cement. *ACS Omega* **2019**, *4*, 20237–20243.